

STUDY OF REACTIVE INTERMEDIATES: 1. TRANSIENT STANNYLENES IN  
SOLUTION; 2. TIME-RESOLVED SPECTROSCOPIC STUDIES OF DI-*TERT*-  
BUTYLSILYLENE IN SOLUTION

STUDY OF REACTIVE INTERMEDIATES: 1. TRANSIENT STANNYLENES IN  
SOLUTION; 2. TIME-RESOLVED SPECTROSCOPIC STUDIES OF DI-*TERT*-  
BUTYLSILYLENE IN SOLUTION

By: IAN RUIXIANG DUFFY, B.Sc. (Honours)

A Thesis

Submitted to the School of Graduate Studies  
in Partial Fulfillment of the Requirements  
for the Degree Doctor of Philosophy

McMaster University

© Ian Ruixiang Duffy, April 2018

DOCTOR OF PHILOSOPHY (2018)

McMaster University

(Chemistry)

Hamilton, Ontario

TITLE: Study of Reactive Intermediates: 1. Transient Stannylenes in Solution; 2. Time-resolved Spectroscopic Studies of Di-*tert*-butylsilylene in Solution

AUTHOR: Ian Ruixiang Duffy

*B.Sc. (Honours, University of British Columbia)*

SUPERVISOR: Professor William J. Leigh

NUMBER OF PAGES: xxxviii, 298

ABSTRACT:

The transient Sn(II) compounds dimethyl-, diphenyl-, methylphenyl-, and dimesitylstannylene ( $\text{SnMe}_2$ ,  $\text{SnPh}_2$ ,  $\text{SnMePh}$ , and  $\text{SnMes}_2$ , respectively) have been successfully detected and characterized in solution. The stannylenes were generated by photolysis of appropriately substituted 1-stannacyclopent-3-ene derivatives, which have each been shown to extrude the respective stannylene cleanly, through stannylene trapping studies using dichlorodimethylstannane ( $\text{Me}_2\text{SnCl}_2$ ) as the substrate. Quantum yields for stannylene extrusion have been measured in three cases, and found to be in the range of 0.4 - 0.8.

Laser flash photolysis of the stannacyclopent-3-ene derivatives in deoxygenated hexanes affords promptly-formed transient absorptions assigned to  $\text{SnMe}_2$  ( $\lambda_{\text{max}} = 500 \text{ nm}$ ;  $\epsilon_{500} = 1,800 \pm 600 \text{ M}^{-1}\text{cm}^{-1}$ ),  $\text{SnPh}_2$  ( $\lambda_{\text{max}} = 300, 505 \text{ nm}$ ;  $\epsilon_{500} = 2,500 \pm 600 \text{ M}^{-1}\text{cm}^{-1}$ ),  $\text{SnMePh}$  ( $\lambda_{\text{max}} = 280, 500 \text{ nm}$ ) and  $\text{SnMes}_2$  ( $\lambda_{\text{max}} < 270, 330(\text{sh}), 550 \text{ nm}$ ), which decay on the microsecond timescale with second order kinetics, consistent with dimerization being the major reaction in the absence of a substrate. Dimerization of  $\text{SnMe}_2$  and  $\text{SnMes}_2$  affords species exhibiting  $\lambda_{\text{max}} = 465 \text{ nm}$  and  $\lambda_{\text{max}} = 490 \text{ nm}$ , respectively, which were assigned to the expected Sn=Sn doubly-bonded dimers, tetramethyl- and tetramesityldistannene, respectively. In contrast, the spectrum of the dimer formed from  $\text{SnPh}_2$  exhibits strong absorptions in the 280 - 380 nm range and a very weak absorption at 650 nm, on the basis of which it is assigned to phenyl(triphenylstannyl)stannylene ( $\text{SnPh}(\text{SnPh}_3)$ ).

The reaction of acetic acid ( $\text{AcOH}$ ) with  $\text{SnPh}_2$  and  $\text{SnMes}_2$  proceeds via arene elimination. With  $\text{SnMe}_2$ , the products are derived from the elimination of methane and O-



H insertion, while SnMePh reacts to afford both benzene and methane in a ca. 3:2 molar ratio.  $\sigma$ -Bond insertion of SnMe<sub>2</sub> with tributylchlorostannane (Bu<sub>3</sub>SnCl) yields the formal Sn-Cl insertion product, Bu<sub>3</sub>SnSnMe<sub>2</sub>Cl.

Lewis acid-base complexation with simple aliphatic O, S, and N donors proceeds rapidly and reversibly, generating the corresponding stannylene-donor pairs, and exhibiting absorption maxima  $\lambda_{\text{max}} \sim 310 - 385$  nm. Equilibrium constants ( $K_{\text{eq}}$ ) upon O-donor coordination afford stabilization energies of -1.9 to -4.0 kcal mol<sup>-1</sup> for SnMe<sub>2</sub> and SnPh<sub>2</sub>, and suggesting a Lewis acidity order SiR<sub>2</sub> > SnR<sub>2</sub> > GeR<sub>2</sub> (R = Me, Ph). Complexation of SnMe<sub>2</sub> with O, S and N donors proceed with a reduction in reaction exergonicity relative to SnPh<sub>2</sub>. Reactions of SnMe<sub>2</sub> and SnPh<sub>2</sub> with Bu<sub>3</sub>SnH and C-C unsaturated compounds proceed with the characteristics of reversible complexation, affording short-lived Lewis acid-base products detectable by transient UV-vis spectroscopy ( $\lambda_{\text{max}} = 375 - 430$  nm).

Di-*tert*-butylsilylene (Sit-Bu<sub>2</sub>) has also been successfully detected and characterized in solution by laser flash photolysis methods, via the photolysis of 7,7-di-*tert*-butyl-7-silabicyclo[4.1.0]heptane and hexa-*tert*-butylcyclotrisilane. This transient silylene exhibits a UV-vis absorption band centred at  $\lambda_{\text{max}} = 515$  nm and decays with second order kinetics to afford a long-lived product assigned to tetra-*tert*-butyldisilene ( $\lambda_{\text{max}} = 290, 435$  nm). Absolute rate constants ( $k_{\text{Q}}$ ) were determined for the reactions of Sit-Bu<sub>2</sub> with several silylene substrates in hexanes at 25 °C. Sit-Bu<sub>2</sub> is seen to react slower compared to SiMe<sub>2</sub>, with  $k_{\text{rel}} (= k_{\text{Q}}^{\text{SiMe}_2}/k_{\text{Q}}^{\text{SitBu}_2})$  ranging between 0.8 - 310, cycloaddition reactions having exhibited the largest sensitivity to the *tert*-butyl for methyl substitution.

#### ACKNOWLEDGEMENTS:

First and foremost, I would like to express my sincere thanks to my supervisor, Dr. William Leigh, for his mentorship and endless patience over the years. Willie helped me develop the rigor and attention to detail that is required to become a good scientist. I believe I was most successful and productive working in this environment as I was given the freedom and encouragement to pursue and follow through with my own ideas. I would also like to express my gratitude to my committee members: Dr. Emslie and Dr. Brook for their helpful guidance during my committee meetings, and to my external examiner Dr. Rivard from the University of Alberta for his constructive feedback.

I have had the pleasure of working with some outstanding undergraduate students on several projects concerning the chemistry of silicon, germanium and tin: Laura Smith, Peter Ho, Joanna Leake, Ryan Maar, Claire Browne, Jasper Woodard, and Brianna Nguyen. Good luck to all of you in your future endeavours. Thank you to my colleagues whom I have had the pleasure of knowing and working with over the years. I have always appreciated the camaraderie and fruitful scientific discussion with my former group members: Dr. Saurabh Chitnis, Dr. Farah Lollmahomed, Dr. Lawrence Huck, Adroha Bhattacharya, Saed Isaac, Sam Saeidi, Dr. Svetlana Kostina, Ketha Jeyakanthan, and Michael Son. A special thank you also goes out to Dr. Peng Wang, Dr. Stephen Wang, Dr. Corey Thompson, Dr. Amir Mohtasebi, Darryl Fong and Ayodele Fatona for their continued friendship and advice over the years. The door to ABB111 is always open; please feel free to disturb.

Completing this thesis would not have been possible without the support of my parents, who have always encouraged me to follow my passion and taught me the value of persistence and perseverance. Thank you to my brother, Tim, who is always someone that I could talk to about anything anytime. Finally, I save my most important thank you to my wife, Heran, and son, Sean. 2017-2018 were productive years for us! I look forward to starting the next chapter of our lives together.

TABLE OF CONTENTS:

List of Figures	xii	
List of Tables	xxxi	
List of Compound Numbers	xxxiv	
<b>Chapter 1 - Introduction</b>		
<b>1.1.</b>	Foreword	1
<b>1.2.</b>	Nomenclature	2
<b>1.3.</b>	Structure and Properties of Stannylenes	2
<b>1.4.1.</b>	Stable Stannylenes - An Overview	4
<b>1.4.2.</b>	Structural Properties of Stannylenes	4
<b>1.4.3.</b>	Reactions of Stannylenes	6
<b>1.4.3(a)</b>	Dimerization	7
<b>1.4.3(b)</b>	Coordination	8
<b>1.4.3(c)</b>	Cycloaddition	10
<b>1.4.3(d)</b>	Insertion (oxidative addition)	11
<b>1.4.3(e)</b>	Substitution (elimination)	12
<b>1.4.3(f)</b>	Applications of Stannylene Chemistry	14
<b>1.4.4.</b>	Intramolecular and Intermolecular Donor-stabilized Stannylenes	16
<b>1.4.5.</b>	Stannylenes Stabilized by Group 15-16 Elements	17
<b>1.4.6.</b>	Donor-acceptor Stabilized Stannylenes	18
<b>1.4.7.</b>	Divalent Tin Hydrides	19
<b>1.5.1.</b>	Studies of Transient Stannylenes in Frozen Matrix, Gas and Solution	20

	Phases - An Overview	
1.5.2.	Chemical Trapping Studies of Transient Stannylenes	21
1.5.3.	Direct Detection and Reactivity Studies of Transient Stannylenes	27
1.6.	Theoretical Studies of Transient Stannylenes	30
1.7.	Techniques used in Reactivity Studies	35
1.8.	Thesis Objectives - Goals of the Work Presented in this Thesis	36
1.9.	Thesis Summary	38
1.10.	References	41
<b>Chapter 2: Direct Detection, Dimerization and Chemical Trapping of Dimethyl- and Diphenylstannylene from Photolysis of Stannacyclopent-3-enes in Solution</b>		
2.1.	Overview	50
2.2.	Results and Discussion	51
2.2.1.	Stannacyclopent-3-ene Photochemistry – Trapping of Transient Stannylenes	51
2.2.2.	Direct Detection of Transient Stannylenes by Laser Flash Photolysis	60
2.2.3.	Computational Studies <sup>55</sup>	69
2.3.	Summary and Conclusions	78
2.4.	Supporting Information	81
2.5.	References	93
<b>Chapter 3: Reactivity of Transient Stannylenes in Solution 1) Direct Detection of SnMePh and Reactions of SnMe<sub>2</sub>, SnPh<sub>2</sub>, and SnMePh with Chlorostannanes and Acetic Acid</b>		
3.1.	Overview	97

3.2.	Direct Detection and Chemical Trapping of SnMePh in Solution	98
3.2.1.	Results	98
3.2.2.	Discussion	108
3.3.	The Reactions of Transient Stannylenes with Tri- <i>n</i> -butyltin Chloride	110
3.3.1.	Results	110
3.3.2.	Discussion	115
3.4.	The Reactions of SnMe <sub>2</sub> , SnPh <sub>2</sub> and SnMePh with Acetic Acid	119
3.4.1.	Results	119
3.4.2.	Discussion	128
3.5.	Summary and Conclusions	133
3.6.	Supporting Information	134
3.7.	References	141
 <b>Chapter 4: Reactivity of Transient Stannylenes in Solution (2) Lewis Acid-Base Complexation of SnMe<sub>2</sub> and SnPh<sub>2</sub> with O-, S-, and N-Donors, C-C Unsaturated Compounds, and Trialkyltin Hydrides</b>		
4.1.	Overview	143
4.2.	Results	144
4.2.1.	Lewis Acid-Base Complexation of SnMe <sub>2</sub> and SnPh <sub>2</sub> with O-, S-, and N-Donors	147
4.2.2.	Arrested Reaction with Alkenes, Alkynes, Dienes, and Trialkyltin hydrides: Direct Detection of Stannylene $\pi$ - and Tin-Hydride Complexes	151
4.3.	Discussion	155
4.4.	Summary and Conclusions	173

4.5.	Supporting Information	174
4.6.	References	181
<b>Chapter 5: Direct detection of Dimesitylstannylene and Tetramesityldistannene in Solution and Studies of Some of Their Reactions</b>		
5.1.	Overview	184
5.2.	Results	185
5.2.1.	Steady State Photolysis Experiments	185
5.2.2.	Laser Flash Photolysis Experiments	193
5.3.	Discussion	201
5.4.	Summary and Conclusions	216
5.5.	Supporting Information	217
5.6.	References	223
<b>Chapter 6: Photochemical Generation and Characterization of Di-<i>tert</i>-butylsilylene in Solution</b>		
6.1.	Introduction	226
6.2.	Results and Discussion	229
6.3.	Summary and Conclusions	250
6.4.	Supporting Information	252
6.5.	References	256
<b>Chapter 7 - Future Directions</b>		
7.1.	Intra- and Intermolecular $\pi$ -Complexes with Unsaturated Hydrocarbons and Arenes	260
7.1a.	Intermolecular $\pi$ -Complexes with Unsaturated Hydrocarbons	260

<b>7.1b.</b>	Intramolecular Stannylene Arene Interactions	261
<b>7.2.</b>	Stannylenes Stabilized by N-heterocyclic Carbenes	262
<b>7.3.</b>	Reaction of Stannylenes with H <sub>2</sub>	263
<b>7.4.</b>	σ-Bond Insertion of Stannylenes into the M-Cl Bond of Chlorosilanes and Chlorogermanes	264
<b>7.5.</b>	References	265
<b>Chapter 8 - Experimental Details</b>		
<b>8.1.</b>	General	267
<b>8.2.</b>	Steady State Photolysis Experiments	268
<b>8.3.</b>	Laser Flash Photolysis Experiments	269
<b>8.4.</b>	Reagents Used	270
<b>8.4.1.</b>	Solvents	270
<b>8.4.2.</b>	Reagents used in Synthesis	271
<b>8.4.3.</b>	Reagents used in Steady State and Laser Flash Photolysis Experiments	271
<b>8.5.</b>	Synthesis and Characterization of Photoprecursors	273
<b>8.5.1.</b>	Synthesis of 1,1,3-trimethyl-4-phenyl-1-stannacyclopent-3-ene ( <b>1</b> )	273
<b>8.5.2.</b>	3,4-Dimethyl-1,1-diphenyl-1-stannacyclopent-3-ene ( <b>2</b> ) <sup>3</sup>	276
<b>8.5.3.</b>	Synthesis of 1,3,4-trimethyl-1-phenyl-1-stannacyclopent-3-ene ( <b>3</b> )	278
<b>8.5.4.</b>	Synthesis of 1,3-dimethyl-1,4-diphenyl-1-stannacyclopent-3-ene ( <b>4</b> )	281
<b>8.5.5.</b>	Synthesis of 1,1-dimesityl-3,4-dimethyl-1-stannacyclopent-3-ene ( <b>5</b> )	283
<b>8.5.6.</b>	Hexa- <i>tert</i> -butylcyclotrisilane ( <b>6</b> )	286
<b>8.6.</b>	UV-Visible Spectra of Photoprecursors	286

<b>8.7.</b>	Identification of Compounds in Steady State Photolysis Experiments	287
<b>8.7.1.</b>	Compounds Identified by Spiking the Photolyzate using Commercially Available Authentic Samples:	287
<b>8.7.2.</b>	Compounds Identified by Spiking the Photolyzate using Independently Prepared Authentic Samples:	288
<b>8.7.3.</b>	Compounds Identified <i>In-situ</i> by Comparison with Literature Data:	294
<b>8.7.4.</b>	New Compounds Identified <i>In-situ</i> :	296
<b>8.8.</b>	References	297



## LIST OF FIGURES:

- Figure 2.1.** Concentration versus time plots for the photolysis of a deaerated 0.04 M solution of **2** in C<sub>6</sub>D<sub>12</sub> containing Me<sub>2</sub>SnCl<sub>2</sub> (0.031 M). The initial slopes, determined from the first five data points in each of the plots, of the plots for the various components of the reaction mixture are: **2**,  $-0.93 \pm 0.09$ ; Me<sub>2</sub>SnCl<sub>2</sub> (not shown),  $-0.89 \pm 0.07$ ; **4a**,  $0.89 \pm 0.07$ ; **5** (ClMe<sub>2</sub>SnSnMe<sub>2</sub>Cl),  $0.47 \pm 0.03$ ; **6** (ClMe<sub>2</sub>SnOSnMe<sub>2</sub>Cl)<sub>2</sub>,  $0.19 \pm 0.04$ ; **7** (Me<sub>3</sub>SnCl),  $0.08 \pm 0.01$  (units, mM min<sup>-1</sup>). The inset shows an expansion of the plots for **5**, **6**, and **7**. 54
- Figure 2.2.** Concentration versus time plots for the photolysis of a solution of **2** (ca. 0.04 M) and Me<sub>2</sub>SnCl<sub>2</sub> (0.033 M) in C<sub>6</sub>D<sub>12</sub>, which was saturated with air prior to irradiation. The inset shows an expanded plot, detailing the formation of dichlorodistannane **5**, distannoxane dimer **6**, and Me<sub>3</sub>SnCl (**7**) with photolysis time. The initial slopes, determined from the first five data points in each of the plots, are (in units of mM min<sup>-1</sup>): **2**,  $-1.02 \pm 0.04$ ; Me<sub>2</sub>SnCl<sub>2</sub>,  $-1.28 \pm 0.06$ ; **4a**,  $1.08 \pm 0.04$ ; **5**,  $0.012 \pm 0.005$ ; **6**,  $0.51 \pm 0.03$  (< 4 min); **7**,  $0.033 \pm 0.003$  (< 4 min). The slopes of the second half (> 4 min) of the plots for **5-7** are: **5**,  $0.37 \pm 0.02$ ; **6**,  $0.055 \pm 0.007$ ; **7**,  $0.10 \pm 0.01$ . 56
- Figure 2.3.** Concentration versus time plots for the photolysis of an undeaerated 0.04 M solution of **3** in C<sub>6</sub>D<sub>12</sub> containing 0.037 M Me<sub>2</sub>SnCl<sub>2</sub>. The initial ( $\leq 2.5$  min) slopes of the plots (in mM min<sup>-1</sup>) are: **3**,  $-0.91 \pm 0.01$ ; Me<sub>2</sub>SnCl<sub>2</sub>,  $-1.84 \pm 0.07$ ; **4b**,  $0.74 \pm 0.01$ ; **8**,  $0.69 \pm 0.04$ ; **6**,  $0.34 \pm 0.02$ ; **9** ( $\geq 3.3$  min),  $0.08 \pm 0.04$ ; **13a** ( $\geq 3.3$  min),  $0.036 \pm 0.003$ . No attempt was made to replenish the air in the photolyzate as the experiment proceeded. 57
- Figure 2.4.** (a) Transient UV-vis absorption spectra from laser flash photolysis of rapidly flowed solutions of (a) **2** ( $2 \times 10^{-4}$  M) and (b) **3** ( $7 \times 10^{-4}$  M) in anhydrous hexanes at 25 °C. The spectra in (a) were recorded 0.10 - 0.26  $\mu$ s (○), 1.06 - 1.15  $\mu$ s (□) and 17.2 - 17.3  $\mu$ s (Δ) after the laser pulse, while those in (b) were recorded 0.42 - 0.51  $\mu$ s (○) and 17.1 - 17.3  $\mu$ s (Δ) after the pulse; the insets show absorbance versus time profiles recorded at selected wavelengths in the two spectra. The spectra in (a) were recorded at reduced laser intensity in order to maximize the temporal resolution between the primary and secondary product spectra. 62

- Figure 2.5.** Plots of  $k_{\text{decay}}$  versus substrate concentration for the stannylenes absorptions from laser photolysis of hexanes solutions of (a) **2** (○) and (b) **3** (□) containing varying concentrations of  $\text{Me}_2\text{SnCl}_2$  at 25 °C. The monitoring wavelengths were 530 nm and 500 nm for **2** and **3**, respectively. The solid lines are the linear least squares fits of the data to eq. 2.16. 65
- Figure 2.6.** (a) Time-resolved UV-vis spectra from laser photolysis of  $\text{SnPh}_2$  precursor **3** in hexanes containing 0.025 M MeOH, 0.26-0.38  $\mu\text{s}$  (○), 4.93-5.18  $\mu\text{s}$  (□) and 35.3-35.7  $\mu\text{s}$  (Δ) after the laser pulse (25 °C), and absorbance-time profiles at selected wavelengths (inset). (b) Plots of  $k_{\text{decay}}$  (□) and  $(\Delta A_0)_0 / (\Delta A_0)_Q$  (○) of the  $\text{SnPh}_2$  absorption (at 500 nm) versus [MeOH], in hexanes solution at 25 °C; the solid lines are the linear least squares fits of the data to equations 2.16 and 2.20, respectively. 68
- Figure 2.7.** Electronic Energy versus Reaction Coordinate Diagram for the dimerization of  $\text{SnPh}_2$  and interconversion of the  $(\text{SnPh}_2)_2$  isomers, calculated at the  $\omega\text{B97XD}/6\text{-}31\text{+G(d,p)}^{\text{C,H,O}}$ -LANL2DZdp<sup>Sn</sup> level of theory. The vertical placement of the various structures is defined by their calculated electronic energy relative to (twice) that of  $\text{SnPh}_2$  (1 atm gas phase, 0 K), as indicated on the y-axis; the numbers in parentheses are the corresponding standard free energies (see Table 2.1). 78
- Figure S2.1.**  $^1\text{H}$  NMR spectra of an argon-degassed 0.04 M solution of **2** in  $\text{C}_6\text{D}_{12}$  (a) before and (b) after 10 minutes photolysis with 254 nm light. The insets in B show an expansion of the  $\delta$  0.23-0.48 region of the spectrum and the portion of the  $^{119}\text{Sn}\{^1\text{H}\}$  spectrum containing product peaks. 81
- Figure S2.2.** Concentration versus time plots for the photolysis of the solution of Fig. S2.1. The initial slopes of the three plots are **2**,  $-0.84 \pm 0.03$ ; **4a**,  $0.82 \pm 0.05$ ;  $[\text{SnMe}_2]_n$  ( $\delta$  0.407)  $0.75 \pm 0.07$  (units,  $\text{mM min}^{-1}$ ). 81
- Figure S2.3.**  $^1\text{H}$  NMR spectra of a deaerated 0.04 M solution of **3** in  $\text{C}_6\text{D}_{12}$  (a) before and (b) after 8.3 minutes photolysis with 254 nm light. The resonances marked with ● disappeared after allowing the photolyzed solution to stand for 18 hours in the dark. 82
- Figure S2.4.** Concentration versus time plots for photolysis of ca. 0.04 M solutions of **3** in  $\text{C}_6\text{D}_{12}$ , (a) deaerated (slopes (in units of mM 82

min<sup>-1</sup>): **3** (○),  $-0.32 \pm 0.02$ ; **4b**, (□),  $0.30 \pm 0.01$ ; (SnPh<sub>2</sub>)<sub>6</sub> (Δ),  $0.0057 \pm 0.0005$ ); (b) air-saturated (slopes: **3**(○),  $-0.52 \pm 0.01$ ; **4b**, (□),  $0.55 \pm 0.02$ ).

- Figure S2.5.** <sup>1</sup>H NMR spectra of a deaerated 0.04 M solution of **2** in C<sub>6</sub>D<sub>12</sub> containing Me<sub>2</sub>SnCl<sub>2</sub> (0.031 M) (a) before and (b) after 10 minutes photolysis with 254 nm light. The inset in B shows the <sup>119</sup>Sn{<sup>1</sup>H} NMR spectrum of the photolyzed mixture. 83
- Figure S2.6.** <sup>1</sup>H NMR spectra of an undeaerated 0.04 M solution of **3** in C<sub>6</sub>D<sub>12</sub> containing Me<sub>2</sub>SnCl<sub>2</sub> (0.037 M) (a) before, (b) after 2.5 minutes, and (c) after 6.7 minutes photolysis with 254 nm light. No attempt was made to replenish the air in the photolyzate as the experiment proceeded. 84
- Figure S2.7.** Plots of the concentration ratios of cyclodistannoxanes **6**, **11**, and **12** (i.e. [**6**]/[**12**] and [**12**]/[**11**]) versus the dichlorostannane concentration ratio [Me<sub>2</sub>SnCl<sub>2</sub>]/[**8**], measured from the <sup>1</sup>H NMR spectra of a ca. 0.012 M solution of **6** in CDCl<sub>3</sub> to which sequential portions of Ph<sub>2</sub>SnCl<sub>2</sub> (**8**) and Me<sub>2</sub>SnCl<sub>2</sub> were added at ca. 22 °C. The solid lines are the linear least squares fits of the data to [**6**]/[**12**] =  $K_{12 \leftrightarrow 6}$ [Me<sub>2</sub>SnCl<sub>2</sub>]/[**8**] (○) and [**12**]/[**11**] =  $K_{11 \leftrightarrow 12}$ [Me<sub>2</sub>SnCl<sub>2</sub>]/[**8**] (□); errors are quoted as the standard errors from the least squares analysis. 86
- Figure S2.8.** Partial <sup>1</sup>H NMR spectra of a deaerated 0.038 M solution of **3** in C<sub>6</sub>D<sub>12</sub> containing Me<sub>2</sub>SnCl<sub>2</sub> (0.034 M) (a) before, (b) after 2.5 minutes, and (c) after 6.7 minutes of photolysis. 86
- Figure S2.9.** Concentration versus time plots for the solution of Figure S2.8. The initial slopes of the plots (in mM min<sup>-1</sup>) are: **3**,  $-0.48 \pm 0.05$ ; Me<sub>2</sub>SnCl<sub>2</sub>,  $-0.77$ ; **4b**,  $0.38 \pm 0.04$ ; **6**,  $0.057 \pm 0.003$ ; **8**,  $0.12 \pm 0.01$ ; **9**,  $0.199 \pm 0.006$ ; **13a**,  $0.039 \pm 0.001$ ; **13b** (not shown),  $0.022 \pm 0.002$ ; **7** (not shown),  $0.017 \pm 0.001$ . 87
- Figure S2.10.** Concentration versus time plots for the photolysis of air-saturated C<sub>6</sub>D<sub>12</sub> solutions of (a) **2** and (b) **3** containing ca. 0.04 M Me<sub>2</sub>SnCl<sub>2</sub>, and of (c) a deoxygenated C<sub>6</sub>D<sub>12</sub> solution of **14** containing 0.05 M MeOH; all three solutions also contained Si<sub>2</sub>Me<sub>6</sub> (ca. 0.01 M) as an internal integration standard. The initial slopes of the plots for the various compounds are (in mM min<sup>-1</sup>): (a) **2**,  $-1.06 \pm 0.09$ ; Me<sub>2</sub>SnCl<sub>2</sub>,  $-1.16 \pm 0.05$ ; **4a**,  $1.01 \pm 0.04$ ; **6**,  $0.51 \pm 0.01$  (A solid, presumed to be **6**, began to precipitate halfway through the experiment, therefore only the 88

first 4 points were used to evaluate the yield of this product); (b) **3**,  $-0.97 \pm 0.07$ ;  $\text{Me}_2\text{SnCl}_2$ ,  $-1.74 \pm 0.40$ ; **4b**,  $0.83 \pm 0.01$ ; **6**,  $0.38 \pm 0.02$ ; **8**,  $0.76 \pm 0.03$ ; **12**,  $0.03 \pm 0.01$ ; (c) **14**,  $-0.781 \pm 0.002$ ; **4b**,  $0.713 \pm 0.006$ ; **15**,  $0.716 \pm 0.012$ .

- Figure S2.11.** (a) Transient UV-vis absorption spectra from laser flash photolysis of a rapidly flowed, deoxygenated solution of **3** ( $7 \times 10^{-4}$  M) in anhydrous hexanes at 25 °C, recorded over a longer timescale than that shown in Figure 2.2. The spectra were recorded 0.64 - 0.96  $\mu\text{s}$  (○) and 81.1 - 81.9  $\mu\text{s}$  (Δ) after the pulse, using a Pyrex filter in the monitoring beam at wavelengths above 310 nm; the inset shows absorbance versus time profiles recorded at 340 and 500 nm. (b) Transient absorbance-time profiles recorded for a flowed solution of **3** in deoxygenated hexanes, under similar conditions to those used for the experiment shown in (a). The 340 nm  $\Delta A$ -time profile was recorded as in (a) and is the average of 10 laser shots, while the 650 nm profile was recorded with a 520 nm cutoff filter (Corning 3-69) in the monitoring beam to filter out overtone absorptions, and is the average of 70 laser shots. The  $\Delta A$ -time profile at 500 nm (recorded with a Pyrex filter) was quite similar to that obtained in the experiment of (a). 89
- Figure S2.12.** Plots of initial transient absorbance ( $(\Delta A)_0$ ) versus laser pulse energy from optically matched (at 248 nm), deoxygenated hexanes solutions of (a) benzophenone and **2**, and (b) benzophenone and **3**, for determination of the extinction coefficients of the  $\text{SnMe}_2$  and  $\text{SnPh}_2$  absorption bands at 500 nm. The benzophenone triplet ( $^3\text{BP}$ ;  $\Phi = 1.0$ ) was monitored at 525 nm ( $\epsilon = 6,250 \pm 1,250 \text{ M}^{-1}\text{cm}^{-1}$ ).<sup>76</sup> The slopes of the plots are (a)  $^3\text{BP}$ ,  $(6.0 \pm 0.1) \times 10^{-4}$ ,  $\text{SnMe}_2$   $(1.43 \pm 0.02) \times 10^{-4}$ ; (b)  $^3\text{BP}$ ,  $(4.61 \pm 0.08) \times 10^{-4}$ ,  $\text{SnPh}_2$   $(1.13 \pm 0.03) \times 10^{-4}$ . 90
- Figure S2.13.** (a) Time-resolved UV-vis spectra recorded by laser photolysis of  $\text{SnMe}_2$  precursor **2** in hexanes containing 7 mM MeOH, 0.22-0.29  $\mu\text{s}$  (○), 1.25-1.31  $\mu\text{s}$  (□) and 17.5-17.7  $\mu\text{s}$  (Δ) after the laser pulse (25 °C), and absorbance-time profiles at selected wavelengths (inset). (b) Plot of  $(\Delta A)_0 / (\Delta A)_Q$  for complexation of  $\text{SnMe}_2$  with MeOH in hexanes at 25 °C; the solid line is the linear least squares fit of the data to equation 2.20. 90
- Figure S2.14.** Selected geometric parameters, electronic energies and standard free energies (in parentheses) for  $\text{SnPh}_2$  and the  $\text{SnPh}_2$ -dimers 92

- 16b, 17b, 19** and (*trans*-) **20**, calculated at the  $\omega$ B97XD/6-31+G(d,p)<sup>C,H,O</sup>-LANL2DZdp<sup>Sn</sup> level (hydrogen atoms omitted for clarity).
- Figure S2.15.** Plots of  $\Delta E$  versus geometry from relaxed PES scans of (A) the C1-Sn2-Sn3-C4 dihedral angle in **16b** and (B) the Sn-C bond distance involving the bridging phenyl group in stannylidenestannylene **19**, carried out at the  $\omega$ B97XD/6-31+G(d,p)<sup>C,H</sup>-LANL2DZdp<sup>Sn</sup> level of theory. 92
- Figure S2.16.** Plot of calculated relative electronic energies ( $\Delta E$ ; relative to two SnPh<sub>2</sub> moieties at infinite separation) versus Sn-Sn bond distance, from relaxed potential energy surface scans of the Sn-Sn bond distances ( $d_{\text{Sn-Sn}}$ ) in **17b** and **19** at the  $\omega$ B97XD/6-31+G(d,p)<sup>C,H</sup>-LANL2DZdp<sup>Sn</sup> level of theory. The calculated structures at various  $d_{\text{Sn-Sn}}$  values in the calculations are also shown. 93
- Figure 3.1.** Concentration versus time plots for the photolysis of a 0.04 M solution of **3** in C<sub>6</sub>D<sub>12</sub> containing 0.04 M Me<sub>2</sub>SnCl<sub>2</sub>. The inset shows an expanded plot, illustrating the formation of compounds **9** ( $\diamond$ ) and **10** ( $\bullet$ ) with photolysis time. The initial slopes determined from the first four data points are **3**,  $-0.77 \pm 0.02$  ( $\circ$ ); Me<sub>2</sub>SnCl<sub>2</sub>,  $-1.9 \pm 0.1$  ( $\Delta$ ) (slope not shown); **6**,  $0.69 \pm 0.07$  ( $\square$ ); **5**,  $0.57 \pm 0.05$  ( $\blacktriangle$ ); **8**,  $0.29 \pm 0.05$  ( $\nabla$ ) (units, mM min<sup>-1</sup>). 102
- Figure 3.2.** Time-resolved UV-vis spectra from laser photolysis of (a) **3** and (b) **4** in hexanes solution, 0.58 - 0.70  $\mu$ s ( $\circ$ ), 4.16 - 4.35  $\mu$ s ( $\square$ ), and 34.4 - 34.7  $\mu$ s ( $\Delta$ ) after the laser pulse (25 °C). Absorbance-time profiles are shown at selected wavelengths (inset). (*Data in (b) recorded by B. Nguyen*) 105
- Figure 3.3.** (a) Plot of  $k_{\text{decay}}$  for the reaction of SnMePh with THF ( $\square$ ) and Me<sub>2</sub>SnCl<sub>2</sub> ( $\circ$ ) in hexanes at 25 °C; the solid lines are the linear least squares fit of the data to equation 3.10. (b) Plot of  $\Delta A_0/\Delta A_Q$  for the reaction of SnMePh with MeOH in hexanes at 25 °C; the solid line is the linear least squares fit of the data to equation 3.11. (c) Time-resolved UV-vis spectra from laser photolysis of **4** in hexanes containing ca. 7.3 mM MeOH, 0.27 - 0.28  $\mu$ s ( $\circ$ ) and 1.58 - 1.61  $\mu$ s ( $\square$ ) after the laser pulse (25 °C). Absorbance-time profiles at selected wavelengths (inset). (*Data from Fig 3.3a-c recorded by B. Nguyen using 4*) 107
- Figure 3.4.** <sup>1</sup>H NMR spectra (0.1 - 0.8 ppm) of a deaerated 0.04 M solution 112

of **1** in C<sub>6</sub>D<sub>12</sub> containing Bu<sub>3</sub>SnCl (0.04 M) (a) before and (b) after 10 minutes photolysis with 254 nm light. (c) <sup>119</sup>Sn NMR spectrum of a deaerated 0.04 M solution of **1** in C<sub>6</sub>D<sub>12</sub> containing Bu<sub>3</sub>SnCl (0.04 M) after 10 minutes photolysis with 254 nm light. <sup>13</sup>C NMR spectra (0 - 15 and 27 - 32 ppm) of a deaerated 0.04 M solution of **1** in C<sub>6</sub>D<sub>12</sub> containing Bu<sub>3</sub>SnCl (0.04 M) (d) before and (e) after 10 minutes photolysis with 254 nm light. (<sup>‡</sup>Bu<sub>3</sub>SnCl; \*Bu<sub>4</sub>Sn)

- Figure 3.5.** Plot of  $k_{\text{decay}}$  for the SnMe<sub>2</sub> absorption (530 nm) versus [Bu<sub>3</sub>SnCl], from flash photolysis of **1** in hexanes at 25 °C; the solid line is the linear least squares fit of the data to equation 3.10. 113
- Figure 3.6.** Time-resolved UV-vis spectra from laser photolysis of **2** in hexanes containing 0.0 mM Bu<sub>3</sub>SnCl at 0.42 - 0.51 μs (Δ), and 15.0 mM Bu<sub>3</sub>SnCl at 0.22 - 0.32 μs (○) and 5.86 - 6.02 μs (□) after the laser pulse (25 °C). 113
- Figure 3.7.** Plots of  $k_{\text{decay}}$  for reaction of (a) SnPh<sub>2</sub> (500 nm) and the (b) 410 nm absorption with Bu<sub>3</sub>SnCl in hexanes at 25 °C. (c) Overlap of the  $k_{\text{decay}}$  data for the SnPh<sub>2</sub> (○) and 410 nm (□) absorptions as a function of [Bu<sub>3</sub>SnCl]. The solid lines are the non-linear least squares fit of the data to equation 3.16. 114
- Figure 3.8.** <sup>1</sup>H NMR spectra of a deaerated 0.05 M solution of **1** in C<sub>6</sub>D<sub>12</sub> containing AcOH (0.21 M) (a) before and (b) after 30 minutes of photolysis with 254 nm light. 120
- Figure 3.9.** Concentration versus time plots for the photolysis of a deaerated 0.05 M solution of **1** in C<sub>6</sub>D<sub>12</sub> containing AcOH (0.21 M). The inset shows an expanded plot, detailing the formation of compounds **21** - **22** with photolysis time. The initial slopes (determined from the first three data points for **20** and **21**, and first four data points otherwise) are **1**,  $-1.210 \pm 0.009$  (○); **7**,  $1.12 \pm 0.06$  (□); **20**,  $0.48 \pm 0.05$  (◇); **23**,  $0.160 \pm 0.001$  (●); **21**,  $0.09 \pm 0.01$  (Δ); **22**,  $0.162 \pm 0.007$  (▽) (units, mM min<sup>-1</sup>). 121
- Figure 3.10.** (a) <sup>1</sup>H NMR spectrum (-0.05 - 0.40 ppm) and (b) <sup>13</sup>C{<sup>1</sup>H} NMR spectrum (-6.0 - -1.0 ppm) of a deaerated 0.05 M solution of **1** in C<sub>6</sub>D<sub>12</sub> containing a mixture of AcOH/AcOD (total concentration 0.20 M) after 30 minutes photolysis with 254 nm light. 122
- Figure 3.11.** <sup>1</sup>H NMR spectra of a deaerated 0.05 M solution of **2** in C<sub>6</sub>D<sub>12</sub> 123

containing AcOH (0.20 M) (a) before and (b) after 30 minutes photolysis with 254 nm light.

- Figure 3.12.** Concentration versus time plots for the photolysis of a solution of **2** (ca. 0.05 M) in C<sub>6</sub>D<sub>12</sub> and AcOH (ca. 0.2 M). The initial slopes of each of the plots, determined from the first four data points for **6** and the first six data points otherwise, are (in units of mM min<sup>-1</sup>) **2**,  $-0.59 \pm 0.02$  (○); **6**,  $0.72 \pm 0.06$  (□); **24**,  $0.71 \pm 0.06$  (Δ). 124
- Figure 3.13.** Inverse-gate <sup>13</sup>C{<sup>1</sup>H} NMR spectrum (128.0 - 129.5 ppm) of a deaerated 0.05 M solution of **2** in C<sub>6</sub>D<sub>12</sub> containing a mixture of AcOH:AcOD (total concentration 0.20 M) after 30 minutes photolysis with 254 nm light (**2'** denote satellite resonances from **2**). 125
- Figure 3.14.** <sup>1</sup>H NMR spectra of a deaerated ca. 0.05 M solution of **4** in C<sub>6</sub>D<sub>12</sub> containing AcOH (0.20 M) (a) before and (b) after 30 minutes photolysis with 254 nm light (\*unreactive impurity). (*Data recorded by B. Nguyen*) 126
- Figure 3.15.** Concentration versus time plots for the photolysis of a solution of **4** (ca. 0.05 M) in C<sub>6</sub>D<sub>12</sub> and AcOH (ca. 0.2 M). The initial slopes in each of the plots, determined from the first four data points for **7** and **24** and first five data points otherwise, are (in units of mM min<sup>-1</sup>) **4**,  $-0.81 \pm 0.07$  (○); **7**,  $0.94 \pm 0.14$  (□); **24**,  $0.46 \pm 0.01$  (Δ); **20**,  $0.32 \pm 0.04$  (◇); **22**,  $0.09 \pm 0.01$  (∇). (*Data recorded by B. Nguyen*) 126
- Figure 3.16.** (a) Time-resolved UV-vis spectra from laser photolysis of **1** in hexanes containing 0.5 mM AcOH, 0.07 - 0.10 μs (○), 0.30 - 0.32 μs (□), and 3.50 - 3.53 μs (Δ) after the laser pulse (25 °C); data recorded using a neutral density filter (43 % transmittance). Plot of  $k_{\text{decay}}$  for reaction of SnMe<sub>2</sub> (530 nm) with (b) AcOH and (c) AcOD in hexanes at 25 °C; the solid lines are the linear least squares fit of the data to equation 3.10. (*Data in (c) recorded by B. Nguyen*) 128
- Figure S3.1.** Concentration versus time plots for the photolysis of a deaerated 0.05 M solution of **3** in C<sub>6</sub>D<sub>12</sub>. The initial slopes determined from the first four data points are **3**,  $-0.66 \pm 0.04$  (○); **6**,  $0.61 \pm 0.07$  (□) (units, mM min<sup>-1</sup>). 134
- Figure S3.2.** <sup>1</sup>H NMR spectra of a deaerated 0.05 M solution of **3** in C<sub>6</sub>D<sub>12</sub> (a) before and (b) after 10 minutes of photolysis with 254 nm light. 134

- (\*Unreactive impurity)
- Figure S3.3.**  $^1\text{H}$  NMR spectra of a 0.04 M solution of **3** in  $\text{C}_6\text{D}_{12}$  containing 0.04 M  $\text{Me}_2\text{SnCl}_2$ , (a) before and (b) after 10 minutes photolysis with 254 nm light, and (c) after spiking the resulting photolyzate with an authentic sample of **5**. (\*Unreactive impurity) 135
- Figure S3.4.**  $^{119}\text{Sn}\{^1\text{H}\}$  NMR spectra of a 0.04 M solution of **3** in  $\text{C}_6\text{D}_{12}$  containing 0.04 M  $\text{Me}_2\text{SnCl}_2$  (a) after 10 minutes photolysis with 254 nm light, and (b) after spiking the resulting photolyzate with an authentic sample of **5**. 135
- Figure S3.5.** (a) Time-resolved UV-vis spectra from laser photolysis of **4** in hexanes solution containing 0.90 mM THF, 0.64 - 0.96  $\mu\text{s}$  ( $\circ$ ) and 34.4 - 34.7  $\mu\text{s}$  ( $\Delta$ ) after the laser pulse (25  $^\circ\text{C}$ ). (b) Time-resolved UV-vis spectra from laser photolysis of **3** in hexanes solution containing 10 mM THF, 0.64 - 0.96  $\mu\text{s}$  ( $\circ$ ) and 34.2 - 34.7  $\mu\text{s}$  ( $\Delta$ ) after the laser pulse (25  $^\circ\text{C}$ ). Absorbance-time profiles shown at selected wavelengths (inset). (Data in (a) recorded by B. Nguyen) 136
- Figure S3.6.**  $^1\text{H}$  NMR spectra of a deaerated 0.04 M solution of **1** in  $\text{C}_6\text{D}_{12}$  containing  $\text{Bu}_3\text{SnCl}$  (0.040 M) (a) before and (b) after 10 minutes of photolysis with 254 nm light. (\* $\text{Bu}_4\text{Sn}$ ) 136
- Figure S3.7.** Concentration versus time plots for the photolysis of a deaerated 0.04 M solution of **1** in  $\text{C}_6\text{D}_{12}$  containing  $\text{Bu}_3\text{SnCl}$  (0.040 M). The initial slopes determined from the first four data points are **1**,  $-0.93 \pm 0.02$  ( $\circ$ ); **7**,  $0.81 \pm 0.03$  ( $\square$ ); **18**,  $0.61 \pm 0.02$  ( $\Delta$ ) (units,  $\text{mM min}^{-1}$ ). 137
- Figure S3.8.** (a) Time-resolved UV-vis spectra from the laser photolysis of **4** in hexanes containing 0.0 mM  $\text{Bu}_3\text{SnCl}$  at 0.42 - 0.51  $\mu\text{s}$  ( $\Delta$ ) and 15.0 mM  $\text{Bu}_3\text{SnCl}$  at 0.22 - 0.32  $\mu\text{s}$  ( $\circ$ ) and 5.86 - 6.02  $\mu\text{s}$  ( $\square$ ) after the laser pulse (25  $^\circ\text{C}$ ). (b) Transient decay profiles recorded at 500 nm and 410 nm from the laser photolysis of a hexanes solution of **4** containing 15.0 mM  $\text{Bu}_3\text{SnCl}$ . 137
- Figure S3.9.** Plots of  $k_{\text{decay}}$  for reaction of (a)  $\text{SnMePh}$  (500 nm) and the (b) 410 nm absorption with  $\text{Bu}_3\text{SnCl}$  in hexanes at 25  $^\circ\text{C}$ . (c) Overlap of the  $k_{\text{decay}}$  data for the  $\text{SnMePh}$  ( $\circ$ ) and 410 nm ( $\square$ ) absorptions as a function of  $[\text{Bu}_3\text{SnCl}]$ . The solid lines are the non-linear least squares fit of the data to equation 3.16. (Data recorded by B. Nguyen) 138



- Figure S3.10.**  $^{119}\text{Sn}$  NMR spectra of a deaerated 0.05 M solution of **1** in  $\text{C}_6\text{D}_{12}$  containing AcOH (0.21 M) after 30 minutes of photolysis with 254 nm light. 138
- Figure S3.11.** (a) GC-MS chromatogram (0 - 5.6 minutes retention time) and (b) mass spectrum of the peak at ca. 3.3 minutes retention time of a 0.05 M solution of **2** in  $\text{C}_6\text{D}_{12}$  containing 0.2 M AcOH after 30 minutes of photolysis with 254 nm UV light. 139
- Figure S3.12.** Plot of  $k_{\text{decay}}$  for the reaction of  $\text{SnPh}_2$  (500 nm) with (a) AcOH and (b) AcOD in hexanes at 25 °C. (c) Plot of  $k_{\text{decay}}$  for the reaction of  $\text{SnMePh}$  (500 nm) with AcOH in hexanes at 25 °C. The solid lines are the linear least squares fit of the data to equation 3.10. (d) Time-resolved UV-vis spectra from laser photolysis of **2** in hexanes containing 0.6 mM AcOH, 0.35-0.42  $\mu\text{s}$  ( $\circ$ ), and 0.86-1.02  $\mu\text{s}$  ( $\square$ ) after the laser pulse (25 °C). (e) Time-resolved UV-vis spectra from laser photolysis of **4** in hexanes containing 1.1 mM AcOH, 0.10 - 0.13  $\mu\text{s}$  ( $\circ$ ) and 1.22 - 1.25  $\mu\text{s}$  ( $\Delta$ ) after the laser pulse (25 °C). Absorbance-time profiles are at selected wavelengths (inset). (*Data in (b),(c) and (e) recorded by B. Nguyen*) 140
- Figure 4.1.** Representative transient decay profiles recorded from a hexanes solution of (a) **1** containing 0 and 0.2 mM  $\text{Et}_2\text{NH}$ , (b) **2** containing 0, 0.3, and 1.0 mM EtOAc, and (c) **1** containing 0 and 1.4 mM EtOAc. 146
- Figure 4.2.** (a) Plot of  $k_{\text{decay}}$  for reaction of  $\text{SnMe}_2$  with  $\text{Et}_2\text{NH}$  in hexanes at 25 °C; the solid line is the linear least squares fit of the data to eq. 4.3. (b) Time-resolved UV-vis spectra from laser photolysis of **1** in hexanes containing 1.0 mM  $\text{Et}_2\text{NH}$ , 0.16 - 0.32  $\mu\text{s}$  ( $\circ$ ), 3.52 - 4.16  $\mu\text{s}$  ( $\square$ ), and 85.9 - 86.6  $\mu\text{s}$  ( $\Delta$ ) after the laser pulse (25 °C), and absorbance-time profiles at selected wavelengths (inset). 147
- Figure 4.3.** (a) Plots of  $k_{\text{decay}}$  ( $\square$ ) and  $(\Delta A_0)_0 / (\Delta A_{\text{res}})_Q$  ( $\circ$ ) for reaction of  $\text{SnPh}_2$  and  $(\Delta A_0)_0 / (\Delta A_0)_Q$  ( $\Delta$ ) for reaction of  $\text{SnMe}_2$  versus  $[\text{EtOAc}]$  in hexanes solution at 25 °C; the solid lines are the linear least-squares fits of the data to equations 4.3, 4.5 and 4.4, respectively. (b) Time-resolved UV-vis spectra from laser photolysis of **2** in hexanes containing 0.50 mM EtOAc, 0.42-0.51  $\mu\text{s}$  ( $\circ$ ), and 17.8-18.0  $\mu\text{s}$  ( $\square$ ) after the laser pulse (25 °C), and absorbance-time profiles at selected wavelengths (inset). (c) Time-resolved UV-vis spectra from laser photolysis of **1** in 148

- hexanes containing 25 mM EtOAc, 0.51 - 0.70  $\mu\text{s}$  ( $\circ$ ), and 34.7 - 35.0  $\mu\text{s}$  ( $\square$ ) after the laser pulse (25  $^{\circ}\text{C}$ ), and absorbance-time profiles at selected wavelengths (inset). The spectra in (c) were recorded using a neutral density filter (43 % transmittance).
- Figure 4.4.**  $^1\text{H}$  NMR spectra of a deaerated 0.05 M solution of **2** in  $\text{C}_6\text{D}_{12}$  containing isoprene (0.096 M) (a) before and (b) after 10 minutes of photolysis with 254 nm light. 152
- Figure 4.5.** Plots of  $(\Delta A_0)_0 / (\Delta A_0)_Q$  for the reactions of (a)  $\text{SnMe}_2$  and (b)  $\text{SnPh}_2$  with 1-hexene in hexanes at 25  $^{\circ}\text{C}$ ; the solid lines are the linear least squares fits of the data to eq. 4.4. (c) Time-resolved UV-vis spectra from laser photolysis of **1** in hexanes containing 1.5 M 1-hexene, 0.16 - 0.48  $\mu\text{s}$  ( $\circ$ ), and 89.1 - 89.8  $\mu\text{s}$  ( $\square$ ) after the laser pulse (25  $^{\circ}\text{C}$ ), and absorbance-time profiles at selected wavelengths (inset). (d) Time-resolved UV-vis spectra from laser photolysis of **2** in hexanes containing 1.52 M 1-hexene, 1.3 - 2.6  $\mu\text{s}$  ( $\circ$ ), and 50.2 - 51.5  $\mu\text{s}$  ( $\square$ ) after the laser pulse (25  $^{\circ}\text{C}$ ), and absorbance-time profiles at selected wavelengths (inset). 153
- Figure 4.6.** Plots of  $\Delta G_{\text{SnMe}_2}$  versus (a) gas phase basicity (GB), (b) proton affinity (PA) and (c)  $\text{BF}_3$  affinity. 158
- Figure 4.7.** Representative transient decay profiles recorded with a hexanes solution of **1** (a) containing 0, 0.8 and 2.9 mM  $\text{Et}_2\text{O}$ , and (b) containing 0, 0.3 and 0.8 mM  $\text{Et}_2\text{S}$ . 164
- Figure 4.8.** Time-resolved UV-vis spectra recorded 0.4 - 2.6  $\mu\text{s}$  after the laser pulse (25  $^{\circ}\text{C}$ ) from laser photolysis of **2** in hexanes containing (a) 0 ( $\Delta$ ), 0.2 ( $\square$ ), and 1.52 M ( $\circ$ ) 1-hexene and (b) 0 ( $\Delta$ ), 0.04 ( $\square$ ) and 0.2 M ( $\circ$ ) 1-hexyne. Each of the three spectra in (a) and (b) are normalized at 460 nm to account for differences in laser intensity between different experiments. 170
- Figure S4.1.** (a) Plots of  $(\Delta A_0)_0 / (\Delta A_0)_Q$  for reaction of  $\text{SnMe}_2$  ( $\circ$ ) and  $\text{SnPh}_2$  ( $\square$ ) with  $\text{Et}_2\text{O}$  in hexanes at 25  $^{\circ}\text{C}$ ; the solid lines are the linear least squares fits of the data to eq. 4.4. (b) Time-resolved UV-vis spectra from laser photolysis of **1** in hexanes containing 25 mM  $\text{Et}_2\text{O}$ , 0.32 - 0.46  $\mu\text{s}$  ( $\circ$ ), and 17.3 - 17.5  $\mu\text{s}$  ( $\square$ ) after the laser pulse (25  $^{\circ}\text{C}$ ), and absorbance-time profiles at selected wavelengths (inset). The spectra in (b) were recorded using a neutral density filter (43 % transmittance). (c) Time-resolved UV-vis spectra recorded by laser photolysis of **2** in hexanes containing 25 mM  $\text{Et}_2\text{O}$ , 0.96 - 1.6  $\mu\text{s}$  ( $\circ$ ), and 22.6 - 23.0  $\mu\text{s}$  ( $\square$ ) 174

after the laser pulse (25 °C), and absorbance-time profiles at selected wavelengths (inset).

- Figure S4.2.** (a) Plots of  $k_{\text{decay}}$  of the SnMe<sub>2</sub> (□) and SnPh<sub>2</sub> (Δ) absorption and  $(\Delta A_0)_0/(\Delta A_{\text{res}})_Q$  (○) of the SnMe<sub>2</sub> absorption versus [THF], in hexanes solution at 25 °C; the solid lines are the linear least-squares fits of the data to equations 4.3 and 4.5, respectively (*data for SnPh<sub>2</sub> (Δ) recorded by B. Nguyen*). (b) Time-resolved UV-vis spectra from laser photolysis of **1** in hexanes containing 25.0 mM THF, 0.51 - 0.70 μs (○), and 34.7 - 35.0 μs (□) after the laser pulse (25 °C), and absorbance-time profiles at selected wavelengths (inset). The spectra in (b) were recorded using a neutral density filter (43 % transmittance). (c) Time-resolved UV-vis spectra recorded by laser photolysis of **2** in hexanes containing 1.23 mM THF, 0.64 - 1.28 μs (○), and 34.7 - 35.6 μs (□) after the laser pulse (25 °C), and absorbance-time profiles at selected wavelengths (inset). 175
- Figure S4.3.** (a) Plots of  $k_{\text{decay}}$  (□) and  $(\Delta A_0)_0/(\Delta A_{\text{res}})_Q$  (○) for reaction of SnPh<sub>2</sub> and  $(\Delta A_0)_0 / (\Delta A_0)_Q$  (Δ) for reaction of SnMe<sub>2</sub> versus [acetone] in hexanes solution at 25 °C; the solid lines are the linear least-squares fits of the data to equations 4.3, 4.5 and 4.4, respectively. (b) Time-resolved UV-vis spectra from laser photolysis of **1** in hexanes containing 25 mM acetone, 0.26 - 0.45 μs (○), and 10.1 - 10.4 μs (□) after the laser pulse (25 °C), and absorbance-time profiles at selected wavelengths (inset). (c) Time-resolved UV-vis spectra from laser photolysis of **2** in hexanes containing 25.0 mM acetone, 0.42 - 0.96 μs (○), and 21.9 - 22.2 μs (□) after the laser pulse (25 °C), and absorbance-time profiles at selected wavelengths (inset). Data from (b) and (c) were recorded using a neutral density filter (67 % transmittance). 175
- Figure S4.4.** (a) Plots of  $k_{\text{decay}}$  for reaction of SnMe<sub>2</sub> (○) and SnPh<sub>2</sub> (□) with Et<sub>2</sub>S in hexanes at 25 °C; the solid lines are the linear least squares fit of the data to eq. 4.3. (b) Time-resolved UV-vis spectra from laser photolysis of **1** in hexanes containing 1.0 mM Et<sub>2</sub>S, 0.16 - 0.48 μs (○), and 11.2 - 11.8 μs (□) after the laser pulse (25 °C), and absorbance-time profiles at selected wavelengths (inset). (c) Time-resolved UV-vis spectra from laser photolysis of **2** in hexanes containing 1.0 mM Et<sub>2</sub>S, 0.32 - 0.64 μs (○), and 85.9 - 86.7 μs (□) after the laser pulse (25 °C), and absorbance-time profiles at selected wavelengths (inset). 176
- Figure S4.5.** (a) Plots of  $k_{\text{decay}}$  for reaction of SnMe<sub>2</sub> (○) and SnPh<sub>2</sub> (□) with 176

THT in hexanes at 25 °C; the solid lines are the linear least squares fit of the data to eq. 4.3. (b) Time-resolved UV-vis spectra from laser photolysis of SnMe<sub>2</sub> precursor **1** in hexanes containing 1.0 mM THT, 0.26 - 0.38 μs (○), and 35.7 - 35.9 μs (□) after the laser pulse (25 °C), and absorbance-time profiles at selected wavelengths (inset). (c) Time-resolved UV-vis spectra from laser photolysis of **2** in hexanes containing 0.6 mM THT, 2.2 - 3.2 μs (○), and 172 - 173 μs (□) after the laser pulse (25 °C), and absorbance-time profiles at selected wavelengths (inset).

- Figure S4.6.** Plots of  $k_{\text{decay}}$  for reaction of (a) SnMe<sub>2</sub> and (b) SnPh<sub>2</sub> with BuNH<sub>2</sub> in hexanes at 25 °C; the solid lines are the linear least squares fit of the data to eq. 4.3 (*data in (a) recorded by B. Nguyen*). (c) Time-resolved UV-vis spectra from laser photolysis of **1** in hexanes containing 1.0 mM BuNH<sub>2</sub>, 0.32 - 0.48 μs (○), 1.28 - 1.76 μs (□), and 26.7 - 27.5 μs (Δ) after the laser pulse (25 °C), and absorbance-time profiles at selected wavelengths (inset). (d) Time-resolved UV-vis spectra from laser photolysis of **2** in hexanes containing 0.49 mM BuNH<sub>2</sub>, 5.8 - 7.7 μs (○), and 357 - 358 μs (□) after the laser pulse (25 °C), and absorbance-time profiles at selected wavelengths (inset). 177
- Figure S4.7.** (a) Plot of  $k_{\text{decay}}$  for reaction of SnPh<sub>2</sub> with Et<sub>2</sub>NH in hexanes at 25 °C; the solid line is the linear least squares fit of the data to eq. 4.3. (b) Time-resolved UV-vis spectra from laser photolysis of **2** in hexanes containing 5.0 mM Et<sub>2</sub>NH, 3.8 - 5.1 μs (○), 16.6 - 19.8 μs (□), and 357 - 359 μs (Δ) after the laser pulse (25 °C), and absorbance-time profiles at selected wavelengths (inset). 177
- Figure S4.8.** Plots of  $k_{\text{decay}}$  for reaction of (a) SnMe<sub>2</sub> and (b) SnPh<sub>2</sub> with Et<sub>3</sub>N in hexanes at 25 °C; the solid lines are the linear least squares fit of the data to eq. 4.3. (c) Time-resolved UV-vis spectra from laser photolysis of **1** in hexanes containing 1.0 mM Et<sub>3</sub>N, 3.97 - 4.16 μs (○), 10.3 - 10.5 μs (□), and 34.4 - 34.6 μs (Δ) after the laser pulse (25 °C), and absorbance-time profiles at selected wavelengths (inset). (d) Time-resolved UV-vis spectra from laser photolysis of **2** in hexanes containing 1.0 mM Et<sub>3</sub>N, 4.5 - 5.8 μs (○), and 344 - 347 μs (□) after the laser pulse (25 °C), and absorbance-time profiles at selected wavelengths (inset). 178
- Figure S4.9.** <sup>1</sup>H NMR spectra of a deaerated 0.05 M solution of **2** in C<sub>6</sub>D<sub>12</sub> containing 1-hexyne (0.096 M) (a) before and (b) after 10 minutes photolysis with 254 nm light. 178

- Figure S4.10.**  $^1\text{H}$  NMR spectra of a deaerated 0.05 M solution of **2** in  $\text{C}_6\text{D}_{12}$  containing  $\text{Bu}_3\text{SnH}$  (0.053 M) (a) before and (b) after 15 minutes photolysis with 254 nm light. 179
- Figure S4.11.** (a) Concentration versus time plots for the photolysis of a solution of **2** (ca. 0.05 M) in  $\text{C}_6\text{D}_{12}$  and isoprene (ca. 0.1 M). The initial slopes, determined from the first eight data points in each of the plots, are (in units of  $\text{mM min}^{-1}$ ) **2**,  $-0.56 \pm 0.02$  ( $\circ$ ); **6**,  $0.54 \pm 0.03$  ( $\square$ ). (b) Concentration versus time plots for the photolysis of a solution of **2** (ca. 0.05 M) in  $\text{C}_6\text{D}_{12}$  and 1-hexyne (ca. 0.1 M). The initial slopes, determined from the first seven data points in each of the plots, are (in units of  $\text{mM min}^{-1}$ ) **2**,  $-0.46 \pm 0.01$  ( $\circ$ ); **6**,  $0.43 \pm 0.01$  ( $\square$ ). (c) Concentration versus time plots for the photolysis of a solution of **2** (ca. 0.05 M) in  $\text{C}_6\text{D}_{12}$  and  $\text{Bu}_3\text{SnH}$  (ca. 0.05 M). The initial slopes, determined from the first six data points in each of the plots, are (in units of  $\text{mM min}^{-1}$ ) **2**,  $-0.47 \pm 0.03$  ( $\circ$ ); **6**,  $0.50 \pm 0.04$  ( $\square$ ). 179
- Figure S4.12.** Plots of  $(\Delta A_0)_0 / (\Delta A_0)_Q$  for the reactions of (a)  $\text{SnMe}_2$  and (b)  $\text{SnPh}_2$  with cyclohexene in hexanes at  $25^\circ\text{C}$ ; the solid lines are the linear least squares fits of the data to eq. 4.4. (c) Time-resolved UV-vis spectra from laser photolysis of **1** in hexanes containing 0.5 M cyclohexene,  $0.64 - 1.12 \mu\text{s}$  ( $\circ$ ), and  $85.9 - 86.7 \mu\text{s}$  ( $\square$ ) after the laser pulse ( $25^\circ\text{C}$ ), and absorbance-time profiles at selected wavelengths (inset). (d) Time-resolved UV-vis spectra from laser photolysis of **2** in hexanes containing 0.5 M cyclohexene,  $0.32 - 0.80 \mu\text{s}$  ( $\circ$ ), and  $85.9 - 86.7 \mu\text{s}$  ( $\square$ ) after the laser pulse ( $25^\circ\text{C}$ ), and absorbance-time profiles at selected wavelengths (inset). 180
- Figure S4.13.** (a) Plots of  $(\Delta A_0)_0 / (\Delta A_0)_Q$  for reaction of the  $\text{SnMe}_2$  ( $\circ$ ) and  $\text{SnPh}_2$  ( $\square$ ) absorption with 1-hexyne in hexanes at  $25^\circ\text{C}$ ; the solid lines are the linear least squares fit of the data to eq. 4.4. (b) Time-resolved UV-vis spectra from laser photolysis of **1** in hexanes containing 0.25 M 1-hexyne,  $0.16 - 0.48 \mu\text{s}$  ( $\circ$ ), and  $21.6 - 22.1 \mu\text{s}$  ( $\square$ ) after the laser pulse ( $25^\circ\text{C}$ ), and absorbance-time profiles at selected wavelengths (inset). (c) Time-resolved UV-vis spectra from laser photolysis of **2** in hexanes containing 0.2 M 1-hexyne,  $0.64 \mu\text{s}$  ( $\circ$ ), and  $77.9 - 78.7 \mu\text{s}$  ( $\square$ ) after the laser pulse ( $25^\circ\text{C}$ ), and absorbance-time profiles at selected wavelengths (inset). 180
- Figure S4.14.** (a) Plots of  $(\Delta A_0)_0 / (\Delta A_0)_Q$  for reaction of the  $\text{SnMe}_2$  ( $\circ$ ) and  $\text{SnPh}_2$  ( $\square$ ) absorption with  $\text{Bu}_3\text{SnH}$  in hexanes at  $25^\circ\text{C}$ ; the solid 181

lines are the linear least squares fit of the data to eq. 4.4. (b) Time-resolved UV-vis spectra from laser photolysis of **2** in hexanes containing 7.8 mM Bu<sub>3</sub>SnH, 0.45 - 0.54 μs (○), and 17.8 - 18.0 μs (□) after the laser pulse (25 °C), and absorbance-time profiles at selected wavelengths (inset). (c) Time-resolved UV-vis spectra from laser photolysis of **1** in hexanes containing 14 mM Bu<sub>3</sub>SnH, 0.42 - 0.54 μs (○), and 17.8 - 18.0 μs (□) after the laser pulse (25 °C), and absorbance-time profiles at selected wavelengths (inset).

- Figure 5.1.** <sup>1</sup>H NMR spectra of an air saturated C<sub>6</sub>D<sub>12</sub> 0.04 M solution of **1** (a) before and (b) after 10 minutes of photolysis with 254 nm light, and (c) after spiking the resulting photolyzate with an authentic sample of **5**. (*Samples prepared by J. Woodard*) 187
- Figure 5.2.** (a) Concentration versus time plots for the photolysis of a solution of **1** (ca. 0.04 M) in air-saturated C<sub>6</sub>D<sub>12</sub>, with periodic replenishment of depleted air (eq. 5.3a). The slopes of the plots are (in units of mM min<sup>-1</sup>) **1**, -0.40 ± 0.03 (○); **3**, 0.40 ± 0.01 (□); **5**, 0.14 ± 0.01 (Δ); **4**, 0.019 ± 0.007 (∇; see expansion). (b) Concentration versus time plots for the photolysis of an incompletely deoxygenated solution of **1** (ca. 0.04 M) in C<sub>6</sub>D<sub>12</sub>, without periodic replenishment of depleted O<sub>2</sub> (eq. 5.3b). The slopes of the plots are (in units of mM min<sup>-1</sup>) **1**, -0.35 ± 0.01 (○); **3**, 0.29 ± 0.01 (□); **5**, 0.121 ± 0.003 (< 3 min) (Δ); **4**, 0.082 ± 0.004 (∇; see expansion). (*Samples prepared by J. Woodard*) 188
- Figure 5.3.** <sup>1</sup>H NMR spectra of a deoxygenated 0.04 M solution of **1** in C<sub>6</sub>D<sub>12</sub> (a) before and (b) after 30 minutes photolysis with 254 nm light, and (c) after spiking the sample of (b) with an authentic sample of **4**. 189
- Figure 5.4.** Concentration versus time plots for the photolysis of a deoxygenated solution of **1** (ca. 0.04 M) in C<sub>6</sub>D<sub>12</sub> and AcOH (ca. 0.2 M). The initial slopes, determined over the first 12 minutes of photolysis, are (in units of mM min<sup>-1</sup>) AcOH, -1.03 ± 0.06 (Δ); **1**, -0.66 ± 0.02 (○); **3**, 0.51 ± 0.02 (□); **4**, 0.97 ± 0.04 (∇). 190
- Figure 5.5.** <sup>1</sup>H NMR spectra of a 0.045 M solution of **1** in C<sub>6</sub>D<sub>12</sub> containing Me<sub>2</sub>SnCl<sub>2</sub> (0.035 M) (a) before and (b) after 10 minutes photolysis with 254 nm UV light (*\*Unreactive impurity*) (*Samples prepared by J. Woodard*) 191
- Figure 5.6.** (a) Concentration versus time plots for the photolysis of a 193

solution of **1** (ca. 0.045 M) and  $\text{Me}_2\text{SnCl}_2$  (ca. 0.035 M) in  $\text{C}_6\text{D}_{12}$  as described in eq. 5.5. The slopes of each of the plots are (in units of  $\text{mM min}^{-1}$ )  $\text{Me}_2\text{SnCl}_2$ ,  $-1.57 \pm 0.06$  ( $\Delta$ ); **1**,  $-0.86 \pm 0.05$  ( $\circ$ ); **3**,  $0.75 \pm 0.03$  ( $\square$ ); **2**,  $0.49 \pm 0.01$  ( $\odot$ ); **6**,  $0.17 \pm 0.01$  ( $\diamond$ ); **4**,  $0.62 \pm 0.03$  ( $\nabla$ ). The slope for **2** was determined using the first seven data points. (b) Concentration versus time plots for the photolysis of a solution of **8** (ca. 0.04 M) and MeOH (ca. 0.04 M) in  $\text{C}_6\text{D}_{12}$  as described in eq. 5.6. The initial slopes, determined from the first seven data points in each of the plots, are (in units of  $\text{mM min}^{-1}$ ) **8**,  $-1.00 \pm 0.05$  ( $\circ$ ); **3**,  $0.87 \pm 0.01$  ( $\square$ ); **7**,  $0.75 \pm 0.03$  ( $\Delta$ ). *Samples prepared by J. Woodard*

- Figure 5.7.** Time-resolved UV-vis spectra recorded by laser photolysis of  $\text{SnMes}_2$  precursor **1** in hexanes solution, 0.16 - 0.32  $\mu\text{s}$  ( $\circ$ ), and 9.4 - 9.9  $\mu\text{s}$  ( $\square$ ) after the laser pulse (25  $^\circ\text{C}$ ), and absorbance-time profiles at selected wavelengths (inset). 194
- Figure 5.8.** Representative transient decay profiles recorded at 570 nm from a hexanes solution of **1** containing (a) 0 and 0.05 mM AcOH, (b) 0 and 0.3 mM  $\text{Et}_2\text{NH}$ , and (c) 0 and 35 mM THF. (*Data recorded by J. Woodard*) 196
- Figure 5.9.** Time-resolved UV-vis spectra from laser photolysis of **1** in hexanes containing 5.0 mM  $\text{BuNH}_2$ , 0.0-2.6  $\mu\text{s}$  ( $\circ$ ), and 12.2-12.7  $\mu\text{s}$  ( $\square$ ) after the laser pulse (25  $^\circ\text{C}$ ), and absorbance-time profiles at selected wavelengths (inset). (b) Time-resolved UV-vis spectra from laser photolysis of **1** in hexanes containing 5.0 mM THT, 0.0 - 0.64  $\mu\text{s}$  ( $\circ$ ), 5.8 - 7.0  $\mu\text{s}$  ( $\square$ ), and 111 - 113  $\mu\text{s}$  ( $\Delta$ ) after the laser pulse (25  $^\circ\text{C}$ ), and absorbance-time profiles at selected wavelengths (inset). (*Data recorded by J. Woodard*) 199
- Figure 5.10.** (a) Representative transient decay profiles recorded at 490 nm from a hexanes solution of **1** containing 0.0 mM, 3.1 mM, and 14.7 mM  $\text{O}_2$ . (b) Plot of  $k_{\text{decay}}$  for the reaction of **9** with  $\text{O}_2$  in hexanes at 25  $^\circ\text{C}$ ; the solid line is the linear least squares fit of the data to equation 5.9. (*Data recorded by J. Woodard*) 201
- Figure S5.1.**  $^{119}\text{Sn}$  NMR spectra of an air-saturated 0.045 M solution of **1** in  $\text{C}_6\text{D}_{12}$  (a) after 10 minutes photolysis with 254 nm light, and (b) after spiking the resulting photolyzate with an authentic sample of **5**. (*\*Unreactive Impurity*) (*Samples prepared by J. Woodard*) 217
- Figure S5.2.** (a) GC-MS chromatogram (0 - 9.5 minutes retention time) and (b) mass spectrum of the peak at ca. 5.8 minutes retention time 218

- from a 0.04 M solution of **1** in C<sub>6</sub>D<sub>12</sub> containing 0.2 M AcOH after 30 minutes photolysis with 254 nm UV light.
- Figure S5.3.** <sup>13</sup>C{<sup>1</sup>H} NMR spectra of a 0.04 M solution of **1** in C<sub>6</sub>D<sub>12</sub> containing 0.2 M AcOH (a) after 30 minutes photolysis with 254 nm UV light and (b) after spiking the photolyzate of (a) with an authentic sample of **4**. 218
- Figure S5.4.** <sup>1</sup>H NMR spectra of a 0.045 M solution of **1** in C<sub>6</sub>D<sub>12</sub> containing Me<sub>2</sub>SnCl<sub>2</sub> (0.035 M) (a) after 10 minutes photolysis with 254 nm light, and (b) after spiking the photolyzate of (a) with an authentic sample of **2**. (\*Unreactive Impurity) (Samples prepared by J. Woodard) 219
- Figure S5.5.** <sup>119</sup>Sn{<sup>1</sup>H} NMR spectra of a 0.045 M solution of **1** in C<sub>6</sub>D<sub>12</sub> containing Me<sub>2</sub>SnCl<sub>2</sub> (0.035 M) (a) after 10 minutes photolysis with 254 nm light, and (b) after spiking the photolyzate of (a) with an authentic sample of **2**. (\*Unreactive Impurity; ? unidentified tin-containing compound) (Samples prepared by J. Woodard) 219
- Figure S5.6.** Plot of  $(\Delta A_0)_0 / (\Delta A_0)_Q$  for reaction of SnMes<sub>2</sub> (570 nm) with (a) Et<sub>2</sub>O, (b) THF and (c) MeOH in hexanes at 25 °C; the solid lines are the linear least squares fit of the data to equation 5.11. (d) Time-resolved UV-vis spectra recorded by laser photolysis of **1** in hexanes containing 2.0 M Et<sub>2</sub>O, 0.4-0.5 μs (○), and 17.3-17.6 μs (□) after the laser pulse (25 °C), and absorbance-time profiles at selected wavelengths (inset). (e) Time-resolved UV-vis spectra recorded by laser photolysis of **1** in hexanes containing 0.12 M THF, 0.32-1.0 μs (○), and 172-173 μs (□) after the laser pulse (25 °C), and absorbance-time profiles at selected wavelengths (inset). (f) Time-resolved UV-vis spectra recorded by laser photolysis of **1** in hexanes containing 41 mM MeOH, 0.58-0.70 μs (○), and 34.4-34.6 μs (□) after the laser pulse (25 °C), and absorbance-time profiles at selected wavelengths (inset). (Data in (a)-(c) recorded by J. Woodard) 220
- Figure S5.7.** Plots of  $k_{\text{decay}}$  (□) and  $(\Delta A_0)_0 / (\Delta A_{\text{res}})_Q$  (○) of SnMes<sub>2</sub> (570 nm) versus (a) [THT] and (e) [Et<sub>2</sub>NH], in hexanes solution at 25 °C; the solid lines are the linear least-squares fits of the data to equations 5.9 and 5.10, respectively. (b) Plot of  $(\Delta A_0)_0 / (\Delta A_0)_Q$  for reaction of SnMes<sub>2</sub> (570 nm) with Et<sub>2</sub>S in hexanes at 25 °C; the solid line is the linear least squares fit of the data to eq. 5.11. (c) Time-resolved UV-vis spectra from laser photolysis of **1** in 221



hexanes containing 7.0 mM Et<sub>2</sub>S, 0.0 - 0.64 μs (○), and 87.7 - 90.9 μs (□) after the laser pulse (25 °C), and absorbance-time profiles at selected wavelengths (inset). (d) Plot of  $k_{\text{decay}}$  for reaction of SnMes<sub>2</sub> (570 nm) with BuNH<sub>2</sub> in hexanes at 25 °C; the solid line is the linear least squares fit of the data to equation 5.9. (f) Time-resolved UV-vis spectra from laser photolysis of **1** in hexanes containing 1.0 mM Et<sub>2</sub>NH, 0.32 - 0.80 μs (○), 5.92 - 6.56 μs (□), and 85.9 - 86.6 μs (Δ) after the laser pulse (25 °C), and absorbance-time profiles at selected wavelengths (inset). (Data recorded by J. Woodard)

- Figure S5.8.** Plots of  $k_{\text{decay}}$  for reaction of SnMes<sub>2</sub> (570 nm) with (a) AcOH, 222  
(b) Me<sub>2</sub>SnCl<sub>2</sub>, and (c) molecular oxygen in hexanes at 25 °C; the solid lines are the linear least squares fit of the data to equation 5.9. (d) Time-resolved UV-vis spectra from laser photolysis of **1** in hexanes containing 0.3 mM AcOH, 0.16 - 0.32 μs (○), 1.3 - 1.6 μs (□), and 85.9 - 86.7 μs (Δ) after the laser pulse (25 °C), and absorbance-time profiles at selected wavelengths (inset). (e) Time-resolved UV-vis spectra from laser photolysis of **1** in hexanes containing 1.0 mM Me<sub>2</sub>SnCl<sub>2</sub>, 0.27 - 0.35 μs (○), and 6.6 - 6.7 μs (□) after the laser pulse (25 °C), and absorbance-time profiles at selected wavelengths (inset). (f) Time-resolved UV-vis spectra from laser photolysis of **1** in hexanes containing 14.7 mM O<sub>2</sub>, 0.16 - 0.32 μs (○), 4.8 - 5.1 μs (□), and 87.5 - 88.3 μs (Δ) after the laser pulse (25 °C), and absorbance-time profiles at selected wavelengths (inset); data from (f) recorded using a neutral density filter (67 % transmittance). (Data in (a)-(e) recorded by J. Woodard)
- Figure S5.9.** Plots of  $k_{\text{decay}}$  for the reactions of **9** with (a) Me<sub>2</sub>SnCl<sub>2</sub>, (b) AcOH, 223  
and (c) MeOH in hexanes at 25 °C; the solid lines are the linear least squares fit of the data to eq. 5.9. (Data recorded by J. Woodard)
- Figure 6.1.** Transient absorption spectra from laser photolysis of **6** in hexanes 230  
solution (ca. 4 × 10<sup>-3</sup> M) recorded 0.13 - 0.16 μs (○) and 17.7 - 17.8 μs (□) after the laser pulse. The inset shows absorbance-time profiles recorded at 290 nm and 510 nm.
- Figure 6.2.** (a) Transient absorption spectra from laser photolysis of **7** in 233  
hexanes solution (ca. 4 × 10<sup>-5</sup> M) recorded 0.16 - 0.64 μs (○) and 7.2 - 7.7 μs (□) after the laser pulse. The dashed spectrum (--) shows the difference between spectra recorded 0.16 - 0.64 μs and 42.1 - 43.0 μs after the laser pulse scaled by a factor of 5. The

insets show magnified versions of the spectra at 420 - 460 nm and 490 - 550 nm. (b) Absorbance-time profiles recorded at 430 nm and 530 nm.

- Figure 6.3.** Plot of  $k_{\text{decay}}$  versus [cyclohexene] for the reaction of *Sit*-Bu<sub>2</sub> with cyclohexene in a hexanes solution of **7** at 25 °C, the silylene is monitored at 530 nm. The solid line is the linear least squares fit of the data to eq. 6.11. 236
- Figure 6.4.** (a) Plot of  $(\Delta A_0)_0 / (\Delta A_0)_Q$  versus [Et<sub>2</sub>O] for the reaction of *Sit*-Bu<sub>2</sub> with Et<sub>2</sub>O from a hexanes solution of **7** at 25 °C, the silylene is monitored at 530 nm. The solid line is the linear least squares fit of the data to eq. 6.12. (b) Transient absorption spectra from laser photolysis of **6** in hexanes solution (ca.  $4 \times 10^{-3} \text{ M}^{-1}$ ) containing 0.40 M Et<sub>2</sub>O recorded 0.35 - 0.43  $\mu\text{s}$  ( $\circ$ ) and 8.6 - 8.7  $\mu\text{s}$  ( $\square$ ) after the laser pulse. The inset shows the transient profile recorded at 300 nm. (c) Transient absorption spectra from laser photolysis of **7** in hexanes solution (ca. 0.04 mM) containing 0.20 M Et<sub>2</sub>O recorded 0.25 - 0.30  $\mu\text{s}$  ( $\circ$ ) and 8.6 - 8.7  $\mu\text{s}$  ( $\square$ ) after the laser pulse. The dashed spectrum (--) shows the difference between the spectra recorded 0.25 - 0.30  $\mu\text{s}$  and 8.6 - 8.7  $\mu\text{s}$  after the laser pulse. The inset shows the transient profile recorded at 290 nm and 430 nm. 238
- Figure 6.5.** (a) Plot of  $k_{\text{fast}}$  versus [acetone] for the reaction of **8** with acetone in a hexanes solution of **7** at 25 °C, the disilene is monitored at 440 nm. The solid line is the linear least squares fit of the data to eq. 6.11; (b) Transient absorption spectra from laser photolysis of **7** in hexanes solution (ca. 0.04 mM) containing 50 mM acetone recorded 0.64 - 1.28  $\mu\text{s}$  ( $\circ$ ) and 344 - 347  $\mu\text{s}$  ( $\square$ ) after the laser pulse. The inset shows the transient profile recorded at 300 nm and 440 nm. The apparent negative absorption in the 340 - 430 nm regions of the UV-vis spectra is due to bleaching of **7**, which exhibits absorption maxima in this wavelength region.<sup>52</sup> 249
- Figure S6.1.** (a) Plot of  $(\Delta A_0)_0 / (\Delta A_0)_Q$  versus [THF] for the reaction of *Sit*-Bu<sub>2</sub> with THF from flash photolysis of hexanes solutions of **7** at 25 °C. Plots of  $k_{\text{decay}}$  versus [Q] for the reactions of *Sit*-Bu<sub>2</sub> with (b) Q = Et<sub>3</sub>N and (c) Q = THT in hexanes solution of **7** at 25 °C. The solid lines are the linear least squares fits of the data to eq. 6.12 (a) and 6.11 (b,c), respectively. 252
- Figure S6.2.** Plot of  $k_{\text{decay}}$  versus [Q] for the reaction of *Sit*-Bu<sub>2</sub> with (a) Q = methanol, (b) Q = Et<sub>2</sub>NH and (c) Q = triethylsilane in hexanes 252

solutions of **7** at 25 °C. The solid lines are the linear least squares fits of the data to eq. 6.11.

- Figure S6.3.** Plot of  $k_{\text{decay}}$  versus [Q] for the reaction of *Sit*-Bu<sub>2</sub> with (a) Q = AcOH, (b) Q = acetone and (c) Q = molecular oxygen from flash photolysis of hexanes solutions of **7** at 25 °C. The solid lines are the linear least squares fit of the data to eq. 6.11. 253
- Figure S6.4.** Plot of  $k_{\text{decay}}$  versus [Q] for the reaction of *Sit*-Bu<sub>2</sub> with (a) Q = 1-hexene, (b) Q = *cis*-cyclooctene and (c) Q = TME in hexanes solutions of **7** at 25 °C. The solid lines are the linear least squares fit of the data to eq. 6.11. 253
- Figure S6.5.** Plot of  $k_{\text{decay}}$  versus [Q] for the reaction of *Sit*-Bu<sub>2</sub> with (a) Q = cyclohexene and (b) Q = triethylsilane in hexanes solutions of **6** at 25 °C. The solid lines are the linear least squares fits of the data to eq. 6.11. 253
- Figure S6.6.** (a) Plot of  $k_{\text{decay}}$  versus [*cis*-cyclooctene] for the reaction of SiMe<sub>2</sub> with *cis*-cyclooctene in a hexanes solution of **2** at 25 °C. (b) Plot of  $k_{\text{decay}}$  versus [1-hexene] for the reaction of SiPh<sub>2</sub> with 1-hexene in hexanes solutions of **3** at 25 °C. (c) Plot of  $k_{\text{decay}}$  versus [1-hexene] for the reaction of SiMe<sub>2</sub> with 1-hexene in hexanes solutions of **4** at 25 °C. The solid lines are the linear least squares fit of the data to eq. 6.11. (*Data from (b) recorded by M. Reid*) 254
- Figure S6.7.** Plots of  $k_{\text{decay}}$  versus [TME] for the reaction of (a) SiMe<sub>2</sub>, (b) SiPh<sub>2</sub>, and (c) SiMe<sub>2</sub> with TME in hexanes solutions of (a) **2**, (b) **3**, and (c) **4** at 25 °C. The solid lines are the linear least squares fit of the data to eq. 6.11. (*Data from (a) and (b) recorded by M. Reid*) 254
- Figure S6.8.** Transient absorption spectra from laser photolysis of **7** in hexanes solution (ca. 0.04 mM) containing 5.0 mM THF recorded 0.16 - 0.64 μs (○) and 45.9 - 46.6 μs (□) after the laser pulse. The dashed spectrum (--) shows the difference between the spectra recorded 0.16 - 0.64 μs and 45.9 - 46.6 μs after the laser pulse. The inset shows the transient profile recorded at 310 nm and 430 nm. The apparent negative absorption in the 340 - 430 nm regions of the UV-vis spectra in (a) and (b) is due to bleaching of **7**, which exhibits absorption maxima in this wavelength region.<sup>52</sup> 255

<b>Figure S6.9.</b>	(a) Transient absorption spectra from laser photolysis of <b>6</b> in hexanes solution (ca. 4 mM) containing 5.1 mM THT recorded 0.32 - 1.28 $\mu\text{s}$ ( $\circ$ ) and 172 - 173 $\mu\text{s}$ ( $\square$ ) after the laser pulse. The inset shows the transient profile recorded at 340 nm; (b) Transient absorption spectra from laser photolysis of <b>6</b> in hexanes solution (ca. 4 mM) containing 5.0 mM $\text{Et}_2\text{NH}$ recorded 0.22 - 0.32 $\mu\text{s}$ ( $\circ$ ) and 17.2 - 17.3 $\mu\text{s}$ ( $\square$ ) after the laser pulse. The inset shows the transient profile recorded at 290 nm.	255
<b>Figure S6.10.</b>	(a) Plot of $k_{\text{decay}}$ versus $[\text{O}_2]$ for the reaction of the 310 nm ( $\circ$ ) and 440 nm ( $\square$ ) transient signals with molecular oxygen in a hexanes solution of <b>7</b> at 25 $^\circ\text{C}$ . The solid lines are the linear least squares for of the data to eq. 6.11. (b) Transient absorption spectra from laser photolysis of <b>7</b> in $\text{O}_2$ saturated hexanes solution (ca. 0.04 mM) recorded 0.19 - 0.38 $\mu\text{s}$ ( $\circ$ ) and 35.3 - 35.6 $\mu\text{s}$ ( $\square$ ) after the laser pulse. The inset shows the transient profile recorded at 300 nm and 430 nm. The apparent negative absorption in the 340 - 430 nm regions of the UV-vis spectra is due to bleaching of <b>7</b> , which exhibits absorption maxima in this wavelength region. <sup>52</sup>	256
<b>Figure 8.1.</b>	UV-visible absorption spectra of 1-stannacyclopent-3-enes (a) <b>2</b> and <b>3</b> , (b) <b>1</b> and <b>4</b> , and (c) <b>5</b> , recorded between 220 - 300 nm in hexanes solution.	287
<b>Figure 8.2.</b>	UV-visible absorption spectra of <i>Sit</i> - $\text{Bu}_2$ precursors (a) <b>6</b> and (b) <b>7</b> recorded between 220 - 300 nm in hexanes solution.	287

## LIST OF TABLES:

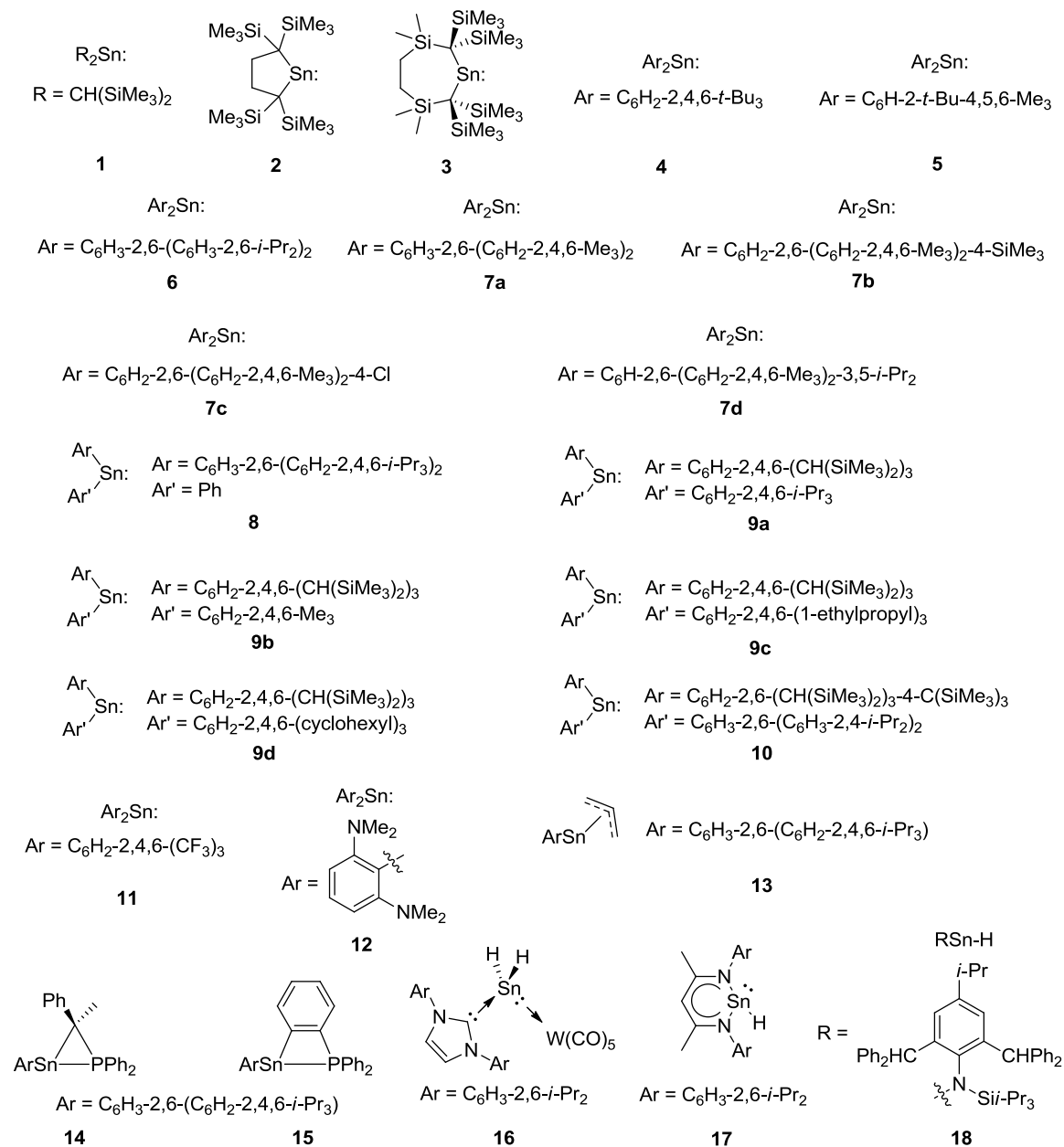
<b>Table 1.1.</b>	Diagnostic Spectral Properties and Spectral Features of Persistent Stannylenes.	5
<b>Table 1.2.</b>	Absolute Rate Constants for the Reactions of $\text{SnMe}_2$ in the Gas Phase at $296 \pm 2 \text{ K}$ . <sup>a,b</sup>	29
<b>Table 2.1.</b>	Absolute Rate ( $k$ , $\text{M}^{-1} \text{ s}^{-1}$ ) and/or Equilibrium Constants ( $K_{\text{eq}}$ , $\text{M}^{-1}$ ) for Dimerization and Reactions of Dimethylstannylene ( $\text{SnMe}_2$ ) and Diphenylstannylene ( $\text{SnPh}_2$ ) with $\text{Me}_2\text{SnCl}_2$ and $\text{MeOH}$ , Determined by Laser Flash Photolysis of <b>2</b> and <b>3</b> in Hexanes at 25 $^\circ\text{C}$ .	69

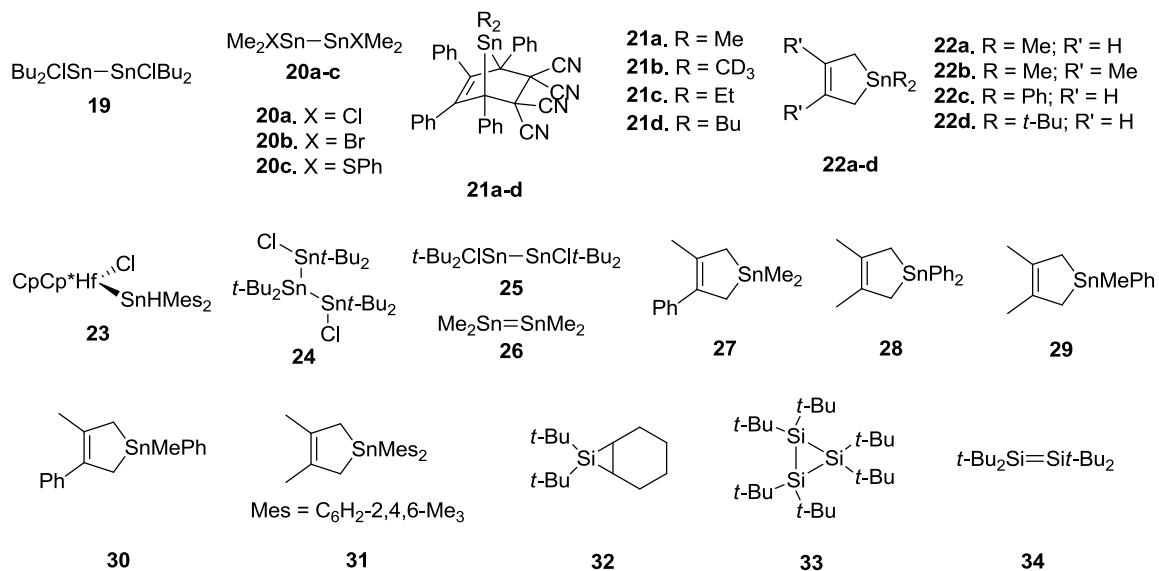
<b>Table 2.2.</b>	Calculated Electronic Energies, Enthalpies (298.15 K), and Free Energies (298.15 K) of Stationary Points in the Dimerization of SnMe <sub>2</sub> and SnPh <sub>2</sub> and their Lewis acid-base Complexation with Methanol, Calculated at the $\omega$ B97XD/6-31+G(d,p) <sup>C,H,O</sup> -LANL2DZdp <sup>Sn</sup> Level of Theory Relative to the Isolated Reactants (in kcal mol <sup>-1</sup> ). <sup>a</sup>	72
<b>Table 2.3.</b>	Calculated <sup>a</sup> and Experimental UV-Vis Absorption Maxima of Stannylenes and Stannylene-derived Dimers and Methanol Complexes.	74
<b>Table S2.1.</b>	Calculated Electronic Energies, Standard Enthalpies (298.15 K), and Standard Free Energies (298.15 K) of Stationary Points in the Dimerization of SnMe <sub>2</sub> and SnPh <sub>2</sub> , Calculated at the $\omega$ B97X/6-31+G(d,p) <sup>C,H,O</sup> -LANL2DZdp <sup>Sn</sup> Level of Theory Relative to the Isolated Reactants (in kcal mol <sup>-1</sup> ).	91
<b>Table 3.1.</b>	Absolute Rate ( $k_Q$ ) and Equilibrium Constants ( $K_{eq}$ ) for the Reactions of SnMe <sub>2</sub> , SnPh <sub>2</sub> and SnMePh with Stannylene Substrates in Hexanes Solution at 25 °C.	110
<b>Table 3.2.</b>	Summary of $K_1$ (M <sup>-1</sup> ), $k_2$ (10 <sup>6</sup> s <sup>-1</sup> ) and $k_Q$ (10 <sup>9</sup> M <sup>-1</sup> s <sup>-1</sup> ) for the Reactions of SnMe <sub>2</sub> , SnPh <sub>2</sub> and SnMePh with Bu <sub>3</sub> SnCl in Hexanes Solution at 25 °C.	118
<b>Table 3.3.</b>	Absolute Rate Constants ( $k_Q$ ) for the Reactions of SnMe <sub>2</sub> , SnPh <sub>2</sub> and SnMePh with AcOH and AcOD in Hexanes Solution at 25 °C. <sup>a</sup>	127
<b>Table 4.1.</b>	Absolute Rate Constants ( $k_Q$ ) and Equilibrium Constants ( $K_{eq}$ ) for the Reactions of SnMe <sub>2</sub> and SnPh <sub>2</sub> with Various Lewis Bases and UV-vis Absorption Maxima of the Stannylene-donor Complexes in Hexanes Solution at 25 °C.	150
<b>Table 4.2.</b>	Equilibrium Constants ( $K_{eq}$ ) and Calculated and Experimental UV-vis Absorption Maxima ( $\lambda_{max}$ ) of the Lewis Acid - Base Complexes for the Reactions of SnMe <sub>2</sub> and SnPh <sub>2</sub> with Various Stannylene Substrates in Hexanes Solution at 25 °C.	155
<b>Table 4.3.</b>	Standard Gibbs Free Energies ( $\Delta G$ ; kcal mol <sup>-1</sup> ) for the Reactions of SnMe <sub>2</sub> with O-donor Substrates and Gas Phase Basicities (GB), Proton Affinities (PA) and BF <sub>3</sub> Affinities (kcal mol <sup>-1</sup> ) of Et <sub>2</sub> O, EtOAc, Acetone, MeOH, and THF.	159

<b>Table 4.4.</b>	Absolute Rate ( $k_Q$ ) and Equilibrium Constants ( $K_{eq}$ ) for the Reactions of $MMe_2$ and $MPh_2$ ( $M = Si, Ge, Sn$ ) with Various Lewis bases in Hexanes Solution at 25 °C.	161
<b>Table 4.5.</b>	Long Wavelength UV-vis Absorption Maxima of the $MMe_2$ and $MPh_2$ -Donor Complexes ( $M = Si, Ge, Sn$ ) with various Lewis Bases in Hexanes Solution at 25 °C.	163
<b>Table 5.1.</b>	Absolute Rate and Equilibrium Constants ( $k_Q$ and $K_{eq}$ ) for the Reactions of $SnMes_2$ with Various Stannylyene Substrates in Hexanes Solution at 25 °C and Long-Wavelength Absorption Maxima ( $\lambda_{max}$ ) of the Observed New Transient Absorptions.	197
<b>Table 5.2.</b>	Long Wavelength Absorption Maxima ( $\lambda_{max}$ (nm and eV)) of Tetrylenes $MR_2$ ( $M = Si, Ge, Sn; R = Mes, Ph, Me, - (Me_3Si)_2C(CH_2)_2C(SiMe_3)_2-$ ). <sup>a</sup>	203
<b>Table 5.3.</b>	Absolute Rate ( $k_Q$ ) and Equilibrium Constants ( $K_{eq}$ ) for the Reactions of $MMes_2$ ( $M = Si, Ge, Sn$ ) and $SnPh_2$ with Various Substrates in Hexanes Solution at 25 °C.	212
<b>Table 5.4.</b>	Long Wavelength Absorption Maxima ( $\lambda_{max}$ (nm) and eV in parenthesis) of the Stannylyene-Donor Complexes ( $SnR_2$ ; $R = Mes, Ph, Me$ ) in Hexanes Solution at 25 °C. <sup>a</sup>	213
<b>Table 6.1.</b>	Absolute Rate Constants ( $k_Q$ ) and Equilibrium Constants ( $K_{eq}$ ) for the Reactions of <i>Sit</i> -Bu <sub>2</sub> and SiMe <sub>2</sub> with Various Silylene Substrates in Hydrocarbon Solution at 20 - 25 °C. <sup>a</sup>	240
<b>Table 6.2.</b>	UV-vis Absorption Maxima ( $\lambda_{max}$ , nm) and Lifetimes ( $\tau$ , $\mu s$ ) of the Lewis Acid-Base Complexes of <i>Sit</i> -Bu <sub>2</sub> and SiMe <sub>2</sub> with Chalcogen and Pnictogen Donors in Hydrocarbon Solution at 20 - 25 °C.	242
<b>Table 6.3.</b>	Ratio of Absolute Rate Constants ( $k_Q$ ) and Equilibrium Constants ( $K_{eq}$ ) Between the Silylene Pairs SiMe <sub>2</sub> : <i>Sit</i> -Bu <sub>2</sub> and SiPh <sub>2</sub> :SiMes <sub>2</sub> with Various Silylene Substrates in Hydrocarbon Solution at Ambient Temperatures.	247
<b>Table 6.4.</b>	Absolute Rate Constants ( $k_Q$ ; $10^6 M^{-1} s^{-1}$ ) for the Reactions of Disilenes with Substrates in Hexane Solution at Ambient Temperatures.	249

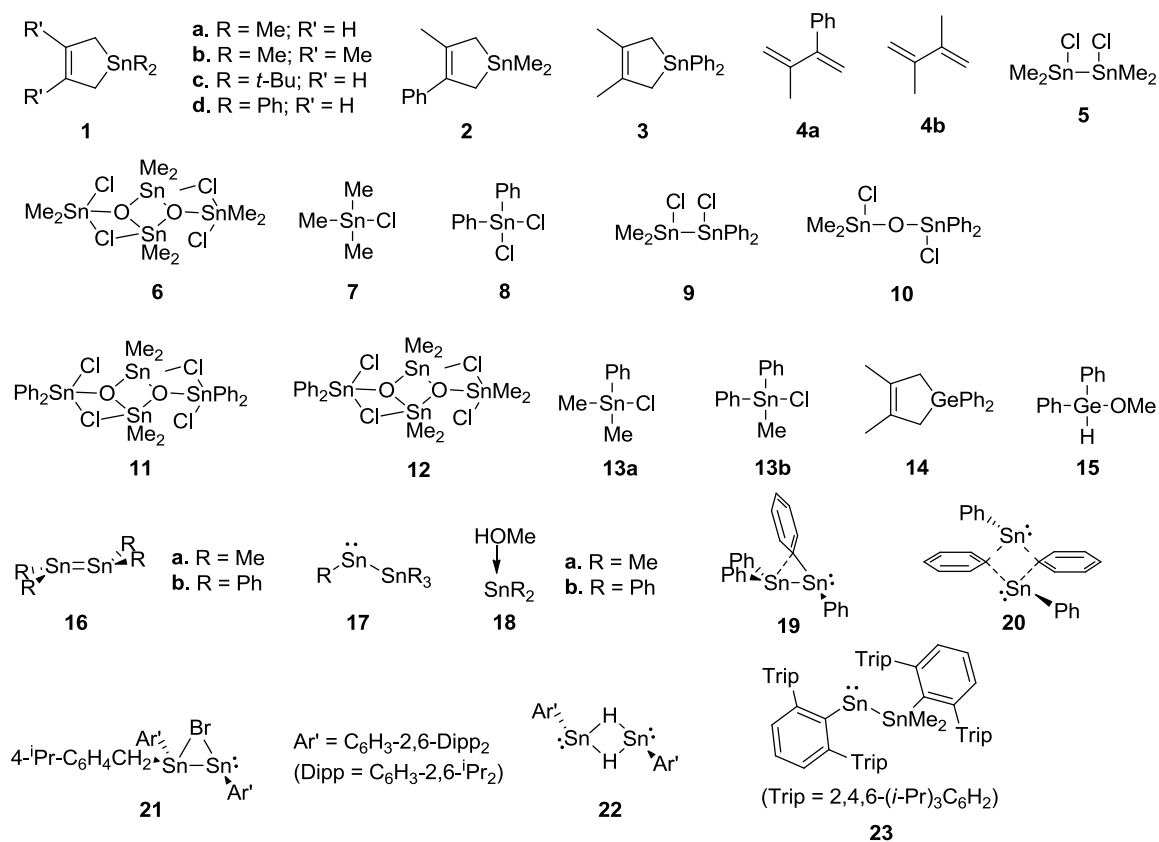
COMPOUND NUMBERS:

Chapter 1



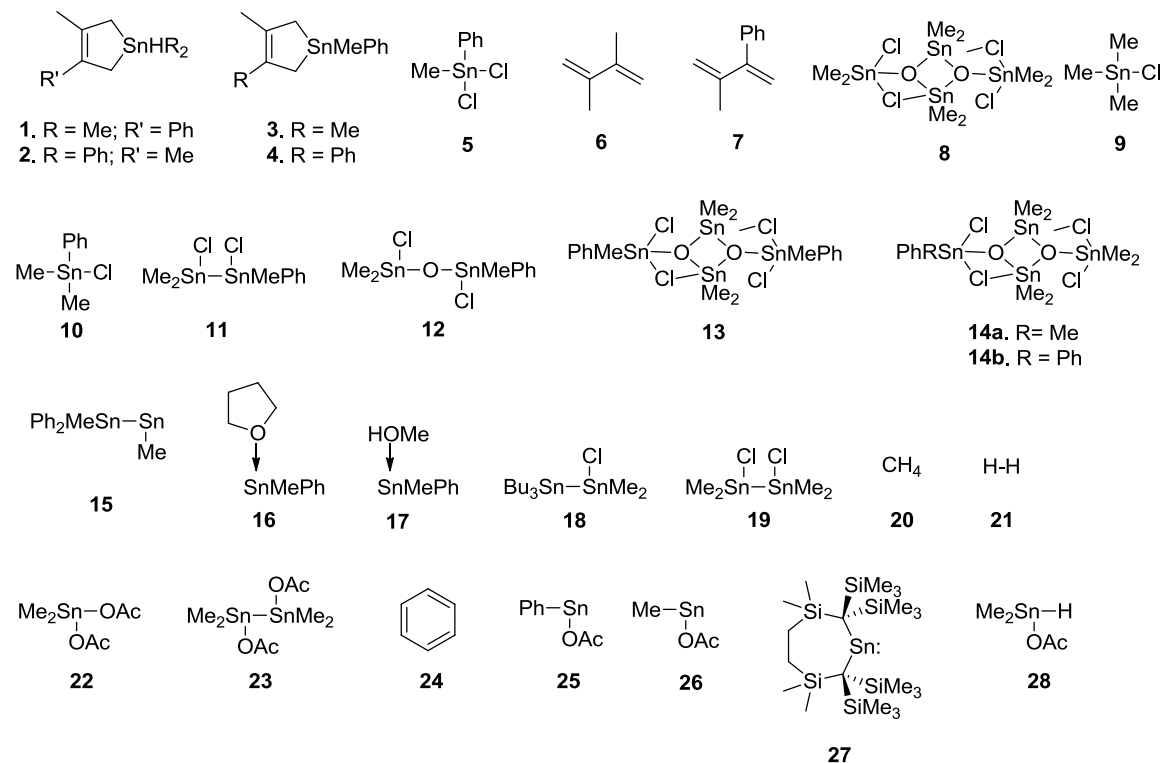


## Chapter 2

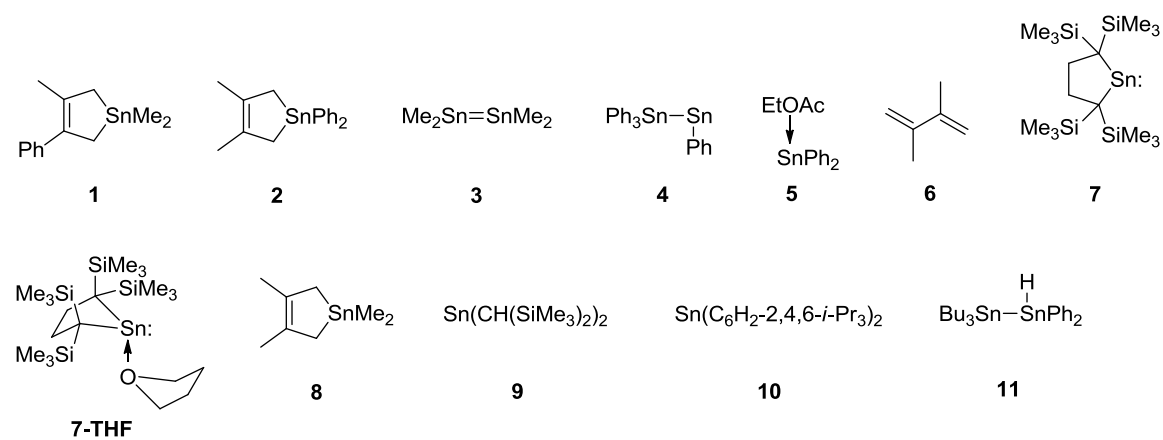




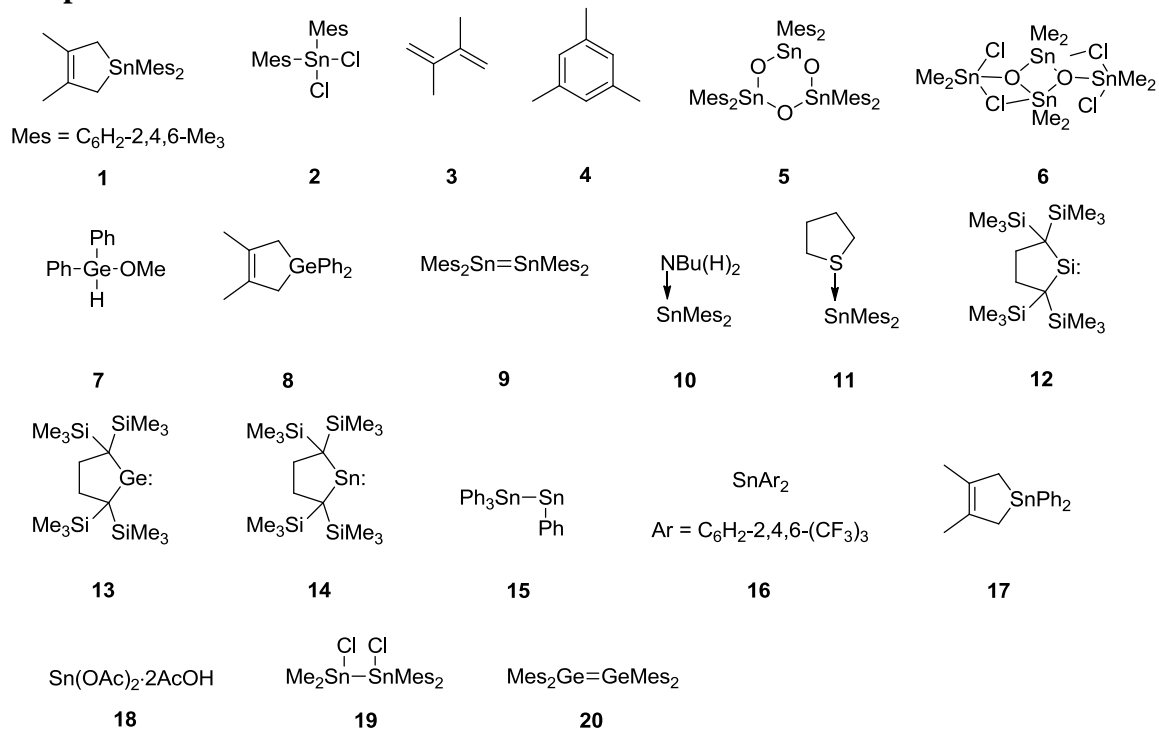
### Chapter 3



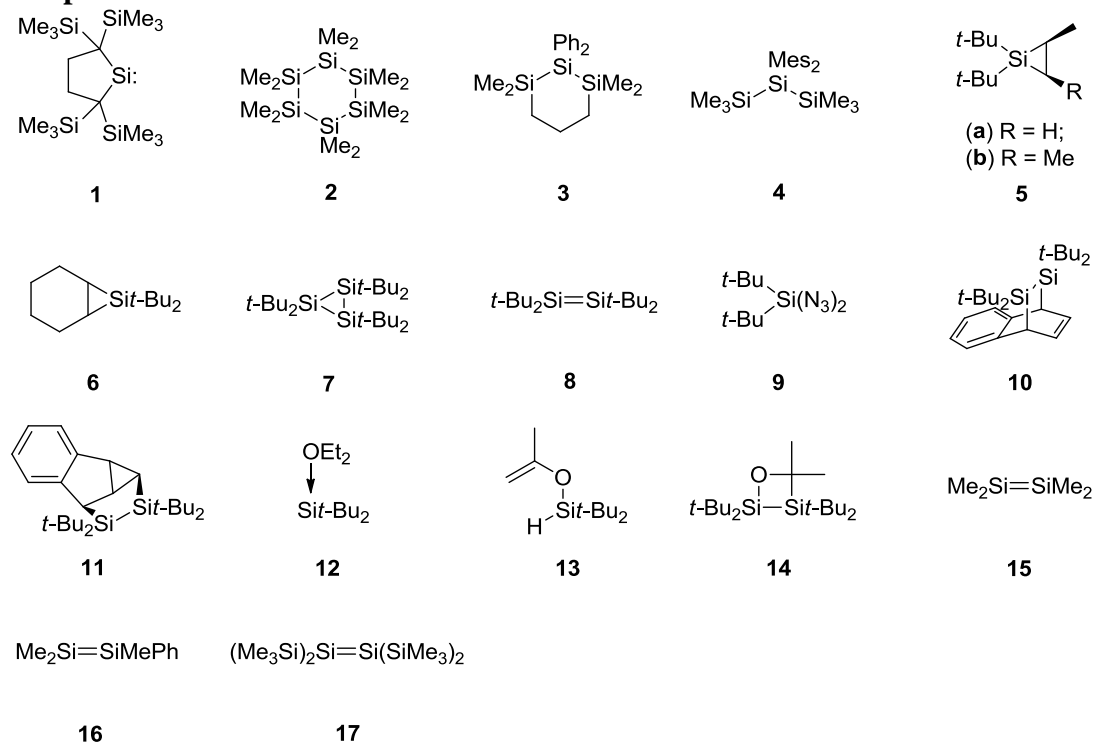
### Chapter 4



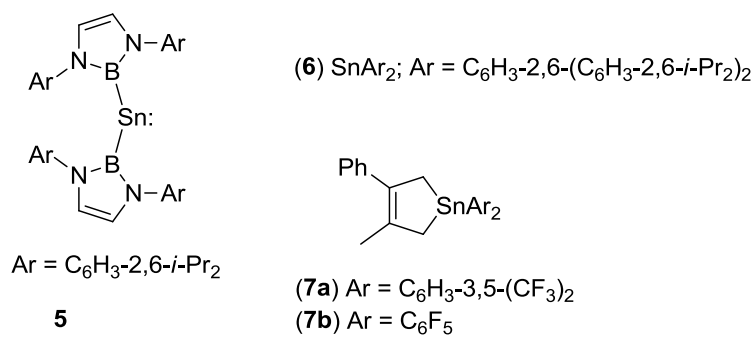
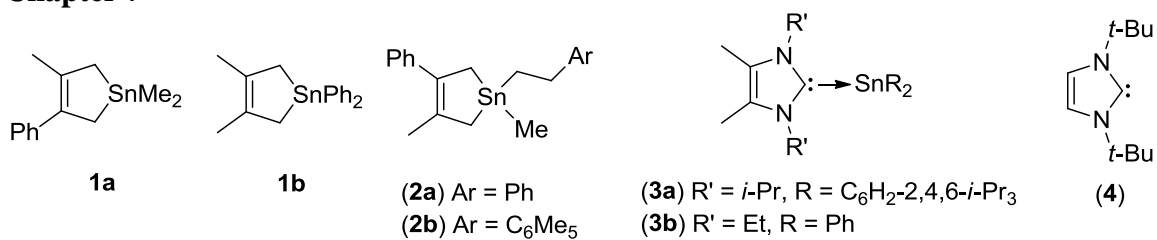
## Chapter 5



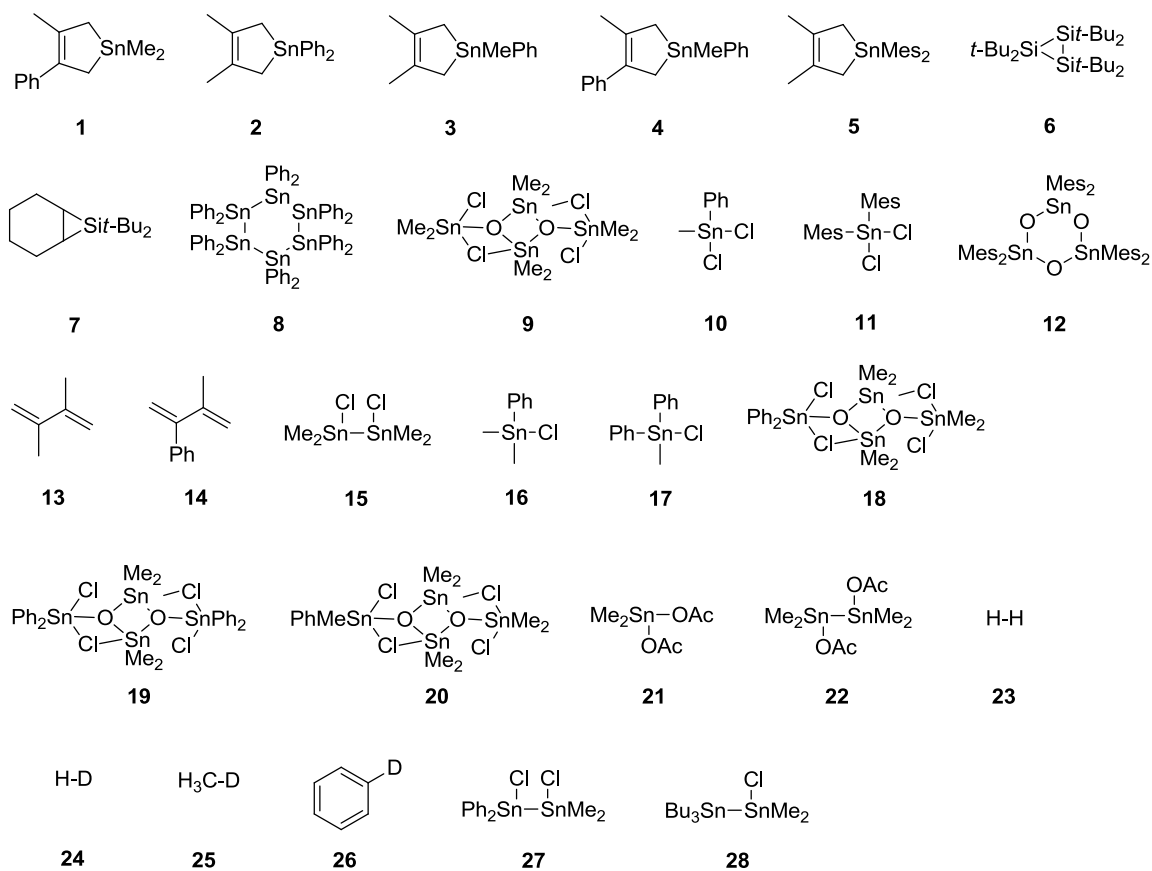
## Chapter 6



### Chapter 7



### Chapter 8



## Chapter 1 - Introduction

### 1.1. Foreword

There has been a growing interest in the twenty-first century in understanding the chemistry of carbon-substituted divalent Sn(II) compounds (stannylenes); this is currently an active research topic in the ongoing studies of organotin chemistry.<sup>1-3</sup> Stannylenes, the tin homologs of carbenes, are an important class of compounds within the larger group collectively known as the organometallic compounds of low coordinate Si, Ge, Sn, and Pb.<sup>4-8</sup> These include the heavier analogues of carbenium ions, organic free radicals, carbanions, carbenes, multiply bonded derivatives (alkenes, 1,3-dienes, allenes and alkynes), and aromatic compounds.<sup>7,9,10</sup> The recent interest in stannylenes has been motivated in part by the potential application of such compounds in catalysis<sup>11</sup> and small molecule activation: stannylenes are one of relatively few p-block element compounds that react readily with H<sub>2</sub>, NH<sub>3</sub>, PH<sub>3</sub>, CS<sub>2</sub> and other small molecules of fundamental importance.<sup>12-16</sup> The attention afforded to stannylenes is part of a larger renaissance in the chemistry of the heavier p-block elements, particularly in light of the growing understanding of parallels between the chemistry of the main group compounds and those of transition metal elements.<sup>17-19</sup>

Despite the great strides already achieved in understanding the fundamental characteristics of these compounds and maximizing their utility, very little is known still of the simplest transient derivatives: SnMe<sub>2</sub>, SnPh<sub>2</sub>, SnMePh and SnMes<sub>2</sub> (Mes = C<sub>6</sub>H<sub>2</sub>-2,4,6-Me<sub>3</sub>).<sup>20-22</sup> In 1991, the early chemistry of transient stannylenes was reviewed by W. P. Neumann, who stated "simple stannylenes like Me<sub>2</sub>Sn, Bu<sub>2</sub>Sn, and Ph<sub>2</sub>Sn polymerize very rapidly,  $k = 10^8 \text{ M}^{-1} \text{ s}^{-1}$  ... the presently restricted number of insertions of Me<sub>2</sub>Sn, Ph<sub>2</sub>Sn, etc. certainly is handicapped by the rapid polymerization of these stannylenes."<sup>20</sup>

Indeed, efforts to study the chemistry of simple stannylenes in the condensed phase are made difficult by their transient nature; direct detection of these compounds under ambient conditions requires specialized time-resolved spectroscopic equipment.<sup>23</sup>

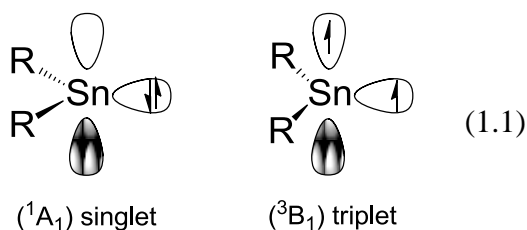
The main focus of this thesis is to detect the simplest  $\sigma$ -bonded alkyl and/or aryl substituted stannylenes in hydrocarbon solution by means of transient UV-visible spectroscopy, and then to characterize their bimolecular reactions in solution with a selection of substrates. This is achieved through a combination of chemical trapping and laser flash photolysis studies, utilizing photoprecursors that generate the respective stannylene of interest using 248 or 254 nm UV irradiation. Useful inferences can then be made by comparing the kinetic and thermodynamic aspects of their reactions with those of silylenes and germylenes, and identifying trends amongst the group 14 carbene homologs.

## 1.2. Nomenclature

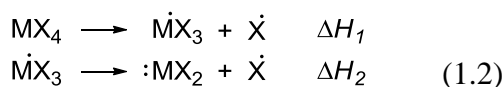
Compounds that possess the element Si, Ge, Sn, and Pb use the prefixes sil-, germ-, stann-, and plumb-, respectively. The suffixes -ylene, -ane, -ene and -yne refer to the divalent species and the formally singly, doubly and triply bonded compounds, respectively. The prefixes di- and tri- are used to denote compounds with two or three of the elements. For example, the doubly bonded dimer of tin is referred to as a di-stann-ene, while the triply bonded derivative is named di-stann-yne. Thus, the term stannylene typically refers to divalent tin(II) compounds. While some publications still use the term stannanediyl, this is less common.<sup>24,25</sup> Similarly, divalent Si(II), Ge(II), Sn(II) and Pb(II) compounds are referred to as silylenes, germylenes, stannylenes, and plumbylenes respectively; they are collectively referred to as tetrylenes, metallylenes, or heavy carbenes.

## 1.3. Structure and Properties of Stannylenes

Monomeric stannylenes  $\text{SnR}_2$  adopt a bent geometry. The central tetrel element may, in theory, adopt a singlet ( $^1\text{A}_1$ ) or triplet ( $^3\text{B}_1$ ) electron configuration depending on the substitution, as is also the case with carbenes (eq. 1.1).<sup>26,27</sup> Theoretical calculations indicate that stannylenes tend to adopt a ground-state singlet multiplicity and the singlet/triplet states are often separated by a large energy difference:  $\Delta E_{\text{ST}} = 29 \text{ kcal mol}^{-1}$  for  $\text{SnMe}_2$ <sup>28</sup> and  $26 \text{ kcal mol}^{-1}$  for  $\text{SnH}_2$ .<sup>29</sup> Experimentally, stannylenes exhibit reactivity consistent with a singlet ground state: the central Sn element possesses both an open coordination site and valence electron pair, and can (in principle) behave as both an electrophile and as a nucleophile. The triplet state would be expected to exhibit reactivity consistent with a biradical. The global electrophilicities and nucleophilicities of  $\text{SnH}_2$  and  $\text{SnMe}_2$  were calculated by De Proft and coworkers;<sup>30</sup> their results support the conclusion that stannylenes exhibit primarily electrophilic character, while the non-bonding electron pair maintains an orbital of high s-character and generally plays a lesser role in its reactions.



Stabilization of the +2 oxidation state of the group 14 elements can be quantified by its divalent state stabilization energy (DSSE), defined as the difference in enthalpies for the homolytic M-X (M = C, Si, Ge, Sn) bond cleavage reactions shown in eq. 1.2.<sup>31</sup>



$$\text{DSSE} = \Delta H_1 - \Delta H_2$$

Allendorf and Melius calculated the DSSE for  $\text{SnH}_2$  and  $\text{SnMe}_2$ , obtaining values of 26.7 and 30.7  $\text{kcal mol}^{-1}$  respectively.<sup>32</sup> This, compared to the values 21.8 and 29.2 kcal

$\text{mol}^{-1}$  calculated for  $\text{SiH}_2$  and  $\text{SiMe}_2$ ,<sup>33</sup> suggests the stability of the divalent state is similar amongst the heavier group 14 elements.

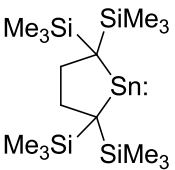
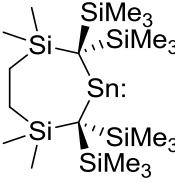
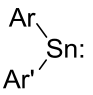
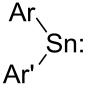
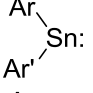
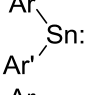
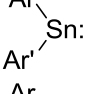
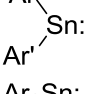
#### 1.4.1. Stable Stannylenes - An Overview

The term "stable stannylene" generally refers to 2-coordinate  $\sigma$ -bonded alkyl, aryl or alkylaryl substituted Sn(II) derivatives that persist in solution, the solid state or both at room temperature in an air-and-moisture free environment. The isolation of such compounds has been achieved by utilizing sterically demanding alkyl<sup>34-41</sup> or aryl<sup>12-14,25,42-51</sup> substituents that protect the molecule from dimerization, without greatly altering the intrinsic electrophilic character of the Sn(II) centre. More recently stannylenes substituted with silyl,<sup>52</sup> germyl,<sup>53</sup> stannyl,<sup>54</sup> and boryl<sup>55</sup> substituents have been prepared and found to exhibit similar chemistry as the  $\sigma$ -bonded carbon substituted derivatives. Stannylenes that are  $\sigma$ -bonded to a group 15 or 16 element are discussed separately (see 1.4.5).

#### 1.4.2. Structural Properties of Stannylenes

The first kinetically stabilized  $\sigma$ -bonded carbon substituted stannylene ( $\text{Sn}(\text{CH}(\text{SiMe}_3)_2)_2$ , **1**) was reported by Lappert and coworkers.<sup>34</sup> The first dialkylstannylene to be monomeric in both solution and in the solid state, 2,2,5,5-tetrakis(trimethylsilyl)-1-stannacyclopentane-1,1-diyl (**2**), was later reported by Kira and coworkers.<sup>39</sup> Development of the Ge and Pb homologues of **1**<sup>36</sup> and the Si and Ge homologues of **2**<sup>41</sup> allowed for the determination of systematic trends in structural characteristics, spectral properties, and reactivities with changes in the central group 14 element for systems bearing the same substitution pattern. A number of isolable diarylstannylenes have also since been characterized in solution and/or the solid state.<sup>25,42,44,46-49,56,57</sup> The kinetic stabilization is imparted primarily by *ortho*-substitution on the aryl ring. Diagnostic spectral properties and structural features of some stable stannylenes that have been reported are summarized in Table 1.1.

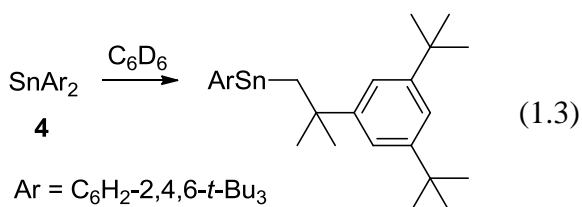
**Table 1.1.** Diagnostic Spectral Properties and Spectral Features of Persistent Stannylenes.

$R_2Sn$	Compound Number (#)	ref.	$\lambda_{max}$ (nm)	$\delta_{Sn}$ (ppm)	C-Sn-C bond angle ( $^\circ$ )
$R_2Sn$ : R = CH(SiMe <sub>3</sub> ) <sub>2</sub>	<b>1</b>	34,58	495	2328	97 <sup>a</sup>
	<b>2</b>	39	486	2323	86.16(9)
	<b>3</b>	59	546	2299	117.6(1)
$Ar_2Sn$ : Ar = C <sub>6</sub> H <sub>2</sub> -2,4,6- <i>t</i> -Bu <sub>3</sub>	<b>4</b>	25	476	980	103.6(1)
$Ar_2Sn$ : Ar = C <sub>6</sub> H-2- <i>t</i> -Bu-4,5,6-Me <sub>3</sub>	<b>5</b>	56	479	1331	<sup>b</sup>
$Ar_2Sn$ : Ar = C <sub>6</sub> H <sub>3</sub> -2,6-(C <sub>6</sub> H <sub>3</sub> -2,6- <i>i</i> -Pr <sub>2</sub> ) <sub>2</sub>	<b>6</b>	48	600	2235	117.6
$Ar_2Sn$ : Ar = C <sub>6</sub> H <sub>3</sub> -2,6-(C <sub>6</sub> H <sub>2</sub> -2,4,6-Me <sub>3</sub> ) <sub>2</sub>	<b>7a</b>	46	553	1971	114.7(2)
$Ar_2Sn$ : Ar = C <sub>6</sub> H <sub>2</sub> -2,6-(C <sub>6</sub> H <sub>2</sub> -2,4,6-Me <sub>3</sub> ) <sub>2</sub> -4-SiMe <sub>3</sub>	<b>7b</b>	57	555	1975	115.37(2)
$Ar_2Sn$ : Ar = C <sub>6</sub> H <sub>2</sub> -2,6-(C <sub>6</sub> H <sub>2</sub> -2,4,6-Me <sub>3</sub> ) <sub>2</sub> -4-Cl	<b>7c</b>	57	544	1891	115.12(8)
$Ar_2Sn$ : Ar = C <sub>6</sub> H-2,6-(C <sub>6</sub> H <sub>2</sub> -2,4,6-Me <sub>3</sub> ) <sub>2</sub> -3,5- <i>i</i> -Pr <sub>2</sub>	<b>7d</b>	57	591	2081	123.4(2)
 Ar = C <sub>6</sub> H <sub>3</sub> -2,6-(C <sub>6</sub> H <sub>2</sub> -2,4,6- <i>i</i> -Pr <sub>3</sub> ) <sub>2</sub> Ar' = Ph	<b>8</b>	47	462	1518	96.87(10)
 Ar = C <sub>6</sub> H <sub>2</sub> -2,4,6-(CH(SiMe <sub>3</sub> ) <sub>2</sub> ) <sub>3</sub> Ar' = C <sub>6</sub> H <sub>2</sub> -2,4,6- <i>i</i> -Pr <sub>3</sub>	<b>9a</b>	42	561	2208	<sup>b</sup>
 Ar = C <sub>6</sub> H <sub>2</sub> -2,4,6-(CH(SiMe <sub>3</sub> ) <sub>2</sub> ) <sub>3</sub> Ar' = C <sub>6</sub> H <sub>2</sub> -2,4,6-Me <sub>3</sub>	<b>9b</b>	44	527	<sup>c</sup>	<sup>c</sup>
 Ar = C <sub>6</sub> H <sub>2</sub> -2,4,6-(CH(SiMe <sub>3</sub> ) <sub>2</sub> ) <sub>3</sub> Ar' = C <sub>6</sub> H <sub>2</sub> -2,4,6-(1-ethylpropyl) <sub>3</sub>	<b>9c</b>	44	563	<sup>c</sup>	<sup>c</sup>
 Ar = C <sub>6</sub> H <sub>2</sub> -2,4,6-(CH(SiMe <sub>3</sub> ) <sub>2</sub> ) <sub>3</sub> Ar' = C <sub>6</sub> H <sub>2</sub> -2,4,6-(cyclohexyl) <sub>3</sub>	<b>9d</b>	44	586	<sup>c</sup>	<sup>c</sup>
 Ar = C <sub>6</sub> H <sub>2</sub> -2,6-(CH(SiMe <sub>3</sub> ) <sub>2</sub> ) <sub>3</sub> -4-C(SiMe <sub>3</sub> ) <sub>3</sub> Ar' = C <sub>6</sub> H <sub>3</sub> -2,6-(C <sub>6</sub> H <sub>3</sub> -2,4- <i>i</i> -Pr <sub>2</sub> ) <sub>2</sub>	<b>10</b>	49	547	1657	106.4(2)
$Ar_2Sn$ : Ar = C <sub>6</sub> H <sub>2</sub> -2,4,6-(CF <sub>3</sub> ) <sub>3</sub>	<b>11</b>	60	345	723	98.2

<sup>a</sup>Determined by gas phase electron diffraction; <sup>b</sup>Crystallizes as a dimer; <sup>c</sup>not reported



Divalent tin compounds that are monomeric in solution are often coloured and exhibit values of  $\lambda_{\max} \sim 460 - 600$  nm, significantly deshielded  $^{119}\text{Sn}$  NMR resonances between 1000 - 2300 ppm, and a C-Sn-C bond angle between  $86.16(9)^\circ$  and  $123.4(2)^\circ$ . Additional coordination to the tin centre by inter- or intramolecular electron donors normally results in both a hypsochromic shift of the lowest energy UV-vis absorption band and an upfield chemical shift of the Sn(II) resonances in the  $^{119}\text{Sn}$  NMR spectrum; such is the case in **11** ( $\lambda_{\max} = 345$  nm;  $\delta_{\text{Sn}} = 723$  ppm), which exhibits long range intramolecular Sn-F contacts in the solid state.<sup>60</sup> A red-shift in  $\lambda_{\max}$  is generally associated with a widening of the C-Sn-C bond angle.<sup>44,57</sup> Such a correlation is most evident when comparing stannylenes with differing degrees of steric bulk, for instance between **7a** ( $\lambda_{\max} = 553$  nm;  $\angle_{\text{C-Sn-C}} = 114.7(2)^\circ$ ) and **7d** ( $\lambda_{\max} = 591$  nm;  $\angle_{\text{C-Sn-C}} = 123.4(2)^\circ$ ).<sup>57</sup> Compounds **1-11** persist in solution at room temperature under an inert atmosphere with the exception of **4**, which rearranges to a sterically less encumbered alkylarylstannylene in solution (eq. 1.3).<sup>25,61</sup>

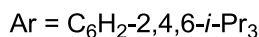
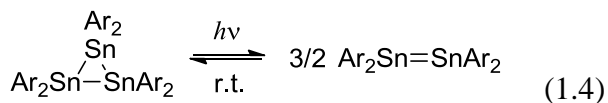


### 1.4.3. Reactions of Stannylenes

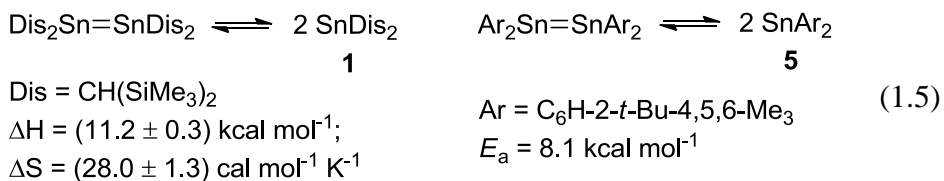
Stannylenes have been found to undergo a wide range of reactions, which in general are analogous to those of their silicon and germanium homologues. These reactions are categorized into the following sections: (a) dimerization, (b) coordination, (c) cycloaddition, (d) insertion, and (e) substitution. Finally, section (f) discusses applications of stannylene reactions, in particular the preparation of low-coordinate compounds of tin.

**(a) Dimerization**

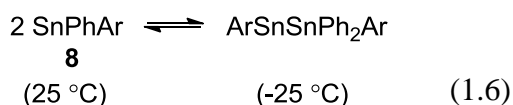
Without sufficient kinetic stabilization, alkyl and aryl substituted stannylenes predominantly form self-association dimers ( $\text{Sn}_2\text{R}_4$ ) or higher cyclic oligomers ( $\text{SnR}_2$ )<sub>n</sub>. Variation in the size and nature of the substituent R is responsible for different solution phase behaviour. Examples are known of stannylene-distannene equilibrium (eq. 1.5),<sup>62,63</sup> distannene-cyclotristannane interconversion (eq. 1.4),<sup>64,65</sup> solid-state dimers that rapidly dissociate in solution,<sup>56,66</sup> and cyclic oligostannanes that exhibit reactivity characteristic of stannylene monomers.<sup>65,67,68</sup>



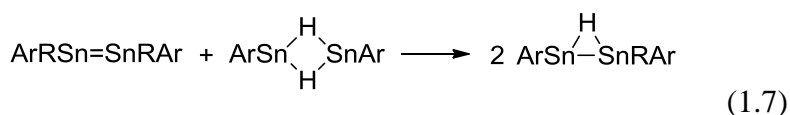
Further examination of **1** has found it to crystallize as the corresponding doubly bonded distannene, exist as a monomer in the gas phase,<sup>58</sup> and exhibit dimer $\rightleftharpoons$ monomer equilibrium in solution.<sup>62</sup> Thermodynamic parameters for the equilibrium in solution ( $\Delta H = 11.2 \pm 0.3 \text{ kcal mol}^{-1}$  and  $\Delta S = 28.0 \pm 1.3 \text{ cal mol}^{-1} \text{ K}^{-1}$ ) have been measured from the temperature dependence of the NMR chemical shifts (eq. 1.5). A recent theoretical study of the dimerization of **1** suggests electrostatic and dispersion interactions impart significant stabilization to the dimeric species relative to the monomer.<sup>69</sup> A similar monomer-dimer equilibrium exists for **5** in toluene-*d*<sub>8</sub>, for which an Arrhenius activation energy of ca.  $8.1 \text{ kcal mol}^{-1}$  for the dissociation of the distannene was measured (eq. 1.5).<sup>63</sup>



Stannylene dimers ( $\text{Sn}_2\text{R}_4$ ) can exhibit great structural diversity, especially if stannylenes incorporating hydride groups are considered. A stannylene possessing one phenyl substituent resulted in valence equilibrium with a stannylstannylene (eq. 1.6).<sup>47</sup>



Ar =  $\text{C}_6\text{H}_3\text{-2,6-(C}_6\text{H}_2\text{-2,4,6-}i\text{-Pr}_3)_2$   
Hydrido stannylenes typically exist as doubly bridged dimers,<sup>70,71</sup> while a mono-hydrido bridged isomer is generated from the 1:1 treatment of two different stannylene dimers, one of which is a Sn(II) hydride (eq. 1.7).<sup>72</sup>



R =  $\text{CH}_2\text{CH}_2t\text{-Bu}$

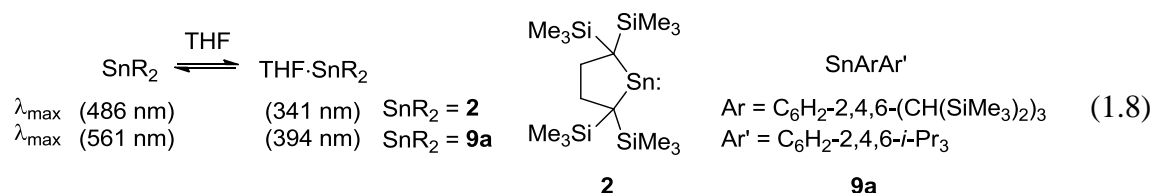
Ar =  $\text{C}_6\text{H}_3\text{-2,6-(C}_6\text{H}_3\text{-2,6-}i\text{-Pr}_2)_2$

The foregoing examples illustrate four different isomers of the dimeric structure  $\text{Sn}_2\text{R}_4$  that have been isolated; the specific form generated depends on the nature of the substituent pattern. This is anticipated given the shallow potential energy surface of the parent dimer  $\text{Sn}_2\text{H}_4$  and its various isomeric forms (see eq. 1.39), which were predicted to be separated by only  $10 \text{ kcal mol}^{-1}$ .<sup>73,74</sup> When substituent groups are large or their migratory aptitudes low, it is distannene that is typically isolated. Formation of organic substituted silylene and germylene dimers, by contrast, invariably adopt the doubly bonded disilene and digermene forms, respectively.<sup>75</sup>

### (b) Coordination

As with their lighter Group 14 homologs, the reactivity of stannylenes is governed by the intrinsic dual functionality associated with the divalent tin centre. In principle, it possesses the ability to exhibit reactivity as both a Lewis base as well as a Lewis acid.

Reversible solvent complexation of **2** is observed in THF (eq. 1.8).<sup>76</sup> The Lewis acid-base complex **2**·THF is observed as a UV absorption band at  $\lambda_{\max} = 341$  nm. The thermodynamic parameters ( $\Delta H = -7.0$  kcal mol<sup>-1</sup> and  $\Delta S = -48$  cal mol<sup>-1</sup> K<sup>-1</sup>) indicate reversible complexation is favored enthalpically but hindered entropically. Similar reactivity was not observed with the silylene and germylene homologs. This was proposed to be due to a decrease in steric crowding about the reactive Sn(II) site in **2**. Similarly, a 1:6 hexanes:THF solution of **9a** at -40 °C also exhibits a new absorption at  $\lambda_{\max} = 394$  nm, assigned to adduct **9a**·THF.<sup>43</sup> Both stannylenes **2** and **9a** exhibit a hypsochromic shift upon complexation with THF (eq. 1.8). This effect has been ascribed to the population of the stannylene's vacant p-orbital upon complexation, resulting in an increased HOMO-LUMO transition energy.<sup>43</sup>

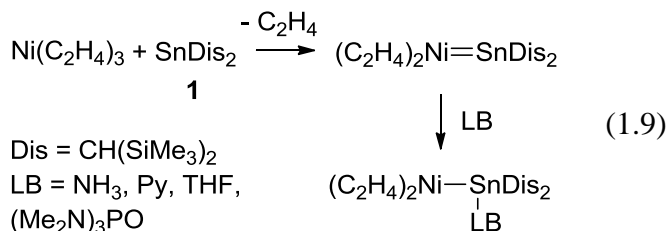


The complexes of halo and amino substituted stannylenes have also been characterized and representative examples are discussed briefly. The vibrational spectra and solid state structures of SnCl<sub>2</sub> with 1,4-dioxane and PPh<sub>3</sub> have been characterized.<sup>77</sup> Complexes with 1,4-dioxane are polymeric while with PPh<sub>3</sub> the 1:1 adduct is monomeric. The Sn(II) oxidation state is retained in both cases. <sup>119</sup>Sn NMR spectra of Lappert's amino stannylene (eq. 1.23) were recorded in cyclohexane-*d*<sub>12</sub>, benzene-*d*<sub>6</sub>, toluene-*d*<sub>8</sub>, THF-*d*<sub>8</sub> and pyridine-*d*<sub>5</sub> solutions. The differences in chemical shift were interpreted as being a measure for the interaction strength between the N-, O-, or arene- donor and the central Sn(II) element.<sup>78</sup>

The coordination of stannylenes to a transition metal element has been well studied, and (with germylenes and plumbylenes) has been the subject of a recent review.<sup>79</sup> Many

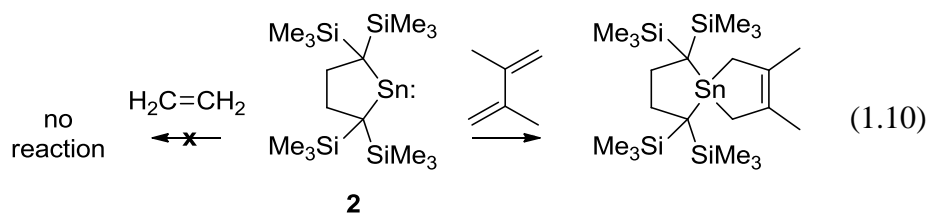
examples have been prepared from the direct treatment of a stannylene with a transition metal compound, with **1** being a commonly employed derivative. The Sn(II) centre in the resulting compounds may also undergo further adduct formation with Lewis bases.

Treatment of **1** ( $\text{SnDis}_2$ ; Dis =  $\text{CH}(\text{SiMe}_3)_2$ ) with metal carbonyls  $\text{M}(\text{CO})_6$  ( $\text{M} = \text{Cr}, \text{Mo}$ ) under UV irradiation furnish a mixture of the 1:1 and 2:1 complexes  $\text{M}(\text{CO})_5(\text{SnDis}_2)$  and *trans*- $[\text{M}(\text{CO})_4(\text{SnDis}_2)_2]$  respectively.<sup>35</sup> More recently, treatment of **1** with  $\text{Ni}(\text{C}_2\text{H}_4)_3$  has been observed to afford the 1:1 adduct  $\text{Ni}(\text{C}_2\text{H}_4)_2(\text{SnDis}_2)$ , which can undergo further coordination with Lewis bases such as THF,  $\text{NH}_3$ , pyridine and  $(\text{Me}_2\text{N})_3\text{PO}$  (eq. 1.9).<sup>80</sup>



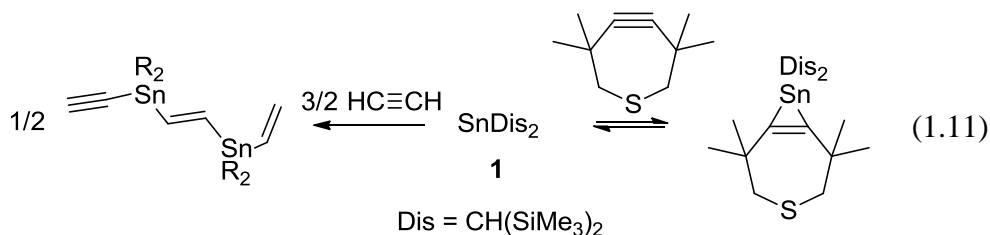
### (c) Cycloaddition

A number of stannylenes undergo [1+4]-chelotropic cycloaddition with 1,3-butadiene derivatives, forming 1-stannacyclopent-3-enes (eq. 1.10).<sup>41,43,44,53,65</sup> The [1+4] cycloaddition of **1** has also been demonstrated for bis(allenes), 1,2-diketones, and  $\alpha,\beta$ -unsaturated carbonyl compounds.<sup>38,81</sup>



The (1+2) addition of a cycloheptyne derivative to **1** (eq. 1.11) and a cyclotristannane *cyclo*- $(\text{SnTip})_3$  (a source of  $\text{SnTip}_2$ ; Tip =  $\text{C}_6\text{H}_2$ -2,4,6-*i*-Pr<sub>3</sub>) proceeds reversibly to furnish a stannirene.<sup>82,83</sup> The reaction of **1** with a slightly less sterically protected cyclooctyne affords a 1,2-distannacyclobut-3-ene.<sup>84</sup> Reaction of acetylene and **1**

proceeds slowly at room temperature to yield a mixture of products, the highest yielding product contains three equivalents of acetylene and two equivalents of **1**.<sup>85</sup>

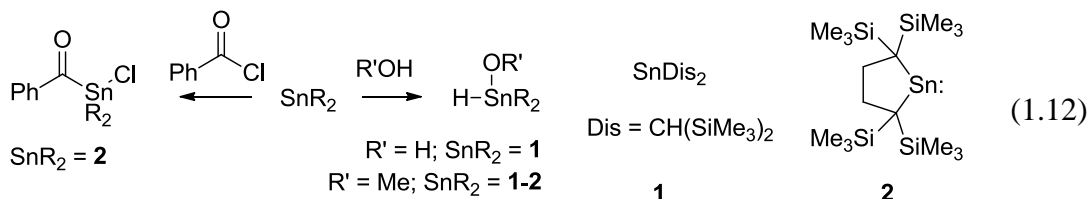


No reaction is observed between ethylene and **2** at room temperature<sup>41</sup> (eq. 1.10).

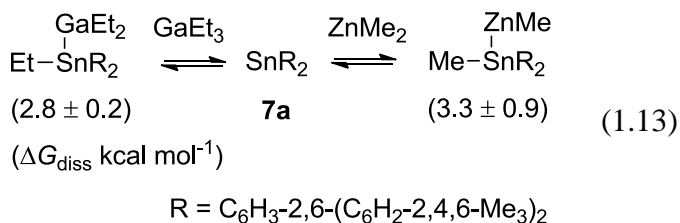
As yet, no examples are known of stanniranes, formally the [1+2] cycloaddition product of the C=C bond and stannylene. The lack of products containing the stannirane moiety is consistent with the larger trend of decreasing thermodynamic stability of the three membered ring compounds (i.e. *cyclo*-[C-C-M-]; M = C > Si > Ge > Sn > Pb) with increasing atomic number of the group 14 element, which was predicted theoretically for ethylene and MR<sub>2</sub> (M = C-Pb; R = H, Me).<sup>28,86</sup>

**(d) Insertion** (oxidative addition)

$\sigma$ -Bond insertion reactions of stannylenes are promoted by the formation of two bonds at the expense of one.<sup>31</sup> This process is also referred to as oxidative addition as the corresponding Sn(IV) compounds are generated.<sup>55</sup> Insertion of **1** (SnDis<sub>2</sub>; Dis = CH(SiMe<sub>3</sub>)<sub>2</sub>) into the R-X (X = halogen) bond of halogenated reagents such as HCl, MeI and Br<sub>2</sub> generate compounds of the type R-(SnDis<sub>2</sub>)-X.<sup>35</sup> Treatment of **3** with MeI also results in the formation of the C-I insertion product.<sup>59</sup> Both methanol and water in THF solution undergo O-H bond insertion reactions with **1** to form the methoxy- and hydroxystannane, respectively.<sup>37</sup> Similarly, the O-H insertion of MeOH with **2** has also been reported (eq. 1.12).<sup>41</sup> Stannylene **2** reportedly undergoes C-Cl insertion with acyl chlorides (eq. 1.12).<sup>87</sup>

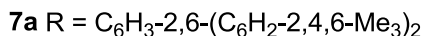
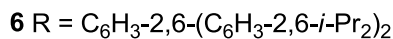
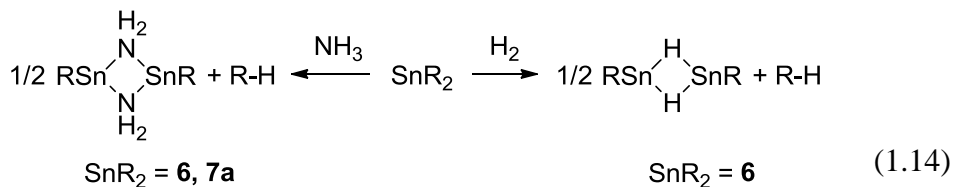


Reactions of **7a** with the organometallic compounds  $\text{ZnMe}_2$  and  $\text{GaMe}_3$  generate M-C (M = Zn, Ga) insertion products. Both reactions are reversible in hydrocarbon solvent at room temperature, and are characterized by  $\Delta G_{\text{diss}} = 3.3 \pm 0.9 \text{ kcal mol}^{-1}$  ( $\text{C}_6\text{D}_6$  at 298 K) and  $2.8 \pm 0.2 \text{ kcal mol}^{-1}$  (for  $\text{GaEt}_3$ , toluene- $d_8$  at 299 K) for the dissociation of the respective insertion products (eq. 1.13).<sup>88,89</sup>



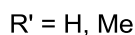
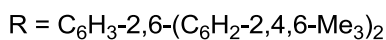
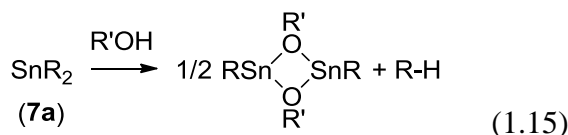
**(e) Substitution (elimination)**

Some stannylene reactions result in cleavage of one or both of the organic ligands without any formal change to the oxidation state of the Sn(II) centre. This has been observed when the co-reactant is a source of hydrogen, for instance in compounds such as  $\text{H}_2$ ,  $\text{NH}_3$ ,<sup>12</sup>  $\text{MeOH}$ ,<sup>16</sup> and *p*-toluenethiol.<sup>90</sup> The substitution is most commonly observed in aryl substituted stannylenes and has thus been referred to in the literature as arene elimination. For example, **6** undergoes reaction with  $\text{H}_2$  and  $\text{NH}_3$  to yield the arene R-H along with doubly bridged dimers of the stannylenes  $\text{SnRH}$  and  $\text{SnR}(\text{NH}_2)$  (eq. 1.14). The less sterically crowded stannylene **7a** was recovered unreacted in a  $\text{H}_2$  atmosphere.<sup>12,13</sup>

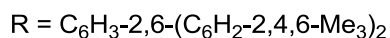
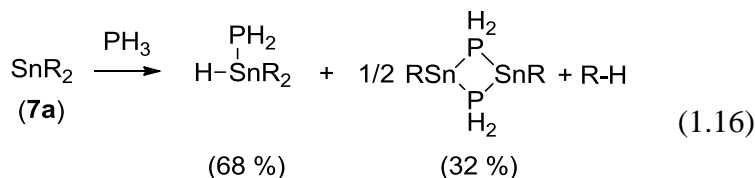


The reaction of **7a** with one equivalent of methanol or water in diethyl ether

solution also proceeds via arene elimination (eq. 1.15).<sup>16</sup>



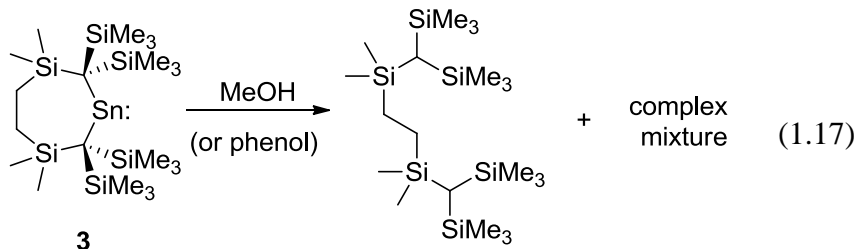
As the above examples illustrate, the reactions of **1** and **7a** with ROH (R = H, Me) proceed by either oxidative addition or arene elimination, depending on the nature of the substitution on the stannylene. In other instances, both  $\sigma$ -bond insertion and arene elimination were observed as competitive pathways. For example, the reaction of **7a** and PH<sub>3</sub> in toluene solution affords both oxidative addition and arene elimination products in relative yields of 68 % and 32 %, respectively (eq. 1.16).<sup>14</sup>



The cleavage of both organic groups has been observed with **11** (SnR<sub>2</sub>; R = C<sub>6</sub>H<sub>2</sub>-2,4,6-(CF<sub>3</sub>)<sub>3</sub>), which reacts with two equivalents of *t*-BuOH to yield (*t*-BuO)<sub>2</sub>Sn and 1,3,5-tris(trifluoromethyl)benzene.<sup>91</sup> Stannylene SnAr<sub>2</sub> (Ar = C<sub>6</sub>H<sub>3</sub>-2,6-(CF<sub>3</sub>)<sub>2</sub>; characterized only by Mössbauer spectroscopy) on the other hand, undergoes consecutive ring cleavage with two equivalents *p*-toluenethiol.<sup>90</sup>



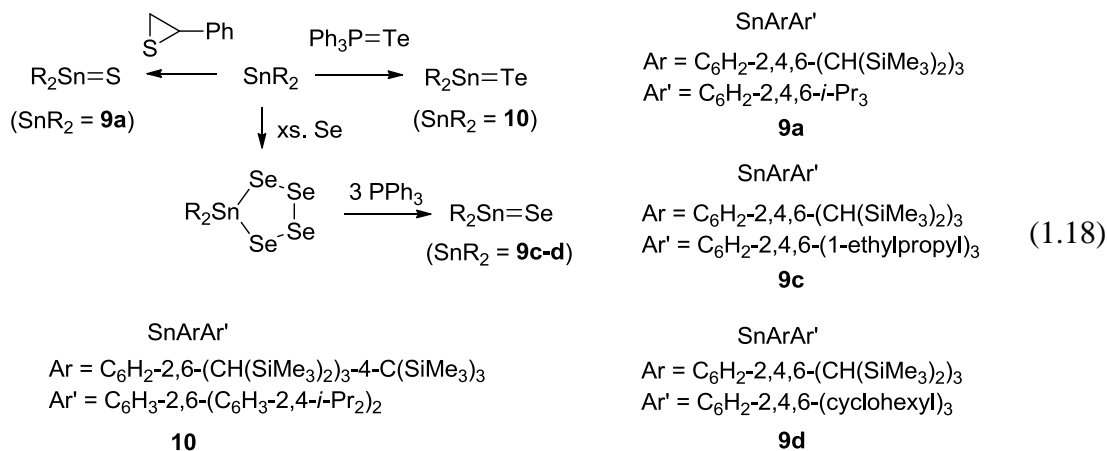
The cleavage of an alkyl group with dialkylstannylenes has not been established unequivocally, although the addition of water, methanol and phenol to **3** was reported to lead to the ring opening of the cyclic stannylene and not O-H insertion. With the alcohols, the protonated ligand was identified within a complicated reaction mixture (eq. 1.17).<sup>92</sup>



Theoretical calculations suggest the reaction between **1** ( $\text{SnDis}_2$ ;  $\text{Dis} = \text{CH}(\text{SiMe}_3)_2$ ) and  $\text{H}_2\text{O}$  favour the elimination of  $\text{H}_2\text{C}(\text{SiMe}_3)_2$ ,<sup>16</sup> yet treatment of **1** with  $\text{H}_2\text{O}$  in THF yields the hydroxystannane, and none of the alkane is formed (eq. 1.12).<sup>37</sup> The authors speculate that the use of an excess (14 equivalents) of  $\text{H}_2\text{O}$  at molar concentrations in the experimental study appears to promote oxidative addition.<sup>16</sup>

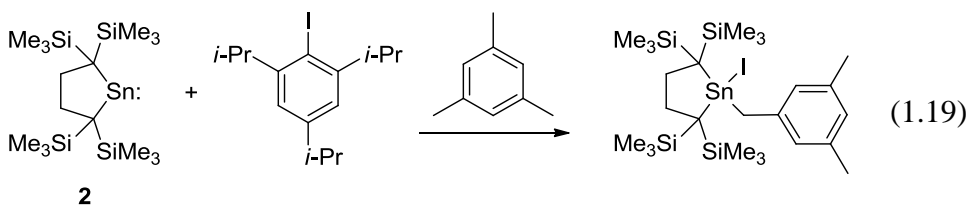
### (f) Applications of Stannylene Chemistry

Stannylenes can be particularly useful as reagents for the synthesis of other low coordinate compounds of tin that would otherwise be very difficult to prepare. The most ubiquitous example is the preparation of distannenes as previously discussed in 1.4.3(a). Stannylenes **9a** and **10** are also reactive towards chalcogen abstraction to form tin-chalcogen multiply bonded compounds  $\text{R}_2\text{Sn}=\text{X}$  ( $\text{X} = \text{S}$  and  $\text{Te}$ ).<sup>42,49</sup> Stannaselenones ( $\text{R}_2\text{Sn}=\text{Se}$ ) can be prepared in two steps starting from stannylenes **9c-d** (eq. 1.18).<sup>45</sup>

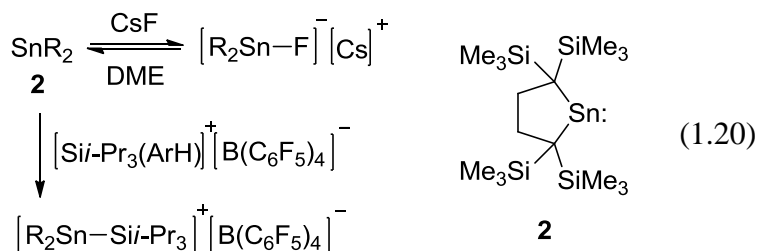


Stannaethene, or stannene (a compound containing a Sn=C double bond)

derivatives, were prepared from the treatment of **1** or **5** ( $\text{SnR}_2$ ;  $\text{R} = \text{C}_6\text{H-2-}t\text{-Bu-4,5,6-Me}_3$ ) with an electrophilic cryptodiborylcarbene ( $(\text{Me}_3\text{Si})_2\text{C(B}t\text{-Bu)}_2\text{C:}$ ) by the groups of Berndt<sup>93</sup> and Weidenbruch,<sup>94</sup> respectively. The selective C-H activation of both saturated and unsaturated hydrocarbons was observed using a mixture of **2** and an aryl halide (eq. 1.19).<sup>95-97</sup> A radical intermediate between **2** and the aryl halide has been proposed to abstract the homolytically weakest hydrogen from the hydrocarbon.<sup>96</sup>



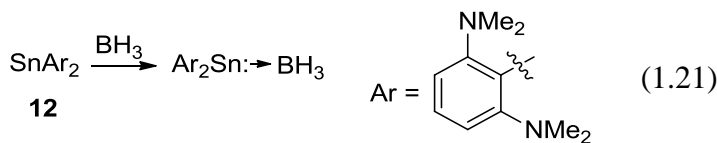
Stannylium ions can be prepared from the treatment of **2** (or **5**<sup>67</sup>) with silylarenium ions  $[\text{R}_3\text{Si(ArH)}]^+[\text{B(C}_6\text{F}_5)_4]^-$  ( $\text{Ar} = \text{Ph}, \text{C}_6\text{H}_4\text{-4-Me}$ ) (eq. 1.20).<sup>98</sup> A fluorostannyl anion is generated reversibly from the treatment of **2** with CsF in THF or DME solution (eq. 1.20). In hydrocarbon solvent the starting reagents are regenerated.<sup>99</sup>



Halogen or hydride substituted stannylenes possess another reactive site that can undergo further functionalization. Only a few representative examples are given here of their potential utility. Reduction of chlorostannylene ( $\text{SnArCl}$ ;  $\text{Ar} = \text{C}_6\text{H}_3\text{-}2,6\text{-}(\text{C}_6\text{H}_3\text{-}2,6\text{-}i\text{-Pr}_2)_2$ ) by a stoichiometric amount of potassium in benzene at room temperature affords the distannyne  $\text{ArSn}\equiv\text{SnAr}$ , a tin analogue of an alkyne.<sup>100</sup> Thermolysis of Sn(II) hydrides also provides a new route for the preparation of tin-clusters.<sup>70,101,102</sup>

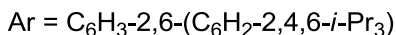
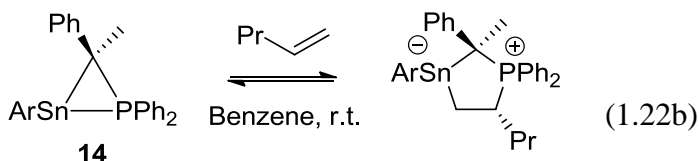
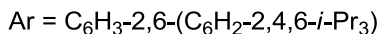
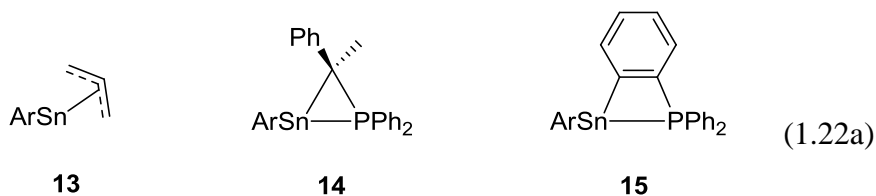
#### 1.4.4. Intramolecular and Intermolecular Donor-stabilized Stannylenes

Another common method used for the stabilization of monomeric diorganostannylenes utilizes electronic stabilization of the vacant 5p orbital by intramolecular or intermolecular electron donors.<sup>103-105</sup> Such an approach serves to reduce electrophilicity and enhance nucleophilicity at the central element and is another technique by which modulation of the electronic properties of the Sn(II) centre can be achieved. One common group of such compounds are diarylstannylenes that feature a heteroatom at the ortho position of the aromatic ring, such as in **11** ( $\text{SnR}_2$ ;  $\text{R} = \text{C}_6\text{H}_2\text{-}2,4,6\text{-}(\text{CF}_3)_3$ ) and **12** ( $\text{SnAr}_2$ ;  $\text{Ar} = \text{C}_6\text{H}_3\text{-}2,6\text{-}(\text{NMe}_2)_2$ ).<sup>106</sup> Such compounds appear to have enhanced nucleophilicity, as is exemplified by the formation of a stable Lewis acid-base adduct from reaction of **12** with  $\text{BH}_3$  (eq. 1.21).<sup>107</sup>



In allyl-substituted stannylene **13**, the allyl group is bonded to the Sn(II) centre in a  $\eta^3$  fashion (eq. 1.22a).<sup>51</sup> Compounds containing the phosphorus-stannylene Lewis pair

coordinated in an intramolecular fashion have been investigated in recent years by Wesemann and coworkers utilizing benzylphosphido- (**14**)<sup>108</sup> or *o*-phenylphosphido- (**15**)<sup>104</sup> substituted stannylenes (eq. 1.22a). Phosphorus-stabilized stannylene **14** reacts with 1-pentene reversibly at room temperature to yield a phosphastannacyclopentane (eq. 1.22b).<sup>108</sup> As the above example illustrates, the intramolecular donor-acceptor approach to small molecule activation allows for reactivity that normally would not be observed with an uncoordinated stannylene. Likewise, the reactions of **14** and **15** with alkynes and azides result in the insertion of these substrates into the dative Sn-P bond.<sup>104,109</sup> Recently, such compounds have been found to be active as catalysts in the hydroboration of aldehydes and ketones.<sup>11</sup>



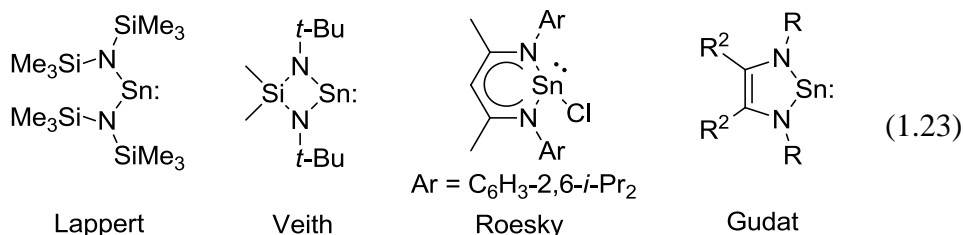
N-heterocyclic carbenes have been used to isolate stannylenes that would normally be transient species in solution. For instance, the NHC adducts of SnPh<sub>2</sub><sup>105</sup> and SnR<sub>2</sub> (R = C<sub>6</sub>H<sub>2</sub>-2,4,6-*i*-Pr<sub>3</sub>)<sup>105,110,111</sup> have been prepared.

#### 1.4.5. Stannylenes Stabilized by Group 15-16 Elements

Numerous examples exist of Sn(II) compounds that are  $\sigma$ -bonded to a heteroatom such as a N, O, S, or P element, where such ligands may be acyclic or cyclic.<sup>6,112,113</sup> Additional thermodynamic stabilization is imparted by delocalization of the electron pair

from the heteroatom into the empty p-orbital on Sn. These compounds frequently retain the +2 oxidation state of tin without the use of sterically demanding substituents; however, they require some degree of steric bulk in order to persist as monomeric species in solution.<sup>114</sup> Numerous applications have been found for such compounds: for example, as catalysts in the production of biodegradable polymers,<sup>115-118</sup> or as single source precursors in the chemical vapour deposition (CVD) of Sn(II) chalcogenides.<sup>2,119-121</sup> Stannylenes have themselves been utilized as monomers, as exemplified by the copolymerization of the Lappert diamino stannylenes (eq. 1.23) with *p*-benzoquinones.<sup>122</sup>

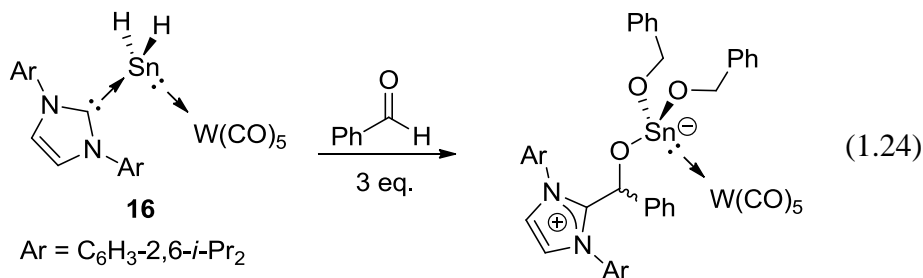
The chemistry of heterocyclic Sn(II) compounds has been the subject of numerous reviews.<sup>6,123-126</sup> Some representative examples of Sn(II) compounds that fall within this class are shown in eq. 1.23, along with the names of their principal investigators: Lappert,<sup>127</sup> Veith,<sup>128</sup> and Roesky.<sup>129,130 131</sup> The tin analogue of the Arduengo carbene has also been reported by Gudat and coworkers.<sup>132</sup>



#### 1.4.6. Donor-acceptor Stabilized Stannylenes

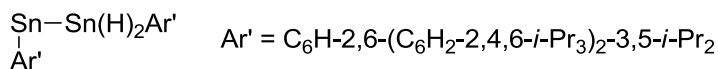
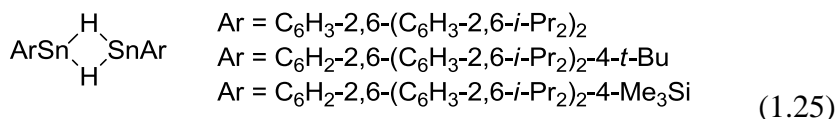
Reactive stannylenes (i.e. stannylenes that would normally be transient intermediates in solution) can be isolated in the form of donor-acceptor adducts. Isolation of SnMe<sub>2</sub>, SnPh<sub>2</sub> and Sn*t*-Bu<sub>2</sub> adducts of this type were initially reported in the 1970s by Marks and coworkers.<sup>133-135</sup> Such examples utilized pyridine and THF as donors and transition metal carbonyls as acceptors. Stannylene donor-acceptor adducts have received renewed attention since the isolation and characterization of a novel Lewis acid-base adduct of SnH<sub>2</sub> (**16**) by Rivard and coworkers.<sup>136-138</sup> The isolation of SnH<sub>2</sub> also allows for

subsequent reactivity studies, as in the hydrostannylation/insertion of benzaldehyde to **16** (eq. 1.24). The donor-acceptor chemistry of the main group elements has been the subject of a recent review by Rivard.<sup>139</sup>



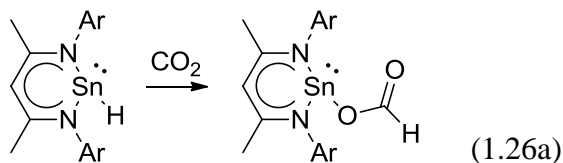
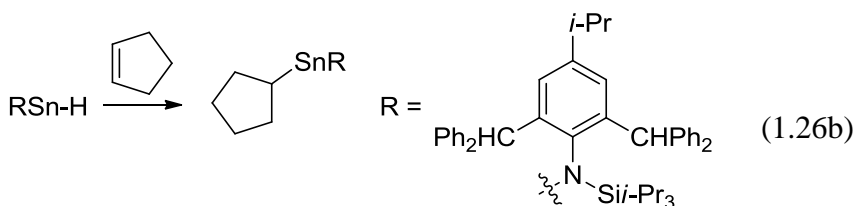
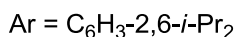
#### 1.4.7. Divalent Tin Hydrides

The chemistry of tin(II) hydrides has garnered particular interest recently. This is due, in part, to the ability of the Sn-H bond to add across the unsaturated bonds of unactivated alkenes, alkynes and carbonyl compounds.<sup>72,140,141</sup> In the absence of electronic stabilization, aryltin(II) hydrides will form doubly-bridged dimers in solution, as discussed in Section 1.4.3a. Bulkier aryl groups, however, favour the stannylstannylene Ar'SnSn(H)<sub>2</sub>Ar (eq. 1.25).<sup>71</sup>



Alkyl and aryltin(II) hydrides stabilized by N-heterocyclic carbenes (NHCs) have appeared more frequently in the literature recently. This is due, in part, to their convenient preparation from the dehydrogenation reactions of alkyl and aryltin trihydrides (R<sub>3</sub>SnH<sub>3</sub>) using 2 equivalents of NHC.<sup>105,142,143</sup> Alternatively, nitrogen bases can be used in place of NHCs.<sup>144</sup> These compounds have found utility as precursors to cationic stannylenes<sup>145</sup> and platinum complexes.<sup>146</sup>

A tin(II) hydride supported by a  $\beta$ -diketiminato ligand (**17**) has been reported by Roesky and coworkers.<sup>147,148</sup> **17** has been found to hydrostannylate various ketones, aldehydes, alkynes, and carbodiimides, as well as undergo facile CO<sub>2</sub> insertion (eq. 1.26a).<sup>148,149</sup> For comparison, the dialkylstannylene **2** was found to be unreactive with CO<sub>2</sub>.<sup>15</sup> Divalent tin hydrides stabilized by a bulky amino group (RSnH (**18**), R = N(C<sub>6</sub>H<sub>2</sub>-2,6-(C(H)Ph<sub>2</sub>)<sub>2</sub>-4-*i*-Pr)(Si*i*-Pr<sub>3</sub>)) have been found by Jones and coworkers to be very active in the hydrostannylation of unactivated alkenes and alkynes (eq. 1.26b).<sup>140,150</sup> **18** has also found utility as a catalyst for the hydroboration of carbonyl compounds<sup>151</sup> and the reduction of CO<sub>2</sub> to a methanol derivative (MeOBcat; cat = catecholato).<sup>152</sup> These examples highlight the use of Sn(II) hydrides to activate and perform catalytic transformations of small molecules and serve as viable alternatives to more expensive transition metal-based systems.

**17****18**

### 1.5.1. Studies of Transient Stannylenes in Frozen Matrix, Gas and Solution Phases - An Overview

In the absence of sufficient electronic stabilization, stannylenes bearing only small organic substituents (SnR<sub>2</sub>; R = Me, Et, *n*-Bu, *t*-Bu, Ph) are known to be short-lived and highly reactive intermediates.<sup>20,23,153,154</sup> Despite the emerging interest in utilizing isolable

derivatives (see 1.4.1-1.4.7), relatively little is known still about the chemistry of transient stannylenes. This contrasts with the substantial literature available regarding the chemistry of transient silylenes and germynes, the heavy carbene analogues of silicon and germanium, respectively.<sup>20,31,155-157</sup>

As early as the mid-nineteenth century, there was interest in the preparation and characterization of divalent organotin compounds: the first reports of isolated 'diethyltin' (Lowig, 1852) and 'diphenyltin' (Krause, 1920)<sup>158</sup> were followed by a number of reports regarding the preparation of such compounds.<sup>159</sup> Re-examination of these early experiments in the 1960s concluded that the structures reported were most likely mixtures of oligomeric organotin compounds.<sup>160-163</sup>

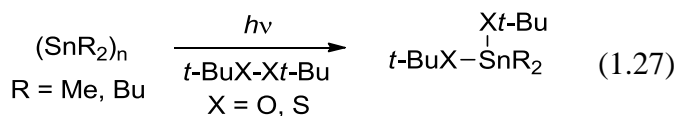
### 1.5.2. Chemical Trapping Studies of Transient Stannylenes

Efforts to study the chemistry of simple stannylenes in the condensed phase are rendered difficult by the transient nature of these compounds. They have thus traditionally relied on indirect methods, such as chemical trapping experiments, in which the species of interest is (ostensibly) generated in the presence of the trapping agent by thermolysis or photolysis of an appropriate precursor. The most comprehensive set of studies of transient stannylenes was conducted by means of chemical trapping experiments by W.P. Neumann and coworkers.<sup>24,164-168</sup> Extrusion of small dialkylstannylenes in the absence of a suitable co-reactant leads predominantly to the isolation of cyclic oligostannanes of the structure *cyclo*-(SnR<sub>2</sub>)<sub>n</sub>.<sup>20,154</sup> Despite much effort, relatively few reaction types have been identified that proceed rapidly enough to compete productively with oligomerization.

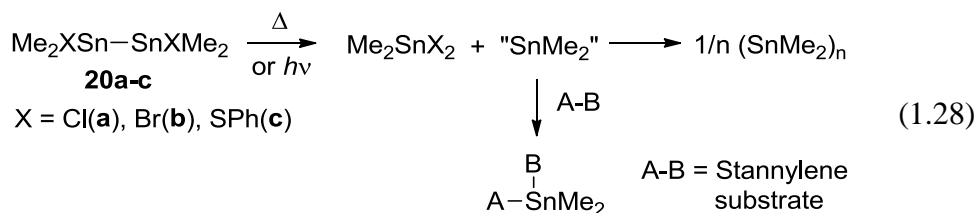
Photolysis of (SnBu<sub>2</sub>)<sub>n</sub> and (SnPh<sub>2</sub>)<sub>n</sub> oligomers in the presence of alkyl halides R'-X afforded the insertion products R'R<sub>2</sub>Sn-X (R= Bu, Ph).<sup>169,170</sup> Similarly, the photolysis of



$(\text{SnR}_2)_n$  ( $\text{R} = \text{Me}, \text{Bu}$ ) in the presence of disulfides and peroxides yielded the O-O and S-S bond insertion products of  $\text{SnR}_2$ , respectively, in yields greater than 80% (eq. 1.27).<sup>164</sup>



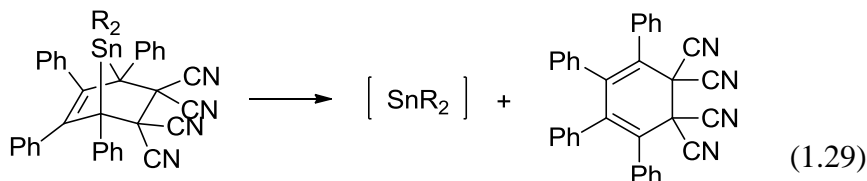
Thermolysis (120 - 130 °C) or room temperature UV photolysis of 1,2-dichlorotetrabutylstannane (**19**) afforded stannylene derived products in the presence of alkyl halides, along with the co-product  $\text{Bu}_2\text{SnCl}_2$ .<sup>24</sup> Similarly, the thermolysis and/or photolysis of  $\text{Me}_2(\text{X})\text{Sn-Sn}(\text{X})\text{Me}_2$  (**20a-c**;  $\text{X} = \text{Cl}(\mathbf{a}), \text{Br}(\mathbf{b}), \text{SPh}(\mathbf{c})$ ) was found to afford  $(\text{SnMe}_2)_n$  oligomers according to the scheme shown in eq. 1.28.<sup>165,168</sup>



While it was initially proposed that free stannylenes were generated in the earlier studies of **19**<sup>24</sup> and **20a**,<sup>165</sup> the authors later acknowledged that the reactions could instead proceed through a 'stannulenoid mechanism', where transfer of the  $\text{SnR}_2$  moiety to the stannylene substrate may not necessarily reflect the chemistry of the uncoordinated transient stannylene.<sup>20,168</sup>

Thermolysis of 7-stannanorbornenes (**21a-d** with  $\text{SnR}_2$ ;  $\text{R} = \text{Me}(\mathbf{a}), \text{CD}_3(\mathbf{b}), \text{Et}(\mathbf{c}), \text{Bu}(\mathbf{d})$ ) above -10 °C follows a first order decomposition process, affording a quantitative yield of 1,1,2,2-tetracyano-3,4,5,6-tetraphenylcyclohexa-3,5-diene (eq. 1.29).<sup>167</sup> As the decomposition of **21a-d** proceeded without <sup>119</sup>Sn CIDNP (chemically induced dynamic nuclear polarization) signals and was not accelerated by the presence of scavengers, Neumann and coworkers concluded it resulted in the extrusion of free uncoordinated stannylene via a concerted mechanism (eq. 1.29).<sup>166</sup> The corresponding Si and Ge

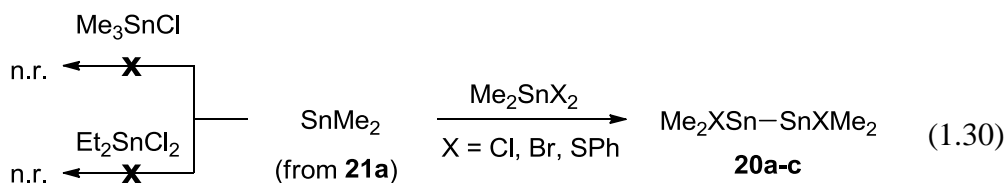
homologs have been established as precursors to the transient silylenes<sup>171</sup> and germynes.<sup>172-174</sup>



**21a-d**

R = Me(**a**), CD<sub>3</sub>(**b**), Et(**c**), Bu(**d**)

Sn-Cl bond insertion of SnMe<sub>2</sub> (from **21a**) with Me<sub>2</sub>SnCl<sub>2</sub> proceeds smoothly at room temperature. Under the same conditions however, the Sn-Cl insertion product with Me<sub>3</sub>SnCl or Et<sub>2</sub>SnCl<sub>2</sub> was not observed.<sup>167</sup> Similar Sn-X (X = Br, SPh) insertion reactions of SnMe<sub>2</sub> into compounds of the type Me<sub>2</sub>SnX<sub>2</sub> have been observed (eq. 1.30).<sup>167</sup> Mixtures of Sn-Sn and Sn-X insertion products were observed with Me<sub>2</sub>XSn-SnXMe<sub>2</sub> (X = Cl, Br) as co-reactant using **21b** as precursor for Sn(CD<sub>3</sub>)<sub>2</sub>.

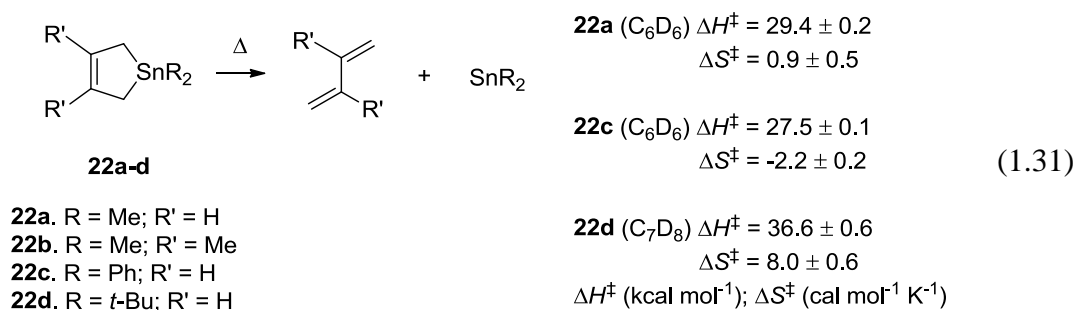


n.r. = no reaction

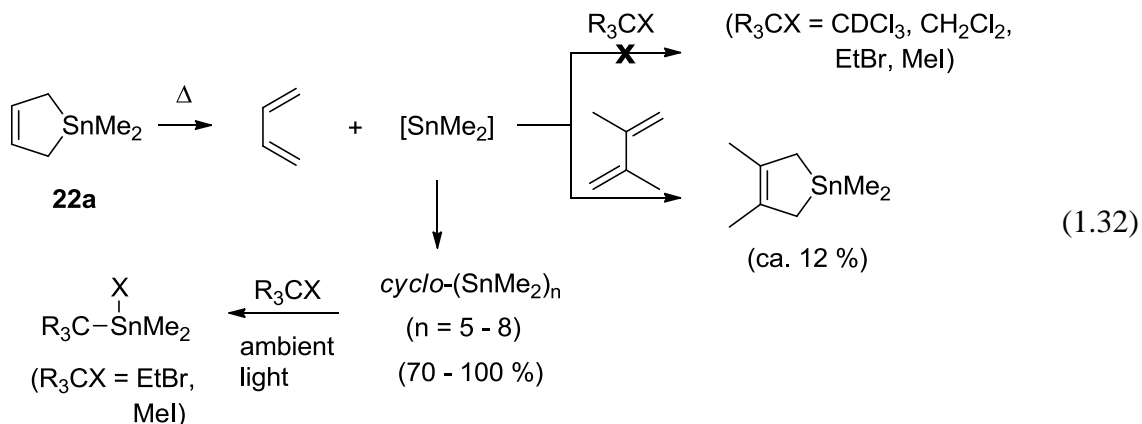
The  $\sigma$ -bond insertion reactions of SnMe<sub>2</sub> into the Sn-Cl bond of Me<sub>2</sub>SnCl<sub>2</sub> and Me<sub>3</sub>SnCl were investigated computationally by Dewar and coworkers using the MNDO SCF MO model. The authors predicted a larger activation barrier (by 4.1 kcal mol<sup>-1</sup>) for the reaction with Me<sub>3</sub>SnCl, and thus concluded these results to be qualitatively consistent with the experimental results of Neumann et al.<sup>175</sup>

Efforts to characterize transient stannylenes by chemical trapping methods have received renewed attention since the finding that 1,1-diorgano-1-stannacyclopent-3-enes serve as robust thermal precursors to the compounds.<sup>154</sup> P. P. Gaspar and coworkers in

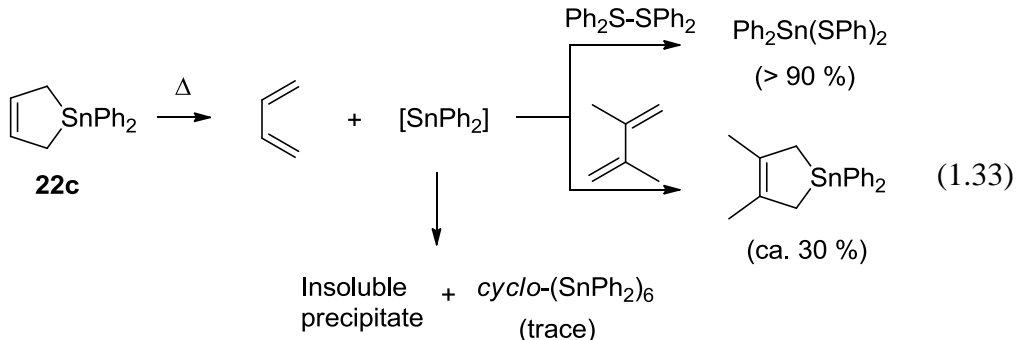
2009 examined several 1-stannacyclopent-3-enes **22a-d** as thermal precursors to SnMe<sub>2</sub> (**22a-b**), SnPh<sub>2</sub> (**22c**) and Sn*t*-Bu<sub>2</sub> (**22d**), respectively (eq. 1.31). Heating solutions of **22a-d** (ca. 80 - 130 °C for **22a-c**, ca. 140 - 180 °C for **22d**) containing 1,3-butadiene (BD) or 2,3-dimethyl-1,3-butadiene (DMB) resulted in first order loss of stannacyclopent-3-ene, and high yields of the respective diene co-product. Activation parameters were determined for the thermolysis reactions (eq. 1.31). The small effect of radical scavengers on the activation parameters was taken as further evidence for unimolecular dissociation to the transient stannylene and diene.



Thermolysis of **22a-b** in benzene-*d*<sub>6</sub> or cyclohexane-*d*<sub>12</sub> led to the formation of the respective diene and cyclic SnMe<sub>2</sub> oligomers (SnMe<sub>2</sub>)<sub>n</sub>; n = 5 - 8. SnMe<sub>2</sub> was trapped by butadienes (DMB from **22a**, BD from **22b** using neat solutions of the dienes) in yields of 12 and 5 %, respectively. SnMe<sub>2</sub> extruded from **22a** did not afford C-X (X = halogen) insertion products when pyrolysis was performed in neat solutions of CDCl<sub>3</sub>, CH<sub>2</sub>Cl<sub>2</sub>, or EtBr, or cyclohexane-*d*<sub>12</sub> solutions containing 2.1 M MeI (eq. 1.32). An authentic sample of (SnMe<sub>2</sub>)<sub>n</sub> (n = 5 - 8) was found to serve as a stannylene source, forming SnMe<sub>2</sub> insertion products with EtBr and MeI under ambient light at room temperature. The formation of Sn<sub>2</sub>Me<sub>5</sub>H from the pyrolysis of **22a** in neat Me<sub>3</sub>SnH solution was also attributed to a reaction with (SnMe<sub>2</sub>)<sub>n</sub> under thermolysis conditions.<sup>154</sup>



Thermolysis of **22c** (80 - 130 °C) in  $C_6D_6$  afforded BD along with oligomers of  $SnPh_2$ , the bulk of which were insoluble, and only a trace of the cyclic hexamer  $cyclo-(SnPh_2)_6$  observed. Pyrolysis in  $C_6D_6$  solutions containing DMB (0.44 M) or diphenyldisulfide (0.5 M) afforded the corresponding [1+4] cycloaddition or S-S insertion products in yields of ca. 30 % and > 90 %, respectively (eq. 1.33).<sup>154</sup>

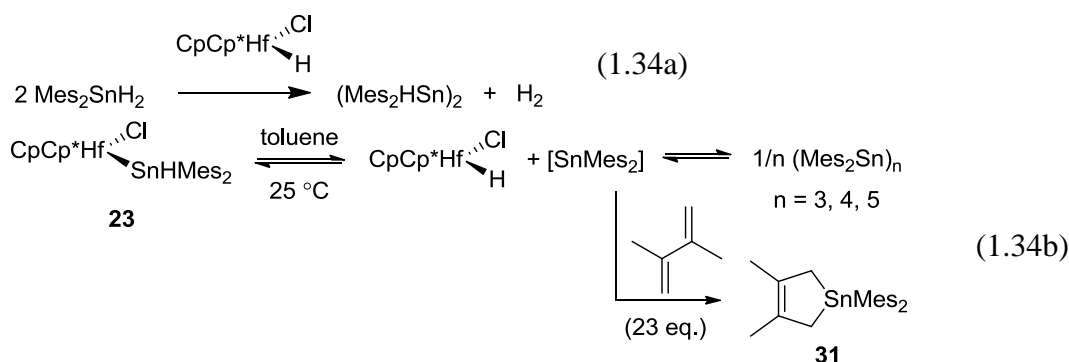


Finally, pyrolysis of **22d** in toluene solution resulted in the formation of 1,3-butadiene and Sn-containing oligomers. The cyclic oligomer  $cyclo-(Snt-Bu_2)_4$  was not detected in the product mixture; however, an independently prepared sample of the oligomer was shown to be unstable under the pyrolysis conditions (140 - 180 °C). Thermolysis in the presence of DMB afforded a high yield of the [1+4] adduct; however, heating a solution of  $cyclo-(Snt-Bu_2)_4$  under the same conditions also led to the same product, resulting in some ambiguity as to the source of the [1+4] adduct.<sup>154</sup> The pyrolysis experiments of **22a-d** generally show that simple Sn(II) derivatives strongly prefer

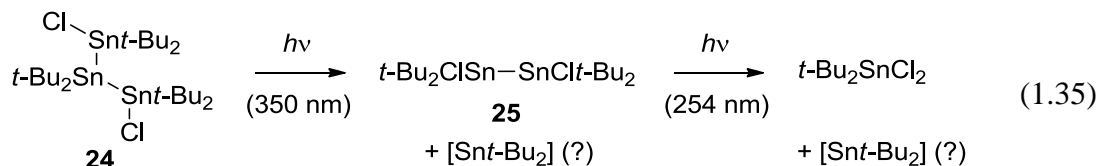
oligomerization over bimolecular reactions with added substrates. The results also indicate that oligomers of  $\text{SnMe}_2$  may also afford stannylene-derived products and could ultimately have been responsible for several reactions previously ascribed to free  $\text{SnMe}_2$ .

Photolysis (214 nm Zn resonance lamp) of a cyclohexane- $d_{12}$  solution of **22b** in the presence of methanol (0.5 M) led to the formation of BD (80 - 90 %) and a collection of peaks in the 0.5-0.8 ppm range of the spectrum consistent with that from  $(\text{Me}_2\text{Sn})_n$  oligomers. Virtually identical results were obtained in solutions of **22b** in the absence of the alcohol.<sup>23</sup> Photolysis (254 nm) of a hexanes solution containing **22a** (0.08 M) and  $\text{Me}_3\text{SnH}$  (0.17 M) gave GC-MS evidence for the anticipated insertion product  $\text{Sn}_2\text{Me}_5\text{H}$ .<sup>23</sup> The interpretation of the result however, should be accepted with caution as it was later discovered by Gaspar and coworkers<sup>154</sup> that  $(\text{Me}_2\text{Sn})_n$  can also contribute to its formation under thermolysis conditions.

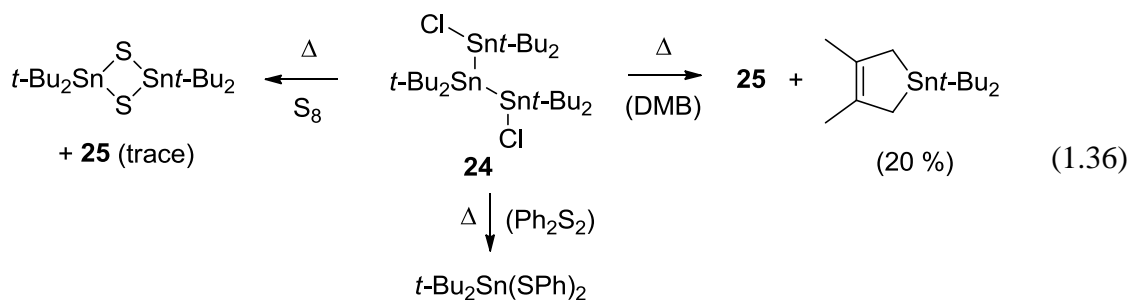
Dimesitylstannylene ( $\text{SnMes}_2$ ; Mes =  $\text{C}_6\text{H}_2$ -2,4,6- $\text{Me}_3$ ) was proposed as an intermediate in the transition metal catalyzed stannane dehydrocoupling of  $\text{Mes}_2\text{SnH}_2$  (eq. 1.34a).<sup>176</sup> Attempts to trap  $\text{SnMes}_2$  by stirring a toluene solution of  $\text{CpCp}^*\text{Hf}(\text{SnHMes}_2)\text{Cl}$  (**23**) at room temperature in the presence of DMB (23 equivalents) afforded the [1+4] cycloadduct (**31**) in 92 % yield by  $^1\text{H}$  NMR spectroscopy. In the absence of DMB, new  $^{119}\text{Sn}$  NMR resonances appear that are consistent with the formation of cyclic oligomers  $(\text{SnMes}_2)_n$ ;  $n = 3 - 5$  (eq. 1.34b).



1,3-Dichlorohexa-*tert*-butyltristannane (**24**) was found to undergo wavelength-dependent photochemical transformations, generating first 1,2-dichlorotetra-*tert*-butyldistannane (**25**) followed by dichlorodi-*tert*-butylstannane according to eq. 1.35.<sup>177</sup>



To date, attempts to trap  $\text{Sn}t\text{-Bu}_2$  from the photolysis of **24** have proven unsuccessful; however, the thermolysis of **24** in solution ( $\text{C}_6\text{D}_6$ , 110 °C) with DMB affords the (1+4) adduct in 20 % yield (eq. 1.36). Thermolysis in the presence of  $\text{Ph}_2\text{S}_2$  and  $\text{S}_8$  affords  $t\text{-Bu}_2\text{Sn}(\text{SPh})_2$  and  $(t\text{-Bu}_2\text{SnS})_2$ , respectively, as the initial products; however, the absence of co-product **25** raises the possibility that a stannylene mechanism may be involved (eq. 1.36). Attempts to trap  $\text{Sn}t\text{-Bu}_2$  with MeI and benzil did not afford the expected<sup>165,168</sup> stannylene-derived products.<sup>178</sup>



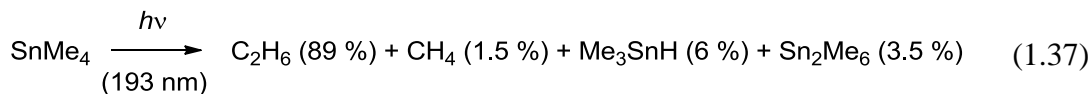
### 1.5.3. Direct Detection and Reactivity Studies of Transient Stannylenes

Only a handful of studies have aimed to identify and characterize transient stannylenes directly using spectroscopic methods. These studies have been performed in frozen matrices,<sup>179-181</sup> gas<sup>22,153</sup> and condensed phases.<sup>23</sup> Direct evidence for the existence of free  $\text{SnMe}_2$  as well as  $\text{Sn}(\text{CD}_3)_2$  was given by their IR spectra in an argon matrix at 5 K from the pyrolysis of *cyclo*- $(\text{Sn}(\text{CH}_3)_2)_6$  and *cyclo*- $(\text{Sn}(\text{CD}_3)_2)_6$ , respectively, or by microwave discharge from  $\text{Me}_2\text{SnH}_2$ .<sup>179,180</sup>  $\text{SnMe}_2$  and  $\text{SnMeH}$  were subsequently identified from the photodissociation of  $\text{Me}_3\text{SnH}$  and  $\text{Me}_2\text{SnH}_2$ , respectively in argon

matrices at 20 K, and assigned on the basis of Mössbauer and IR spectroscopy.<sup>182</sup> The existence of SnH<sub>2</sub> was further established from laser ablation experiments: laser-ablated Sn atoms and H<sub>2</sub> produce SnH<sub>2</sub> as well as SnH, SnH<sub>3</sub>, and SnH<sub>4</sub> (the deuterated analogues SnD<sub>1-4</sub> are produced from D<sub>2</sub>). These were identified on the basis of infrared spectra in solid neon and argon.<sup>183</sup> Using a similar procedure, laser-ablated Sn atoms react with CH<sub>4</sub> to produce SnMeH in a solid argon matrix at 4 K.<sup>184</sup>

Characteristic stretching frequencies of SnF<sub>2</sub><sup>185</sup> and SnCl<sub>2</sub><sup>186</sup> were characterized at 15 K in an Ar matrix. Subsequently, low temperature matrix IR spectroscopy was utilized by the groups of Margrave,<sup>187</sup> Tevault<sup>188</sup> and Nefedov<sup>189-192</sup> to identify a series of coordination complexes between SnCl<sub>2</sub> or SnF<sub>2</sub> and several small molecules. New IR stretching frequencies were assigned to the  $\pi$ -complexes between SnF<sub>2</sub> and the unsaturated hydrocarbons ethylene<sup>187</sup> and 1-heptyne.<sup>190</sup> Similarly, complexes were identified between SnF<sub>2</sub> and aromatic systems such as benzene, toluene and chlorobenzene,<sup>189</sup> as well as with methyl chloride<sup>191</sup> and N<sub>2</sub>.<sup>192</sup> The complexes of SnF<sub>2</sub> were assigned on the basis of their IR stretching frequencies, and supported by the results of theoretical calculations. Tevault et al. similarly identified shifts in the IR stretching frequencies of SnCl<sub>2</sub> in solid argon matrices in the presence of CO, NO, and N<sub>2</sub>, and assigned the new bands to complexes between SnCl<sub>2</sub> and the added substrates.<sup>188</sup>

The first reported study to characterize the reaction kinetics of transient stannylenes was carried out by Walsh and Becerra. It also focussed on SnMe<sub>2</sub> generated photochemically in the gas-phase.<sup>153</sup> The 193 nm photolysis of SnMe<sub>4</sub>, Sn<sub>2</sub>Me<sub>6</sub>, Me<sub>3</sub>SnH, and PhSnMe<sub>2</sub>H all generate visible wavelength absorptions in the 450-520 nm region that were assigned to SnMe<sub>2</sub>. Evaluation of the photoproducts suggested SnMe<sub>4</sub> is the cleanest source of the stannylene under the conditions employed (eq. 1.37).



Evaluation of the stannylene's reaction kinetics was carried out through the determination of gas-phase rate constants for reaction with an extensive selection of potential substrates including alkenes, alkynes, dienes, silyl and germlyl hydrides, MeOH, HCl, alkyl halides, N<sub>2</sub>O, SO<sub>2</sub>, and O<sub>2</sub>.<sup>153</sup> This study also allowed for the first quantitative comparison of the reaction kinetics of stannylenes with those of silylenes and germlylenes under similar conditions.<sup>22,153</sup> The gas-phase rate constants for the reactions of SnMe<sub>2</sub>, converted from molecular units, are summarized in Table 1.2.

**Table 1.2.** Absolute Rate Constants for the Reactions of SnMe<sub>2</sub> in the Gas Phase at 296 ± 2 K.<sup>a,b</sup>

substrate	SnMe <sub>2</sub> (10 <sup>9</sup> M <sup>-1</sup> s <sup>-1</sup> )	substrate	SnMe <sub>2</sub> (10 <sup>9</sup> M <sup>-1</sup> s <sup>-1</sup> )
1,3-Butadiene	36 ± 1	Propane	≤ 0.02
2-Butyne	4.72 ± 0.07	Me <sub>3</sub> SiH	≤ 0.04
MeOH	1.57 ± 0.06	GeH <sub>4</sub>	≤ 0.02
HCl	0.49 ± 0.02	Me <sub>2</sub> GeH <sub>2</sub>	≤ 0.06
BuBr	1.7 ± 0.2	Ethylene	≤ 0.006
SO <sub>2</sub>	20.2 ± 0.7	N <sub>2</sub> O	≤ 0.06

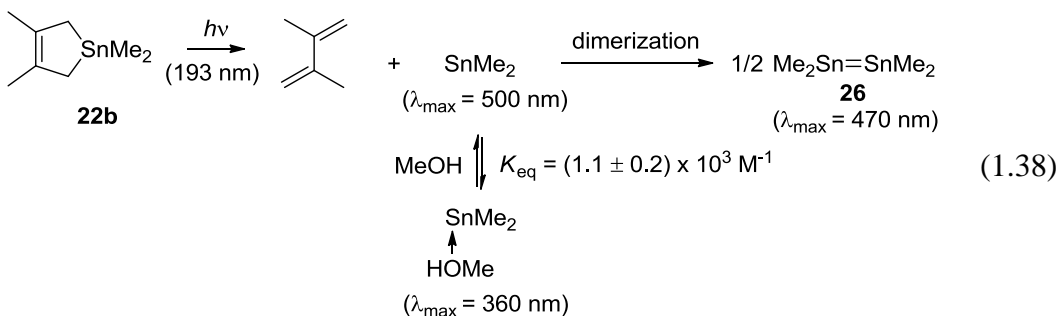
<sup>a</sup>Data from ref<sup>153</sup>; <sup>b</sup> gas phase rate constants converted from molecular units

This study revealed that SnMe<sub>2</sub> does not react with hydridosilanes or -germanes, alkanes, alkenes or N<sub>2</sub>O; however, it does exhibit reactivity toward alkynes, dienes and a variety of donor molecules (MeOH, HCl, a bromoalkane and SO<sub>2</sub>). Walsh and Becerra classified SnMe<sub>2</sub> as the least reactive in the series of the "heavy carbene" homologs, SiMe<sub>2</sub>, GeMe<sub>2</sub>, and SnMe<sub>2</sub>.<sup>153</sup> The stannacyclopent-3-ene **22a** was later used<sup>23</sup> as the photoprecursor to



reproduce the rate constants obtained for SO<sub>2</sub>, HCl, MeOH and 2-butyne using SnMe<sub>4</sub> as precursor.

The first detection of SnMe<sub>2</sub>, or of any transient stannylene, in solution at room temperature was achieved by the 193 nm flash photolysis of **22b** in hexanes solution.<sup>23</sup> SnMe<sub>2</sub> was detected using transient UV-vis spectroscopy; it was found to exhibit a transient absorption band at  $\lambda_{\text{max}} \approx 500$  nm which decayed over ca. 10  $\mu$ s to afford a new transient at  $\lambda_{\text{max}} \approx 470$  nm. The latter absorption was assigned to tetramethyldistannene Me<sub>2</sub>Sn=SnMe<sub>2</sub> (**26**). When the reactivity of SnMe<sub>2</sub> with methanol was studied, it was found to complex reversibly to afford a species assigned to the Lewis acid-base complex ( $\lambda_{\text{max}} \approx 360$  nm) with an equilibrium constant  $K_{\text{eq}} = (1.1 \pm 0.2) \times 10^3 \text{ M}^{-1}$  (eq. 1.38). Time-dependent DFT calculations support the spectral assignments made for SnMe<sub>2</sub> and **26**, and suggest dimerization to be, in effect, an irreversible process under the conditions of these experiments.

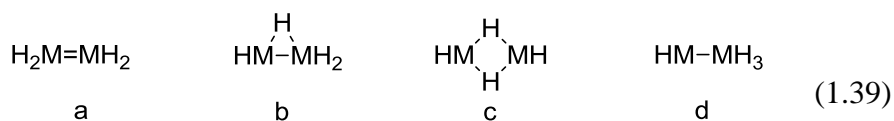


## 1.6. Theoretical Studies of Transient Stannylenes

Experimental studies of transient stannylenes (as well as kinetically stabilized derivatives) have often been complemented by theoretical calculations of the stannylenes' electronic structure, spectroscopic properties and bimolecular reactions.<sup>28,30,57,86,175,193-200</sup> These studies aim to provide support and additional insight into experimental findings. They have often been carried out alongside those using silylenes, germylenes, and plumblylenes with the goal of comparing the results with those derived for other divalent

Group 14 homologs.<sup>21</sup> The structure and properties of  $\text{SnH}_2$ ,<sup>201,202</sup>  $\text{SnMe}_2$ <sup>23,58,179</sup> and tin(II) dihalides<sup>29</sup> have received the most attention theoretically. More recently, the properties of more elaborately substituted stannylene derivatives have been investigated,<sup>198,203-205</sup> including examples of unsaturated stannylenes  $\text{Y}_2\text{Z}=\text{Sn}$ : ( $\text{Z} = \text{C}, \text{Si}, \text{Ge}, \text{Sn}$ ;  $\text{Y} = \text{F}, \text{MeNCH}_2\text{-}$  and  $\text{MeNCH-}$ ),<sup>205</sup> and dicoordinate stannylenes ( $\text{L}_2\text{Sn}(0)$ ;  $\text{L} = \text{:PMe}_3, \text{:C(NMe}_2)_2$ ).<sup>204</sup>

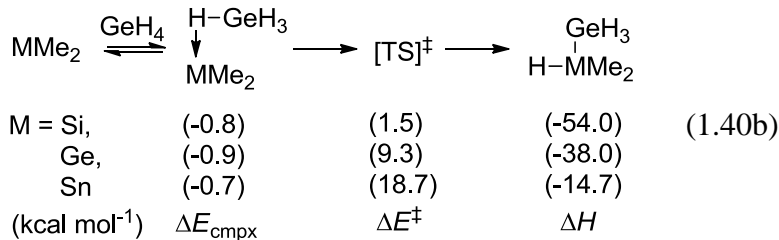
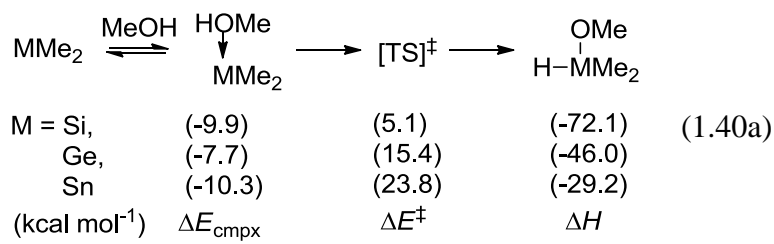
The structures, relative energies, and interconversion of the four isomeric forms of the  $\text{SnH}_2$  dimer ( $\text{Sn}_2\text{H}_4$ ) were investigated by Trinquier in the early 1990s (eq. 1.39) using ab initio methods.<sup>73,74</sup> While the silicon and germanium analogs were found to prefer the doubly bonded dimers (eq. 1.39 structure a), the most stable isomer for the tin and lead analogs was found to be the doubly bridged dimer (eq. 1.39 structure c). According to the calculations, the four isomers of  $\text{Sn}_2\text{H}_4$  are separated by no more than  $10 \text{ kcal mol}^{-1}$ , which is consistent with the structural diversity of the dimers of the sterically stabilized Sn(II) hydrides that have been reported recently (see 1.4.3a).<sup>71,72</sup>



$\text{M} = \text{C}, \text{Si}, \text{Ge}, \text{Sn}, \text{Pb}$

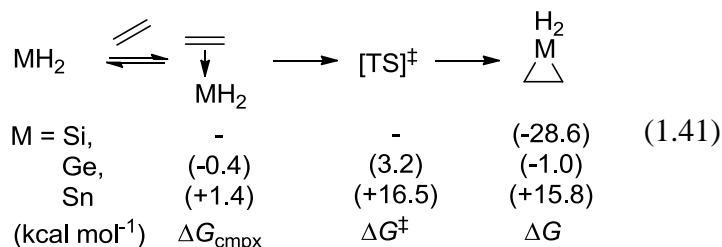
The dimerization of diorganostannylenes has also been the subject of recent theoretical interest. The thermodynamics of distannene formation from  $\text{SnR}_2$  ( $\text{R} = \text{H}, \text{Me}, \text{Ph}$ ) were calculated at the PW91/TZ2P level of theory, and compared to those of the corresponding reactions for the Si and Ge derivatives.<sup>23</sup> The trends from the data suggest dimerization to be a thermodynamically favoured process in all instances. There is, however, a consecutive decrease in  $\text{M}=\text{M}$  bond strength with increasing size of the group 14 element (i.e.  $\text{Si} > \text{Ge} > \text{Sn}$ ), suggesting the formation of the doubly-bonded dimer becomes less thermodynamically favorable as the central element becomes larger.<sup>23</sup>

M. D. Su investigated the  $\sigma$ -bond insertion reactions of heavy carbenes  $MMe_2$  ( $M = C, Si, Ge, Sn, Pb$ ) with silane, germane, and methanol, as well as [1+2] cycloaddition with ethylene and acetylene, with calculations at the CCSD(T)/LANL2DZdp//B3LYP/LANL2DZ and B3LYP/LANL2DZ levels of theory.<sup>28</sup> The results of this research suggest the reactions of  $SnMe_2$  all proceeded with the initial formation of weak  $\sigma$ -donor complexes with silane, germane and methanol, and  $\pi$ -complexes with ethylene and acetylene. The calculations suggest that the energies of the pre-reaction complexes for  $SnMe_2$  are comparable to those of the Si and Ge derivatives. For example, the calculated reaction energies of  $MMe_2$  with MeOH and  $GeH_4$  are shown in eq. 1.40a-b (calculated at the CCSD(T)/LANL2DZdp//B3LYP/LANL2DZ levels of theory). The general lack of reactivity of stannylenes toward typical tetrylene substrates observed experimentally<sup>153</sup> was attributed either to prohibitively high reaction barriers with respect to Si-H, Ge-H bond insertion, or to unfavourable overall reaction thermochemistries in the case of (1+2) cycloaddition to the C=C bond.<sup>28</sup>



The interactions of stannylenes with alkenes, alkynes and dienes have received theoretical interest on numerous occasions.<sup>28,86,193,195</sup> Similar to the results of Su, stannirane formation from the addition of  $SnH_2$  to ethylene was predicted by Sakai to be

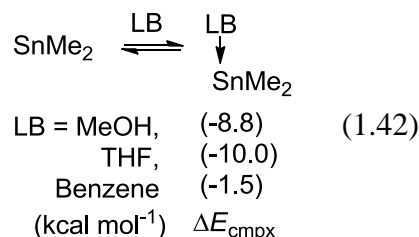
endergonic ( $\Delta G = 15.8 \text{ kcal mol}^{-1}$ ) on the basis of ab initio calculations, while the formation of a  $\pi$ -complex was expected to be close to thermoneutral relative to the constituent reagents (eq. 1.41, calculated at the MP4/6-31G(d,p) level of theory).<sup>86</sup>



The cycloaddition of  $\text{SnH}_2$  to acetylene to form stannirene is also predicted to be enthalpically favored ( $\Delta H = -12.5 \text{ kcal mol}^{-1}$ ) based on the calculations of Boatz et al. (computed at the MP2/3-21G(d)//RHF/3-21G(d) level of theory).<sup>195</sup> One consistent trend that emerges from the data is the stabilities of metalliranes and metallirenes (relative to free tetrylene + alkene / alkyne) decrease with increasing atomic number of the group 14 element (see eq. 1.41).<sup>28,86,195</sup> The cycloaddition of  $\text{SnMe}_2$  with  $\text{C}_{60}$  has also been investigated theoretically; the reaction is predicted to be enthalpically favored ( $\Delta H = -7.3 \text{ kcal mol}^{-1}$ ) but has not been probed experimentally.<sup>200</sup> The addition of  $\text{SnMe}_2$  to Single Walled Carbon Nanotubes (SWCNT), on the other hand, is predicted to be endothermic (calculated at the B3LYP/LANL2DZ level of theory).<sup>206</sup> The [1+4] cycloaddition of  $\text{SnMe}_2$  to 1,3-butadiene has been the subject of theoretical investigations by Nag and Gaspar.<sup>154,193</sup> The calculations predict the addition of  $\text{SnMe}_2$  proceeds via concerted [1+4] cycloaddition, without participation from the vinylstannirane (i.e. the [1+2] cycloadduct). The calculations also provide insight into the reverse process, the thermal extrusion of  $\text{SnMe}_2$  from **22a** (see 1.5.2).<sup>154</sup>

The Lewis acid-base complexes of various chalcogen and pnictogen donors with  $\text{SnH}_2$  (along with  $\text{SiH}_2$  and  $\text{GeH}_2$ ) have been calculated. The complexes were found to be weakly bound and the binding energies for the donor complexes were predicted to

decrease in the order silylene > germylene > stannylene.<sup>196</sup> Broeckaert et al. explored the possibility of  $\pi$ -complexation of  $\text{SnMe}_2$  with aromatic systems, where it was found an interaction with benzene to be weakly stable by  $\Delta E = -1.5 \text{ kcal mol}^{-1}$ . Complexation with  $\sigma$ -donors like methanol and THF, however, exhibit much stronger interactions (see eq. 1.42).<sup>30</sup>



The electrophilicity of  $\text{SnMe}_2$  was established as the dominant mode of reactivity (relative to its nucleophilic character; see 1.3). The local electrophilicity of the central metal element was found to be higher for  $\text{SnMe}_2$  relative to  $\text{GeMe}_2$ .<sup>30</sup> Referring to the calculated pathway for the reaction of  $\text{GeMe}_2$  and  $\text{SnMe}_2$  with methanol reported earlier by Su (eq. 1.40a),<sup>28</sup> the authors suggest the reaction barrier for insertion is higher for  $\text{SnMe}_2$  due to greater stability of the pre-reaction complex and the higher (local) electrophilicity at tin compared to the situation with  $\text{GeMe}_2$ .<sup>30</sup>

The oxygen abstraction reactions between oxirane and heavy carbene analogs ( $\text{MH}_2$ ,  $\text{M} = \text{Si}, \text{Ge}, \text{Sn}, \text{Pb}$ ) was studied theoretically by Su.<sup>197</sup> The results suggest a trend towards higher activation barriers and less stable products with increasing size of the group 14 element. The reaction between oxirane and  $\text{SnH}_2$ , to generate stannanone ( $\text{H}_2\text{Sn}=\text{O}$ ), was predicted not to proceed. Competition between bond insertion (i.e. oxidative addition) and substituent exchange of  $\text{SnHX}$  ( $\text{X} = \text{H}, \text{F}, \text{Cl}, \text{Br}$ ) with  $\text{HX}$  ( $\text{X} = \text{H}, \text{F}, \text{Cl}, \text{Br}$ ) has also been investigated theoretically.<sup>207</sup> The existence of two competing pathways for reaction with protic compounds is analogous to the competing arene elimination and oxidative addition of diarylstannylenes (see 1.4.3.).

### 1.7. Techniques Used in Reactivity Studies

The characterization of reactive intermediates in this thesis utilizes a combination of chemical trapping and laser flash photolysis experiments, as well as input from theoretical calculations. This three-pronged approach helps to develop a more comprehensive picture of stannylene and silylene reactivity, as often the results from any one method alone can be ambiguous. Furthermore, chemical trapping and flash photolysis experiments are complementary as they characterize a reaction both within the first several  $\mu$ s and several minutes after the reaction takes place.

The aim of product-study (i.e. chemical trapping) experiments is to identify the primary products from the ca. 254 nm photolysis of the photoprecursor in question in hydrocarbon solvent at room temperature in the presence of an appropriate trapping agent. Ideally, the products are identified by spiking the photolyzate with authentic samples of the suspected compounds, obtained either commercially (in rare cases) or by independent synthesis using known literature procedures. Synthesized authentic samples were characterized using  $^1\text{H}$ ,  $^{13}\text{C}\{^1\text{H}\}$  and  $^{119}\text{Sn}\{^1\text{H}\}$  NMR spectroscopy, FT-IR spectroscopy, High-Resolution Mass Spectrometry (HRMS) and melting point analysis if applicable. If this is not possible, then tentative characterization of the products is carried out on the crude photolysis mixtures using multinuclear ( $^1\text{H}$ ,  $^{13}\text{C}$ , and  $^{119}\text{Sn}$ ) NMR techniques and GC/MS (when applicable). Some additional questions that must also be considered include: Is the solution mixture containing precursor and trapping agent unchanged in the absence of light? What are the product yields? Are the products formed the primary photolysis products? Control samples of the reaction mixture prior to photolysis can be kept in the dark during the course of the photolysis experiment to assess possible dark (that is, thermal) reactions. Product yields are determined from the relative slopes of concentration-versus-time plots of the products relative to the consumed

precursor in the early stages of photolysis. Upwards curvature in concentration-versus-time plots for products usually indicates they are formed at least to some extent via secondary photolysis of a primary product.

Laser Flash Photolysis<sup>208</sup> experiments aim to detect the reactive intermediates formed during or after a ca. 25 ns pulse of UV light from a 248 nm KrF excimer laser, and follow their time evolution on the microsecond timescale after they are produced. The photoproducts were identified using time-resolved UV-vis spectroscopy in the 270-650 nm spectral range, up to 360  $\mu$ s after irradiation. The transient tetrylene compounds studied in this work exhibit absorption maxima within the 480-580 nm spectral range, that are sufficiently resolved from other absorbing compounds, in order to carry out detailed reactivity studies. Information about the kinetic and thermodynamic aspects of tetrylene reactivity can be obtained by observing the changes in the kinetic traces caused by variable concentrations of an added reactive substrate. The formation of new transient products observed in the UV-vis spectral range can also provide additional insight.

### **1.8. Thesis Objectives - Goals of the Work Presented in this Thesis**

Few studies have been reported on the chemistry of transient stannylenes (see 1.5). They have not kept in step with recent advances in the understanding and utility of isolable Sn(II) compounds (see 1.4). The ultimate goal of this thesis is to detect and characterize the solution-phase behaviour and reactivity of simple carbon substituted transient stannylenes.

Several inconsistencies are apparent in the transient stannylene literature that does exist. Chemical trapping studies have been reported by Neumann and coworkers;<sup>24,164,165</sup> however, the authors acknowledge that such reactions do not necessarily establish the involvement of free uncoordinated stannylenes and suggest reactions may proceed via stannulenoid mechanisms.<sup>20,168,180</sup> More recently, Gaspar and coworkers suggest that

dimethyltin oligomers may function as stannylenoids and were ultimately responsible for several reactions previously attributed to the free stannylene.<sup>154</sup> The difficulties in interpreting such reactivity studies are that they have relied solely on indirect methods such as chemical trapping experiments in which the species of interest is (ostensibly) generated in the presence of the trapping agent by thermolysis or by the photolysis of an appropriate precursor. This work aims to avoid these problems by studying stannylene reactivity using a combination of chemical trapping and direct detection methods in order to develop a more unified picture.

Experimental (and theoretical) studies of stannylene chemistry have often been carried out in conjunction with studies of silylenes and germylenes under the same conditions to examine trends amongst the heavy carbene series. The opportunity exists to make such comparisons in this thesis. Studies by Leigh and coworkers over the last thirteen years have characterized the transient diorganosilylenes ( $\text{SiMe}_2$ ,  $\text{SiMePh}$ ,<sup>209</sup>  $\text{SiPh}_2$ <sup>210,211</sup> and  $\text{SiMes}_2$ ) and germylenes ( $\text{GeMe}_2$ ,<sup>212,213</sup>  $\text{GeMePh}$ ,<sup>214</sup>  $\text{GePh}_2$ ,<sup>212,215</sup> and  $\text{GeMes}_2$ <sup>212,216</sup>) in solution, and studied the mechanistic aspects of several of their known reactions in solution at ambient temperatures.<sup>217-227</sup> Thus far, only  $\text{SnMe}_2$  had been studied by direct spectroscopic methods,<sup>23</sup> and only a basic characterization had been made of its dimerization and complexation with methanol. The necessity of employing 193 nm light to excite the precursor that was used in that study severely restricted the scope of the study of the stannylene's reactivity, since most substrates of interest (alkenes, alkynes, amines, sulfides, ethers, etc.) also absorb significantly at the excitation wavelength.

Detailed mechanistic studies of silylenes and germylenes in solution using laser flash photolysis methods have relied on the availability of photoprecursors to generate the transient molecules cleanly and efficiently using a pulsed laser with a 248 nm excitation

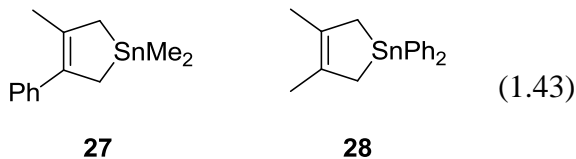


wavelength. This expands the scope of reactivity studies to include a greater variety of substrates (alkenes, alkynes, amines, sulphides, ethers, etc.) than are possible with 193 nm excitation. Thus, the first goal of this thesis was to develop compounds that will produce transient stannylenes cleanly and efficiently with 248 nm excitation light, to enable studies to be carried out at the same level of detail as used in our work on silylene and germylene chemistry. The most appropriate compounds satisfying these criteria appear to be stannacyclopent-3-ene derivatives: **22b** has already been demonstrated to be an effective photoprecursor for  $\text{SnMe}_2$ ,<sup>23</sup> while compounds **22a-d** have been shown to be useful thermal precursors to transient stannylenes.<sup>154</sup> In addition, the preparative procedures for these compounds appear conveniently amenable to modification.<sup>154</sup> Such compounds bear analogy to the germacyclopent-3-ene derivatives that yield transient germylenes cleanly and with high photochemical efficiency<sup>212</sup> (note, however, that the silicon analogue does not extrude  $\text{SiPh}_2$ <sup>228</sup> cleanly under similar conditions).

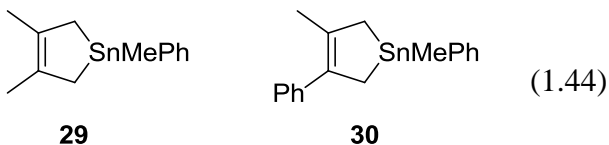
### 1.9. Thesis Summary

The second chapter describes the direct detection and preliminary characterization of the benchmark stannylenes  $\text{SnMe}_2$  and  $\text{SnPh}_2$  using transient UV-vis spectroscopy. The stannacyclopent-3-ene derivatives **27** and **28** (eq. 1.43) are synthesized and established to be clean, highly efficient photoprecursors for the transient stannylenes utilizing pulsed laser (248 nm) or lamp (254 nm) excitation.  $\text{SnPh}_2$  is detected directly for the first time under any set of conditions; while  $\text{SnMe}_2$  is successfully generated using an excitation wavelength that allows for more detailed reactivity studies than previously had been possible using 193 nm excitation. The dimerization of both  $\text{SnMe}_2$  and  $\text{SnPh}_2$  is characterized kinetically and the products identified on the basis of their UV-vis spectra and computational studies. This is further complemented by the results of end product analysis and theoretical calculations of the stannylenes' dimerization pathways. The Sn-Cl

bond insertion reaction of chlorostannanes is investigated by a combination of steady state trapping and laser flash photolysis experiments, using  $\text{Me}_2\text{SnCl}_2$  as the reactant. Rate and equilibrium constants are reported for the reactions of the two stannylenes with MeOH.



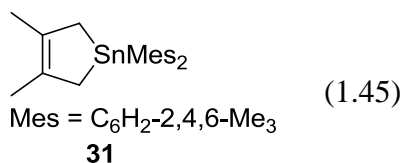
The third chapter begins by introducing the mixed alkylarylstannylene,  $\text{SnMePh}$ , using two novel precursors **29** and **30** (eq. 1.44) to generate the molecule. The free stannylene is characterized in solution and its dimerization behaviour characterized. A combination of chemical trapping and laser flash photolysis studies are used to characterize the Sn-Cl bond insertion of  $\text{SnMePh}$  with  $\text{Me}_2\text{SnCl}_2$ , and an equilibrium constant is determined for its reaction with MeOH. Two additional stannylene reactions are then investigated with  $\text{SnMe}_2$ ,  $\text{SnPh}_2$  and  $\text{SnMePh}$  that are found to lead to stable products in chemical trapping experiments. In the first, investigation of the Sn-Cl bond insertion reaction of chlorostannanes is extended to include  $\text{Bu}_3\text{SnCl}$  as the stannylene scavenger. The second reaction investigates the reaction of stannylenes with acetic acid, and the competition between O-H insertion, alkane-, and arene- elimination pathways that give rise to the major products.



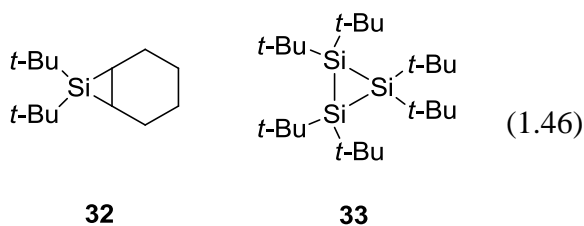
In Chapter Four, the Lewis acid-base complexation of  $\text{SnMe}_2$  and  $\text{SnPh}_2$  with O-, S-, and N- donors and their reactions with alkenes, alkynes, dienes and trialkyltin hydrides are investigated. Rate and equilibrium constants are measured for the coordination of the stannylenes with the donor substrates. These are accompanied in each instance by the

identification of the stannylene-donor complexes by transient UV-vis spectroscopy. In addition, comparison of the thermodynamic aspects of stannylene complexation with those of transient silylenes and germylenes allows for the determination of a Lewis acidity scale for the tetrylene series  $MR_2$  ( $M = Si, Ge, Sn$ ;  $R = Me, Ph$ ). The characteristics of the reactions of stannylenes with alkenes, alkynes, dienes and trialkyltin hydrides closely resemble those of the O-, S-, and N- donors in that these reactions do not proceed beyond initial Lewis acid-base coordination of the stannylene and the substrate. Such behaviour differs dramatically from those of the homologous silylenes and germylenes.

Chapter Five describes the direct detection of dimesitylstannylene ( $SnMes_2$ ) and its dimer, tetramesityldistannene, in solution for the first time via the photolysis of **31** (eq. 1.45) in hydrocarbon solution. The Sn-Cl bond insertion of  $SnMes_2$  with  $Me_2SnCl_2$  and the arene elimination with AcOH are studied through a combination of chemical trapping and laser flash photolysis studies. Product-studies experiments in aerated solution also afford stannylene-derived products, while  $SnMes_2$  and its doubly bonded dimer  $Sn_2Mes_4$  appear to be reactive with  $O_2$  in time resolved flash photolysis measurements. The reactions of  $SnMes_2$  with ethers, alcohols, sulfides and amines afford the stannylene-donor pairs; the rate and equilibrium constants are measured for these reactions. The kinetic and thermodynamic aspects of the reactions of  $SnMes_2$  are compared to the solution-phase reactivity of  $SnPh_2$ . This provides a model for sterically hindered diarylstannylene derivatives.



In Chapter Six the direct detection of  $\text{Si}t\text{-Bu}_2$  in solution by transient UV-vis spectroscopy, using two well known photoprecursors **32** and **33** (eq. 1.46) to generate the molecule, is reported. Detailed reactivity studies of the silylene are next carried out with respect to Lewis acid-base complexation, ene-addition,  $\sigma$ -bond insertion and cycloaddition reactions. The rate and equilibrium constants obtained for the reactions of  $\text{Si}t\text{-Bu}_2$  in solution provide a model for the reactivity for the sterically more crowded dialkylsilylenes relative to the parent derivative  $\text{SiMe}_2$ . This model ultimately aims to develop kinetic benchmarks describing the sensitivity of various silylene reaction types to steric effects. Finally, the kinetics of the reactions of tetra-*tert*-butyldisilene (**34**) with molecular oxygen and acetone are studied using precursor **33** which also produces the disilene as a primary photoproduct.



## 1.10. References

- (1) Davies, A. G. In *Organotin Chemistry*; 2nd ed.; Wiley-VCH Verlag GmbH & Co. KGaA: 2004, p 351.
- (2) de Lima, G. M. In *Tin Chemistry: Fundamentals, Frontiers, and Applications*; Davies, A. G., Gielen, M., Pannell, K. H., Tiekink, E., Eds.; John Wiley & Sons, Ltd: New York, 2008, p 285.
- (3) Veith, M.; Recktenwald, O. *Top. Curr. Chem.* **1982**, *104*, 1.
- (4) Tokitoh, N.; Okazaki, R. *Coord. Chem. Rev.* **2000**, *210*, 251.
- (5) Tokitoh, N.; Ando, W. In *Reactive Intermediate Chemistry*; Moss, R. A., Platz, M. S., Jones, M., Jr., Eds.; John Wiley & Sons: New York, 2004, p 651.
- (6) Mizuhata, Y.; Sasamori, T.; Tokitoh, N. *Chem. Rev.* **2009**, *109*, 3479.
- (7) Lee, V. Y.; Sekiguchi, A. In *Organometallic Compounds of Low-Coordinate Si, Ge, Sn and Pb*; John Wiley & Sons, Ltd: Chichester, 2010, p 139.
- (8) Rivard, E. *Chem. Soc. Rev.* **2016**, *45*, 989.
- (9) Driess, M.; Grützmacher, H. *Angew. Chem. Int. Ed. Engl.* **1996**, *35*, 828.

- (10) Weidenbruch, M. *Eur. J. Inorg. Chem.* **1999**, 1999, 373.
- (11) Schneider, J.; Sindlinger, C. P.; Freitag, S. M.; Schubert, H.; Wesemann, L. *Angew. Chem. Int. Ed. Engl.* **2017**, 56, 333.
- (12) Peng, Y.; Ellis, B. D.; Wang, X.; Power, P. P. *J. Am. Chem. Soc.* **2008**, 130, 12268.
- (13) Peng, Y.; Guo, J.-D.; Ellis, B. D.; Zhu, Z.; Fettingner, J. C.; Nagase, S.; Power, P. P. *J. Am. Chem. Soc.* **2009**, 131, 16272.
- (14) Dube, J. W.; Brown, Z. D.; Caputo, C. A.; Power, P. P.; Ragogna, P. J. *Chem. Commun.* **2014**, 50, 1944.
- (15) Yan, C.; Xu, Z.; Xiao, X.-Q.; Li, Z.; Lu, Q.; Lai, G.; Kira, M. *Organometallics* **2016**, 35, 1323.
- (16) Erickson, J. D.; Vasko, P.; Riparetti, R. D.; Fettingner, J. C.; Tuononen, H. M.; Power, P. P. *Organometallics* **2015**, 34, 5785.
- (17) Power, P. P. *Nature* **2010**, 463, 171.
- (18) Power, P. P. *Chem. Record* **2012**, 12, 238.
- (19) Power, P. P. *Acc. Chem. Res.* **2011**, 44, 627.
- (20) Neumann, W. P. *Chem. Rev.* **1991**, 91, 311.
- (21) Boganov, S. E.; Egorov, M. P.; Faustov, V. I.; Nefedov, O. M. In *The chemistry of organic germanium, tin and lead compounds - Vol. 2*; Rappoport, Z., Ed.; John Wiley and Sons: New York, 2002, p 749.
- (22) Boganov, S. E.; Egorov, M. P.; Faustov, V. I.; Krylova, I. V.; Nefedov, O. M.; Becerra, R.; Walsh, R. *Russ. Chem. Bull. Int. Ed.* **2005**, 54, 483.
- (23) Becerra, R.; Harrington, C. R.; Gaspar, P. P.; Leigh, W. J.; Vargas-Baca, I.; Walsh, R.; Zhou, D. *J. Am. Chem. Soc.* **2005**, 127, 17469.
- (24) Schröer, U.; Neumann, W. P. *Angew. Chem. Int. Ed. Engl.* **1975**, 14, 246.
- (25) Weidenbruch, M.; Schlaefke, J.; Schafer, A.; Peters, K.; Schnering, H. G. v.; Marsmann, H. *Angew. Chem. Int. Ed. Engl.* **1994**, 33, 1846.
- (26) Jones, M., Jr.; Moss, R. A. In *Reactive Intermediate Chemistry*; Moss, R. A., Platz, M. S., Jones, M., Jr., Eds.; John Wiley & Sons: New York, 2004, p 273.
- (27) Tomioka, H. In *Reactive Intermediate Chemistry*; Moss, R. A., Platz, M. S., Maitland, J. J., Eds.; John Wiley & Sons: New York, 2004, p 1071.
- (28) Su, M. D. *Chem. Eur. J.* **2004**, 10, 6073.
- (29) Szabados, A.; Hargittai, M. *J. Phys. Chem. A* **2003**, 107, 4314.
- (30) Broeckaert, L.; Geerlings, P.; Růžička, A.; Willem, R.; De Proft, F. *Organometallics* **2012**, 31, 1605.
- (31) Becerra, R.; Walsh, R. *Phys. Chem. Chem. Phys.* **2007**, 9, 2817.
- (32) Allendorf, M. D.; Melius, C. F. *J. Phys. Chem. A* **2005**, 109, 4939.
- (33) Allendorf, M. D.; Melius, C. F. *J. Phys. Chem.* **1993**, 97, 720.
- (34) Davidson, P. J.; Lappert, M. F. *Chem. Commun.* **1973**, 317a.
- (35) Cotton, J. D.; Davidson, P. J.; Lappert, M. F. *J. Chem. Soc., Dalton Trans.* **1976**, 2275.
- (36) Davidson, P. J.; Harris, D. H.; Lappert, M. F. *Dalton Trans.* **1976**, 2268.
- (37) Schager, F.; Goddard, R.; Seevogel, K.; Porschke, K. R. *Organometallics* **1998**, 17, 1546.

- (38) Hillner, K.; Neumann, W. P. *Tetrahedron Lett.* **1986**, *27*, 5347.
- (39) Kira, M.; Yauchibara, R.; Hirano, R.; Kabuto, C.; Sakurai, H. *J. Am. Chem. Soc.* **1991**, *113*, 7785.
- (40) Eaborn, C.; Hill, M. S.; Hitchcock, P. B.; Patel, D.; Smith, J. D.; Zhang, S. *Organometallics* **1999**, *19*, 49.
- (41) Kira, M.; Ishida, S.; Iwamoto, T. *Chem. Record* **2004**, *4*, 243.
- (42) Tokitoh, N.; Saito, M.; Okazaki, R. *J. Am. Chem. Soc.* **1993**, *115*, 2065.
- (43) Saito, M.; Tokitoh, N.; Okazaki, R. *Organometallics* **1996**, *15*, 4531.
- (44) Saito, M.; Tokitoh, N.; Okazaki, R. *Chem. Lett.* **1996**, *25*, 265.
- (45) Saito, M.; Tokitoh, N.; Okazaki, R. *J. Am. Chem. Soc.* **1997**, *119*, 11124.
- (46) Simons, R. S.; Pu, L.; Olmstead, M. M.; Power, P. P. *Organometallics* **1997**, *16*, 1920.
- (47) Phillips, A. D.; Hino, S.; Power, P. P. *J. Am. Chem. Soc.* **2003**, *125*, 7520.
- (48) Spikes, G. H.; Peng, Y.; Fettingner, J. C.; Power, P. P. *Z. Anorg. Allg. Chem.* **2006**, *632*, 1005.
- (49) Tajima, T.; Takeda, N.; Sasamori, T.; Tokitoh, N. *Organometallics* **2006**, *25*, 3552.
- (50) Lips, F.; Mansikkamäki, A.; Fettingner, J. C.; Tuononen, H. M.; Power, P. P. *Organometallics* **2014**, *33*, 6253.
- (51) Krebs, K. M.; Wiederkehr, J.; Schneider, J.; Schubert, H.; Eichele, K.; Wesemann, L. *Angew. Chem. Int. Ed.* **2015**, *54*, 5502.
- (52) Arp, H.; Baumgartner, J.; Marschner, C.; Muller, T. *J. Am. Chem. Soc.* **2011**, *133*, 5632.
- (53) Setaka, W.; Sakamoto, K.; Kira, M.; Power, P. P. *Organometallics* **2001**, *20*, 4460.
- (54) Eichler, B. E.; Phillips, A. D.; Power, P. P. *Organometallics* **2003**, *22*, 5423.
- (55) Protchenko, A. V.; Bates, J. I.; Saleh, L. M. A.; Blake, M. P.; Schwarz, A. D.; Kolychev, E. L.; Thompson, A. L.; Jones, C.; Mountford, P.; Aldridge, S. *J. Am. Chem. Soc.* **2016**, *138*, 4555.
- (56) Weidenbruch, M.; Kilian, H.; Peters, K.; von Schnering, H. G.; Marsmann, H. *Chem. Ber.* **1995**, *128*, 983.
- (57) Wilfling, P.; Schittelkopf, K.; Flock, M.; Herber, R. H.; Power, P. P.; Fischer, R. C. *Organometallics* **2015**, *34*, 2222.
- (58) Fjeldberg, T.; Haaland, A.; Schilling, B. E. R.; Lappert, M. F.; Thorne, A. J. *J. Chem. Soc., Dalton Trans.* **1986**, *1986*, 1551.
- (59) Eaborn, C.; Hill, M. S.; Hitchcock, P. B.; Patel, D.; Smith, J. D.; Zhang, S. *Organometallics* **2000**, *19*, 49.
- (60) Grützmacher, H.; Pritzkow, H.; Edelman, F. T. *Organometallics* **1991**, *10*, 23.
- (61) Weidenbruch, M.; Stilter, A.; Schlaefke, J.; Peters, K.; Schnering, H. G. v. J. *Organomet. Chem.* **1995**, *501*, 67.
- (62) Zilm, K. W.; Lawless, G. A.; Merrill, R. M.; Millar, J. M.; Webb, G. G. *J. Am. Chem. Soc.* **1987**, *109*, 7236.
- (63) Della Bona, M. A.; Cassani, M. C.; Keates, J. M.; Lawless, G. A.; Lappert, M. F.; Sturmman, M.; Weidenbruch, M. *J. Chem. Soc., Dalton Trans.* **1998**, 1187.

- (64) Masamune, S.; Sita, L. R. *J. Am. Chem. Soc.* **1985**, *107*, 6390.
- (65) Weidenbruch, M.; Schäfer, A.; Kilian, H.; Pohl, S.; Saak, W.; Marsmann, H. *Chem. Ber.* **1992**, *125*, 563.
- (66) Lay, U.; Pritzkow, H.; Grützmacher, H. *Chem. Commun.* **2005**, 1992, 260.
- (67) Schäfer, A.; Winter, F.; Saak, W.; Haase, D.; Pöttgen, R.; Müller, T. *Chem. Eur. J.* **2011**, *17*, 10979.
- (68) Cardin, C. J.; Cardin, D. J.; Convery, M. A.; Devereux, M. M.; Twamley, B.; Silver, J. *J. Chem. Soc., Dalton Trans.* **1996**, 1145.
- (69) Guo, J.-D.; Liptrot, D. J.; Nagase, S.; Power, P. P. *Chem. Sci.* **2015**, *6*, 6235.
- (70) Rivard, E.; Steiner, J.; Fettingner, J. C.; Giuliani, J. R.; Augustine, M. P.; Power, P. P. *Chem. Commun.* **2007**, 4919.
- (71) Rivard, E.; Fischer, R. C.; Wolf, R.; Peng, Y.; Merrill, W. A.; Schley, N. D.; Zhu, Z.; Pu, L.; Fettingner, J. C.; Teat, S. J.; Nowik, I.; Herber, R. H.; Takagi, N.; Nagase, S.; Power, P. P. *J. Am. Chem. Soc.* **2007**, *129*, 16197.
- (72) Wang, S.; McCrea-Hendrick, M. L.; Weinstein, C. M.; Caputo, C. A.; Hoppe, E.; Fettingner, J. C.; Olmstead, M. M.; Power, P. P. *J. Am. Chem. Soc.* **2017**, *139*, 6586
- (73) Trinquier, G. *J. Am. Chem. Soc.* **1991**, *113*, 144.
- (74) Trinquier, G. *J. Am. Chem. Soc.* **1990**, *112*, 2130.
- (75) Lee, V. Y.; Sekiguchi, A. In *Organometallic Compounds of Low-Coordinate Si, Ge, Sn and Pb*; John Wiley & Sons, Ltd: Chichester, 2010, p 199.
- (76) Kira, M.; Ishida, S.; Iwamoto, T.; Yauchibara, R.; Sakurai, H. *J. Organomet. Chem.* **2001**, *636*, 144.
- (77) Leites, L. A.; Zabula, A. V.; Bukalov, S. S.; Korlyukov, A. A.; Koroteev, P. S.; Maslennikova, O. S.; Egorov, M. P.; Nefedov, O. M. *J. Mol. Struct.* **2005**, *750*, 116.
- (78) Broeckaert, L.; Turek, J.; Olejník, R.; Růžička, A.; Biesemans, M.; Geerlings, P.; Willem, R.; De Proft, F. *Organometallics* **2013**, *32*, 2121.
- (79) Baumgartner, J.; Marschner, C. In *Rev. Inorg. Chem.* 2014; Vol. 34, p 119.
- (80) Pluta, C.; Pörschke, K. R.; Mynott, R.; Betz, P.; Krüger, C. *Chem. Ber.* **1991**, *124*, 1321.
- (81) Marx, R.; Neumann, W. P.; Hillner, K. *Tetrahedron Lett.* **1984**, *25*, 625.
- (82) Sita, L. R.; Bickerstaff, R. D. *J. Am. Chem. Soc.* **1988**, *110*, 5208.
- (83) Sita, L. R.; Bickerstaff, R. D. *Phosph. Sulf. Sil. Rel. Elem.* **1989**, *41*, 31.
- (84) Sita, L. R.; Kinoshita, I.; Lee, S. P. *Organometallics* **1990**, *9*, 1644.
- (85) Pluta, C.; Pörschke, K.-R. *J. Organomet. Chem.* **1993**, *453*, C11.
- (86) Sakai, S. *Int. J. Quantum Chem.* **1998**, *70*, 291.
- (87) Lu, Q.; Yan, C.; Xiao, X.-Q.; Li, Z.; Wei, N.; Lai, G.; Kira, M. *Organometallics* **2017**, *36*, 3633.
- (88) Erickson, J. D.; Riparetti, R. D.; Fettingner, J. C.; Power, P. P. *Organometallics* **2016**, *35*, 2124.
- (89) Erickson, J. D.; Fettingner, J. C.; Power, P. P. *Inorg. Chem.* **2015**, *54*, 1940.
- (90) Bigwood, M. P.; Corvan, P. J.; Zuckerman, J. J. *J. Am. Chem. Soc.* **1981**, *103*, 7643.

- (91) Grützmacher, H.; Freitag, S.; Herbst-Irmer, R.; Sheldrick, G. S. *Angew. Chem. Int. Ed. Engl.* **1992**, *31*, 437.
- (92) Asadi, A.; Eaborn, C.; Hill, M. S.; Hitchcock, P. B.; Meehan, M. M.; Smith, J. D. *Organometallics* **2002**, *21*, 2430.
- (93) Meyer, H.; Baum, G.; Massa, W.; Berger, S.; Berndt, A. *Angew. Chem. Int. Ed. Engl.* **1987**, *26*, 546.
- (94) Weidenbruch, M.; Kilian, H.; Stürmann, M.; Pohl, S.; Saak, W.; Marsmann, H.; Steiner, D.; Berndt, A. *J. Organomet. Chem.* **1997**, *530*, 255.
- (95) Kavara, A.; Cousineau, K. D.; Rohr, A. D.; Kampf, J. W.; Banaszak Holl, M. M. *Organometallics* **2008**, *27*, 1041.
- (96) Kavara, A.; Boron, T. T.; Ahsan, Z. S.; Banaszak Holl, M. M. *Organometallics* **2010**, *29*, 5033.
- (97) Kavara, A.; Kheir, M. M.; Kampf, J. W.; Banaszak Holl, M. M. *J. Inorg. Organomet. Polym.* **2014**, *24*, 250.
- (98) Schäfer, A.; Saak, W.; Haase, D.; Müller, T. *J. Am. Chem. Soc.* **2011**, *133*, 14562.
- (99) Yan, C.; Li, Z.; Xiao, X.-Q.; Wei, N.; Lu, Q.; Kira, M. *Angew. Chem. Int. Ed.* **2016**, *55*, 14784.
- (100) Phillips, A. D.; Wright, R. J.; Olmstead, M. M.; Power, P. P. *J. Am. Chem. Soc.* **2002**, *124*, 5930.
- (101) Richards, A. F.; Eichler, B. E.; Brynda, M.; Olmstead, M. M.; Power, P. P. *Angew. Chem. Int. Ed.* **2005**, *44*, 2546.
- (102) Rivard, E.; Power, P. P. *Dalton Trans.* **2008**, 4336.
- (103) Padelkova, Z.; Svec, P.; Pejchal, V.; Růžička, A. *Dalton Trans.* **2013**, *42*, 7660.
- (104) Freitag, S.; Krebs, K. M.; Henning, J.; Hirdler, J.; Schubert, H.; Wesemann, L. *Organometallics* **2013**, *32*, 6785.
- (105) Sindlinger, C. P.; Wesemann, L. *Chem. Sci.* **2014**, *5*, 2739.
- (106) Drost, C.; Hitchcock, P. B.; Lappert, M. F.; Pierssens, L. J.-M. *Chem. Commun.* **1997**, 1141.
- (107) Drost, C.; Hitchcock, P. B.; Lappert, M. F. *Organometallics* **1998**, *17*, 3838.
- (108) Freitag, S.; Henning, J.; Schubert, H.; Wesemann, L. *Angew. Chem. Int. Ed.* **2013**, *52*, 5640.
- (109) Schneider, J.; Krebs, K. M.; Freitag, S.; Eichele, K.; Schubert, H.; Wesemann, L. *Chem. Eur. J.* **2016**, *22*, 9812.
- (110) Schafer, A.; Weidenbruch, M.; Saak, W.; Pohl, S. *Chem. Commun.* **1995**, 1157.
- (111) Sindlinger, C. P.; Weiß, S.; Schubert, H.; Wesemann, L. *Angew. Chem. Int. Ed.* **2015**, *54*, 4087.
- (112) Kultyshev, R. G.; Prakash, G. K. S.; Olah, G. A.; Faller, J. W.; Parr, J. *Organometallics* **2004**, *23*, 3184.
- (113) Rekken, B. D.; Brown, T. M.; Fettingner, J. C.; Lips, F.; Tuononen, H. M.; Herber, R. H.; Power, P. P. *J. Am. Chem. Soc.* **2013**, *135*, 10134.
- (114) Veith, M. *Chem. Rev.* **1990**, *90*, 3.
- (115) Wang, L.; Rosca, S.-C.; Poirier, V.; Sinbandhit, S.; Dorcet, V.; Roisnel, T.; Carpentier, J.-F.; Sarazin, Y. *Dalton Trans.* **2014**, *43*, 4268.



- (116) Wang, L.; Poirier, V.; Ghiotto, F.; Bochmann, M.; Cannon, R. D.; Carpentier, J.-F.; Sarazin, Y. *Macromolecules* **2014**, *47*, 2574.
- (117) Dechy-Cabaret, O.; Martin-Vaca, B.; Bourissou, D. *Chem. Rev.* **2004**, *104*, 6147.
- (118) Dove, A. P.; Gibson, V. C.; Marshall, E. L.; Rzepa, H. S.; White, A. J. P.; Williams, D. J. *J. Am. Chem. Soc.* **2006**, *128*, 9834.
- (119) Knapp, C. E.; Carmalt, C. J. *Chem. Soc. Rev.* **2016**, *45*, 1036.
- (120) Ahmet, I. Y.; Hill, M. S.; Johnson, A. L.; Peter, L. M. *Chem. Mater.* **2015**, *27*, 7680.
- (121) Wildsmith, T.; Hill, M. S.; Johnson, A. L.; Kingsley, A. J.; Molloy, K. C. *Chem. Commun.* **2013**, *49*, 8773.
- (122) Kobayashi, S.; Iwata, S.; Abe, M.; Yajima, K.; Kim, H. J.; Shoda, S. *Makromol. Chem. Macromol. Symp.* **1992**, *54*, 225.
- (123) Asay, M.; Jones, C.; Driess, M. *Chem. Rev.* **2011**, *111*, 354.
- (124) Zabula, A. V.; Hahn, F. E. *Eur. J. Inorg. Chem.* **2008**, *33*, 5165.
- (125) Cabeza, J. A.; García-Álvarez, P.; Polo, D. *Eur. J. Inorg. Chem.* **2016**, *2016*, 10.
- (126) Álvarez-Rodríguez, L.; Cabeza, J. A.; García-Álvarez, P.; Polo, D. *Coord. Chem. Rev.* **2015**, *300*, 1.
- (127) Harris, D. H.; Lappert, M. F. *J. Chem. Soc., Chem. Comm.* **1974**, 895.
- (128) Veith, M. *Angew. Chem. Int. Ed. Engl.* **1987**, *26*, 1.
- (129) Ding, Y.; Roesky, H. W.; Noltemeyer, M.; Schmidt, H.-G.; Power, P. P. *Organometallics* **2001**, *20*, 1190.
- (130) Jana, A.; Roesky, H. W.; Schulzke, C.; Döring, A.; Beck, T.; Pal, A.; Herbst-Irmer, R. *Inorg. Chem.* **2009**, *48*, 193.
- (131) Jana, A.; Roesky, H. W.; Schulzke, C.; Samuel, P. P. *Inorg. Chem.* **2010**, *49*, 3461.
- (132) Gans-Eichler, T.; Gudat, D.; Nieger, M. *Angew. Chem. Int. Ed.* **2002**, *41*, 1888.
- (133) Marks, T. J.; Newman, A. R. *J. Am. Chem. Soc.* **1973**, *95*, 769.
- (134) Petz, W. *Chem. Rev.* **1986**, *86*, 1019.
- (135) Marks, T. J. *J. Am. Chem. Soc.* **1971**, *93*, 7090.
- (136) Al-Rafia, S. M. I.; Malcolm, A. C.; Liew, S. K.; Ferguson, M. J.; Rivard, E. *J. Am. Chem. Soc.* **2011**, *133*, 777.
- (137) Al-Rafia, S. M. I.; Shynkaruk, O.; McDonald, S. M.; Liew, S. K.; Ferguson, M. J.; McDonald, R.; Herber, R. H.; Rivard, E. *Inorg. Chem.* **2013**, *52*, 5581.
- (138) Swarnakar, A. K.; McDonald, S. M.; Deutsch, K. C.; Choi, P.; Ferguson, M. J.; McDonald, R.; Rivard, E. *Inorg. Chem.* **2014**, *53*, 8662.
- (139) Rivard, E. *Dalton Trans.* **2014**, *43*, 8577.
- (140) Zhao, L.; Hermann, M.; Jones, C.; Frenking, G. *Chem. Eur. J.* **2016**, *22*, 11728.
- (141) Wang, S.; McCrea-Hendrick, M. L.; Weinstein, C. M.; Caputo, C. A.; Hoppe, E.; Fetting, J. C.; Olmstead, M. M.; Power, P. P. *J. Am. Chem. Soc.* **2017**, *139*, 6596.
- (142) Maudrich, J.-J.; Sindlinger, C. P.; Aicher, F. S. W.; Eichele, K.; Schubert, H.; Wesemann, L. *Chem. Eur. J.* **2017**, *23*, 2192.
- (143) Sindlinger, C. P.; Grahneis, W.; Aicher, F. S. W.; Wesemann, L. *Chem. Eur. J.* **2016**, *22*, 7554.

- (144) Sindlinger, C. P.; Stasch, A.; Bettinger, H. F.; Wesemann, L. *Chem. Sci.* **2015**, *6*, 4737.
- (145) Sindlinger, C. P.; Aicher, F. S. W.; Wesemann, L. *Inorg. Chem.* **2017**, *56*, 548.
- (146) Sindlinger, C. P.; Wesemann, L. *Chem. Commun.* **2015**, *51*, 11421.
- (147) Pineda, L. W.; Jancik, V.; Starke, K.; Oswald, R. B.; Roesky, H. W. *Angew. Chem. Int. Ed.* **2006**, *45*, 2602.
- (148) Mandal, S. K.; Roesky, H. W. *Acc. Chem. Res.* **2011**, *45*, 298.
- (149) Jana, A.; Roesky, H. W.; Schulzke, C.; Döring, A. *Angew. Chem. Int. Ed.* **2009**, *48*, 1106.
- (150) Hadlington, T. J.; Hermann, M.; Frenking, G.; Jones, C. *Chem. Sci.* **2015**, *6*, 7249.
- (151) Hadlington, T. J.; Hermann, M.; Frenking, G.; Jones, C. *J. Am. Chem. Soc.* **2014**, *136*, 3028.
- (152) Hadlington, T. J.; Kefalidis, C. E.; Maron, L.; Jones, C. *ACS Catalysis* **2017**, *7*, 1853.
- (153) Becerra, R.; Boganov, S. E.; Egorov, M. P.; Faustov, V. I.; Krylova, I. V.; Nefedov, O. M.; Walsh, R. *J. Am. Chem. Soc.* **2002**, *124*, 7555.
- (154) Zhou, D.; Reiche, C.; Nag, M.; Soderquist, J. A.; Gaspar, P. P. *Organometallics* **2009**, *28*, 2595.
- (155) Gaspar, P. P. In *Reactive Intermediates, Vol. 3*; Jones, M., Jr., Moss, R. A., Eds.; John Wiley & Sons: New York, 1985; Vol. 3, p 333.
- (156) Gaspar, P. P.; West, R. In *The chemistry of organic silicon compounds, Vol. 2*; Rappoport, Z., Apeloig, Y., Eds.; John Wiley and Sons: New York, 1998; Vol. 2, p 2463.
- (157) Becerra, R.; Walsh, R. *Dalton Trans.* **2010**, *39*, 9217.
- (158) Krause, E.; Becker, R. *Ber. Deutsch. Chem. Ges.* **1920**, *53*, 173.
- (159) Kuivila, H. G.; Jakusik, E. R. *J. Org. Chem.* **1961**, *26*, 1430.
- (160) Neumann, W. P.; Burkhardt, G.; Heymann, E.; Kleiner, F.; König, K.; Niermann, H.; Pedain, J.; Schick, R.; Sommer, R.; Weller, H. *Angew. Chem. Int. Ed. Engl.* **1963**, *2*, 165.
- (161) Neumann, W. P.; König, K. *Angew. Chem. Int. Ed. Engl.* **1962**, *1*, 212.
- (162) Olson, D. H.; Rundle, R. E. *Inorg. Chem.* **1963**, *2*, 1310.
- (163) Neumann, W. P.; König, K. *J. Liebigs Ann. Chem.* **1964**, *677*, 1.
- (164) Neumann, W. P.; Schwarz, A. *Angew. Chem. Int. Ed. Engl.* **1975**, *14*, 812.
- (165) Grugel, C.; Neumann, W. P.; Seifert, P. *Tetrahedron Lett.* **1977**, *18*, 2205.
- (166) Grugel, C.; Neumann, W. P.; Schriewer, M. *Angew. Chem. Int. Ed. Engl.* **1979**, *18*, 543.
- (167) Gross, L. W.; Moser, R.; Neumann, W. P.; Scherping, K. H. *Tetrahedron Lett.* **1982**, *23*, 635.
- (168) Scherping, K. H.; Neumann, W. P. *Organometallics* **1982**, *1*, 1017.
- (169) Kozima, S.; Kobayashi, K.; Kawanisi, M. *Bull. Chem. Soc. Jpn.* **1976**, *49*, 2837.
- (170) Kobayashi, K.; Kunô, K.; Kawanisi, M.; Kozima, S. *Bull. Chem. Soc. Jpn.* **1977**, *50*, 1353.
- (171) Hawari, J. A.; Griller, D. *Organometallics* **1984**, *3*, 1123.
- (172) Neumann, W. P.; Schriewer, M. *Tetrahedron Lett.* **1980**, *21*, 3273.

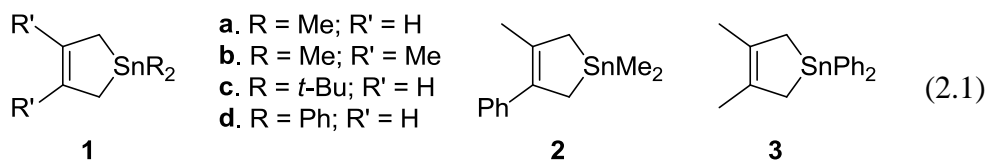
- (173) Ando, W.; Tsumuraya, T.; Sekiguchi, A. *Chem. Lett.* **1987**, *16*, 317.
- (174) Harrington, C. R.; Leigh, W. J.; Chan, B. K.; Gaspar, P. P.; Zhou, D. *Can. J. Chem.* **2005**, *83*, 1324.
- (175) Dewar, M. J. S.; Friedheim, J. E.; Grady, G. L. *Organometallics* **1985**, *4*, 1784.
- (176) Neale, N. R.; Tilley, T. D. *J. Am. Chem. Soc.* **2002**, *124*, 3802.
- (177) Sharma, H. K.; Miramontes, A.; Metta-Magaña, A. J.; Pannell, K. H. *Organometallics* **2011**, *30*, 4501.
- (178) Sharma, H. K.; Metta-Magaña, A.; Pannell, K. H. *Inorg. Chim. Acta* **2018**, *475*, 3.
- (179) Bleckmann, P.; Maly, H.; Minkwitz, R.; Neumann, W. P.; Watta, B.; Olbrich, G. *Tetrahedron Lett.* **1982**, *23*, 4655.
- (180) Watta, B.; Neumann, W. P.; Sauer, J. *Organometallics* **1985**, *4*, 1954.
- (181) Boganov, S. E.; Faustov, V. I.; Egorov, M. P.; Nefedov, O. M. *Russ. Chem. Bull. Int. Ed.* **2004**, *53*, 960.
- (182) Yamada, Y.; Kumagawa, T.; Yamada, Y. T.; Tominaga, T. *J. Radioanal. Nucl. Chem.* **1995**, *201*, 417.
- (183) Wang, X.; Andrews, L.; Chertihin, G. V.; Souter, P. F. *J. Phys. Chem. A* **2002**, *106*, 6302.
- (184) Cho, H.-G.; Andrews, L. *J. Phys. Chem. A* **2012**, *116*, 8500.
- (185) Hauge, R. H.; Hastie, J. W.; Margrave, J. L. *J. Mol. Spectrosc.* **1973**, *45*, 420.
- (186) Andrews, L.; Frederick, D. L. *J. Am. Chem. Soc.* **1970**, *92*, 775.
- (187) Meier, P. F.; Perry, D. L.; Hauge, R. H.; Margrave, J. L. *Inorg. Chem.* **1979**, *18*, 2051.
- (188) Tevault, D.; Nakamoto, K. *Inorg. Chem.* **1976**, *15*, 1282.
- (189) Boganov, S. E.; Egorov, M. P.; Nefedov, O. M. *Russ. Chem. Bull.* **1999**, *48*, 98.
- (190) Boganov, S. E.; Faustov, V. I.; Egorov, M. P.; Nefedov, O. M. *Russ. Chem. Bull.* **1994**, *43*, 47.
- (191) Boganov, S. E.; Faustov, Y. I.; Rudyak, S. G.; Egorov, M. P.; Nefedov, O. M. *Russ. Chem. Bull.* **1996**, *45*, 1061.
- (192) Boganov, S. E.; Faustov, V. I.; Egorov, M. P.; Nefedov, O. M. *Russ. Chem. Bull.* **1998**, *47*, 1054.
- (193) Nag, M.; Gaspar, P. P. *Organometallics* **2009**, *28*, 5612.
- (194) Sedlak, R.; Stasyuk, O. A.; Fonseca Guerra, C.; Řezáč, J.; Růžička, A.; Hobza, P. *J. Chem. Theor. Comp.* **2016**, *12*, 1696.
- (195) Boatz, J. A.; Gordon, M. S.; Sita, L. R. *J. Phys. Chem.* **1990**, *94*, 5488.
- (196) Schoeller, W. W.; Schneider, R. *Chem. Ber.* **1997**, *130*, 1013.
- (197) Su, M. D. *J. Phys. Chem. A* **2002**, *106*, 9563.
- (198) Oláh, J.; De Proft, F.; Veszprémi, T.; Geerlings, P. *J. Phys. Chem. A* **2004**, *108*, 490.
- (199) Tsai, M.-L.; Su, M.-D. *J. Phys. Chem. A* **2006**, *110*, 6216.
- (200) Lan, C.-Y.; Su, M.-D. *J. Phys. Chem. A* **2007**, *111*, 6232.
- (201) Olbrich, G. *Chem. Phys. Lett.* **1980**, *73*, 110.
- (202) Fjeldberg, T.; Haaland, A.; Schilling, B. E. R.; Volden, H. V.; Lappert, M. F.; Thorne, A. J. *J. Organomet. Chem.* **1985**, *280*, c43.

- (203) Bundhun, A.; Ramasami, P.; Gaspar, P. P.; Schaefer, H. F. *Inorg. Chem.* **2012**, *51*, 851.
- (204) Broeckert, L.; Frenking, G.; Geerlings, P.; De Proft, F. *ChemPhysChem* **2013**, *14*, 3233.
- (205) Bundhun, A.; Momeni, M. R.; Shakib, F. A.; Ramasami, P.; Gaspar, P. P.; Schaefer III, H. F. *RSC Advances* **2016**, *6*, 53749.
- (206) Su, M.-D. *J. Phys. Chem. B* **2005**, *109*, 21647.
- (207) Boganov, S. E.; Promyslov, V. M.; Faustov, V. I.; Egorov, M. P.; Nefedov, O. M. *Russ. Chem. Bull.* **2011**, *60*, 2147.
- (208) Scaiano, J. C. In *Reactive Intermediate Chemistry*; Moss, R. A., Platz, M. S., Jones, M., Jr., Eds.; John Wiley & Sons, Inc.: New York, 2004, p 847.
- (209) Moiseev, A. G.; Coulais, E.; Leigh, W. J. *Chem. Eur. J.* **2009**, *15*, 8485.
- (210) Moiseev, A. G.; Leigh, W. J. *J. Am. Chem. Soc.* **2006**, *128*, 14442.
- (211) Moiseev, A. G.; Leigh, W. J. *Organometallics* **2007**, *26*, 6268.
- (212) Leigh, W. J.; Harrington, C. R.; Vargas-Baca, I. *J. Am. Chem. Soc.* **2004**, *126*, 16105.
- (213) Leigh, W. J.; Lollmahomed, F.; Harrington, C. R. *Organometallics* **2006**, *25*, 2055.
- (214) Leigh, W. J.; Dumbrava, I. G.; Lollmahomed, F. *Can. J. Chem.* **2006**, *84*, 934.
- (215) Leigh, W. J.; Harrington, C. R. *J. Am. Chem. Soc.* **2005**, *127*, 5084.
- (216) Toltl, N. P.; Leigh, W. J.; Kollegger, G. M.; Stibbs, W. G.; Baines, K. M. *Organometallics* **1996**, *15*, 3732.
- (217) Leigh, W. J.; Lollmahomed, F.; Harrington, C. R.; McDonald, J. M. *Organometallics* **2006**, *25*, 5424.
- (218) Huck, L. A.; Leigh, W. J. *Organometallics* **2007**, *26*, 1339.
- (219) Moiseev, A. G.; Leigh, W. J. *Organometallics* **2007**, *26*, 6277.
- (220) Lollmahomed, F.; Huck, L. A.; Harrington, C. R.; Chitnis, S. S.; Leigh, W. J. *Organometallics* **2009**, *28*, 1484.
- (221) Huck, L. A.; Leigh, W. J. *Organometallics* **2009**, *28*, 6777.
- (222) Leigh, W. J.; Kostina, S. S.; Bhattacharya, A.; Moiseev, A. G. *Organometallics* **2010**, *29*, 662.
- (223) Huck, L. A.; Leigh, W. J. *Can. J. Chem.* **2011**, *89*, 241.
- (224) Kostina, S. S.; Leigh, W. J. *J. Am. Chem. Soc.* **2011**, *133*, 4377.
- (225) Kostina, S. S.; Singh, T.; Leigh, W. J. *J. Phys. Org. Chem.* **2011**, *24*, 937.
- (226) Kostina, S. S.; Singh, T.; Leigh, W. J. *Organometallics* **2012**, *31*, 3755.
- (227) Kostina, S. S.; Leigh, W. J. *Can. J. Chem.* **2014**, *93*, 435.
- (228) Leigh, W. J.; Huck, L. A.; Held, E.; Harrington, C. R. *Silicon Chem.* **2005**, *3*, 139.

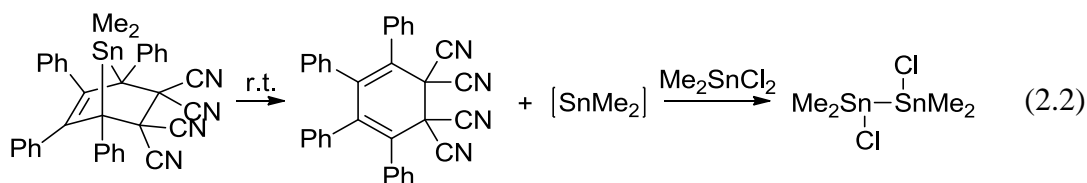
## Chapter 2: Direct Detection, Dimerization and Chemical Trapping of Dimethyl- and Diphenylstannylene from Photolysis of Stannacyclopent-3-enes in Solution

### 2.1. Overview

The preparation and thermal chemistry of stannacyclopent-3-enes (**1a-d**) was described by Gaspar and coworkers:<sup>1</sup> the pyrolysis of **1a,b** afforded cyclic oligomers  $(\text{SnMe}_2)_n$  ( $n = 5 - 8$ ), while **1d** afforded insoluble oligomers of  $\text{SnPh}_2$ . Such compounds have also been shown to be potentially suitable for photochemical studies, as **1b** was used to detect  $\text{SnMe}_2$  directly in hydrocarbon solution using 193 nm laser flash photolysis.<sup>2</sup> In this chapter, stannacyclopent-3-enes **2** and **3** have been synthesized and used to directly detect  $\text{SnMe}_2$  and  $\text{SnPh}_2$ , respectively, and study their dimerization behaviour in hydrocarbon solution at room temperature.

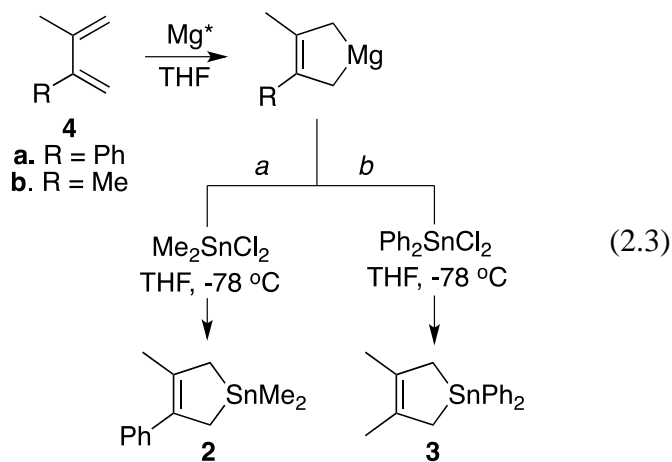


We next studied the reactions of  $\text{SnMe}_2$  and  $\text{SnPh}_2$  with  $\text{Me}_2\text{SnCl}_2$  in the presence and absence of oxygen. The Sn-Cl insertion reaction of  $\text{SnMe}_2$  with this substrate has been investigated previously by Neumann and coworkers<sup>3</sup> (eq. 2.2), and later investigated computationally by Dewar.<sup>4</sup> The main goal of this part of the work was to show through chemical trapping experiments that photolysis of **2** and **3** results in the extrusion of the desired stannylenes, to measure the quantum yields of the extrusion process, and to support the assignments made in the flash photolysis studies.



## 2.2. Results and Discussion

Compounds **2** and **3** were prepared by reaction of the magnesium complexes of 2-methyl-3-phenyl-1,3-butadiene (**4a**) and 2,3-dimethyl-1,3-butadiene (**4b**), respectively, with the appropriate dichlorostannane ( $\text{Me}_2\text{SnCl}_2$  for **2** and  $\text{Ph}_2\text{SnCl}_2$  for **3**; see equation 2.3), using procedures adapted from those reported by Gaspar and coworkers.<sup>1</sup> The two compounds were obtained in overall (crude) yields of 30-50%, and were each purified by repeated distillation and/or column chromatography to  $\geq 98\%$  purity (as estimated by  $^1\text{H}$  NMR spectroscopy) prior to being used in photochemical experiments.

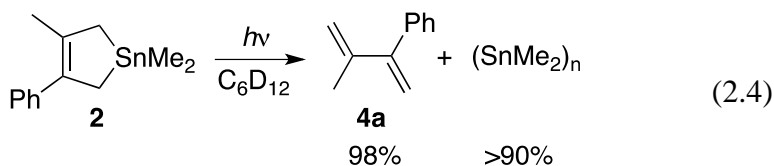


### 2.2.1. Stannacyclopent-3-ene Photochemistry – Trapping of Transient Stannylenes

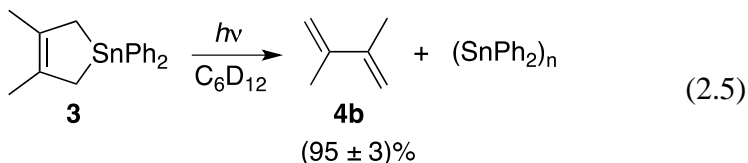
Steady state photolysis experiments were carried out in quartz NMR tubes with low pressure mercury lamps (254 nm), on  $\text{C}_6\text{D}_{12}$  solutions of **2** and **3** (ca. 0.04 M) containing  $\text{Si}_2\text{Me}_6$  as internal standard, both alone and in the presence of 0.03-0.04 M  $\text{Me}_2\text{SnCl}_2$ . Neumann and coworkers identified this stannane reagent as an efficient substrate for  $\text{SnMe}_2$ , with which it reacts via formal Sn-Cl bond insertion to afford the corresponding 1,2-dichlorodistannane (**5**) as the primary product.<sup>3</sup> Although  $\text{Me}_2\text{SnCl}_2$  has limited solubility in cyclohexane, it has the advantage of being transparent at 254 nm, unlike most of the other potential stannylenes substrates that earlier studies suggested might be useful as trapping agents.<sup>1,5,6</sup> The photolyses were monitored at selected time intervals

throughout the photolysis by  $^1\text{H}$  NMR spectroscopy, and taken to a maximum conversion of ca. 25% in stannacyclopentene (**2** or **3**); product yields were calculated from the initial slopes of concentration versus time plots for the various products relative to the initial slopes of the corresponding plots for **2** or **3**. The peaks used to calculate concentrations for **2** ( $\delta_{\text{H}}$  7.04) and **3** ( $\delta_{\text{H}}$  7.21) are indicated in the parenthesis. This was supplemented with the  $^{119}\text{Sn}\{^1\text{H}\}$  NMR spectra of the photolyzed mixtures at the end of each experiment, to further aid in product identification. Most photolyses were carried out both with and without deaeration of the solution prior to photolysis, as the presence of air led to significantly higher photolysis rates (particularly with **3**) owing to oxidation of the primary tin-containing (distannane) photoproducts to the corresponding distannoxanes, which (in contrast to the distannanes) are non-absorbing and/or non-photoreactive under the conditions of our experiments.

Steady state photolysis of **2** as a deaerated 0.04 M solution in cyclohexane- $d_{12}$  led to the efficient consumption of the stannacyclopentene and the formation of diene **4a**, in addition to a collection of compounds exhibiting  $^1\text{H}$  and  $^{119}\text{Sn}$  NMR resonances in the ranges characteristic of  $[\text{SnMe}_2]_n$  oligomers ( $\delta_{\text{H}}$  0.35 - 0.46 (m);  $\delta_{\text{Sn}}$  -242.0, -245.6, -243.8) (Fig. S2.1).<sup>1,7</sup> Exposure of the photolyzed solution to air resulted in the formation of a colorless precipitate, as expected for these materials.<sup>1,7</sup> Chemical yields of  $(89 \pm 5)\%$  and  $(98 \pm 5)\%$  for the major  $[\text{SnMe}_2]_n$  oligomer and diene **4a**, respectively, were determined from the relative slopes of the concentration versus time plots for the products relative to consumed **2** (eq. 2.4; Figure S2.2).



In contrast, photolysis of a deaerated solution of **3** in  $C_6D_{12}$  under similar conditions resulted in the immediate precipitation of a solid and the development of a yellow color that deepened with continued irradiation.  $^1H$  NMR spectra of the mixture (Fig. S2.3) indicated that **3** was consumed with the concomitant formation of diene **4b** and small amounts of at least three compounds (one at  $\delta_H$  6.91, another at  $\delta_H$  6.96 and 7.29, and a third characterized by a broadening of the  $^1H$  NMR spectrum between  $\delta_H$  6.6 - 7.5) whose spectral characteristics and reactivity are consistent with  $(SnPh_2)_n$  oligomers (eq. 2.5). Two of the three product-derived multiplets (at  $\delta_H$  6.96 and 7.29) that were present in the aromatic region of the NMR spectrum of the photolyzate (Fig. S2.3) disappeared after allowing the solution to stand for 18 h in the dark, most likely due to oxidation resulting from gradual contact with air. The multiplet that remained (at  $\delta_H$  6.91), was identified as due to dodecaphenylcyclohexastannane ( $c-Sn_6Ph_{12}$ ), by spiking the mixture (in benzene- $d_6$ ) with an authentic sample. The concentration versus time plot for this compound (Fig. S2.4a) exhibits positive curvature, consistent with it being derived (at least partially) from secondary photolysis; the initial slope of the plot indicates an upper limit of ca. 10% for the chemical yield relative to consumed **3** (on a per- $SnPh_2$  unit basis). The consumption of **3** and formation of **4b** proceeded faster upon irradiation of an air-saturated solution under similar conditions (Figure S2.4b), as did the precipitation of insoluble material, and the solution remained colorless throughout the photolysis up to ca. 8% conversion of **3**. No other products could be detected (by NMR) under the conditions employed for the analysis.



Photolysis of a deaerated 0.04 M solution of **2** in  $C_6D_{12}$  containing  $Me_2SnCl_2$  (0.033 M) resulted in the consumption of **2** and the formation of **4a** ( $98 \pm 9\%$ ) along with three



major tin-containing products (eq. 2.6), which were identified as 1,2-dichlorotetramethyldistannane (**5**,  $\delta_{\text{H}}$  0.807,  $\delta_{\text{Sn}}$  99.2 ( $^2J_{\text{SnH}} = 53.5$  Hz,  $^3J_{\text{SnH}} = 13.0$  Hz);  $51 \pm 6\%$ ),<sup>8,9</sup> the association dimer of 1,2-dichlorotetramethyldistannoxane (**6**,  $\delta_{\text{H}}$  1.05 and 1.14;  $\delta_{\text{Sn}}$  -63.3 and -125.4;  $39 \pm 6\%$ ),<sup>39,40</sup> and chlorotrimethylstannane (**7**,  $\delta_{\text{H}}$  0.524;  $9 \pm 2\%$ ); Figure S2.5 shows  $^1\text{H}$  NMR spectra of the mixture before and after photolysis to ca. 20% conversion of **2**. Concentration versus time plots for **2**, **4a**, and **5-7** are shown in Figure 2.1; that for **7** exhibits upward curvature, consistent with it being formed as a secondary photolysis product of distannane **5**.<sup>3</sup> Compound **6** is ascribed to oxidation of **5** by residual oxygen in the solvent.<sup>10-12</sup>

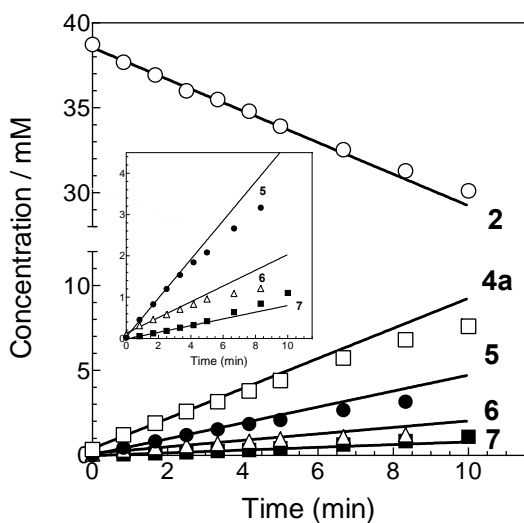
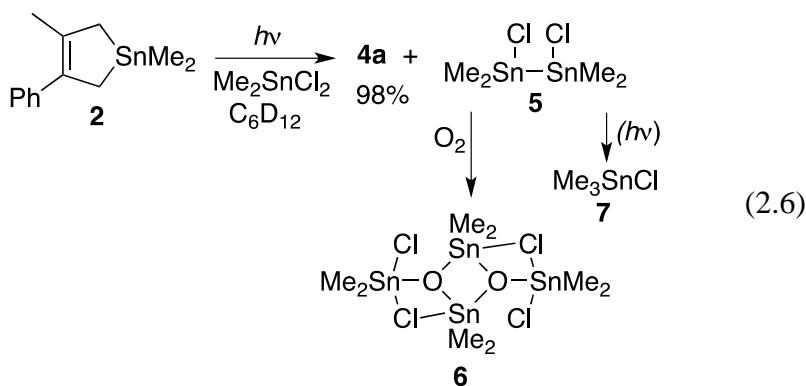


**Figure 2.1.** Concentration versus time plots for the photolysis of a deaerated 0.04 M solution of **2** in  $\text{C}_6\text{D}_{12}$  containing  $\text{Me}_2\text{SnCl}_2$  (0.031 M). The initial slopes, determined from the first five data points in each of the plots, of the plots for the various components of the reaction mixture are: **2**,  $-0.93 \pm 0.09$ ;  $\text{Me}_2\text{SnCl}_2$  (not shown),  $-0.89 \pm 0.07$ ; **4a**,  $0.89 \pm 0.07$ ; **5** ( $\text{ClMe}_2\text{SnSnMe}_2\text{Cl}$ ),  $0.47 \pm 0.03$ ; **6** ( $\text{ClMe}_2\text{SnOSnMe}_2\text{Cl}$ )<sub>2</sub>,  $0.19 \pm 0.04$ ; **7** ( $\text{Me}_3\text{SnCl}$ ),  $0.08 \pm 0.01$  (units,  $\text{mM min}^{-1}$ ). The inset shows an expansion of the plots for **5**, **6**, and **7**.



Indeed, photolysis of an undeaerated solution of **2** and  $\text{Me}_2\text{SnCl}_2$  in  $\text{C}_6\text{D}_{12}$  produced **4a** and **6** in close to quantitative yields, and only trace amounts of **5** and **7** during the initial few minutes of irradiation. Upon continued photolysis the formation of **6** slowed significantly and was supplanted by the formation of **5** and **7**, which proceeded at a combined total rate roughly equal to the initial rate of formation of **6**. The concentration versus time plots from the experiment are shown in Figure 2.2; it should be noted that the break-points in the plots for the three tin-containing products (see inset) occurs at the point where the concentration of **6** is roughly 80% of the (initial) oxygen concentration in air-saturated cyclohexane (ca.  $2.4 \text{ mM}^{13}$ ). The presence of air caused a barely significant increase in the initial rates of photolysis of **2** and formation of **4a** compared to those in deaerated solution, which allows the conclusion that  $\text{O}_2$  (at a concentration of ca. 3 mM or less) interacts only with the primary photoproducts and does not interact with the reactive excited state of the stannacyclopentene (**2**).

Photolysis of an undeaerated 0.04 M solution of **3** in  $\text{C}_6\text{D}_{12}$  containing  $\text{Me}_2\text{SnCl}_2$  (0.037 M) afforded diene **4b**,  $\text{Ph}_2\text{SnCl}_2$  (**8**), and distannoxane dimer **6** as the major products at low (< 6%) conversions of **3** (eq. 2.7); Fig. S2.6 shows representative  $^1\text{H}$  NMR spectra recorded throughout the photolysis, while the concentration versus time plots from which the initial yields were calculated are shown in Fig. 2.3.

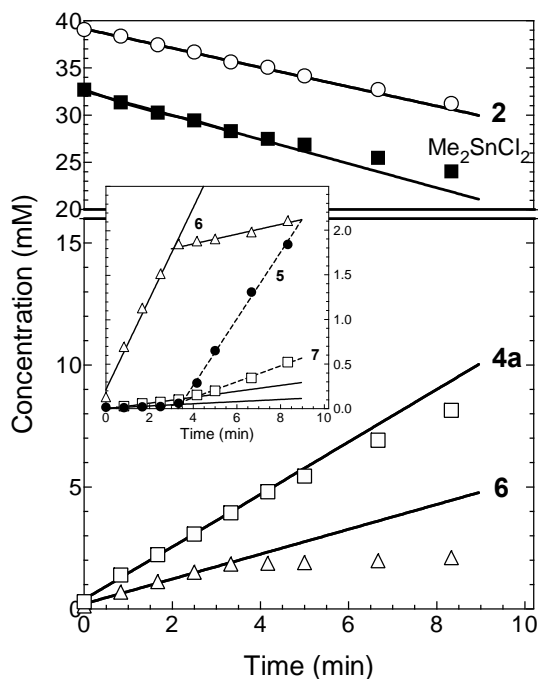


**Figure 2.2.** Concentration versus time plots for the photolysis of a solution of **2** (ca. 0.04 M) and Me<sub>2</sub>SnCl<sub>2</sub> (0.033 M) in C<sub>6</sub>D<sub>12</sub>, which was saturated with air prior to irradiation. The inset shows an expanded plot, detailing the formation of dichlorodistannane **5**, distannoxane dimer **6**, and Me<sub>3</sub>SnCl (**7**) with photolysis time. The initial slopes, determined from the first five data points in each of the plots, are (in units of mM min<sup>-1</sup>): **2**,  $-1.02 \pm 0.04$ ; Me<sub>2</sub>SnCl<sub>2</sub>,  $-1.28 \pm 0.06$ ; **4a**,  $1.08 \pm 0.04$ ; **5**,  $0.012 \pm 0.005$ ; **6**,  $0.51 \pm 0.03$  (< 4 min); **7**,  $0.033 \pm 0.003$  (< 4 min). The slopes of the second half (> 4 min) of the plots for **5-7** are: **5**,  $0.37 \pm 0.02$ ; **6**,  $0.055 \pm 0.007$ ; **7**,  $0.10 \pm 0.01$ .

The plots exhibit good linearity over the first 2.5 minutes of photolysis, and also reveal that the consumption of Me<sub>2</sub>SnCl<sub>2</sub> proceeds at roughly twice the rate of consumption of **3** during the initial (2.5 minute) photolysis period, as expected considering that **6** is a major product of the reaction. Continuation of the photolysis past ca. 5% conversion of **3** – and the point where the O<sub>2</sub> concentration had been reduced by 80-90% from its initial level (*vide supra*) – resulted in significant yellowing of the solution, sharp downward curvature in the concentration versus time plots for **4b**, **6**, and **8**, and the enhanced growth of several of the minor product resonances in the <sup>1</sup>H NMR spectra. One of the minor product peaks was a singlet at  $\delta$  0.90, which we assign tentatively to 1,2-dichlorodistannane **9**, the expected primary product of insertion of SnPh<sub>2</sub> into a Sn-Cl bond of the substrate.

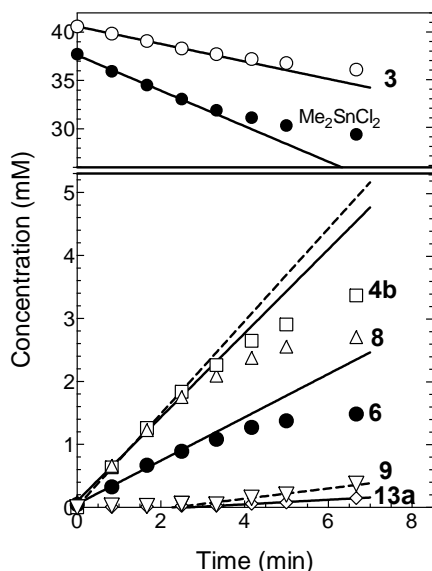
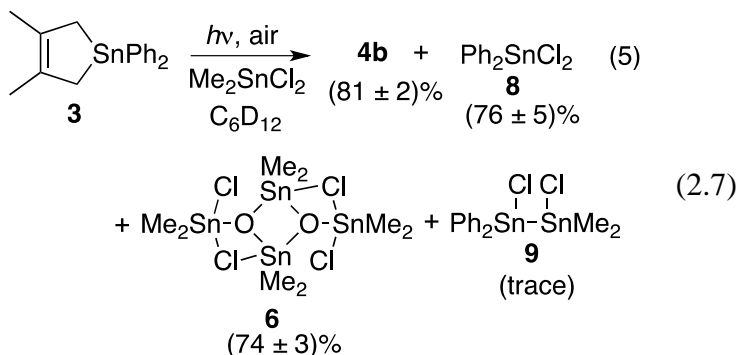
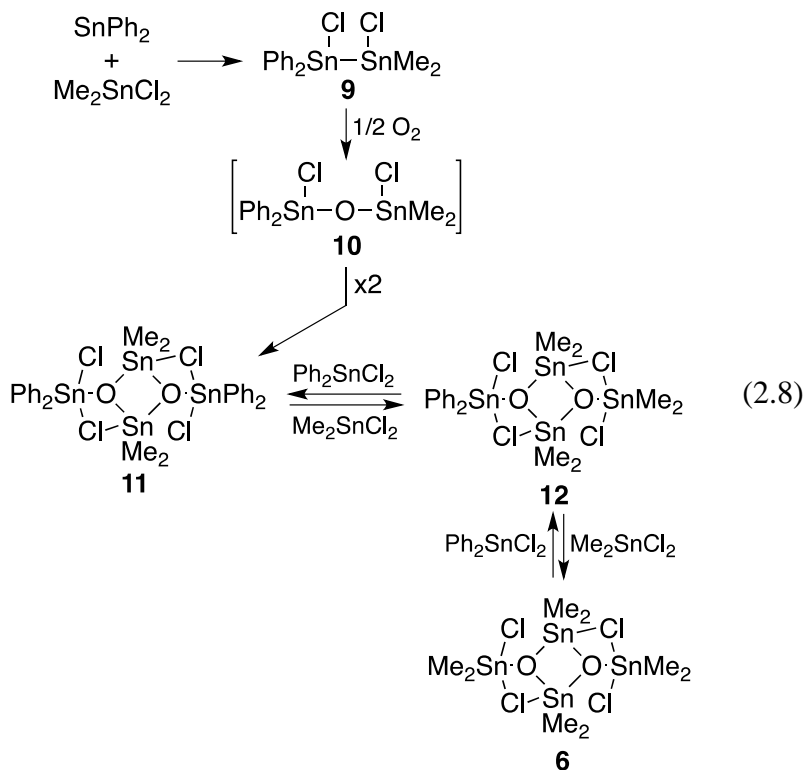


**Figure 2.3.** Concentration versus time plots for the photolysis of an undeaerated 0.04 M solution of **3** in  $C_6D_{12}$  containing 0.037 M  $Me_2SnCl_2$ . The initial ( $\leq 2.5$  min) slopes of the plots (in  $mM\ min^{-1}$ ) are: **3**,  $-0.91 \pm 0.01$ ;  $Me_2SnCl_2$ ,  $-1.84 \pm 0.07$ ; **4b**,  $0.74 \pm 0.01$ ; **8**,  $0.69 \pm 0.04$ ; **6**,  $0.34 \pm 0.02$ ; **9** ( $\geq 3.3$  min),  $0.08 \pm 0.04$ ; **13a** ( $\geq 3.3$  min),  $0.036 \pm 0.003$ . No attempt was made to replenish the air in the photolyzate as the experiment proceeded.



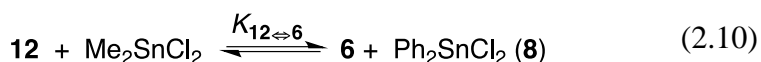
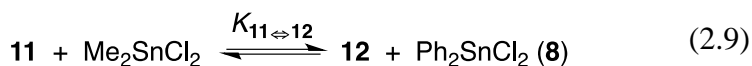
A reasonable mechanism for the formation of **6** and **8** in this experiment involves air-oxidation of 1,2-dichlorodistannane **9** to afford the corresponding 1,3-dichlorodistannoxane (**10**), which dimerizes to the corresponding association dimer (**11**) and then liberates **8** by exchange with excess  $Me_2SnCl_2$  (eq. 2.8); exchange processes in compounds of this type are known to proceed rapidly in solution at ambient temperatures.<sup>14,15</sup> Assuming that the equilibration of **6**, **11**, and the intermediate cyclodistannoxane (**12**) is rapid and that the three species have similar thermodynamic stabilities under the conditions of our experiments, then the mechanism predicts that the mixed dimer (**12**) should be present at 10-20% the concentration of **6** at the highest conversion (of **3**) examined, where **6**, **8** and  $Me_2SnCl_2$  are present at concentrations of ca.

1.5, 2.7, and 29 mM, respectively (see Fig. 2.3). Indeed, the  $^1\text{H}$  NMR spectrum of the photolyzed mixture shows a weak doublet at  $\delta$  8.09 (Fig. S2.6c), which is consistent with the presence of **12** as a minor component in the photolyzate;<sup>16</sup> integration of the spectrum indicates that **12** and **6** are present in relative concentrations of  $[\mathbf{12}]:[\mathbf{6}] = 0.14 \pm 0.02$ . Addition of aliquots of  $\text{Ph}_2\text{SnCl}_2$  (**8**) to the photolyzate caused an increase in the relative intensity of a weaker doublet at  $\delta$  8.06 (relative to the  $\delta$  8.09 doublet), which has been tentatively assigned to cyclodistannoxane **11**, formed by exchange of **8** with the exocyclic  $\text{Me}_2\text{SnCl}_2$  moiety in **12**.



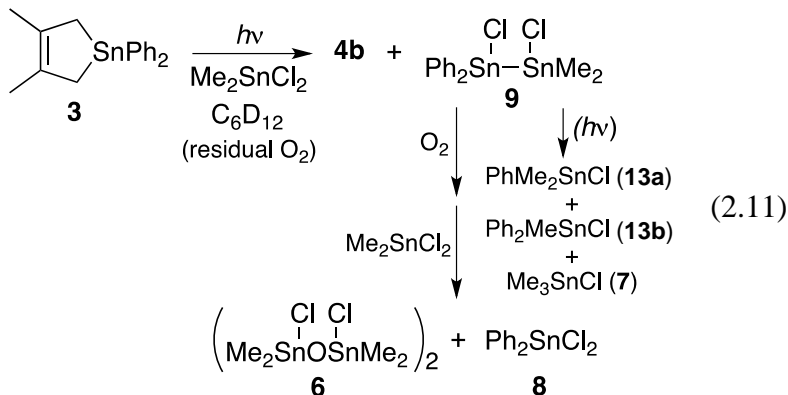
Additional support for these assignments was obtained by analysis of the  $^1\text{H}$  NMR spectra of a series of mixtures of  $\text{Me}_2\text{SnCl}_2$ , **8**, and authentic **6** in  $\text{CDCl}_3$  solution. These spectra also showed two doublets in the aromatic region assignable to **11** ( $\delta$  8.03) and **12** ( $\delta$  8.06), in relative intensities (i.e. **11**:**12**) that increased as the  $[\mathbf{8}]:[\text{Me}_2\text{SnCl}_2]$  ratio was increased (see Supporting Information). Analysis of the compositions of four different

synthetic mixtures according to the expressions for the equilibrium constants for interconversion of **11**, **12** and **6** (equations 2.9 and 2.10) afforded values of  $K_{12\leftrightarrow 6} = 0.46 \pm 0.03$  and  $K_{11\leftrightarrow 12} = 0.81 \pm 0.14$  in  $\text{CDCl}_3$  at 22 °C (see Figure S2.7). The values predict that at the highest conversion of **3** achieved in the photolysis with 0.037 M  $\text{Me}_2\text{SnCl}_2$  in undeaerated  $\text{C}_6\text{D}_{12}$  (Fig. 2.3), cyclodistannoxanes **6** and **12** should be present in the ratio  $[\mathbf{12}]:[\mathbf{6}] \approx 0.11$ , given the relative concentrations of **8** and  $\text{Me}_2\text{SnCl}_2$  at this point ( $[\text{Me}_2\text{SnCl}_2]:[\mathbf{8}] \approx 10.7$ ) and assuming a negligible solvent effect on the equilibrium constants. Considering the uncertainties, the estimate is in reasonable agreement with the value determined from the  $^1\text{H}$  NMR spectrum of the photolyzate.

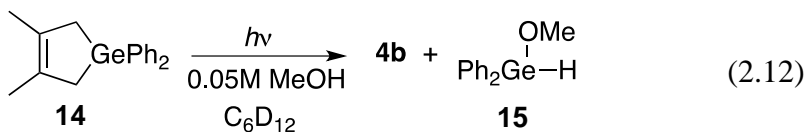


Photolysis of a deaerated<sup>17</sup> solution of **3** in  $\text{C}_6\text{D}_{12}$  containing  $\text{Me}_2\text{SnCl}_2$  (0.035 M) resulted in rapid yellowing of the solution and the appearance of the singlet at  $\delta$  0.90 assigned above to distannane **9** (Fig. S2.8), which was the major Sn-containing product over the first 3% conversion of **3**. It was formed in an estimated yield of  $(42 \pm 10)$  % along with diene **4b** (ca. 79%), **6** (ca. 24%), and **8** (ca. 25%) (eq. 2.11), based on the relative slopes of the concentration versus time plots between 0 and 3% conversion of **3** (Fig. S2.9). At conversions >3% the plot for **9** curved sharply downward while those for **7** and several minor Sn-containing products increased sharply, indicating that secondary photolysis of **9** competes with the primary photolysis of **3** as the former builds up in solution. Two of the minor products were identified as  $\text{Me}_2\text{PhSnCl}$  (**13a**,  $\delta_{\text{H}}$  0.69; 8%) and  $\text{MePh}_2\text{SnCl}$  (**13b**,  $\delta_{\text{H}}$  0.84; 5%) on the basis of their  $^1\text{H}$  NMR spectra (Fig. S2.8),<sup>18,19</sup> while **7** (3.5%) was identified by comparison with an authentic sample. These compounds, along with  $(\text{SnMe}_2)_n$  oligomers (which were also tentatively identified in the spectrum;

see Fig. S2.8) and a portion of the amount of **8** that is formed, are the products expected from photolysis of diaryldistannane **9**, which can be expected to absorb quite strongly at 254 nm.<sup>20</sup> The formation of **6** and the majority of **8** that is formed can be ascribed to incomplete deaeration of the solution prior to photolysis.



Quantum yields for the formation of **6** from photolysis of **2** and **3** as air-saturated, 0.04 M solutions in C<sub>6</sub>D<sub>12</sub> containing 0.03-0.04 M Me<sub>2</sub>SnCl<sub>2</sub> were determined using the photolysis of 3,4-dimethyl-1,1-diphenylgermacyclopent-3-ene **14** ( $\Phi_{\text{GePh}_2} = 0.55 \pm 0.07$  in methanolic C<sub>6</sub>D<sub>12</sub>;<sup>21</sup> equation 2.12) as an actinometer. The values obtained for **2** ( $\Phi_{\text{SnMe}_2} = 0.78 \pm 0.10$ ) and **3** ( $\Phi_{\text{SnPh}_2} = 0.61 \pm 0.09$ ) were calculated from the initial slopes ( $\times 2$ ) of the concentration versus time plots for **6** relative to that of **15** from the photolysis of the actinometer (Fig S2.10). In the case of **3**, the value of  $\Phi_{\text{SnPh}_2}$  obtained is the same regardless of which of the two major Sn-containing products (**6** or **8**) is used for the calculation, as expected (Fig. S2.10b).



### 2.2.2. Direct Detection of Transient Stannylenes by Laser Flash Photolysis

Laser flash photolysis experiments were carried out with rapidly flowed, deoxygenated solutions of **2** and **3** in anhydrous hexanes, using the pulses from a KrF

excimer laser (248 nm, 95-105 mJ, ca. 25 ns) for excitation. In both cases laser photolysis gave rise to readily detectable transient absorptions throughout the 270 - 600 nm spectral range, one set of absorptions that were formed during the laser pulse (and are thus assignable to a primary photoproduct), and a second set that grew in concomitantly with the decay of the primary absorptions, and are thus assignable to secondary products formed via (ground state) reaction of the primary transient; with **2**, the decay of the secondary products was accompanied by the growth of a third set of absorptions, as we found in the earlier study with **1b** as SnMe<sub>2</sub>-precursor.<sup>2</sup> In both cases, but particularly with **3**, the quality of the signals tended to degrade steadily throughout the course of an experiment due to the gradual appearance of periodic spikes in the absorbance versus time profiles. These result from the build-up of particulate material on the inner walls of the sample cell, which worsens as the experiment progresses.<sup>22</sup> They did not interfere with the recording of transient UV-vis spectra, and did not compromise the determination of decay rate coefficients from the absorbance versus time profiles, provided that data acquisition was limited to timescales of 4 μs (full-scale) or greater.

The decay of the prompt absorption produced upon laser photolysis of **2** (monitored at 540 nm to avoid overlap with the secondary absorption) was found to proceed with clean second order kinetics and rate coefficient  $2k/\epsilon_{540} = (3.0 \pm 0.3) \times 10^7$  cm s<sup>-1</sup> (obtained by fitting the absorbance-time plot of the prompt absorption at 540 nm to eq. 2.13), in good agreement with the value reported in the earlier solution phase study.<sup>2</sup>

$$\Delta A_t = \Delta A_0 / (1 + (2k_{\text{dim}}\Delta A_0 / \epsilon l)t) \quad (2.13)$$

Figure 2.4a shows representative transient absorption spectra and absorbance-time profiles obtained with this compound. As in the earlier work, we assign the prompt absorption to SnMe<sub>2</sub>, the secondary absorption centred at  $\lambda_{\text{max}} \approx 465$  nm to



tetramethyldistannene ( $\text{Me}_2\text{Sn}=\text{SnMe}_2$ , **16a**), and the tertiary absorption below 320 nm to a product of further reaction of the distannene.<sup>2</sup> The apparent  $\lambda_{\text{max}}$ -value of 490 nm for  $\text{SnMe}_2$  is in acceptable agreement with the earlier-reported value ( $\lambda_{\text{max}} = 500$  nm), the apparent blue shift occurring most likely because the higher transient concentrations achieved in the present work result in faster second order decays, which compromises our ability to isolate temporally the spectrum of the prompt transient from that of the dimerization product (**16a**). The value of  $\lambda_{\text{max}} = 465$  nm observed in the present work for the absorption maximum of the latter species, and the timescale over which it decays, are also in good agreement with the previously reported data.<sup>2</sup>

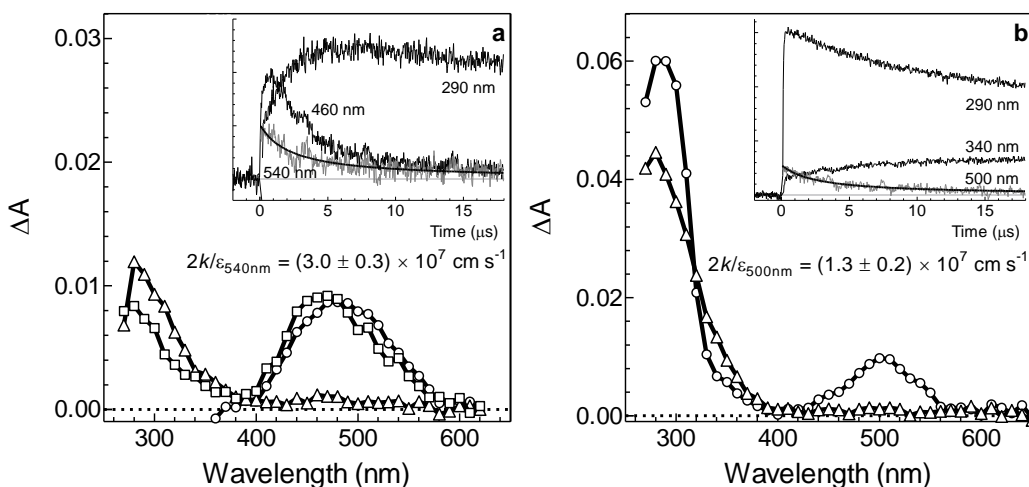
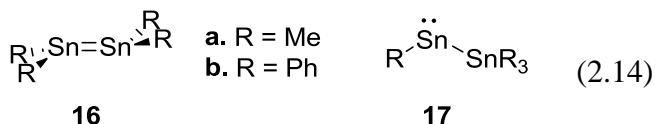


**Figure 2.4.** (a) Transient UV-vis absorption spectra from laser flash photolysis of rapidly flowed solutions of (a) **2** ( $2 \times 10^{-4}$  M) and (b) **3** ( $7 \times 10^{-4}$  M) in anhydrous hexanes at 25 °C. The spectra in (a) were recorded 0.10 - 0.26  $\mu\text{s}$  (○), 1.06 - 1.15  $\mu\text{s}$  (□) and 17.2 - 17.3  $\mu\text{s}$  (Δ) after the laser pulse, while those in (b) were recorded 0.42 - 0.51  $\mu\text{s}$  (○) and 17.1 - 17.3  $\mu\text{s}$  (Δ) after the pulse; the insets show absorbance versus time profiles recorded at selected wavelengths in the two spectra. The spectra in (a) were recorded at reduced laser intensity in order to maximize the temporal resolution between the primary and secondary product spectra.



Laser photolysis of **3** also led to at least two sequentially formed transient products. The initially-formed species exhibits absorption bands centred at  $\lambda_{\text{max}} = 300$  nm and 505 nm that decay together over ca. 20  $\mu\text{s}$ , leaving behind a longer-lived species exhibiting a broad absorption with  $\lambda_{\text{max}} < 280$  nm, and tailing out to ca. 400 nm (Figure 2.4b). The 505 nm species (monitored at 500 nm) decays with clean second order kinetics and rate coefficient  $2k/\epsilon_{500} = (1.3 \pm 0.2) \times 10^7 \text{ cm s}^{-1}$ , consistent with dimerization as the main mode of decay, and we thus assign it to  $\text{SnPh}_2$ . Notably, the absorption maximum of the species is blue-shifted compared to those of the sterically hindered diarylstannylenes that have been reported,<sup>23-27</sup> which is a feature that is also shared by diarylsilylene and –germylene systems.<sup>21,28-30</sup> An absorbance versus time profile recorded at 340 nm, on the long wavelength tail of the broad 280 nm absorption, consists of a growth that occurs over a similar timescale as the decay of the 505 nm  $\text{SnPh}_2$ -absorption (Fig. 2.4b), suggesting it is associated with the product of the dimerization reaction. Importantly, there is no evidence of a strong product absorption anywhere throughout the 450-600 nm spectral range, the range characteristic of tetraaryldistannenes.<sup>26,31</sup> We thus conclude that, in contrast to the behavior of  $\text{SnMe}_2$  (*vide supra*) and the higher diphenyltetrylenes,  $\text{SiPh}_2$ <sup>29,32</sup> and  $\text{GePh}_2$ ,<sup>21</sup> the dimerization of  $\text{SnPh}_2$  does *not* afford the corresponding (Sn=Sn) doubly-bonded dimer (**16b**) in detectable amounts, but rather some other  $\text{Sn}_2\text{Ph}_4$  isomer, formed perhaps via (rapid) isomerization of **16b**; the most reasonable candidate, based on computational<sup>33,34</sup> and experimental<sup>35</sup> precedent, is phenyltriphenylstannylstannylene (**17b**). The latter can be expected to exhibit a very weak  $n \rightarrow 5p$  absorption in the 600-800 nm range of the visible spectrum,<sup>26,36</sup> which is unfortunately in a region of relatively low sensitivity for our spectrometer. Nevertheless, careful probing in this spectral range did reveal a barely detectable product absorption

centred apparently at  $\lambda_{\max} \approx 650$  nm, which appeared to grow in over a similar timescale as the growth of the absorption at 340 nm (see Fig. S2.11). The result cannot be considered conclusive, but is nevertheless consistent with the tentative assignment of the observed dimer to stannylstannylene **17b**. The assignment is also supported by the results of computational studies of the  $\text{Sn}_2\text{Ph}_4$  potential energy surface, as discussed later in the chapter.

The steady state photolysis experiments suggest that both stannylenes can be trapped efficiently by  $\text{Me}_2\text{SnCl}_2$  (*vide supra*), so we carried out transient quenching experiments with **2** and **3** using the dichlorostannane as the substrate, monitoring the prompt absorptions assigned to the stannylenes (at 530 and 500 nm, respectively) as a function of  $\text{Me}_2\text{SnCl}_2$  concentration. Indeed, addition of sub-millimolar concentrations of  $\text{Me}_2\text{SnCl}_2$  in hexanes caused the decays to accelerate and proceed with clean pseudo-first order kinetics in both cases, in a manner consistent with irreversible reaction. Accompanying this was a reduction in the intensities of the signals due to the dimerization products, indicating dimerization is suppressed in the presence of the added substrate, as might be expected. Plots of the pseudo-first order rate constants for decay of the prompt absorptions ( $k_{\text{decay}}$ ; obtained by fitting the absorbance-time plot of the prompt absorption to eq. 2.15) versus  $\text{Me}_2\text{SnCl}_2$  concentration according to equation 2.16 were both linear (see Figure 2.5), consistent with an overall second-order reaction. The slopes of the plots afford bimolecular rate constants of  $k_{\text{Q}} = (1.9 \pm 0.3) \times 10^{10}$  and  $(3.6 \pm 0.2) \times 10^9 \text{ M}^{-1}\text{s}^{-1}$  for the reactions of  $\text{Me}_2\text{SnCl}_2$  with  $\text{SnMe}_2$  and  $\text{SnPh}_2$ , respectively. A transient spectrum recorded with **2** in hexanes containing 0.3 mM  $\text{Me}_2\text{SnCl}_2$ , where the lifetime of  $\text{SnMe}_2$  is reduced to ca. 230 ns and dimerization is suppressed almost completely, exhibited  $\lambda_{\max} = 500$  nm, which is in excellent agreement with the earlier reported

spectrum of SnMe<sub>2</sub> in hexanes solution.<sup>2</sup> No other transient products could be detected in the experiment.

$$\Delta A_t = \Delta A_{\text{res}} + (\Delta A_0 - \Delta A_{\text{res}}) \exp(-k_{\text{decay}}t) \quad (2.15)$$

$$k_{\text{decay}} = k_0 + k_Q[Q] \quad (2.16)$$

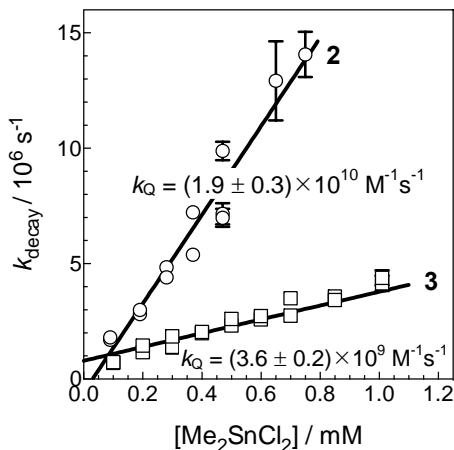
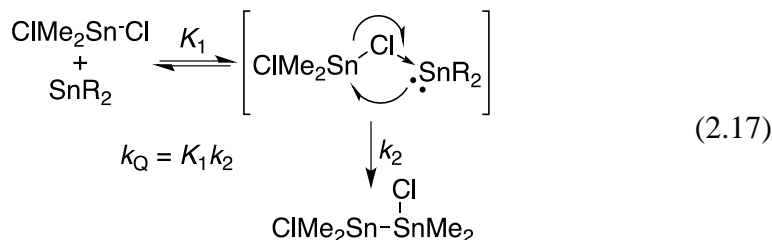


**Figure 2.5.** Plots of  $k_{\text{decay}}$  versus substrate concentration for the stannylene absorptions from laser photolysis of hexanes solutions of (a) **2** (O) and (b) **3** (□) containing varying concentrations of Me<sub>2</sub>SnCl<sub>2</sub> at 25 °C. The monitoring wavelengths were 530 nm and 500 nm for **2** and **3**, respectively. The solid lines are the linear least squares fits of the data to eq. 2.16.

The kinetic data for the reactions with the dichlorostannane are consistent with a two-step mechanism involving reversible Lewis acid-base complexation of the stannylene with the halostannane, followed by unimolecular insertion of the Sn(II) site into the (complexed) Sn-Cl bond (equation 2.17). The mechanism is analogous to that for Si-Cl bond insertions by silylenes, which has been studied extensively by Kira and coworkers.<sup>37-39</sup> By this mechanism, the rate constant  $k_Q$  is the product of the individual terms  $K_1$  and  $k_2$  at the low substrate limit (i.e.  $k_{\text{decay}} \ll k_2$ ; see Figure 2.5).



The extinction coefficients of SnMe<sub>2</sub> and SnPh<sub>2</sub> at 500 nm were determined by benzophenone actinometry, according to eq. 2.18 and in conjunction with the

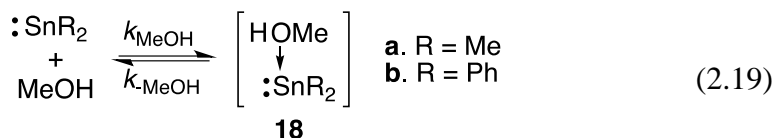
photoproduct quantum yields determined in the previous section.  $S_{\text{SnR2}}$  and  $S_{3\text{BP}^*}$  (eq. 2.18) are the slopes for the linear least squares analysis of the plots of initial transient absorbance ( $(\Delta A)_0$ ) versus laser pulse energy for the stannylene and the benzophenone triplet, respectively (see Fig. S2.12).<sup>40,41</sup>

$$\Phi_{\text{SnR2}} \cdot \epsilon_{\text{SnR2}} / S_{\text{SnR2}} = \Phi_{3\text{BP}^*} \cdot \epsilon_{3\text{BP}^*} / S_{3\text{BP}^*} \quad (2.18)$$

The values obtained –  $\epsilon_{500} = 1,800 \pm 600 \text{ M}^{-1} \text{ cm}^{-1}$  for  $\text{SnMe}_2$  and  $\epsilon_{500} = 2,500 \pm 600 \text{ M}^{-1} \text{ cm}^{-1}$  for  $\text{SnPh}_2$  – are in the range typical of the  $n(\text{M})\text{-}\pi\pi(\text{M})$  absorption bands of dialkyl- and diaryltetraylenes ( $\text{M} = \text{Si}, \text{Ge}, \text{or Sn}$ ) in solution.<sup>21,26,27,42-49</sup> Use of these data with the second order decay rate coefficients reported above affords  $k_{\text{dim}} = (1.4 \pm 0.4) \times 10^{10} \text{ M}^{-1} \text{ s}^{-1}$  for the absolute second order rate constant for dimerization of  $\text{SnMe}_2$ ,<sup>50</sup> and  $k_{\text{dim}} = (1.6 \pm 0.4) \times 10^{10} \text{ M}^{-1} \text{ s}^{-1}$  as the corresponding value for  $\text{SnPh}_2$ . It can thus be concluded that the dimerization of both stannylenes proceeds with absolute second order rate constants that are very close to the diffusional limit ( $k_{\text{diff}} = 2.2 \times 10^{10} \text{ M}^{-1} \text{ s}^{-1}$ )<sup>13</sup> in solution.

A final set of laser photolysis experiments was carried out using methanol (MeOH) as the substrate, a reagent found in our earlier study to react with  $\text{SnMe}_2$  *reversibly* to form a transient product exhibiting  $\lambda_{\text{max}} \approx 360 \text{ nm}$ , which was assigned to the  $\text{Me}_2\text{Sn-O(H)Me}$  Lewis acid-base complex (**18a**; eq. 2.19).<sup>2</sup> Indeed, addition of 0.1-1.5 mM MeOH to hexanes solutions of **2** caused closely analogous behavior to what was observed in the earlier study of stannacyclopentene **1b**;<sup>2</sup> the intensities of the signals due to both  $\text{SnMe}_2$  and  $\text{Sn}_2\text{Me}_4$  were reduced in a manner consistent with a moderately favorable, reversible reaction of the alcohol with the stannylene,<sup>51,52</sup> giving rise to a new transient product exhibiting a similar lifetime to the stannylene (as expected if the complex is in mobile equilibrium with the free stannylene) and a UV-vis spectrum centred at  $\lambda_{\text{max}} = 355$

nm (Fig. S2.13a). A plot of the relative stannylene signal intensities as a function of MeOH concentration according to eq. 2.20, where  $(\Delta A_0)_0$  and  $(\Delta A_0)_Q$  are the initial signal intensities (at 530 nm) in the absence and presence of the substrate at concentration [Q] and  $K_{\text{MeOH}} (= k_{\text{MeOH}} / k_{-\text{MeOH}})$  is the equilibrium constant, was linear (Fig. S2.13b) with slope  $K_{\text{MeOH}} = (2.4 \pm 0.2) \times 10^3 \text{ M}^{-1}$ . The value is larger than the earlier reported value by a factor of about two,<sup>2</sup> but can be considered to be the more accurate of the two determinations. Interestingly, a time-resolved spectrum recorded with **2** in hexanes containing 0.025 M MeOH exhibited an absorption band centred at  $\lambda_{\text{max}} = 335 \text{ nm}$ , blue-shifted significantly compared to that obtained in the presence of 7 mM of the alcohol. This may be the result of the formation of dicoordinate complexes (i.e.  $\text{SnMe}_2\text{-(MeOH)}_2$ ) at the higher alcohol concentration.<sup>53</sup> It should be noted that distannene **16a** is evidently not formed in the presence of the alcohol.



$$(\Delta A_0)_0 / (\Delta A_0)_Q = 1 + K_{\text{eq}}[\text{Q}] \quad (2.20)$$

A transient UV-vis spectrum recorded with **3** in hexanes containing 3 mM MeOH (Figure 2.6a) showed a prompt absorption centred at  $\lambda_{\text{max}} = 370 \text{ nm}$ , which decayed over ca. 5  $\mu\text{s}$  to afford similar long-lived oligomer absorptions as were observed in the absence of substrate;  $\text{SnPh}_2$  itself could not be detected under these conditions. We assign the 370 nm species to the  $\text{SnPh}_2\text{-MeOH}$  Lewis acid-base complex (**18b**; eq. 2.19). The stannylene could be detected at lower concentrations of MeOH, where it was found to exhibit bimodal decays consisting of a rapid initial decay component and a slowly-decaying residual absorbance. The initial decay became more rapid and the intensity of the residual absorbance was reduced as the MeOH concentration was increased, which is consistent

with a reversible reaction characterized by an equilibrium constant in the approximate range of  $2 \times 10^3 \text{ M}^{-1} < K_{\text{MeOH}} < 3 \times 10^4 \text{ M}^{-1}$ .<sup>51,52</sup> Analysis of the transient decay and residual signal intensity data in the usual manner<sup>51,52</sup> (see Fig. 2.6b) afforded rate and equilibrium constants of  $k_{\text{MeOH}} = (6 \pm 1) \times 10^9 \text{ M}^{-1} \text{ s}^{-1}$  and  $K_{\text{MeOH}} = (7.6 \pm 0.8) \times 10^3 \text{ M}^{-1}$ , respectively.

The threefold higher value of  $K_{\text{MeOH}}$  for  $\text{SnPh}_2$  compared to  $\text{SnMe}_2$  corresponds to a difference in binding free energies of ca.  $0.7 \text{ kcal mol}^{-1}$ , which is similar to that reported for complexation of MeOH with the corresponding Ge(II) homologs ( $\text{GeMe}_2$ ,  $K_{\text{MeOH}} = 900 \text{ M}^{-1}$ ;  $\text{GePh}_2$ ,  $K_{\text{MeOH}} = 3,300 \text{ M}^{-1}$ ).<sup>52,54</sup>

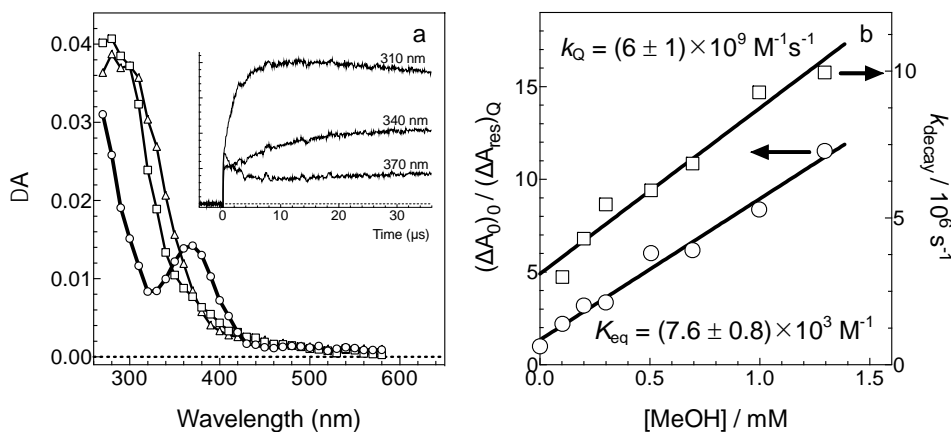


**Figure 2.6.** (a) Time-resolved UV-vis spectra from laser photolysis of  $\text{SnPh}_2$  precursor **3** in hexanes containing 0.025 M MeOH, 0.26-0.38  $\mu\text{s}$  ( $\circ$ ), 4.93-5.18  $\mu\text{s}$  ( $\square$ ) and 35.3-35.7  $\mu\text{s}$  ( $\triangle$ ) after the laser pulse (25 °C), and absorbance-time profiles at selected wavelengths (inset). (b) Plots of  $k_{\text{decay}}$  ( $\square$ ) and  $(\Delta A_0)_0 / (\Delta A_{\text{res}})_Q$  ( $\circ$ ) of the  $\text{SnPh}_2$  absorption (at 500 nm) versus [MeOH], in hexanes solution at 25 °C; the solid lines are the linear least squares fits of the data to equations 2.16 and 2.20, respectively.

The data indicate that with both the methyl- and phenyl-substituted  $\text{MR}_2$  ( $\text{M} = \text{Si}$ , Ge or Sn) systems, the Lewis acidity at the central M(II) atom is modestly higher for the stannylenes than the germlylenes, the difference in binding free energies of the Sn(II) and Ge(II) complexes (all else being equal) amounting to about  $0.5 \text{ kcal mol}^{-1}$  for both substituents. The acidity-enhancing effect of phenyl substitution at the M(II) centre is also

observed with the corresponding silylene derivatives, which (based on our earlier estimates of  $K_{\text{MeOH}}^{52}$ ) are modestly stronger Lewis acids than the stannylenes. Thus, Lewis acidity decreases in the order  $\text{SiR}_2 > \text{SnR}_2 > \text{GeR}_2$  for both substituents. Interestingly, the UV-vis spectra of the stannylene-MeOH complexes are both red-shifted significantly compared to those of the corresponding  $\text{SiR}_2\text{-MeOH}$  and  $\text{GeR}_2\text{-MeOH}$  complexes.<sup>51,54</sup> The absolute rate and equilibrium constants determined above for the dimerization of  $\text{SnMe}_2$  and  $\text{SnPh}_2$  and their reactions with  $\text{Me}_2\text{SnCl}_2$  and MeOH in hexanes at 25 °C are summarized in Table 2.1.

**Table 2.1.** Absolute Rate ( $k$ ,  $\text{M}^{-1} \text{s}^{-1}$ ) and/or Equilibrium Constants ( $K_{\text{eq}}$ ,  $\text{M}^{-1}$ ) for Dimerization and Reactions of Dimethylstannylene ( $\text{SnMe}_2$ ) and Diphenylstannylene ( $\text{SnPh}_2$ ) with  $\text{Me}_2\text{SnCl}_2$  and MeOH, Determined by Laser Flash Photolysis of **2** and **3** in Hexanes at 25 °C.

Substrate	$k$ ( $\text{M}^{-1}\text{s}^{-1}$ ) [ $K$ ( $\text{M}^{-1}$ )]	
	$\text{SnMe}_2$	$\text{SnPh}_2$
$\text{SnR}_2$ (dimerization)	$(1.4 \pm 0.4) \times 10^{10}$	$(1.6 \pm 0.4) \times 10^{10}$
$\text{Me}_2\text{SnCl}_2$	$(1.9 \pm 0.3) \times 10^{10}$	$(3.6 \pm 0.2) \times 10^9$
MeOH	<sup>a</sup> $[(2.4 \pm 0.2) \times 10^3]$	$(6 \pm 1) \times 10^9$ $[(7.6 \pm 0.8) \times 10^3]$

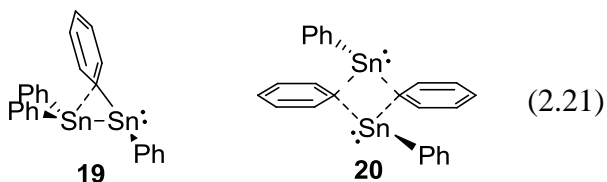
<sup>a</sup>rate constant is indeterminable

### 2.2.3. Computational Studies<sup>55</sup>

Density functional theory (DFT) calculations were carried out to model the structures, relative energies, and electronic spectra of  $\text{SnMe}_2$ ,  $\text{SnPh}_2$ , the corresponding distannene and stannylstannylene dimers, and the Lewis acid-base complexes of the two  $\text{SnR}_2$  species with MeOH, and to attempt to identify a possible mechanism for the apparent diffusion-controlled formation of stannylstannylene **17b** from dimerization of  $\text{SnPh}_2$ . The calculations employed the dispersion-corrected hybrid density functional of Chai and Head-Gordon ( $\omega\text{B97XD}$ )<sup>56</sup> in conjunction with the 6-31+G(d,p) basis set for

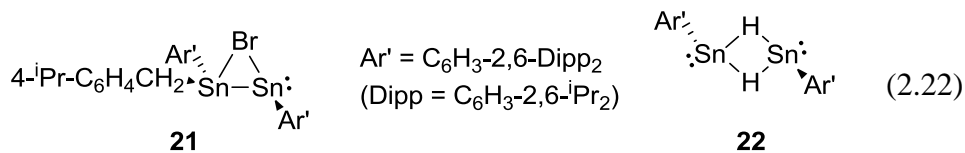


first and second-row elements and the LANL2DZdp basis set and effective core potential for Sn.<sup>57</sup> Energy minima were identified by the absence of negative eigenvalues of the Hessian matrix, while transition state structures (*vide infra*) were identified as such by the presence of a single negative eigenvalue. A total of four Sn<sub>2</sub>Ph<sub>4</sub> isomers were located (*vide infra*) – distannene **16b**, stannylstannylene **17b**, and the mono- and di-bridged SnPh<sub>2</sub> dimers **19** and **20**, respectively. All four of these structures corresponded to energy minima except for **17b**, which gave rise to one imaginary frequency associated with a coupled rocking vibration of two of the phenyl groups. Despite many attempts, we were unsuccessful at locating a minimum-energy geometry for this structure with the ωB97XD density functional. All energies are referenced relative to the isolated stannylenes (+ MeOH, where appropriate) at 298.15K; those for the complexes with MeOH are corrected for basis set superposition errors (BSSE), which were computed using the counterpoise correction method.<sup>58</sup> Vibrational frequencies were not scaled. Table 2.2 lists the calculated (ωB97XD/6-31+G(d,p)<sup>C,H,O</sup>-LANL2DZdp<sup>Sn</sup>) electronic energies and thermochemical parameters of the various structures that were located computationally, relative to the isolated reactants. The structures and selected geometrical parameters of the various SnPh<sub>2</sub>-dimers studied are shown in Figure S2.14, and in the reaction coordinate diagram of Figure 2.7 (*vide infra*).



The stannylidenestannylene structure **19** is analogous to the “zwitterionic, donor-acceptor” stannylene-dimers that have been reported by various groups,<sup>59-63</sup> the bridging phenyl group in the present case providing  $\pi$ -stabilization of the increased positive charge at the neighbouring Sn-atom that results from the donor-acceptor interaction between the

two Sn-atoms. Indeed, NBO calculations afforded charges of +0.80 and +1.09 at the Sn<sup>1</sup> and Sn<sup>2</sup> atoms in **19**, respectively, indicating discrete polarization of the Sn-Sn bond in the molecule.<sup>64</sup> The structure and bonding situation in both **19** and **20** are somewhat analogous to the sterically-stabilized halogen- and hydride-bridged stannylene dimers (**21** and **22**, respectively) that have been reported by Power and coworkers.<sup>65,66</sup> All of the possible SnPh<sub>2</sub>-dimer isomers have precedent in the early theoretical studies of Trinquier of the dimers of SnH<sub>2</sub> and the other parent divalent Group 14 hydrides.<sup>33,34,67</sup>



A parallel set of calculations was carried out using the  $\omega$ B97X<sup>68</sup> density functional and the same basis set combination (see Table S2.1), to assess the effects of dispersion-correction on the calculated energies. For the stannylene-dimers, the inclusion of dispersion corrections lowered the calculated energies by 1.5-6 kcal mol<sup>-1</sup>, with the largest effects being on the bridged dimers **19** and **20**. As might be expected, it had little impact on the binding energies of the stannylene-MeOH complexes.

The calculated structures of SnMe<sub>2</sub>, SnPh<sub>2</sub> and their doubly-bonded dimers (**16a** and **16b**, respectively) compare favorably with previously reported structures at other levels of theory.<sup>2,69,70</sup> Similarly, the calculated Sn-Sn bond distances in the distannenes (2.74 and 2.77 Å for **16a** and **16b**, respectively) and the stannylstannylenes (2.91 and 2.90 Å for **17a** and **17b**, respectively) are in very good agreement with experimental data for the tetraalkyl- and tetraaryldistannene and stannylstannylene derivatives for which structural data exist.<sup>35,65,71-73</sup> As is the case with the parent hydrido-systems,<sup>33,34</sup> the stannylstannylenes are in both cases predicted to be significantly lower in energy than the corresponding distannene isomer. The difference is larger for the phenylated systems,

presumably reflecting a weakening effect of phenyl substitution on the Sn=Sn bond strength (see Table 2.2).<sup>2</sup>

**Table 2.2.** Calculated Electronic Energies, Enthalpies (298.15 K), and Free Energies (298.15 K) of Stationary Points in the Dimerization of SnMe<sub>2</sub> and SnPh<sub>2</sub> and their Lewis acid-base Complexation with Methanol, Calculated at the  $\omega$ B97XD/6-31+G(d,p)<sup>C,H,O</sup>-LANL2DZdp<sup>Sn</sup> Level of Theory Relative to the Isolated Reactants (in kcal mol<sup>-1</sup>).<sup>a</sup>

Species	$\Delta E_{\text{elec}}$	$\Delta H^\circ$	$\Delta G^\circ$
Me <sub>2</sub> Sn=SnMe <sub>2</sub> ( <b>16a</b> )	-24.9	-22.1	-11.9
MeSnSnMe <sub>3</sub> ( <b>17a</b> )	-32.7	-30.3	-21.1
Ph <sub>2</sub> Sn=SnPh <sub>2</sub> ( <b>16b</b> )	-22.7	-21.1	-11.4
PhSnSnPh <sub>3</sub> ( <b>17b</b> ) <sup>b</sup>	-34.0	-33.0	-21.1
PhSn(C <sub>6</sub> H <sub>5</sub> )SnPh <sub>2</sub> ( <b>19</b> )	-29.8	-28.3	-16.3
<i>trans</i> -PhSn(C <sub>6</sub> H <sub>5</sub> ) <sub>2</sub> SnPh ( <b>20</b> )	-19.5	-18.0	-5.8
Transition state <b>24</b> <sup>‡</sup>	+0.4	+1.0	+14.4
Transition state <b>25</b> <sup>‡c</sup>	-29.2	-28.5	-15.7
Me <sub>2</sub> Sn-O(H)Me ( <b>18a</b> ) <sup>d</sup>	-13.5 (-14.4)	-11.8 (-12.8)	-1.9 (-2.9)
Ph <sub>2</sub> Sn-O(H)Me ( <b>18b</b> ) <sup>d</sup>	-16.0 (-17.3)	-14.3 (-15.6)	-3.3 (-5.0)

<sup>a</sup>Thermodynamic parameters were computed at 298.15 K from unscaled vibrational frequencies; <sup>b</sup>Structure gives rise to one low-energy imaginary frequency (= 8.21*i* cm<sup>-1</sup>); <sup>c</sup>An IRC calculation showed that **25**<sup>‡</sup> is in fact not the correct transition state for the formation of **17b** from **19**. However, its calculated energies define upper limits for those of the true transition state for the process; <sup>d</sup>Corrected for BSSE; values in parentheses are the corresponding uncorrected values.

Excellent agreement is also observed between the calculated (BSSE-corrected, gas phase) free energies of complexation of MeOH with SnMe<sub>2</sub> ( $\Delta G = -1.9$  kcal mol<sup>-1</sup>) and SnPh<sub>2</sub> ( $\Delta G = -3.3$  kcal mol<sup>-1</sup>) and the experimental (solution phase) values of  $\Delta G = -2.7$  and  $-3.3$  kcal mol<sup>-1</sup>, respectively, where the latter were calculated from the equilibrium constants after adjustment to the gas-phase reference state (1 atm, 298.15K). This gives

some confidence in the chemical accuracy of the  $\omega$ B97XD/6-31+G(d,p)<sup>C,H</sup>-

LANL2DZdp<sup>Sn</sup> method for the prediction of reaction thermochemistries for transient Sn(II) systems, at least as applied to Lewis acid-base complexation reactions.

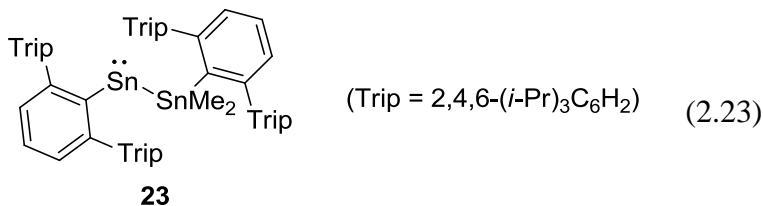
Electronic spectra were modeled using the time-dependent (TD) extension of the  $\omega$ B97XD functional and the same basis set combination as was employed for the geometry optimizations; the results of the calculations are listed in Table 2.3 along with the corresponding experimental values where known. Again, reasonable agreement between theory and experiment is observed in all cases for which comparisons are possible; these include SnMe<sub>2</sub>, SnPh<sub>2</sub>, Me<sub>2</sub>Sn=SnMe<sub>2</sub> (**16a**), and the two stannylene-MeOH complexes, for which the TD-DFT predictions of the lowest energy electronic transitions agree with the experimental values to within 0.15 eV in every case. The calculated absorption maximum for Ph<sub>2</sub>Sn=SnPh<sub>2</sub> (**16b**;  $\lambda_{\text{max}} \approx 503$  nm) is within the range of reported values for kinetically stable tetraaryldistannenes,<sup>26,31</sup> and supports the conclusion that the SnPh<sub>2</sub>-dimer detected by laser photolysis of **3** is *not* the distannene. As mentioned above, the most likely alternative based on thermodynamic considerations is stannylstannylene **17b**,<sup>35</sup> for which the TD-DFT calculation predicts a very weak HOMO→LUMO (n→5p) absorption centred at  $\lambda_{\text{max}} \approx 730$  nm, in reasonable agreement with the value reported for the stable derivative **23** ( $\lambda_{\text{max}} \approx 689$  nm;  $\epsilon = 271 \text{ M}^{-1} \text{ cm}^{-1}$ ),<sup>73</sup> and consistent with the weak secondary product absorption at 650 nm observed by laser photolysis of **3** (*vide supra*). It should be noted that the calculated oscillator strength of the n→5p transition in **17b** is an order of magnitude smaller than that calculated for the corresponding transition in SnPh<sub>2</sub> (see Table 2.3), which is also in good agreement with the difference between the experimental extinction coefficients of the stable stannylstannylene **23**<sup>35</sup> and SnPh<sub>2</sub> ( $\epsilon_{\text{max}} = 2500 \pm 600 \text{ M}^{-1} \text{ cm}^{-1}$ ). The long wavelength n→5p absorption band in the spectrum of **17b**

is thus expected to be inherently quite difficult to detect under the conditions of our laser photolysis experiments.

**Table 2.3.** Calculated<sup>a</sup> and Experimental UV-Vis Absorption Maxima of Stannylenes and Stannylene-derived Dimers and Methanol Complexes.

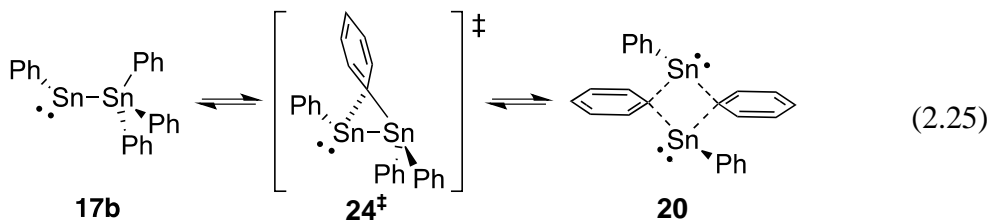
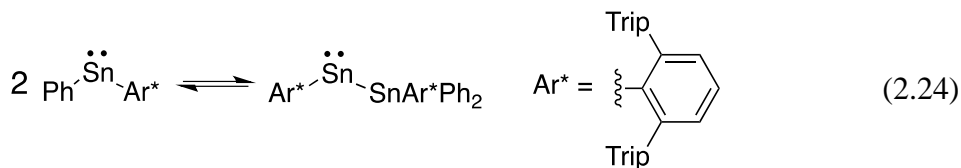
Compound	$\lambda_{\max} / \text{nm} (f)$	
	Calculated <sup>a</sup>	Experimental
SnMe <sub>2</sub>	515(0.029)	500
SnPh <sub>2</sub>	331(0.143), 495(0.027)	300, 505
Me <sub>2</sub> Sn=SnMe <sub>2</sub> ( <b>16a</b> )	440(0.351)	465
MeSnSnMe <sub>3</sub> ( <b>17a</b> )	270(0.095), 400(0.011), 800(0.002)	–
Ph <sub>2</sub> Sn=SnPh <sub>2</sub> ( <b>16b</b> )	275(0.123), 503(0.353)	–
PhSnSnPh <sub>3</sub> ( <b>17b</b> )	288(0.149), 383(0.016), 730 (0.001)	<280, ~340(sh), 650 <sup>b</sup>
PhSn(C <sub>6</sub> H <sub>5</sub> )SnPh <sub>2</sub> ( <b>19</b> )	284(0.318), 337(0.013), 386(0.115)	–
PhSn(C <sub>6</sub> H <sub>5</sub> ) <sub>2</sub> SnPh ( <b>20</b> )	279(0.070), 323(0.242), 338(0.186)	–
Me <sub>2</sub> Sn←O(H)Me ( <b>18a</b> )	254(0.19), 348(0.08)	355
Ph <sub>2</sub> Sn←O(H)Me ( <b>18b</b> )	241(0.23), 354(0.05)	370

<sup>a</sup>TD-ωB97XD/6-31+G(d,p)<sup>C,H,O</sup>-LANL2DZdp<sup>Sn</sup> // ωB97XD/6-31+G(d,p)<sup>C,H,O</sup>-LANL2DZdp<sup>Sn</sup>; the numbers in parentheses are the calculated oscillator strengths (*f*) of each of the transitions; <sup>b</sup>The UV-vis spectrum of the experimentally observed SnPh<sub>2</sub>-dimer consists of a broad absorption extending from 270-400 nm (Figs. 2.2 and S2.13a). A very weak absorption at 650 nm, with similar growth/decay characteristics to those recorded at 340-360 nm, was also detected (Fig. S2.13b) and is tentatively ascribed to the same species.



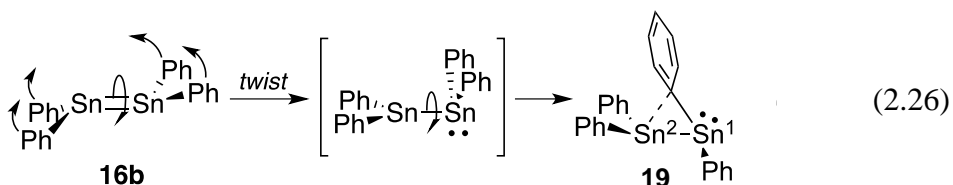
We next probed possible mechanisms for the formation of **17b** via rearrangement of

distannene **16b**, which we assumed to be the first-formed product in the dimerization of  $\text{SnPh}_2$ . We began by modeling transition state structure **24**<sup>‡</sup>, using a starting geometry derived from the structure reported by Tsai and Su<sup>74</sup> in their computational study of the reversible dimerization / valence isomerization of a bulky arylphenylstannylene derivative reported in 2003 by Power and coworkers (eq. 2.24).<sup>35</sup> The structure that was located (**24**<sup>‡</sup>) indeed corresponds closely to that reported in the earlier study.<sup>74</sup> However, it is much too high in energy (see Figure 2.7) to be compatible with the kinetic data, which indicate that the initial dimerization step is the rate-determining step in the sequence, and all subsequent unimolecular rearrangement steps must occur on the nanosecond (or shorter) time scale. Indeed, an intrinsic reaction coordinate (IRC) calculation showed that **24**<sup>‡</sup> links stannylstannylene **17b** to the doubly-bridged dimer **20** (eq. 2.25) and not to distannene **16b**.

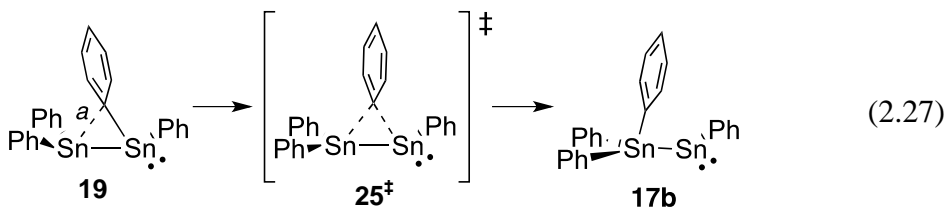


We then carried out a relaxed potential energy surface (PES) scan of the trans  $\text{C}_{\text{Ph}}\text{-Sn-Sn-C}_{\text{Ph}}$  dihedral angles in **16b**, based on the hypothesis that the [1,2]-phenyl migration that leads to **17b** is likely to be preceded by twisting about the  $\text{Sn}=\text{Sn}$  bond, to allow the migrating  $\text{Sn-C}$  bond to adopt an orientation in which it roughly bisects the  $\text{C-Sn-C}$  angle at the second  $\text{Sn}$  atom. Interestingly, contracting either of the trans dihedral angles in  $10^\circ$  increments from the equilibrium geometry resulted in initial flattening of one end of the  $\text{Sn}=\text{Sn}$  bond, and concomitant flipping of the substituents at the other end into a near-

perpendicular relative orientation, as the dihedral was contracted through the initial 50-60° of the rotation. The process (see eq. 2.26 and Figure S2.15a) resulted in less than a 2 kcal mol<sup>-1</sup> rise in energy as the molecule approached the perpendicular orientation, after which continued rotation resulted in an abrupt drop in energy and the formation of the singly-bridged dimer **19**. Structure **19** evidently occupies a rather shallow minimum on the Sn<sub>2</sub>Ph<sub>4</sub> PES, as various attempts to locate an analogous structure at the B3LYP/LANL2DZ level of theory all failed, most of them leading instead to the global minimum, stannylstannylene **17b**.



A relaxed PES scan of the bridging Sn-C bond distance in **19** was then carried out in an attempt to locate a transition state for migration of the bridging phenyl group to form **17b**. Decreasing the bridging Sn-C distance (bond “a” in eq. 2.27) in increments of 0.03 Å from its equilibrium value (of 2.56 Å) in **19** resulted in a rise in  $\Delta E$  of only 0.5 kcal mol<sup>-1</sup> at the highest energy point in the migration, which was successfully optimized to transition state structure **25<sup>‡</sup>** (see eq. 2.27 and Fig. S2.15b). While an IRC calculation revealed that **25<sup>‡</sup>** is in fact not the correct transition state linking **19** and **17b**, it nevertheless represents an upper energetic limit in the reaction profile for interconversion of the two isomers, which is shown in Figure S2.15b along with the computed structures at selected points in the transformation.



Finally, relaxed scan calculations of the Sn-Sn bond distances in **16b** and **19** were carried out in a search for potential transition states for their direct formation *via* SnPh<sub>2</sub>-dimerization. Incremental lengthening of the Sn-Sn bond distances ( $d_{\text{Sn-Sn}}$ ) in the two molecules to values in excess of 4 Å resulted simply in a continuous rise in energy in both cases (see Figure S2.16). The calculation for **16b** essentially collapsed once the Sn-Sn distance exceeded 4 Å, but with **19** stabilizing non-bonded ( $\pi$ - $\pi$ ) interactions between the bridging phenyl group and the neighbouring Sn-atom persisted even at Sn-Sn distances as large as 6.5 Å.<sup>75</sup> In neither case could any indication of a possible transition state be found. This suggests there are *two* distinct barrierless pathways for dimerization of SnPh<sub>2</sub>, one involving exo-approach of one stannylene toward the other and leading to distannene **16b**, and the other involving an endo-approach and leading to the polarized stannylidenestannylene structure, **19**. With a predicted barrier of less than 1 kcal mol<sup>-1</sup> for the phenyl-migration that converts **19** to **17b**, the endo-dimerization pathway comes very close to the limit of concerted insertion of one SnPh<sub>2</sub> unit into a Sn-C(Ph) bond of another, assisted by  $\pi_{\text{Ph}} \rightarrow p_{\text{Sn}}$  dative bonding interactions.

Thus, the calculations support a multi-step mechanism for the formation of stannylstannylene **17b** via dimerization of SnPh<sub>2</sub>, in which the initial diffusional encounter of the two stannylene moieties is the rate-determining step in the sequence. The two possible products of the initial step - distannene **16b** and stannylidenestannylene **19** - are each formed by barrierless pathways and represent shallow minima on the (SnPh<sub>2</sub>)<sub>2</sub> energy surface, according to the calculations. Both species are predicted to have lifetimes in the nanosecond range or less, due to the ultrafast phenyl-migration process that leads from distannene **16b** to stannylstannylene **17b** via the intermediacy of the phenyl-bridged isomer, **19**. The calculations, which are summarized in Figure 2.7 in the form of a



reaction coordinate diagram for interconversion of the various  $(\text{SnPh}_2)_2$  dimer structures, are fully consistent with the experimental kinetic data.

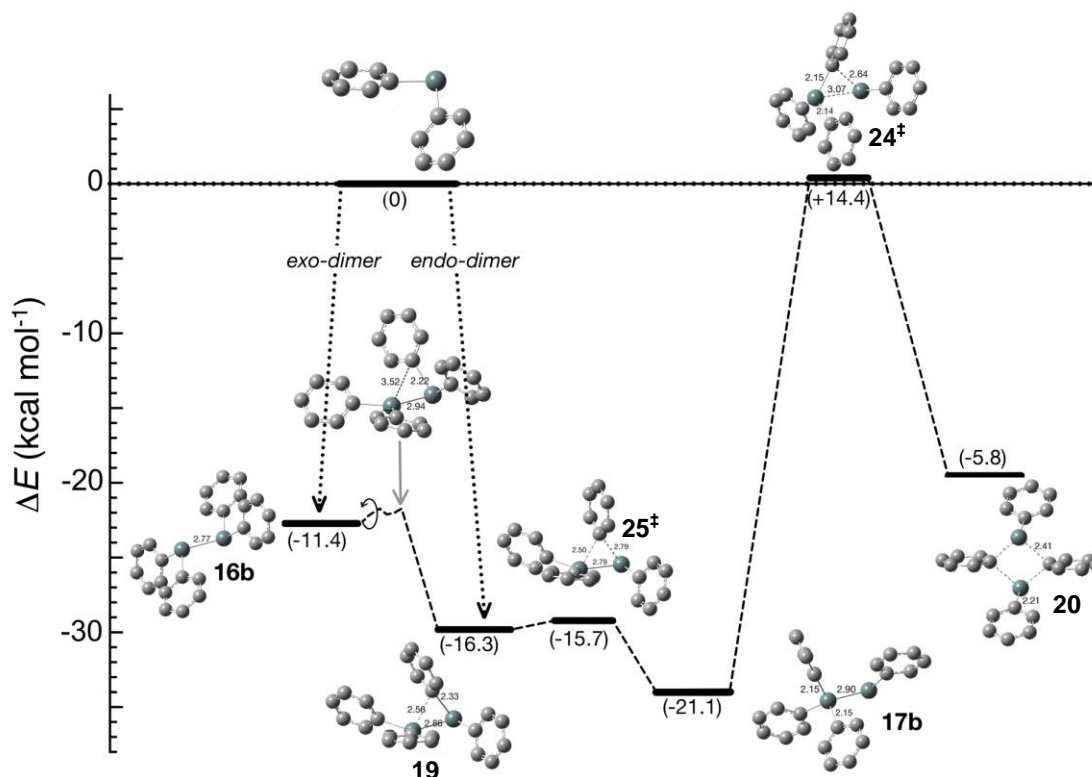


**Figure 2.7.** Electronic Energy versus Reaction Coordinate Diagram for the dimerization of  $\text{SnPh}_2$  and interconversion of the  $(\text{SnPh}_2)_2$  isomers, calculated at the  $\omega\text{B97XD}/6\text{-}31+\text{G}(\text{d},\text{p})^{\text{C,H,O}}\text{-LANL2DZdp}^{\text{Sn}}$  level of theory. The vertical placement of the various structures is defined by their calculated electronic energy relative to (twice) that of  $\text{SnPh}_2$  (1 atm gas phase, 0 K), as indicated on the y-axis; the numbers in parentheses are the corresponding standard free energies (see Table 2.1).

### 2.3. Summary and Conclusions

The transient stannylenes  $\text{SnMe}_2$  and  $\text{SnPh}_2$  are formed cleanly and efficiently by UV-lamp or –laser photolysis of the 1-stannacyclopent-3-ene derivatives **2** and **3**, respectively, according to the results of chemical trapping and laser flash photolysis experiments. The stannylenes can both be trapped cleanly by Sn-Cl insertion with  $\text{Me}_2\text{SnCl}_2$  in aerated solution, the presence of air facilitating the reaction by oxidizing the initially produced 1,2-dichlorostannanes, which absorb relatively strongly at the

excitation wavelength and are themselves highly photolabile; the corresponding 1,3-dichlorodistannoxanes that are formed in the oxidation absorb relatively weakly at the photolysis wavelength and in any event exhibit very low photoreactivity. The ultimate product of trapping *both* SnMe<sub>2</sub> and SnPh<sub>2</sub> with Me<sub>2</sub>SnCl<sub>2</sub> under these conditions is the association dimer of 1,3-dichlorotetramethyldistannoxane (**6**), along with Ph<sub>2</sub>SnCl<sub>2</sub> (**8**) in the case of SnPh<sub>2</sub>. In the latter case, dichlorostannane **8** is liberated from the initially-formed dichlorodistannoxane dimer (**11**) by exchange with excess Me<sub>2</sub>SnCl<sub>2</sub>; this process has been verified to be rapid and reversible under conditions similar to those employed in our photolysis experiments. The two-step exchange reaction is characterized by equilibrium constants that indicate that phenyl-substitution on the peripheral Sn-atoms leads to increased stabilization of the dimer compared to methyl substitution.

Both transient stannylenes are detectable by laser flash photolysis, their long-wavelength (n→5p) absorption bands centred at  $\lambda_{\max} = 500$  nm (SnMe<sub>2</sub>;  $\epsilon_{500} = 1,800 \pm 600$  M<sup>-1</sup> cm<sup>-1</sup>) and  $\lambda_{\max} = 505$  nm (SnPh<sub>2</sub>;  $\epsilon_{500} = 2,400 \pm 600$  M<sup>-1</sup> cm<sup>-1</sup>). They each decay with a second order rate constant approaching the diffusional limit, with the concomitant growth of secondary transient absorptions assignable to the corresponding dimers. Both stannylenes react rapidly with added Me<sub>2</sub>SnCl<sub>2</sub>, SnMe<sub>2</sub> with an absolute rate constant of  $k_Q = (1.9 \pm 0.3) \times 10^{10}$  and SnPh<sub>2</sub> with  $k_Q = (3.6 \pm 0.2) \times 10^9$  M<sup>-1</sup>s<sup>-1</sup> in hexanes at 25 °C.

The UV-vis spectrum and dimerization behavior of SnMe<sub>2</sub> agrees well with earlier solution phase results,<sup>2</sup> the species decaying with clean second order kinetics ( $k_{\text{dim}} = (1.4 \pm 0.4) \times 10^{10}$  M<sup>-1</sup>s<sup>-1</sup>) to afford tetramethyldistannene (Me<sub>2</sub>Sn=SnMe<sub>2</sub>, **16a**;  $\lambda_{\max} = 465$  nm). The distannene absorption decays on a similar timescale as those due to SnMe<sub>2</sub>, to afford one or more longer-lived product(s) exhibiting absorptions below 360 nm. Diphenylstannylene also dimerizes at close to the diffusion-controlled rate ( $k_{\text{dim}} = (1.6 \pm$

$0.4) \times 10^{10} \text{ M}^{-1} \text{ s}^{-1}$ ), but in contrast to the behavior exhibited by the dialkyl derivative, the UV-vis spectrum of the observed  $\text{SnPh}_2$ -dimer lacks the strong absorption in the 450 - 600 nm range that is expected for tetraphenyldistannene ( $\text{Ph}_2\text{Sn}=\text{SnPh}_2$ , **16b**). The observed dimer ( $\lambda_{\text{max}} = 280, 340(\text{sh}) \text{ nm}$ ) is instead assigned to phenyltriphenylstannylstannylene (**17b**), based on the observation of a weak transient product absorption centred at 650 nm, which is in the range expected for such a species, and the results of DFT calculations carried out at the  $\omega\text{B97XD}/6\text{-}31\text{+G(d,p)}^{\text{C,H,O-LANL2DZdp}^{\text{Sn}}}$  level of theory. The latter indicate that **17b** is the global minimum on the  $\text{Sn}_2\text{Ph}_4$  potential energy surface, and suggest it can be formed from the higher-energy distannene isomer via an ultrafast rearrangement process involving the intermediacy of a phenyl-bridged, donor-acceptor dimer (**19**). The calculated reaction barriers are consistent with the experimental finding that diffusion is the rate-controlling step in the decay of  $\text{SnPh}_2$  and the formation of **17b** in hexanes at 25 °C. The calculations further suggest that the phenyl-bridged dimer can also be formed via a direct endo-dimerization pathway, which should compete with the exo-pathway that produces the isomeric distannene. According to the calculations, the barrier for migration of the bridging phenyl group in **19** is so low that the endo-dimerization mode represents an essentially *direct* (formal Sn-C(Ph) insertion) pathway for the formation of **17b** from  $\text{SnPh}_2$ .

## 2.4. Supporting Information

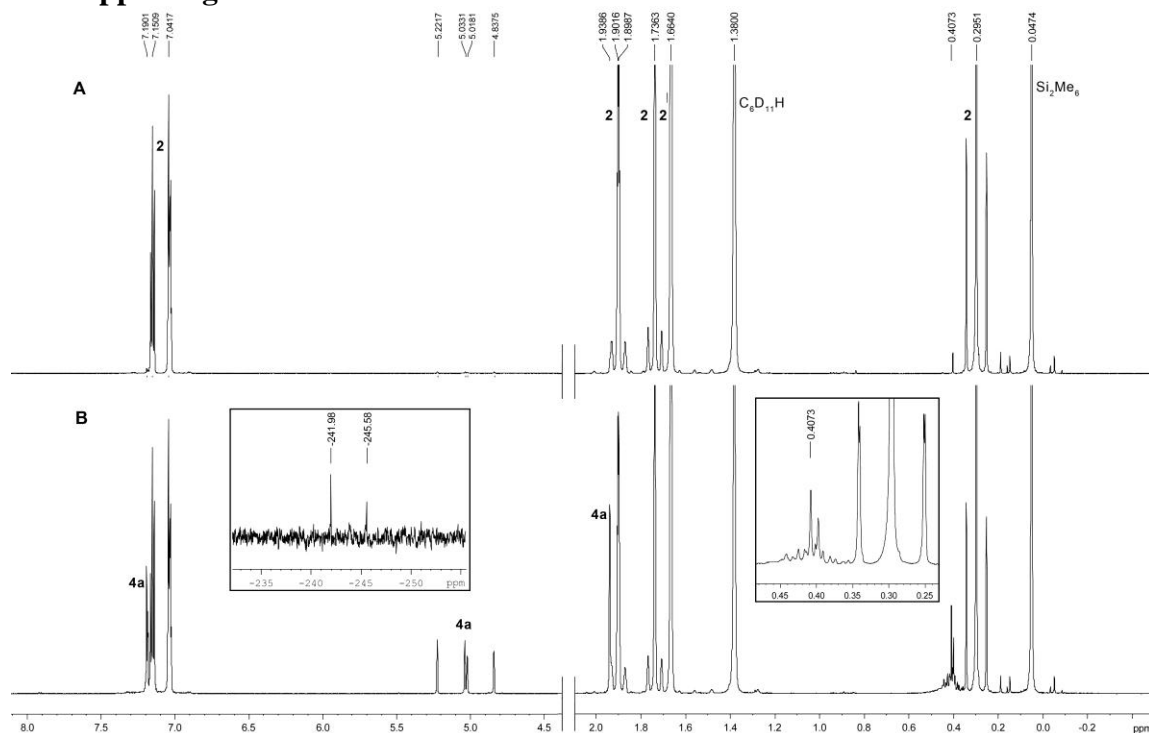


**Figure S2.1.**  $^1\text{H}$  NMR spectra of an argon-degassed 0.04 M solution of **2** in  $\text{C}_6\text{D}_{12}$  (a) before and (b) after 10 minutes photolysis with 254 nm light. The insets in B show an expansion of the  $\delta$  0.23-0.48 region of the spectrum and the portion of the  $^{119}\text{Sn}\{^1\text{H}\}$  spectrum containing product peaks.

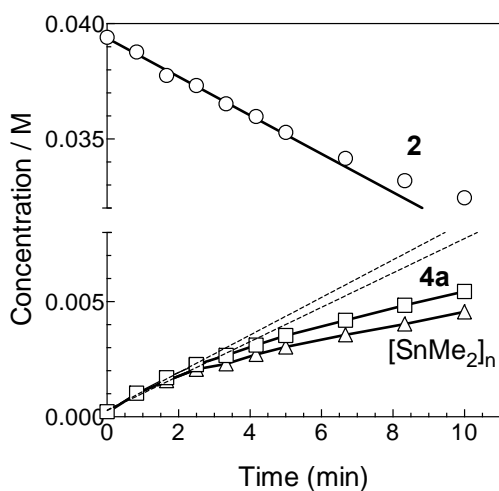


**Figure S2.2.** Concentration versus time plots for the photolysis of the solution of Fig. S2.1. The initial slopes of the three plots are **2**,  $-0.84 \pm 0.03$ ; **4a**,  $0.82 \pm 0.05$ ;  $[\text{SnMe}_2]_n$  ( $\delta$  0.407)  $0.75 \pm 0.07$  (units,  $\text{mM min}^{-1}$ ).

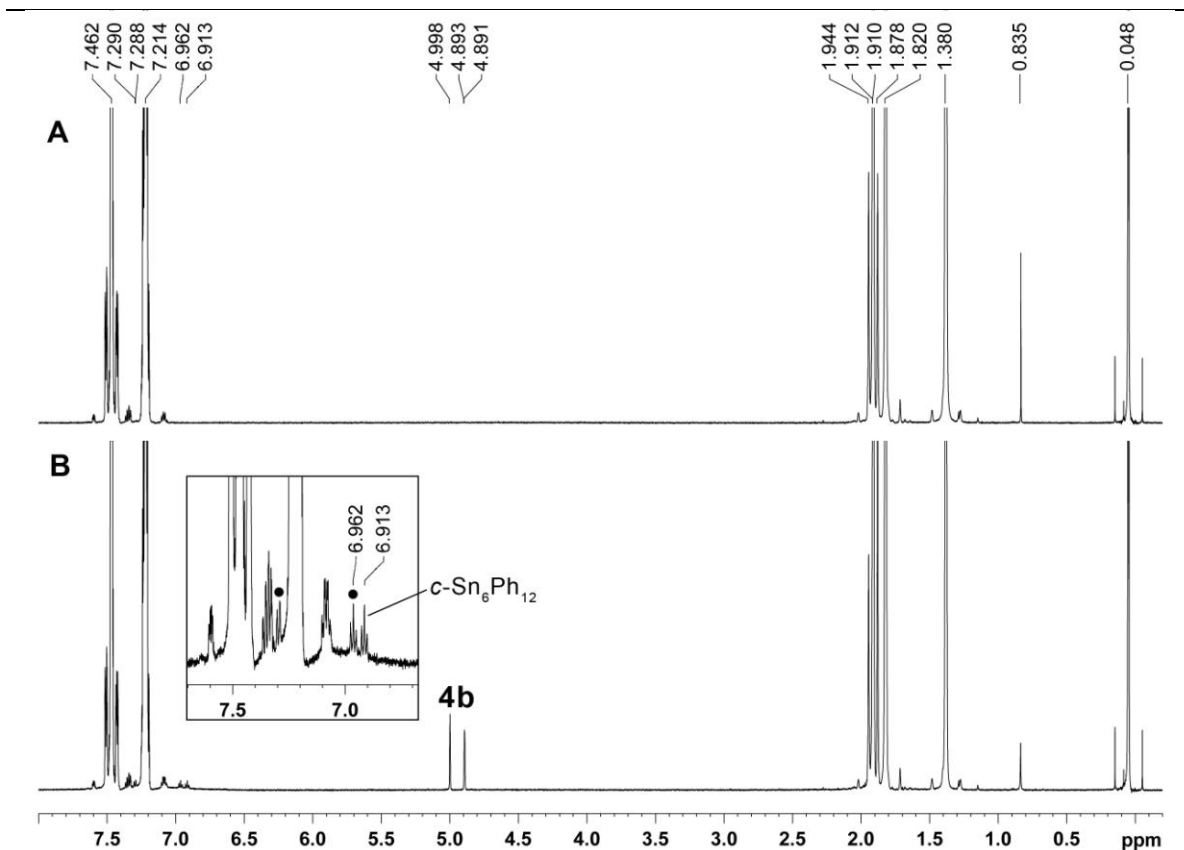


**Figure S2.3.**  $^1\text{H}$  NMR spectra of a deaerated 0.04 M solution of **3** in  $\text{C}_6\text{D}_{12}$  (a) before and (b) after 8.3 minutes photolysis with 254 nm light. The resonances marked with ● disappeared after allowing the photolyzed solution to stand for 18 hours in the dark.

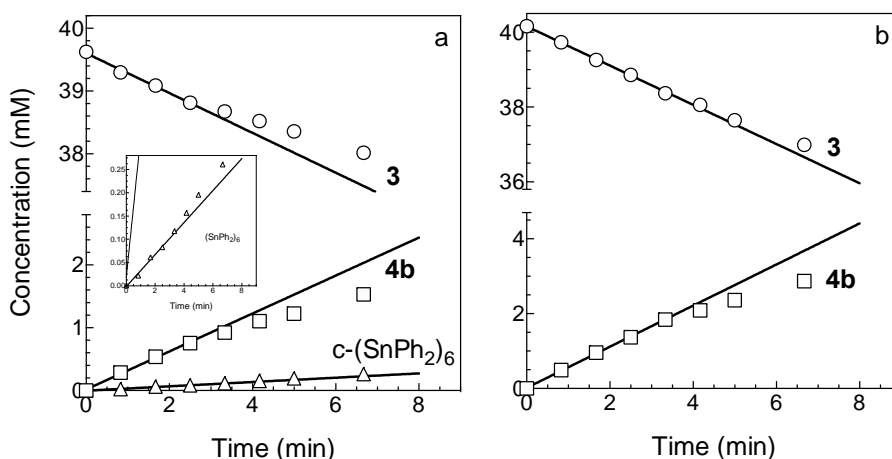


**Figure S2.4.** Concentration versus time plots for photolysis of ca. 0.04 M solutions of **3** in  $\text{C}_6\text{D}_{12}$ , (a) deaerated (slopes (in units of  $\text{mM min}^{-1}$ ): **3** (O),  $-0.32 \pm 0.02$ ; **4b**, (□),  $0.30 \pm 0.01$ ;  $(\text{SnPh}_2)_6$  (Δ),  $0.0057 \pm 0.0005$ ); (b) air-saturated (slopes: **3**(O),  $-0.52 \pm 0.01$ ; **4b**, (□),  $0.55 \pm 0.02$ ).

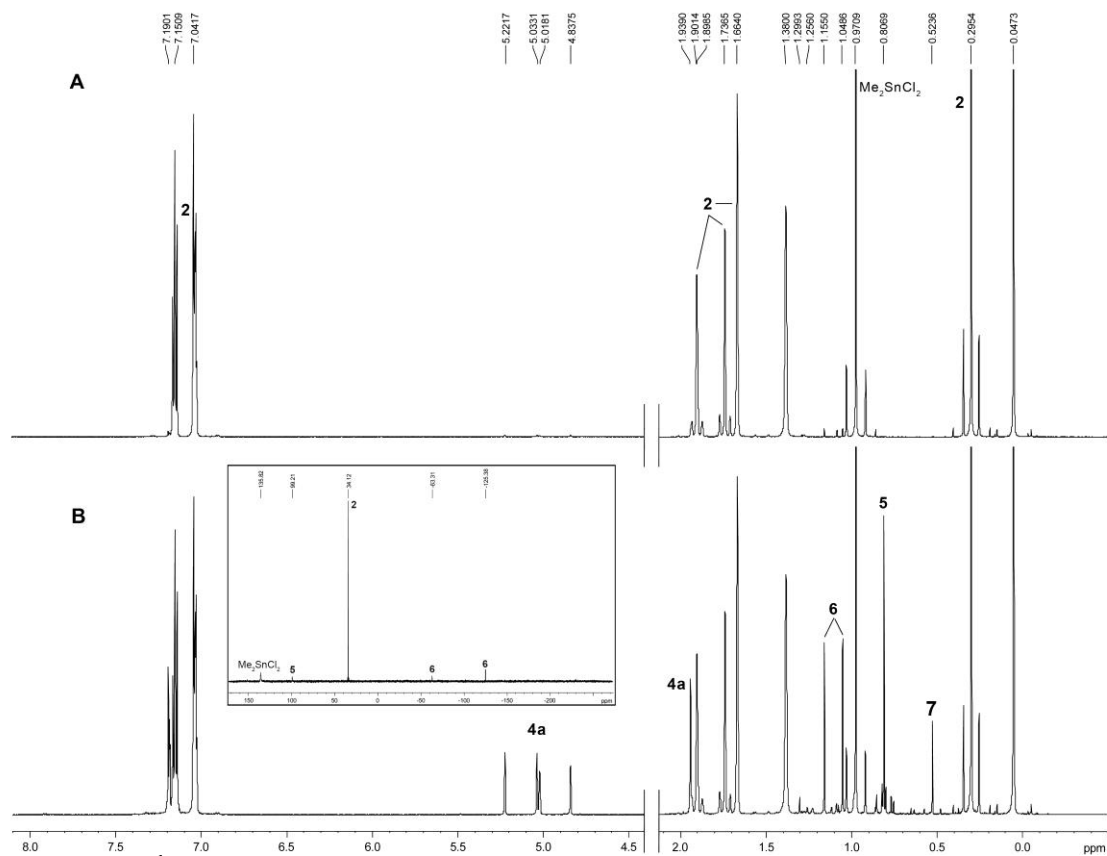


**Figure S2.5.**  $^1\text{H}$  NMR spectra of a deaerated 0.04 M solution of **2** in  $\text{C}_6\text{D}_{12}$  containing  $\text{Me}_2\text{SnCl}_2$  (0.031 M) (a) before and (b) after 10 minutes photolysis with 254 nm light. The inset in B shows the  $^{119}\text{Sn}\{^1\text{H}\}$  NMR spectrum of the photolyzed mixture.

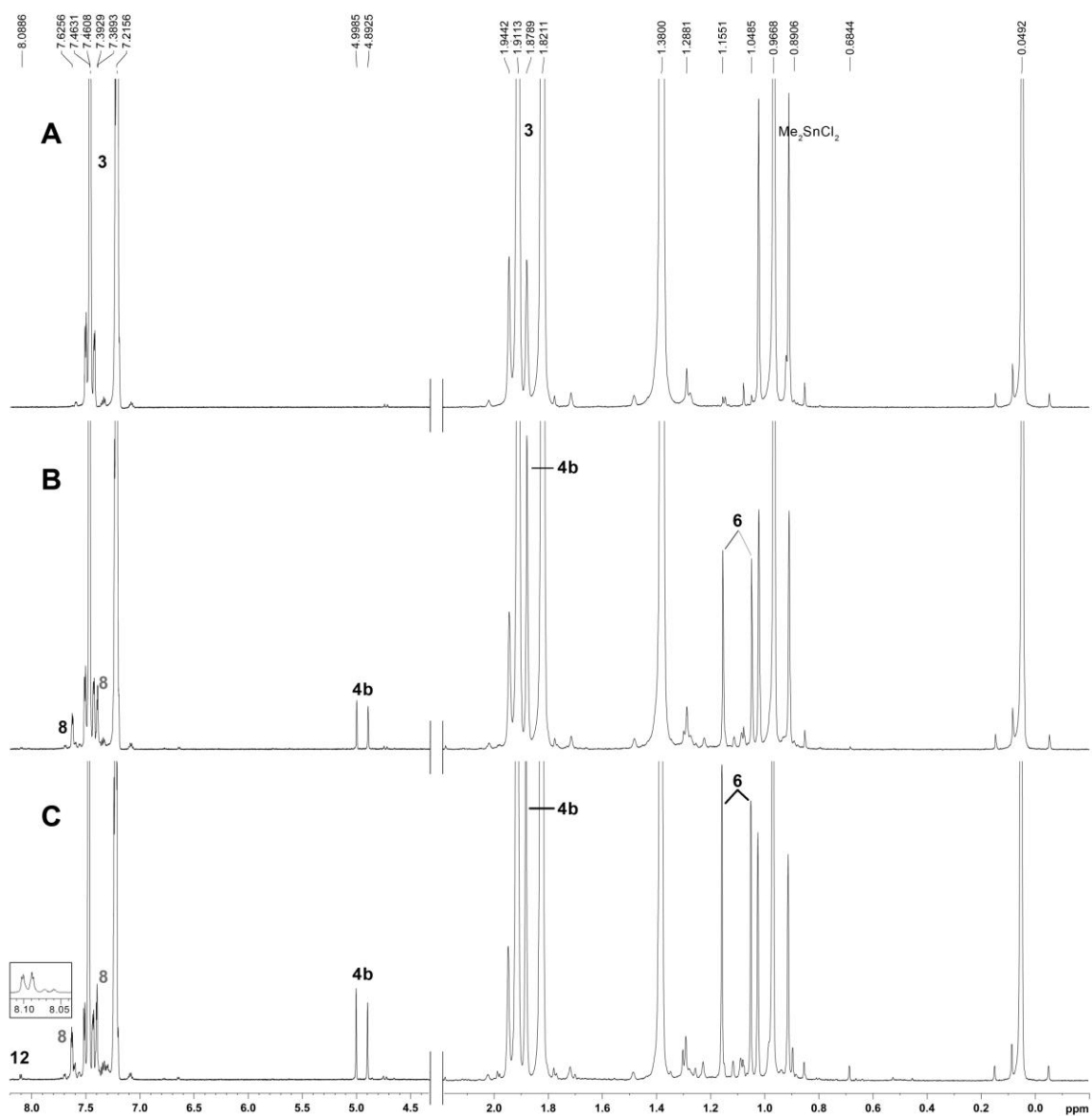


**Figure S2.6.**  $^1\text{H}$  NMR spectra of an undeaerated 0.04 M solution of **3** in  $\text{C}_6\text{D}_{12}$  containing  $\text{Me}_2\text{SnCl}_2$  (0.037 M) (a) before, (b) after 2.5 minutes, and (c) after 6.7 minutes photolysis with 254 nm light. No attempt was made to replenish the air in the photolyzate as the experiment proceeded.

Equilibrium Constants for Interconversion of Cyclodistannoxanes **6**, **12**, and **11** (CDCl<sub>3</sub>, 22 °C).

A mixture of **6** (13.7 mg, 11.9 mM) and hexamethyldisilane (4.00  $\mu$ L, 13.0 mM) in CDCl<sub>3</sub> (1.50 mL) was ultrasonicated in a 5 mL screw cap glass vial at 22 °C, and then the <sup>1</sup>H NMR spectrum of the resulting opaque solution was recorded. The NMR sample was recombined with the bulk of the solution, **8** (24.2 mg, 46.9 mM) was added, the solution was shaken briefly, and the <sup>1</sup>H NMR spectrum of the resulting clear colourless solution (solution ‘a’) was recorded. The procedure was repeated with an additional amount of **8** (26.7 mg, 51.8 mM; solution ‘b’), and again with two successive additions of Me<sub>2</sub>SnCl<sub>2</sub> (31.8 mg, 96.5 mM (solution ‘c’) and 31.5 mg, 95.6 mM (solution ‘d’)).

The relative concentrations of the five components of each of the mixtures (see Table below) were calculated from the NMR integrals, using the signals at  $\delta$  1.19 (s, 12 H),  $\delta$  8.06 (d, 4 H),  $\delta$  8.03 (d, 8 H),  $\delta$  1.21 (s, 6 H), and  $\delta$  7.71 (d, 4 H) for **6**, **12**, **11**, Me<sub>2</sub>SnCl<sub>2</sub>, and Ph<sub>2</sub>SnCl<sub>2</sub> (**8**), respectively. The equilibrium constants  $K_{11 \rightleftharpoons 12}$  and  $K_{12 \rightleftharpoons 6}$  were then calculated by least squares analysis of plots of the concentration ratios of the cyclodistannoxanes versus those of the dichlorostannanes (Fig. S2.7).

Solution	Quantities Mixed / mM			([ <b>6</b> ]/[ <b>12</b> ]) <sub>e</sub>	([ <b>12</b> ]/[ <b>11</b> ]) <sub>e</sub>	([Me <sub>2</sub> SnCl <sub>2</sub> ]/[ <b>8</b> ]) <sub>e</sub>
	<b>6</b>	Me <sub>2</sub> SnCl <sub>2</sub>	<b>8</b>			
(a)	11.9	0	46.9	0.266	0.758	0.383
(b)	11.9	0	98.7	0.205	0.560	0.191
(c)	11.9	96.5	98.7	0.780	1.90	1.32
(d)	11.9	192	98.7	1.23	2.43	2.45



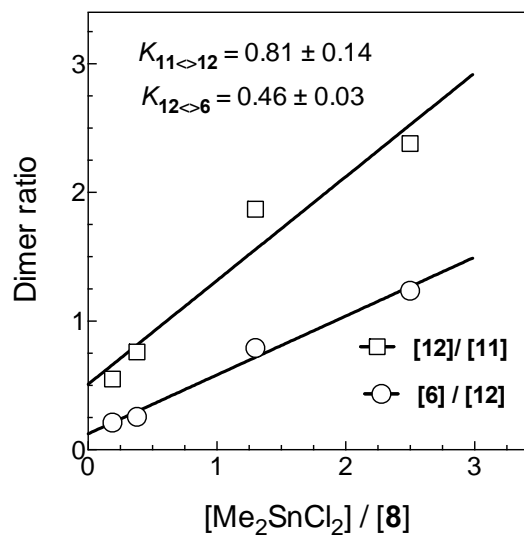


**Figure S2.7.** Plots of the concentration ratios of cyclodistannoxanes **6**, **11**, and **12** (i.e. [6]/[12] and [12]/[11]) versus the dichlorostannane concentration ratio [Me<sub>2</sub>SnCl<sub>2</sub>]/[8], measured from the <sup>1</sup>H NMR spectra of a ca. 0.012 M solution of **6** in CDCl<sub>3</sub> to which sequential portions of Ph<sub>2</sub>SnCl<sub>2</sub> (**8**) and Me<sub>2</sub>SnCl<sub>2</sub> were added at ca. 22 °C. The solid lines are the linear least squares fits of the data to [6]/[12] =  $K_{12 \rightarrow 6}$ [Me<sub>2</sub>SnCl<sub>2</sub>]/[8] (○) and [12]/[11] =  $K_{11 \rightarrow 12}$ [Me<sub>2</sub>SnCl<sub>2</sub>]/[8] (□); errors are quoted as the standard errors from the least squares analysis.

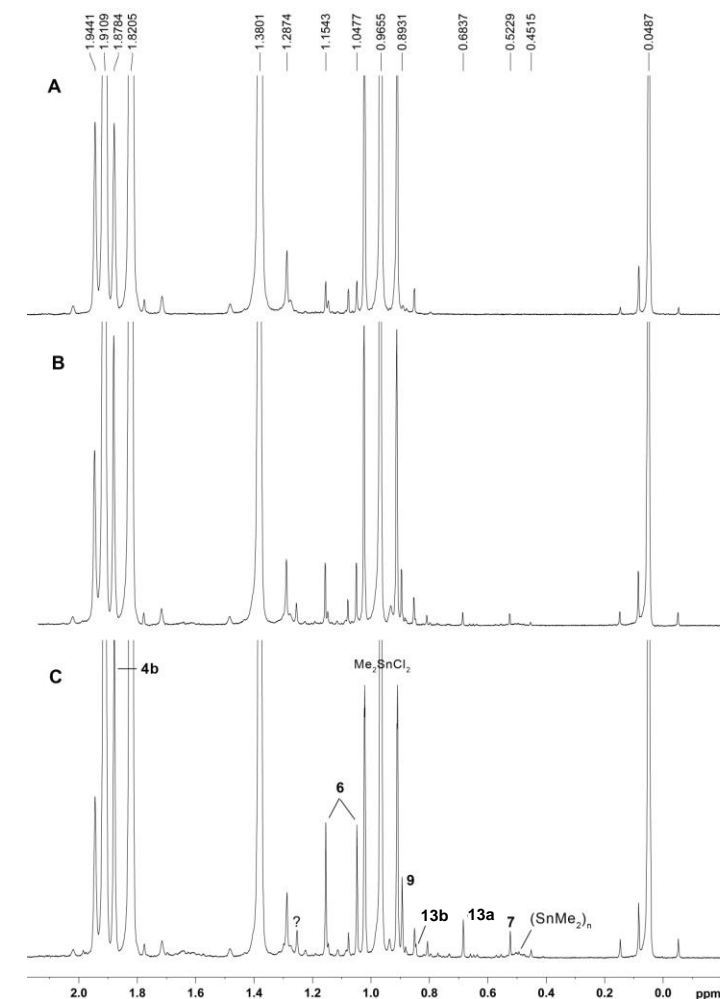


**Figure S2.8.** Partial <sup>1</sup>H NMR spectra of a deaerated 0.038 M solution of **3** in C<sub>6</sub>D<sub>12</sub> containing Me<sub>2</sub>SnCl<sub>2</sub> (0.034 M) (a) before, (b) after 2.5 minutes, and (c) after 6.7 minutes of photolysis.

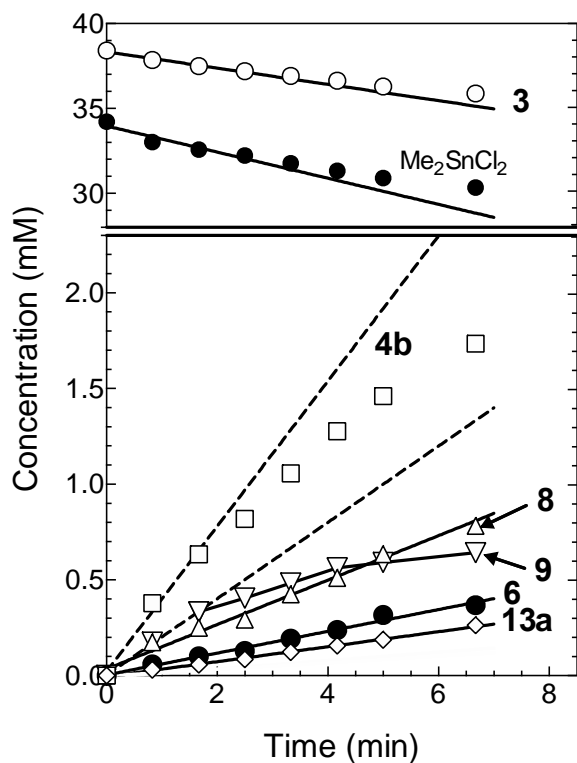


**Figure S2.9.** Concentration versus time plots for the solution of Figure S2.8. The initial slopes of the plots (in  $\text{mM min}^{-1}$ ) are: **3**,  $-0.48 \pm 0.05$ ;  $\text{Me}_2\text{SnCl}_2$ ,  $-0.77$ ; **4b**,  $0.38 \pm 0.04$ ; **6**,  $0.057 \pm 0.003$ ; **8**,  $0.12 \pm 0.01$ ; **9**,  $0.199 \pm 0.006$ ; **13a**,  $0.039 \pm 0.001$ ; **13b** (not shown),  $0.022 \pm 0.002$ ; **7** (not shown),  $0.017 \pm 0.001$ .

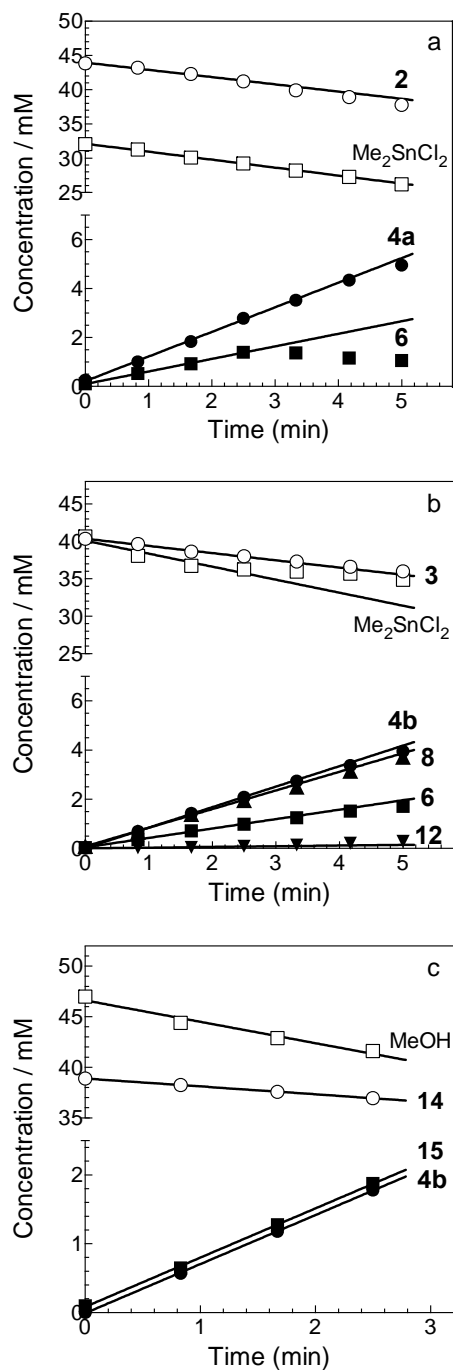


**Figure S2.10.** Concentration versus time plots for the photolysis of air-saturated  $C_6D_{12}$  solutions of (a) **2** and (b) **3** containing ca. 0.04 M  $Me_2SnCl_2$ , and of (c) a deoxygenated  $C_6D_{12}$  solution of **14** containing 0.05 M MeOH; all three solutions also contained  $Si_2Me_6$  (ca. 0.01 M) as an internal integration standard. The initial slopes of the plots for the various compounds are (in  $mM\ min^{-1}$ ): (a) **2**,  $-1.06 \pm 0.09$ ;  $Me_2SnCl_2$ ,  $-1.16 \pm 0.05$ ; **4a**,  $1.01 \pm 0.04$ ; **6**,  $0.51 \pm 0.01$  (A solid, presumed to be **6**, began to precipitate halfway through the experiment, therefore only the first 4 points were used to evaluate the yield of this product); (b) **3**,  $-0.97 \pm 0.07$ ;  $Me_2SnCl_2$ ,  $-1.74 \pm 0.40$ ; **4b**,  $0.83 \pm 0.01$ ; **6**,  $0.38 \pm 0.02$ ; **8**,  $0.76 \pm 0.03$ ; **12**,  $0.03 \pm 0.01$ ; (c) **14**,  $-0.781 \pm 0.002$ ; **4b**,  $0.713 \pm 0.006$ ; **15**,  $0.716 \pm 0.012$ .

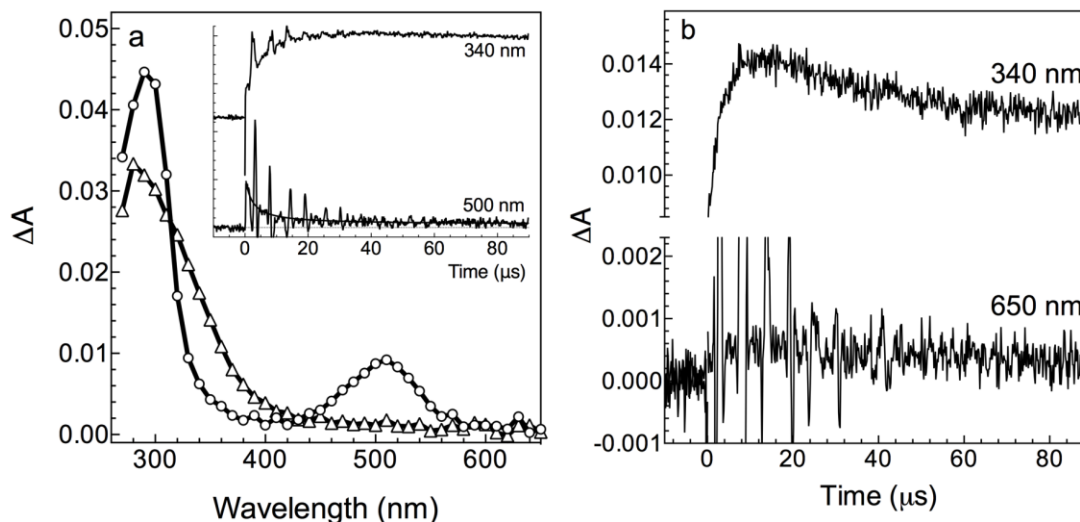


**Figure S2.11.** (a) Transient UV-vis absorption spectra from laser flash photolysis of a rapidly flowed, deoxygenated solution of **3** ( $7 \times 10^{-4}$  M) in anhydrous hexanes at 25 °C, recorded over a longer timescale than that shown in Figure 2.2. The spectra were recorded 0.64 - 0.96  $\mu$ s ( $\circ$ ) and 81.1 - 81.9  $\mu$ s ( $\Delta$ ) after the pulse, using a Pyrex filter in the monitoring beam at wavelengths above 310 nm; the inset shows absorbance versus time profiles recorded at 340 and 500 nm. (b) Transient absorbance-time profiles recorded for a flowed solution of **3** in deoxygenated hexanes, under similar conditions to those used for the experiment shown in (a). The 340 nm  $\Delta A$ -time profile was recorded as in (a) and is the average of 10 laser shots, while the 650 nm profile was recorded with a 520 nm cutoff filter (Corning 3-69) in the monitoring beam to filter out overtone absorptions, and is the average of 70 laser shots. The  $\Delta A$ -time profile at 500 nm (recorded with a Pyrex filter) was quite similar to that obtained in the experiment of (a).

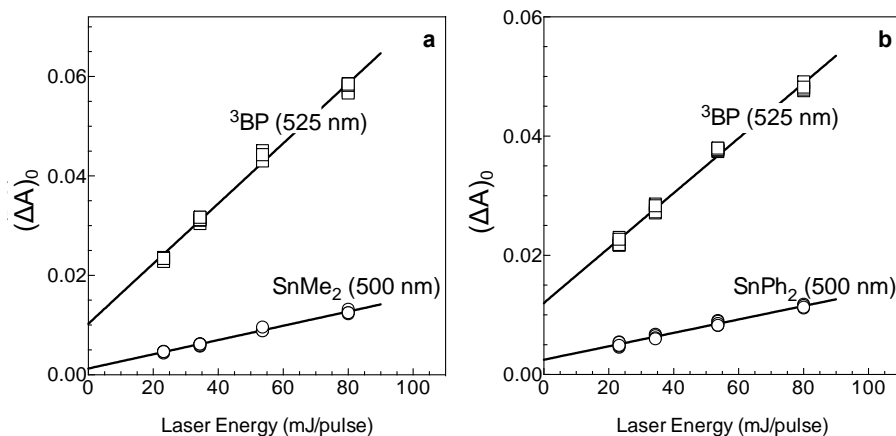


**Figure S2.12.** Plots of initial transient absorbance  $(\Delta A)_0$  versus laser pulse energy from optically matched (at 248 nm), deoxygenated hexanes solutions of (a) benzophenone and **2**, and (b) benzophenone and **3**, for determination of the extinction coefficients of the  $\text{SnMe}_2$  and  $\text{SnPh}_2$  absorption bands at 500 nm. The benzophenone triplet ( $^3\text{BP}$ ;  $\Phi = 1.0$ ) was monitored at 525 nm ( $\epsilon = 6,250 \pm 1,250 \text{ M}^{-1} \text{ cm}^{-1}$ ).<sup>76</sup> The slopes of the plots are (a)  $^3\text{BP}$ ,  $(6.0 \pm 0.1) \times 10^{-4}$ ,  $\text{SnMe}_2$   $(1.43 \pm 0.02) \times 10^{-4}$ ; (b)  $^3\text{BP}$ ,  $(4.61 \pm 0.08) \times 10^{-4}$ ,  $\text{SnPh}_2$   $(1.13 \pm 0.03) \times 10^{-4}$ .

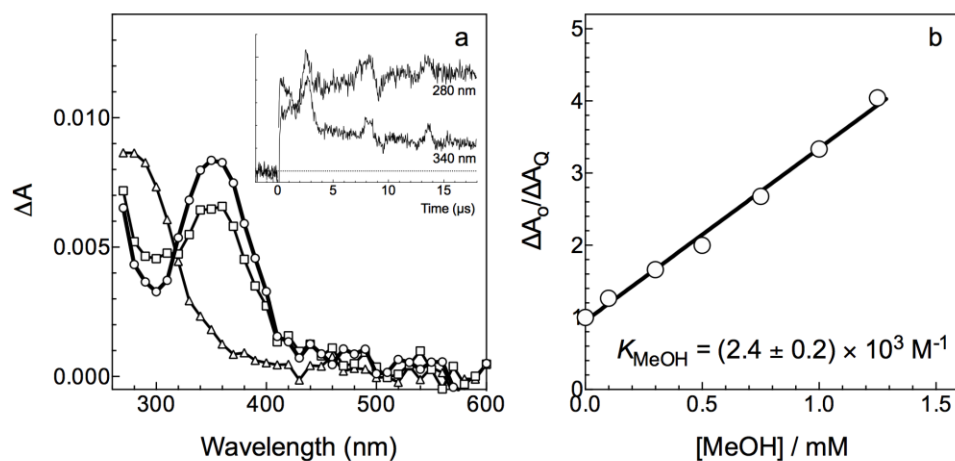


**Figure S2.13.** (a) Time-resolved UV-vis spectra recorded by laser photolysis of  $\text{SnMe}_2$  precursor **2** in hexanes containing 7 mM MeOH, 0.22-0.29  $\mu\text{s}$  ( $\circ$ ), 1.25-1.31  $\mu\text{s}$  ( $\square$ ) and 17.5-17.7  $\mu\text{s}$  ( $\Delta$ ) after the laser pulse (25 °C), and absorbance-time profiles at selected wavelengths (inset). (b) Plot of  $(\Delta A)_0 / (\Delta A)_Q$  for complexation of  $\text{SnMe}_2$  with MeOH in hexanes at 25 °C; the solid line is the linear least squares fit of the data to equation 2.20.

## Computational Studies

Theoretical calculations were carried out using the Gaussian09 (Rev. B.01) suite of programs.<sup>77</sup>

**Table S2.1.** Calculated Electronic Energies, Standard Enthalpies (298.15 K), and Standard Free Energies (298.15 K) of Stationary Points in the Dimerization of SnMe<sub>2</sub> and SnPh<sub>2</sub>, Calculated at the  $\omega$ B97X/6-31+G(d,p)<sup>C,H,O</sup>-LANL2DZdp<sup>Sn</sup> Level of Theory Relative to the Isolated Reactants (in kcal mol<sup>-1</sup>).

Species	$\omega$ B97X/6-31+G(d,p) <sup>C,H,O</sup> -LANL2DZdp <sup>Sn</sup>				
	$\Delta E_{\text{elec}}$	$\Delta H^\circ$	$\Delta G^\circ$	$\Delta(\Delta H^\circ)^a$	$\Delta(\Delta G^\circ)^a$
Me <sub>2</sub> Sn=SnMe <sub>2</sub> ( <b>16a</b> )	-23.4	-20.7	-10.4	-1.4	-1.5
MeSnSnMe <sub>3</sub> ( <b>17a</b> )	-32.2	-29.8	-20.3	-0.5	-0.8
Ph <sub>2</sub> Sn=SnPh <sub>2</sub> ( <b>16b</b> )	-19.5	-18.0	-8.3	-3.1	-3.1
PhSnSnPh <sub>3</sub> ( <b>17b</b> )	-30.8	-29.3	-20.4	-3.7	-0.7
PhSn(C <sub>6</sub> H <sub>5</sub> )SnPh <sub>2</sub> ( <b>19</b> )	-24.2	-22.9	-11.1	-5.4	-5.2
<i>trans</i> -PhSn(C <sub>6</sub> H <sub>5</sub> ) <sub>2</sub> SnPh ( <b>20</b> )	-14.0	-12.6	-0.2	-5.4	-5.6
Transition state <b>24</b> <sup>‡</sup>	+8.1	+8.6	+21.7	-7.6	-7.3
Transition state <b>25</b> <sup>‡</sup>	-24.2	-23.5	-10.3	-5.0	-5.4
Me <sub>2</sub> Sn←O(H)Me ( <b>18a</b> ) <sup>b</sup>	-14.0	-12.5	-2.6	+0.7	+0.7
Ph <sub>2</sub> Sn←O(H)Me ( <b>18b</b> ) <sup>b</sup>	-15.9	-14.4	-4.0	+0.1	+0.7

a. Defined as  $\Delta(\Delta E) = \Delta E(\omega$ B97XD) -  $\Delta E(\omega$ B97X).

b. Corrected for Basis Set Superposition Error (BSSE).

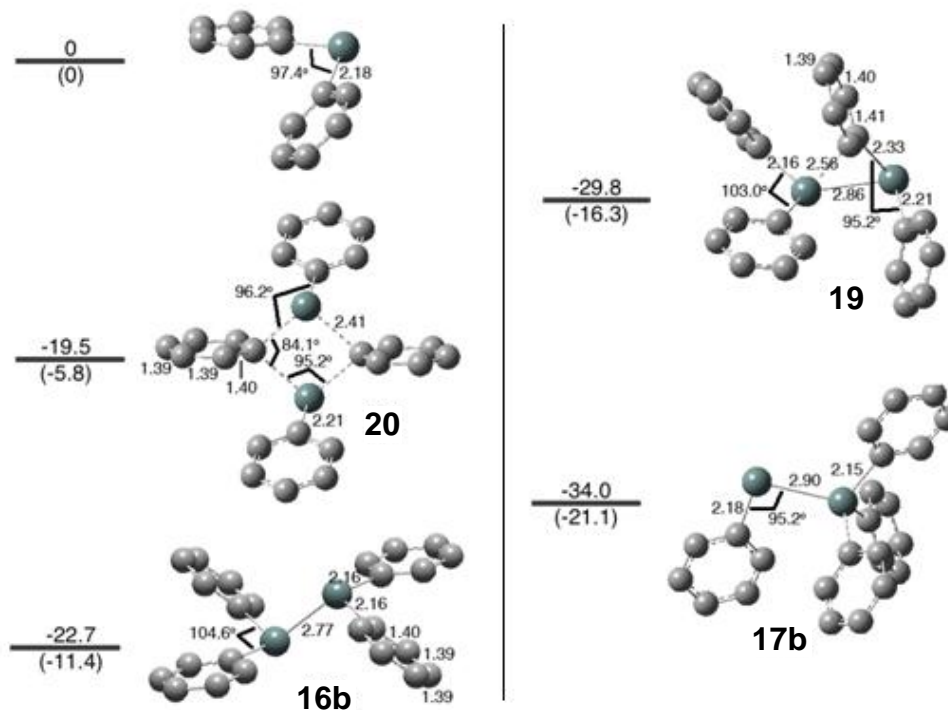


**Figure S2.14.** Selected geometric parameters, electronic energies and standard free energies (in parentheses) for  $\text{SnPh}_2$  and the  $\text{SnPh}_2$ -dimers **16b**, **17b**, **19** and (*trans*-) **20**, calculated at the  $\omega\text{B97XD}/6\text{-}31+\text{G}(\text{d},\text{p})^{\text{C,H,O}}\text{-LANL2DZdp}^{\text{Sn}}$  level (hydrogen atoms omitted for clarity).

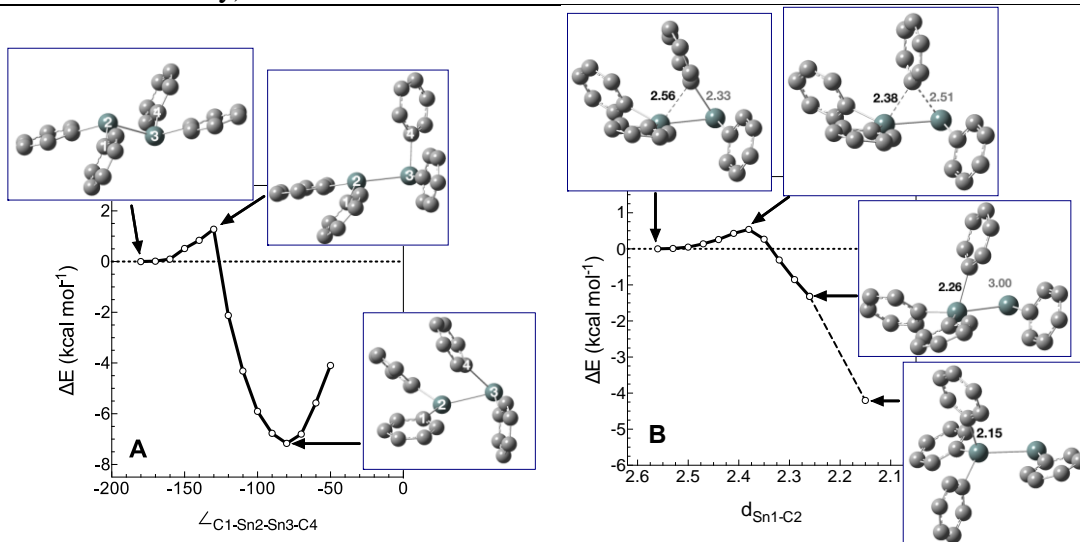


**Figure S2.15.** Plots of  $\Delta E$  versus geometry from relaxed PES scans of (A) the C1-Sn2-Sn3-C4 dihedral angle in **16b** and (B) the Sn-C bond distance involving the bridging phenyl group in stannylidenestannylene **19**, carried out at the  $\omega\text{B97XD}/6\text{-}31+\text{G}(\text{d},\text{p})^{\text{C,H}}\text{-LANL2DZdp}^{\text{Sn}}$  level of theory.

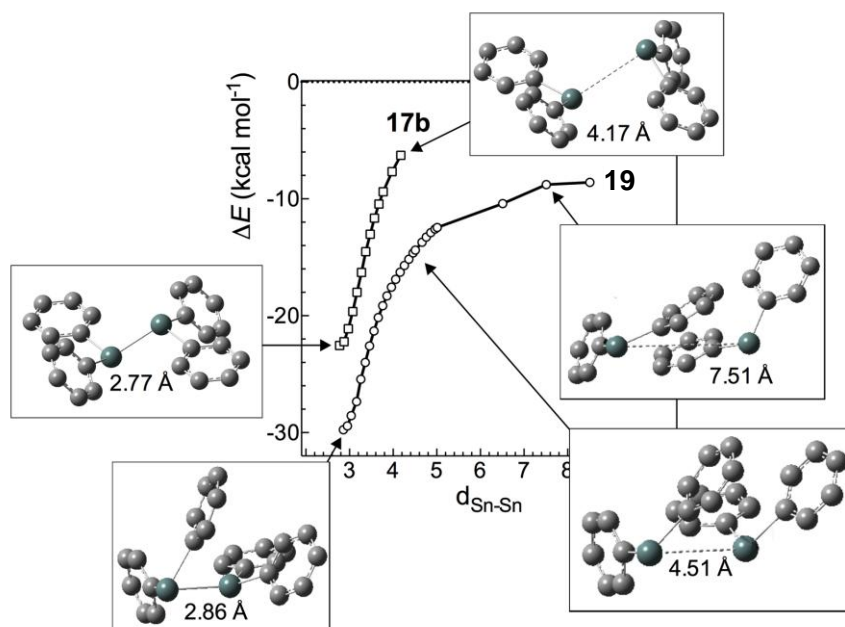


**Figure S2.16.** Plot of calculated relative electronic energies ( $\Delta E$ ; relative to two  $\text{SnPh}_2$  moieties at infinite separation) versus Sn-Sn bond distance, from relaxed potential energy surface scans of the Sn-Sn bond distances ( $d_{\text{Sn-Sn}}$ ) in **17b** and **19** at the  $\omega\text{B97XD/6-31+G(d,p)}^{\text{C,H}}\text{-LANL2DZdp}^{\text{Sn}}$  level of theory. The calculated structures at various  $d_{\text{Sn-Sn}}$  values in the calculations are also shown.

## 2.5. References

- (1) Zhou, D.; Reiche, C.; Nag, M.; Soderquist, J. A.; Gaspar, P. P. *Organometallics* **2009**, *28*, 2595.
- (2) Becerra, R.; Harrington, C. R.; Gaspar, P. P.; Leigh, W. J.; Vargas-Baca, I.; Walsh, R.; Zhou, D. *J. Am. Chem. Soc.* **2005**, *127*, 17469.
- (3) Gross, L. W.; Moser, R.; Neumann, W. P.; Scherping, K. H. *Tetrahedron Lett.* **1982**, *23*, 635.
- (4) Dewar, M. J. S.; Friedheim, J. E.; Grady, G. L. *Organometallics* **1985**, *4*, 1784.
- (5) Neumann, W. P.; Schwarz, A. *Angew. Chem. Int. Ed. Engl.* **1975**, *14*, 812.
- (6) Neumann, W. P. *Chem. Rev.* **1991**, *91*, 311.
- (7) Watta, B.; Neumann, W. P.; Sauer, J. *Organometallics* **1985**, *4*, 1954.
- (8) Mathiasch, B. *Inorg. Nucl. Chem. Lett.* **1977**, *13*, 13.
- (9) Adams, S.; Dräger, M.; Mathiasch, B. *Z. Anorg. Allg. Chem.* **1986**, *532*, 81.
- (10) Gibbons, A. J.; Sawyer, A. K.; Ross, A. *J. Org. Chem.* **1961**, *26*, 2304.
- (11) Sawyer, A. K.; Brown, Y. E.; Hanson, E. L. *J. Organomet. Chem.* **1965**, *3*, 464.
- (12) Davies, A. G. *J. Chem. Res.* **2004**, 309.



- (13) Murov, S. L.; Carmichael, I.; Hug, G. L. *Handbook of photochemistry*; 2nd ed.; Dekker: New York, 1993.
- (14) Dakternieks, D.; Jurkschat, K.; van Dreumel, S.; Tiekink, E. R. T. *Inorg. Chem.* **1997**, *36*, 2023.
- (15) Davies, A. G. *Organotin Chemistry*; 2nd ed.; Wiley-VCH, 2004.
- (16) Patel, Y.; George, J.; Pillai, S. M.; Munshi, P. *Green Chem.* **2009**, *11*, 1056.
- (17) Our initial experiments employed a method of air-purging that proved to be capable of removing only 60-70% of the dissolved oxygen in the air-saturated solvent.
- (18) Apodaca, P.; Cervantes-Lee, F.; Pannell, K. H. *Main Group Metal Chem.* **2001**, *24*, 597.
- (19) Kapoor, R. N.; Apodaca, P.; Montes, M.; Gomez, F. D.; Pannell, K. H. *Appl. Organomet. Chem.* **2005**, *19*, 518.
- (20) Scherping, K. H.; Neumann, W. P. *Organometallics* **1982**, *1*, 1017.
- (21) Leigh, W. J.; Harrington, C. R.; Vargas-Baca, I. *J. Am. Chem. Soc.* **2004**, *126*, 16105.
- (22) The spikes in the absorbance-time profiles are attributed to thermal shock waves, generated by the release of a pulse of heat following absorption of the laser pulse by the solid particulate, which resonate back and forth through the cell. See Scaiano, J. C. in *Reactive Intermediate Chemistry*; Moss, R. A., Platz, M. S., Jones, M., Jr., Eds.; John Wiley & Sons: New York, 2004, p 847.
- (23) Tokitoh, N.; Saito, M.; Okazaki, R. *J. Am. Chem. Soc.* **1993**, *115*, 2065.
- (24) Weidenbruch, M.; Schlaefke, J.; Schafer, A.; Peters, K.; Schnering, H. G. v.; Marsmann, H. *Angew. Chem. Int. Ed. Engl.* **1994**, *33*, 1846.
- (25) Saito, M.; Tokitoh, N.; Okazaki, R. *Chem. Lett.* **1996**, *25*, 265.
- (26) Henning, J.; Eichele, K.; Fink, R. F.; Wesemann, L. *Organometallics* **2014**, *33*, 3904.
- (27) Wilfling, P.; Schittelkopf, K.; Flock, M.; Herber, R. H.; Power, P. P.; Fischer, R. C. *Organometallics* **2015**, *34*, 2222.
- (28) Tokitoh, N.; Ando, W. In *Reactive Intermediate Chemistry*; Moss, R. A., Platz, M. S., Jones, M., Jr., Eds.; John Wiley & Sons: New York, 2004, p 651.
- (29) Moiseev, A. G.; Leigh, W. J. *Organometallics* **2007**, *26*, 6268.
- (30) Mizuhata, Y.; Sasamori, T.; Tokitoh, N. *Chem. Rev.* **2009**, *109*, 3479.
- (31) Masamune, S.; Sita, L. R. *J. Am. Chem. Soc.* **1985**, *107*, 6390.
- (32) Moiseev, A. G.; Leigh, W. J. *J. Am. Chem. Soc.* **2006**, *128*, 14442.
- (33) Trinquier, G. *J. Am. Chem. Soc.* **1990**, *112*, 2130.
- (34) Trinquier, G. *J. Am. Chem. Soc.* **1991**, *113*, 144.
- (35) Phillips, A. D.; Hino, S.; Power, P. P. *J. Am. Chem. Soc.* **2003**, *125*, 7520.
- (36) Drost, C.; Hildebrand, M.; Lonneck, P. *Main Group Metal Chem.* **2002**, *25*, 93.
- (37) Lai, G.; Xu, Z.; Li, Z.; Jiang, J.; Kira, M.; Qiu, H. *Organometallics* **2009**, *28*, 3591.
- (38) Xu, Z.; Jin, J.; Li, Z.; Qiu, H.; Jiang, J.; Lai, G.; Kira, M. *Chem. Eur. J.* **2009**, *15*, 8605.

- (39) Xu, Z.; Jin, J.; Zhang, H.; Li, Z.; Jiang, J.; Lai, G.; Kira, M. *Organometallics* **2011**, *30*, 3311.
- (40) Wintgens, V.; Johnston, L. J.; Scaiano, J. C. *J. Am. Chem. Soc.* **1988**, *110*, 511.
- (41) Carmichael, I.; Hug, G. L.; Scaiano, J. C. In *CRC handbook of organic photochemistry, Vol. I*; CRC Press: Boca Raton, 1989, p 369.
- (42) Conlin, R. T.; Netto-Ferreira, J. C.; Zhang, S.; Scaiano, J. C. *Organometallics* **1990**, *9*, 1332.
- (43) Kira, M.; Yauchibara, R.; Hirano, R.; Kabuto, C.; Sakurai, H. *J. Am. Chem. Soc.* **1991**, *113*, 7785.
- (44) Yamaji, M.; Hamanishi, K.; Takahashi, T.; Shizuka, H. *J. Photochem. Photobiol. A: Chem.* **1994**, *81*, 1.
- (45) Kira, M.; Ishida, S.; Iwamoto, T.; Kabuto, C. *J. Am. Chem. Soc.* **1999**, *121*, 9722.
- (46) Tokitoh, N.; Kishikawa, K.; Okazaki, R.; Sasamori, T.; Nakata, N.; Takeda, N. *Polyhedron* **2003**, *21*, 563.
- (47) Leigh, W. J.; Lollmahomed, F.; Harrington, C. R. *Organometallics* **2006**, *25*, 2055.
- (48) Spikes, G. H.; Peng, Y.; Fettinger, J. C.; Power, P. P. *Z. Anorg. Allg. Chem.* **2006**, *632*, 1005.
- (49) Davidson, P. J.; Harris, D. H.; Lappert, M. F. *Dalton Trans.* **1976**, 2268.
- (50) The rate coefficient was measured at 540 nm, at which the extinction coefficient is roughly half the value at the absorption maximum (see Fig. 4).
- (51) Leigh, W. J.; Lollmahomed, F.; Harrington, C. R.; McDonald, J. M. *Organometallics* **2006**, *25*, 5424.
- (52) Kostina, S. S.; Singh, T.; Leigh, W. J. *Organometallics* **2012**, *31*, 3755.
- (53) Lollmahomed, F.; Huck, L. A.; Harrington, C. R.; Chitnis, S. S.; Leigh, W. J. *Organometallics* **2009**, *28*, 1484.
- (54) Leigh, W. J.; Kostina, S. S.; Bhattacharya, A.; Moiseev, A. G. *Organometallics* **2010**, *29*, 662.
- (55) Computational studies were carried out by Prof. W.J. Leigh.
- (56) Chai, J.-D.; Head-Gordon, M. *Phys. Chem. Chem. Phys.* **2008**, *10*, 6615.
- (57) Check, C. E.; Faust, T. O.; Bailey, J. M.; Wright, B. J.; Gilbert, T. M.; Sunderlin, L. S. *J. Phys. Chem. A* **2001**, *105*, 8111.
- (58) Boys, S. F.; Bernardi, F. *Mol. Phys.* **1970**, *19*, 553.
- (59) Leung, W. P.; Kwok, W. H.; Xue, F.; Mak, T. C. W. *J. Am. Chem. Soc.* **1997**, *119*, 1145.
- (60) Drost, C.; Hitchcock, P. B.; Lappert, M. F. *Angew. Chem. Int. Ed.* **1999**, *38*, 1113.
- (61) Weidenbruch, M.; Stilter, A.; Marsmann, H.; Peters, K.; von Schnering, H. G. *Eur. J. Inorg. Chem.* **1998**, 1333.
- (62) Lee, V. Y.; Sekiguchi, A. In *Organometallic Compounds of Low-Coordinate Si, Ge, Sn and Pb*; John Wiley & Sons, Ltd: Chichester, 2010, p 199.
- (63) Leung, W.-P.; Cheng, H.; Huang, R.-B.; Yang, Q.-C.; Mak, T. C. W. *Chem. Commun.* **2000**, 451.

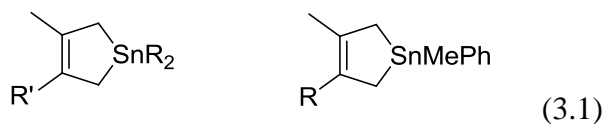
- (64) The corresponding Hirshfeld charges at Sn1 and Sn2 in 23 are +0.21 and +0.45, respectively.
- (65) Stanciu, C.; Richards, A. F.; Power, P. P. *J. Am. Chem. Soc.* **2004**, *126*, 4106.
- (66) Rivard, E.; Fischer, R. C.; Wolf, R.; Peng, Y.; Merrill, W. A.; Schley, N. D.; Zhu, Z.; Pu, L.; Fettinger, J. C.; Teat, S. J.; Nowik, I.; Herber, R. H.; Takagi, N.; Nagase, S.; Power, P. P. *J. Am. Chem. Soc.* **2007**, *129*, 16197.
- (67) Trinquier, G.; Malrieu, J. P. *J. Am. Chem. Soc.* **1991**, *113*, 8634.
- (68) Chai, J.-D.; Head-Gordon, M. *J. Chem. Phys.* **2008**, *128*, 08410610.1063/1.2834918
- (69) Malcolm, N. O. J.; Gillespie, R. J.; Popelier, P. L. A. *J. Chem. Soc., Dalton Trans.* **2002**, *2002*, 3333.
- (70) Su, M. D. *Chem. Eur. J.* **2004**, *10*, 6073.
- (71) Goldberg, D. E.; Harris, D. H.; Lappert, M. F.; Thomas, K. M. *Chem. Commun.* **1976**, 261.
- (72) Fischer, R. C.; Power, P. P. *Chem. Rev.* **2010**, *110*, 3877.
- (73) Eichler, B. E.; Power, P. P. *Inorg. Chem.* **2000**, *39*, 5444.
- (74) Tsai, M.-L.; Su, M.-D. *J. Phys. Chem. A* **2006**, *110*, 6216.
- (75) Broeckert, L.; Geerlings, P.; Růžička, A.; Willem, R.; De Proft, F. *Organometallics* **2012**, *31*, 1605.
- (76) Carmichael, I.; Helman, W. P.; Hug, G. L. *J. Phys. Chem. Ref. Data* **1987**, *16*, 239.
- (77) Frisch, M. J.; Trucks, G. W.; Schlegel, H. B.; Scuseria, G. E.; Robb, M. A.; Cheeseman, J. R.; Scalmani, G.; Barone, V.; Mennucci, B.; Petersson, G. A.; Nakatsuji, H.; Caricato, M.; Li, X.; Hratchian, H. P.; Izmaylov, A. F.; Bloino, J.; Zheng, G.; Sonnenberg, J. L.; Hada, M.; Ehara, M.; Toyota, K.; Fukuda, R.; Hasegawa, J.; Ishida, M.; Nakajima, T.; Honda, Y.; Kitao, O.; Nakai, H.; Vreven, T.; Montgomery, J., J. A.; Peralta, J. E.; Ogliaro, F.; Bearpark, M.; Heyd, J. J.; Brothers, E.; Kudin, K. N.; Staroverov, V. N.; Kobayashi, R.; Normand, J.; Raghavachari, K.; Rendell, A.; Burant, J. C.; Iyengar, S. S.; Tomasi, J.; Cossi, M.; Rega, N.; Millam, N. J.; Klene, M.; Knox, J. E.; Cross, J. B.; Bakken, V.; Adamo, C.; Jaramillo, J.; Gomperts, R.; Stratmann, R. E.; Yazyev, O.; Austin, A. J.; Cammi, R.; Pomelli, C.; Ochterski, J. W.; Martin, R. L.; Morokuma, K.; Zakrzewski, V. G.; Voth, G. A.; Salvador, P.; Dannenberg, J. J.; Dapprich, S.; Daniels, A. D.; Farkas, Ö.; Foresman, J. B.; Ortiz, J. V.; Cioslowski, J.; Fox, D. J.; Gaussian, I., Wallingford CT, 2009; Gaussian, Inc.: Wallingford CT, 2009.

### Chapter 3: Reactivity of Transient Stannylenes in Solution

#### 1) Direct Detection of SnMePh and Reactions of SnMe<sub>2</sub>, SnPh<sub>2</sub>, and SnMePh with Chlorostannanes and Acetic Acid

##### 3.1. Overview

As discussed in the previous chapter,<sup>1</sup> laser flash photolysis experiments carried out with solutions of **1** or **2** in anhydrous hexanes, using the pulses from a KrF excimer laser (248 nm) for excitation, result in the observation of SnMe<sub>2</sub> and SnPh<sub>2</sub> as promptly formed, short-lived transients, exhibiting UV-vis absorption bands centred at  $\lambda_{\text{max}} = 500$  nm ( $\tau \sim 10$   $\mu\text{s}$ ) and  $\lambda_{\text{max}} = 290, 505$  nm ( $\tau \sim 20$   $\mu\text{s}$ ), respectively.



1. R = Me; R' = Ph

2. R = Ph; R' = Me

3. R = Me

4. R = Ph

This chapter discusses the reactions of transient stannylenes with tributyltin chloride (Bu<sub>3</sub>SnCl) and acetic acid (AcOH), where the results of product studies and laser flash photolysis experiments suggest rapid and irreversible reaction of the stannylenes leading to discrete product formation. In carrying out this study, it became apparent the differing observations between alkyl and aryl substituted stannylenes, suggesting the behaviour of methylphenylstannylene (SnMePh) would be particularly informative.

The initial motivation to study SnMePh was to provide additional insight into the dimerization of SnMe<sub>2</sub> and SnPh<sub>2</sub>, as well as their reactions with Me<sub>2</sub>SnCl<sub>2</sub>. Thus, this chapter begins by discussing the preparation of stannacyclopent-3-enes **3** and **4**, which were used as photoprecursors of SnMePh in order to characterize the stannylenes' behaviour in solution and carry out chemical trapping studies with Me<sub>2</sub>SnCl<sub>2</sub> as the scavenger. Next, reactivity studies involving Sn-Cl insertion of SnMe<sub>2</sub>, SnMePh and

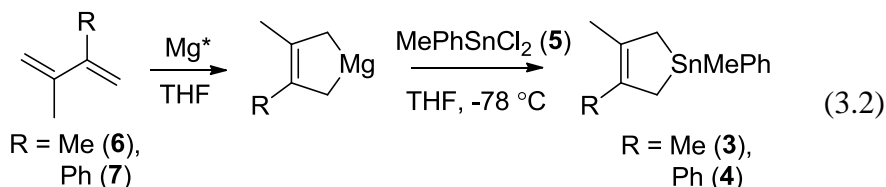
$\text{SnPh}_2$  with  $\text{Bu}_3\text{SnCl}$  were conducted, which expands on the insertion reaction of  $\text{Me}_2\text{SnCl}_2$  described in the previous chapter. In the final section, the reaction of  $\text{SnMe}_2$ ,  $\text{SnMePh}$  and  $\text{SnPh}_2$  with  $\text{AcOH}$  was studied through a combination of product studies, deuterium labelling, and laser flash photolysis methods. The results indicate competing ligand substitution and oxidative addition reaction channels, which has precedent in the reactions of kinetically stabilized diarylstannylenes with small protic molecules like  $\text{NH}_3$ ,  $\text{H}_2\text{O}$  and  $\text{MeOH}$ .<sup>2,3</sup>

## 3.2. Direct Detection and Chemical Trapping of $\text{SnMePh}$ in Solution

### 3.2.1. Results

Compounds **3** and **4** were prepared by an adaptation of the method of Gaspar and coworkers<sup>4</sup> by treatment of methylphenyltin dichloride ( $\text{MePhSnCl}_2$ , **5**) with the magnesacycle generated from Rieke magnesium ( $\text{Mg}^*$ ) and either 2,3-dimethyl-1,3-butadiene (**6**) for **3** or 2-methyl-3-phenyl-1,3-butadiene (**7**) for **4** (eq. 3.2). Compound **3** was obtained as a clear colourless oil in 2 % yield by silica gel column chromatography using a gradient elution method (0 to 30% dichloromethane / hexane). Samples used for steady state and laser flash photolysis studies of **3** contain additional  $^1\text{H}$  and  $^{13}\text{C}$  NMR resonances that suggest the presence of an aliphatic hydrocarbon that was found to be unchanged in steady state photolysis experiments. Without knowing the exact structure of the impurity, integration of the  $\delta_{\text{H}} = 0.88$  ppm resonance relative to the  $\delta_{\text{H}} = 0.43$  ppm resonance due to **3** (see Figure S3.2a) indicates it is present at the level of 12 mol % relative to **3**, assuming the 0.88 ppm resonance is due to 6 equivalent protons. In addition, a small quantity of naphthalene is present (ca. 0.2 mol % relative to **3** as determined by  $^1\text{H}$  NMR spectroscopy) that could not be removed. Compound **4** was isolated as a clear colourless oil in 45 % yield by applying a vacuum to remove both excess naphthalene and **7**, followed by column chromatography using basic alumina as the stationary phase and

10 % dichloromethane / pentane as the eluant. Samples of **4** used for steady state and laser flash photolysis studies contain (as determined by  $^1\text{H}$  and  $^{13}\text{C}$  NMR spectroscopy) an unknown impurity ( $\leq 10$  mol %) that was also found to be unchanged in steady state photolysis experiments.



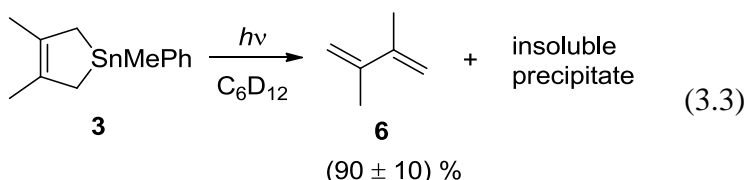
Compounds **3** and **4** were identified on the basis of their  $^1\text{H}$ ,  $^{13}\text{C}$  and  $^{119}\text{Sn}$  NMR spectra, and high resolution mass spectrometry (HRMS). Diagnostic resonances in the  $^1\text{H}$  NMR ( $\text{CDCl}_3$ ) spectrum of **3** include a singlet at 0.50 (s, 3 H,  $^2J_{\text{SnH}} = 57.0$  Hz) that is assigned to the SnMe resonance, in addition to two aromatic resonances at 7.52 (m, 2 H,  $^3J_{\text{SnH}} = 45.5$  Hz, *o*-Ph) and 7.33 (m, 3 H, *m,p*-Ph). The  $^{13}\text{C}$  NMR ( $\text{CDCl}_3$ ) spectrum also exhibits a diagnostic resonance at -11.5 ( $^1J_{119\text{SnC}} = 340.8$  Hz,  $^1J_{117\text{SnC}} = 325.2$  Hz) assigned to the SnMe carbon. Other peaks at 21.8 ( $^1J_{119\text{SnC}} = 335.3$  Hz,  $^1J_{117\text{SnC}} = 320.4$  Hz,  $-\text{CH}_2\text{C}(\text{Me})\text{C}(\text{Me})\text{CH}_2-$ ) and 131.8 ( $^2J_{\text{SnC}} = 20.6$  Hz,  $-\text{CH}_2\text{C}(\text{Me})\text{C}(\text{Me})\text{CH}_2-$ ) are assigned to the respective stannacyclopentene ring carbons, while the aromatic ring carbons are found at 140.8 ( $^1J_{\text{SnC}} = 452$  Hz, *ipso*-Ph), 136.2 ( $^2J_{\text{SnC}} = 36.4$  Hz, *o*-Ph), 128.4 ( $^4J_{\text{SnC}} = 10.6$  Hz, *p*-Ph), and 128.2 ( $^3J_{\text{SnC}} = 46.2$  Hz, *m*-Ph). The  $^{119}\text{Sn}\{^1\text{H}\}$  NMR ( $\text{CDCl}_3$ ) spectrum shows a peak at -4.8 ppm. The EI-MS, *m/z* (relative intensity; Sn-containing isotopomeric clusters are represented by the  $^{120}\text{Sn}$  isotopomer) exhibits major peaks at 294.0 (22,  $\text{M}^+$ ), 279.0 (30,  $\text{M}^+ - \text{CH}_3$ ), 212.0 (53,  $\text{M}^+ - \text{C}_6\text{H}_{10}$ ), 196.9 (98,  $\text{PhSn}^+$ ), and 119.9 (41,  $\text{Sn}^+$ ). A HRMS of the molecular ion gave an exact mass of 294.0454 (calculated for  $\text{C}_{13}\text{H}_{18}^{120}\text{Sn}$ , 294.0430).

The  $^1\text{H}$  NMR ( $\text{CDCl}_3$ ) spectrum of **4** shows a singlet at 0.58 (s, 3 H,  $^2J_{119\text{SnH}} = 57.4$  Hz,  $^2J_{117\text{SnH}} = 55.0$  Hz) that is assigned to the SnMe protons. The SnPh resonances

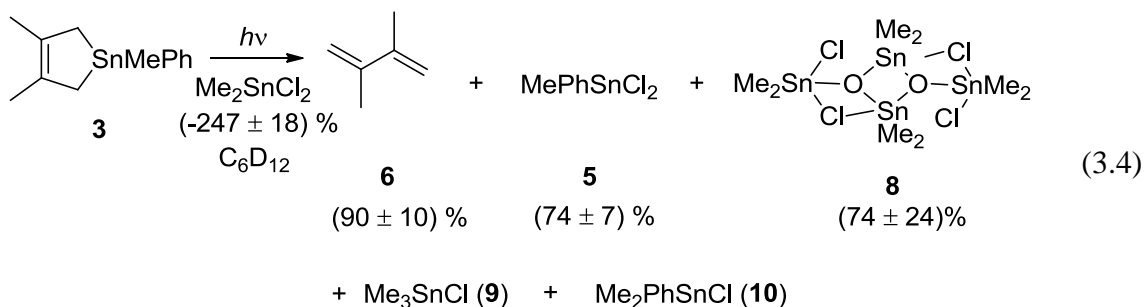
are identified at 7.37 (m, 3 H, *m,p*-PhSn) and 7.57 (m, 2 H,  $^3J_{\text{SnH}} = 45.6$  Hz, *o*-PhSn), while the phenyl resonances on the stannacyclopentene ring are located at 7.19 (d, 2 H,  $^3J = 7.9$  Hz, *o*-Ph), 7.20 (t, 1 H,  $^3J = 6.6$  Hz, *p*-Ph), and 7.31 (t, 2 H,  $^3J = 7.9$  Hz, *m*-Ph). The  $^{13}\text{C}$  NMR ( $\text{CDCl}_3$ ) spectrum shows a diagnostic resonance at -11.2 ( $^1J_{119\text{SnC}} = 343.8$  Hz,  $^1J_{117\text{SnC}} = 328.7$  Hz) that is assigned to SnMe. Furthermore, aromatic carbons at 125.7 (*p*-Ph), 127.9 (*m*-Ph), 128.1 (*o*-Ph), and 145.8 ( $^3J_{\text{SnC}} = 57.3$  Hz, *ipso*-Ph) are assigned to C=C-Ph, while 128.3 ( $^3J_{\text{SnC}} = 46.5$  Hz, *m*-PhSn), 128.6 ( $^4J_{\text{SnC}} = 11.8$  Hz, *p*-PhSn), 136.2 ( $^2J_{\text{SnC}} = 36.7$  Hz, *o*-PhSn) and 140.7 ( $^1J_{119\text{SnC}} = 455.8$  Hz,  $^1J_{117\text{SnC}} = 438.4$  Hz, *ipso*-PhSn) are assigned to SnPh. The  $^{119}\text{Sn}\{^1\text{H}\}$  NMR ( $\text{CDCl}_3$ ) spectrum exhibits a resonance at 5.1 ppm. The electron impact mass spectrum exhibits diagnostic peaks at  $m/z(\text{I}) = 356.1^*$  (3,  $\text{M}^+$ ), 341.0\* (17,  $\text{M}^+ - \text{CH}_3$ ), 196.9\* (63,  $\text{PhSn}^+$ ), 144.1 (78,  $\text{C}_{11}\text{H}_{12}^+$ ), and 129.0 (100,  $\text{C}_{10}\text{H}_9^+$ ). HRMS of the molecular ion (calculated for  $\text{C}_{18}\text{H}_{20}^{120}\text{Sn}$ , 356.0566) affords an exact mass of 356.0587.

Photolysis of an air-saturated  $\text{C}_6\text{D}_{12}$  solution of **3** (0.04 M) using two low pressure mercury vapour lamps (254 nm) led to the disappearance of the stannacyclopent-3-ene, concurrent with the formation of **6** and an insoluble white precipitate. The average of all resolved  $^1\text{H}$  NMR resonances for **3** ( $\delta_{\text{H}} = 7.40$  (2 H), 7.18 (3 H), 0.43 (3 H)) and **6** ( $\delta_{\text{H}} = 4.89$  (2 H) and 5.00 (2 H)) were used to calculate their concentrations. Thus, the collection of resonances at  $\delta_{\text{H}} = 1.6 - 1.9$  ppm for **3** and  $\delta_{\text{H}} = 1.88$  ppm for **6** were not used. Concentration versus time plots for **3** and **6** are shown in Figure S3.1, while the  $^1\text{H}$  NMR spectra before and after 10 minutes photolysis are shown in Figure S3.2. No attempts were made to replenish the oxygen content of the sample as photolysis proceeded, or to identify the insoluble precipitate. Continued irradiation beyond 2.5 minutes results in a decrease in both the rates of consumption of **3** and formation of **6**. The breakpoint at ca. 2.5 minutes coincides with the consumption of roughly 2.4 mM of

**3**, which corresponds to the concentration of molecular oxygen in air-saturated cyclohexane solution at 25 °C.<sup>5</sup> Similarly curved concentration versus time plots were obtained in the photolysis of **2** under similar conditions (see Chapter 2).<sup>1</sup> The results of the experiment are summarized in eq. 3.3; the yield of **6** was estimated from the relative slopes of the concentration versus time plots of **3** and **6** over the first ca. 2.5 minutes of photolysis.



Photolysis of an undeaerated C<sub>6</sub>D<sub>12</sub> solution of **3** (0.04 M) containing dichlorodimethylstannane (Me<sub>2</sub>SnCl<sub>2</sub>, 0.04 M) led to the formation of **6** (89 ± 10 %) and several tin-containing compounds, the most abundant of which were identified as MePhSnCl<sub>2</sub> (**5**; 74 ± 7 %) and the association dimer of 1,3-dichlorotetramethyldistannoxane (**8**, 74 ± 24 %); yields of tin containing products were calculated from the average of their respective methyltin resonances. Two additional products, which were identified by NMR as chlorotrimethylstannane (Me<sub>3</sub>SnCl, **9**; δ<sub>H</sub> 0.52) and chlorodimethylphenylstannane (Me<sub>2</sub>PhSnCl, **10**; δ<sub>H</sub> 0.69), are formed in lower yields (eq. 3.4). The identity of **5** was verified by spiking the photolyzate with an authentic sample, while **6**, **8**, **9** and **10** were identified by comparison of the <sup>1</sup>H and/or <sup>119</sup>Sn spectra of the crude photolyzate with the literature spectra.<sup>1,6,7</sup>





The  $^1\text{H}$  NMR spectrum of the solution mixture before and after 10 minutes of photolysis time, as well as the latter after the addition of an authentic sample of **5** is shown in Figure S3.3, while the  $^{119}\text{Sn}$  NMR spectrum after 10 minutes of photolysis with and without added **5**, is shown in Figure S3.4. The concentration versus time plots showing the consumption of **3** and  $\text{Me}_2\text{SnCl}_2$  and the formation of the various identified products are shown in Figure 3.1. No attempts were made to replenish the oxygen content in the sample as the photolysis proceeded. In the first 2.5 minutes of photolysis, the major products formed, concurrent with the consumption of **3** and  $\text{Me}_2\text{SnCl}_2$  ( $-250 \pm 20\%$ ), are **5**, **6**, and **8**. Continued photolysis between 2.5 - 10 minutes resulted in no further (net) formation of **5**, **6**, or **8**, and the linear growth of the resonances due to **9** and **10** (*vide infra*).

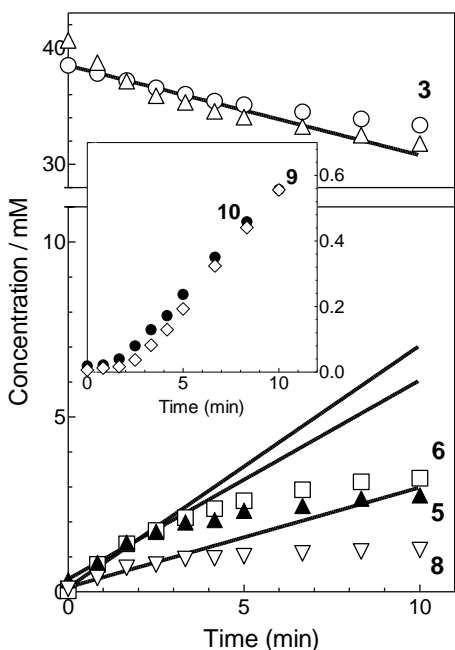
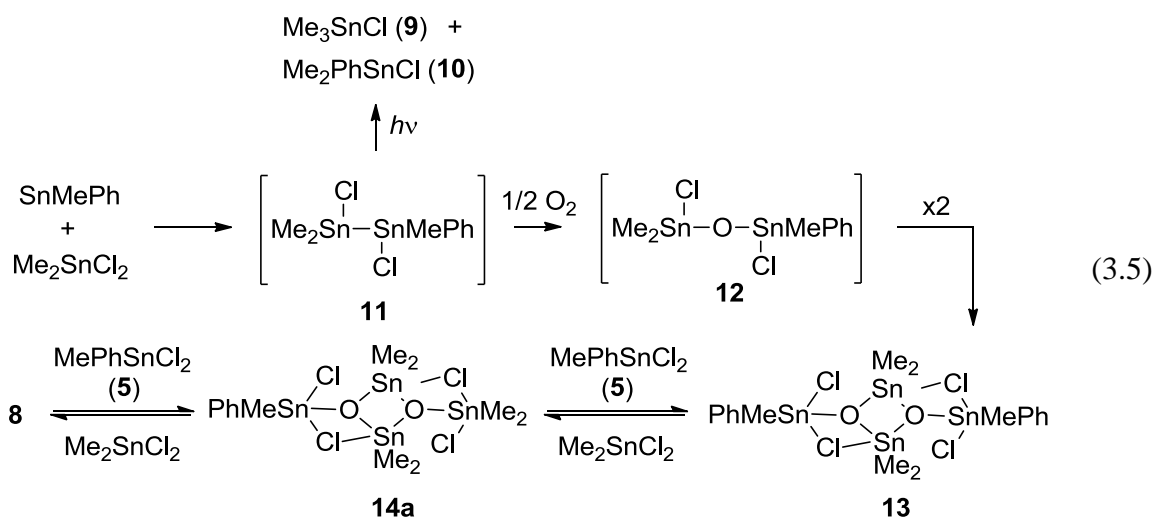


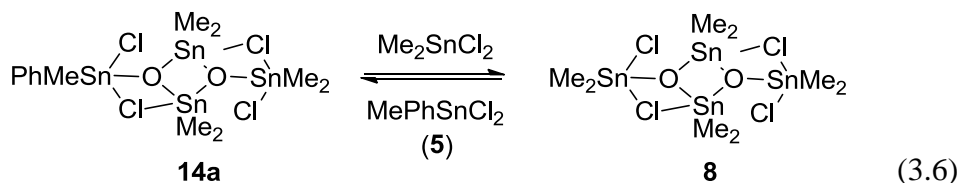
**Figure 3.1.** Concentration versus time plots for the photolysis of a 0.04 M solution of **3** in  $\text{C}_6\text{D}_{12}$  containing 0.04 M  $\text{Me}_2\text{SnCl}_2$ . The inset shows an expanded plot, illustrating the formation of compounds **9** ( $\diamond$ ) and **10** ( $\bullet$ ) with photolysis time. The initial slopes determined from the first four data points are **3**,  $-0.77 \pm 0.02$  ( $\circ$ );  $\text{Me}_2\text{SnCl}_2$ ,  $-1.9 \pm 0.1$  ( $\Delta$ ) (slope not shown); **6**,  $0.69 \pm 0.07$  ( $\square$ ); **5**,  $0.57 \pm 0.05$  ( $\blacktriangle$ ); **8**,  $0.29 \pm 0.05$  ( $\nabla$ ) (units,  $\text{mM min}^{-1}$ ).

A reasonable mechanism for the formation of the various Sn-containing products of the photolysis is shown in equation 3.5, which is analogous to the proposed mechanism for product formation in the photolysis of an air saturated  $\text{C}_6\text{D}_{12}$  solution of **2** in the

presence of  $\text{Me}_2\text{SnCl}_2$ .<sup>1</sup> The insertion of  $\text{SnMePh}$  into the  $\text{Sn}-\text{Cl}$  bond in  $\text{Me}_2\text{SnCl}_2$  generates **11** which, in the presence of oxygen, is converted to **12**. Distannoxane **12** dimerizes to form **13**, which undergoes exchange with excess  $\text{Me}_2\text{SnCl}_2$  to afford **5** and **8**.



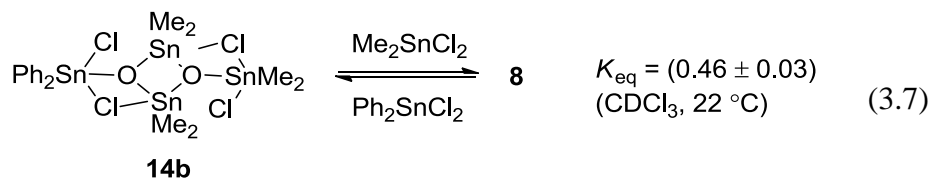
The mechanism of eq. 3.5 suggests that distannoxane dimers **13** and **14a** should be present, and indeed a resonance at  $\delta_{\text{H}}$  8.07 ppm is observed that has been assigned tentatively to **14a**.<sup>1,8</sup> It and distannoxane dimer **8** are present in the ratio **14a**:**8** = 5.03 after 10 minutes irradiation time together with the ratio **5**: $\text{Me}_2\text{SnCl}_2$  = 11.5 that is present, this allows an equilibrium constant  $K_{\text{eq}} \sim 0.44$  to be approximated for the **14a**↔**8** equilibrium in  $\text{C}_6\text{D}_{12}$  at 22 °C (eq. 3.6).



$$K_{\text{eq}} = \frac{[\text{8}] \cdot [\text{MePhSnCl}_2]}{[\text{14a}] \cdot [\text{Me}_2\text{SnCl}_2]} \sim 0.50 \\
 (\text{C}_6\text{D}_{12}, 22 \text{ }^\circ\text{C})$$

Also in agreement with both the assignment and the mechanism, the concentration of **14a** increased when an authentic sample of **5** was added to the photolyzate (Figure S3.3c): the

new ratio of **14a**:**8** = 1.9, together with the ratio of **5**: $\text{Me}_2\text{SnCl}_2$  = 3.3, affords an estimate of  $K_{\text{eq}} \sim 0.57$ . The average ( $K_{\text{eq}} \sim 0.50$ ) is nearly identical to the value measured for the interconversion of **8** and the  $\text{SnPh}_2$  derived species **14b** under similar conditions (eq. 3.7; see also Chapter 2).<sup>1</sup>



The change in the slopes of the concentration versus time plots after ca. 2.5 minutes (Figure 3.1) coincides with the point at which ca. 2.0 mM of **3** has been consumed, which corresponds to roughly 80 % of the concentration of  $\text{O}_2$  in air-saturated cyclohexane solution.<sup>5</sup> After which, the formation of mixed chlorostannanes **9** and **10** results from the photolysis of **11**; 1,2-dichlorotetraorganodistannanes are known to absorb strongly at 254 nm and also be highly photolabile to form triorganotin chlorides.<sup>9-11</sup> The levelling of the concentration versus time plots for **1** and **6** is also consistent with **11** absorbing some of the incident light.

Laser flash photolysis studies were performed using excitation from a 248 nm KrF excimer laser, on continuously flowing argon-saturated solutions of **3** (ca.  $9.2 \times 10^{-4}$  M) or **4** (ca.  $1.1 \times 10^{-4}$  M) in anhydrous hexanes. Transient UV-Vis absorption spectra recorded over the 270 - 600 nm region at selected time intervals after excitation are shown in Figures 3.2a and 3.2b for **3** and **4**, respectively.

The absorption spectra recorded of a hexanes solution of **4**, 0.58 - 0.70  $\mu\text{s}$  after the laser pulse, reveals the prompt formation of a transient species exhibiting an absorption maximum at  $\lambda_{\text{max}} = 500$  nm (Fig 3.2b) and more intense absorptions below 300 nm. The decay of the promptly formed species fits reasonably well to second-order kinetics (eq. 3.8) with  $2k/\epsilon_{500} = (3.6 \pm 0.2) \times 10^7 \text{ cm s}^{-1}$ , consistent with an assignment to  $\text{SnMePh}$ .

The decay of the promptly formed species is concurrent with the formation of a new transient absorption exhibiting an absorption band between 270 - 400 nm with  $\lambda_{\text{max}} = 290$  nm.

$$\Delta A_t = \Delta A_0 / (1 + (2k_{\text{dim}}\Delta A_0 / \epsilon I)t) \quad (3.8)$$

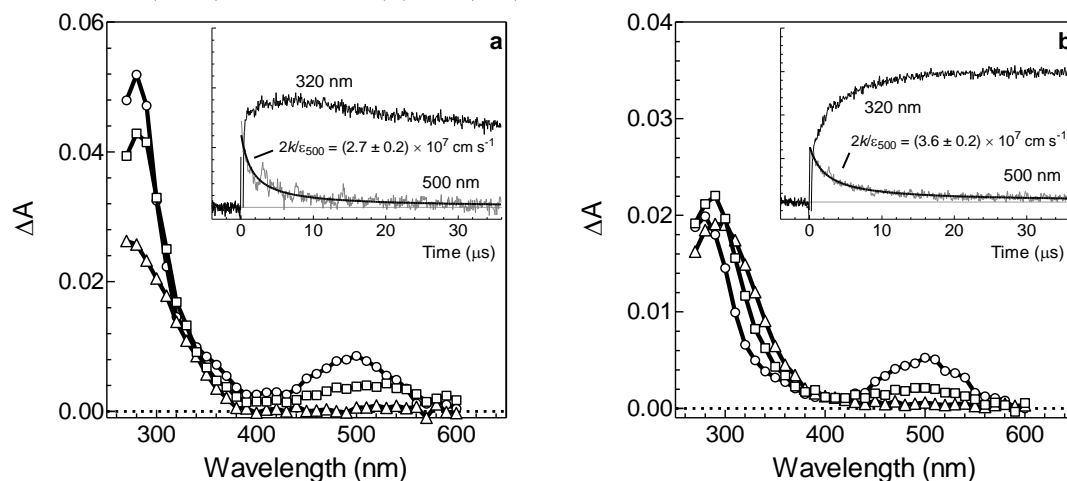


**Figure 3.2.** Time-resolved UV-vis spectra from laser photolysis of (a) **3** and (b) **4** in hexanes solution, 0.58 - 0.70  $\mu\text{s}$  ( $\circ$ ), 4.16 - 4.35  $\mu\text{s}$  ( $\square$ ), and 34.4 - 34.7  $\mu\text{s}$  ( $\triangle$ ) after the laser pulse (25  $^{\circ}\text{C}$ ). Absorbance-time profiles are shown at selected wavelengths (inset). (Data in (b) recorded by B. Nguyen)

Laser flash photolysis of a hexanes solution of **3** (Fig 3.2a) afforded similar transient absorption spectra to those obtained from **4**. The promptly-formed transient exhibits an absorption band at  $\lambda_{\text{max}} = 500$  nm and decays with 2nd order rate coefficient  $2k/\epsilon_{500} = (2.7 \pm 0.2) \times 10^7 \text{ cm s}^{-1}$ , to afford a secondary species exhibiting a broad absorption between 270 - 380 nm. Comparison of the transient absorption spectra from **3** and **4** verifies that common transient products are formed from the two precursors, and thus support the assignment of the promptly formed transient to SnMePh. An additional weak absorption appears in the 350 - 430 nm region of the spectra, and is attributed to the triplet-triplet absorption spectrum of the small amount of residual naphthalene that is present in the samples of **3**.<sup>12,13</sup>

As was discussed in the previous chapter, the addition of a stannylene substrate (Q) results in changes to the stannylene absorbance-time profiles in a manner that depends on the magnitude of the absolute rate ( $k_Q$ ) and/or equilibrium ( $K_{eq}$ ) constants of the interaction. Reactions that proceed to pre-pulse level with pseudo first order decay character are modelled according to eq. 3.9 and afford  $k_{decay}$ , while the slopes of linear plots of  $k_{decay}$  versus substrate concentration [Q] affords  $k_Q$ , consistent with an overall second-order reaction (eq. 3.10). Rapid and reversible reactions are characterized by a drop in apparent yield of the stannylene ( $(\Delta A_0)_Q$ ) with [Q] according to eq. 3.11, the slope of the linear correlation affords  $K_{eq}$ .

$$\Delta A_t = \Delta A_{res} + (\Delta A_0 - \Delta A_{res}) \exp(-k_{decay}t) \quad (3.9)$$

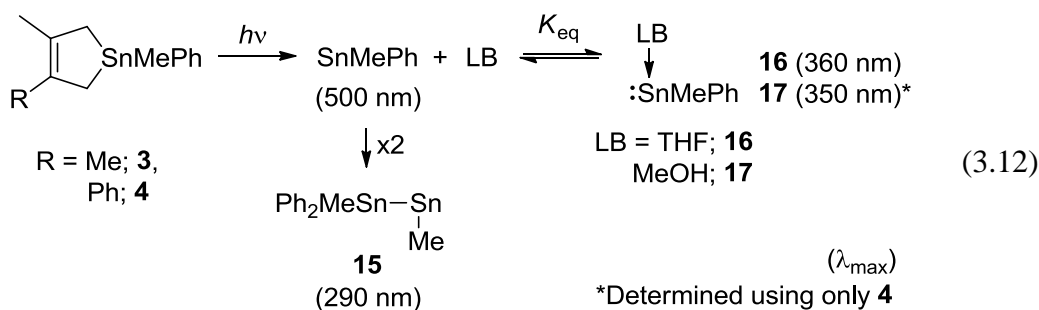
$$k_{decay} = k_{-Q} + k_Q[Q] \quad (3.10)$$

$$(\Delta A_0)_0/(\Delta A_0)_Q = 1 + K_{eq}[Q] \quad (3.11)$$

Transient absorption spectra recorded of hexanes solutions of **3** or **4** containing millimolar concentrations of THF reveal a new absorption band centred at  $\lambda_{max} = 360$  nm, in place of the absorption band due to SnMePh (Figure S3.5). The new absorption band is assigned to the SnMePh-THF Lewis acid-base complex **16** (eq. 3.12). Addition of smaller amounts of THF to a hexanes solution of **4** resulted in acceleration of the decay of SnMePh and a change to pseudo-first order decay kinetics. Analysis of  $k_{decay}$  versus [THF] data according to equation 3.10 affords the bimolecular rate constant  $k_Q = (1.8 \pm 0.1) \times 10^{10} \text{ M}^{-1} \text{ s}^{-1}$  (Figure 3.3a).

The addition of MeOH in sub-millimolar concentrations to hexanes solutions of **4** resulted in a decrease in the initial signal intensity of SnMePh ( $(\Delta A_0)_0$ ), consistent with a rapid and reversible reaction between SnMePh and MeOH. Analysis of the stannylene traces at 500 nm according to equation 3.11 affords the equilibrium constant  $K_{eq} = (5.0 \pm 0.6) \times 10^3 \text{ M}^{-1}$  (Figure 3.3b). Transient UV-Vis absorption spectra recorded in the

presence of 7.3 mM MeOH show a transient absorption centred at  $\lambda_{\max} = 350$  nm in place of the stannylene absorption, which can be assigned to the Lewis acid-base complex SnMePh-O(H)Me (**17**) (Figure 3.3c).



The addition of  $\text{Me}_2\text{SnCl}_2$  in sub-millimolar concentrations to hexanes solutions of **4** also resulted in acceleration of the decay of SnMePh and a change to pseudo-first order decay kinetics. Analysis of  $k_{\text{decay}}$  versus  $[\text{Me}_2\text{SnCl}_2]$  data according to equation 3.10 affords the bimolecular rate constant  $k_Q = (5.6 \pm 0.9) \times 10^9 \text{ M}^{-1} \text{ s}^{-1}$  (Figure 3.3a) for the reaction of SnMePh with this substrate.

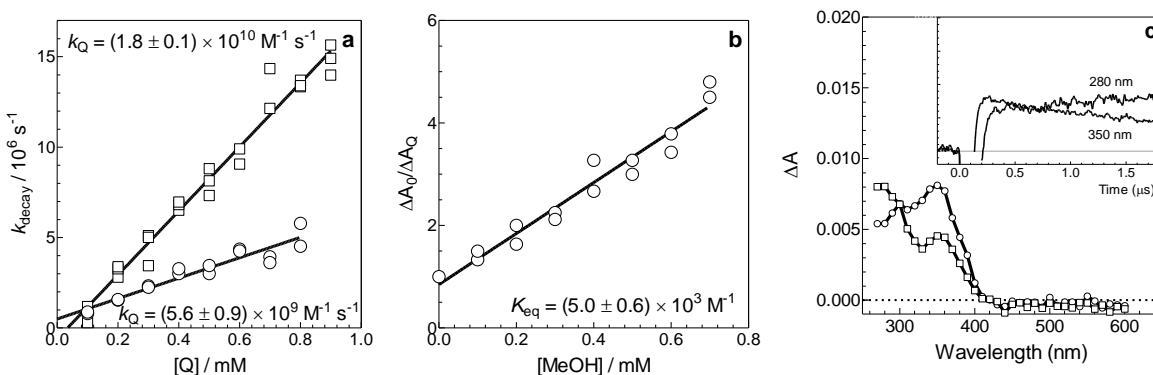


**Figure 3.3.** (a) Plot of  $k_{\text{decay}}$  for the reaction of SnMePh with THF ( $\square$ ) and  $\text{Me}_2\text{SnCl}_2$  ( $\circ$ ) in hexanes at 25 °C; the solid lines are the linear least squares fit of the data to equation 3.10. (b) Plot of  $\Delta A_0/\Delta A_Q$  for the reaction of SnMePh with MeOH in hexanes at 25 °C; the solid line is the linear least squares fit of the data to equation 3.11. (c) Time-resolved UV-vis spectra from laser photolysis of **4** in hexanes containing ca. 7.3 mM MeOH, 0.27 - 0.28  $\mu\text{s}$  ( $\circ$ ) and 1.58 - 1.61  $\mu\text{s}$  ( $\square$ ) after the laser pulse (25 °C). Absorbance-time profiles at selected wavelengths (inset). (Data from Fig 3.3a-c recorded by B. Nguyen using **4**)

### 3.2.2. Discussion

Laser flash photolysis of **3** and **4** results in the prompt formation of new absorption bands, centred at  $\lambda_{\text{max}} = 500$  nm, which are assigned to SnMePh. This represents the first time that SnMePh has been detected directly under any set of conditions. The transient exhibits similar decay characteristics from the two precursors, leading to an average second order decay rate coefficient of  $2k/\epsilon_{500} = (3.1 \pm 0.5) \times 10^7$  cm s<sup>-1</sup>. While both **3** and **4** produce adequate transient signals of SnMePh in order to carry out solution phase studies, **4** has the added advantage of having a ca. 10 fold higher molar absorptivity at the excitation wavelength, meaning a smaller quantity of material is required for an experiment. Transient absorption spectra recorded in the presence of millimolar concentrations of THF also showed a similar transient ( $\lambda_{\text{max}} = 360$  nm) from both precursors. The similarities outlined above confirm the expectation that **3** and **4** should generate the same transient product upon photolysis (eq. 3.12).

To a first approximation, the properties of SnMePh can be expected to fall in between with those of SnMe<sub>2</sub> and SnPh<sub>2</sub>. Indeed the long wavelength absorption maxima does not vary between the transient stannylenes, and the rate coefficients match those obtained for SnMe<sub>2</sub> and SnPh<sub>2</sub>, which exhibit rate coefficients between  $1.3 - 3.0 \times 10^7$  cm s<sup>-1</sup>.<sup>1</sup> The decay of SnMePh takes place concurrently with the formation of new transient absorptions that we assign to a (SnMePh)<sub>2</sub> dimer. As in the dimer detected for SnPh<sub>2</sub>, the spectrum of the species is devoid of an absorption band in the 460 - 500 nm range, where (*E*)- and/or (*Z*)-1,2-dimethyl-1,2-diphenyldistannene is expected to absorb, based on the spectra of the alkyl or aryl substituted distannenes that have been reported.<sup>14,15</sup> The absorption spectrum of the dimer (the portion of it that is detectable under our conditions) instead bears closer resemblance to the SnPh<sub>2</sub> dimer (Ph<sub>3</sub>Sn)SnPh,<sup>1</sup> and is assigned tentatively to (methylphenylstannyl)methylstannylene

((MePh<sub>2</sub>Sn)SnMe, **15**) (eq. 3.13). We did not attempt to detect the weak absorption band in the 650 - 750 nm region that is expected for the compound, however.

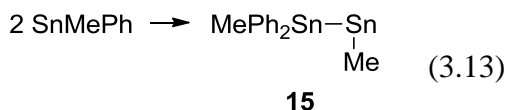


Table 3.1 summarizes the rate and equilibrium constants for the reactions of SnMePh along with the values for SnMe<sub>2</sub> and SnPh<sub>2</sub>. The reaction of SnMePh with methanol shows characteristics that closely resemble those exhibited by SnMe<sub>2</sub> and SnPh<sub>2</sub> in the presence of the substrate. The behaviour is consistent with a rapid and reversible reaction, characterized by an equilibrium constant ( $K_{\text{eq}} = (5.0 \pm 0.6) \times 10^3 \text{ M}^{-1}$ ) and absorption maximum for **17** ( $\lambda_{\text{max}} = 350 \text{ nm}$ ) that falls intermediate to the values obtained for SnMe<sub>2</sub> and SnPh<sub>2</sub>.<sup>1,14</sup> The values of  $K_{\text{eq}}$  allow one to establish a Lewis acidity scale for the three stannylenes, which follows the order: SnPh<sub>2</sub> > SnMePh > SnMe<sub>2</sub>.

The formation of **6** as the major product (ca. 90 %) from the photolysis of **3** in C<sub>6</sub>D<sub>12</sub> (eq. 3.3) is consistent with the clean extrusion of SnMePh, which the evidence suggests polymerizes in the absence of a stannylene substrate such as Me<sub>2</sub>SnCl<sub>2</sub>. Photolysis of an air-saturated C<sub>6</sub>D<sub>12</sub> solution of **3** containing Me<sub>2</sub>SnCl<sub>2</sub> affords **5** and **8** as the major tin-containing compounds, most likely via the mechanism outlined in eq. 3.5. The results are quite similar to those obtained from the chemical trapping of SnPh<sub>2</sub> as Ph<sub>2</sub>SnCl<sub>2</sub> in air saturated solution.<sup>1</sup> The flash photolysis results for **3** in hexanes containing Me<sub>2</sub>SnCl<sub>2</sub> is consistent with a rapid and irreversible reaction between the stannylene and the substrate. The resulting bimolecular rate constant ( $k_{\text{Q}} = (5.6 \pm 0.9) \times 10^9 \text{ M}^{-1} \text{ s}^{-1}$ ) falls between that for reaction of Me<sub>2</sub>SnCl<sub>2</sub> with SnMe<sub>2</sub> ( $k_{\text{Q}} = (1.9 \pm 0.3) \times 10^{10} \text{ M}^{-1} \text{ s}^{-1}$ ) and SnPh<sub>2</sub> ( $k_{\text{Q}} = (3.6 \pm 0.2) \times 10^9 \text{ M}^{-1} \text{ s}^{-1}$ ),<sup>1</sup> as might be expected.



**Table 3.1.** Absolute Rate ( $k_Q$ ) and Equilibrium Constants ( $K_{eq}$ ) for the Reactions of SnMe<sub>2</sub>, SnPh<sub>2</sub> and SnMePh with Stannylenes Substrates in Hexanes Solution at 25 °C.

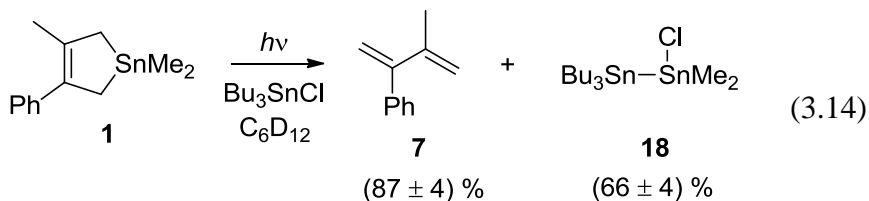
Substrate	$k_Q (10^9 \text{ M}^{-1} \text{ s}^{-1}) / [K_{eq} (10^3 \text{ M}^{-1})]$		
	SnMe <sub>2</sub>	SnPh <sub>2</sub>	SnMePh
MeOH	$[2.4 \pm 0.2]^{a,b}$	$6 \pm 1^b$ $[7.6 \pm 0.8]^b$	$[5.0 \pm 0.6]^{a,c}$
THF	$25 \pm 5^e$ $[19 \pm 5]^e$	$15 \pm 3^{c,d,e}$	$19 \pm 0.1^{c,d}$
Me <sub>2</sub> SnCl <sub>2</sub>	$19 \pm 3^b$	$3.6 \pm 0.2^b$	$5.6 \pm 0.9^c$

Errors are quoted as twice the standard error obtained from the least-squares analyses unless otherwise specified. <sup>a</sup> $k_Q$  indeterminable; <sup>b</sup>ref<sup>1</sup>; <sup>c</sup>Data recorded by B. Nguyen; <sup>d</sup> $K_{eq} > 25000 \text{ M}^{-1}$ ; <sup>e</sup>Data from Chapter 4.

### 3.3. The Reactions of Transient Stannylenes with Tri-*n*-butyltin Chloride

#### 3.3.1. Results

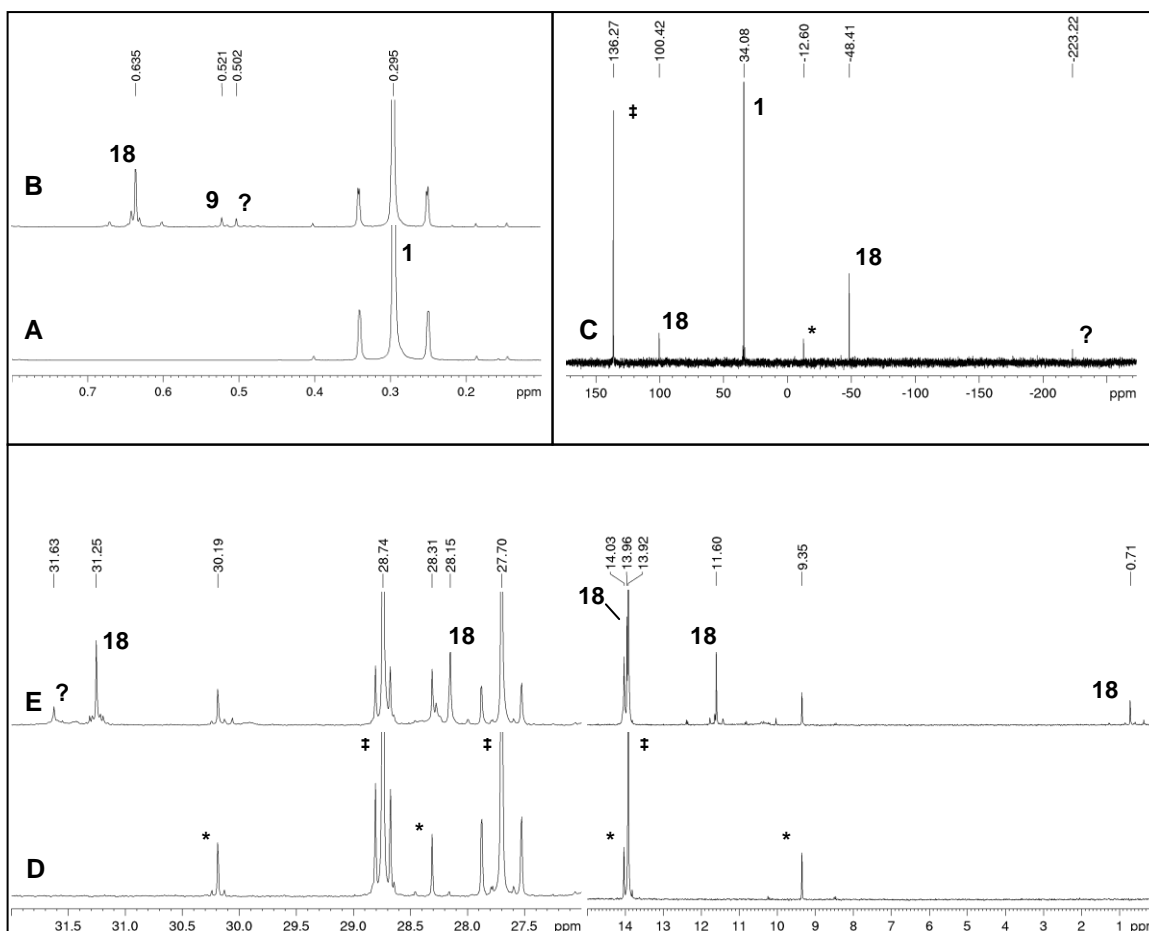
Photolysis of a deaerated solution of **1** in the presence of Bu<sub>3</sub>SnCl (0.04 M) results in the formation of diene **7** ( $87 \pm 4\%$ ) and a product identified by NMR as 1,1,1-tributyl-2-chloro-2,2-dimethyldistannane (**18**,  $66 \pm 4\%$ ), the formal insertion product of SnMe<sub>2</sub> into Bu<sub>3</sub>SnCl (eq. 3.14). At least two additional products were also formed, for which the concentration versus time plots exhibited upwards-curvature characteristic of secondary photolysis products (see Fig. S3.6). One of these can be assigned tentatively to Me<sub>3</sub>SnCl (**9**;  $9 \pm 5\%$ ) on the basis of its <sup>1</sup>H and <sup>119</sup>Sn NMR spectra. The other product could not be identified and disappeared gradually after allowing air to diffuse into the NMR tube over four days. Distannane **18** also disappeared after allowing air to diffuse into the NMR tube over the same period of time. This is consistent with its anticipated air sensitivity, based on the reported characteristics of a structurally comparable derivative (Bu<sub>3</sub>SnSnR<sub>2</sub>Cl, R = C<sub>6</sub>H<sub>4</sub>-2-(CH<sub>2</sub>N(CH<sub>3</sub>)<sub>2</sub>)).<sup>16</sup> Exposure of the photolyzed sample to air also resulted in a gradual clouding of the solution.



Compound **18** was assigned on the basis of its  $^1\text{H}$ ,  $^{13}\text{C}\{^1\text{H}\}$  and  $^{119}\text{Sn}\{^1\text{H}\}$  NMR spectral characteristics in the NMR spectra of the crude photolyzate mixture (see Figure 3.4; the full  $^1\text{H}$  NMR spectrum is shown in Figure S3.6). It exhibits  $\delta_{\text{H}}$  0.64 ( $^2J_{\text{SnH}} = 41.6$  Hz,  $^3J_{\text{SnH}} = 6.4$  Hz), and  $\delta_{\text{Sn}}$  100.4, -48.4; the  $^{119}\text{Sn}$  resonance at 100.4 ppm falls in the range characteristic of chlorodimethylstannylstannanes,<sup>1</sup> while the  $^{119}\text{Sn}$  resonance at -48.4 ppm agrees with the chemical shift reported for the tributyltin atom in a similar derivative ( $\text{Bu}_3\text{SnSnR}_2\text{Cl}$ ,  $\text{R} = \text{C}_6\text{H}_4\text{-2-(CH}_2\text{N(CH}_3)_2)$ ).<sup>16</sup> Diagnostic resonances consistent with **18** are also evident in the  $^{13}\text{C}$  NMR spectrum of the photolyzate; in particular, the Sn-*Me* and n-Bu( $\text{C}^\alpha$ ) carbons exhibit Sn-C coupling constants of  $^1J_{^{119}\text{SnC}} = 198.6$  Hz,  $^1J_{^{117}\text{SnC}} = 190.4$  Hz,  $^2J_{\text{SnC}} = 44.2$  Hz and  $^1J_{^{119}\text{SnC}} = 277.2$  Hz,  $^1J_{^{117}\text{SnC}} = 264.7$  Hz,  $^2J_{\text{SnC}} = 59.4$  Hz, respectively, consistent with the presence of a Sn-Sn bond in the compound.<sup>17</sup> The expected  $^1J_{\text{SnSn}}$  coupling constants were not observed in the  $^{119}\text{Sn}$  NMR spectrum for **18**, likely due to an insufficient concentration. Complete NMR data for **18** are as follows:

$^1\text{H}$  NMR ( $\text{C}_6\text{D}_{12}$ ):  $\delta$  0.64 (s, 6 H,  $^2J_{\text{SnH}} = 41.6$  Hz,  $^3J_{\text{SnH}} = 6.4$  Hz, Sn-*Me*), 0.89-0.94 (t, 9 H, n-Bu( $\text{C}^\delta\text{H}_3$ )), 1.11-1.26 (m, 6 H, n-Bu( $\text{C}^\alpha\text{H}_2$ )), 1.32-1.40 (m, 6 H, n-Bu( $\text{C}^\gamma\text{H}_2$ )), 1.57-1.65 (m, 6 H, n-Bu( $\text{C}^\beta\text{H}_2$ )).

$^{13}\text{C}\{^1\text{H}\}$  NMR ( $\text{C}_6\text{D}_{12}$ ):  $\delta$  0.7 ( $^1J_{^{119}\text{SnC}} = 198.6$  Hz,  $^1J_{^{117}\text{SnC}} = 190.4$  Hz,  $^2J_{\text{SnC}} = 44.2$  Hz, Sn-*Me*), 11.6 ( $^1J_{^{119}\text{SnC}} = 277.2$  Hz,  $^1J_{^{117}\text{SnC}} = 264.7$  Hz,  $^2J_{\text{SnC}} = 59.4$  Hz, n-Bu( $\text{C}^\alpha$ )), 14.0 (n-Bu( $\text{C}^\delta$ )), 28.2 ( $^3J_{\text{SnC}} = 54.9$  Hz, n-Bu( $\text{C}^\gamma$ )), 31.3 ( $^2J_{\text{SnC}} = 20.5$  Hz,  $^3J_{\text{SnC}} = 6.4$  Hz, n-Bu( $\text{C}^\beta$ )).

$^{119}\text{Sn}\{^1\text{H}\}$  NMR ( $\text{C}_6\text{D}_{12}$ ):  $\delta$  100.4, -48.4

**Figure 3.4.**  $^1\text{H}$  NMR spectra (0.1 - 0.8 ppm) of a deaerated 0.04 M solution of **1** in  $\text{C}_6\text{D}_{12}$  containing  $\text{Bu}_3\text{SnCl}$  (0.04 M) (a) before and (b) after 10 minutes photolysis with 254 nm light. (c)  $^{119}\text{Sn}$  NMR spectrum of a deaerated 0.04 M solution of **1** in  $\text{C}_6\text{D}_{12}$  containing  $\text{Bu}_3\text{SnCl}$  (0.04 M) after 10 minutes photolysis with 254 nm light.  $^{13}\text{C}$  NMR spectra (0 - 15 and 27 - 32 ppm) of a deaerated 0.04 M solution of **1** in  $\text{C}_6\text{D}_{12}$  containing  $\text{Bu}_3\text{SnCl}$  (0.04 M) (d) before and (e) after 10 minutes photolysis with 254 nm light. ( $\ddagger\text{Bu}_3\text{SnCl}$ ;  $\ast\text{Bu}_4\text{Sn}$ )

Laser flash photolysis of a hexanes solution of **1** in the presence of millimolar concentrations of  $\text{Bu}_3\text{SnCl}$  resulted in behaviour consistent with a fast and irreversible reaction between the stannylene and the substrate, and a plot of  $k_{\text{decay}}$  for the  $\text{SnMe}_2$  absorption versus  $[\text{Bu}_3\text{SnCl}]$  (Fig. 3.5) is linear with slope  $k_Q = (8.3 \pm 0.8) \times 10^8 \text{ M}^{-1} \text{ s}^{-1}$ .

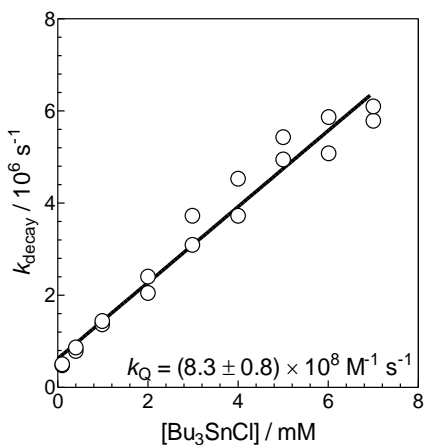


**Figure 3.5.** Plot of  $k_{\text{decay}}$  for the  $\text{SnMe}_2$  absorption (530 nm) versus  $[\text{Bu}_3\text{SnCl}]$ , from flash photolysis of **1** in hexanes at 25 °C; the solid line is the linear least squares fit of the data to equation 3.10.

Addition of  $\text{Bu}_3\text{SnCl}$  to a solution of **2** led to a simultaneous decrease in the initial signal intensity of  $\text{SnPh}_2$  ( $(\Delta A_0)_0$ ) and a shortening of the stannylene lifetime. Increasing the concentration of the substrate caused the decay rate coefficient of the stannylene to plateau asymptotically (Figure 3.7a). Transient absorption spectra recorded of solutions containing 15 mM  $\text{Bu}_3\text{SnCl}$  (Figure 3.6a) revealed the formation of a new transient product exhibiting  $\lambda_{\text{max}} \sim 410$  nm. Monitoring its absorbance-time profile (at 410 nm) as a function of increasing substrate concentration shows that the species exhibits an increase in its yield as well as a first order decay profile, with decay rate coefficients that are very similar to that of the stannylene (Figure 3.7b) at the same substrate concentration.

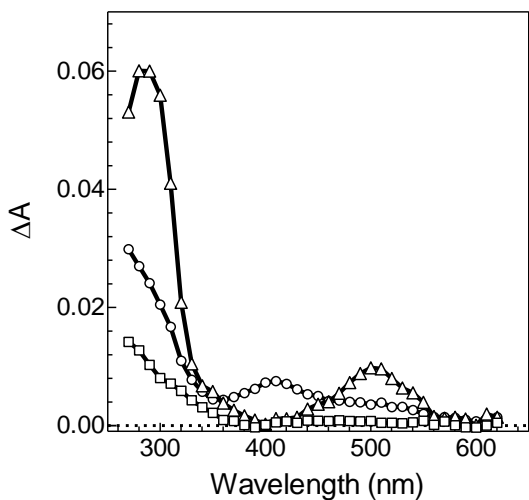


**Figure 3.6.** Time-resolved UV-vis spectra from laser photolysis of **2** in hexanes containing 0.0 mM  $\text{Bu}_3\text{SnCl}$  at 0.42 - 0.51  $\mu\text{s}$  ( $\Delta$ ), and 15.0 mM  $\text{Bu}_3\text{SnCl}$  at 0.22 - 0.32  $\mu\text{s}$  ( $\circ$ ) and 5.86 - 6.02  $\mu\text{s}$  ( $\square$ ) after the laser pulse (25 °C).

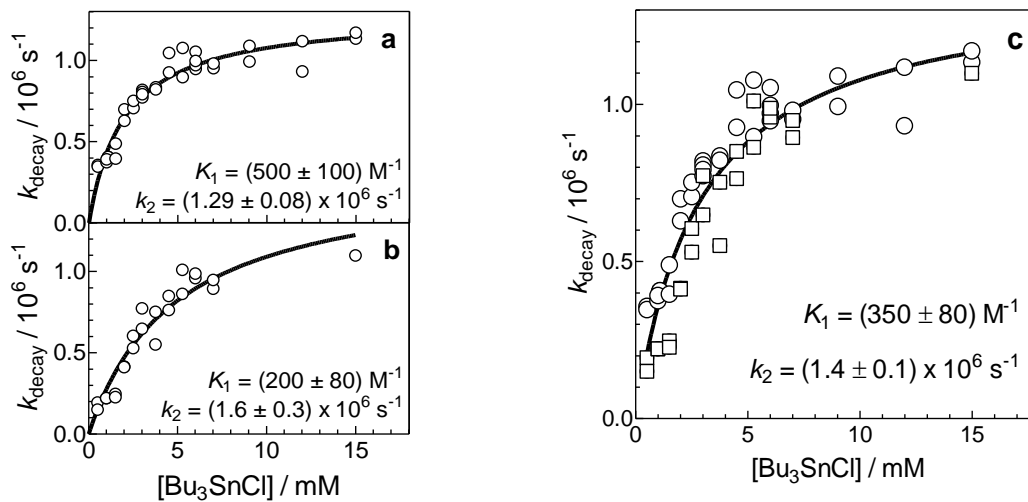
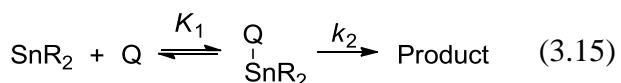


**Figure 3.7.** Plots of  $k_{\text{decay}}$  for reaction of (a)  $\text{SnPh}_2$  (500 nm) and the (b) 410 nm absorption with  $\text{Bu}_3\text{SnCl}$  in hexanes at 25 °C. (c) Overlap of the  $k_{\text{decay}}$  data for the  $\text{SnPh}_2$  (○) and 410 nm (□) absorptions as a function of  $[\text{Bu}_3\text{SnCl}]$ . The solid lines are the non-linear least squares fit of the data to equation 3.16.

The addition of  $\text{Bu}_3\text{SnCl}$  to a solution of **4** resulted in very similar behaviour to that exhibited by **2**. Transient absorption spectra recorded of solutions of **4** containing 15 mM  $\text{Bu}_3\text{SnCl}$  (Figure S3.8a) reveal the formation of a new transient absorption band centred at  $\lambda_{\text{max}} \sim 410 \text{ nm}$ , which overlaps with the absorption due to  $\text{SnMePh}$  at  $\lambda_{\text{max}} = 500 \text{ nm}$ . Plots of  $k_{\text{decay}}$  measured at 500 nm and at 410 nm appear also to approach a constant value asymptotically with increasing substrate concentration (Figure S3.9a-b). These observations for the reactions of both  $\text{SnMePh}$  and  $\text{SnPh}_2$  are consistent with a scenario wherein the stannylene, substrate and an intermediate complex rapidly establish equilibrium ( $K_1$ ), followed by an irreversible, unimolecular reaction of the intermediate complex ( $k_2$ ) to form the final product (eq. 3.15). In such a scenario, the relationship between the decay rate coefficients for the stannylene, and for the complex, versus substrate concentration  $[\text{Q}]$  can both be modelled using eq. 3.16.<sup>18</sup>



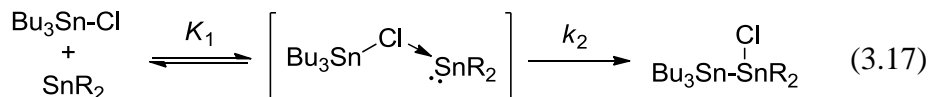
$$k_{\text{decay}} = \frac{k_2 K_1 [\text{Q}]}{1 + K_1 [\text{Q}]} \quad (3.16)$$

### 3.3.2. Discussion

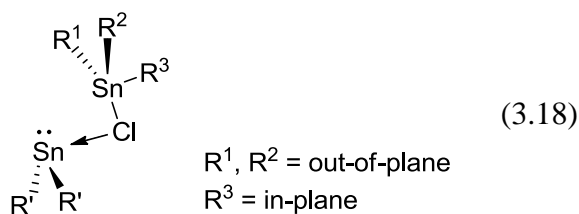
The insertion of  $\text{SnR}_2$  ( $\text{R} = \text{C}_6\text{H}_4\text{-2-CH}_2\text{N}(\text{CH}_3)_2$ ) into  $\text{Bu}_3\text{SnCl}$  was demonstrated recently by Ružička and coworkers.<sup>16</sup> We also found in our previous study that transient stannylenes undergo facile  $\sigma$ -bond insertion with  $\text{Me}_2\text{SnCl}_2$  to generate the corresponding 1,2-dichlorodistannane; for example the reaction with  $\text{SnMe}_2$  produces  $\text{Me}_2\text{ClSnSnClMe}_2$  (**19**).<sup>1</sup> These results are in agreement with previous studies by Neumann and coworkers, who also demonstrated the insertion of  $\text{SnMe}_2$  into the Sn-Cl bond of  $\text{Me}_2\text{SnCl}_2$  under ambient conditions.<sup>19</sup> However, the same study showed that  $\text{Me}_3\text{SnCl}$  was unreactive towards  $\text{SnMe}_2$  under the same conditions, so it was somewhat surprising to find evidence of reaction of both  $\text{SnMe}_2$  and  $\text{SnPh}_2$  with  $\text{Bu}_3\text{SnCl}$ . While **19** was found to form distannoxane **8** upon air oxidation,<sup>1</sup> we could not detect any new resonances in the  $^1\text{H}$  NMR spectrum of the photolyzate containing **18**, upon air oxidation, that would be consistent with the distannoxane of **18**.<sup>16,20</sup>

Laser flash photolysis studies of the quenching of  $\text{SnMe}_2$  by  $\text{Bu}_3\text{SnCl}$  showed the addition of  $\text{Bu}_3\text{SnCl}$  caused the decay of  $\text{SnMe}_2$  to accelerate and change to pseudo-first order kinetics, affording a bimolecular rate constant of  $k_{\text{Q}} = (8.3 \pm 0.8) \times 10^8 \text{ M}^{-1} \text{ s}^{-1}$  (Fig 3.5). In contrast to what was observed in experiments with the phenylstannylenes and the substrate, no new transient absorptions in the 270 - 620 nm spectral range could be detected in this case. The rate constant is roughly 20-fold smaller than that for reaction with  $\text{Me}_2\text{SnCl}_2$ , corresponding to a difference of  $\Delta\Delta G^\ddagger = 1.9 \text{ kcal mol}^{-1}$ . The difference in reactivity is consistent with the results of Dewar et al.<sup>21</sup> who predicted a 4.1 kcal mol<sup>-1</sup> difference in activation energy for the reactions of  $\text{SnMe}_2$  with  $\text{Me}_2\text{SnCl}_2$  and  $\text{Me}_3\text{SnCl}$ . The greater reactivity of  $\text{Me}_2\text{SnCl}_2$  compared to  $\text{Bu}_3\text{SnCl}$  can be attributed to the

increased Lewis acidity of the central tin atom in the substrate,<sup>19,21</sup> which would be expected to accelerate the second step in the proposed mechanism for the reaction (eq. 3.17).



Increased steric crowding from the *n*-butyl substituents may also play a role in increasing the activation barrier for the second step of the reaction with  $\text{Bu}_3\text{SnCl}$  compared to that with  $\text{Me}_2\text{SnCl}_2$ .<sup>22</sup> In a related study, the Si-Cl bond insertion of  $\text{SiMe}_2$  into compounds of the type  $\text{R}_3\text{SiCl}$  ( $\text{R} = \text{H}, \text{Me}, \text{Cl}$  etc.) was investigated theoretically by Kira and coworkers;<sup>22</sup> the results were interpreted as suggesting that one 'in-plane' electron withdrawing substituent accelerates the reaction (conversely, an in-plane electron donating substituent decelerates the reaction), while the two remaining 'out-of-plane' substituents influence the reaction mainly through sterics (eq. 3.18). The plane is defined as the two dimensional space occupied by the  $\text{Sn-Cl} \rightarrow \text{Sn}$  atoms. The two factors should combine to produce a larger rate constant for reaction of  $\text{Me}_2\text{SnCl}_2$  compared to  $\text{Bu}_3\text{SnCl}$  in the present work.



The addition of  $\text{Bu}_3\text{SnCl}$  to a hexanes solution of **2** led to a simultaneous shortening of the lifetime of  $\text{SnPh}_2$  and an apparent decrease in its photochemical yield. The decays fit reasonably well to first order exponentials, affording  $k_{\text{decay}}$  values that appear to approach a constant value ( $k_2$ ) with increasing concentration of substrate. Transient absorption spectra revealed the presence of a new transient product with  $\lambda_{\text{max}} \sim 410$  nm in addition to the stannylene absorption band in solutions of **2** containing 15.0

mM  $\text{Bu}_3\text{SnCl}$ . The new transient also decays with first order kinetics, and exhibits a simultaneous increase in its maximum yield and decay coefficient with increasing substrate concentration, the latter following a similar concentration dependence as that on the stannylene decay rate coefficient. The 410 nm transient is assigned to the Lewis acid-base complex of  $\text{SnPh}_2$  with  $\text{Bu}_3\text{SnCl}$ . The plot of  $k_{\text{decay}}$  vs.  $\text{Bu}_3\text{SnCl}$  for this species follows a similar form as the stannylene trace, and both can be modelled using the pre-equilibrium approximation,<sup>18</sup> which becomes applicable in instances wherein a rapid equilibrium is established between the stannylene and substrate with constant  $K_1$ , followed by a slow unimolecular rearrangement characterized by the rate constant  $k_2$ . At low substrate concentration,  $k_{\text{decay}}$  is linear with respect to substrate concentration with limiting slope given by the product  $K_1k_2$ , while at the high concentration limit  $k_{\text{decay}}$  is given by  $k_2$ , and is independent of concentration.

The non-linear least squares fit of the  $\text{SnPh}_2$  decay values to eq. 3.16 affords the values  $K_1 = (500 \pm 100) \text{ M}^{-1}$  and  $k_2 = (1.3 \pm 0.1) \times 10^6 \text{ s}^{-1}$  (Figure 3.7a), analysis of  $k_{\text{decay}}$  at 410 nm similarly affords values of  $K_1 = (200 \pm 80) \text{ M}^{-1}$  and  $k_2 = (1.6 \pm 0.3) \times 10^6 \text{ s}^{-1}$  (Figure 3.7b). As expected, reasonable agreement is found between the data obtained at 500 nm and 410 nm; although a marginally smaller  $K_1$  is obtained in the latter case. The composite values, obtained by analyzing the 410 nm and 500 nm data together (Figure 3.7c), afford values of  $K_1 = (350 \pm 80) \text{ M}^{-1}$  and  $k_2 = (1.4 \pm 0.1) \times 10^6 \text{ s}^{-1}$ .

A similar analysis of  $k_{\text{decay}}$  for  $\text{SnMePh}$  (Figure S3.9a-b) affords nearly identical values for  $K_1$  and  $k_2$  from analysis of the 500 nm and 410 nm data (see Table 3.2). Analysis of the composite data (Figure S3.9c) affords values of  $K_1 = (500 \pm 100) \text{ M}^{-1}$  and  $k_2 = (1.5 \pm 0.1) \times 10^6 \text{ s}^{-1}$ . The values for  $K_1$  and  $k_2$  for the reactions of  $\text{Bu}_3\text{SnCl}$  with  $\text{SnPh}_2$  and  $\text{SnMePh}$  are summarized in Table 3.2. Also included in the table are the values



of  $k_Q$  for SnMe<sub>2</sub>, SnPh<sub>2</sub> and SnMePh, in the latter two cases these are calculated as the product of the terms  $K_1k_2$  from the composite data.

**Table 3.2.** Summary of  $K_1$  (M<sup>-1</sup>),  $k_2$  (10<sup>6</sup> s<sup>-1</sup>) and  $k_Q$  (10<sup>9</sup> M<sup>-1</sup> s<sup>-1</sup>) for the Reactions of SnMe<sub>2</sub>, SnPh<sub>2</sub> and SnMePh with Bu<sub>3</sub>SnCl in Hexanes at 25 °C.

	SnMe <sub>2</sub> <sup>b</sup> (530 nm)	SnPh <sub>2</sub> (500 nm)	SnPh <sub>2</sub> (410 nm)	SnMePh <sup>c</sup> (500 nm)	SnMePh <sup>c</sup> (410 nm)
$K_1$ (M <sup>-1</sup> )	-	500 ± 100	(200 ± 80)	600 ± 100	(200 ± 100)
$k_2$ (10 <sup>6</sup> s <sup>-1</sup> )	-	1.3 ± 0.1	(1.6 ± 0.3)	1.46 ± 0.09	(1.8 ± 0.3)
Composite (i.e. both data sets analyzed as one)					
$K_1$ (M <sup>-1</sup> )	-	350 ± 80		500 ± 100	
$k_2$ (10 <sup>6</sup> s <sup>-1</sup> )	-	1.4 ± 0.1		1.5 ± 0.1	
$k_Q$ (10 <sup>9</sup> M <sup>-1</sup> s <sup>-1</sup> )	0.83 ± 0.08	0.5 ± 0.1 <sup>d</sup>		0.7 ± 0.2 <sup>d</sup>	

<sup>a</sup>Errors are quoted as twice the standard error obtained from the least-squares analyses unless otherwise specified; <sup>b</sup>no intermediate detected; <sup>c</sup>Data recorded by B. Nguyen; <sup>d</sup> $k_Q$  calculated as the product of separately measured values  $K_1$  and  $k_2$ :  $k_Q = K_1k_2$ ;

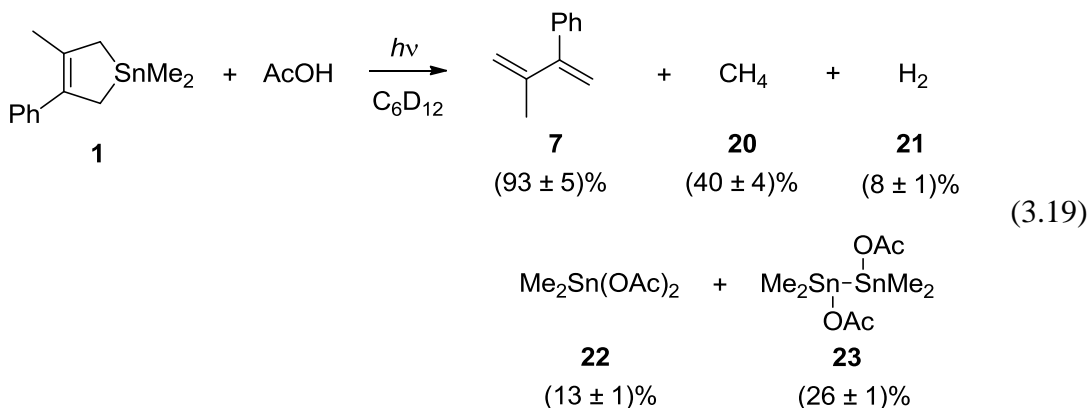
The transient spectral behaviour of the stannylenes with Bu<sub>3</sub>SnCl is consistent with the general reaction scheme shown in eq. 3.17. With SnMePh and SnPh<sub>2</sub> the intermediate complex was observed directly, whereas with SnMe<sub>2</sub> the complex does not build up to a high enough concentration for it to be detected. This presumably occurs because SnMe<sub>2</sub> is a weaker Lewis acid than SnPh<sub>2</sub> and SnMePh (decreasing  $K_1$ ) but leads to a more reactive complex owing to steric factors (increasing  $k_2$ ). With the knowledge that SnMe<sub>2</sub> consistently forms less stable Lewis acid-base complexes than SnPh<sub>2</sub> - the ratio  $K_{eq}^{SnPh_2} / K_{eq}^{SnMe_2}$  varies between 2 to 6 in the substrates where both equilibrium constants can be measured (see Chapter 4) - an equilibrium constant of the first step can be estimated to be  $K_1 \sim 10^2$  M<sup>-1</sup>, and by extension (using the relationship  $k_Q = K_1k_2$ ) the subsequent insertion to proceed at a rate  $k_2 \sim 10^7$  s<sup>-1</sup>. Comparison of the composite data for SnPh<sub>2</sub> and SnMePh reveal negligible differences in the equilibrium ( $K_1$ ) and insertion

( $k_2$ ) steps. Similarly, a comparison of  $K_1k_2$  at the low substrate limit suggests (within error) a negligible difference in overall reactivity between the three stannylenes, all of which range between  $(6 - 8) \times 10^8 \text{ M}^{-1} \text{ s}^{-1}$ .

### 3.4. The Reactions of $\text{SnMe}_2$ , $\text{SnPh}_2$ and $\text{SnMePh}$ with Acetic Acid

#### 3.4.1. Results

Photolysis of a deaerated  $\text{C}_6\text{D}_{12}$  solution of **1** (ca. 0.05 M) in the presence of AcOH (ca. 0.21 M) affords diene **7**, methane (**20**), molecular hydrogen (**21**) and two tin-containing products that were tentatively identified as dimethyltin diacetate (**22**) and 1,2-diacetoxytetramethyldistannane (**23**) (eq. 3.19). The  $^1\text{H}$  and  $^{119}\text{Sn}$  NMR spectra of the photolyzate after 30 minutes of photolysis are shown in Figures 3.8b and S3.10, respectively.  $\text{H}_2$  ( $\delta_{\text{H}}$  4.54) was identified by comparison of the chemical shift to that reported in the same solvent,<sup>23</sup> while the identity of methane ( $\delta_{\text{H}}$  0.18;  $\delta_{\text{C}}$  -4.70) was confirmed by spiking the photolyzate with an authentic sample. Compounds **22** and **23** were identified by comparison of the  $^1\text{H}$ ,  $^{13}\text{C}\{^1\text{H}\}$  and  $^{119}\text{Sn}\{^1\text{H}\}$  NMR spectra of the photolyzate to their reported spectra,<sup>24,25</sup> after evaporation of solvent and redissolution in  $\text{CDCl}_3$  or  $\text{C}_6\text{D}_6$  as appropriate (see 8.7.3).



Product yields were determined from the initial (first three or four data points, see Figure 3.9) slopes of concentration versus time plots constructed for the starting materials

and products from  $^1\text{H}$  NMR spectra recorded of the reaction mixture at selected time intervals during the photolysis. The yield of molecular hydrogen is adjusted to account for the 3:1 ratio of *ortho*- $\text{H}_2$  to *para*- $\text{H}_2$  (the latter is NMR inactive<sup>26</sup>), while that of the distannane **23** was calculated on a per-SnMe<sub>2</sub>-unit basis. Concentration versus time plots for **20**, **21** and **22** in particular are strongly curved at prolonged photolysis times. Evaporation of volatile compounds  $\text{H}_2$  (**21**) and  $\text{CH}_4$  (**20**) during prolonged photolysis could account for some of the curvature. Product formation was also accompanied by a rapid yellowing of the reaction solution, consistent with the build-up of distannane **23** in the mixture.<sup>11</sup> The mixture of **1** and AcOH remains unchanged after sitting for roughly 30 minutes prior to irradiation, suggesting product formation is initiated by photolysis.

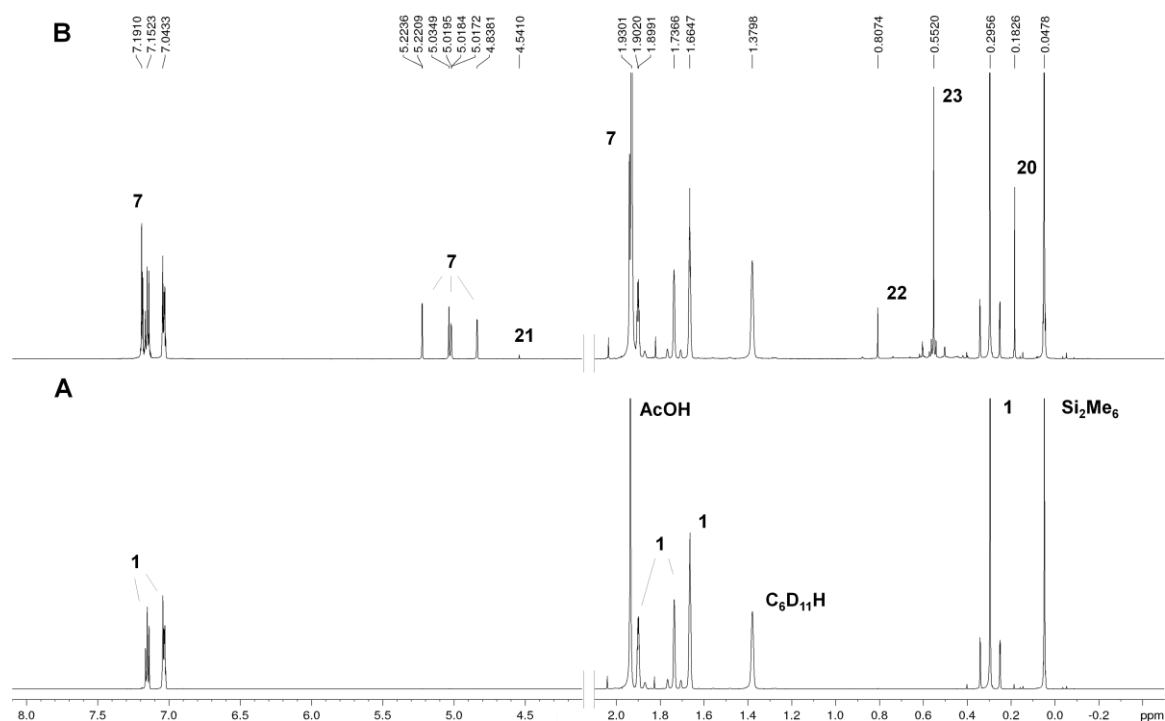


**Figure 3.8.**  $^1\text{H}$  NMR spectra of a deaerated 0.05 M solution of **1** in  $\text{C}_6\text{D}_{12}$  containing AcOH (0.21 M) (a) before and (b) after 30 minutes of photolysis with 254 nm light.

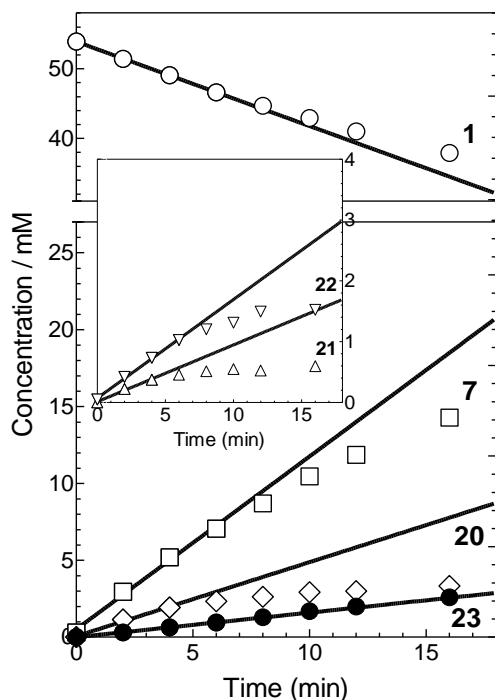


**Figure 3.9.** Concentration versus time plots for the photolysis of a deaerated 0.05 M solution of **1** in  $C_6D_{12}$  containing AcOH (0.21 M). The inset shows an expanded plot, detailing the formation of compounds **21** - **22** with photolysis time. The initial slopes (determined from the first three data points for **20** and **21**, and first four data points otherwise) are **1**,  $-1.210 \pm 0.009$  ( $\circ$ ); **7**,  $1.12 \pm 0.06$  ( $\square$ ); **20**,  $0.48 \pm 0.05$  ( $\diamond$ ); **23**,  $0.160 \pm 0.001$  ( $\bullet$ ); **21**,  $0.09 \pm 0.01$  ( $\Delta$ ); **22**,  $0.162 \pm 0.007$  ( $\nabla$ ) (units,  $mM \text{ min}^{-1}$ ).

When the photolysis of **1** is repeated using a mixture of AcOH:AcOD ( $24 \pm 1\%$  AcOH, calculated from the relative integrals of the OH and  $CH_3$  resonances in the  $^1H$  NMR spectrum), the resulting product mixture after 30 minutes of irradiation (Fig 3.10) was very similar to that described above except for the presence of additional signals (all triplets) in the  $^{13}C$  and/or  $^1H$  NMR spectra assignable to HD ( $\delta_H$  4.50 (t),  $^1J_{HD} = 42.5$  Hz) and  $CH_3D$  ( $\delta_H$  0.17 (t),  $^2J_{HD} = 1.9$  Hz;  $\delta_C$  -4.9 (t),  $^1J_{CD} = 19.6$  Hz). The  $^1H$  NMR spectrum after 30 minutes photolysis indicates the ratio of  $CH_4$  and  $CH_3D$  present was  $CH_4:CH_3D = 2.8 \pm 0.3$ . By comparison, a ratio of  $CH_4:CH_3D \sim 0.3$  would be predicted in the absence of an isotope effect on the reaction. The kinetic isotope effect ( $k_H/k_D$ ) can thus be calculated according to eq. 3.20 from the relative ratios of AcOH:AcOD and  $CH_4:CH_3D$ , affording a value of  $k_H/k_D = 8.7 \pm 0.9$  for the isotope effect on the reaction rate.

$$\frac{k_H}{k_D} = \frac{[AcOD]}{[AcOH]} \cdot \frac{[CH_4]}{[CH_3D]} \quad (3.20)$$

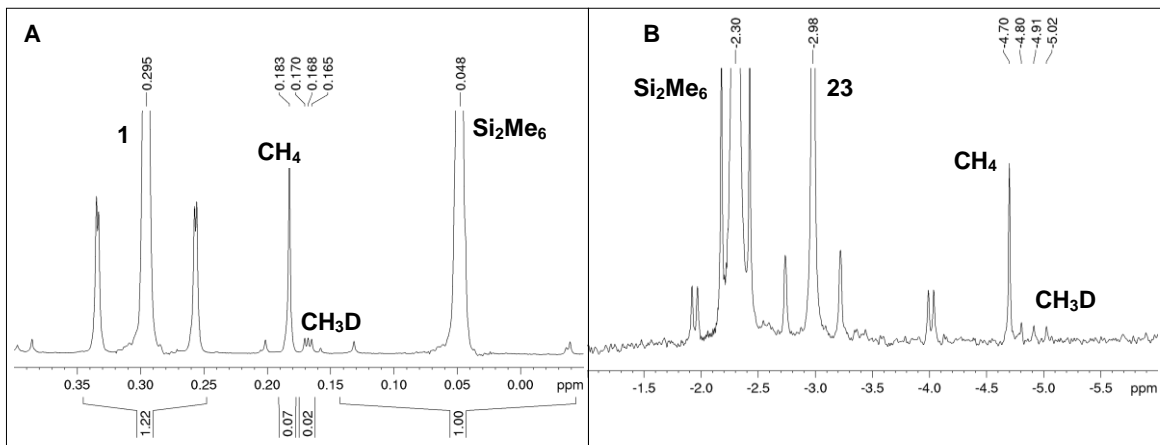
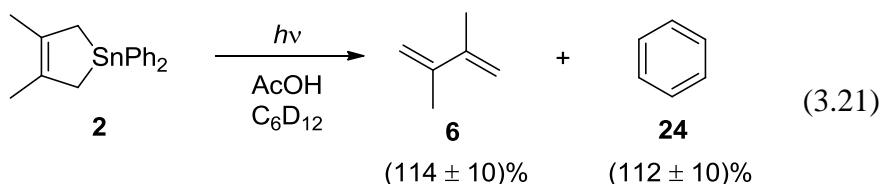


**Figure 3.10.** (a)  $^1\text{H}$  NMR spectrum (-0.05 - 0.40 ppm) and (b)  $^{13}\text{C}\{^1\text{H}\}$  NMR spectrum (-6.0 - -1.0 ppm) of a deaerated 0.05 M solution of **1** in  $\text{C}_6\text{D}_{12}$  containing a mixture of AcOH/AcOD (total concentration 0.20 M) after 30 minutes photolysis with 254 nm light.

Photolysis of **2** in the presence of AcOH (0.20 M) resulted in the formation of **6** and benzene (**24**) as the major products (eq. 3.21). One additional unidentified product containing aromatic resonances was observed to be formed in minor yield; however, its formation levels off after ca. 4% conversion of **2**. The presence of **24** was confirmed by GC-MS analysis of the photolyzate (Figure S11), in addition to analysis of  $^1\text{H}$  and  $^{13}\text{C}$  NMR spectra of the photolysis mixture after addition of an authentic sample of **24**.



Continued photolysis led to the formation of a white precipitate and broadening of the aromatic and aliphatic regions of the  $^1\text{H}$  NMR spectrum; no new resonances were observed in the  $^{119}\text{Sn}$  NMR spectrum of the photolyzate after 30 minutes photolysis and ca. 30 % conversion of **2**. The  $^1\text{H}$  NMR spectrum contained no resonances in the ( $\delta_{\text{H}}$  5 - 6.5) Sn-H region or ( $\delta_{\text{H}}$  4.54) where  $\text{H}_2$  resonates, indicating the O-H insertion product ( $\text{Ph}_2\text{Sn}(\text{H})\text{OAc}$ ) is not formed in the reaction. The generation of benzene in quantitative

yield suggests the primary reaction to be analogous to that of the aryl substitution channel reported for the reactions of kinetically stabilized diarylstannylenes with MeOH or water.<sup>3</sup> The mixture was allowed to sit for roughly 1 hour prior to photolysis and resulted in no changes in the  $^1\text{H}$  NMR spectrum, which rules out the possibility of a dark reaction. Representative  $^1\text{H}$  NMR spectra are presented in Figure 3.11, while concentration versus time plots showing the formation of **6** and **24** at the expense of **2** are shown in Figure 3.12.

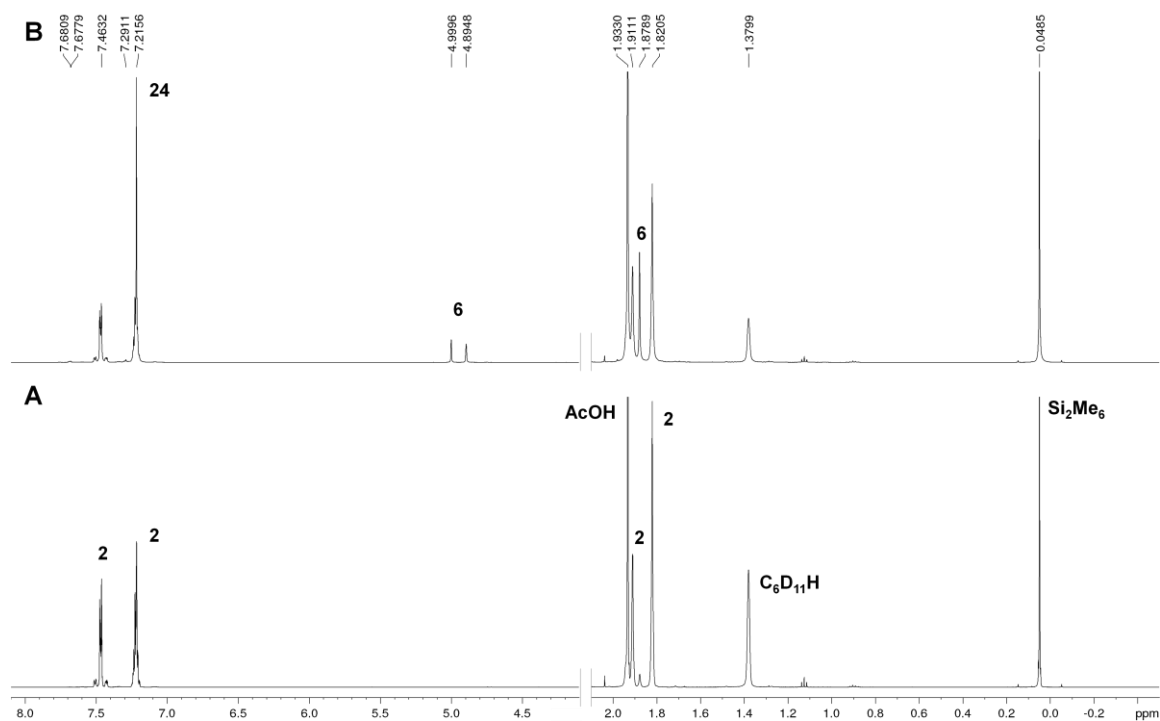


**Figure 3.11.**  $^1\text{H}$  NMR spectra of a deaerated 0.05 M solution of **2** in  $\text{C}_6\text{D}_{12}$  containing AcOH (0.20 M) (a) before and (b) after 30 minutes photolysis with 254 nm light.

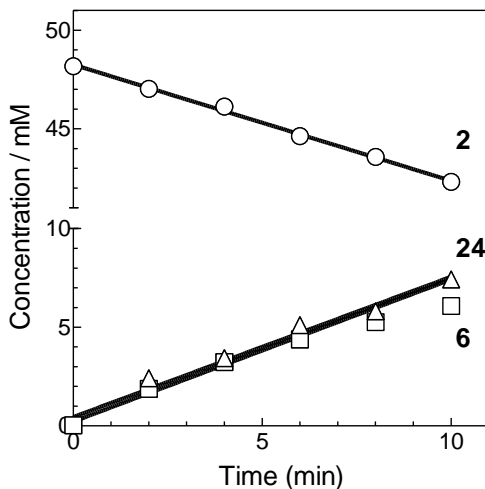


**Figure 3.12.** Concentration versus time plots for the photolysis of a solution of **2** (ca. 0.05 M) in  $C_6D_{12}$  and AcOH (ca. 0.2 M). The initial slopes of each of the plots, determined from the first four data points for **6** and the first six data points otherwise, are (in units of  $mM\ min^{-1}$ ) **2**,  $-0.59 \pm 0.02$  ( $\circ$ ); **6**,  $0.72 \pm 0.06$  ( $\square$ ); **24**,  $0.71 \pm 0.06$  ( $\Delta$ ).

Repeating the photolysis of **2** under the same conditions but using a mixture of AcOH and AcOD ( $22 \pm 1\%$  AcOH) results in a similar  $^1H$  NMR spectrum to the one obtained from the photolysis with AcOH. The inverse-gate proton-decoupled  $^{13}C$  NMR spectrum after 30 minutes of irradiation exhibits new resonances assigned to  $C_6H_5D$  ( $\delta_C$  128.4 ( $^1J_{CD} = 24.5$  Hz; *ipso*-Ph), 128.6 (*o*-Ph), 128.7 (*m,p*-Ph)).  $C_6H_5D$  was identified based on agreement of its deuterium isotope effects on  $\delta_C$  (i.e. the differences in  $\delta_C$  relative to  $C_6H_6$  which is also present in the spectrum; see Fig. 3.13) with those previously reported.<sup>27</sup> The ratio  $[C_6H_6]:[C_6H_5D]$  was calculated from the integral ratio of the resonance at 128.7 (after subtracting additional resonances due to **2'** and  $C_6H_5D$ ) relative to the resonance at 128.6 due to  $C_6H_5D$ , and adjusting for the number of carbons. Integration of the spectrum afforded an estimate of  $C_6H_6:C_6H_5D = 1.4 \pm 0.1$  for the ratio of benzene:benzene-*d* formed in the photolysis. From this and the AcOH:AcOD concentration ratio was calculated a value of  $k_H/k_D = 5.2 \pm 0.3$  for the kinetic isotope effect.

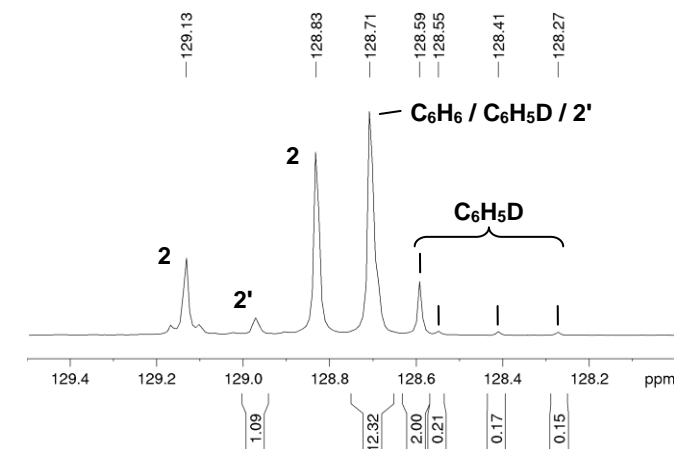
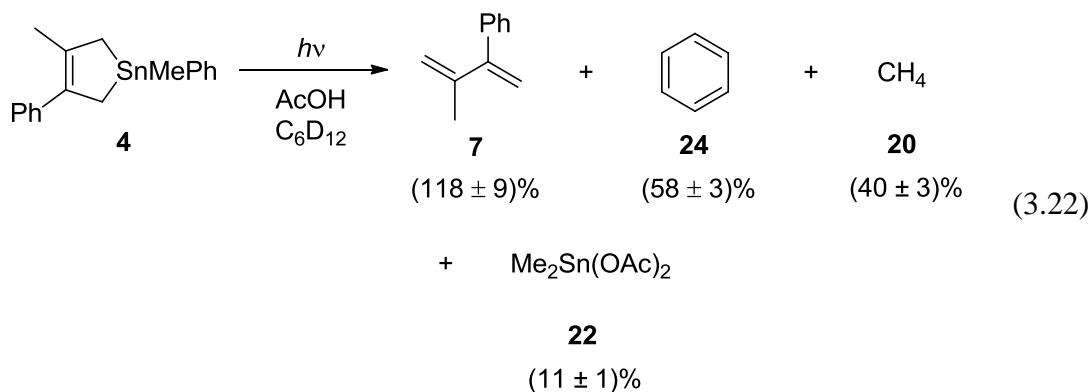


**Figure 3.13.** Inverse-gate <sup>13</sup>C{<sup>1</sup>H} NMR spectrum (128.0 - 129.5 ppm) of a deaerated 0.05 M solution of **2** in C<sub>6</sub>D<sub>12</sub> containing a mixture of AcOH:AcOD (total concentration 0.20 M) after 30 minutes photolysis with 254 nm light (**2'** denote satellite resonances from **2**).

Photolysis of a C<sub>6</sub>D<sub>12</sub> solution of **4** (0.05 M) containing AcOH (0.20 M) resulted in the formation of **7** (118 ± 9 %), benzene (**24**, 58 ± 3 %), and methane (**20**, 40 ± 3 %) as the major products (eq. 3.22); one additional product was formed in relatively low yield and is tentatively assigned to **22** (11 ± 1 %) on the basis of its <sup>1</sup>H, <sup>13</sup>C{<sup>1</sup>H} and <sup>119</sup>Sn{<sup>1</sup>H} NMR resonances in comparison with the spectra obtained from the photolysis of **1** with AcOH. A small collection of additional resonances was also observed in the 0.6 - 0.8 and 7.5 - 7.7 ppm regions of the <sup>1</sup>H NMR spectrum but could not be identified. Continued photolysis was accompanied by the formation of a white precipitate.



Concentration versus time plots for **4** and the identified products are shown in Figure 3.15, while the <sup>1</sup>H NMR spectrum of the photolyzate after ca. 30 minutes photolysis is shown in Figure 3.14b. The presence of methane and benzene was confirmed by <sup>1</sup>H and <sup>13</sup>C NMR spectroscopy after spiking the photolyzate with an authentic sample of each



compound. A separate solution containing the same mixture and kept in the dark was found not to change over the course of the photolysis experiment. The products observed (eq. 3.22) suggest that SnMePh and diene **7** are generated cleanly from **4**, and the stannylene reacts with AcOH to produce methane and benzene competitively.

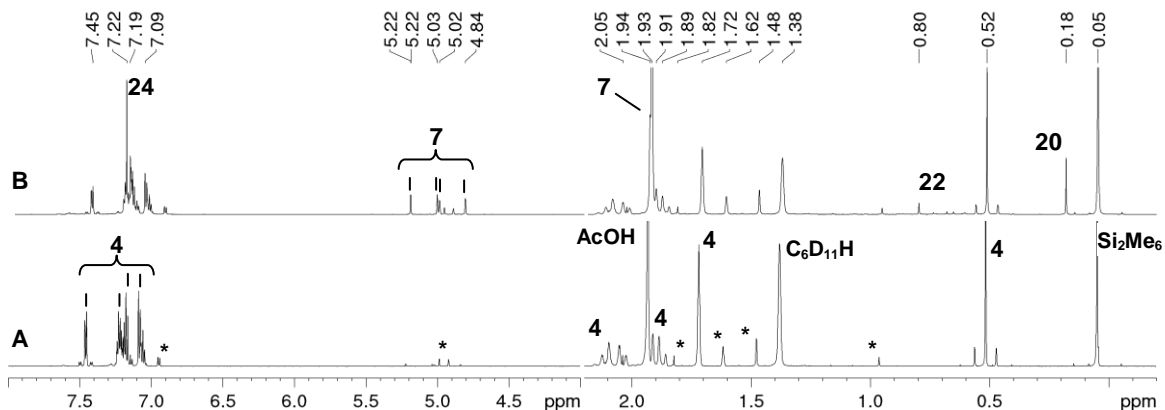


**Figure 3.14.**  $^1\text{H}$  NMR spectra of a deaerated ca. 0.05 M solution of **4** in  $\text{C}_6\text{D}_{12}$  containing AcOH (0.20 M) (a) before and (b) after 30 minutes photolysis with 254 nm light (\*unreactive impurity). (Data recorded by B. Nguyen)

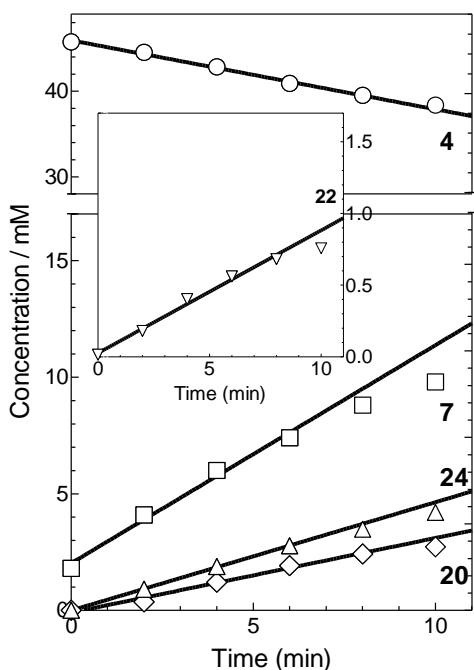


**Figure 3.15.** Concentration versus time plots for the photolysis of a solution of **4** (ca. 0.05 M) in  $\text{C}_6\text{D}_{12}$  and AcOH (ca. 0.2 M). The initial slopes in each of the plots, determined from the first four data points for **7** and **24** and first five data points otherwise, are (in units of  $\text{mM min}^{-1}$ ) **4**,  $-0.81 \pm 0.07$  ( $\circ$ ); **7**,  $0.94 \pm 0.14$  ( $\square$ ); **24**,  $0.46 \pm 0.01$  ( $\triangle$ ); **20**,  $0.32 \pm 0.04$  ( $\diamond$ ); **22**,  $0.09 \pm 0.01$  ( $\nabla$ ). (Data recorded by B. Nguyen)

The absolute rate constants for the reactions of SnMe<sub>2</sub>, SnPh<sub>2</sub>, and SnMePh with AcOH and AcOD determined in this work are summarized in Table 3.3. The same bimolecular rate constants within error were obtained for SnMe<sub>2</sub> and SnPh<sub>2</sub>, while a ca. 50 % larger rate constant was measured for the reaction with SnMePh relative to SnMe<sub>2</sub>. Quenching experiments with SnMe<sub>2</sub> and SnPh<sub>2</sub> were also carried out using AcOD as the stannylene substrate (Figure 3.16c and S3.12b). In both cases rate constants were obtained that were the same within error as those for quenching by AcOH, suggesting a negligible kinetic isotope effect:  $k_H/k_D = 1.2 \pm 0.3$  for SnMe<sub>2</sub> and  $0.9 \pm 0.1$  for SnPh<sub>2</sub>. Laser flash photolysis experiments show that the addition of AcOH to hexanes solutions of **1**, **2** and **4** results in kinetic quenching of the stannylene signals, and the appearance of new, relatively long-lived transient absorptions in the 270 - 340 nm region of the spectrum. (See Figure 3.16 for **1** and Figure S3.12 for **2** and **4**) In all cases, formation of the dimer absorptions observed in the absence of substrate is eliminated in the presence of added AcOH.

**Table 3.3.** Absolute Rate Constants ( $k_Q$ ) for the Reactions of SnMe<sub>2</sub>, SnPh<sub>2</sub> and SnMePh with AcOH and AcOD in Hexanes Solution at 25 °C.<sup>a</sup>

Substrate	$k_Q$ ( $10^9 \text{ M}^{-1} \text{ s}^{-1}$ )		
	SnMe <sub>2</sub>	SnPh <sub>2</sub>	SnMePh <sup>b</sup>
AcOH	$3.5 \pm 0.8$	$4.2 \pm 0.4$	$6.5 \pm 0.5$
AcOD	$2.9 \pm 0.3^b$	$4.6 \pm 0.5^b$	<sup>c</sup>

<sup>a</sup>Errors are quoted as twice the standard error obtained from the least-squares analyses unless otherwise specified; <sup>b</sup>Data recorded by B. Nguyen; <sup>c</sup>not measured

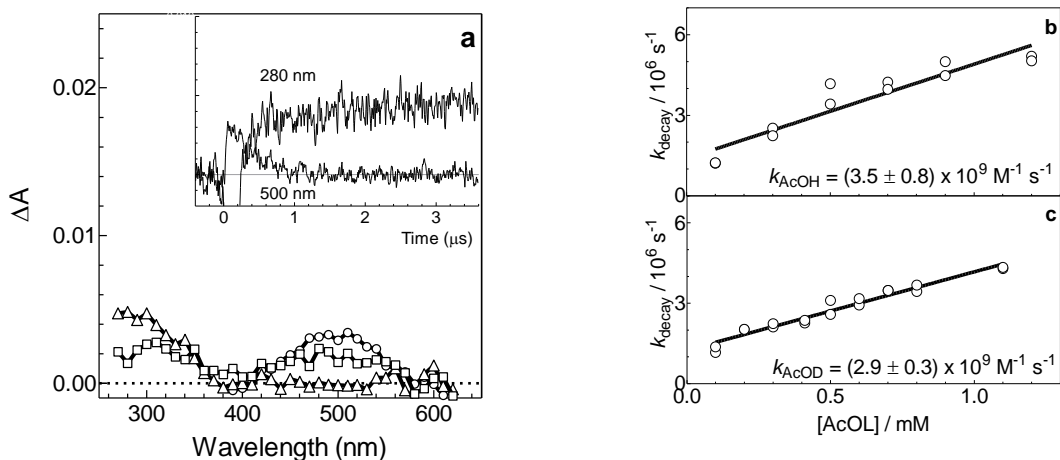


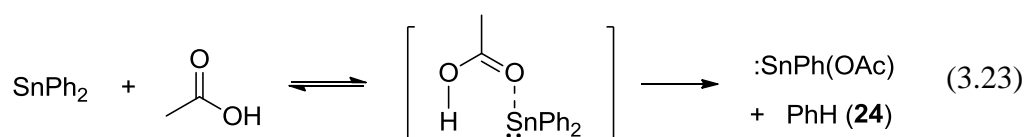
**Figure 3.16.** (a) Time-resolved UV-vis spectra from laser photolysis of **1** in hexanes containing 0.5 mM AcOH, 0.07 - 0.10  $\mu\text{s}$  ( $\circ$ ), 0.30 - 0.32  $\mu\text{s}$  ( $\square$ ), and 3.50 - 3.53  $\mu\text{s}$  ( $\triangle$ ) after the laser pulse (25  $^\circ\text{C}$ ); data recorded using a neutral density filter (43 % transmittance). Plot of  $k_{\text{decay}}$  for reaction of SnMe<sub>2</sub> (530 nm) with (b) AcOH and (c) AcOD in hexanes at 25  $^\circ\text{C}$ ; the solid lines are the linear least squares fit of the data to equation 3.10. (Data in (c) recorded by B. Nguyen)

### 3.4.2. Discussion

Previous work with transient silylenes and germynes indicates that they react with HOAc to afford the corresponding acetoxysilane or -germane ( $\text{R}_2(\text{H})\text{MOAc}$ ; R = Me, Ph; M= Si, Ge), respectively, as the major products in all cases.<sup>28-30</sup> Substituent effects on the rate constant for reaction of AcOH strongly implicate the involvement of a pre-reaction complex in the case of diarylgermylenes,<sup>31</sup> although they do not build up to sufficiently high concentrations for their transient spectra to be detected directly. In the present cases, addition of sub-millimolar concentrations of AcOH resulted in acceleration of the stannylene decays, and a change to (pseudo) first order decay kinetics, in a manner consistent with kinetic quenching. Plots of the decay rate coefficient versus  $[\text{AcOH}]$  are linear up to 1.2 mM, and afford rate constants of  $k_{\text{Q}} = (3.5 \pm 0.8) \times 10^9 \text{ M}^{-1} \text{ s}^{-1}$ ,  $k_{\text{Q}} = (4.2 \pm 0.4) \times 10^9 \text{ M}^{-1} \text{ s}^{-1}$  and  $k_{\text{Q}} = (6.5 \pm 0.5) \times 10^9 \text{ M}^{-1} \text{ s}^{-1}$  for SnMe<sub>2</sub>, SnPh<sub>2</sub>, and SnMePh respectively. The spectra showed no evidence of transient absorptions in the 350 - 370 nm range, where the corresponding stannylene-HOAc complexes would be expected to

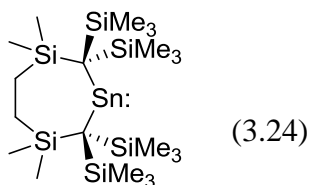
absorb based on the spectra of the  $\text{SnR}_2\text{-EtOAc}$  complexes (for  $\text{SnMe}_2$  and  $\text{SnPh}_2$ ; see Chapter 4). This suggests the stannylene-HOAc complexes, if they are formed, exist as steady state intermediates. Transient absorption spectra of solutions of **1**, **2** and **4** containing 0.5 - 1.1 mM AcOH, recorded at the end of the stannylene decays, in all cases show a transient product with absorption bands in the short wavelength region of the UV-vis spectrum, and a maximum absorbance below 280 - 290 nm (see Figures 3.16a and S3.12d-e).

It was also found in the reaction mixtures of **2** and AcOH that benzene (**24**) formed in high yield as the major product. The photolyzate is stable in the absence of UV irradiation, which rules out a direct reaction between **2** and AcOH as the source of benzene. The finding from flash photolysis studies that  $\text{SnPh}_2$  reacts rapidly and (by all indications) irreversibly with AcOH, coupled with the equivalent product yields of benzene and **6**, leads us to attribute the formation of benzene to a direct reaction between  $\text{SnPh}_2$  and AcOH. The formation of benzene is analogous to the aryl substitution channel found for kinetically stabilized diarylstannylenes and small protic molecules ( $\text{NH}_3$ ,  $\text{H}_2\text{O}$  and  $\text{MeOH}$ ),<sup>3,32</sup> as well as  $\text{H}_2$  elimination between  $\text{GeH}_2$  and AcOH.<sup>23</sup> In principle, the elimination of benzene should also afford acetoxyphenylstannylene ( $\text{SnPh(OAc)}$ ; **25**)<sup>33-35</sup> as the co-product (eq. 3.23); however, evidence for its formation was not found in the transient UV-vis absorption spectrum.

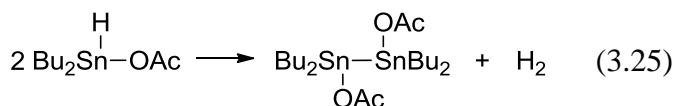


The flash photolysis behaviour of **1** in the presence of AcOH is also consistent with a fast, direct reaction between  $\text{SnMe}_2$  and AcOH, which the results of product studies experiments suggest is due to two competing reactions. The formation of methane is attributed to a substitution channel analogous to the aryl substitution pathway that

produces benzene from  $\text{SnPh}_2$ . The elimination of methane should also produce a stoichiometric quantity of acetoxymethylstannylene ( $\text{SnMe}(\text{OAc})$ ; **26**). However, as with the phenyl analogue, **26** could not be identified in the transient UV-vis spectrum. The only precedent for acid-promoted cleavage of an alkyl group from a dialkylstannylene to our knowledge is a report that treatment of the sterically hindered stannylene **27** (eq. 3.24) with MeOH or water led to the formation of "acyclic products" that were not specifically identified.<sup>36</sup>

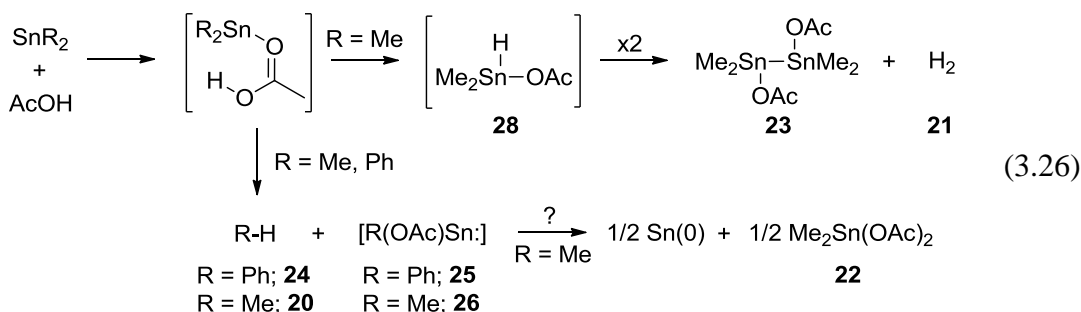
**27**

No indication of diagnostic Sn-H and Sn-Me resonances attributable to acetoxymethylstannylene ( $\text{Me}_2\text{Sn}(\text{H})\text{OAc}$ ; **28**) (through comparison with structurally related compounds  $\text{R}_2\text{M}(\text{H})\text{OAc}$  ( $\text{R}_2\text{M} = \text{Me}_2\text{Ge}^{29}$  and  $\text{Bu}_2\text{Sn}^{37}$ )) could be detected in the  $^1\text{H}$  NMR spectrum of the photolyzate. The formation of  $\text{H}_2$  and distannane **23** can be tentatively ascribed to a secondary reaction of **28**. The dehydrogenative coupling of dialkyltin hydrides has been previously demonstrated with the di-*n*-butyl derivatives of **23** and **28** (eq. 3.25).<sup>37</sup>



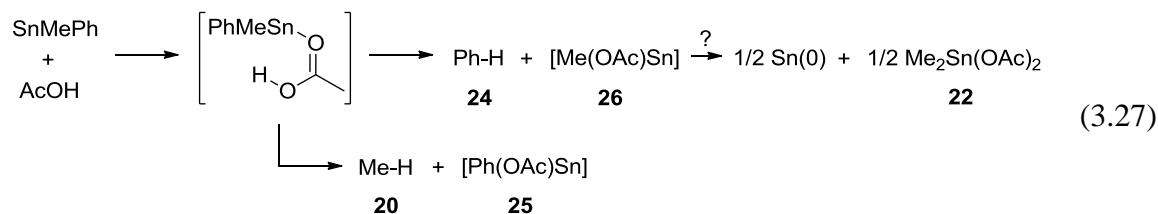
Based on the reaction stoichiometry shown in eq. 3.25, the chemical yield of  $\text{H}_2$  should be considered on a per 'H' basis (i.e. if taken as straight concentration affords a maximum yield of 50 %), affording a yield  $16 \pm 2$  %. The primary yield of **28** can also be approximated as twice the product yield of **23**, which affords a value of ca. 26 %.

Equation 3.26 illustrates the two reaction channels between  $\text{SnMe}_2$  and  $\text{AcOH}$  (i.e. O-H insertion and methane elimination), as well as the aryl substitution pathway for  $\text{SnPh}_2$  and  $\text{AcOH}$ . With  $\text{SnMe}_2$ , the ratio of product yields  $\mathbf{20}/\mathbf{23} = 1.5 \pm 0.2$  suggests a slight preference for alkane elimination over O-H insertion, consistent with a difference in activation energy of  $\Delta\Delta G^\ddagger \sim 0.3 \text{ kcal mol}^{-1}$ . Continued photolysis leads to a levelling of the concentration versus time plot for  $\mathbf{21}$ , but not for  $\mathbf{23}$ , perhaps because of evaporation of  $\text{H}_2$  during prolonged photolysis.<sup>38</sup> The formation of  $\mathbf{22}$  is ascribed to a disproportionation reaction of  $\mathbf{26}$  (eq. 3.26). This is analogous to the reported reaction between the Lappert dialkylstannylene  $\text{SnR}_2$  ( $\text{R} = \text{CH}(\text{SiMe}_3)_2$ ) and  $\text{SnCl}_2$  to produce  $\text{R}_2\text{SnCl}_2$  and tin metal;<sup>39</sup> the process can be formally represented as  $2 \text{ Sn(II)} \rightarrow \text{Sn(IV)} + \text{Sn(0)}$ .



In principle, the reaction of  $\text{SnMePh}$  with  $\text{AcOH}$  can proceed via three competing pathways: the elimination of  $\text{CH}_4$  ( $\mathbf{20}$ ), elimination of benzene ( $\mathbf{24}$ ), and O-H bond insertion. Indeed, the product studies indicate that  $\mathbf{20}$  and  $\mathbf{24}$  are formed (eq. 3.27) in a ratio  $\mathbf{24}:\mathbf{20} = 1.5 \pm 0.1$ , indicating a preference for aryl over alkyl substitution. Evidence for O-H insertion, either in the form of the acetoxystannane ( $\text{MePhSn(H)OAc}$ ) or the formation of  $\text{H}_2$ , was not found for this compound. The formation of  $\mathbf{22}$  is attributed again to the disproportionation of  $\mathbf{26}$  (eq. 3.27). The scheme outlined in eq. 3.27 predicts the product ratio  $\mathbf{22}/\mathbf{24} \sim 0.5$ , which is roughly twice the value obtained from the ratio of

product yields  $22/24 \sim 0.2$ . This discrepancy suggests the formation of **22** from **26** to be ca. 40 % efficient.



The flash photolysis results indicate the rate constant for reaction of AcOH with SnMePh is modestly greater than those for either SnMe<sub>2</sub> or SnPh<sub>2</sub>. The first comparison ( $k_{\text{SnMePh}} > k_{\text{SnMe}_2}$ ) suggests aryl substitution to be the preferred pathway over methane elimination, while the latter result ( $k_{\text{SnMePh}} > k_{\text{SnPh}_2}$ ) is consistent with the electron donating character of the methyl group in SnMePh (relative to the phenyl group in SnPh<sub>2</sub>) facilitating aryl substitution.

The kinetic isotope effects calculated from the CH<sub>4</sub>/CH<sub>3</sub>D and C<sub>6</sub>H<sub>6</sub>/C<sub>6</sub>H<sub>5</sub>D ratios from the reaction of SnMe<sub>2</sub> and SnPh<sub>2</sub> with AcOH/AcOD mixtures indicate a large primary isotope effect in both cases, consistent with proton transfer in the rate determining step. This appears at odds with the  $k_{\text{AcOH}}/k_{\text{AcOD}}$  ratios determined by laser flash photolysis, of which indicates a negligible isotope effect in both cases. The reason for the discrepancy may be related to the difference in AcOL (L = H, D) concentration employed in the two methods, as it is known that AcOH exists in a variety of oligomeric forms in hydrocarbon solvents. In particular, acetic acid at 0.2 M molar concentration in cyclohexane (as employed in the product studies) is expected to exist as oligomeric structures<sup>40</sup> while in hexanes solution at 0.1 - 1.2 mM it is expected to be present mostly as a mixture of monomer and hydrogen bonded dimer.<sup>41</sup> The lack of a significant kinetic isotope effect in the flash photolysis experiments is attributed to the rapid rate of proton transfer, as was observed previously in the O-L insertion of diarylgermylenes with

AcOL.<sup>31</sup> In other words, the initial complexation that precedes proton transfer is rate determining. At higher concentrations, the reacting species may be an oligomer of much lower acidity than the monomer, or there may be an additional pre-reaction equilibrium involving dissociation of AcOH oligomers on which there is a large isotope effect.

### 3.5. Summary and Conclusions

Laser flash photolysis of **3** and **4** both generate SnMePh cleanly and efficiently in solution. Analysis of the stannylene's reactivity towards Me<sub>2</sub>SnCl<sub>2</sub> using a combination of product and kinetic studies suggests facile Sn-Cl bond insertion of the stannylene via a two-step mechanism initiated by reversible Lewis acid-base complexation between SnMePh and the substrate, followed by the bond insertion step. SnMePh was found to be reactive towards Lewis acid-base complexation with THF and MeOH. The  $K_{eq}$  for complexation with MeOH is intermediate between those of SnPh<sub>2</sub> and SnMe<sub>2</sub> under similar conditions.

The reaction of acetic acid with SnPh<sub>2</sub> proceeds via arene elimination, affording benzene as the primary product; no evidence is found for the formation of the O-H insertion product Ph<sub>2</sub>Sn(H)OAc. Conversely, the reaction of acetic acid with SnMe<sub>2</sub> produces methane, molecular hydrogen, and the acetoxytin compounds **23** and **22**. H<sub>2</sub> and **23** are proposed to be formed as decomposition products of the formal O-H insertion product Me<sub>2</sub>Sn(H)OAc **28** based on literature precedent. The reaction of acetic acid with SnMePh generates benzene and methane in roughly 3:2 relative yields, indicating a small preference for arene over alkane elimination. The fate of the presumed co-products of ligand substitution, MeSnOAc (**26**) or PhSnOAc (**25**), could not be conclusively ascertained, nor could they be identified conclusively by laser photolysis methods.

The reaction of SnMe<sub>2</sub> with tributylchlorostannane affords the formal Sn-Cl insertion product, Bu<sub>3</sub>SnSnMe<sub>2</sub>Cl (**18**). Kinetics experiments suggest the reaction



proceeds via a two-step coordination-insertion pathway, and with SnMePh and SnPh<sub>2</sub> the intermediate complex was detected alongside the stannylene by its UV-vis absorption at  $\lambda_{\text{max}} = 410 \text{ nm}$ .

### 3.6. Supporting Information

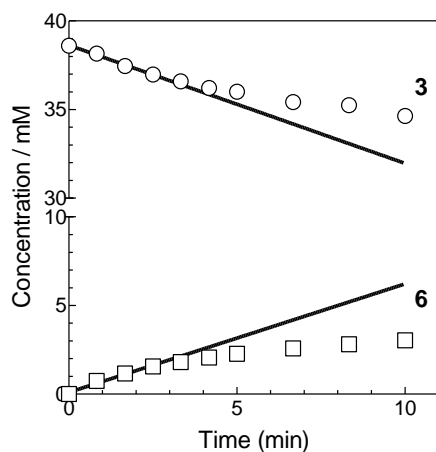


**Figure S3.1.** Concentration versus time plots for the photolysis of a deaerated 0.05 M solution of **3** in C<sub>6</sub>D<sub>12</sub>. The initial slopes determined from the first four data points are **3**,  $-0.66 \pm 0.04$  (○); **6**,  $0.61 \pm 0.07$  (□) (units, mM min<sup>-1</sup>).

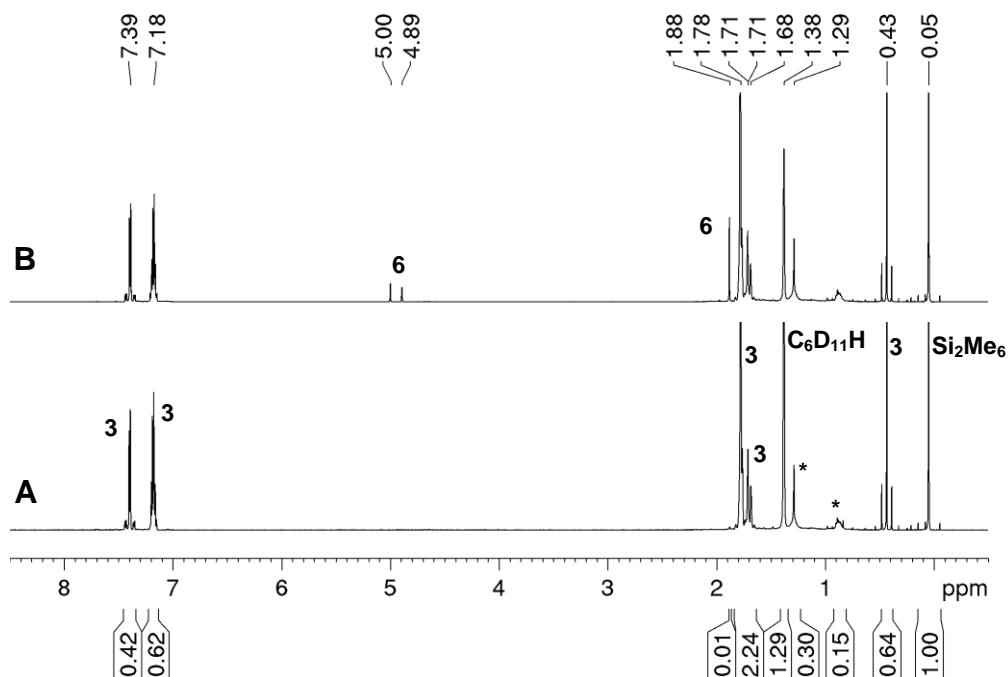


**Figure S3.2.** <sup>1</sup>H NMR spectra of a deaerated 0.05 M solution of **3** in C<sub>6</sub>D<sub>12</sub> (a) before and (b) after 10 minutes of photolysis with 254 nm light. (\*Unreactive impurity)

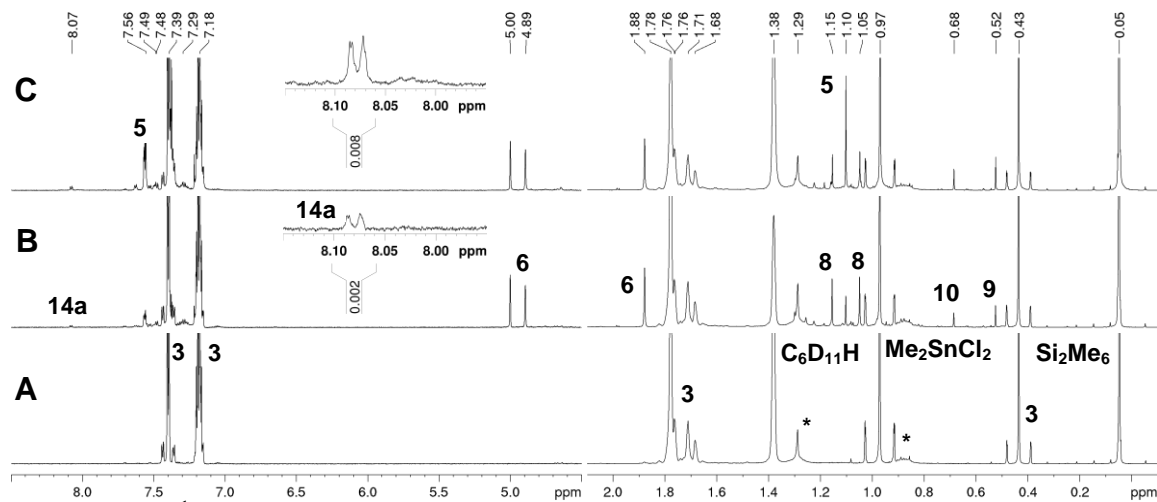


**Figure S3.3.**  $^1\text{H}$  NMR spectra of a 0.04 M solution of **3** in  $\text{C}_6\text{D}_{12}$  containing 0.04 M  $\text{Me}_2\text{SnCl}_2$ , (a) before and (b) after 10 minutes photolysis with 254 nm light, and (c) after spiking the resulting photolyzate with an authentic sample of **5**. (\*Unreactive impurity)

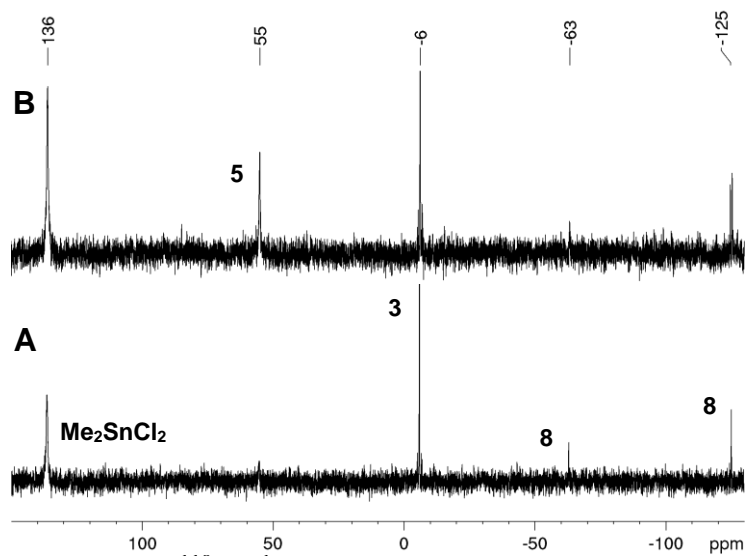


**Figure S3.4.**  $^{119}\text{Sn}\{^1\text{H}\}$  NMR spectra of a 0.04 M solution of **3** in  $\text{C}_6\text{D}_{12}$  containing 0.04 M  $\text{Me}_2\text{SnCl}_2$  (a) after 10 minutes photolysis with 254 nm light, and (b) after spiking the resulting photolyzate with an authentic sample of **5**.

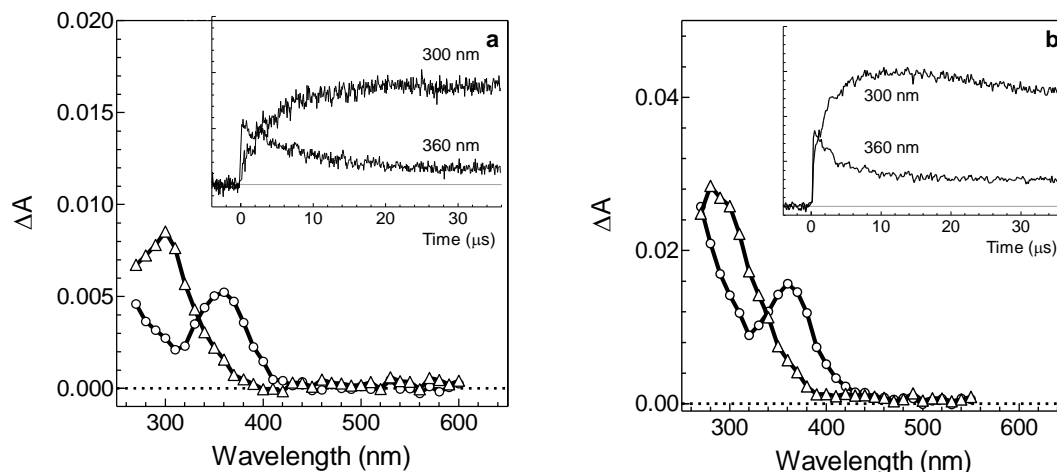


**Figure S3.5.** (a) Time-resolved UV-vis spectra from laser photolysis of **4** in hexanes solution containing 0.90 mM THF, 0.64 - 0.96  $\mu\text{s}$  ( $\circ$ ) and 34.4 - 34.7  $\mu\text{s}$  ( $\Delta$ ) after the laser pulse (25  $^{\circ}\text{C}$ ). (b) Time-resolved UV-vis spectra from laser photolysis of **3** in hexanes solution containing 10 mM THF, 0.64 - 0.96  $\mu\text{s}$  ( $\circ$ ) and 34.2 - 34.7  $\mu\text{s}$  ( $\Delta$ ) after the laser pulse (25  $^{\circ}\text{C}$ ). Absorbance-time profiles shown at selected wavelengths (inset). (*Data in (a) recorded by B. Nguyen*)

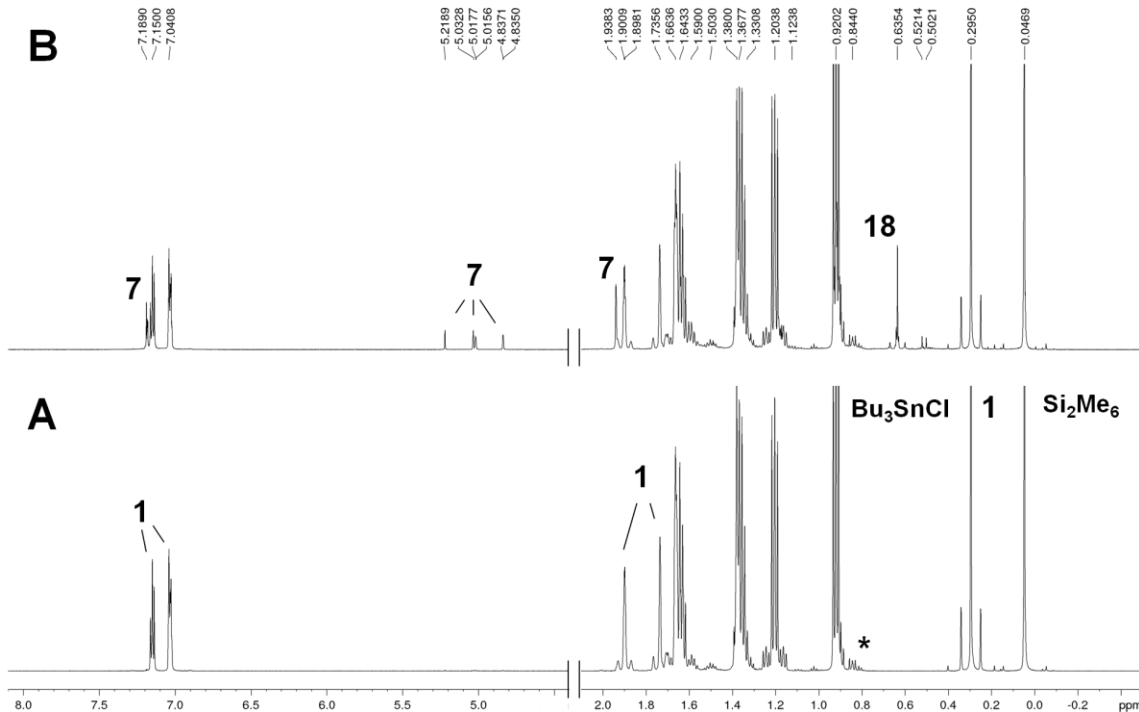


**Figure S3.6.**  $^1\text{H}$  NMR spectra of a deaerated 0.04 M solution of **1** in  $\text{C}_6\text{D}_{12}$  containing  $\text{Bu}_3\text{SnCl}$  (0.040 M) (a) before and (b) after 10 minutes of photolysis with 254 nm light. (\* $\text{Bu}_4\text{Sn}$ )

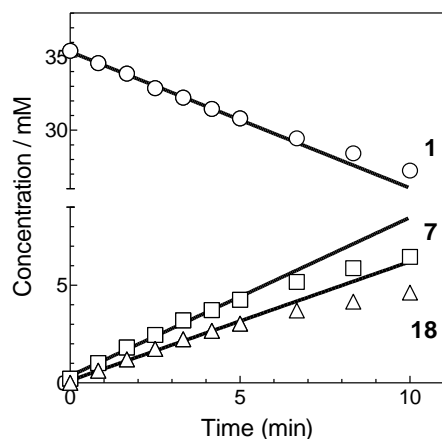


**Figure S3.7.** Concentration versus time plots for the photolysis of a deaerated 0.04 M solution of **1** in  $C_6D_{12}$  containing  $Bu_3SnCl$  (0.040 M). The initial slopes determined from the first four data points are **1**,  $-0.93 \pm 0.02$  ( $\circ$ ); **7**,  $0.81 \pm 0.03$  ( $\square$ ); **18**,  $0.61 \pm 0.02$  ( $\Delta$ ) (units,  $mM\ min^{-1}$ ).

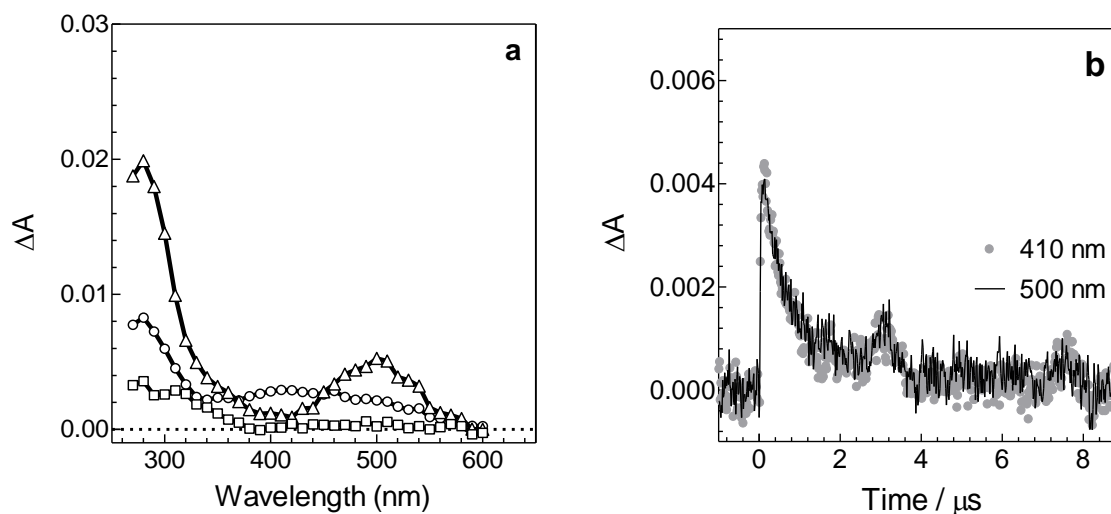


**Figure S3.8.** (a) Time-resolved UV-vis spectra from the laser photolysis of **4** in hexanes containing 0.0 mM  $Bu_3SnCl$  at 0.42 - 0.51  $\mu s$  ( $\Delta$ ) and 15.0 mM  $Bu_3SnCl$  at 0.22 - 0.32  $\mu s$  ( $\circ$ ) and 5.86 - 6.02  $\mu s$  ( $\square$ ) after the laser pulse (25  $^{\circ}C$ ). (b) Transient decay profiles recorded at 500 nm and 410 nm from the laser photolysis of a hexanes solution of **4** containing 15.0 mM  $Bu_3SnCl$ .

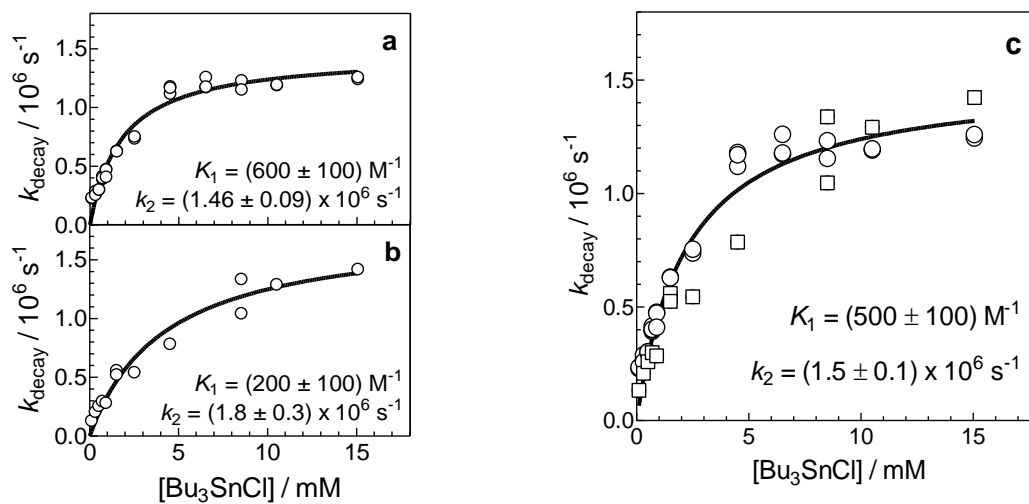


**Figure S3.9.** Plots of  $k_{\text{decay}}$  for reaction of (a) SnMePh (500 nm) and the (b) 410 nm absorption with  $\text{Bu}_3\text{SnCl}$  in hexanes at 25 °C. (c) Overlap of the  $k_{\text{decay}}$  data for the SnMePh ( $\circ$ ) and 410 nm ( $\square$ ) absorptions as a function of  $[\text{Bu}_3\text{SnCl}]$ . The solid lines are the non-linear least squares fit of the data to equation 3.16. (Data recorded by B. Nguyen)

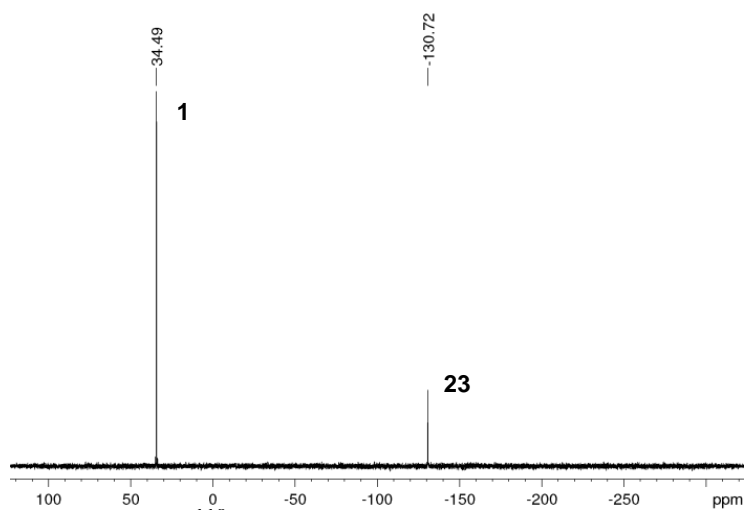


**Figure S3.10.**  $^{119}\text{Sn}$  NMR spectra of a deaerated 0.05 M solution of **1** in  $\text{C}_6\text{D}_{12}$  containing AcOH (0.21 M) after 30 minutes of photolysis with 254 nm light.

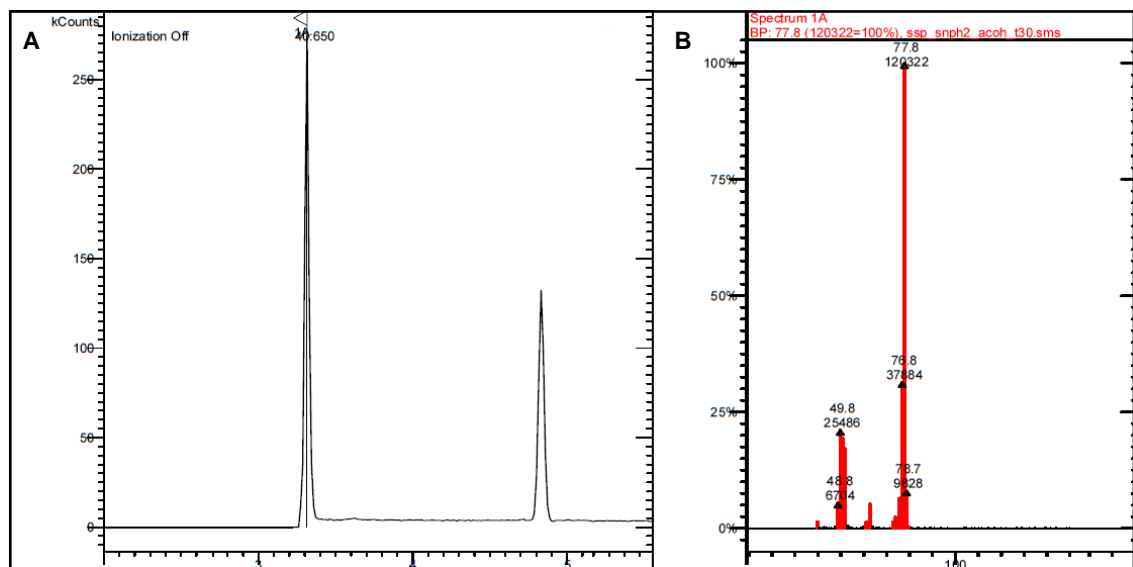


**Figure S3.11.** (a) GC-MS chromatogram (0 - 5.6 minutes retention time) and (b) mass spectrum of the peak at ca. 3.3 minutes retention time of a 0.05 M solution of **2** in  $C_6D_{12}$  containing 0.2 M AcOH after 30 of minutes photolysis with 254 nm UV light.

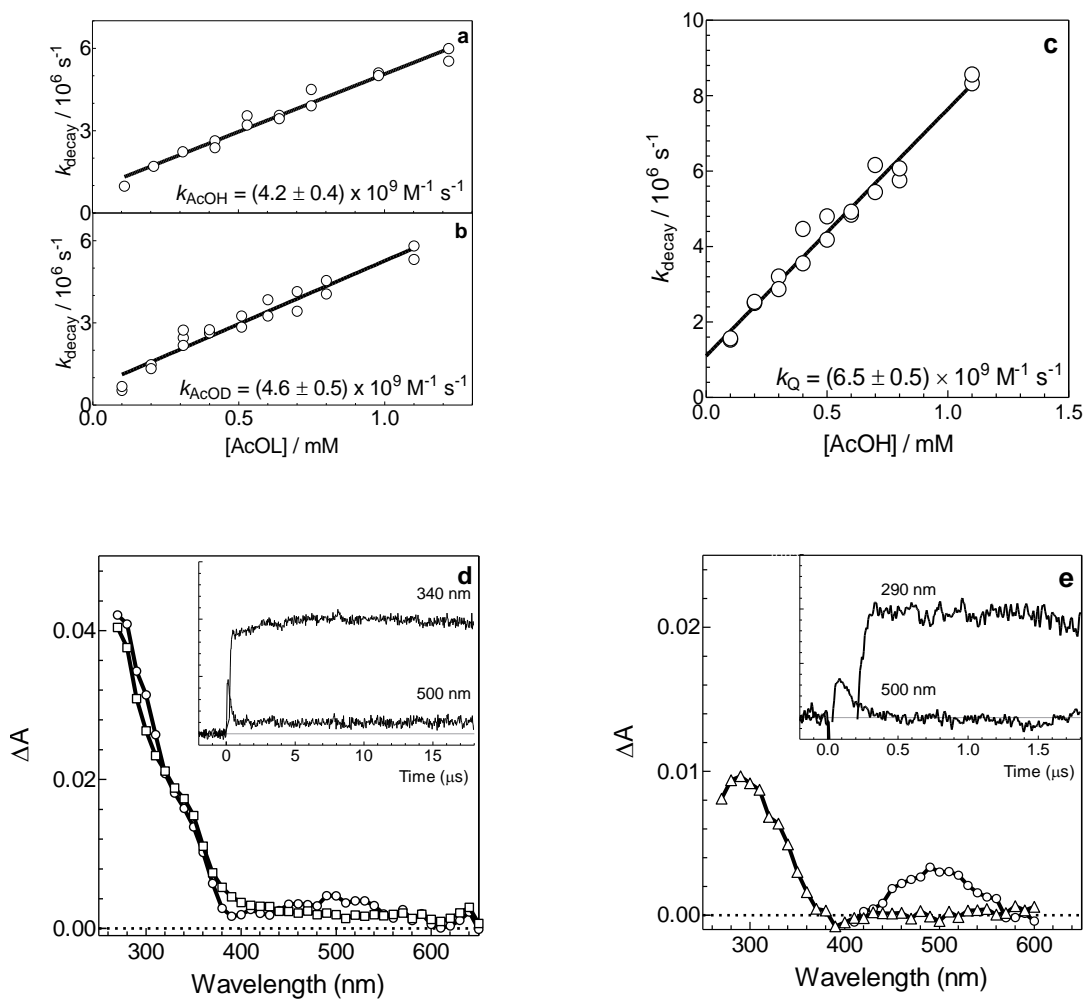


**Figure S3.12.** Plot of  $k_{\text{decay}}$  for the reaction of SnPh<sub>2</sub> (500 nm) with (a) AcOH and (b) AcOD in hexanes at 25 °C. (c) Plot of  $k_{\text{decay}}$  for the reaction of SnMePh (500 nm) with AcOH in hexanes at 25 °C. The solid lines are the linear least squares fit of the data to equation 3.10. (d) Time-resolved UV-vis spectra from laser photolysis of **2** in hexanes containing 0.6 mM AcOH, 0.35-0.42  $\mu\text{s}$  ( $\circ$ ), and 0.86-1.02  $\mu\text{s}$  ( $\square$ ) after the laser pulse (25 °C). (e) Time-resolved UV-vis spectra from laser photolysis of **4** in hexanes containing 1.1 mM AcOH, 0.10 - 0.13  $\mu\text{s}$  ( $\circ$ ) and 1.22 - 1.25  $\mu\text{s}$  ( $\Delta$ ) after the laser pulse (25 °C). Absorbance-time profiles are at selected wavelengths (inset). (Data in (b),(c) and (e) recorded by B. Nguyen)

### 3.7. References

- (1) Duffy, I. R.; Leigh, W. J. *Organometallics* **2015**, *34*, 5029.
- (2) Peng, Y.; Ellis, B. D.; Wang, X.; Power, P. P. *J. Am. Chem. Soc.* **2008**, *130*, 12268.
- (3) Erickson, J. D.; Vasko, P.; Riparetti, R. D.; Fettinger, J. C.; Tuononen, H. M.; Power, P. P. *Organometallics* **2015**, *34*, 5785.
- (4) Zhou, D.; Reiche, C.; Nag, M.; Soderquist, J. A.; Gaspar, P. P. *Organometallics* **2009**, *28*, 2595.
- (5) Murov, S. L.; Carmichael, I.; Hug, G. L. *Handbook of Photochemistry*; 2nd ed.; Dekker: New York, 1993.
- (6) Kapoor, R. N.; Apodaca, P.; Montes, M.; Gomez, F. D.; Pannell, K. H. *Appl. Organomet. Chem.* **2005**, *19*, 518.
- (7) Apodaca, P.; Cervantes-Lee, F.; Pannell, K. H. *Main Group Metal Chem.* **2001**, *24*, 597.
- (8) Patel, Y.; George, J.; Pillai, S. M.; Munshi, P. *Green Chem.* **2009**, *11*, 1056.
- (9) Sharma, H. K.; Miramontes, A.; Metta-Magaña, A. J.; Pannell, K. H. *Organometallics* **2011**, *30*, 4501.
- (10) Grugel, C.; Neumann, W. P.; Seifert, P. *Tetrahedron Lett.* **1977**, *18*, 2205.
- (11) Scherping, K. H.; Neumann, W. P. *Organometallics* **1982**, *1*, 1017.
- (12) Pabst, M.; Lunkenheimer, B.; Köhn, A. *J. Phys. Chem. C* **2011**, *115*, 8335.
- (13) McClure, D. S. *J. Chem. Phys.* **1951**, *19*, 670.
- (14) Becerra, R.; Harrington, C. R.; Gaspar, P. P.; Leigh, W. J.; Vargas-Baca, I.; Walsh, R.; Zhou, D. *J. Am. Chem. Soc.* **2005**, *127*, 17469.
- (15) Masamune, S.; Sita, L. R. *J. Am. Chem. Soc.* **1985**, *107*, 6390.
- (16) Padelkova, Z.; Svec, P.; Pejchal, V.; Růžička, A. *Dalton Trans.* **2013**, *42*, 7660.
- (17) Mitchell, T. N.; Walter, G. *J. Chem. Soc., Perkin Trans. 2* **1977**, 1842.
- (18) Wright, M. R. *An Introduction to Chemical Kinetics*; John Wiley & Sons: Chichester, 2004.
- (19) Gross, L. W.; Moser, R.; Neumann, W. P.; Scherping, K. H. *Tetrahedron Lett.* **1982**, *23*, 635.
- (20) Davies, A. G.; Harrison, P. G.; Palan, P. R. *J. Chem. Soc. C* **1970**, 2030.
- (21) Dewar, M. J. S.; Friedheim, J. E.; Grady, G. L. *Organometallics* **1985**, *4*, 1784.
- (22) Xu, Z.; Jin, J.; Zhang, H.; Li, Z.; Jiang, J.; Lai, G.; Kira, M. *Organometallics* **2011**, *30*, 3311.
- (23) Billone, P. S.; Beleznyay, K.; Harrington, C. R.; Huck, L. A.; Leigh, W. J. *J. Am. Chem. Soc.* **2011**, *133*, 10523.
- (24) Mathiasch, B.; Mitchell, T. N. *J. Organomet. Chem.* **1980**, *185*, 351.
- (25) Lockhart, T. P.; Calabrese, J. C.; Davidson, F. *Organometallics* **1987**, *6*, 2479.
- (26) Farkas, A. *Orthohydrogen, Parahydrogen and Heavy Hydrogen*; Cambridge University Press: London, 1935.
- (27) Berger, S.; Diehl, B. W. K. *Tetrahedron Lett.* **1987**, *28*, 1243.
- (28) Moiseev, A. G.; Leigh, W. J. *Organometallics* **2007**, *26*, 6277.



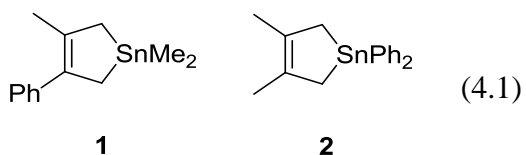
- (29) Leigh, W. J.; Lollmahomed, F.; Harrington, C. R. *Organometallics* **2006**, *25*, 2055.
- (30) Leigh, W. J.; Harrington, C. R.; Vargas-Baca, I. *J. Am. Chem. Soc.* **2004**, *126*, 16105.
- (31) Huck, L. A.; Leigh, W. J. *Organometallics* **2007**, *26*, 1339.
- (32) Peng, Y.; Guo, J.-D.; Ellis, B. D.; Zhu, Z.; Fettinger, J. C.; Nagase, S.; Power, P. *J. Am. Chem. Soc.* **2009**, *131*, 16272.
- (33) Wagner, M.; Dietz, C.; Krabbe, S.; Koller, S. G.; Strohmman, C.; Jurkschat, K. *Inorg. Chem.* **2012**, *51*, 6851.
- (34) Stafeeva, V. S.; Mitiaev, A. S.; Abakumov, A. M.; Tsirlin, A. A.; Makarevich, A. M.; Antipov, E. V. *Polyhedron* **2007**, *26*, 5365.
- (35) Reuter, H. Z. *Kristallogr.* **2004**, *219*, 109.
- (36) Asadi, A.; Eaborn, C.; Hill, M. S.; Hitchcock, P. B.; Meehan, M. M.; Smith, J. D. *Organometallics* **2002**, *21*, 2430.
- (37) Davies, A. G.; Osei-Kissi, D. K. *J. Organomet. Chem.* **1994**, *474*, C8.
- (38) Leigh, W. J.; Potter, G. D.; Huck, L. A.; Bhattacharya, A. *Organometallics* **2008**, *27*, 5948.
- (39) Jolly, B. S.; Lappert, M. F.; Engelhardt, L. M.; White, A. H.; Raston, C. L. *J. Chem. Soc., Dalton Trans.* **1993**, 2653.
- (40) Jentschura, U.; Lippert, E. *Berich. Bunsen. Gesell.* **1971**, *75*, 556.
- (41) Fujii, Y.; Yamada, H.; Mizuta, M. *J. Phys. Chem.* **1988**, *92*, 6768.

## Chapter 4: Reactivity of Transient Stannylenes in Solution

### (2) Lewis Acid-Base Complexation of SnMe<sub>2</sub> and SnPh<sub>2</sub> with O-, S-, and N-Donors, C-C Unsaturated Compounds, and Trialkyltin Hydrides

#### 4.1. Overview

The purpose of this study is to examine the reactivity of transient stannylenes in solution using a much larger substrate scope than had previously been possible. In the present chapter, we examine the reactivities of SnMe<sub>2</sub> and SnPh<sub>2</sub>, generated from 1-stannacyclopent-3-enes **1** and **2** (eq. 4.1), respectively, toward O-donor complexation with diethyl ether (Et<sub>2</sub>O), tetrahydrofuran (THF), acetone and ethyl acetate (EtOAc); S-donor complexation with diethylsulfide (Et<sub>2</sub>S) and tetrahydrothiophene (THT); N-donor complexation with butylamine (BuNH<sub>2</sub>), diethylamine (Et<sub>2</sub>NH) and triethylamine (Et<sub>3</sub>N);  $\sigma$ -bond insertion with tributyltin hydride (Bu<sub>3</sub>SnH); and cycloaddition with cyclohexene, 1-hexene, 1-hexyne, and isoprene.



The [1+4] cycloaddition with dienes is a well studied and seemingly versatile reaction of transient stannylenes,<sup>1-4</sup> although the trapping yields are generally low (ca. 10 - 30 %) at elevated temperatures (ca. 80 - 130 °C). Cycloaddition with alkenes is unknown, while the [1+2] cycloadducts have been observed between strained cyclic alkynes and kinetically stabilized stannylenes.<sup>5,6</sup> The  $\sigma$ -bond insertion with trimethyltin hydride (Me<sub>3</sub>SnH) has been utilized as a scavenger for photochemically generated SnMe<sub>2</sub>. When SnMe<sub>2</sub> is generated thermally however, the cyclic oligomers of SnMe<sub>2</sub> appear to act as a stannylenoid.<sup>1</sup> The reactions of SnMe<sub>2</sub> and SnPh<sub>2</sub> with O-, S-, and N- donors

were found to proceed readily, the data affording rate and equilibrium constants for the coordination of the stannylenes with the donor substrates that allow a general assessment of stannylene complexation to be made. One major goal of the work in this chapter is to provide additional mechanistic insight into these reactions. An additional goal of this chapter is to investigate trends amongst the heavy carbene series, through a comparison of the stannylene reactions with the kinetic and thermodynamic aspects of silylene and germylene complexation,  $\sigma$ -bond insertion and cycloaddition.<sup>7-11</sup>

## 4.2. Results

Laser flash photolysis experiments were carried out with rapidly flowed, deoxygenated solutions of **1** (ca.  $2 \times 10^{-4}$  M) or **2** (ca.  $7 \times 10^{-4}$  M) in anhydrous hexanes, using the pulses from a KrF excimer laser (248 nm, 94-100 mJ, ca. 25 ns) for excitation. As reported in Chapter 2,<sup>12</sup> SnMe<sub>2</sub> and SnPh<sub>2</sub> are observed as promptly formed, short-lived transients, exhibiting UV-vis absorption bands centred at  $\lambda_{\text{max}} = 500$  nm ( $\tau \sim 10$   $\mu$ s) and  $\lambda_{\text{max}} = 505$  nm ( $\tau \sim 20$   $\mu$ s), respectively. In the absence of added substrates, the stannylenes each decay with second order kinetics to afford new transient absorptions assignable to the corresponding dimers, tetramethyldistannene (Me<sub>2</sub>Sn=SnMe<sub>2</sub> (**3**),  $\lambda_{\text{max}} = 465$  nm) and phenyl(triphenylstannyl)stannylene (SnPh(SnPh<sub>3</sub>) (**4**),  $\lambda_{\text{max}} < 280$ ,  $\sim 340$ (sh), 650 nm), respectively. Transient decays for SnMe<sub>2</sub> were recorded at 530 nm in order to minimize spectral overlap with the dimerization product Me<sub>2</sub>Sn=SnMe<sub>2</sub> (**3**); while those for SnPh<sub>2</sub> were recorded near the absorption maximum, at 500 nm.

Addition of a stannylene substrate (Q) results in changes to the stannylene absorbance-time profiles in a manner that depends on the magnitude of the absolute rate ( $k_Q$ ) and/or equilibrium ( $K_{\text{eq}}$ ) constants of the interaction. These observations and the procedures employed for data analysis were discussed in Chapter 2,<sup>7</sup> and are thus summarized only briefly below.

*Kinetic quenching* behaviour is observed with reactions or equilibria that are either irreversible or are characterized by equilibrium constants in excess of ca.  $2.5 \times 10^4 \text{ M}^{-1}$ .<sup>10</sup> In this situation addition of the substrate causes the stannylene signal to decay with pseudo-first order kinetics to the pre-pulse level, and thus absorbance versus time data can be analyzed using eq. 4.2 (with  $\Delta A_{\text{res}} \approx 0$ , in general). The pseudo-first order rate coefficient is proportional to substrate concentration, and a plot of  $k_{\text{decay}}$  versus  $[\text{Q}]$  according to eq. 4.3 is typically linear, the slope affording  $k_{\text{Q}}$ , the forward bimolecular rate constant for the reaction or equilibrium.

$$\Delta A_t = \Delta A_{\text{res}} + (\Delta A_0 - \Delta A_{\text{res}}) \exp(-k_{\text{decay}}t) \quad (4.2)$$

$$k_{\text{decay}} = k_{-\text{Q}} + k_{\text{Q}}[\text{Q}] \quad (4.3)$$

*Equilibrium quenching* behaviour is observed with reversible reactions characterized by equilibrium constants smaller than ca.  $10^3 \text{ M}^{-1}$ .<sup>10</sup> In this situation, the addition of an appropriate concentration of substrate causes only a reduction in the *apparent* initial signal intensity ( $(\Delta A_0)_{\text{Q}}$ ), which is now associated with free stannylene at equilibrium, its concentration reduced relative to the total amount produced in the laser pulse (as approximated by the value of  $\Delta A_0$  in the absence of substrate,  $(\Delta A_0)_0$ ); the approach to equilibrium cannot be resolved from the laser pulse. The equilibrium constant for the reaction ( $K_{\text{eq}}$ ) is determined from the concentration dependence of the apparent initial signal intensities, as defined by eq. 4.4.

$$(\Delta A_0)_0 / (\Delta A_0)_{\text{Q}} = 1 + K_{\text{eq}}[\text{Q}] \quad (4.4)$$

*Mixed kinetic/equilibrium quenching* behaviour is observed when  $K_{\text{eq}}$  falls within the intermediate range  $10^3 \text{ M}^{-1} < K_{\text{eq}} < 2.5 \times 10^4 \text{ M}^{-1}$ .<sup>10</sup> This results in two-phase decay of the stannylene signal upon addition of the substrate, consisting of an initial, approximately first-order decay to a residual absorbance level ( $(\Delta A_{\text{res}})_{\text{Q}}$ ), which then decays on an extended time scale with concomitant formation of stannylene oligomer(s).

The fast initial decay accelerates and the residual absorbance decreases with increasing [Q]; the former is associated with the pseudo-first order approach to equilibrium between the free stannylene (and substrate) and the reaction product, while the latter is associated with free stannylene remaining after equilibrium has been established. Absorbance-time profiles are generally analyzed by non-linear least squares fitting of the initial rapidly decaying portions to single exponential decays according to eq. 4.2, treating the residual absorption  $\Delta A_{\text{res}}$  as "infinity" levels.<sup>9</sup> The residual absorbance values ( $(\Delta A_{\text{res}})_Q$ ) are estimated manually from the decay profiles as the break point in the 2-phase decay, and analyzed as a function of substrate concentration according to eq. 4.5, where  $(\Delta A_0)_0$  is the apparent initial transient absorbance at the beginning of the experiment, in the absence of added substrate.

$$(\Delta A_0)_0 / (\Delta A_{\text{res}})_Q = 1 + K_{\text{eq}}[Q] \quad (4.5)$$

Kinetic traces illustrating each type of behaviour are displayed in Figure 4.1, and show examples of (a) kinetic quenching, (b) mixed kinetic/equilibrium quenching and (c) equilibrium quenching. Examples of the resulting linear plots of the data according to equations 4.3 - 4.5 are shown in Figures 4.2a and 4.3a.

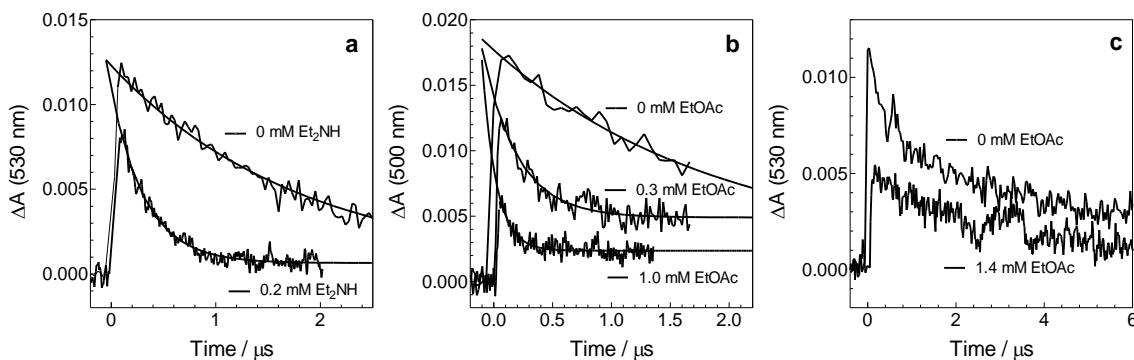


**Figure 4.1.** Representative transient decay profiles recorded from a hexanes solution of (a) **1** containing 0 and 0.2 mM  $\text{Et}_2\text{NH}$ , (b) **2** containing 0, 0.3, and 1.0 mM EtOAc, and (c) **1** containing 0 and 1.4 mM EtOAc.

#### 4.2.1. Lewis Acid-Base Complexation of $\text{SnMe}_2$ and $\text{SnPh}_2$ with *O*-, *S*-, and *N*-Donors

Addition of representative aliphatic ethers, sulfides, amines, ethyl acetate, and acetone to hexanes solutions of **1** and **2** results in quenching of the stannylene transient absorptions and the concomitant formation of new long-lived transient absorptions assignable to the corresponding Lewis acid-base complexes, similar to what was observed earlier for  $\text{SnMe}_2$  and  $\text{SnPh}_2$  and MeOH (see Chapter 2).<sup>12</sup> Kinetic quenching was observed with the sulfides ( $\text{Et}_2\text{S}$  and tetrahydrothiophene (THT)) and amines ( $\text{BuNH}_2$ ,  $\text{Et}_2\text{NH}$ , and  $\text{Et}_3\text{N}$ ), which allowed the forward rate constants for complexation and well-defined UV-vis spectra of the resulting complexes to be determined over the sub-millimolar concentration range in added substrate. For example, Figure 4.2 shows a plot of  $k_{\text{decay}}$  versus  $[\text{Et}_2\text{NH}]$  (Fig 4.2a), along with transient UV-vis absorption spectra recorded with a solution of **1** containing 1.0 mM  $\text{Et}_2\text{NH}$  (Fig 4.2b).

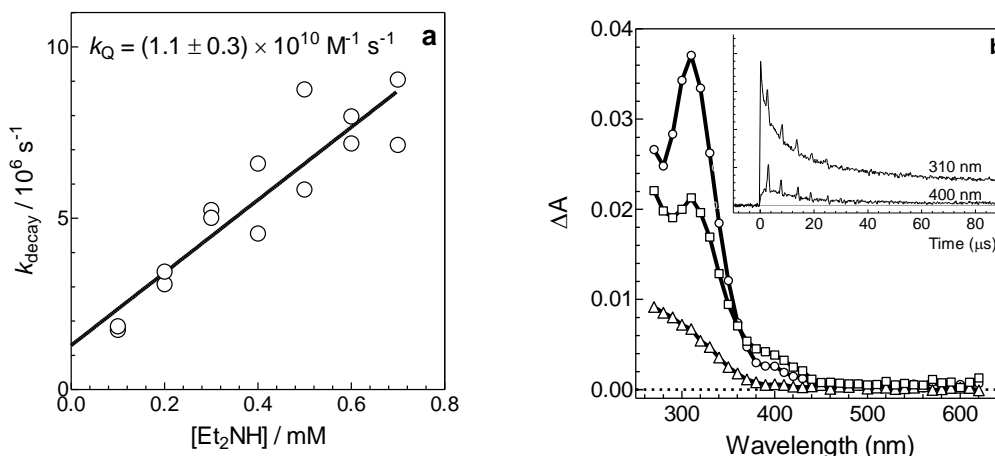


**Figure 4.2.** (a) Plot of  $k_{\text{decay}}$  for reaction of  $\text{SnMe}_2$  with  $\text{Et}_2\text{NH}$  in hexanes at 25 °C; the solid line is the linear least squares fit of the data to eq. 4.3. (b) Time-resolved UV-vis spectra from laser photolysis of **1** in hexanes containing 1.0 mM  $\text{Et}_2\text{NH}$ , 0.16 - 0.32  $\mu\text{s}$  ( $\circ$ ), 3.52 - 4.16  $\mu\text{s}$  ( $\square$ ), and 85.9 - 86.6  $\mu\text{s}$  ( $\triangle$ ) after the laser pulse (25 °C), and absorbance-time profiles at selected wavelengths (inset).

In contrast, the O-donors ( $\text{Et}_2\text{O}$ , THF, EtOAc, and acetone), exhibited behaviour characteristic of equilibrium or mixed kinetic/equilibrium quenching, consistent with the weaker Lewis basicity of these substrates compared to the sulfides and amines,<sup>13-15</sup> and

similar to the behaviour elicited by MeOH.<sup>12</sup> Illustrative examples are shown in Figure 4.3, which shows transient UV-vis absorption spectra recorded with a solution of **2** containing 0.5 mM EtOAc (Fig 4.3b), a solution of **1** containing 25 mM EtOAc (Fig 4.3c), and plots of  $k_{\text{decay}}$  and  $((\Delta A_0)_0/(\Delta A_{\text{res}})_Q)$  versus [Q]; the latter affords an equilibrium constant of  $K_{\text{eq}} = 4400 \pm 900 \text{ M}^{-1}$  for the reaction with SnPh<sub>2</sub> (Fig 4.3a). The transient spectrum (Fig 4.3b) recorded 0.42 - 0.51  $\mu\text{s}$  after the laser pulse reveals the presence of transient absorption bands centred at  $\lambda_{\text{max}} \approx 370 \text{ nm}$ , which we assign to the Lewis acid-base complex of SnPh<sub>2</sub> with EtOAc (**5**), and at  $\lambda_{\text{max}} = 500 \text{ nm}$  due to the free stannylene. On the other hand, SnMe<sub>2</sub> exhibits equilibrium quenching with this substrate, forming a complex with equilibrium constant ca. 6 times smaller than that of SnPh<sub>2</sub> (Fig. 4.3a) and a UV-vis absorption band centred at  $\lambda_{\text{max}} \approx 355 \text{ nm}$  (Fig. 4.3c).

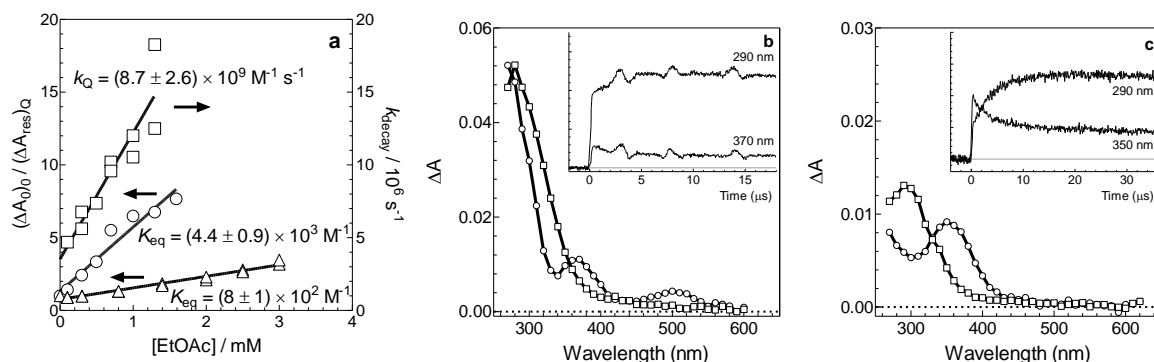


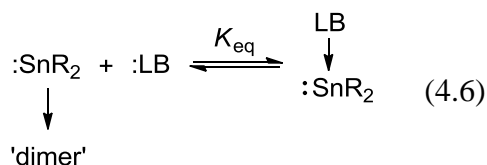
**Figure 4.3.** (a) Plots of  $k_{\text{decay}}$  ( $\square$ ) and  $(\Delta A_0)_0/(\Delta A_{\text{res}})_Q$  ( $\circ$ ) for reaction of SnPh<sub>2</sub> and  $(\Delta A_0)_0/(\Delta A_0)_Q$  ( $\Delta$ ) for reaction of SnMe<sub>2</sub> versus [EtOAc] in hexanes solution at 25 °C; the solid lines are the linear least-squares fits of the data to equations 4.3, 4.5 and 4.4, respectively. (b) Time-resolved UV-vis spectra from laser photolysis of **2** in hexanes containing 0.50 mM EtOAc, 0.42-0.51  $\mu\text{s}$  ( $\circ$ ), and 17.8-18.0  $\mu\text{s}$  ( $\square$ ) after the laser pulse (25 °C), and absorbance-time profiles at selected wavelengths (inset). (c) Time-resolved UV-vis spectra from laser photolysis of **1** in hexanes containing 25 mM EtOAc, 0.51 - 0.70  $\mu\text{s}$  ( $\circ$ ), and 34.7 - 35.0  $\mu\text{s}$  ( $\square$ ) after the laser pulse (25 °C), and absorbance-time profiles at selected wavelengths (inset). The spectra in (c) were recorded using a neutral density filter (43 % transmittance).

---

Transient intermediates from the reaction of the stannylene with the remaining

Lewis bases studied in this work can be readily detected in all instances in time-resolved

UV-vis spectra recorded by flash photolysis of solutions of **1** and **2** containing moderate concentrations of the substrate, and are shown in Figures S4.1 - S4.8. Transient absorption spectra recorded of a hexanes solution of **1** containing 1.0 mM Et<sub>2</sub>S (0.16 - 0.48 μs after the laser pulse; Figure S4.4b) and 1.0 mM THT (0.26 - 0.38 μs after the laser pulse; Figure S4.5b) show an additional transient band at ca. 440 - 450 nm due to the formation of **3**, since the growth portion of **3** could not be resolved from the laser pulse. The new transient products that are observed can be assigned in each instance to the stannylene-donor Lewis pairs (eq. 4.6). The rate and equilibrium constants for complexation of SnMe<sub>2</sub> and SnPh<sub>2</sub> with the nine Lewis bases studied in this work are summarized in Table 4.1, along with the UV-vis absorption maxima of the corresponding complexes and the data for complexation with MeOH, which was reported in Chapter 2.<sup>12</sup>



Transient absorption spectra of hexanes solutions of **1** containing 1.0 mM of the amines (BuNH<sub>2</sub>, Et<sub>2</sub>NH and Et<sub>3</sub>N) were also accompanied by the formation and disappearance of additional transient products exhibiting λ<sub>max</sub> = 380 - 400 nm, red-shifted from the bands due to the SnMe<sub>2</sub>-amine complexes (see Figures 4.2b, S4.6b and S4.8c). These absorptions are assigned tentatively to the amine-stabilized stannylene dimers R<sub>3</sub>N<sup>(+)</sup>-SnMe<sub>2</sub>-Sn<sup>(-)</sup>Me<sub>2</sub>. These assignments are supported by the results of theoretical calculations of the free energies (298.15 K; relative to uncoordinated **3** and amine) and long wavelength absorption maxima for the above structures: R<sub>3</sub>N = MeNH<sub>2</sub>: ΔG° = -7.9 kcal mol<sup>-1</sup>, λ<sub>max</sub> = 377 nm; R<sub>3</sub>N = Me<sub>2</sub>NH: ΔG° = -8.3 kcal mol<sup>-1</sup>, λ<sub>max</sub> = 374 nm. Calculations were performed at the (TD)ωB97XD/def2-TZVP//ωB97XD/def2-TZVP level of theory.<sup>16</sup>



**Table 4.1.** Absolute Rate Constants ( $k_Q$ ) and Equilibrium Constants ( $K_{eq}$ ) for the Reactions of SnMe<sub>2</sub> and SnPh<sub>2</sub> with Various Lewis Bases and UV-vis Absorption Maxima of the Stannylene-donor Complexes in Hexanes at 25 °C.

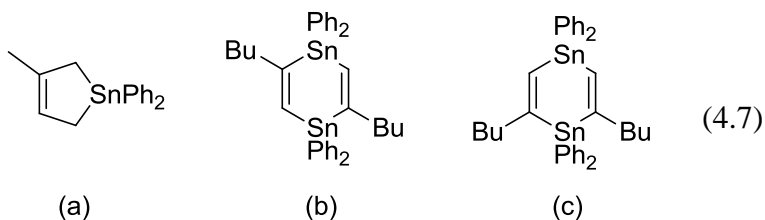
substrate	$k_Q$ ( $10^9$ M <sup>-1</sup> s <sup>-1</sup> ) / [ $K_{eq}$ (M <sup>-1</sup> )]		$\lambda_{max}$ (nm)		Figure.
	SnMe <sub>2</sub>	SnPh <sub>2</sub>	SnMe <sub>2</sub>	SnPh <sub>2</sub>	
Et <sub>2</sub> O	[510 ± 20] <sup>b</sup>	[1200 ± 100] <sup>b</sup>	345	370	S4.1
THF	25 ± 5 [19000 ± 5000]	15 ± 3 <sup>a, d</sup>	345	365	S4.2
MeOH	[2400 ± 200] <sup>b, c</sup>	6 ± 1 <sup>c</sup> [7600 ± 800] <sup>c</sup>	355 <sup>c, e</sup>	370 <sup>c</sup>	c
EtOAc	[800 ± 100] <sup>b</sup>	8.7 ± 2.6 [4400 ± 900]	355	365	4.3
Acetone	[1300 ± 100] <sup>b</sup>	11 ± 4 [8000 ± 2000]	355	365	S4.3
Et <sub>2</sub> S	20 ± 3 <sup>a</sup>	11 ± 1 <sup>a</sup>	345	365	S4.4
THT	18 ± 3 <sup>a</sup>	11 ± 2 <sup>a</sup>	350	370	S4.5
BuNH <sub>2</sub>	19 ± 2 <sup>a</sup>	19 ± 2 <sup>a, d</sup>	320	340	S4.6
Et <sub>2</sub> NH	11 ± 3 <sup>a</sup>	12 ± 1 <sup>a</sup>	310	340	4.2, S4.7
Et <sub>3</sub> N	7.1 ± 1.5 <sup>a</sup>	6.4 ± 1.1 <sup>a</sup>	315	350	S4.8

<sup>a</sup> $K_{eq} > 25000$  M<sup>-1</sup>; <sup>b</sup> $k_Q$  indeterminable; <sup>c</sup>ref<sup>12</sup>; <sup>d</sup>(Data recorded by B. Nguyen); <sup>e</sup>Transient absorption spectrum recorded in hexanes solutions of **1** containing 7 mM MeOH. The spectrum repeated with 25 mM MeOH exhibits an absorption band at 335 nm.

4.2.2. Arrested Reaction with Alkenes, Alkynes, Dienes, and Trialkyltin hydrides: Direct Detection of Stannylyene  $\pi$ - and Tin-Hydride Complexes

Steady state photolysis experiments were performed with the goal of determining the fate of  $\text{SnMe}_2$  and  $\text{SnPh}_2$  in the presence of moderate concentrations (0.05 - 0.1 M) of tributyltin hydride ( $\text{Bu}_3\text{SnH}$ ), isoprene and 1-hexyne, as similar derivatives ( $\text{Me}_3\text{SnH}$ , 2,3-dimethyl-1,3-butadiene (**6**)) had previously been identified as trapping agents for transient stannylenes<sup>1,17</sup> and are also effective traps for transient silylenes<sup>8,18</sup> and germylenes.<sup>9,19,20</sup> Photolysis experiments were carried out in quartz NMR tubes on deaerated solutions of cyclohexane- $d_{12}$  containing **2** (0.04 - 0.05 M), the respective substrate (0.05 - 0.1 M), and  $\text{Si}_2\text{Me}_6$  (ca. 0.01 M) as an internal standard. The photolysis samples were irradiated using low-pressure mercury lamps and monitored periodically by  $^1\text{H}$  NMR spectroscopy. The yields of photoproducts were calculated relative to the disappearance of **2**, determined from the initial slopes of concentration versus time plots.

Photolysis of deaerated  $\text{C}_6\text{D}_{12}$  solutions of **2** containing isoprene (0.1 M) or 1-hexyne (0.1 M) resulted in the formation of **6** in near quantitative yields and a broadening of the 7.1 - 7.4 ppm region of the  $^1\text{H}$  NMR spectra after ca. 9 % conversion of **2**. However, no evidence was found for the formation of additional low molecular weight products. In particular, no additional peaks were observed in the vinylic region of the  $^1\text{H}$  NMR spectrum that would signal the formation of cycloaddition products between  $\text{SnPh}_2$  and isoprene (see eq. 4.7a)<sup>1</sup> or 1-hexyne (see eq. 4.7b-c).<sup>1,21</sup>



Analogous results were obtained from the photolysis of **2** in the presence of (0.05 M)  $\text{Bu}_3\text{SnH}$ , in that the NMR spectrum of the photolyzate after ca. 8 % conversion of **2** showed no evidence of an Sn-H resonance consistent with the formation of  $\text{Bu}_3\text{SnSn(H)Ph}_2$  (**11**).<sup>1,17</sup> Figure 4.4 shows representative  $^1\text{H}$  NMR spectra of the  $\text{C}_6\text{D}_{12}$  solution of **2** containing 0.1 M isoprene prior to and after 10 minutes of photolysis, while those containing 1-hexyne and  $\text{Bu}_3\text{SnH}$  are shown in Figures S4.9 and S4.10, respectively. Concentration versus time plots showing the consumption of **2** and the formation of **6** in the three experiments are shown in Figure S4.11.

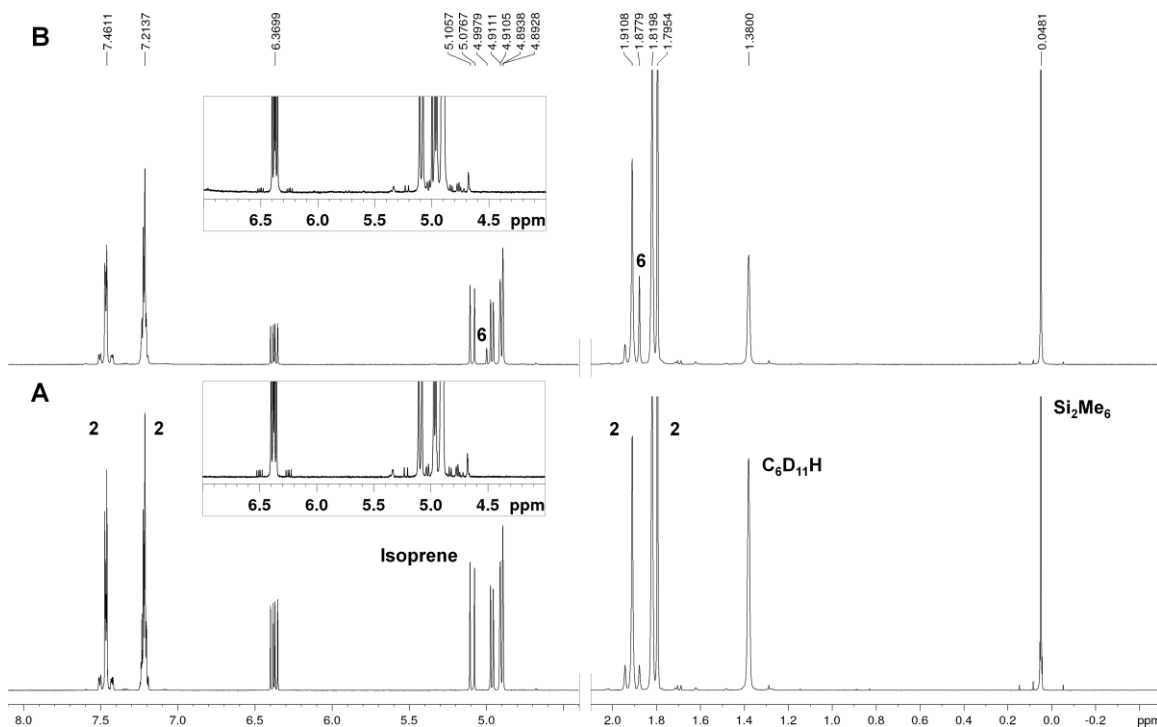


**Figure 4.4.**  $^1\text{H}$  NMR spectra of a deaerated 0.05 M solution of **2** in  $\text{C}_6\text{D}_{12}$  containing isoprene (0.096 M) (a) before and (b) after 10 minutes of photolysis with 254 nm light.

The addition of 1-hexene in near molar quantities to hexanes solutions of **1** and **2** led in both cases to a reduction in the initial intensity of the stannylene absorption  $(\Delta A_0)_0$  with characteristics consistent with equilibrium quenching. A plot of  $(\Delta A_0)_0/(\Delta A_0)_Q$  is linear with respect to [1-hexene] according to eq. 4.4 and affords the equilibrium

constants  $K_{\text{eq}} = (4.2 \pm 0.3) \text{ M}^{-1}$  and  $(4.1 \pm 0.3) \text{ M}^{-1}$  for the reactions with  $\text{SnMe}_2$  and  $\text{SnPh}_2$  respectively (see Figure 4.5a-b). Transient absorption spectra of hexanes solutions of **1** and **2** (Figures 4.5c and 4.5d, respectively) containing ca. 1.5 M 1-hexene showed new absorption bands, exhibiting maxima at  $\lambda_{\text{max}} = 380 \text{ nm}$  and  $405 \text{ nm}$ , respectively, which decay on a timescale of tens of microseconds. Both species exhibit characteristics that bear resemblance to the stannylene-donor complexes with O-, S- and N-donors described earlier, and are assigned to the corresponding  $\pi$ -complexes between 1-hexene and  $\text{SnMe}_2$  and  $\text{SnPh}_2$ .

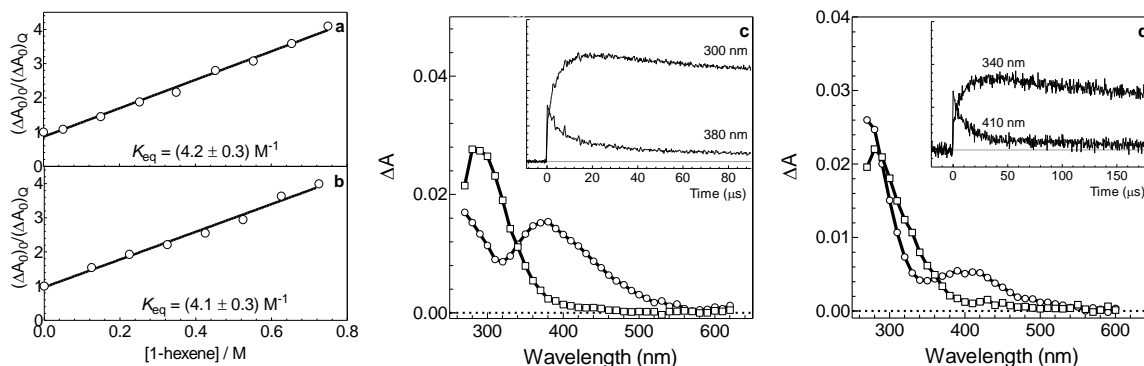


**Figure 4.5.** Plots of  $(\Delta A_0)_0 / (\Delta A_0)_Q$  for the reactions of (a)  $\text{SnMe}_2$  and (b)  $\text{SnPh}_2$  with 1-hexene in hexanes at 25 °C; the solid lines are the linear least squares fits of the data to eq. 4.4. (c) Time-resolved UV-vis spectra from laser photolysis of **1** in hexanes containing 1.5 M 1-hexene, 0.16 - 0.48  $\mu\text{s}$  ( $\circ$ ), and 89.1 - 89.8  $\mu\text{s}$  ( $\square$ ) after the laser pulse (25 °C), and absorbance-time profiles at selected wavelengths (inset). (d) Time-resolved UV-vis spectra from laser photolysis of **2** in hexanes containing 1.52 M 1-hexene, 1.3 - 2.6  $\mu\text{s}$  ( $\circ$ ), and 50.2 - 51.5  $\mu\text{s}$  ( $\square$ ) after the laser pulse (25 °C), and absorbance-time profiles at selected wavelengths (inset).

The addition of cyclohexene to hexanes solutions of **1** and **2** led to similar effects on the stannylene transient signals. Linear plots of  $(\Delta A_0)_0 / (\Delta A_0)_Q$  versus [cyclohexene] afford the equilibrium constants  $K_{\text{eq}} = (7.4 \pm 0.3) \text{ M}^{-1}$  and  $(6.4 \pm 0.8) \text{ M}^{-1}$  for the reactions with  $\text{SnMe}_2$  and  $\text{SnPh}_2$  respectively, according to eq. 4.4 (Figure S4.12a-b). Also similar to the results of 1-hexene were the detection of new transient absorption bands from

hexanes solutions of **1** and **2** containing ca. 0.5 M cyclohexene, exhibiting maxima at  $\lambda_{\max}$  = 390 nm and 400 nm (Figures S4.12c and S4.12d, respectively).

Similar results were obtained in laser photolysis experiments with **1** and **2** in hexanes containing up to 0.20 - 0.25 M 1-hexyne. The addition of the alkyne to solutions of **1** and **2** led to equilibrium quenching in both instances, allowing the determination of the equilibrium constants  $K_{\text{eq}} = (17.4 \pm 0.9) \text{ M}^{-1}$  and  $(63 \pm 5) \text{ M}^{-1}$ , respectively. New transient absorptions centred at  $\lambda_{\max} = 380 \text{ nm}$  were observed in both cases in the presence of 0.20 - 0.25 M 1-hexyne, which are assigned to the corresponding stannylene 1-hexyne  $\pi$ -complexes. Equilibrium quenching plots and transient absorption spectra are shown in Figure S4.13.

The addition of tributyltin hydride ( $\text{Bu}_3\text{SnH}$ ) also resulted in equilibrium quenching of the stannylene traces (Figure S4.14a). A plot of  $(\Delta A_0)_0/(\Delta A_0)_Q$  versus  $[\text{Bu}_3\text{SnH}]$  for  $\text{SnPh}_2$  affords the equilibrium constant  $K_{\text{eq}} = (2.0 \pm 0.1) \times 10^2 \text{ M}^{-1}$  coinciding with a new transient product formed with  $\lambda_{\max} = 430 \text{ nm}$  (Figure S4.14b), assigned to the donor-acceptor pair between  $\text{SnPh}_2$  and  $\text{Bu}_3\text{SnH}$ . The addition of  $\text{Bu}_3\text{SnH}$  to a solution of **1** also resulted in equilibrium quenching of the  $\text{SnMe}_2$  kinetic trace, affording  $K_{\text{eq}} = (63 \pm 5) \text{ M}^{-1}$  (Figure S4.14a). Transient absorption spectra of a solution of **1** containing ca. 0.014 M  $\text{Bu}_3\text{SnH}$  (Figure S4.14c) did not show evidence of a new transient species, although this is likely due to an insufficient concentration of substrate, given the small equilibrium constant for the reaction. We did not measure spectra at higher concentrations of  $\text{Bu}_3\text{SnH}$  because it absorbs appreciably at the incident wavelength ( $\epsilon_{248\text{nm}} = 36 \text{ M}^{-1} \text{ cm}^{-1}$ ).

The assignments for the Lewis acid-base complexes between the stannylenes  $\text{SnR}_2$  ( $\text{R} = \text{Me}, \text{Ph}$ ) and 1-hexene, 1-hexyne, and  $\text{Bu}_3\text{SnH}$  are supported by the results of theoretical calculations for the corresponding long wavelength absorption maxima of the

stannylene complexes with propene, propyne, and  $\text{Me}_3\text{SnH}$ . Calculations were performed at the (TD) $\omega$ B97XD/def2-TZVP// $\omega$ B97XD/def2-TZVP level of theory. In all instances, the predicted long wavelength maxima are within 26 nm (0.19 eV) of the experimental value. The equilibrium constants and UV-visible absorption maxima of the Lewis acid-base complexes for the reactions of  $\text{SnMe}_2$  and  $\text{SnPh}_2$  with alkenes, alkynes and trialkyltin hydrides are summarized in Table 4.2, alongside the calculated absorption maxima shown in parenthesis.

**Table 4.2.** Equilibrium Constants ( $K_{\text{eq}}$ ) and Calculated and Experimental UV-vis Absorption Maxima ( $\lambda_{\text{max}}$ ) of the Lewis Acid - Base Complexes for the Reactions of  $\text{SnMe}_2$  and  $\text{SnPh}_2$  with Various Stannylene Substrates in Hexanes Solution at 25 °C.

substrate	$[K_{\text{eq}} (\text{M}^{-1})]$		$\lambda_{\text{max}} (\text{nm})$		Figure.
	$\text{SnMe}_2$	$\text{SnPh}_2$	$\text{SnMe}_2$	$\text{SnPh}_2$	
1-hexene	$[4.2 \pm 0.3]$	$[4.1 \pm 0.3]$	375 (374) <sup>c</sup>	405 (386) <sup>c</sup>	4.5
cyclohexene	$[7.4 \pm 0.3]$	$[6.4 \pm 0.8]$	390	400	S4.12
1-hexyne	$[17.4 \pm 0.9]$	$[63 \pm 5]$	380 (370) <sup>c</sup> <sup>b</sup>	380 (378) <sup>c</sup>	S4.13
$\text{Bu}_3\text{SnH}$	$[63 \pm 5]$	$[200 \pm 10]^{\text{a}}$	(400) <sup>c</sup>	430 (404) <sup>c</sup>	S4.14

<sup>a</sup> $\text{SnPh}_2$  monitored at 520 nm; <sup>b</sup>Complex not detected; <sup>c</sup>Calculated at the (TD) $\omega$ B97XD/def2-TZVP// $\omega$ B97XD/def2-TZVP level of theory using propene, propyne, and  $\text{Me}_3\text{SnH}$  in place of 1-hexene, 1-hexyne, and  $\text{Bu}_3\text{SnH}$ , respectively.

### 4.3. Discussion

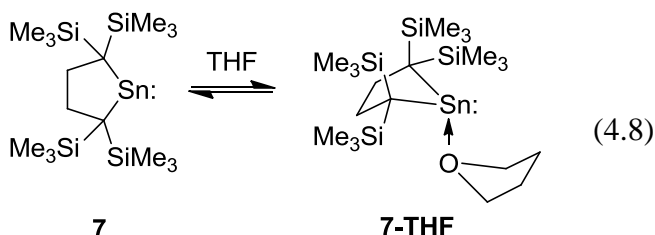
The reactions of  $\text{SnMe}_2$  and  $\text{SnPh}_2$  with  $\text{Et}_2\text{O}$ , THT, EtOAc, acetone, MeOH,  $\text{Et}_2\text{S}$ , THT,  $\text{BuNH}_2$ ,  $\text{Et}_2\text{NH}$ , and  $\text{Et}_3\text{N}$  all result in Lewis acid-base complexation between the stannylene and the O, S, or N donor. Within this set of reagents, the oxygen donors mostly exhibit equilibrium constants of a magnitude appropriate for measurement under the conditions of our experiments (ca.  $0.1 \text{ M}^{-1} < K_{\text{eq}} < 25000 \text{ M}^{-1}$ ).<sup>7</sup> The values obtained are shown in Table 4.1, and span a range of less than 2 orders of magnitude. With each

substrate, the equilibrium constant is consistently higher for SnPh<sub>2</sub> than SnMe<sub>2</sub> by a factor of 2.4 - 6.2. This indicates that phenyl-for-methyl substitution leads to enhancement in the Lewis acidity of the Sn(II) centre, which is analogous to the trends observed with the homologous silylene and germylene systems.<sup>7</sup> The data obtained for the complexation of SnPh<sub>2</sub> with THF indicates that  $K_{\text{eq}} > 2.5 \times 10^4 \text{ M}^{-1}$ , which is consistent with the value obtained for SnMe<sub>2</sub> with this substrate ( $K_{\text{eq}} = (19000 \pm 5000) \text{ M}^{-1}$ ) and the consistently higher  $K_{\text{eq}}$  values that characterize the complexation of SnPh<sub>2</sub> with the other O-donors, relative to SnMe<sub>2</sub>.

Table 4.4 summarizes the rate and equilibrium constants for the complexation of SnMe<sub>2</sub> and SnPh<sub>2</sub>, along with the corresponding values for the silylene and germylene homologs. The equilibrium constants for complexation of SnMe<sub>2</sub> and SnPh<sub>2</sub> lie between those exhibited by the corresponding silylenes and germylenes, establishing the general trend in Lewis acidities  $\text{SiR}_2 > \text{SnR}_2 > \text{GeR}_2$  (R = Me, Ph).<sup>7</sup> These findings indicate that our preliminary assessment of tetrylene Lewis acidity with MeOH as the substrate<sup>12</sup> can be generalized to a broader range of O-donors, and in particular with Et<sub>2</sub>O, where all six equilibrium constants fall within the range that allows for direct experimental measurement. Furthermore, a comparison of  $K_{\text{Et}_2\text{O}}$  reveals the values for MPh<sub>2</sub> ( $K^{\text{Si}} \sim 6 K^{\text{Sn}} \sim 44 K^{\text{Ge}}$ ) span a wider range than the values for the MMe<sub>2</sub> series (i.e.  $K^{\text{Si}} \sim 2.5 K^{\text{Sn}} \sim 11.5 K^{\text{Ge}}$ ).

The higher Lewis acidity of stannylenes relative to the germylenes is supported by theoretical calculations for the reaction of MMe<sub>2</sub> with MeOH,<sup>22</sup> and follows the electrophilicity and electron affinity trends computed for the R<sub>2</sub>M(II) (M = Ge, Sn) systems.<sup>23,24</sup> The relative Lewis acidities of the MMe<sub>2</sub> and MPh<sub>2</sub> systems contrast the theoretical calculations by Schoeller and Schneider,<sup>25</sup> who determined relative binding energies for the complexation of the MH<sub>2</sub> system with H<sub>2</sub>O, H<sub>2</sub>S, NH<sub>3</sub>, and PH<sub>3</sub> to

decrease in the order  $\text{SiH}_2 > \text{GeH}_2 > \text{SnH}_2$ . The findings also contrast with the results of Kira et al.,<sup>26</sup> who found evidence of reversible complexation of dialkylstannylene (**7**) in tetrahydrofuran solution (eq. 4.8) under conditions where the corresponding silylene or germylene derivatives are unreactive. This indicates that the tin derivative **7** is significantly more Lewis acidic than the Si and Ge homologues in the series. Steric hindrance was suggested as the determining factor here, whereas the results of our work represent cases where steric factors are minimized. Close agreement is found for the absorption maxima observed for the  $\text{Me}_2\text{Sn}$ -THF complex in hexanes solution ( $\lambda_{\text{max}} = 345$  nm), and the corresponding Lewis acid-base complex (**7**-THF) observed for **7**, which exhibits an absorption maximum at  $\lambda_{\text{max}} = 341$  nm in THF solution between  $-100$  -  $-60$  °C.<sup>26</sup> This agreement is expected given that both compounds are dialkylstannylene-THF complexes. Extrapolation of the linear relationship between  $\ln(K_{\text{eq}})$  and  $1/T$  for the complexation of **7** with THF<sup>26</sup> affords an approximation for  $K_{\text{eq}} \sim 4 \times 10^{-6} \text{ M}^{-1}$  at  $25$  °C, smaller than the value exhibited by  $\text{SnMe}_2$  ( $K_{\text{eq}} = (1.9 \pm 0.5) \times 10^4 \text{ M}^{-1}$ ) by approximately 10 orders of magnitude, the likely result of steric crowding of the Lewis acidic tin(II) element in **7**.



The equilibrium constants for complexation of  $\text{SnMe}_2$  and  $\text{SnPh}_2$  with O-donor substrates decrease in the order  $K_{\text{THF}} > K_{\text{MeOH}} > K_{\text{acetone}} > K_{\text{EtOAc}} > K_{\text{Et}_2\text{O}}$ ; the same order is followed with both stannylenes (with  $\text{SnPh}_2$  the values for  $K_{\text{MeOH}}$  and  $K_{\text{acetone}}$  are the same within error) and their lighter silylene and germylene homologues as well (where values have been measured).<sup>7</sup> In other words, the variation in the equilibrium constants with the



tetrel centre ( $M = \text{Si, Ge, Sn}$ ) and substituent ( $R = \text{Me, Ph}$ ) is independent of the choice of substrate, at least within the series studied here (THF, MeOH, acetone, EtOAc and Et<sub>2</sub>O). Figure 4.6 shows plots of the standard Gibbs free energies with gas phase basicities (GB; Fig. 4.6a), proton affinities (PA; Fig. 4.6b) and BF<sub>3</sub> affinities (Fig. 4.6c) for the reactions of SnMe<sub>2</sub> with the O-donor substrates examined in this study.<sup>15,27</sup> The values (in kcal mol<sup>-1</sup>) are also summarized in Table 4.3. The experimental  $\Delta G$  values do not correlate well with gas phase basicities (GB) or proton affinities (PA) for the substrates examined.<sup>15</sup> This is likely due to the small range of GB (173.2 - 192.3 kcal mol<sup>-1</sup>) or PA (180.3 - 199.7 kcal mol<sup>-1</sup>) in which these substrates span. For comparison, the substrates examined in a previous combined computational and experimental study of silylene and germylene complexation, in which an approximately linear correlation was found between calculated free energies of complexation ( $\Delta G$ ) and proton affinities, span a much wider range in proton affinity values.<sup>7</sup> A somewhat better correlation is found with correlation with BF<sub>3</sub>-affinity, although the value for MeOH was not available for comparison.<sup>27</sup>

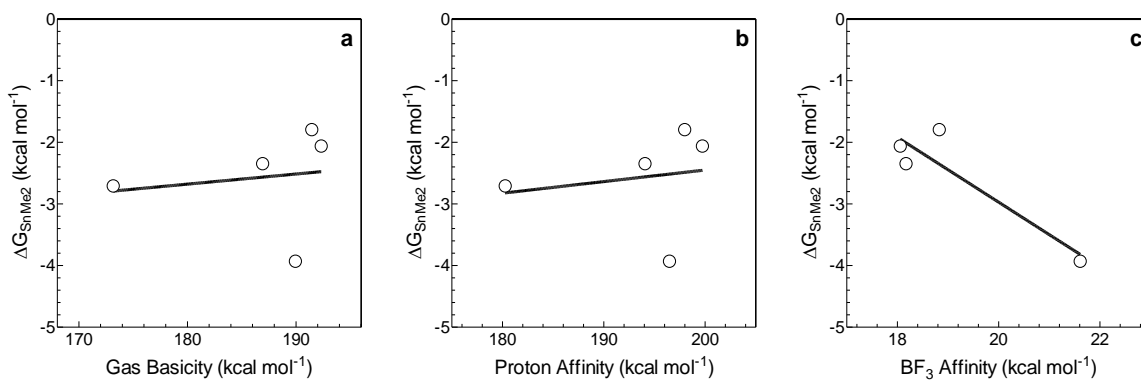


**Figure 4.6.** Plots of  $\Delta G_{\text{SnMe}_2}$  versus (a) gas phase basicity (GB), (b) proton affinity (PA) and (c) BF<sub>3</sub> affinity.

**Table 4.3.** Standard Gibbs Free Energies ( $\Delta G$ ; kcal mol<sup>-1</sup>) for the Reactions of SnMe<sub>2</sub> with O-donor Substrates and Gas Phase Basicities (GB), Proton Affinities (PA) and BF<sub>3</sub> Affinities (kcal mol<sup>-1</sup>) of Et<sub>2</sub>O, EtOAc, Acetone, MeOH, and THF.

Substrate	$\Delta G$ (kcal mol <sup>-1</sup> )	GB (kcal mol <sup>-1</sup> ) <sup>a</sup>	PA (kcal mol <sup>-1</sup> ) <sup>a</sup>	BF <sub>3</sub> affinity (kcal mol <sup>-1</sup> ) <sup>b</sup>
Et <sub>2</sub> O	-1.79	191.4	198.0	18.83
EtOAc	-2.06	192.3	199.7	18.06
Acetone	-2.35	186.9	194.1	18.17
MeOH	-2.71	173.2	180.3	<sup>c</sup>
THF	-3.93	189.9	196.5	21.61

<sup>a</sup>ref<sup>15</sup>; <sup>b</sup>ref<sup>27</sup>; <sup>c</sup>Value not available

Equilibrium constants could not be measured with the S- and N- donors, as addition of the lowest substrate concentration caused the stannylenes signals to decay to their pre-pulse levels, indicating that  $K_{eq} > 25000 \text{ M}^{-1}$  for these reactions. This is not surprising given these are stronger donors based on gas phase basicity and proton affinity scales, and the finding that the silylenes and germylenes also exhibit the same behaviour with these substrates.<sup>7</sup> The higher binding affinity for S- than O-donors is consistent with the classification of stannylenes as soft Lewis acids.

The Lewis acid - base complexation of SnMe<sub>2</sub> and SnPh<sub>2</sub> with O-, S-, and N-donors are all fast reactions with absolute rate constants within a factor of 4 of the diffusional rate constant in hexanes at 25 °C ( $k_{diff} = 2.2 \times 10^{10} \text{ M}^{-1} \text{ s}^{-1}$ )<sup>28</sup> in all cases. The rate constants for complexation of SnMe<sub>2</sub> with the oxygen and sulphur donors are within experimental error of  $k_{diff}$ , indicating an essentially barrierless reaction with no variation between cyclic O- and S-donors (THF and THT) or between cyclic or acyclic S-donors (THT and Et<sub>2</sub>S). The finding that complexation is barrierless is consistent with the reaction proceeding with a minimal rearrangement of atoms and without the breaking of bonds.

Reaction with the primary amine BuNH<sub>2</sub> also appears to be barrierless, however a small but systematic reduction in rate constant is observed with increasing substitution on the nitrogen atom (i.e.  $k_{\text{BuNH}_2} > k_{\text{Et}_2\text{NH}} > k_{\text{Et}_3\text{N}}$ ). Roughly the same variation in  $k_Q$  was found with the corresponding silylenes and germylenes. The trend runs counter to that expected from gas phase basicities and proton affinities of the amines; the increased reaction barrier from mono-, di- and tri- substituted amines can be attributed to increasing steric interactions between the stannylene and alkyl groups on the nitrogen. The absolute rate constants for complexation of the amines with SnPh<sub>2</sub> mirror those for SnMe<sub>2</sub>, while an approximately 2-fold reduction in rate constants was observed for the reaction of SnPh<sub>2</sub> with the sulfides (THT and Et<sub>2</sub>S) compared to those for SnMe<sub>2</sub>. Similar patterns of reactivity are also observed with the homologous silylene and germylene series.<sup>7,11,29</sup>

There was little to differentiate the complexation kinetics of SnMe<sub>2</sub> and SnPh<sub>2</sub> to their lighter analogues when varying the tetrel element (i.e. a comparison of SnMe<sub>2</sub> with SiMe<sub>2</sub> and GeMe<sub>2</sub>, and of SnPh<sub>2</sub> with SiPh<sub>2</sub> and GePh<sub>2</sub>), this is perhaps not surprising as all these reactions proceed with minimal rearrangement of their constituent atoms. The absolute rate constants for SnPh<sub>2</sub> are nearly the same as those for GePh<sub>2</sub> with the sulphur donors, but with the alkylamines are faster roughly by a factor of two, likely due to the increased M-N dative bond length in the stannylenes compared to the germylenes, reducing steric congestion.<sup>25</sup> Both GePh<sub>2</sub> and SnPh<sub>2</sub> react roughly half as fast as SiPh<sub>2</sub> with MeOH, while all three diphenyltetrelenes react with the same rate constant with both sulphur substrates. The pattern of reactivity for SnMe<sub>2</sub> also parallels those for SiMe<sub>2</sub> and GeMe<sub>2</sub>, showing little dependence on the nature of the tetrel centre. For instance, all three MMe<sub>2</sub> tetrelenes (M = Si, Ge, Sn) react within a factor of two of the diffusion controlled rate with ethers, and sulfides, and show the same gradual decrease in rates with increasing substitution of the alkylamines.

**Table 4.4.** Absolute Rate ( $k_Q$ ) and Equilibrium Constants ( $K_{eq}$ ) for the Reactions of  $MMe_2$  and  $MPh_2$  ( $M = Si, Ge, Sn$ ) with Various Lewis bases in Hexanes Solution at 25 °C.

substrate	$k_Q (10^9 M^{-1} s^{-1}) / [K_{eq} (M^{-1})]$					
	SnMe <sub>2</sub>	SnPh <sub>2</sub>	SiMe <sub>2</sub>	SiPh <sub>2</sub>	GeMe <sub>2</sub>	GePh <sub>2</sub>
Et <sub>2</sub> O	[510 ± 20] <sup>a</sup>	[1200 ± 100] <sup>a</sup>	[1260 ± 50] <sup>7,a</sup>	$\frac{15 \pm 4^7}{[7100 \pm 600]^7}$	[110 ± 10] <sup>7,a</sup>	[160 ± 10] <sup>7,a</sup>
THF	$\frac{25 \pm 5}{[19000 \pm 5000]}$	15 ± 3 <sup>b,e</sup>	17.3 ± 1.5 <sup>8,b</sup>	15 ± 1 <sup>8,b</sup>	$\frac{11 \pm 2^{10}}{[9800 \pm 3800]^{10}}$	$\frac{6.3 \pm 0.6^{10}}{[23000 \pm 5000]^{10}}$
MeOH	[2400 ± 200] <sup>a,12</sup>	$\frac{6 \pm 1^{12}}{[7600 \pm 800]^{12}}$	18.1 ± 1.5 <sup>30,b</sup>	13.4 ± 1.0 <sup>30,b</sup>	[900 ± 60] <sup>a,10</sup>	$\frac{6.1 \pm 1.1^{10}}{[3300 \pm 800]^{10}}$
EtOAc	[800 ± 100] <sup>a</sup>	$\frac{8.7 \pm 2.6}{[4400 \pm 900]}$	c	c	c	[405 ± 7] <sup>a,31</sup>
Acetone	[1300 ± 100] <sup>a</sup>	$\frac{11 \pm 4}{[8000 \pm 2000]}$	14.1 ± 1.2 <sup>30,b</sup>	14.4 ± 2.0 <sup>30,b</sup>	[290 ± 50] <sup>a,f</sup>	c
Et <sub>2</sub> S	20 ± 3 <sup>b</sup>	11 ± 1 <sup>b</sup>	22 ± 3 <sup>b,d</sup>	10 ± 1 <sup>b,d</sup>	18 ± 2 <sup>b,32</sup>	8.3 ± 0.4 <sup>b,32</sup>
THT	18 ± 3 <sup>b</sup>	11 ± 2 <sup>b</sup>	21 ± 2 <sup>b,33</sup>	16 ± 2 <sup>b,33</sup>	17 ± 2 <sup>b,7</sup>	10 ± 2 <sup>b,7</sup>
BuNH <sub>2</sub>	19 ± 2 <sup>b</sup>	19 ± 2 <sup>b,e</sup>	17 ± 2 <sup>b,29</sup>	11 ± 3 <sup>b,29</sup>	12 ± 3 <sup>b,11</sup>	10.1 ± 0.6 <sup>b,34</sup>
Et <sub>2</sub> NH	11 ± 3 <sup>b</sup>	12 ± 1 <sup>b</sup>	16 ± 3 <sup>b,29</sup>	8.3 ± 0.7 <sup>b,29</sup>	12 ± 3 <sup>b,7</sup>	7.3 ± 0.9 <sup>b,9</sup>
Et <sub>3</sub> N	7.1 ± 1.5 <sup>b</sup>	6.4 ± 1.1 <sup>b</sup>	9.8 ± 0.8 <sup>b,29</sup>	3.9 ± 0.4 <sup>b,29</sup>	8.7 ± 0.7 <sup>b,11</sup>	2.8 ± 0.9 <sup>b,9</sup>

<sup>a</sup> $k_Q$  indeterminable; <sup>b</sup> $K_{eq} > 25000 M^{-1}$ ; <sup>c</sup> not measured; <sup>d</sup>(unpublished data by S. Kostina); <sup>9</sup><sup>e</sup>(Data recorded by B. Nguyen);  
<sup>f</sup>(unpublished data by K. Jeyakanthan)

Each of the stannylene donor coordination complexes have been characterized by their electronic spectra; all exhibit absorption maxima within the 310 - 370 nm region of the UV-visible spectrum, markedly blue-shifted relative to the spectra of the uncoordinated stannylenes. The absorption maxima of the complexes exhibit a bathochromic shift of 10 - 35 nm with the phenyl-for-methyl substitution. Essentially no variation in  $\lambda_{\text{max}}$  is found between the chalcogen (O, S) donors, whereas the spectra of the stannylene-amine complexes are comparatively blue-shifted by 20 - 30 nm. The absorption maxima are the same within each set of O-donors, amines, and sulfides.

We reported earlier an apparent concentration dependence of  $\lambda_{\text{max}}$  for the  $\text{Me}_2\text{Sn} / \text{MeOH}$  system;<sup>12</sup> the  $\text{Me}_2\text{Sn-O(H)Me}$  adduct exhibits a blue shift from 355 nm in 7 mM MeOH solution to 335 nm when the concentration is increased to 25 mM. This effect was attributed to generation of the dicoordinate complex  $(\text{SnMe}_2\text{-(MeOH)}_2)^{25}$  with increased methanol content. Such a hypsochromic shift is unique to MeOH within the 6 - 25 mM concentration range. This can be rationalized by considering the size of the Lewis bases and suggesting that a preference for a dicoordinate complex at 25 mM occurs only in instances where steric hindrance is not significant. Higher concentrations ( $\geq 25$  mM) may still result in a blue-shift in the absorption maxima however, as was observed for the THF and MeOH complexes of  $\text{GeMe}_2$ .<sup>35</sup>

Table 4.5 summarizes the long wavelength absorption maxima of the  $\text{SnMe}_2$  and  $\text{SnPh}_2$ -donor complexes along with their silylene and germylene homologs to facilitate comparison. While the location of absorption maxima appear largely independent between  $\text{SiMe}_2$  and  $\text{GeMe}_2$ ,<sup>7</sup> the absorption maxima of the  $\text{SnMe}_2$ -donor complexes are consistently 30 - 35 nm to the red of those of the  $\text{SiMe}_2$  and  $\text{GeMe}_2$  complexes. This is an expected trend given the reduced orbital overlap between the  $np$  orbital on  $\text{MMe}_2$  ( $n = 3$  ( $\text{M} = \text{Si}$ ), 4 ( $\text{M} = \text{Ge}$ ), and 5 ( $\text{M} = \text{Sn}$ )) and the  $\sigma$ -donor as  $n$  increases from 3 to 5.<sup>25,36</sup>

Variations in  $\lambda_{\max}$  within the diphenyltetraylene complexes are smaller in magnitude, and those of the GePh<sub>2</sub>-complexes are generally slightly blue shifted relative to the corresponding Si and Sn species. Absorption maxima for each stannylene and their respective substrates (specifically with respect to the N-donors) qualitatively reflect the binding energies of the reaction, similar to the conclusions made of the silylene and germylene complexes.<sup>7</sup>

**Table 4.5.** Long Wavelength UV-vis Absorption Maxima of the MMe<sub>2</sub> and MPh<sub>2</sub>-Donor Complexes (M = Si, Ge, Sn) with various Lewis Bases in Hexanes Solution at 25 °C.

substrate	$\lambda_{\max}$ (nm)					
	SnMe <sub>2</sub>	SnPh <sub>2</sub>	SiMe <sub>2</sub>	SiPh <sub>2</sub>	GeMe <sub>2</sub>	GePh <sub>2</sub>
none	500 <sup>a</sup>	505 <sup>a</sup>	465 <sup>b</sup>	515 <sup>b</sup>	470 <sup>l</sup>	500 <sup>o</sup>
Et <sub>2</sub> O	345	370	305 <sup>c</sup>	375 <sup>k</sup>	300 <sup>k</sup>	360 <sup>k</sup>
THF	345	365	310 <sup>d</sup>	370 <sup>d</sup>	310 <sup>m</sup>	355 <sup>m</sup>
MeOH	355 <sup>a,r</sup>	370 <sup>a</sup>	310 <sup>e</sup>	360 <sup>e</sup>	295 <sup>m</sup>	350 <sup>m</sup>
EtOAc	355	365	f	f	f	350 <sup>p</sup>
Acetone	355	365	g	g	< 310 <sup>s</sup>	f
Et <sub>2</sub> S	345	365	320 <sup>h</sup>	370 <sup>h</sup>	300 <sup>n</sup>	350 <sup>n</sup>
THT	350	370	325 <sup>i</sup>	370 <sup>i</sup>	320 <sup>k</sup>	350 <sup>k</sup>
BuNH <sub>2</sub>	320	340	280 <sup>j</sup>	300 <sup>j</sup>	< 290 <sup>g</sup>	325 <sup>o</sup>
Et <sub>2</sub> NH	310	340	280 <sup>j</sup>	300 <sup>j</sup>	280 <sup>k</sup>	320 <sup>q</sup>
Et <sub>3</sub> N	315	350	270 <sup>j</sup>	310 <sup>j</sup>	290 <sup>l</sup>	340 <sup>q</sup>

<sup>a</sup>ref<sup>12</sup>; <sup>b</sup>ref<sup>30</sup>; <sup>c</sup>cyclohexane 20 °C ref<sup>37</sup>; <sup>d</sup>ref<sup>8</sup>; <sup>e</sup>ref<sup>38</sup>; <sup>f</sup>not measured; <sup>g</sup>complex not detected; <sup>h</sup>(*unpublished data by S. Kostina*); <sup>i</sup>ref<sup>33</sup>; <sup>j</sup>ref<sup>29</sup>; <sup>k</sup>ref<sup>7</sup>; <sup>l</sup>ref<sup>11</sup>; <sup>m</sup>ref<sup>10</sup>; <sup>n</sup>ref<sup>32</sup>; <sup>o</sup>ref<sup>34</sup>; <sup>p</sup>ref<sup>31</sup>; <sup>q</sup>ref<sup>9</sup>; <sup>r</sup>Transient absorption spectrum recorded in hexanes solutions of **1** containing 7 mM MeOH. The spectrum repeated with 25 mM MeOH exhibits an absorption band at 335 nm; <sup>s</sup>(*unpublished data by K. Jeyakanthan*)

The ultimate fate of the  $\text{SnMe}_2\text{-O}$  and  $\text{-S}$  donor complexes can be addressed qualitatively by studying their decay kinetics and the concomitant product absorptions that appear in the transient spectra. We found from earlier steady state photolysis studies that MeOH is an ineffective trap for  $\text{SnMe}_2$ , even at MeOH concentrations as high as 0.5 M.<sup>17</sup> Nevertheless, flash photolysis experiments of **1** indicate that the formation of  $\text{Me}_2\text{Sn}=\text{SnMe}_2$  (**3**) appears to be quenched in the presence of MeOH, the effect increasing with increasing concentration of the alcohol.<sup>12</sup> The presence of  $\text{Et}_2\text{O}$ , THF, EtOAc, acetone, THT and  $\text{Et}_2\text{S}$  led to similar effects on the absorbance-time profile of **3**, showing the effects to be common to both O and S donors. The reduction in the yield of **3** was more pronounced for substrates that formed more stable complexes (i.e. higher  $K_{\text{eq}}$ ) with  $\text{SnMe}_2$ . For example, Figure 4.7 shows absorbance-time profiles for the distannene at 440 nm in the presence of  $\text{Et}_2\text{O}$  (a) and  $\text{Et}_2\text{S}$  (b) at three representative concentrations. Such behaviour contrasts with that of  $\text{GeMe}_2\text{-THF}$  complexes, where the formation of the corresponding digermene is not significantly impacted even in neat THF solution.<sup>35</sup>

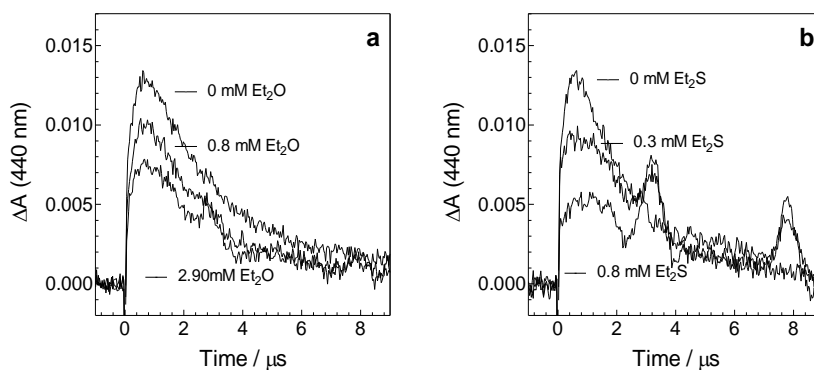
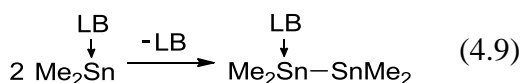


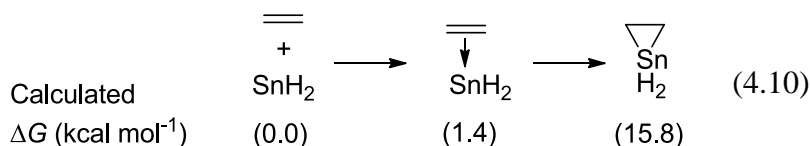
**Figure 4.7.** Representative transient decay profiles recorded with a hexanes solution of **1** (a) containing 0, 0.8 and 2.9 mM  $\text{Et}_2\text{O}$ , and (b) containing 0, 0.3 and 0.8 mM  $\text{Et}_2\text{S}$ .

What accounts for the decrease in distannene yield? The decay of the  $\text{SnMe}_2\text{-N}$  donor pairs was accompanied in each case by the formation and subsequent decay of a new transient product appearing as a shoulder absorption on the long wavelength edge of

the more intense absorption band due to the stannylene-amine complex (see Figures 4.2b, S4.6b, and S4.8c). The absorbance-time profiles of these products are consistent with them being derived from the decay of the  $\text{SnMe}_2\text{-N}$  donor complexes. A structure that is consistent with the experimental evidence is the amine stabilized stannylene dimer  $\text{R}_3\text{N}^{(+)}\text{-SnMe}_2\text{-Sn}^{(-)}\text{Me}_2$ . Similar compounds have been reported previously,<sup>39</sup> and a general scheme for its formation is shown in (eq. 4.9). The existence of such compounds is also supported by the results of theoretical calculations, which suggest their formation to be thermodynamically favorable relative to uncoordinated **3** and amine. We can speculate that these compounds can also account for the reduced yield of distannene with O- and S- donors as well.

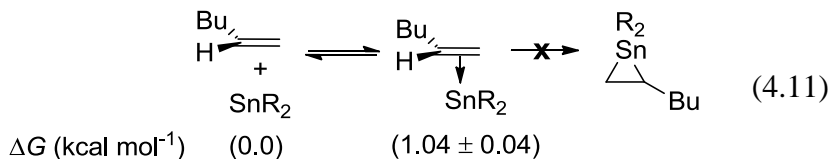


The [2+1] cycloaddition reaction of silylenes with alkenes has been the subject of great interest for many years,<sup>40-43</sup> and subsequent reactions of the corresponding silirane has found utility in preparative organosilicon chemistry.<sup>44</sup> Three examples of isolable germiranes are also known.<sup>45,46</sup> By contrast, no examples of the corresponding three membered tin analogues (stanniranes) have been reported. The [2+1] cycloadditions of ethylene to  $\text{MH}_2$  ( $\text{M} = \text{C}, \text{Si}, \text{Ge}, \text{Sn}$ ) have been studied theoretically by S. Sakai (eq. 4.10).<sup>47</sup> The calculations reveal a systematic decrease in product stability with increasing size of the group 14 element, and the formation of stannirane is predicted to be endergonic.<sup>22,47</sup> The calculations also predict the existence of a pre-reaction  $\pi$ -complex.<sup>47</sup> Similar conclusions were afforded by calculations of the [2+1] cycloaddition of  $\text{MMe}_2$  ( $\text{M} = \text{Si}, \text{Ge}, \text{Sn}$ ) with ethylene<sup>22</sup> and 1,3-butadiene.<sup>2</sup>





Our previous flash photolysis studies of the reactions of transient silylenes and germynes with alkenes have found that the silirane and germirane are the respective kinetic products, and, with aryl containing tetrylenes, are observable as long-lived species exhibiting absorption bands in the 275 - 285 nm region of the UV spectrum.<sup>8,34</sup> The results of the present study indicate that the reactions of SnMe<sub>2</sub> and SnPh<sub>2</sub> with 1-hexene and 1-hexyne (or terminal C=C or C≡C bonds) differ markedly from those of silylenes and germynes. The behaviour of the stannylene transient signals upon addition of 1-hexene is consistent with a rapid and reversible reaction, characterized by equilibrium constants of  $K_{\text{eq}} = (4.2 \pm 0.3) \text{ M}^{-1}$  and  $(4.1 \pm 0.3) \text{ M}^{-1}$  for SnMe<sub>2</sub> and SnPh<sub>2</sub>, respectively (Figure 4.5a and 4.5b). This corresponds to a standard Gibbs free energy difference (standard state: gas phase at 1 atm, 25 °C) of  $\Delta G = (1.04 \pm 0.04) \text{ kcal mol}^{-1}$ . Transient absorption spectra recorded in the presence of molar concentrations of 1-hexene (Figures 4.6c and 4.6d) display new transient products exhibiting broad absorption bands centred at  $\lambda_{\text{max}} = 375 \text{ nm}$  for SnMe<sub>2</sub> and  $\lambda_{\text{max}} = 405 \text{ nm}$  for SnPh<sub>2</sub>. The absorption spectra of these transient products are clearly not consistent with the characteristics expected of the corresponding stanniranes, and are more compatible with those of a complex between 1-hexene and the stannylene, the C-C unsaturated bond acting as a  $\pi$  electron donor to the Sn(II) centre (eq. 4.11). Additional support for this assignment is provided by the close agreement between the observed maxima and the calculated  $\lambda_{\text{max}}$  of the corresponding SnMe<sub>2</sub> and SnPh<sub>2</sub>  $\pi$ -complexes with propene (see Table 4.2).

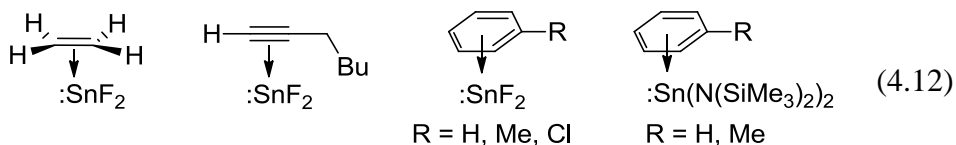


The addition of cyclohexene also results in behaviour consistent with the formation of cyclohexene  $\pi$ -complexes between SnMe<sub>2</sub> and SnPh<sub>2</sub>, both exhibiting UV-

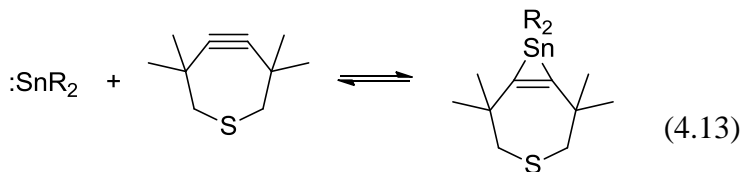
vis absorption maxima between 390 - 400 nm (Figures S4.12c-d). These reactions are characterized by equilibrium constants of  $K_{\text{eq}} = (7.4 \pm 0.3) \text{ M}^{-1}$  and  $(6.4 \pm 0.8) \text{ M}^{-1}$  for  $\text{SnMe}_2$  and  $\text{SnPh}_2$ , respectively (Figures S4.12a and S4.12b), in hexanes at 25 °C. A small increase in  $K_{\text{eq}}$  was observed with both stannylenes compared to their results for 1-hexene. This result is consistent with the increase in electron donating character of the alkene with increased alkyl substitution. The coordination of the alkenes (1-hexene and cyclohexene) with the stannylenes bears some resemblance to that with the  $\sigma$ -donors, in that the spectra of the  $\text{SnPh}_2$ -complexes are red-shifted by 10 - 30 nm compared to those with  $\text{SnMe}_2$ . No difference is found for the equilibrium constants for complexation of the two stannylenes, however, which runs counter to the trend exhibited by complexation with 1-hexyne and the O- donors. Impurity quenching may be responsible for this discrepancy, as reactions characterized by a small  $K_{\text{eq}}$  are especially susceptible to the influence of a small quantity of adventitious water, which would be expected to exhibit reactivity similar to that of  $\text{Et}_2\text{O}$  or  $\text{MeOH}$ . This discrepancy appears for both alkenes however, which would appear to rule out impurity quenching. It is also possible that alkene  $\pi$ -complexes with  $\text{SnPh}_2$  are destabilized by steric factors relative to those of  $\text{SnMe}_2$ . Steric factors appear to play a larger role in the [2+1] cycloaddition reactions of alkenes with diaryl<sup>8</sup> and dialkylsilylenes (see Chapter 6) relative to complexation or  $\sigma$ -bond insertion reactions.

Prior experimental<sup>48</sup> and theoretical<sup>23</sup> studies have concluded that stannylene coordination with  $\pi$ -systems like toluene and benzene is less favorable than coordination with O- and N- donors. Broeckeaert et al.<sup>23</sup> found that the calculated stabilization energies for complexation ( $\Delta E_{\text{complexation}}$ ) for the reactions of  $\text{SnMe}_2$  decrease in the order THF ( $\Delta E = -10.0 \text{ kcal mol}^{-1}$ ) >  $\text{MeOH}$  ( $\Delta E = -8.8 \text{ kcal mol}^{-1}$ ) > benzene ( $\Delta E = -1.5 \text{ kcal mol}^{-1}$ ). This parallels the experimental  $\Delta G$  values for the complexation reactions of  $\text{SnMe}_2$

reported in this work: THF ( $\Delta G = -3.9 \pm 0.2 \text{ kcal mol}^{-1}$ ) > MeOH ( $\Delta G = -2.7 \pm 0.1 \text{ kcal mol}^{-1}$ ) > 1-hexene ( $\Delta G = 1.04 \pm 0.04 \text{ kcal mol}^{-1}$ ). The observation of intermolecular  $\pi$ -donor interactions of stannylenes in this work can be compared to the  $\pi$ -complex between  $\text{SnF}_2$  and 1-heptyne detected using matrix IR spectroscopy by Boganov et al.,<sup>49</sup> and the interaction of stannylenes with aromatic  $\pi$ -systems that have been reported in solution,<sup>48</sup> the crystalline state,<sup>50</sup> and frozen matrices (eq. 4.12).<sup>51,52</sup> The  $\text{SnF}_2$ -ethylene complex has also been reported in an argon matrix (12 K) by Meier and coworkers.<sup>53</sup>



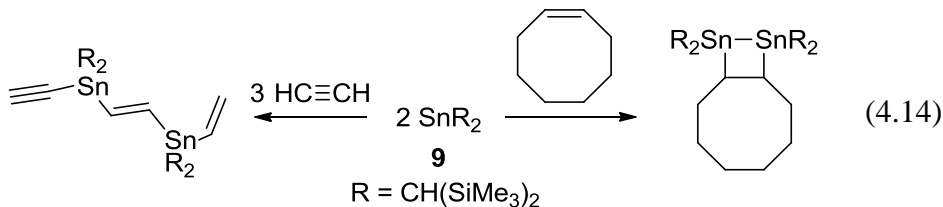
The reactions of alkynes with organostannylenes have been studied experimentally.<sup>5,6,21,54</sup> Most notably, the reversible formation of a stannirene from the Lappert dialkylstannylene ( $\text{SnDis}_2$  (**9**); Dis =  $\text{CH}(\text{SiMe}_3)_2$ )<sup>5</sup> and  $\text{SnTip}_2$  (**10**; Tip =  $\text{C}_6\text{H}_2$ -2,4,6-*i*-Pr<sub>3</sub>)<sup>6</sup> with a strained cycloheptyne has been reported by Sita et al. (eq. 4.13).



**9**; R =  $\text{CH}(\text{SiMe}_3)_2$

**10**; R =  $\text{C}_6\text{H}_2$ -2,4,6-*i*-Pr<sub>3</sub>

The Lappert stannylene **9** also reacts with *cis*-cyclooctene to afford a 1,2-distannacyclobut-3-ene<sup>21</sup> and reacts with acetylene to afford a product containing two equivalents of **9** and three equivalents of acetylene in low yield (eq. 4.14).<sup>54</sup>



Theoretical investigations of the reactions of  $\text{SnH}_2$ <sup>55</sup> and  $\text{SnMe}_2$ <sup>22</sup> with acetylene also predict the existence of a pre-reaction  $\pi$ -complex. DFT calculations on the reactions of  $\text{SnMe}_2$  with  $\text{C}_2\text{H}_2$  and  $\text{C}_2\text{H}_4$  by Su<sup>22</sup> also found evidence for the involvement of pre-reaction complexes, and indicate that stannirene formation is exothermic, while stannirane formation is slightly endothermic.

The reactions of 1-hexyne with both  $\text{SnMe}_2$  and  $\text{SnPh}_2$  follow a similar pattern compared to those with 1-hexene, in that they are also characterized by a  $K_{\text{eq}} < 10^2 \text{ M}^{-1}$  and lead to the formation of transient products exhibiting absorption bands in the 375 - 405 nm region of the UV-vis spectrum. A modest increase is found in the free energy gain upon complexation of the alkyne, represented by the equilibrium constants  $K_{\text{eq}} = (17.4 \pm 0.9) \text{ M}^{-1}$  and  $(63 \pm 5) \text{ M}^{-1}$  measured for  $\text{SnMe}_2$  and  $\text{SnPh}_2$ , respectively (Figure S4.13a). These values of  $K_{\text{eq}}$  correspond to standard Gibbs free energies (standard state: gas phase at 1 atm, 25 °C) of  $\Delta G^\circ = (0.20 \pm 0.03) \text{ kcal mol}^{-1}$  and  $\Delta G^\circ = (-0.56 \pm 0.05) \text{ kcal mol}^{-1}$ , respectively. The ca. 3-fold larger equilibrium constant for  $\text{SnPh}_2$  compared to  $\text{SnMe}_2$  is similar to the differences observed for complexation with O-donor substrates (*vide infra*). This suggests the stannylene behaves as a Lewis acid given the relative electron withdrawing effects of the phenyl substituent versus methyl. New transient products assignable to the corresponding  $\pi$  complexes between 1-hexyne and the stannylene are observed to exhibit absorption maxima at  $\lambda_{\text{max}} = 380 \text{ nm}$  in both cases. Steady state photolysis of a  $\text{C}_6\text{D}_{12}$  solution of **2** and 1-hexyne did not result in the formation of olefinic products; negative results were also reported by Gaspar and coworkers in their attempts to trap thermally generated  $\text{SnMe}_2$  with 3-hexyne.<sup>1</sup> These results are consistent with the flash photolysis studies, which suggest the alkyne acts only as a complexing agent, and further reaction between the components is unfavorable.

Figure 4.8 shows transient absorption spectra recorded of hexanes solutions of **2** containing selected concentrations of 1-hexene (Fig 4.8a) and 1-hexyne (Fig 4.8b). The figures illustrate the similarity in the UV-vis spectra of the SnPh<sub>2</sub>-alkene and -alkyne  $\pi$ -complexes. The transient spectra also illustrate the difference in  $K_{eq}$  between the two substrates, as a much higher concentration of 1-hexene was required to reduce the stannylene signal to an undetectable amount.

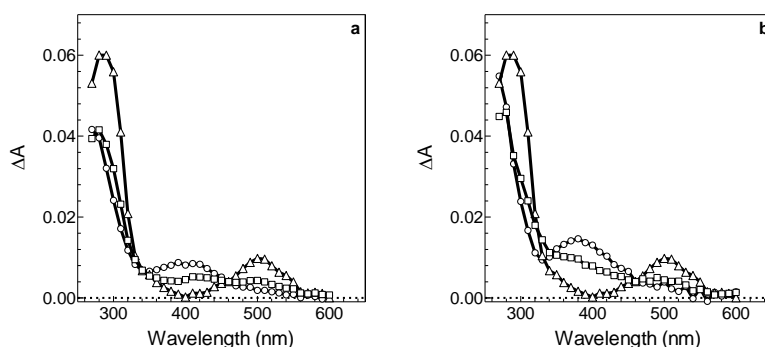
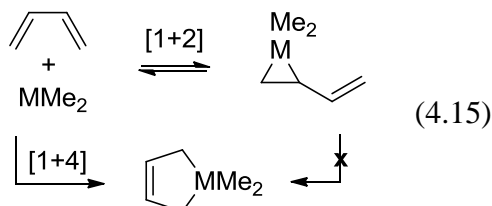


**Figure 4.8.** Time-resolved UV-vis spectra recorded 0.4 - 2.6  $\mu$ s after the laser pulse (25  $^{\circ}$ C) from laser photolysis of **2** in hexanes containing (a) 0 ( $\Delta$ ), 0.2 ( $\square$ ), and 1.52 M ( $\circ$ ) 1-hexene and (b) 0 ( $\Delta$ ), 0.04 ( $\square$ ) and 0.2 M ( $\circ$ ) 1-hexyne. Each of the three spectra in (a) and (b) are normalized at 460 nm to account for differences in laser intensity between different experiments.

Kinetically stable organostannylenes commonly undergo [1+4] cycloaddition with dienes at room temperature in hydrocarbon solution.<sup>3,36,56-60</sup> More recently, thermally generated transient stannylenes SnMe<sub>2</sub> and SnPh<sub>2</sub> were both trapped by **6** to form the corresponding stannacyclopent-3-enes, albeit at high temperatures and in low yields: SnMe<sub>2</sub> was trapped at 100  $^{\circ}$ C from a neat solution of **6** in 12 % yield while SnPh<sub>2</sub> was trapped in 30 % yield from a C<sub>6</sub>D<sub>6</sub> solution containing **6** (0.44 M) at temperatures between 82 - 126  $^{\circ}$ C.<sup>1</sup> The mechanism of 1,3-butadiene addition to MMe<sub>2</sub> (M = Si, Ge, Sn) was investigated theoretically by Nag and Gaspar.<sup>2</sup> The calculations suggest SiMe<sub>2</sub> and GeMe<sub>2</sub> form the corresponding vinyltetriranes as the kinetic product via [1+2] cycloaddition, while the thermodynamic product is formed via a concerted [1+4]

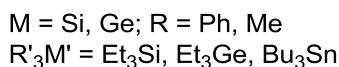
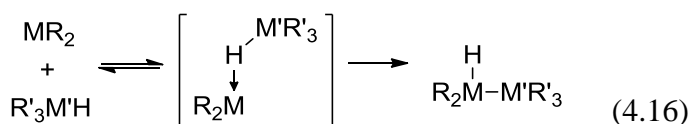
cycloaddition process.  $\text{SnMe}_2$  on the other hand is predicted to react exclusively by the latter route (eq. 4.15), and that formation of vinylstannirane (i.e. [1+2] cycloaddition) is endergonic and does not play a role in the reaction pathway.



Given the reaction of  $\text{SnPh}_2$  and 1-hexene examined in this work, it is expected that the reaction with isoprene would also proceed entirely via [1+4] cycloaddition. However, our steady state photolysis experiments of a  $\text{C}_6\text{D}_{12}$  solution of **2** in the presence of 0.1 M isoprene indicate that neither the [1+4] cycloaddition product, nor any Sn containing low molecular weight products, were formed. From these results, it was concluded that isoprene is inefficient for room temperature trapping of  $\text{SnPh}_2$  generated photochemically. Isoprene was not studied by flash photolysis as the substrate absorbs sufficiently strongly at the incident wavelength ( $\epsilon_{248\text{nm}} = 81 \text{ M}^{-1} \text{ cm}^{-1}$ ) such that it results in significant internal screening effects, meaning that the concentration of the substrate could not be increased sufficiently for an effect on the stannylene signals to be detected, assuming  $K_{\text{eq}}$  is similar to that for complexes with 1-hexene.

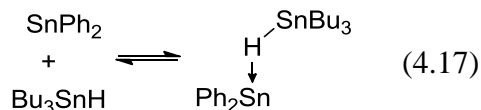
Group 14 metal hydride (M-H; M = Si, Ge, Sn) bond insertions of transient silylenes and germynenes have been proposed to proceed via two step processes involving hydride-bridged complexes as the initially formed intermediates (eq. 4.16).<sup>8,9,11</sup> The involvement of an intermediate complex has been predicted theoretically, while experimentally their existence is implied by the fact that the gas phase reactions of  $\text{SiH}_2$  and  $\text{GeH}_2$  with silane and germane are characterized by negative activation energies.<sup>58</sup> In solution, the reaction of metal hydrides ( $\text{Et}_3\text{SiH}$ ,  $\text{Et}_3\text{GeH}$ , and  $\text{Bu}_3\text{SnH}$ ) with  $\text{SiMe}_2$  and

SiPh<sub>2</sub> proceed readily with bimolecular rate constants  $k_Q \sim 10^9 - 10^{10} \text{ M}^{-1} \text{ s}^{-1}$ .<sup>8</sup> Reactions of GeMe<sub>2</sub> and GePh<sub>2</sub> with the same metal hydrides show a successive increase in rate constant that correlates with M-H bond strengths,<sup>9,11</sup> for instance  $6200k_{\text{Et}_3\text{SiH}} \sim 130k_{\text{Et}_3\text{GeH}} \sim k_{\text{Bu}_3\text{SnH}}$  ( $k_{\text{Bu}_3\text{SnH}} = (3.5 \pm 0.1) 10^9 \text{ M}^{-1} \text{ s}^{-1}$ ) for GePh<sub>2</sub>.<sup>9</sup> Gas phase kinetic studies of the reactions of SiMe<sub>2</sub>, GeMe<sub>2</sub> and SnMe<sub>2</sub> with silanes and germanes showed SnMe<sub>2</sub> to be the least reactive of the tetrelene series with compounds containing Si-H and Ge-H bonds.<sup>61,62</sup> We did not extend the study to include Et<sub>3</sub>MH (M = Si, Ge) as the interaction with the stannylenes was not expected to be strong and because of cost considerations in using large quantities of Et<sub>3</sub>GeH.



The effect of added Bu<sub>3</sub>SnH on the kinetic behaviour of SnMe<sub>2</sub> and SnPh<sub>2</sub> differed quite considerably from that observed with the corresponding silylenes and germylenes, which react rapidly and irreversibly with this substrate in solution at 25 °C.<sup>8,9,11</sup> In both cases, addition of the tin hydride led to a drop in the apparent yield of the stannylene, consistent with a reversible, weakly exergonic reaction with the substrate, characterized by equilibrium constants of  $K_{\text{eq}} = (63 \pm 5) \text{ M}^{-1}$  and  $(200 \pm 10) \text{ M}^{-1}$  for SnMe<sub>2</sub> and SnPh<sub>2</sub>, respectively. The ca. 3-fold higher equilibrium constant exhibited by SnPh<sub>2</sub> compared to SnMe<sub>2</sub> is consistent with the stannylene serving as a Lewis acid in the reaction. The difference is similar to that found for the complexation with O-donors, which exhibit  $K_{\text{SnPh}_2} / K_{\text{SnMe}_2} = 2.4 - 6.2$ . The prompt formation of a new transient product is apparent from transient absorption spectra recorded of a hexanes solution of **2** containing 7.8 mM Bu<sub>3</sub>SnH (Fig S4.14b). The spectrum immediately after the laser pulse

exhibits a long wavelength absorption maximum at  $\lambda_{\text{max}} = 430 \text{ nm}$ , and is consistent with a Lewis acid-base complex between the tin hydride and the stannylene (eq. 4.17).



The product studies with **2** in the presence of  $\text{Bu}_3\text{SnH}$  failed to reveal evidence of an Sn-H insertion product, as there were no new Sn-H resonances within the  $\delta_{\text{H}} 5 - 7 \text{ ppm}$  region of the  $^1\text{H}$  NMR spectrum that would be expected for the putative insertion product,  $\text{Bu}_3\text{SnSn(H)Ph}_2$  (**11**) (Figure S4.10). This contrasts with an earlier report which indicated that the Sn-H insertion product  $\text{Me}_3\text{SnSnMe}_2\text{H}$  was detected from the photochemical generation of  $\text{SnMe}_2$  in hexane containing  $0.17 \text{ M Me}_3\text{SnH}$ .<sup>1,17</sup> However, we cannot conclusively rule out the possibility that **11** is formed in low yields, as it would be expected to be photosensitive under these conditions.<sup>63</sup> Collectively, our results for  $\text{SnPh}_2$  are consistent with simple complexation, as shown in eq. 4.17. The direct detection of an intermediate complex suggests the kinetic barrier for formation of **11** is prohibitively large, and certainly larger than those in the reactions of  $\text{SiPh}_2$  and  $\text{GePh}_2$  with  $\text{Bu}_3\text{SnH}$ .<sup>8</sup>

#### 4.4. Summary and Conclusions

Lewis acid-base complexation of the transient stannylenes  $\text{SnMe}_2$  and  $\text{SnPh}_2$  with a collection of simple aliphatic oxygen, sulfur, and nitrogen containing substrates exhibits characteristics that strongly resemble those exhibited by the silicon and germanium homologs. The reactions afford the corresponding stannylene-donor complexes, whose UV-vis spectrum is in each case blue-shifted relative to the spectrum of the free stannylene. The reactions are rapid and reversible, proceeding with bimolecular rate constants that approach the diffusional limit and (in the cases of O-donors such as  $\text{MeOH}$ , aliphatic ethers, an ester and a ketone) with equilibrium constants that are systematically



larger for SnPh<sub>2</sub> than SnMe<sub>2</sub>. The equilibrium constants for complexation of MMe<sub>2</sub> and MPh<sub>2</sub> with O-donors in hexanes at 25 °C follow the order  $K_{\text{eq}}^{\text{Si}} > K_{\text{eq}}^{\text{Sn}} > K_{\text{eq}}^{\text{Ge}}$ .

Reactions of the transient stannylenes with tri-*n*-butylstannane, cyclohexene, 1-hexene, and 1-hexyne proceed in a manner consistent with rapid reversible reaction with the substrate to afford transient products exhibiting absorption maxima in the 380 - 430 nm wavelength region for SnPh<sub>2</sub> and 375 - 380 nm for SnMe<sub>2</sub>, which are assigned to the corresponding Lewis acid-base complexes. The observation of stannylene donor-acceptor complexes with these substrates provides insight into the mechanisms of the reactions of silylenes and germlyenes with these substrate types, as such complexes have been postulated to be involved as intermediates in the reaction pathways but have never been observed directly. The transient spectroscopic results are consistent with the results of product studies experiments with **2**, which indicate that these substrates are ineffective scavengers of SnPh<sub>2</sub> in solution at ambient temperatures.

#### 4.5. Supporting Information

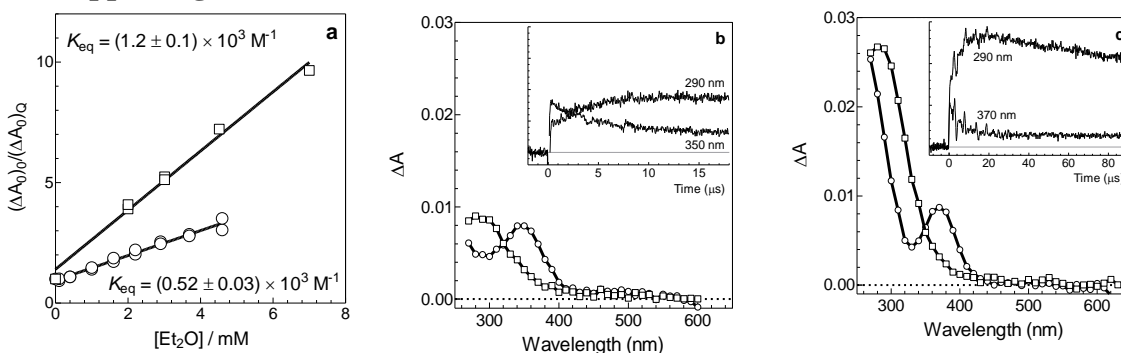


**Figure S4.1.** (a) Plots of  $(\Delta A_0)_0 / (\Delta A_0)_Q$  for reaction of SnMe<sub>2</sub> (○) and SnPh<sub>2</sub> (□) with Et<sub>2</sub>O in hexanes at 25 °C; the solid lines are the linear least squares fits of the data to eq. 4.4. (b) Time-resolved UV-vis spectra from laser photolysis of **1** in hexanes containing 25 mM Et<sub>2</sub>O, 0.32 - 0.46  $\mu\text{s}$  (○), and 17.3 - 17.5  $\mu\text{s}$  (□) after the laser pulse (25 °C), and absorbance-time profiles at selected wavelengths (inset). The spectra in (b) were recorded using a neutral density filter (43 % transmittance). (c) Time-resolved UV-vis spectra recorded by laser photolysis of **2** in hexanes containing 25 mM Et<sub>2</sub>O, 0.96-1.6  $\mu\text{s}$  (○), and 22.6 - 23.0  $\mu\text{s}$  (□) after the laser pulse (25 °C), and absorbance-time profiles at selected wavelengths (inset).

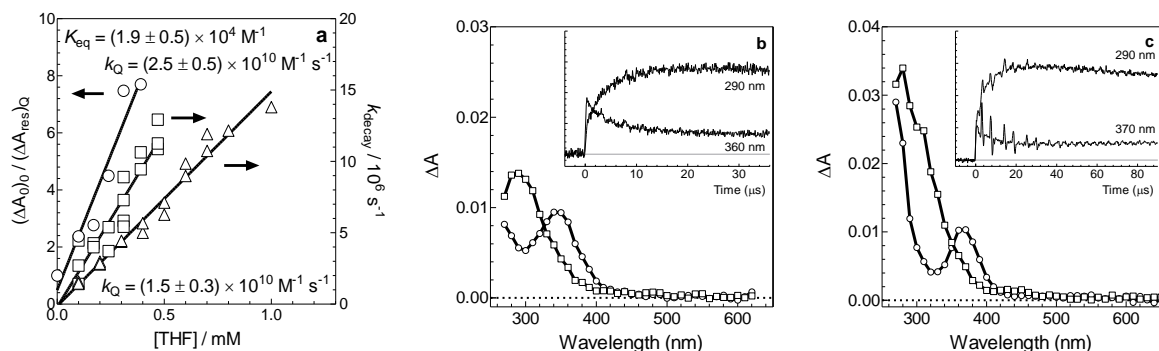


**Figure S4.2.** (a) Plots of  $k_{decay}$  of the SnMe<sub>2</sub> (□) and SnPh<sub>2</sub> (Δ) absorption and  $(\Delta A_0)_0 / (\Delta A_{res})_Q$  (○) of the SnMe<sub>2</sub> absorption versus [THF], in hexanes solution at 25 °C; the solid lines are the linear least-squares fits of the data to equations 4.3 and 4.5, respectively (*data for SnPh<sub>2</sub> (Δ) recorded by B. Nguyen*). (b) Time-resolved UV-vis spectra from laser photolysis of **1** in hexanes containing 25.0 mM THF, 0.51 - 0.70  $\mu\text{s}$  (○), and 34.7 - 35.0  $\mu\text{s}$  (□) after the laser pulse (25 °C), and absorbance-time profiles at selected wavelengths (inset). The spectra in (b) were recorded using a neutral density filter (43 % transmittance). (c) Time-resolved UV-vis spectra recorded by laser photolysis of **2** in hexanes containing 1.23 mM THF, 0.64 - 1.28  $\mu\text{s}$  (○), and 34.7 - 35.6  $\mu\text{s}$  (□) after the laser pulse (25 °C), and absorbance-time profiles at selected wavelengths (inset).

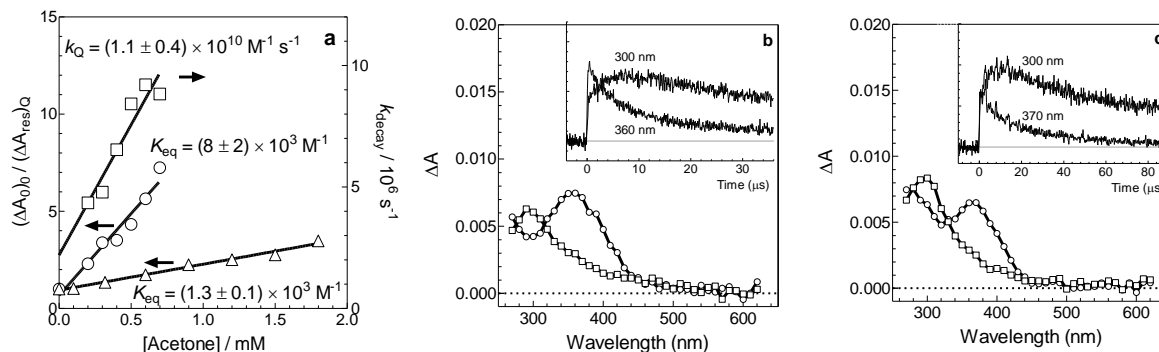


**Figure S4.3.** (a) Plots of  $k_{decay}$  (□) and  $(\Delta A_0)_0 / (\Delta A_{res})_Q$  (○) for reaction of SnPh<sub>2</sub> and  $(\Delta A_0)_0 / (\Delta A_0)_Q$  (Δ) for reaction of SnMe<sub>2</sub> versus [acetone] in hexanes solution at 25 °C; the solid lines are the linear least-squares fits of the data to equations 4.3, 4.5 and 4.4, respectively. (b) Time-resolved UV-vis spectra from laser photolysis of **1** in hexanes containing 25.0 mM acetone, 0.26 - 0.45  $\mu\text{s}$  (○), and 10.1 - 10.4  $\mu\text{s}$  (□) after the laser pulse (25 °C), and absorbance-time profiles at selected wavelengths (inset). (c) Time-resolved UV-vis spectra from laser photolysis of **2** in hexanes containing 25.0 mM acetone, 0.42 - 0.96  $\mu\text{s}$  (○), and 21.9 - 22.2  $\mu\text{s}$  (□) after the laser pulse (25 °C), and absorbance-time profiles at selected wavelengths (inset). Data from (b) and (c) were recorded using a neutral density filter (67 % transmittance).

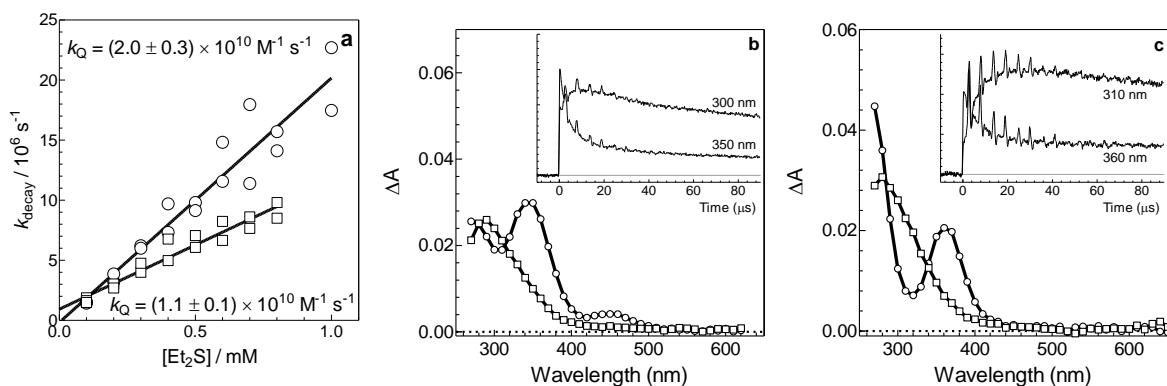


**Figure S4.4.** (a) Plots of  $k_{\text{decay}}$  for reaction of  $\text{SnMe}_2$  ( $\circ$ ) and  $\text{SnPh}_2$  ( $\square$ ) with  $\text{Et}_2\text{S}$  in hexanes at 25 °C; the solid lines are the linear least squares fit of the data to eq. 4.3. (b) Time-resolved UV-vis spectra from laser photolysis of **1** in hexanes containing 1.0 mM  $\text{Et}_2\text{S}$ , 0.16 - 0.48  $\mu\text{s}$  ( $\circ$ ), and 11.2 - 11.8  $\mu\text{s}$  ( $\square$ ) after the laser pulse (25 °C), and absorbance-time profiles at selected wavelengths (inset). (c) Time-resolved UV-vis spectra from laser photolysis of **2** in hexanes containing 1.0 mM  $\text{Et}_2\text{S}$ , 0.32 - 0.64  $\mu\text{s}$  ( $\circ$ ), and 85.9 - 86.7  $\mu\text{s}$  ( $\square$ ) after the laser pulse (25 °C), and absorbance-time profiles at selected wavelengths (inset).

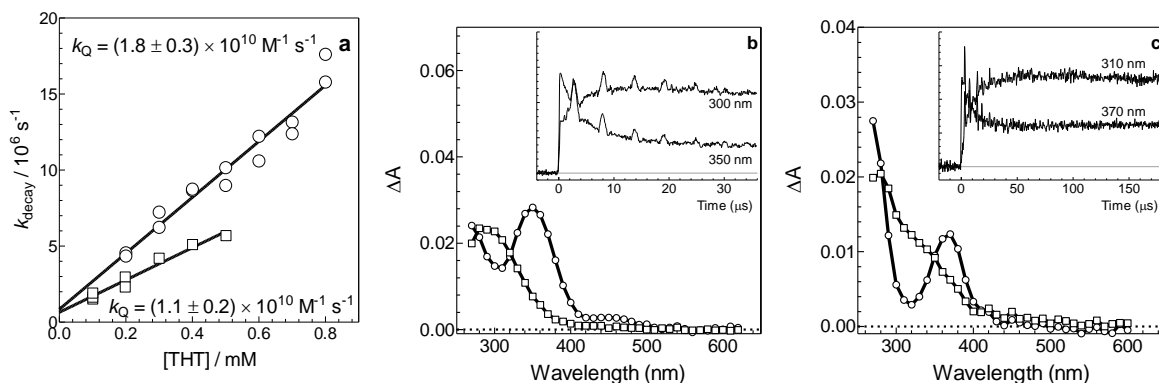


**Figure S4.5.** (a) Plots of  $k_{\text{decay}}$  for reaction of  $\text{SnMe}_2$  ( $\circ$ ) and  $\text{SnPh}_2$  ( $\square$ ) with THT in hexanes at 25 °C; the solid lines are the linear least squares fit of the data to eq. 4.3. (b) Time-resolved UV-vis spectra from laser photolysis of  $\text{SnMe}_2$  precursor **1** in hexanes containing 1.0 mM THT, 0.26 - 0.38  $\mu\text{s}$  ( $\circ$ ), and 35.7 - 35.9  $\mu\text{s}$  ( $\square$ ) after the laser pulse (25 °C), and absorbance-time profiles at selected wavelengths (inset). (c) Time-resolved UV-vis spectra from laser photolysis of **2** in hexanes containing 0.6 mM THT, 2.2 - 3.2  $\mu\text{s}$  ( $\circ$ ), and 172 - 173  $\mu\text{s}$  ( $\square$ ) after the laser pulse (25 °C), and absorbance-time profiles at selected wavelengths (inset).

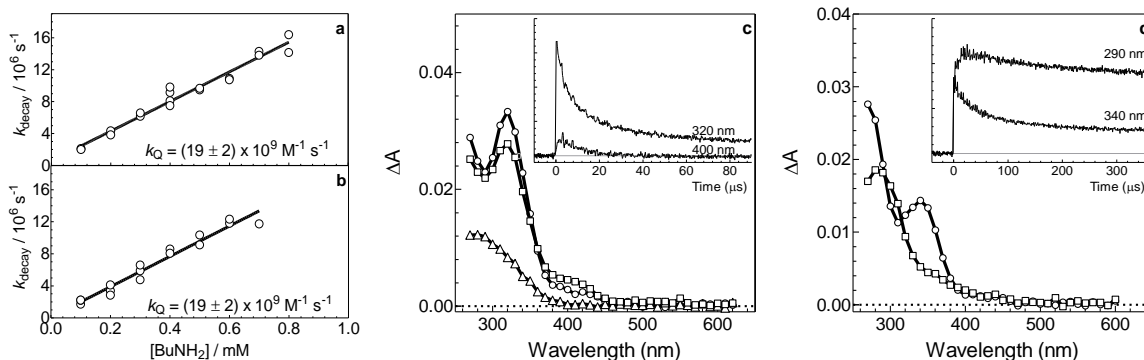


**Figure S4.6.** Plots of  $k_{\text{decay}}$  for reaction of (a)  $\text{SnMe}_2$  and (b)  $\text{SnPh}_2$  with  $\text{BuNH}_2$  in hexanes at  $25^\circ \text{C}$ ; the solid lines are the linear least squares fit of the data to eq. 4.3 (*data in (a) recorded by B. Nguyen*). (c) Time-resolved UV-vis spectra from laser photolysis of **1** in hexanes containing  $1.0 \text{ mM BuNH}_2$ ,  $0.32 - 0.48 \mu\text{s}$  ( $\circ$ ),  $1.28 - 1.76 \mu\text{s}$  ( $\square$ ), and  $26.7 - 27.5 \mu\text{s}$  ( $\Delta$ ) after the laser pulse ( $25^\circ \text{C}$ ), and absorbance-time profiles at selected wavelengths (inset). (d) Time-resolved UV-vis spectra from laser photolysis of **2** in hexanes containing  $0.49 \text{ mM BuNH}_2$ ,  $5.8 - 7.7 \mu\text{s}$  ( $\circ$ ), and  $357 - 358 \mu\text{s}$  ( $\square$ ) after the laser pulse ( $25^\circ \text{C}$ ), and absorbance-time profiles at selected wavelengths (inset).

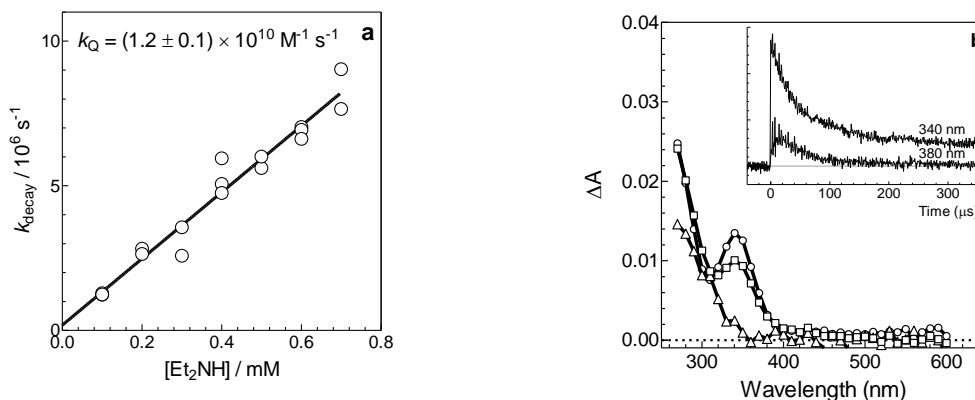


**Figure S4.7.** (a) Plot of  $k_{\text{decay}}$  for reaction of  $\text{SnPh}_2$  with  $\text{Et}_2\text{NH}$  in hexanes at  $25^\circ \text{C}$ ; the solid line is the linear least squares fit of the data to eq. 4.3. (b) Time-resolved UV-vis spectra from laser photolysis of **2** in hexanes containing  $5.0 \text{ mM Et}_2\text{NH}$ ,  $3.8 - 5.1 \mu\text{s}$  ( $\circ$ ),  $16.6 - 19.8 \mu\text{s}$  ( $\square$ ), and  $357 - 359 \mu\text{s}$  ( $\Delta$ ) after the laser pulse ( $25^\circ \text{C}$ ), and absorbance-time profiles at selected wavelengths (inset).

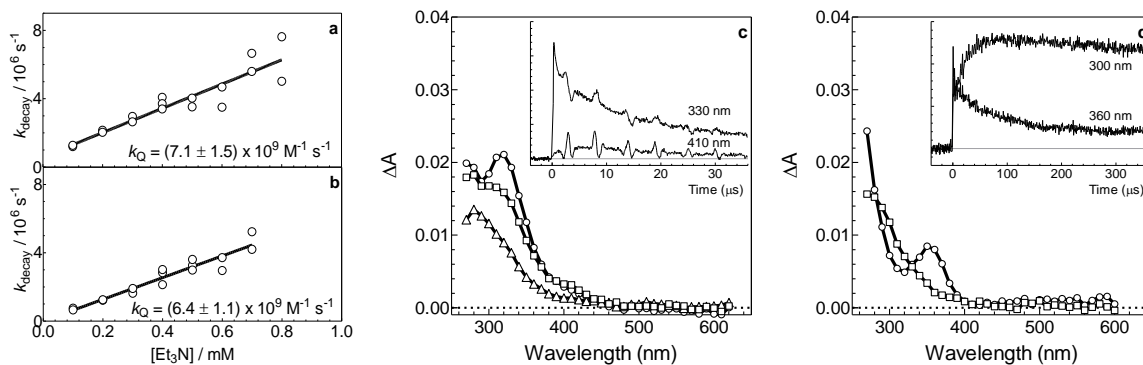


**Figure S4.8.** Plots of  $k_{\text{decay}}$  for reaction of (a)  $\text{SnMe}_2$  and (b)  $\text{SnPh}_2$  with  $\text{Et}_3\text{N}$  in hexanes at 25 °C; the solid lines are the linear least squares fit of the data to eq. 4.3. (c) Time-resolved UV-vis spectra from laser photolysis of **1** in hexanes containing 1.0 mM  $\text{Et}_3\text{N}$ , 3.97 - 4.16  $\mu\text{s}$  ( $\circ$ ), 10.3 - 10.5  $\mu\text{s}$  ( $\square$ ), and 34.4 - 34.6  $\mu\text{s}$  ( $\triangle$ ) after the laser pulse (25 °C), and absorbance-time profiles at selected wavelengths (inset). (d) Time-resolved UV-vis spectra from laser photolysis of **2** in hexanes containing 1.0 mM  $\text{Et}_3\text{N}$ , 4.5 - 5.8  $\mu\text{s}$  ( $\circ$ ), and 344 - 347  $\mu\text{s}$  ( $\square$ ) after the laser pulse (25 °C), and absorbance-time profiles at selected wavelengths (inset).

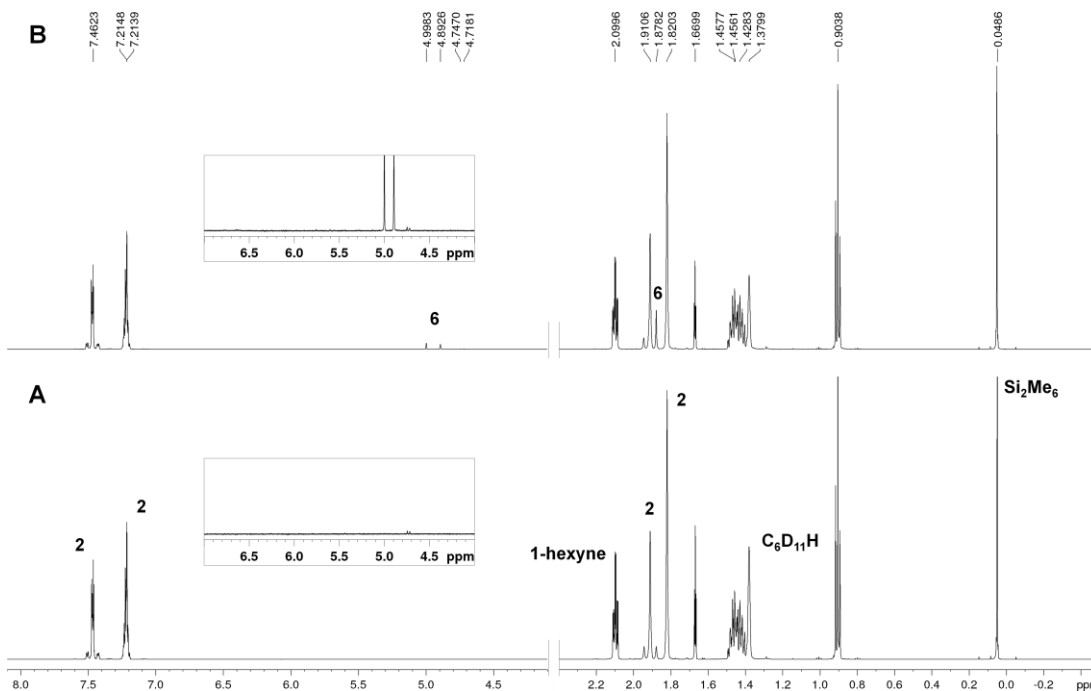


**Figure S4.9.**  $^1\text{H}$  NMR spectra of a deaerated 0.05 M solution of **2** in  $\text{C}_6\text{D}_{12}$  containing 1-hexyne (0.096 M) (a) before and (b) after 10 minutes photolysis with 254 nm light.

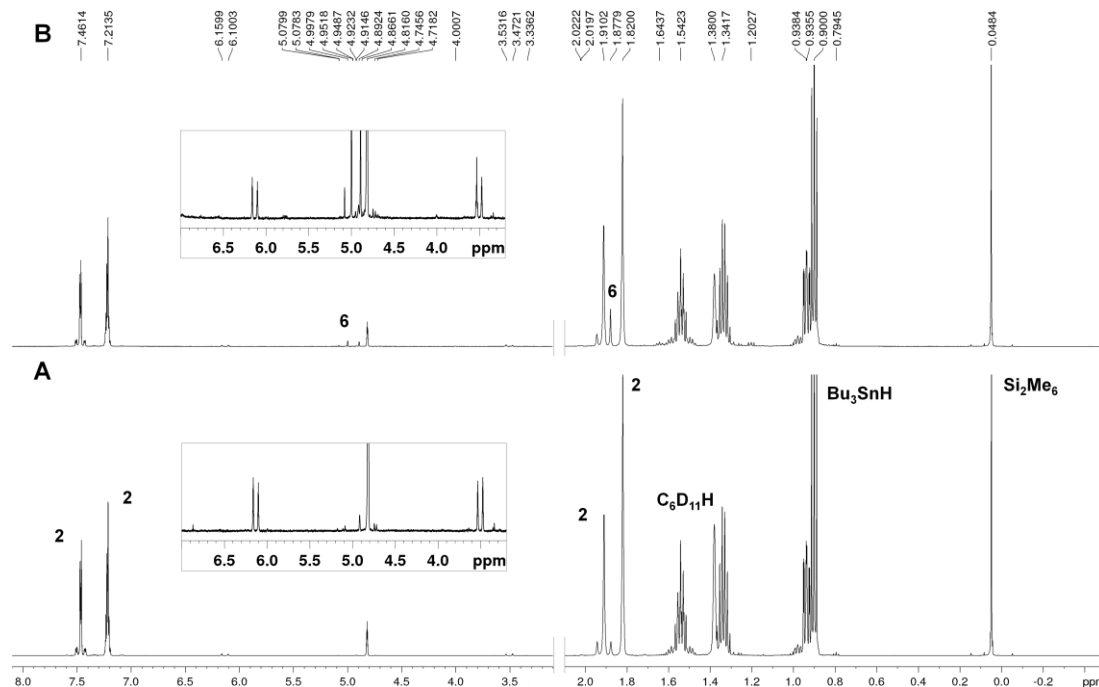


**Figure S4.10.**  $^1\text{H}$  NMR spectra of a deaerated 0.05 M solution of **2** in  $\text{C}_6\text{D}_{12}$  containing  $\text{Bu}_3\text{SnH}$  (0.053 M) (a) before and (b) after 15 minutes photolysis with 254 nm light.

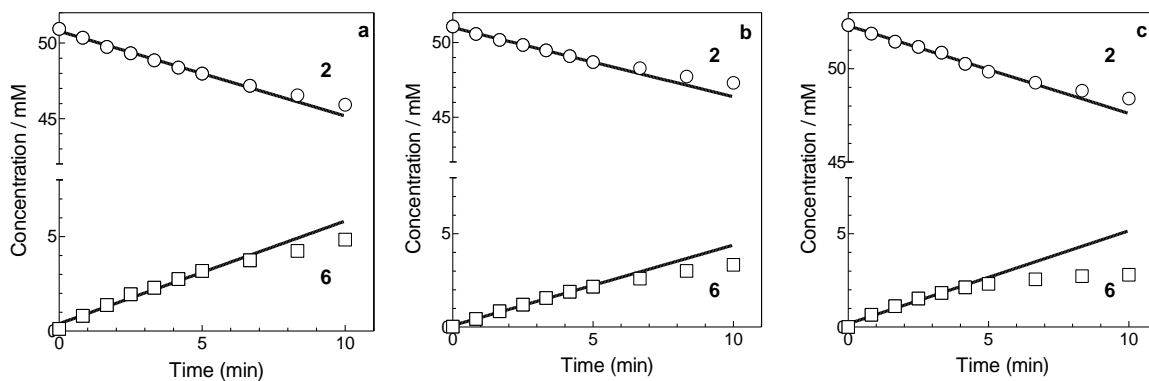


**Figure S4.11.** (a) Concentration versus time plots for the photolysis of a solution of **2** (ca. 0.05 M) in  $\text{C}_6\text{D}_{12}$  and isoprene (ca. 0.1 M). The initial slopes, determined from the first eight data points in each of the plots, are (in units of  $\text{mM min}^{-1}$ ) **2**,  $-0.56 \pm 0.02$  ( $\circ$ ); **6**,  $0.54 \pm 0.03$  ( $\square$ ). (b) Concentration versus time plots for the photolysis of a solution of **2** (ca. 0.05 M) in  $\text{C}_6\text{D}_{12}$  and 1-hexyne (ca. 0.1 M). The initial slopes, determined from the first seven data points in each of the plots, are (in units of  $\text{mM min}^{-1}$ ) **2**,  $-0.46 \pm 0.01$  ( $\circ$ ); **6**,  $0.43 \pm 0.01$  ( $\square$ ). (c) Concentration versus time plots for the photolysis of a solution of **2** (ca. 0.05 M) in  $\text{C}_6\text{D}_{12}$  and  $\text{Bu}_3\text{SnH}$  (ca. 0.05 M). The initial slopes, determined from the first six data points in each of the plots, are (in units of  $\text{mM min}^{-1}$ ) **2**,  $-0.47 \pm 0.03$  ( $\circ$ ); **6**,  $0.50 \pm 0.04$  ( $\square$ ).

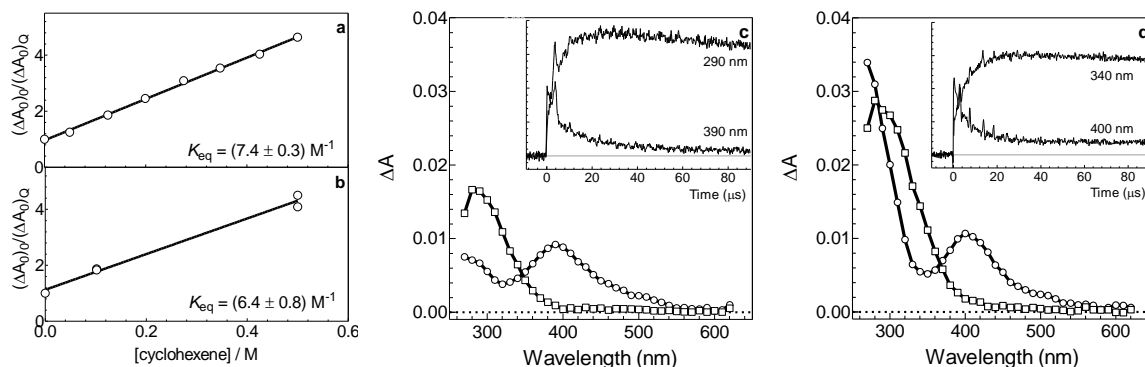


**Figure S4.12.** Plots of  $(\Delta A_0)_0 / (\Delta A_0)_Q$  for the reactions of (a)  $\text{SnMe}_2$  and (b)  $\text{SnPh}_2$  with cyclohexene in hexanes at 25 °C; the solid lines are the linear least squares fits of the data to eq. 4.4. (c) Time-resolved UV-vis spectra from laser photolysis of **1** in hexanes containing 0.5 M cyclohexene, 0.64 - 1.12  $\mu\text{s}$  ( $\circ$ ), and 85.9 - 86.7  $\mu\text{s}$  ( $\square$ ) after the laser pulse (25 °C), and absorbance-time profiles at selected wavelengths (inset). (d) Time-resolved UV-vis spectra from laser photolysis of **2** in hexanes containing 0.5 M cyclohexene, 0.32 - 0.80  $\mu\text{s}$  ( $\circ$ ), and 85.9 - 86.7  $\mu\text{s}$  ( $\square$ ) after the laser pulse (25 °C), and absorbance-time profiles at selected wavelengths (inset).

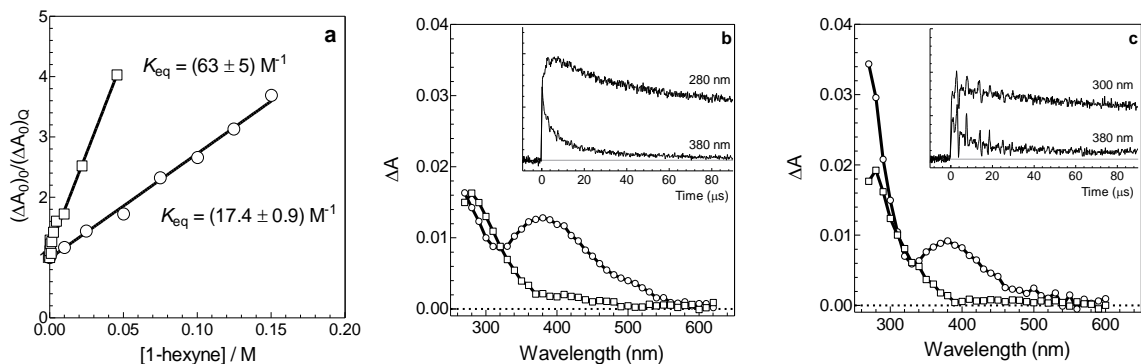


**Figure S4.13.** (a) Plots of  $(\Delta A_0)_0 / (\Delta A_0)_Q$  for reaction of the  $\text{SnMe}_2$  ( $\circ$ ) and  $\text{SnPh}_2$  ( $\square$ ) absorption with 1-hexyne in hexanes at 25 °C; the solid lines are the linear least squares fit of the data to eq. 4.4. (b) Time-resolved UV-vis spectra from laser photolysis of **1** in hexanes containing 0.25 M 1-hexyne, 0.16 - 0.48  $\mu\text{s}$  ( $\circ$ ), and 21.6 - 22.1  $\mu\text{s}$  ( $\square$ ) after the laser pulse (25 °C), and absorbance-time profiles at selected wavelengths (inset). (c) Time-resolved UV-vis spectra from laser photolysis of **2** in hexanes containing 0.2 M 1-hexyne, 0.64  $\mu\text{s}$  ( $\circ$ ), and 77.9 - 78.7  $\mu\text{s}$  ( $\square$ ) after the laser pulse (25 °C), and absorbance-time profiles at selected wavelengths (inset).

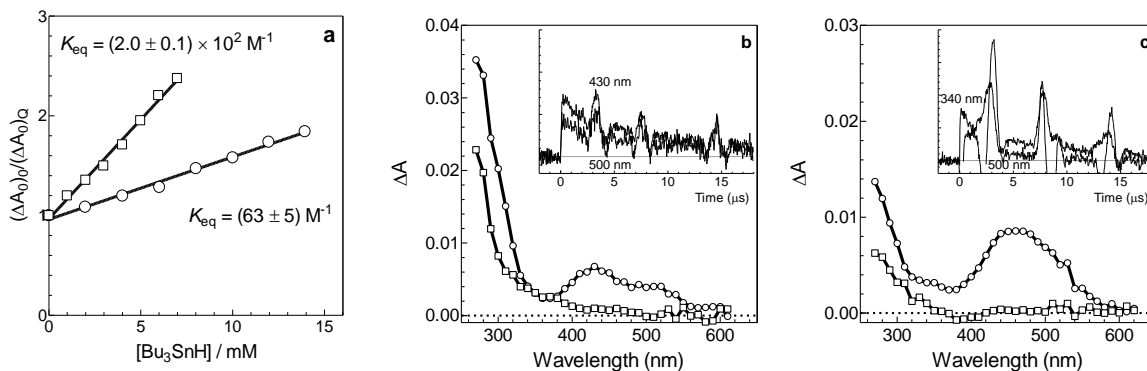


**Figure S4.14.** (a) Plots of  $(\Delta A_0)_0 / (\Delta A_0)_e$  for reaction of the  $\text{SnMe}_2$  ( $\circ$ ) and  $\text{SnPh}_2$  ( $\square$ ) absorption with  $\text{Bu}_3\text{SnH}$  in hexanes at 25 °C; the solid lines are the linear least squares fit of the data to eq. 4.4. (b) Time-resolved UV-vis spectra from laser photolysis of **2** in hexanes containing 7.8 mM  $\text{Bu}_3\text{SnH}$ , 0.45 - 0.54  $\mu\text{s}$  ( $\circ$ ), and 17.8 - 18.0  $\mu\text{s}$  ( $\square$ ) after the laser pulse (25 °C), and absorbance-time profiles at selected wavelengths (inset). (c) Time-resolved UV-vis spectra from laser photolysis of **1** in hexanes containing 14 mM  $\text{Bu}_3\text{SnH}$ , 0.42 - 0.54  $\mu\text{s}$  ( $\circ$ ), and 17.8 - 18.0  $\mu\text{s}$  ( $\square$ ) after the laser pulse (25 °C), and absorbance-time profiles at selected wavelengths (inset).

#### 4.6. References

- (1) Zhou, D.; Reiche, C.; Nag, M.; Soderquist, J. A.; Gaspar, P. P. *Organometallics* **2009**, *28*, 2595.
- (2) Nag, M.; Gaspar, P. P. *Organometallics* **2009**, *28*, 5612.
- (3) Weidenbruch, M.; Schäfer, A.; Kilian, H.; Pohl, S.; Saak, W.; Marsmann, H. *Chem. Ber.* **1992**, *125*, 563.
- (4) Sharma, H. K.; Metta-Magaña, A.; Pannell, K. H. *Inorg. Chim. Acta* **2018**, *475*, 3.
- (5) Sita, L. R.; Bickerstaff, R. D. *J. Am. Chem. Soc.* **1988**, *110*, 5208.
- (6) Sita, L. R.; Bickerstaff, R. D. *Phosph. Sulf. Sil. Rel. Elem.* **1989**, *41*, 31.
- (7) Kostina, S. S.; Singh, T.; Leigh, W. J. *Organometallics* **2012**, *31*, 3755.
- (8) Moiseev, A. G.; Leigh, W. J. *Organometallics* **2007**, *26*, 6277.
- (9) Leigh, W. J.; Harrington, C. R. *J. Am. Chem. Soc.* **2005**, *127*, 5084.
- (10) Leigh, W. J.; Lollmahomed, F.; Harrington, C. R.; McDonald, J. M. *Organometallics* **2006**, *25*, 5424.
- (11) Leigh, W. J.; Lollmahomed, F.; Harrington, C. R. *Organometallics* **2006**, *25*, 2055.
- (12) Duffy, I. R.; Leigh, W. J. *Organometallics* **2015**, *34*, 5029.
- (13) Drago, R. S. *Coord. Chem. Rev.* **1980**, *33*, 251.
- (14) Drago, R. S.; Ferris, D. C.; Wong, N. *J. Am. Chem. Soc.* **1990**, *112*, 8953.
- (15) Hunter, E. P. L.; Lias, S. G. *J. Phys. Chem. Ref. Data* **1998**, *27*, 413.
- (16) Computational studies were carried out by Prof. W. J. Leigh



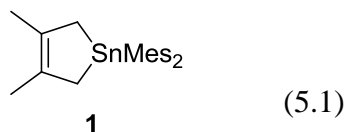
- (17) Becerra, R.; Harrington, C. R.; Gaspar, P. P.; Leigh, W. J.; Vargas-Baca, I.; Walsh, R.; Zhou, D. *J. Am. Chem. Soc.* **2005**, *127*, 17469.
- (18) Appler, H.; Neumann, W. P. *J. Organomet. Chem.* **1986**, *314*, 247.
- (19) Huck, L. A.; Leigh, W. J. *Organometallics* **2009**, *28*, 6777.
- (20) Billeb, G.; Neumann, W. P.; Steinhoff, G. *Tetrahedron Lett.* **1988**, *29*, 5245.
- (21) Sita, L. R.; Kinoshita, I.; Lee, S. P. *Organometallics* **1990**, *9*, 1644.
- (22) Su, M. D. *Chem. Eur. J.* **2004**, *10*, 6073.
- (23) Broeckaert, L.; Geerlings, P.; Růžička, A.; Willem, R.; De Proft, F. *Organometallics* **2012**, *31*, 1605.
- (24) Bundhun, A.; Ramasami, P.; Gaspar, P. P.; Schaefer, H. F. *Inorg. Chem.* **2012**, *51*, 851.
- (25) Schoeller, W. W.; Schneider, R. *Chem. Ber.* **1997**, *130*, 1013.
- (26) Kira, M.; Ishida, S.; Iwamoto, T.; Yauchibara, R.; Sakurai, H. *J. Organomet. Chem.* **2001**, *636*, 144.
- (27) Laurence, C.; Gal, J.-F. In *Lewis Basicity and Affinity Scales*; John Wiley & Sons, Ltd: 2009, p 323.
- (28) Murov, S. L.; Carmichael, I.; Hug, G. L. *Handbook of Photochemistry*; 2nd ed.; Dekker: New York, 1993.
- (29) Kostina, S. S.; Singh, T.; Leigh, W. J. *J. Phys. Org. Chem.* **2011**, *24*, 937.
- (30) Moiseev, A. G.; Leigh, W. J. *Organometallics* **2007**, *26*, 6268.
- (31) Huck, L. A.; Leigh, W. J. *Organometallics* **2007**, *26*, 1339.
- (32) Kostina, S. S.; Leigh, W. J. *Can. J. Chem.* **2014**, *93*, 435.
- (33) Kostina, S. S.; Leigh, W. J. *J. Am. Chem. Soc.* **2011**, *133*, 4377.
- (34) Leigh, W. J.; Harrington, C. R.; Vargas-Baca, I. *J. Am. Chem. Soc.* **2004**, *126*, 16105.
- (35) Lollmahomed, F.; Huck, L. A.; Harrington, C. R.; Chitnis, S. S.; Leigh, W. J. *Organometallics* **2009**, *28*, 1484.
- (36) Kira, M.; Ishida, S.; Iwamoto, T. *Chem. Record* **2004**, *4*, 243.
- (37) Levin, G.; Das, P. K.; Bilgrien, C.; Lee, C. L. *Organometallics* **1989**, *8*, 1206.
- (38) Leigh, W. J.; Kostina, S. S.; Bhattacharya, A.; Moiseev, A. G. *Organometallics* **2010**, *29*, 662.
- (39) Leung, W.-P.; Cheng, H.; Huang, R.-B.; Yang, Q.-C.; Mak, T. C. W. *Chem. Commun.* **2000**, 451.
- (40) Kroke, E.; Willms, S.; Weidenbruch, M.; Saak, W.; Pohl, S.; Marsmann, H. *Tetrahedron Lett.* **1996**, *37*, 3675.
- (41) Gaspar, P. P.; West, R. In *The chemistry of organic silicon compounds, Vol. 2*; Rappoport, Z., Apeloig, Y., Eds.; John Wiley and Sons: New York, 1998; Vol. 2, p 2463.
- (42) Ishida, S.; Iwamoto, T.; Kira, M. *Heteroatom Chem.* **2011**, *22*, 432.
- (43) Lips, F.; Fettinger, J. C.; Mansikkamäki, A.; Tuononen, H. M.; Power, P. P. *J. Am. Chem. Soc.* **2014**, *136*, 634.
- (44) Driver, T. G. In *Silver in Organic Chemistry*; Harmata, M., Ed.; John Wiley & Sons: New York, 2010, p 183.

- (45) Kabe, Y.; Ohgaki, H.; Yamagaki, T.; Nakanishi, H.; Ando, W. *J. Organomet. Chem.* **2001**, *636*, 82.
- (46) Ando, W.; Ohgaki, H.; Kabe, Y. *Angew. Chem. Int. Ed. Engl.* **1994**, *33*, 659.
- (47) Sakai, S. *Int. J. Quantum Chem.* **1998**, *70*, 291.
- (48) Broeckaert, L.; Turek, J.; Olejník, R.; Růžička, A.; Biesemans, M.; Geerlings, P.; Willem, R.; De Proft, F. *Organometallics* **2013**, *32*, 2121.
- (49) Boganov, S. E.; Faustov, V. I.; Egorov, M. P.; Nefedov, O. M. *Russ. Chem. Bull.* **1994**, *43*, 47.
- (50) de Lima, G. M.; Toupance, T.; Arkis, E.; Chaniotakis, N.; Cusack, P. A.; Lacroix, P. G.; Farfán, N.; Jousseau, B.; Sharma, H. K.; Pannell, K. H.; Haiduc, I.; Tiekink, E. R. T.; Zukerman-Schpector, J. In *Tin Chemistry*; John Wiley & Sons, Ltd: 2008, p 285.
- (51) Boganov, S. E.; Egorov, M. P.; Nefedov, O. M. *Russ. Chem. Bull.* **1999**, *48*, 98.
- (52) Boganov, S. E.; Faustov, V. I.; Egorov, M. P.; Nefedov, O. M. *Russ. Chem. Bull. Int. Ed.* **2004**, *53*, 960.
- (53) Meier, P. F.; Perry, D. L.; Hauge, R. H.; Margrave, J. L. *Inorg. Chem.* **1979**, *18*, 2051.
- (54) Pluta, C.; Porschke, K. -R. *J. Organomet. Chem.* **1993**, *453*, C11.
- (55) Boatz, J. A.; Gordon, M. S.; Sita, L. R. *J. Phys. Chem.* **1990**, *94*, 5488.
- (56) Saito, M.; Tokitoh, N.; Okazaki, R. *Organometallics* **1996**, *15*, 4531.
- (57) Saito, M.; Tokitoh, N.; Okazaki, R. *Chem. Lett.* **1996**, *25*, 265.
- (58) Setaka, W.; Sakamoto, K.; Kira, M.; Power, P. P. *Organometallics* **2001**, *20*, 4460.
- (59) Marx, R.; Neumann, W. P.; Hillner, K. *Tetrahedron Lett.* **1984**, *25*, 625.
- (60) Cotton, J. D.; Davidson, P. J.; Lappert, M. F. *J. Chem. Soc., Dalton Trans.* **1976**, 2275.
- (61) Becerra, R.; Boganov, S. E.; Egorov, M. P.; Faustov, V. I.; Krylova, I. V.; Nefedov, O. M.; Walsh, R. *J. Am. Chem. Soc.* **2002**, *124*, 7555.
- (62) Boganov, S. E.; Egorov, M. P.; Faustov, V. I.; Krylova, I. V.; Nefedov, O. M.; Becerra, R.; Walsh, R. *Russ. Chem. Bull. Int. Ed.* **2005**, *54*, 483.
- (63) Lehnig, M.; Neumann, W. P.; Seifert, P. *J. Organomet. Chem.* **1978**, *162*, 145.

## Chapter 5: Direct detection of Dimesitylstannylene and Tetramesityldistannene in Solution and Studies of Some of Their Reactions

### 5.1. Overview

Chapter 5 details the solution phase detection of dimesitylstannylene ( $\text{SnMes}_2$ ; Mes = 2,4,6-trimethylphenyl) and its doubly bonded dimer, tetramesityldistannene. It is well known that *ortho* substitution by alkyl or aryl groups imparts steric effects on the bimolecular reactions of diarylstannylenes.<sup>1-4</sup> As such, comparison of the reactivity of  $\text{SnMes}_2$  to that of  $\text{SnPh}_2$  (described in Chapters 2 - 4) aims to provide information on how steric factors alter the kinetics and thermodynamics of the reactions of diarylstannylenes. The overall goal is to ascertain quantitatively the effects of steric bulk on the solution phase reactivity of transient stannylenes via direct spectroscopic methods. Such a strategy has been employed in our kinetic and thermodynamic analysis of the reactions of transient diarylsilylenes<sup>5-9</sup> and germlyenes.<sup>9-12</sup> Characterization of the doubly bonded dimer is also significant as the lighter Si and Ge homologs are well known as stable and isolable compounds.<sup>13-15</sup>



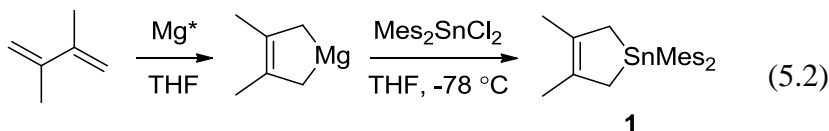
Mes = C<sub>6</sub>H<sub>2</sub>-2,4,6-Me<sub>3</sub>

The direct detection and solution phase characterization of photochemically generated  $\text{SnMes}_2$  was carried out using 1-stannacyclopent-3-ene precursor **1**. The reaction of dichlorodimethylstannane ( $\text{Me}_2\text{SnCl}_2$ ) and acetic acid ( $\text{AcOH}$ ) with  $\text{SnMes}_2$  was studied by a combination of steady state and laser flash photolysis methods, as these substrates were found in Chapters 2 and 3 to lead to discrete product formation with  $\text{SnPh}_2$ . Steady state photolysis of an aerated hydrocarbon solution containing **1** afforded

hexamethylcyclotristannoxane (**5**), which was attributed to the reaction of molecular oxygen ( $O_2$ ) with  $SnMes_2$ . Finally, the kinetics and thermodynamics of Lewis acid-base complexation of  $SnMes_2$  with ethers, alcohols, sulfides and amines have been characterized, allowing for an assessment to be made of the effects of steric bulk on diarylstannylene reactivity.

## 5.2. Results

Compound **1** was prepared according to procedures derived from those of Gaspar and coworkers,<sup>16</sup> by the reaction of dichlorodimesitylstannane ( $Mes_2SnCl_2$ , **2**) with the Rieke magnesium ( $Mg^*$ ) complex of 2,3-dimethyl-1,3-butadiene (**3**) in THF at  $-78\text{ }^\circ\text{C}$  (eq. 5.2). Compound **1** was obtained as an opaque colourless oil in 8 % isolated yield after purification, which was achieved by stirring the crude sample in a mixture of basic alumina and pentane before filtering the solution and subsequent removal of the solvent. Attempted purification by silica gel chromatography resulted in the decomposition of **1** and formation of mesitylene (**4**). Samples used for steady state and flash photolysis experiments contained **4** (4.8 mol %) as the only detectable impurity by  $^1H$  NMR spectroscopy. The presence of **4** is not expected to interfere with the results of photolysis experiments, given the low molar absorptivity of **4** ( $\epsilon_{254nm} \sim 100\text{ M}^{-1}\text{ cm}^{-1}$ )<sup>17</sup> relative to **1** ( $\epsilon_{254nm} \sim 2100\text{ M}^{-1}\text{ cm}^{-1}$ ; see Chapter 8.6), in conjunction with its low concentration (ca. 1  $\mu\text{M}$ ) in laser flash photolysis experiments. Spectroscopic data for **1** is in agreement with those reported by Tilley and coworkers.<sup>18</sup>



### 5.2.1. Steady State Photolysis Experiments

Product studies experiments were carried out on air- or argon-saturated  $C_6D_{12}$  solutions of **1** (0.03 - 0.05 M) containing hexamethyldisilane as internal NMR standard, with and without added  $Me_2SnCl_2$  (ca. 0.035 M) or AcOH (ca. 0.20 M) as stannylene substrates. The  $Me_2SnCl_2$  trapping experiment was performed in air-saturated solution so as to convert the anticipated primary photoproduct ( $Mes_2ClSnSnClMe_2$ , **19**, eq. 3.19) to the corresponding distannoxane, which is expected to be photostable.<sup>19</sup> The oxygen content in the air-saturated samples was replenished at periodic intervals throughout the photolysis. Samples were irradiated with two low pressure mercury lamps (253.7 nm), and the progress of the photolysis was followed by  $^1H$  NMR spectroscopy;  $^{13}C\{^1H\}$  and/or  $^{119}Sn\{^1H\}$  NMR spectra were recorded for each photolysis sample at the end of irradiation to aid further in product identification. Product yields were calculated from the slopes of concentration versus time plots for the products relative to that of the corresponding plot for **1**. Each photolysis experiment was compared to an independent sample that was kept in the dark for an equivalent period of time, and monitored by  $^1H$  NMR along with the photolyzed sample.

Steady state photolysis of an aerated solution of **1** in  $C_6D_{12}$  (0.04 M) resulted in the consumption of the stannacyclopent-3-ene and the formation of **3** ( $99 \pm 9 \%$ ) and hexamesitylcyclotristannoxane (**5**,  $105 \pm 9 \%$ ) (eq. 5.3a). The latter compound was identified by spiking the photolysis mixture with an independently prepared sample (Figure 5.1c).  $^1H$  and  $^{119}Sn$  NMR spectra of the photolyzate after 10 minutes photolysis are shown in Figure 5.1b and S5.1a, respectively, while concentration versus time plots of the identified products are shown in Figure 5.2a. The formation of **3** and **5** in a 1:1 molar ratio as the primary photoproducts suggests the cyclotristannoxane is the sole product of trapping of  $SnMes_2$  under these conditions. The yield of **5** was calculated on a per- $SnMes_2$  basis, but is plotted in Figure 5.2a as straight concentration. The  $^1H$  NMR

spectrum of the "dark" solution of **1** in air saturated  $C_6D_{12}$  - and specifically the estimated concentration of **4** - did not change over the course of the photolysis experiment, showing **1** to be stable in solution in the absence of light.

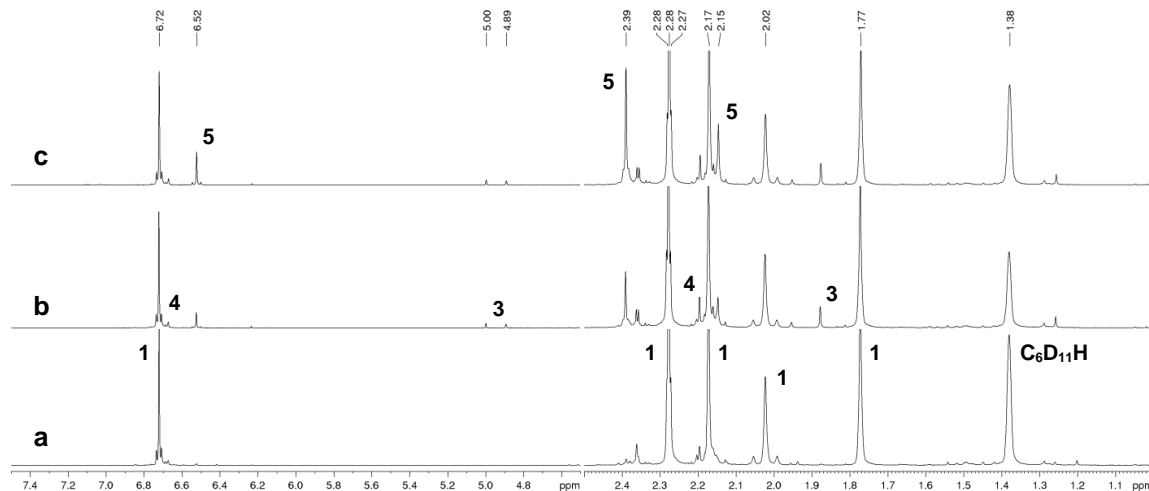


**Figure 5.1.**  $^1H$  NMR spectra of an air saturated  $C_6D_{12}$  0.04 M solution of **1** (a) before and (b) after 10 minutes of photolysis with 254 nm light, and (c) after spiking the resulting photolyzate with an authentic sample of **5**. (Samples prepared by J. Woodard)

Photolysis of an incompletely deoxygenated solution of **1** in  $C_6D_{12}$ , without replenishing the oxygen content throughout the photolysis, results in the formation of **3** ( $83 \pm 2\%$ ), **4** ( $24 \pm 1\%$ ), and **5** ( $93 \pm 7\%$ ) over the first ca. 2.5 min of irradiation. Photolysis for a further 7.5 minutes resulted in a levelling of the concentration versus time plot for **5**, and the formation of multiple resonances in the 6.6 - 6.8 ppm region of the  $^1H$  NMR spectrum. The levelling off of the yield of **5** at approximately 2.5 min likely corresponds to the point where the  $O_2$  in solution is largely depleted; an  $O_2$  concentration of ca. 0.6 mM at the beginning of the photolysis is estimated from the total concentration of **5** produced. The formation of **4** suggests that an additional reaction of  $SnMes_2$  takes over when the concentration of  $O_2$  drops below a threshold level, and is interpreted as being due to a relatively slow reaction of  $SnMes_2$  with adventitious water in the solution (*vide infra*).

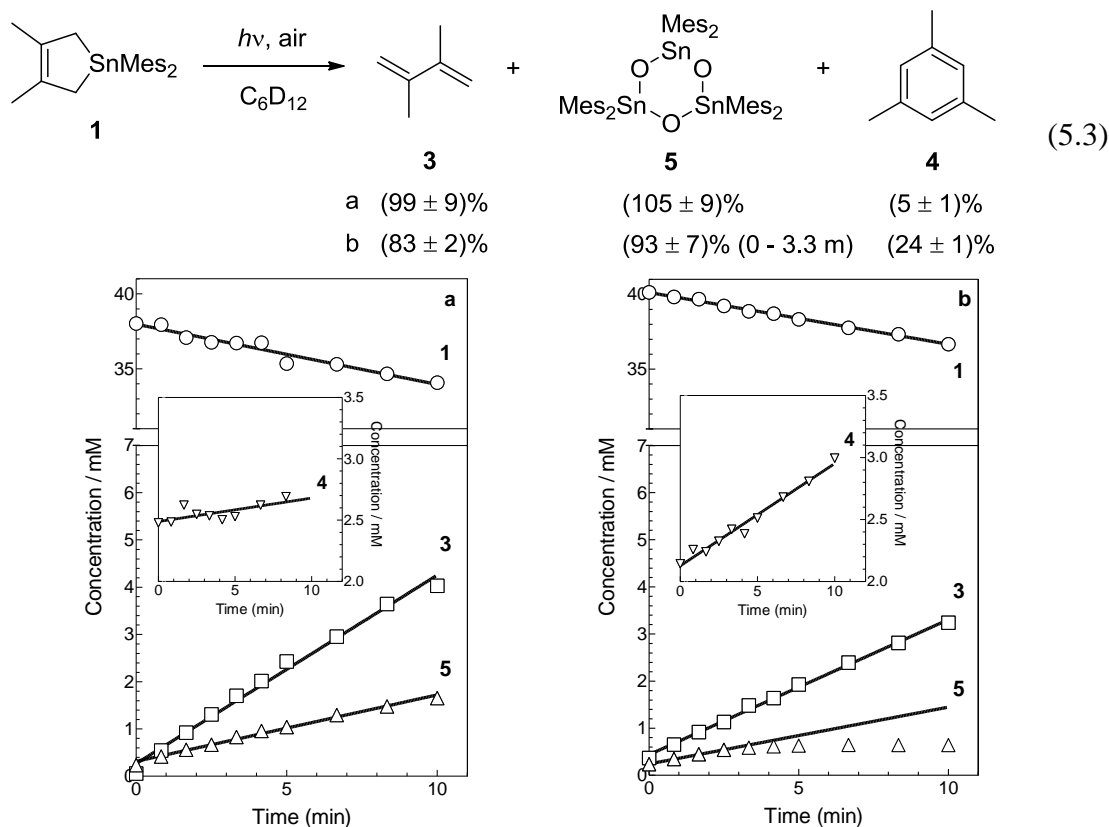


**Figure 5.2.** (a) Concentration versus time plots for the photolysis of a solution of **1** (ca. 0.04 M) in air-saturated  $C_6D_{12}$ , with periodic replenishment of depleted air (eq. 5.3a). The slopes of the plots are (in units of  $mM\ min^{-1}$ ) **1**,  $-0.40 \pm 0.03$  ( $\circ$ ); **3**,  $0.40 \pm 0.01$  ( $\square$ ); **5**,  $0.14 \pm 0.01$  ( $\Delta$ ); **4**,  $0.019 \pm 0.007$  ( $\nabla$ ; see expansion). (b) Concentration versus time plots for the photolysis of an incompletely deoxygenated solution of **1** (ca. 0.04 M) in  $C_6D_{12}$ , without periodic replenishment of depleted  $O_2$  (eq. 5.3b). The slopes of the plots are (in units of  $mM\ min^{-1}$ ) **1**,  $-0.35 \pm 0.01$  ( $\circ$ ); **3**,  $0.29 \pm 0.01$  ( $\square$ ); **5**,  $0.121 \pm 0.003$  ( $< 3\ min$ ) ( $\Delta$ ); **4**,  $0.082 \pm 0.004$  ( $\nabla$ ; see expansion). (Samples prepared by J. Woodard)

Steady state photolysis of a deoxygenated solution of **1** (0.04 M) in  $C_6D_{12}$  containing 0.2 M AcOH resulted in the immediate precipitation of a white solid, and the formation of **3** ( $77 \pm 4\%$ ) and **4** ( $147 \pm 8\%$ ) as the only detectable products after 30 minutes of photolysis (eq. 5.4). Mesitylene (**4**) was identified in the GC-MS spectrum of the resulting photolyzate (Figure S5.2), and was further confirmed by  $^1H$  and  $^{13}C\{^1H\}$  NMR spiking experiments with an authentic sample. The  $^1H$  NMR spectrum at 0 and 30 minutes photolysis, and after the addition of an authentic sample of **4** is shown in Figure

5.3, while the  $^{13}\text{C}\{^1\text{H}\}$  NMR spectrum before and after the addition of **4** is shown in Figure S5.3. Concentration versus time plots for **1**, **3**, and **4** are shown in Figure 5.4. The yield of **4** was found to be well in excess of 100 %. Furthermore, the rate of its formation is equal to the consumption rate of AcOH and twice the rate of formation of **3** within experimental error; these are all consistent with the reaction between  $\text{SnMes}_2$  and AcOH producing two equivalents of **4**. Careful decanting of the solution enabled the collection of the white solid (m.p. > 299 °C). A  $\text{C}_6\text{D}_{12}$  solution of the same mixture that was not photolyzed also shows the gradual formation of **3** and **4** over time, but not at a fast enough rate to significantly affect the yields in the photolysis experiment: from the formation rates of **3** and **4** in the dark reaction, it can be estimated to contribute 1.7 % of the yield for **3** and 1.5 % of the yield for **4** from the photolyzed sample.

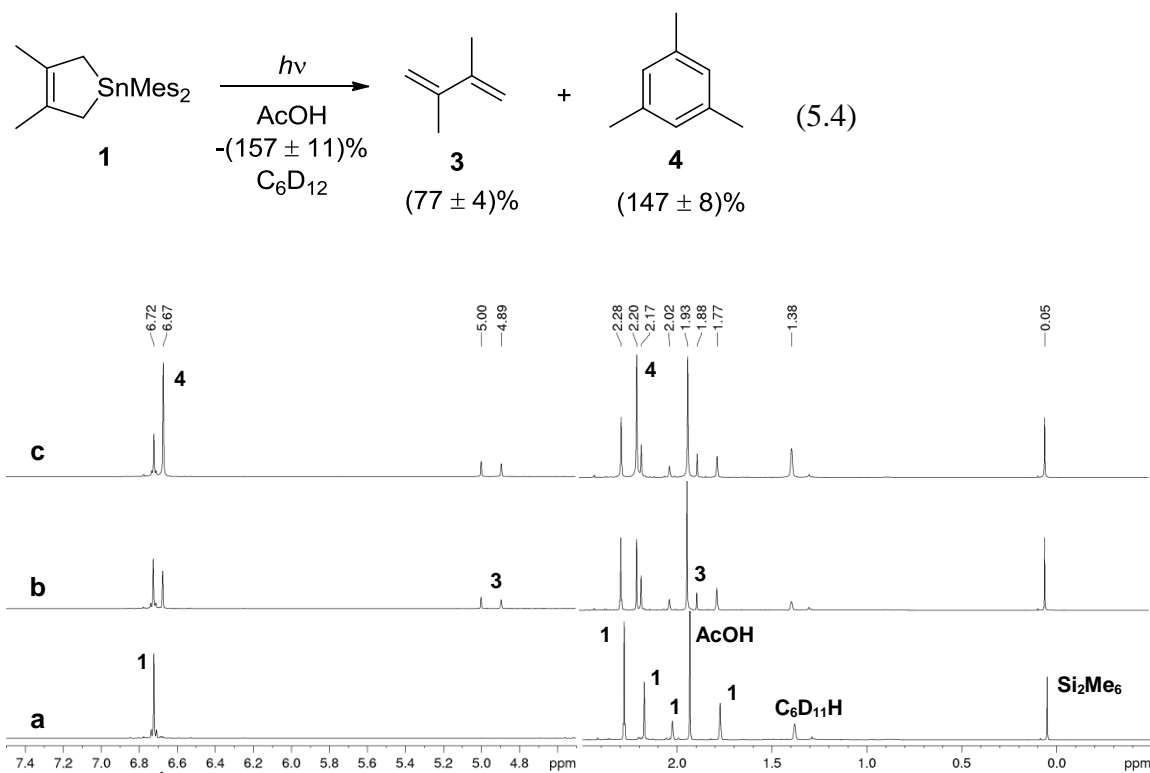


**Figure 5.3.**  $^1\text{H}$  NMR spectra of a deoxygenated 0.04 M solution of **1** in  $\text{C}_6\text{D}_{12}$  (a) before and (b) after 30 minutes photolysis with 254 nm light, and (c) after spiking the sample of (b) with an authentic sample of **4**.



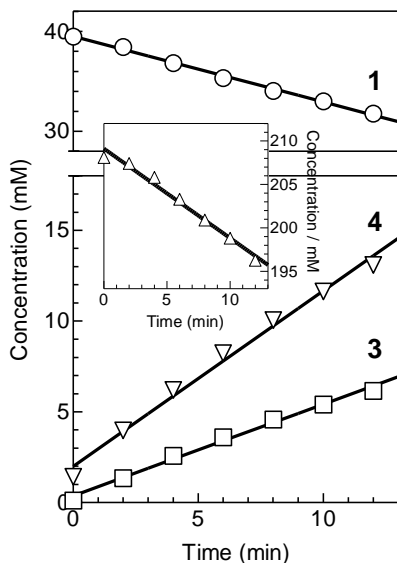


**Figure 5.4.** Concentration versus time plots for the photolysis of a deoxygenated solution of **1** (ca. 0.04 M) in  $C_6D_{12}$  and AcOH (ca. 0.2 M). The initial slopes, determined over the first 12 minutes of photolysis, are (in units of  $mM\ min^{-1}$ ) AcOH,  $-1.03 \pm 0.06$  ( $\Delta$ ); **1**,  $-0.66 \pm 0.02$  ( $\circ$ ); **3**,  $0.51 \pm 0.02$  ( $\square$ ); **4**,  $0.97 \pm 0.04$  ( $\nabla$ ).

Photolysis of an aerated solution of **1** (ca. 0.045 M) in  $C_6D_{12}$  containing  $Me_2SnCl_2$  (ca. 0.035 M) led to the consumption of **1** and the concurrent growth of four products (eq. 5.5): these were identified as **3** ( $88 \pm 5\%$ ), **4** ( $72 \pm 4\%$ ),  $Me_2SnCl_2$  (**2**,  $57 \pm 2\%$ ), and the association dimer of 1,3-dichlorotetramethyldistannoxane (**6**,  $41 \pm 5\%$ ). Representative  $^1H$  and  $^{119}Sn$  NMR spectra are shown in Figure 5.5b and S5.5a, respectively, while concentration versus time plots are shown in Figure 5.6a. Compounds **2** (Figure S5.4) and **4** were identified by spiking the photolyzate with authentic samples, while **6** was identified by comparison of the  $^1H$  and  $^{119}Sn$  NMR spectral data to those previously reported in  $C_6D_{12}$ .<sup>19</sup> The yield of **6** was calculated on a per- $SnMe_2$  basis, but is plotted in Figure 5.6a as straight concentration. An additional unidentified organotin compound is formed ( $\delta_H$  1.07, 1.30;  $\delta_{Sn}$  -90.3) but disappears upon standing after two days. The formation of **2**, **3** and **6** as the major photoproducts is consistent with the extrusion of  $SnMe_2$  from **1** in the presence of  $Me_2SnCl_2$  in air saturated solution, based on the products obtained from previous studies of  $SnPh_2$ .<sup>19</sup>

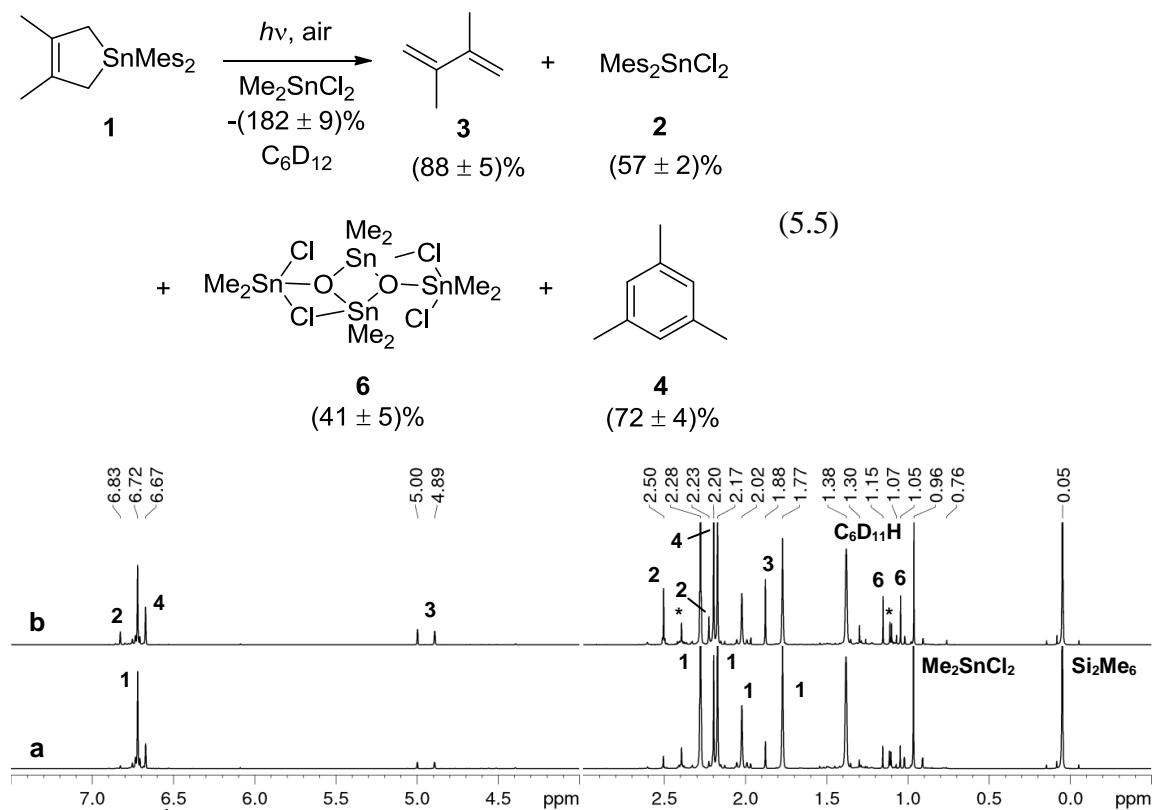
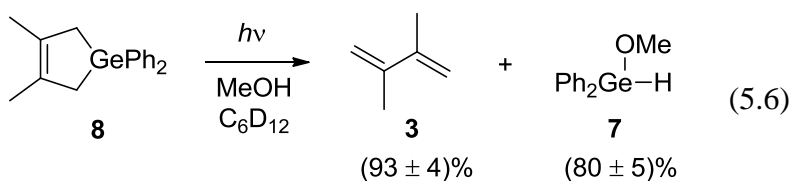


**Figure 5.5.**  $^1\text{H}$  NMR spectra of a 0.045 M solution of **1** in  $\text{C}_6\text{D}_{12}$  containing  $\text{Me}_2\text{SnCl}_2$  (0.035 M) (a) before and (b) after 10 minutes photolysis with 254 nm UV light (\*Unreactive impurity) (Samples prepared by J. Woodard)

Both the  $^1\text{H}$  and  $^{119}\text{Sn}$  spectra indicate the photolysis products are present in the sample prior to irradiation, presumably due to a "dark" reaction. Indeed, the  $^1\text{H}$  NMR spectrum of an identical solution that was kept in the dark for the duration of the photolysis (ca. 4 hours) revealed the consumption of stannacyclopent-3-ene **1** and  $\text{Me}_2\text{SnCl}_2$  in an approximately 1:1 concentration ratio, and the formation of **3**, **4**, **2**, and **6** in concentration ratios of (1):(2):(0.02):(0.2). The very small quantity of **2** that is produced in the absence of light suggests its formation in the photochemical experiment originates solely from irradiation of the solution. In absolute terms, a total of ca. 2.7 mM of **3**, ca. 5.8 mM of **4**, and ca. 0.5 mM of **6** were produced in the dark reaction during the ca. 4 hours. By comparison, a total of ca. 7.5 mM of **3**, ca. 6.3 mM of **4**, and ca. 1.8 mM

of **6** were produced after 10 minutes of photolysis, in addition to ca. 4.3 mM of  $\text{Mes}_2\text{SnCl}_2$  (**2**). The absolute values were calculated from the concentration differences for the respective products between 0 and 10 minutes of photolysis (or during the equivalent amount of time in the dark reaction). It can be concluded from this that a direct (dark) reaction between **1** and  $\text{Me}_2\text{SnCl}_2$  is the exclusive source of **4** during photolysis, and to a lesser extent to the yields of **3** and **6**.

The quantum yield for the formation of **2** from photolysis of an air-saturated solution of **1** in  $\text{C}_6\text{D}_{12}$  containing  $\text{Me}_2\text{SnCl}_2$  (0.04 M) was determined using the formation of methoxydiphenylgermane (**7**) from parallel photolysis of 3,4-dimethyl-1,1-diphenylgermacyclopent-3-ene (**8**; 0.04 M) in deoxygenated  $\text{C}_6\text{D}_{12}$  containing methanol (0.04 M) as the actinometer ( $\Phi_{\text{GePh}_2} = 0.55 \pm 0.07$ ) (eq. 5.6).<sup>10</sup> A value of  $\Phi_{\text{SnMes}_2} = 0.36 \pm 0.05$  was determined from the relative slopes of the concentration versus time plots for **2** and **7** over the first 5 minutes of photolysis (Fig. 5.6). Compound **2** was selected for the quantum yield determination because its formation appears to be derived exclusively from a photochemical route (*vide supra*).



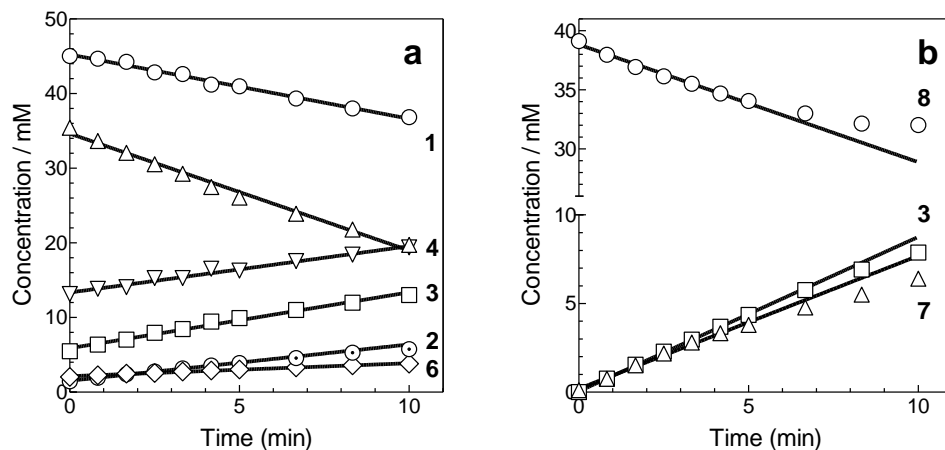


**Figure 5.6.** (a) Concentration versus time plots for the photolysis of a solution of **1** (ca. 0.045 M) and  $\text{Me}_2\text{SnCl}_2$  (ca. 0.035 M) in  $\text{C}_6\text{D}_{12}$  as described in eq. 5.5. The slope of each of the plots is (in units of  $\text{mM min}^{-1}$ )  $\text{Me}_2\text{SnCl}_2$ ,  $-1.57 \pm 0.06$  ( $\Delta$ ); **1**,  $-0.86 \pm 0.05$  ( $\circ$ ); **3**,  $0.75 \pm 0.03$  ( $\square$ ); **2**,  $0.49 \pm 0.01$  ( $\odot$ ); **6**,  $0.17 \pm 0.01$  ( $\diamond$ ); **4**,  $0.62 \pm 0.03$  ( $\nabla$ ). The slope for **2** was determined using the first seven data points. (b) Concentration versus time plots for the photolysis of a solution of **8** (ca. 0.04 M) and  $\text{MeOH}$  (ca. 0.04 M) in  $\text{C}_6\text{D}_{12}$  as described in eq. 5.6. The initial slopes, determined from the first seven data points in each of the plots, are (in units of  $\text{mM min}^{-1}$ ) **8**,  $-1.00 \pm 0.05$  ( $\circ$ ); **3**,  $0.87 \pm 0.01$  ( $\square$ ); **7**,  $0.75 \pm 0.03$  ( $\Delta$ ). (Samples prepared by J. Woodard)

### 5.2.2. Laser Flash Photolysis Experiments

Laser flash photolysis experiments were performed using excitation from a 248 nm KrF excimer laser (98-100 mJ, ca. 25 ns) and continuously flowing argon-saturated solutions of **1** (ca.  $2 \times 10^{-5}$  M) in anhydrous hexanes. Transient UV-vis absorption spectra recorded over the 270 - 650 nm wavelength range at selected time intervals after excitation are shown in Figure 5.7. The first absorption spectrum (recorded 0.16 - 0.32  $\mu\text{s}$  after the laser pulse) reveals the prompt formation of a transient species exhibiting maxima at  $\lambda_{\text{max}} < 270$ ,  $\sim 330$ (sh), and 550 nm. This promptly-formed species decays with clean second order decay kinetics and rate coefficient  $2k_{\text{decay}}/\epsilon_{570\text{nm}} = (7.5 \pm 2.7) \times 10^6$   $\text{cm s}^{-1}$  (monitored at 570 nm to minimize spectral overlap); the promptly formed transient species is assigned to  $\text{SnMes}_2$ . According to the spectrum of Fig 5.7 and Fig S5.8f,  $\epsilon_{570\text{nm}} \sim 0.8\epsilon_{\lambda_{\text{max}}}$  and, provided the extinction coefficient does not differ substantially from those

previously reported for diarylstannylenes in solution -  $\text{SnPh}_2$  ( $\epsilon_{\lambda_{\text{max}}} = 2500 \text{ M}^{-1} \text{ cm}^{-1}$ ),<sup>19</sup>  $\text{SnArPh}$  ( $\text{Ar} = \text{C}_6\text{H}_3\text{-2,6-(C}_6\text{H}_2\text{-2,4,6-}i\text{-Pr}_3)_2$ ;  $\epsilon_{\lambda_{\text{max}}} = 1660 \text{ M}^{-1} \text{ cm}^{-1}$ ),<sup>20</sup> and  $\text{SnAr}'_2$  ( $\text{Ar}' = \text{C}_6\text{H}_3\text{-2,6-(C}_6\text{H}_3\text{-2,6-}i\text{-Pr}_2)_2$ ;  $\epsilon_{\lambda_{\text{max}}} = 1430 \text{ M}^{-1} \text{ cm}^{-1}$ )<sup>21</sup> - an estimate of  $\epsilon_{\lambda_{\text{max}}} \sim 2 \times 10^3 \text{ M}^{-1} \text{ cm}^{-1}$  (and hence  $\epsilon_{570\text{nm}} \sim 1.6 \times 10^3 \text{ M}^{-1} \text{ cm}^{-1}$ ) affords a dimerization rate constant  $k_{\text{dim}} \sim 6 \times 10^9 \text{ M}^{-1} \text{ s}^{-1}$ , which indicates that the dimerization of  $\text{SnMes}_2$  proceeds with a rate constant within a factor of ca. 4 of the diffusional rate constant in hexanes solution at 25 °C ( $k_{\text{diff}} = 2.2 \times 10^{10} \text{ M}^{-1} \text{ s}^{-1}$ ).<sup>22</sup> A second transient absorption spectrum recorded at 9.4 - 9.9  $\mu\text{s}$  shows that the initially formed transient is replaced with a second transient species exhibiting absorption maxima at  $\lambda_{\text{max}} = 290$  and 490 nm, which decays with mixed order kinetics and a lifetime of ca. 60  $\mu\text{s}$ ; the second formed species is assigned to tetramesityldistannene ( $\text{Mes}_2\text{Sn}=\text{SnMes}_2$ , **9**) (eq. 5.7). Assuming the dimerization of  $\text{SnMes}_2$  is quantitative, the spectra of Figure 5.7 provides an estimate of  $\epsilon_{490\text{nm}} \sim 6.5 \times 10^3 \text{ M}^{-1} \text{ cm}^{-1}$  for **9**, in agreement with the reported values for other tetraaryldistannenes.<sup>32</sup>

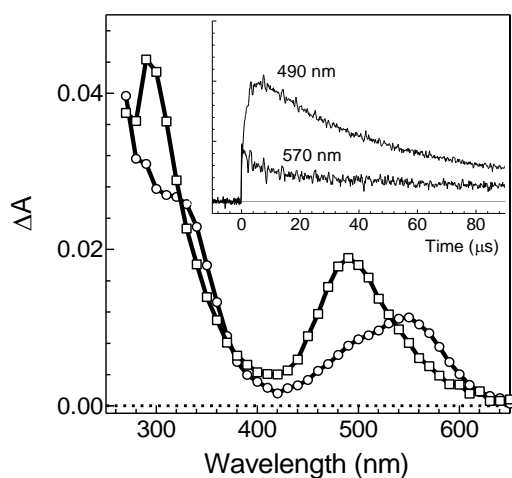
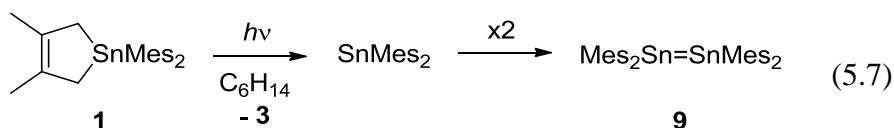


**Figure 5.7.** Time-resolved UV-vis spectra recorded by laser photolysis of  $\text{SnMes}_2$  precursor **1** in hexanes solution, 0.16 - 0.32  $\mu\text{s}$  ( $\circ$ ), and 9.4 - 9.9  $\mu\text{s}$  ( $\square$ ) after the laser pulse (25 °C), and absorbance-time profiles at selected wavelengths (inset).

The reactions of  $\text{SnMes}_2$  with various stannylene substrates in hexanes were investigated by monitoring its absorbance-time profile at 570 nm in order to minimize

spectral overlap with distannene **9**. Most experiments were accompanied by the gradual appearance of repetitive spikes in the absorbance versus time profiles. These result from the accumulation of solid particulate in the sample cells,<sup>23</sup> and care was taken to ensure these did not interfere with the determination of rate and/or equilibrium constants from the data. The first seven substrates investigated behave as simple Lewis bases to produce the corresponding stannylene-donor pairs. They consist of representative examples of ethers and alcohols (diethylether (Et<sub>2</sub>O), tetrahydrofuran (THF) and methanol (MeOH)), sulfides (diethylsulfide (Et<sub>2</sub>S) and tetrahydrothiophene (THT)), and amines (butylamine (BuNH<sub>2</sub>) and diethylamine (Et<sub>2</sub>NH)). Three additional substrates, acetic acid (AcOH), dichlorodimethylstannane (Me<sub>2</sub>SnCl<sub>2</sub>) and molecular oxygen (O<sub>2</sub>), afforded behaviour consistent with irreversible reaction of the stannylene, as recorded in the product studies with these substrates.

Addition of these substrates led to three different types of effects on the stannylene decay profile, depending on the magnitude of the equilibrium constant ( $K_{\text{eq}}$ ) for the reaction between the stannylene and the substrate. Detailed interpretation of these observations has been previously described (see Chapters 2 - 4).<sup>9,12</sup> In the first set of observations, the addition of the substrate (Q) in sub-millimolar concentrations result in an acceleration of the decay of SnMes<sub>2</sub> and a change to first order decay kinetics. Analysis of the decay profiles according to equation 5.8 allows for the determination of the pseudo first-order decay rate coefficients ( $k_{\text{decay}}$ ). A least-squares analysis of  $k_{\text{decay}}$  versus substrate concentration according eq. 5.9 affords the bimolecular rate constant ( $k_{\text{Q}}$ ) for the reaction. Such behaviour is observed in instances wherein the equilibrium constant  $K_{\text{eq}} > 25000 \text{ M}^{-1}$ . The absorbance of SnMes<sub>2</sub> upon equilibrium becomes indistinguishable from its pre-pulse level at the smallest quantity of substrate added.

$$\Delta A_t = \Delta A_{\text{res}} + (\Delta A_0 - \Delta A_{\text{res}}) \exp(-k_{\text{decay}}t) \quad (5.8)$$

$$k_{\text{decay}} = k_{-Q} + k_Q[Q] \quad (5.9)$$

The second and most informative set of observations occurs in instances wherein  $K_{\text{eq}}$  falls within the approximate range  $1000 - 25000 \text{ M}^{-1}$ . In such situations, addition of the reactive substrate results in an acceleration of the stannylene decay, proceeding to a non-zero absorbance  $\Delta A_{\text{res}}$ . Increasing the concentration of substrate further results in the simultaneous increase in  $k_{\text{decay}}$  and decrease in  $\Delta A_{\text{res}}$ ; fitting these response variables with respect to  $[Q]$  according to equations 5.9 and 5.10 respectively affords both  $k_Q$  and  $K_{\text{eq}}$ .

$$(\Delta A_0)_0 / (\Delta A_{\text{res}})_Q = 1 + K_{\text{eq}}[Q] \quad (5.10)$$

In the third set of circumstances, successive addition of the substrate results in a drop in the initial absorbance of the stannylene  $(\Delta A_0)_0$ , unaccompanied by a change in the rate coefficient. This behaviour is observed when  $K_{\text{eq}} < 1000 \text{ M}^{-1}$ , and is consistent with a rapid and reversible reaction between the stannylene and substrate; the approach to equilibrium is unresolved from the excitation by the laser pulse. The equilibrium concentration of the stannylene at a given concentration of substrate is represented by its initial absorbance  $(\Delta A_0)_Q$ . Plotting  $(\Delta A_0)_Q$  as a function of substrate concentration according to equation 5.11 affords the equilibrium constant  $K_{\text{eq}}$ .

$$(\Delta A_0)_0 / (\Delta A_0)_Q = 1 + K_{\text{eq}}[Q] \quad (5.11)$$

Figure 5.8 shows examples of the typical kinetic traces in cases where (a)  $K_{\text{eq}} > 25000 \text{ M}^{-1}$ , (b)  $1000 < K_{\text{eq}} < 25000 \text{ M}^{-1}$  and (c)  $K_{\text{eq}} < 1000 \text{ M}^{-1}$ .

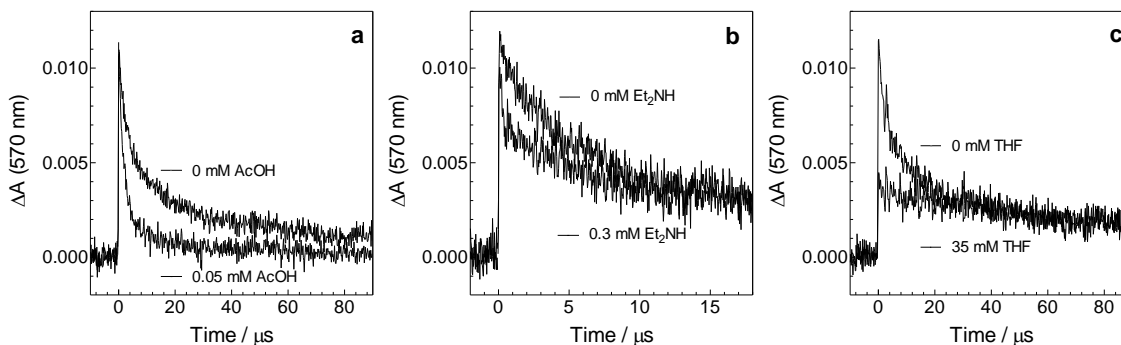


**Figure 5.8.** Representative transient decay profiles recorded at 570 nm from a hexanes solution of **1** containing (a) 0 and 0.05 mM AcOH, (b) 0 and 0.3 mM Et<sub>2</sub>NH, and (c) 0 and 35 mM THF. (Data recorded by J. Woodard)

Analysis of the ten stannylene substrates in this manner allow the determination of six rate constants and six equilibrium constants; these are summarized in Table 5.1, along with the UV-vis absorption maxima of the transient products formed in the presence of substrate, where applicable. The linear plots are shown in Figures S5.6a-c, and S5.7a,b,d,e.

**Table 5.1.** Absolute Rate and Equilibrium Constants ( $k_Q$  and  $K_{eq}$ ) for the Reactions of  $\text{SnMes}_2$  with Various Stannylene Substrates in Hexanes Solution at 25 °C and Long-Wavelength Absorption Maxima ( $\lambda_{max}$ ) of the Observed New Transient Absorptions.

Substrate (Q)	$k_Q$ ( $10^9 \text{ M}^{-1} \text{ s}^{-1}$ ) <sup>a</sup>	$[K_{eq} (\text{M}^{-1})]$ <sup>a</sup>	$\lambda_{max}$ (nm)
none	$\sim 6 \pm 1$ <sup>b</sup>	d	320(sh), 550
Et <sub>2</sub> O	c	$[1.8 \pm 0.1]$ <sup>f</sup>	360
THF	c	$[35 \pm 4]$ <sup>f</sup>	~380
MeOH	c	$[90 \pm 10]$ <sup>f</sup>	360
Et <sub>2</sub> S	c	$[370 \pm 40]$ <sup>f</sup>	370(sh) <sup>f</sup>
THT	$17 \pm 5$ <sup>f</sup>	$[2900 \pm 400]$ <sup>f</sup>	385 <sup>f</sup>
BuNH <sub>2</sub>	$9 \pm 1$ <sup>f</sup>	d	355 <sup>f</sup>
Et <sub>2</sub> NH	$6 \pm 2$ <sup>f</sup>	$[2200 \pm 400]$ <sup>f</sup>	350(sh) <sup>f</sup>
AcOH	$4.3 \pm 0.5$ <sup>f</sup>	d	330 <sup>f</sup>
Me <sub>2</sub> SnCl <sub>2</sub>	$1.7 \pm 0.1$ <sup>f</sup>	d	e
O <sub>2</sub>	$0.0056 \pm 0.0006$ <sup>f</sup>	d	e

<sup>a</sup>Errors are quoted as twice the standard error from the linear least-squares analysis of the data according to equations 5.9 - 5.11; <sup>b</sup>assuming  $\epsilon_{570} \sim 1.6 \times 10^3 \text{ M}^{-1} \text{ cm}^{-1}$ ; <sup>c</sup> $k_Q$  indeterminable; <sup>d</sup> $K_{eq} > 25000 \text{ M}^{-1}$ ; <sup>e</sup>No new transient absorptions produced over 300 - 650 nm range; <sup>f</sup>(Data recorded by J. Woodard)



The reactions between SnMes<sub>2</sub> and the Lewis bases all result in the formation of new transient products exhibiting absorption bands in the 270 - 390 nm region of the UV-vis spectrum, as shown in Figure 5.9 for BuNH<sub>2</sub>, and THT, and in Figures S5.6d-f, and S5.7c,f for the others. The new absorptions are assigned in each instance to the corresponding Mes<sub>2</sub>Sn-donor Lewis acid-base complexes (eq. 5.12). Transient absorption spectra were recorded using sufficiently high concentrations of Lewis base so as to render the stannylene absorptions undetectable or nearly so. The complexes all decay with mixed order kinetics and apparent lifetimes of  $\tau \sim 80\text{-}100 \mu\text{s}$ , with the S- and N- donor complexes exhibiting slower decays.

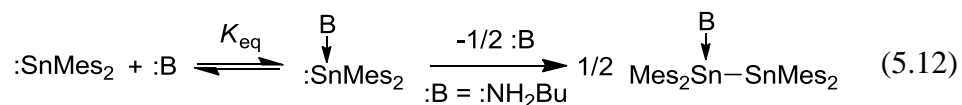
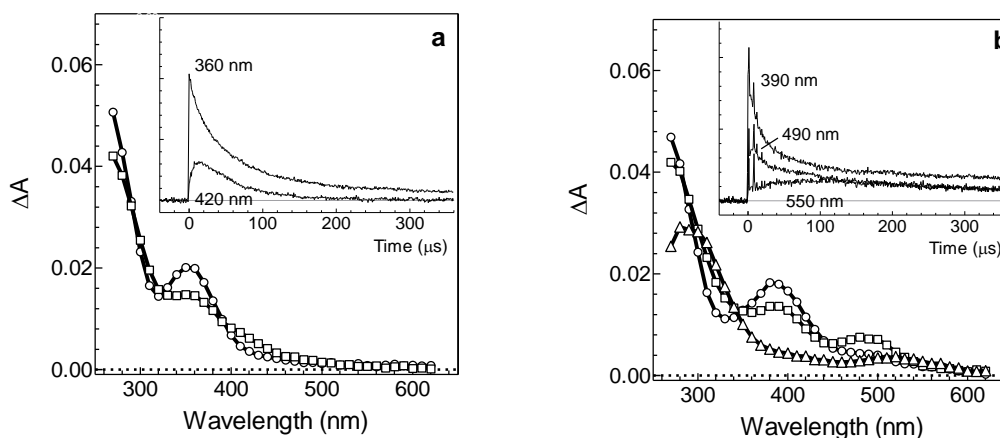


Figure 5.9a shows time-resolved UV-vis absorption spectra of a solution of **1** containing 5.0 mM BuNH<sub>2</sub> recorded 0 - 2.6  $\mu\text{s}$ , and 12.2 - 12.7  $\mu\text{s}$  after excitation. The earlier spectrum indicates that the transient absorption bands attributed to SnMes<sub>2</sub> and **9** have disappeared and have been replaced with a new transient product exhibiting  $\lambda_{\text{max}} < 270$ , 355 nm, which is assigned to the Mes<sub>2</sub>Sn-NH<sub>2</sub>Bu Lewis pair (**10**). Complex **10** decays with mixed order kinetics, concurrent with the formation and disappearance of a new transient product exhibiting a broad absorption from 350 - 450 nm. The temporal behaviour of this new species bears resemblance to the transient products formed from the decay of the SnMe<sub>2</sub> and SnPh<sub>2</sub> complexes with BuNH<sub>2</sub> (see Chapter 4), and is thus assigned tentatively to the amine stabilized stannylene dimer BuH<sub>2</sub>N<sup>(+)</sup>-SnMes<sub>2</sub>-Sn<sup>(-)</sup>Mes<sub>2</sub> (eq. 5.12).

Similarly, transient absorption spectra recorded with a solution of **1** in hexane containing 5.0 mM THT immediately after the laser pulse shows an absorption band assignable to the Mes<sub>2</sub>Sn-THT complex (**11**) at  $\lambda_{\text{max}} < 270$ , 385 nm (Figure 5.9b). Its

disappearance proceeds with mixed order kinetics ( $\tau \sim 100 \mu\text{s}$ ) and is concurrent with the growth and decay of **9** as well as a new, very weak transient at ca. 530 nm that appears over a longer timescale, reaching a maximum ca. 100  $\mu\text{s}$  after the laser pulse before slowly diminishing over the maximum time interval (ca. 360  $\mu\text{s}$ ). While we were not able to conclusively identify this new transient, its growth profile suggests that its appearance coincides with the decay of **9** or **11**, and is not a residual signal from **9** or  $\text{SnMes}_2$  despite appearing in the same spectral region.



**Figure 5.9.** (a) Time-resolved UV-vis spectra from laser photolysis of **1** in hexanes containing 5.0 mM  $\text{BuNH}_2$ , 0.0-2.6  $\mu\text{s}$  ( $\circ$ ), and 12.2-12.7  $\mu\text{s}$  ( $\square$ ) after the laser pulse (25  $^\circ\text{C}$ ), and absorbance-time profiles at selected wavelengths (inset). (b) Time-resolved UV-vis spectra from laser photolysis of **1** in hexanes containing 5.0 mM THT, 0.0 - 0.64  $\mu\text{s}$  ( $\circ$ ), 5.8 - 7.0  $\mu\text{s}$  ( $\square$ ), and 111 - 113  $\mu\text{s}$  ( $\triangle$ ) after the laser pulse (25  $^\circ\text{C}$ ), and absorbance-time profiles at selected wavelengths (inset). (Data recorded by J. Woodard)

Addition of  $\text{Me}_2\text{SnCl}_2$ ,  $\text{AcOH}$  and  $\text{O}_2$  led to acceleration of the stannylene decay and a change to first order decay kinetics, in a manner consistent with reactions characterized by an equilibrium constant in excess of ca.  $3 \times 10^4 \text{ M}^{-1}$ . Bimolecular rate constants ( $k_Q$ ) were thus determined from plots of  $k_{\text{decay}}$  versus  $[\text{Q}]$  according to equation 5.9 (Figure S5.8a-c). Transient absorption spectra recorded of a solution of **1** in the presence of 0.3 mM  $\text{AcOH}$  indicate that the reaction with  $\text{SnMes}_2$  results in the formation of a new transient product with  $\lambda_{\text{max}} < 270, 330 \text{ nm}$  (Figure S5.8d). No new transient

products could be detected in spectra recorded in the presence of 1.0 mM  $\text{Me}_2\text{SnCl}_2$  (Fig S5.8e) or 14.7 mM  $\text{O}_2$  (Fig S5.8f), on the other hand.

By monitoring the absorbance-time profile at 490 nm, changes in the temporal behaviour of distannene **9** that are caused by the addition of the stannylene substrates could also be assessed. The transient absorption from  $\text{SnMes}_2$  provides only a minor (ca. 10 %) contribution to the overall signal at 490 nm, assuming the long wavelength absorption band for  $\text{SnMes}_2$  is symmetric about the maximum. In the presence of the ethers, sulfides and amines, a reduction in the maximum yield of **9** is observed in proportion to the concentration of added substrate, but there are no changes observed in its decay lifetime. This suggests the substrates do not react with **9**, but reduce its yield through a reaction with  $\text{SnMes}_2$ . On the other hand, addition of  $\text{O}_2$ ,  $\text{Me}_2\text{SnCl}_2$ ,  $\text{MeOH}$ , and  $\text{AcOH}$  was accompanied by both a drop in the maximum signal intensity at 490 nm, and acceleration of the rate coefficient for decay ( $k_{\text{decay}}$ ). With  $\text{O}_2$  a bimolecular rate constant was determined by fitting the decay portion of the absorbance-time profiles for **9** and analyzing the  $k_{\text{decay}}$  versus  $[\text{Q}]$  data as single exponential decays (Figure 5.10a) according to equations 5.8 and 5.9. This analysis affords  $k_{\text{Q}} = (5.3 \pm 0.3) \times 10^6 \text{ M}^{-1} \text{ s}^{-1}$  (Figure 5.10b). The analogous  $k_{\text{decay}}$  versus  $[\text{Q}]$  plots for the reactions of  $\text{MeOH}$ ,  $\text{AcOH}$ , and  $\text{Me}_2\text{SnCl}_2$  are shown in Figure S5.9, and afford values of  $k_{\text{MeOH}} = (2.6 \pm 0.4) \times 10^6 \text{ M}^{-1} \text{ s}^{-1}$ ,  $k_{\text{AcOH}} = (7 \pm 2) \times 10^8 \text{ M}^{-1} \text{ s}^{-1}$ , and  $k_{\text{Me}_2\text{SnCl}_2} = (3.4 \pm 0.4) \times 10^8 \text{ M}^{-1} \text{ s}^{-1}$ , respectively. The  $k_{\text{Q}}$  values for  $\text{AcOH}$  and  $\text{Me}_2\text{SnCl}_2$  are derived from data over the initial concentration range ( $< 0.2 \text{ mM}$  and  $\leq 0.5 \text{ mM}$ , respectively) where the yields of **9** were not substantially reduced compared to that in the absence of substrate.

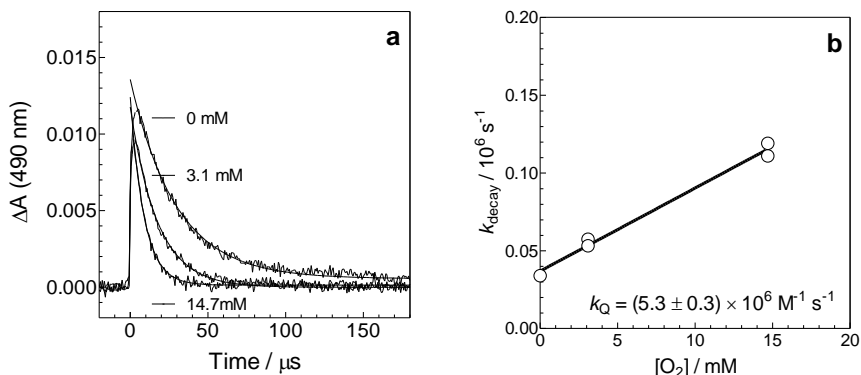


**Figure 5.10.** (a) Representative transient decay profiles recorded at 490 nm from a hexanes solution of **1** containing 0.0 mM, 3.1 mM, and 14.7 mM  $\text{O}_2$ . (b) Plot of  $k_{\text{decay}}$  for the reaction of **9** with  $\text{O}_2$  in hexanes at 25 °C; the solid line is the linear least squares fit of the data to equation 5.9. (Data recorded by J. Woodard)

### 5.3. Discussion

Laser flash photolysis of **1** in hexanes solution leads to the prompt formation of new transient absorption bands assignable to the transient stannylene,  $\text{SnMes}_2$ . Among them, the long wavelength absorption band centred at  $\lambda_{\text{max}} = 550 \text{ nm}$  (assigned to the n-p transition) is the most diagnostic and provides insight into the electronic structure of the stannylene.<sup>4</sup> The absorption maximum is comparable to that reported for  $\text{Tbt}(\text{Mes})\text{Sn}$  ( $\text{Tbt} = \text{C}_6\text{H}_2\text{-}2,4,6\text{-(CH}(\text{SiMe}_3)_2)_3$  at ( $\lambda_{\text{max}} = 527 \text{ nm}$ )<sup>24</sup> as well as those of other kinetically stabilized diarylstannylenes that have been reported in solution (refer to Table 1.1 for a list of  $\lambda_{\text{max}}$  values for kinetically stabilized diarylstannylenes).<sup>4,24-26</sup> It also compares well with the results of TDDFT calculations, which predict  $\lambda_{\text{max}} = 540 \text{ nm}$  for the lowest energy band in the electronic spectrum of the molecule at the TD $\omega$ B97XD/def2-TZVP// $\omega$ B97XD/def2-SVP level of theory.

The lowest energy absorption band for  $\text{SnMes}_2$  is red-shifted ca. 45 nm (0.20 eV) relative to that of the parent derivative  $\text{SnPh}_2$ .<sup>19</sup> The red-shift in the absorption maximum can be attributed to the increase in the twist angle of the aryl groups, which decreases the

degree of conjugation between the aromatic group and the vacant 5p orbital on Sn.<sup>4</sup> Larger red-shifts are observed with the homologous diarylsilylene and germylene derivatives (i.e.  $\text{MMes}_2$  and  $\text{MPh}_2$  ( $\text{M} = \text{Si}, \text{Ge}$ )); these systems exhibit shifts of  $\Delta\lambda_{\text{max}} = 65 \text{ nm}^5$  (0.29 eV) and  $60 \text{ nm}^{10}$  (0.27 eV), respectively. Comparison of  $\text{SnMes}_2$  with its lighter Si and Ge homologs ( $\text{SiMes}_2$  ( $\lambda_{\text{max}} = 580 \text{ nm}^{27}$ ) and  $\text{GeMes}_2$  ( $\lambda_{\text{max}} = 560 \text{ nm}^{10}$ )) reveal a consecutive blue-shift with increase in atomic number of the group 14 element. The trend of decreasing  $\lambda_{\text{max}}$  is attributed to the relative decrease in twist angle of the aryl groups. This coincides with the increase in M-C ( $\text{M} = \text{Si}, \text{Ge}, \text{Sn}$ ) bond length when increasing the size of the group 14 element in the  $\text{MMes}_2$  series, which in turn increases the degree of conjugation between the aromatic group and the vacant  $np$  orbital on the metal centre. The trend of decreasing  $\lambda_{\text{max}}$  has also been observed with other kinetically stabilized diaryltetraylenes (i.e. with  $\text{Ge} > \text{Sn} > \text{Pb}$ ).<sup>4</sup> In contrast, consecutive red-shifts in  $\lambda_{\text{max}}$  with increasing group 14 element ( $\text{Si} < \text{Ge} < \text{Sn}$ ) are observed<sup>28</sup> with the dialkyltetraylenes series  $\text{MMe}_2$  ( $\text{Si}, \text{Ge},$  and  $\text{Sn}$ ) and  $\text{MR}_2$  (**12** - **14**; see eq. 5.13), as summarized in Table 5.2.

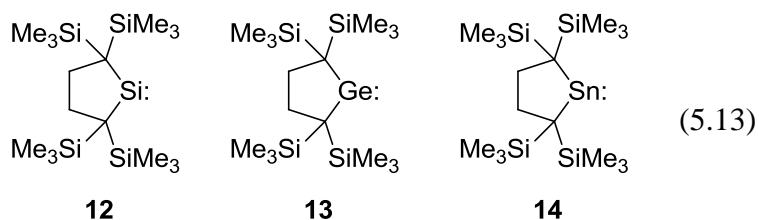


**Table 5.2.** Long Wavelength Absorption Maxima ( $\lambda_{\text{max}}$  (nm and eV)) of Tetrylenes  $\text{MR}_2$  (M = Si, Ge, Sn; R = Mes, Ph, Me,  $-(\text{Me}_3\text{Si})_2\text{C}(\text{CH}_2)_2\text{C}(\text{SiMe}_3)_2-$ ).<sup>a</sup>

$\text{MR}_2$	$\lambda_{\text{max}}$ (nm)	$\lambda_{\text{max}}$ (eV)	ref
SiMes <sub>2</sub>	580	2.14	27
GeMes <sub>2</sub>	560	2.21	11
SnMes <sub>2</sub>	550	2.25	this work
SiPh <sub>2</sub>	515	2.41	5
GePh <sub>2</sub>	500	2.48	10
SnPh <sub>2</sub>	505	2.46	19
SiMe <sub>2</sub>	465	2.67	29
GeMe <sub>2</sub>	470	2.64	10
SnMe <sub>2</sub>	500	2.48	30
<b>12</b>	440	2.82	28
<b>13</b>	450	2.76	28
<b>14</b>	486	2.55	28

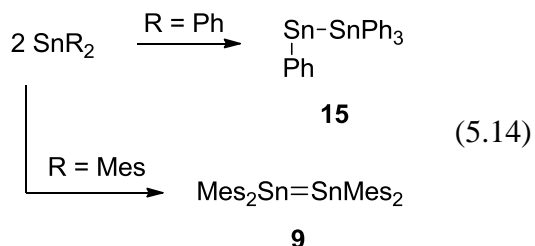
<sup>a</sup>UV-vis absorption spectra recorded in hexanes solution at room temperature

The absorbance-time profile at 570 nm indicates the stannylene decays with clean second order kinetics in the absence of substrates, and with an estimated rate constant of  $k_{\text{dim}} \sim 6 \times 10^9 \text{ M}^{-1} \text{ s}^{-1}$ , assuming a value of  $\epsilon_{570\text{nm}} \sim 1.6 \times 10^3 \text{ M}^{-1} \text{ cm}^{-1}$  at the monitoring wavelength. Such behaviour is consistent with those observed for SnMe<sub>2</sub> and SnPh<sub>2</sub> in solution,<sup>19</sup> and of SiMes<sub>2</sub><sup>27</sup> and GeMes<sub>2</sub>,<sup>10</sup> and indicates the dimerization of SnMes<sub>2</sub> proceeds with a minimal kinetic barrier. The disappearance of SnMes<sub>2</sub> is accompanied by the formation of Mes<sub>2</sub>Sn=SnMes<sub>2</sub> (**9**), which is characterized by absorption maxima centred at  $\lambda_{\text{max}} = 290, 490 \text{ nm}$ . The position of the long wavelength absorption band is in

good agreement with the results of TDDFT calculations, which predict a value of  $\lambda_{\max} = 502$  nm (performed at the (TD)ωB97XD/def2-TZVP//ωB97XD/def2-SVP level of theory). It also agrees well with the spectra of other carbon substituted acyclic distannenes that have been reported in solution:  $\text{Tip}_2\text{Sn}=\text{SnTip}_2$  (Tip =  $\text{C}_6\text{H}_2$ -2,4,6-*i*-Pr<sub>3</sub>),  $\lambda_{\max} = 494$  nm<sup>31</sup> and  $\text{Me}_2\text{Sn}=\text{SnMe}_2$ ,  $\lambda_{\max} = 465$  nm.<sup>30</sup> Cyclic<sup>32,33</sup> and/or silicon<sup>34-36</sup> substituted distannene derivatives that have been reported more recently exhibit long wavelength absorption bands in the 572 - 670 nm region. The spectrum of the distannene is also red-shifted compared to its disilene ( $\lambda_{\max} = 410$  nm<sup>13</sup>) and digermene ( $\lambda_{\max} = 420$  nm<sup>11</sup>) homologs. Similar red-shifts in  $\lambda_{\max}$  are observed for the  $\text{Tip}_2\text{M}=\text{MTip}_2$  (M = Si (432 nm)<sup>37</sup>, Ge (416 nm),<sup>38</sup> Sn (494 nm)<sup>31</sup>) and (*t*-Bu<sub>2</sub>MeSi)<sub>2</sub>M=M(SiMe*t*-Bu<sub>2</sub>)<sub>2</sub> (M = Si (612 nm)<sup>39</sup>, Ge (618 nm),<sup>40</sup> Sn (670 nm)<sup>34</sup>) series of ditetrelenes. Our results suggest **9** is a relatively short-lived species in hydrocarbon solution at ambient temperature, which is consistent with the observations of Tilley and coworkers, who attributed the formation of 3-, 4- and 5- membered cyclic oligostannanes (Mes<sub>2</sub>Sn)<sub>n</sub> to the final products of free SnMes<sub>2</sub> oligomerization in benzene-*d*<sub>6</sub> at 25 °C.<sup>18</sup> The transient nature of **9** suggests that the mesityl substituent provides insufficient steric protection to prevent further oligomerization of the molecule, unlike the Si and Ge homologues,<sup>14,15</sup> which are both isolable at room temperature under appropriate conditions.<sup>77,79</sup>

The formation of **9** also suggests a different oligomerization pathway for SnMes<sub>2</sub> compared to the parent diarylstannylene SnPh<sub>2</sub> (eq. 5.14). We have previously reported that the dimerization of SnPh<sub>2</sub> in solution at 25 °C does not afford tetraphenyldistannene (Ph<sub>2</sub>Sn=SnPh<sub>2</sub>) in detectable amounts, but rather the stannylstannylene, Ph<sub>3</sub>SnSnPh (**15**) instead.<sup>19</sup> The formation of the rearranged dimer is supported by the results of theoretical calculations of the Sn<sub>2</sub>Ph<sub>4</sub> potential energy surface.<sup>19</sup> The dimerization of SnMes<sub>2</sub>

proceeds at a rate ca. 2-3 times slower than that of SnPh<sub>2</sub>, indicating that dimerization is only slightly influenced by mesityl for phenyl substitution.



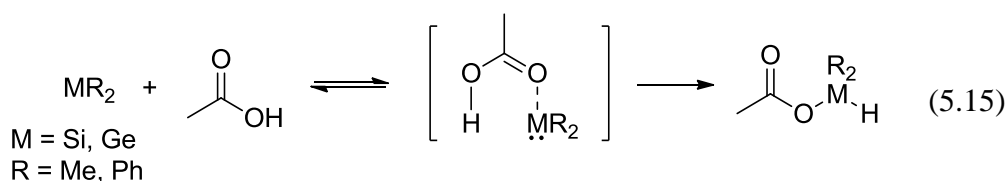
The reaction of SnAr<sub>2</sub> (Ar = C<sub>6</sub>H<sub>2</sub>-2,4,6-(CF<sub>3</sub>)<sub>3</sub>; **16**) and O<sub>2</sub> has been shown to afford the cyclic tristannoxane (Ar<sub>2</sub>SnO)<sub>3</sub> in toluene solution,<sup>41</sup> while the Lappert dialkylstannylene SnR<sub>2</sub> (R = CH(SiMe<sub>3</sub>)<sub>2</sub>) was reported to afford a compound (R<sub>2</sub>SnO)<sub>n</sub> of undetermined structure.<sup>42</sup> The reaction kinetics of O<sub>2</sub> with SnMe<sub>2</sub> was investigated in the gas phase, but the rate constant could not be determined.<sup>43</sup> Determination of *k*<sub>Q</sub> for the reaction of SnMes<sub>2</sub> and O<sub>2</sub> was accomplished by monitoring the stannylene decay in dried argon, air and O<sub>2</sub> saturated hexanes solutions ([O<sub>2</sub>] = 0, 3.1, and 14.7 mM, respectively<sup>22</sup>), affording a bimolecular rate constant *k*<sub>Q</sub> = (5.6 ± 0.6) × 10<sup>6</sup> M<sup>-1</sup> s<sup>-1</sup> (Figure S5.8c). The value is similar to the value reported for GeMes<sub>2</sub> (*k*<sub>O<sub>2</sub></sub> = (7.3 ± 0.8) × 10<sup>6</sup> M<sup>-1</sup> s<sup>-1</sup>),<sup>11</sup> and roughly 6 times smaller than that reported for the silicon homologue (*k*<sub>O<sub>2</sub></sub> = (3.2 ± 0.4) × 10<sup>7</sup> M<sup>-1</sup> s<sup>-1</sup>),<sup>27</sup> suggesting a reactivity order of SiMes<sub>2</sub> > GeMes<sub>2</sub> ~ SnMes<sub>2</sub>. Transient absorption spectra recorded in O<sub>2</sub>-saturated solution do not show any new transient products absorbing in the 270 - 620 nm region of the UV-vis spectrum (Figure S5.8f).

The results of product studies experiments for **1** in air saturated C<sub>6</sub>D<sub>12</sub> solution indicate that diene **3** and cyclic tristannoxane **5** are the major products under these conditions and they are formed in equal chemical yields, suggesting the formation of **5** is derived from the extrusion of SnMes<sub>2</sub>. Compound **5** could also conceivably be generated from the oxidation of distannene **9** or higher oligomers (SnMes<sub>2</sub>)<sub>n</sub> based on the reactions of analogous organotin compounds with O<sub>2</sub> in solution.<sup>44,45</sup> However, the finding that



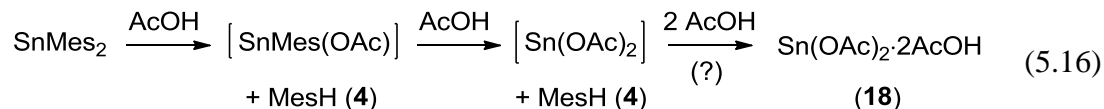
$\text{SnMes}_2$  reacts with  $\text{O}_2$  in flash photolysis experiments, coupled with the much lower steady state concentration of  $\text{SnMes}_2$  that characterizes lamp compared to laser-photolysis experiments (which will reduce the rate of dimerization compared to a pseudo-first order reaction with a substrate), make it most likely that product **5** is derived from reaction of monomeric  $\text{SnMes}_2$  with  $\text{O}_2$ .

The mechanisms for the reactions of transient silylenes and germylenes with acetic acid have been investigated in some detail; the reaction is thought to proceed via a two step complexation-H-migration mechanism, the latter via a 6 membered transition state,<sup>46</sup> to afford the corresponding acetoxysilane<sup>6</sup> or acetoxygermane (eq. 5.15).<sup>10,47</sup>

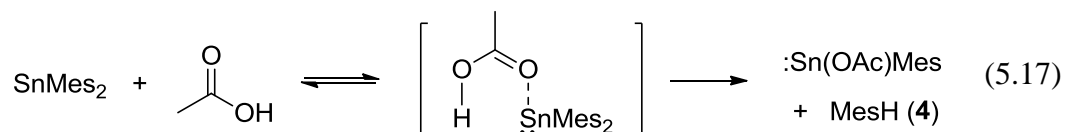


The results of product studies experiments of 1,1-diphenylstannacyclopent-3-ene (**17**) indicate the reaction of  $\text{SnPh}_2$  and  $\text{AcOH}$  affords benzene in quantitative yield (see Chapter 3). The formation of benzene in this reaction is analogous to the arene substitution found with diarylstannylenes and  $\text{H}_2\text{O}$  or  $\text{MeOH}$ .<sup>48</sup> Likewise, the results of steady state photolysis of **1** in the presence of acetic acid indicate that the formation of mesitylene (**4**) proceeds in approximately twice the yield of diene **3**, consistent with the reaction of  $\text{SnMes}_2$  and  $\text{AcOH}$  ultimately producing *two* equivalents of **4**, presumably one equivalent at a time. Diarylstannylenes that undergo consecutive substitution of their arene groups have been reported on two separate occasions, in the reactions of **16** with *t*- $\text{BuOH}$ <sup>49</sup> and of  $\text{SnAr}'_2$  ( $\text{Ar}' = \text{C}_6\text{H}_2\text{-2,6-(CF}_3)_2$ ) with *p*-toluenethiol.<sup>1</sup> Presumably, the reaction with  $\text{SnMes}_2$  also produces  $\text{Sn(II)}$  acetate (eq. 5.16), which would be expected to form the solvated product  $\text{Sn(OAc)}_2 \cdot 2\text{AcOH}$  (**18**) under the conditions of the photolysis experiment.<sup>50</sup> Compound **18** has been described as a white crystalline product (m.p. 295

°C (dec)) that is insoluble in hydrocarbon solvent;<sup>50</sup> this is consistent with the white solid (m.p. > 299 °C) that was isolated in this experiment, although further attempts towards its identification were not performed.

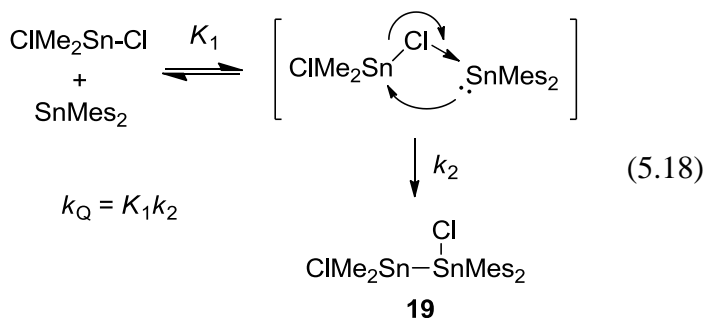


The addition of AcOH in sub-millimolar concentrations to a solution of **1** in laser photolysis experiments results in acceleration of the decay of SnMes<sub>2</sub> and a change to first-order decay kinetics, a plot according to eq. 5.9 affording a bimolecular rate constant  $k_Q = (4.3 \pm 0.5) \times 10^9 \text{ M}^{-1} \text{ s}^{-1}$  (Figure S5.8a). The rate constant is very similar to that measured for SnPh<sub>2</sub> ( $k_Q = (4.2 \pm 0.4) \times 10^9 \text{ M}^{-1} \text{ s}^{-1}$ ; see Chapter 3). Transient absorption spectra recorded in the presence of 0.3 mM AcOH show a new transient product exhibiting an absorption maximum at  $\lambda_{\text{max}} = 330 \text{ nm}$ , which decays with mixed order kinetics and lifetime  $\tau \sim 20 \mu\text{s}$  (Figure S5.8d). The new transient is assigned tentatively to MesSn(OAc), a plausible mechanism for the formation of which is shown in eq. 5.17.

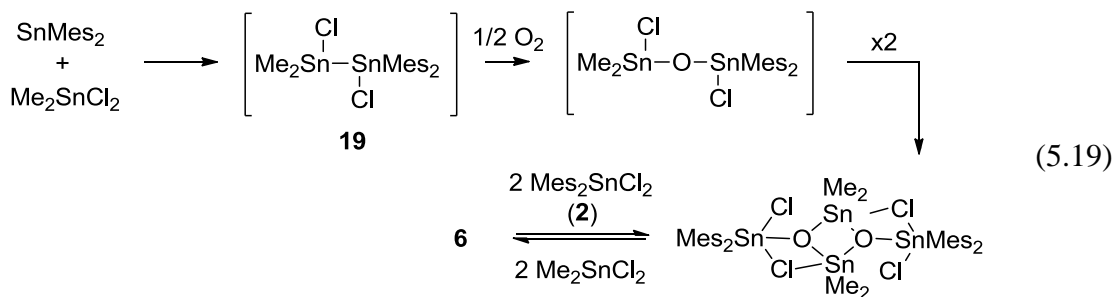


The insertion of SnMe<sub>2</sub> into the Sn-Cl bond of chlorostannanes was originally reported by Neumann and coworkers,<sup>51</sup> while more recently an intramolecularly stabilized diarylstannylene (SnR<sub>2</sub>; R = C<sub>6</sub>H<sub>4</sub>-2-(CH<sub>2</sub>NMe<sub>2</sub>)) has also been reported to undergo the same reaction.<sup>52</sup> Our group has shown that Sn-Cl insertion of SnMe<sub>2</sub> and SnPh<sub>2</sub> with Me<sub>2</sub>SnCl<sub>2</sub> proceeds rapidly, with bimolecular rate constants of  $k_Q = (1.9 \pm 0.3) \times 10^{10} \text{ M}^{-1} \text{ s}^{-1}$  and  $k_Q = (3.6 \pm 0.2) \times 10^9 \text{ M}^{-1} \text{ s}^{-1}$ , respectively (Chapter 2). Product studies experiments carried out for 1,1-diphenylstannacyclopent-3-ene (**17**) and Me<sub>2</sub>SnCl<sub>2</sub> in air saturated C<sub>6</sub>D<sub>12</sub> solution afford the SnPh<sub>2</sub> derived products Ph<sub>2</sub>SnCl<sub>2</sub> and **6**.<sup>19</sup> The reaction of Me<sub>2</sub>SnCl<sub>2</sub> with SnMes<sub>2</sub> also exhibits the characteristics of a rapid and

irreversible process, proceeding without the formation of detectable intermediates (Figure S5.8e), and with rate constant  $k_Q = (1.7 \pm 0.1) \times 10^9 \text{ M}^{-1} \text{ s}^{-1}$  (Figure S5.8b). A reduction in the rate constant is obtained relative to the reaction with  $\text{SnPh}_2$ , i.e.  $k_Q^{\text{SnPh}_2} / k_Q^{\text{SnMes}_2} = 2.1 \pm 0.2$ . The kinetic data is consistent with a two step coordination - insertion mechanism, like that previously proposed for  $\text{SnPh}_2$  (eq. 5.18).<sup>19</sup>



The results of a product study experiment from the photolysis of **1** in an air-saturated  $\text{C}_6\text{D}_{12}$  solution containing  $\text{Me}_2\text{SnCl}_2$  indicate the formation of **2** and **6** as the major tin-containing products. This is consistent with the initial formation of distannane ( $\text{Me}_2\text{ClSnSnClMe}_2$ , **19**) followed by air oxidation and subsequent exchange with  $\text{Me}_2\text{SnCl}_2$  (eq. 5.19). A similar product distribution was obtained from the steady state trapping of  $\text{SnPh}_2$  (see Chapter 2) and  $\text{SnMePh}$  (see Chapter 3), forming **6** and the corresponding dichlorodiorganostannane ( $\text{Ph}_2\text{SnCl}_2$  and  $\text{PhMeSnCl}_2$ , respectively), so it is very likely that the same mechanism is involved in all three instances.<sup>19</sup>



Identification of the photochemically-derived products from photolysis of **1** and  $\text{Me}_2\text{SnCl}_2$  and determination of their yields is made complicated by an apparent dark

reaction of **1** and  $\text{Me}_2\text{SnCl}_2$  (eq. 5.20), which produces some of the same products as are formed in the photochemical reaction. The formation of two equivalents of **4** suggests the presence of a proton source that results in cleavage of the  $\text{Sn-C}_{\text{aryl}}$  bond; the likely culprit is adventitious water, which becomes more acidic as the result of complexation with  $\text{Me}_2\text{SnCl}_2$ .<sup>16</sup> Indeed, **1** was found to be sensitive towards protonolysis to produce **4** when passed through a silica gel column. The formation of **6** in the absence of light may be attributed to the partial hydrolysis of  $\text{Me}_2\text{SnCl}_2$ .<sup>53</sup>

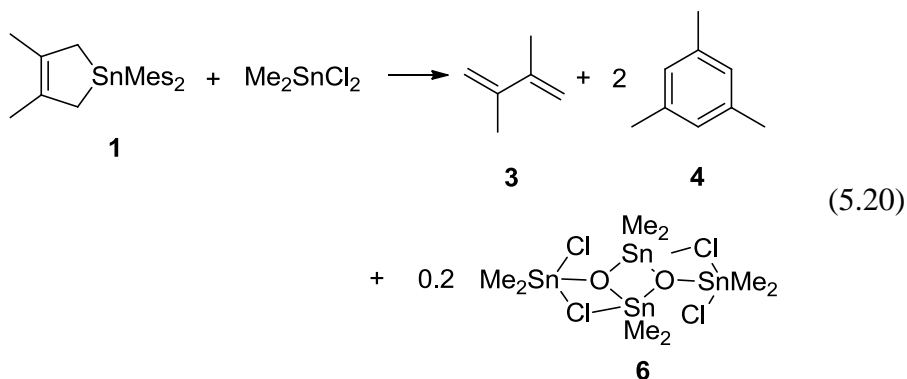


Table 5.3 lists the rate and equilibrium constants for the reactions of  $\text{SnMes}_2$  with the Lewis bases studied in this work, along with those determined previously for  $\text{SnPh}_2$ . Also included in the table are the corresponding values for reactions of  $\text{SiMes}_2$  and  $\text{GeMes}_2$  with the same substrates<sup>7-10,12</sup> to facilitate comparison with the silicon and germanium homologs as well. Comparison of  $K_{\text{eq}}$  for the Lewis acid-base complexation reactions of  $\text{SnMes}_2$  indicate the following order of increasing binding energy:  $\text{Et}_2\text{O} < \text{THF} < \text{MeOH} < \text{Et}_2\text{S} < \text{Et}_2\text{NH} \sim \text{THT} < \text{BuNH}_2$ . Equilibrium constants for complexation were measurable for all these substrates except  $\text{BuNH}_2$ , and correspond to a range in binding free energies of  $-2.8 - 1.5 \text{ kcal mol}^{-1}$ . The O-donor substrates exhibit the least thermodynamically favourable reactions as expected, and are followed by reactions with S and N donors. This includes two comparisons where the substrate differs only by the chalcogen atom, where  $K_{\text{Et}_2\text{S}} / K_{\text{Et}_2\text{O}} = 210 \pm 30$  and  $K_{\text{THT}} / K_{\text{THF}} = 80 \pm 20$ . The finding

that cyclic and acyclic sulfides form stronger complexes than their homologous ethers supports the classification of  $\text{SnMes}_2$  as a soft Lewis acid, similar to the conclusions made for  $\text{SiMes}_2$  and  $\text{GeMes}_2$ .<sup>9</sup> Acyclic ethers and sulfides lead to more weakly-bound complexes than their cyclic derivatives, which may be attributed to entropic effects from the reduced freedom of rotation of the ethyl groups. The complex with the dialkylamine ( $\text{Et}_2\text{NH}$ ) is less stable than the mono-substituted amine  $\text{BuNH}_2$ .

Comparisons between the diarylstannylenes  $\text{SnMes}_2$  and  $\text{SnPh}_2$  reveal a decrease in  $K_{\text{eq}}$  in every instance where comparison is possible. In two instances a quantitative measure is possible, affording values of  $K^{\text{SnPh}_2}/K^{\text{SnMes}_2} = 670 \pm 70$  for  $\text{Et}_2\text{O}$  and  $K^{\text{SnPh}_2}/K^{\text{SnMes}_2} = 80 \pm 10$  for  $\text{MeOH}$ , suggesting a substantial influence in complexation thermodynamics with the mesityl for phenyl substitution. Equilibrium constants for the complexation of O-donor substrates with  $\text{SnPh}_2$  (see Table 5.3), by comparison, increases in the order  $K_{\text{Et}_2\text{O}} < K_{\text{MeOH}} < K_{\text{THF}}$ . The difference in ordering obtained for  $\text{SnMes}_2$  (i.e.  $K_{\text{Et}_2\text{O}} < K_{\text{THF}} < K_{\text{MeOH}}$ ) suggests complexation with THF is more hindered by steric crowding compared to MeOH. The diarylgermylene pair ( $\text{GePh}_2$  and  $\text{GeMes}_2$ ) also exhibits the same differences in ordering.<sup>9,12</sup> The equilibrium constants with the ethers and MeOH define a Lewis acidity scale amongst the transient stannylenes:  $\text{SnMes}_2 < \text{SnMe}_2 < \text{SnPh}_2$ .

With the exception of THT and  $\text{Et}_2\text{NH}$ , which afford the same values of  $K_{\text{eq}}$  within error, the same order of substrates is obtained for both  $\text{SiMes}_2$  and  $\text{GeMes}_2$  when arranged in order of increasing binding energies of complexation. The equilibrium constants allow a Lewis acidity scale to be established for the five donors where  $K_{\text{eq}}$  is measurable for all three tetrylenes (i.e. the ethers, sulfides and  $\text{Et}_2\text{NH}$ ). The finding that the tin derivative is the most Lewis acidic of the  $\text{MMes}_2$  series (i.e.  $\text{SnMes}_2 > \text{SiMes}_2 > \text{GeMes}_2$ ) toward four of the five donors differs from the ordering found with the

dimethyl- and diphenyltetrylenes, for which the equilibrium constants for complexation with O-donors decrease in the order  $\text{SiR}_2 > \text{SnR}_2 > \text{GeR}_2$  ( $\text{R} = \text{Me}, \text{Ph}$ ; see Chapter 4). The latter scale represents instances where the substituent groups offer minimal steric influence on complexation thermodynamics. Comparison with the former scale suggests that mesityl for phenyl substitution has a greater impact on silylene complexation thermodynamics than is the case with the corresponding stannylene reactions. The finding that  $\text{SnMes}_2$  is the most Lewis acidic of the dimesityltetrylene series ( $\text{M} = \text{Si}, \text{Ge}, \text{Sn}$ ) is also consistent with the findings of Kira and coworkers, who reported that the kinetically stable dialkylstannylene **14** undergoes reversible Lewis acid-base complexation with THF, while the silylene and germlyene homologs (**12** and **13**, respectively) do not.<sup>54</sup> Such behaviour was attributed to the greater degrees of steric crowding in **12** and **13** relative to **14** as a result of the decrease in M-C ( $\text{M} = \text{Si}, \text{Ge}, \text{Sn}$ ) bond length with decreasing size of the group 14 element.<sup>54</sup>

Bimolecular rate constants  $k_Q$  could be determined for the complexation reactions of  $\text{SnMes}_2$  with THT,  $\text{BuNH}_2$  and  $\text{Et}_2\text{NH}$ . The values obtained all fall within a factor of 4 of the diffusion controlled rate, indicating that the reactions are invariably quite rapid and thus proceed with minimal kinetic barriers. Using the parent derivative  $\text{SnPh}_2$  as a benchmark, the results suggest that the forward rate constants for Lewis acid-base complexation are not substantially impacted by mesityl for phenyl substitution. For example, no difference in reaction rate constants is observed for complexation with THT, while that for complexation with  $\text{BuNH}_2$  and  $\text{Et}_2\text{NH}$  is slowed by a factor of only ca. 2 for  $\text{SnMes}_2$  compared to  $\text{SnPh}_2$ . When possible, comparison of the  $\text{MMes}_2$  series ( $\text{M} = \text{Si}, \text{Ge}, \text{Sn}$ ) indicate the rate constants do not vary substantially through the series.

**Table 5.3.** Absolute Rate ( $k_Q$ ) and Equilibrium Constants ( $K_{eq}$ ) for the Reactions of  $MMes_2$  ( $M = Si, Ge, Sn$ ) and  $SnPh_2$  with Various Substrates in Hexanes Solution at 25 °C.

Substrate (Q)	$k_Q (10^9 M^{-1} s^{-1}) / [K_{eq} (M^{-1})]$			
	$SnMes_2^a$	$SnPh_2$	$GeMes_2$	$SiMes_2$
$Et_2O$	$[1.8 \pm 0.1]^b$	$[1200 \pm 100]^b$	$[0.09 \pm 0.01]^{e,b}$	$[0.9 \pm 0.1]^{e,b}$
THF	$[35 \pm 4]^b$	$15 \pm 3^{c,n}$	$[1.1 \pm 0.2]^{f,b}$	$[2.4 \pm 0.4]^{e,b}$
MeOH	$[90 \pm 10]^b$	$6 \pm 1^g$ $[7600 \pm 800]^g$	$[15 \pm 6]^{f,b}$	$1.0 \pm 0.1^{h,c}$
$Et_2S$	$[370 \pm 40]^b$	$11 \pm 1^c$	$[40 \pm 4]^{i,b}$	$[54 \pm 3]^{i,b}$
THT	$17 \pm 5$ $[2900 \pm 400]$	$11 \pm 2^c$	$[1000 \pm 100]^{e,b}$	$7 \pm 2$ $[1500 \pm 100]^e$
$BuNH_2$	$9 \pm 1^c$	$19 \pm 2^{c,n}$	$7.0 \pm 0.3^{j,c}$	$10 \pm 3^{k,c}$
$Et_2NH$	$6 \pm 2$ $[2200 \pm 400]$	$12 \pm 1^c$	$[510 \pm 20]^{e,b}$	$3.5 \pm 0.5^k$ $[6300 \pm 600]^k$
AcOH	$4.3 \pm 0.5^c$	$4.2 \pm 0.4^c$	$1.6 \pm 0.3^{j,c}$	$3.5 \pm 0.3^{i,c}$
$Me_2SnCl_2$	$1.7 \pm 0.1^c$	$3.6 \pm 0.2^{f,c}$	d	d
$O_2$	$0.0056 \pm 0.0006^c$	d	$0.0073 \pm 0.0008^{l,c}$	$0.032 \pm 0.004^{m,c}$

Errors are quoted as twice the standard error from the linear least-squares analysis of the data from equations 5.9 - 5.11. <sup>a</sup>(Data recorded by J. Woodard); <sup>b</sup> $k_Q$  undeterminable; <sup>c</sup> $K_{eq} > 25000 M^{-1}$ ; <sup>d</sup>not determined; <sup>e</sup>ref<sup>9</sup>; <sup>f</sup>ref<sup>19</sup>; <sup>g</sup>ref<sup>12</sup>; <sup>h</sup>ref<sup>7</sup>; <sup>i</sup>unpublished results (Data recorded by S. Kostina); <sup>j</sup>ref<sup>10</sup>; <sup>k</sup>ref<sup>8</sup>; <sup>l</sup>ref<sup>11</sup>; <sup>m</sup>ref<sup>27</sup>; <sup>n</sup>(data recorded by B. Nguyen)

Table 5.4 summarizes the long wavelength absorption maxima of the transient stannylene donor complexes. The long wavelength absorption bands of the  $SnMes_2$ -donor complexes are blue-shifted compared to that for the uncoordinated stannylene, falling within the 320 - 440 nm range of the UV-vis spectrum, and appear generally broadened relative to those of the corresponding  $SnPh_2$ -donor complexes. The broadening may indicate that the complexes of  $SnMes_2$  exhibit more fluxional geometries than those with

SnPh<sub>2</sub>. The shifts in absorption maxima do not correlate with the complexation binding energies, similar conclusions were made for the complexes of SiMes<sub>2</sub> and GeMes<sub>2</sub>.<sup>9</sup> The SnMes<sub>2</sub>-amine complexes are blue-shifted compared to those of the chalcogen donors, similar to the trends observed with SnMe<sub>2</sub> and SnPh<sub>2</sub>. The SnMes<sub>2</sub> complexes of THT and BuNH<sub>2</sub> experience a bathochromic shift of 15 nm (0.13 and 0.16 eV) and 35 nm (0.32 and 0.38 eV) relative to the complexes of SnPh<sub>2</sub> and SnMe<sub>2</sub>, respectively. The smaller transition energies (i.e. longer wavelengths) of the SnMes<sub>2</sub> complexes relative to those of SnPh<sub>2</sub> appear to correlate with the difference in transition energies of the uncoordinated stannylenes. This trend is not general however, as the SnMes<sub>2</sub> complexes of Et<sub>2</sub>O and MeOH appear blue-shifted from those of SnPh<sub>2</sub> by ca. 10 nm (0.09 eV).

**Table 5.4.** Long Wavelength Absorption Maxima ( $\lambda_{\text{max}}$  (nm) and eV in parenthesis) of the Stannylene-Donor Complexes (SnR<sub>2</sub>; R = Mes, Ph, Me) in Hexanes Solution at 25 °C.<sup>a</sup>

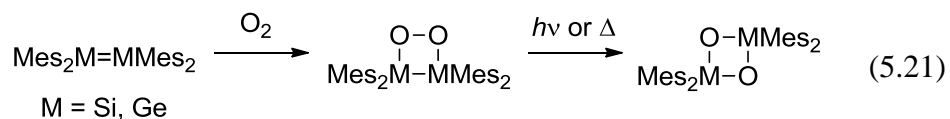
Substrate (Q)	SnMes <sub>2</sub>	SnPh <sub>2</sub>	SnMe <sub>2</sub>
none	550 (2.25)	505 <sup>b</sup> (2.46)	500 <sup>b</sup> (2.48)
Et <sub>2</sub> O	360 (3.44)	370 (3.35)	345 (3.59)
THF	~380 (3.26)	365 (3.40)	345 (3.59)
MeOH	360 (3.44)	370 <sup>b</sup> (3.35)	355 <sup>b</sup> (3.49)
Et <sub>2</sub> S	370(sh) (3.35) <sup>c</sup>	365 (3.40)	345 (3.59)
THT	385 (3.22) <sup>c</sup>	370 (3.35)	350 (3.54)
nBuNH <sub>2</sub>	355 (3.49) <sup>c</sup>	340 (3.65)	320 (3.87)
Et <sub>2</sub> NH	350(sh) (3.54) <sup>c</sup>	340 (3.65)	310 (4.00)

<sup>a</sup>This work unless otherwise noted; <sup>b</sup>ref<sup>19</sup>; <sup>c</sup>(Data recorded by J. Woodard)



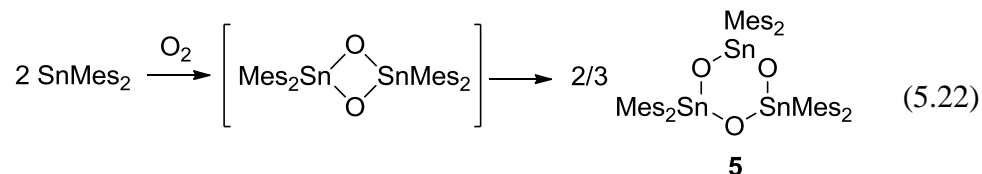
Monitoring the absorbance-time profile at 490 nm upon addition of the stannylene substrates allows the opportunity to explore the reaction kinetics of **9**. Reactivity studies of distannenes have generally been limited in scope<sup>32-34,44,55-58</sup> due to the dissociative nature of most distannenes in solution. The addition of O<sub>2</sub> results in an acceleration of the distannene's decay, where a bimolecular rate constant  $k_Q = (5.3 \pm 0.3) \times 10^6 \text{ M}^{-1} \text{ s}^{-1}$  was obtained. Comparison with the digermene homolog<sup>11</sup> (Mes<sub>2</sub>Ge=GeMes<sub>2</sub>; **20**) indicates the reaction of **9** with O<sub>2</sub> proceeds with a significantly larger rate constant:  $k_{\text{O}_2}^{\text{Sn}}/k_{\text{O}_2}^{\text{Ge}} = 23 \pm 4$ , providing thus far the only quantitative assessment of the differences in reactivity of distannenes and digermenes of otherwise identical substitution. Such a rate difference can be attributed to the Sn derivative being more sterically accessible towards reaction with O<sub>2</sub>.

The reaction of O<sub>2</sub> with tetramesityldisilene<sup>59,60</sup> and **20**<sup>61</sup> affords the corresponding 1,2-disiladioxetane and 1,2-digermadioxetane addition products, respectively, which undergo thermal and/or photochemical rearrangement to the corresponding 1,3-dimetalladioxetane (eq. 5.21).



The results of our product studies experiments in air saturated solution indicate the formation of **5** as the major tin containing product. While this is envisaged as the anticipated product from the addition of oxygen to distannene **9** - the 1,3-distannadioxetane produced from the oxidation of Tip<sub>2</sub>Sn=SnTip<sub>2</sub> with O<sub>2</sub> undergoes further reactivity to *cyclo*-(Tip<sub>2</sub>SnO)<sub>3</sub> (Tip = C<sub>6</sub>H<sub>2</sub>-2,4,6-*i*Pr) over ca. 24 hours at room temperature<sup>44</sup> - its isolation should not be taken as evidence for such a process having occurred. It is in fact unlikely that the products were the result of a reaction of **9**, given the low steady state concentration of SnMes<sub>2</sub> and the knowledge that the stannylene itself

reacts with O<sub>2</sub> with a similar rate constant. A suggested pathway for the formation of **5** from the reaction of SnMes<sub>2</sub> and O<sub>2</sub> is given in eq. 5.22.



The addition of MeOH, AcOH, and Me<sub>2</sub>SnCl<sub>2</sub> also results in a simultaneous drop in yield and acceleration of the distannene decay, affording apparent bimolecular rate constants  $k_{\text{MeOH}} = (2.6 \pm 0.4) \times 10^6 \text{ M}^{-1} \text{ s}^{-1}$ ,  $k_{\text{AcOH}} = (7 \pm 2) \times 10^8 \text{ M}^{-1} \text{ s}^{-1}$ , and  $k_{\text{Me}_2\text{SnCl}_2} = (3.4 \pm 0.4) \times 10^8 \text{ M}^{-1} \text{ s}^{-1}$ , respectively (see Figure S5.9). The rate constants suggest **9** exhibits similar reactivity as SnMes<sub>2</sub>, ranging from the same in the case of O<sub>2</sub> to only 5-6 times lower in the cases of Me<sub>2</sub>SnCl<sub>2</sub> and AcOH. While the course of the reactions of distannenes with the above substrates has not been investigated, the reactions of AcOH and MeOH with tetramesityldigermene (**20**)<sup>15,46</sup> are known to generate the product of RO-H addition across the Ge=Ge bond. In the former case, an upper limit of  $k_{\text{AcOH}} < 10^2 \text{ M}^{-1} \text{ s}^{-1}$  was reported.<sup>10</sup> Comparing the values of  $k_{\text{AcOH}}$  for **9** and **20** suggest the reaction of **9** to be at least 6 orders of magnitude faster. This is consistent with the mesityl group being less effective in shielding **9** from reaction relative to its Ge homolog. Additional mechanistic insight into these reactions is made difficult given the lack of a reported photochemical precursor that would generate **9** directly, in order to carry out product studies experiments.

#### 5.4. Summary and Conclusions

The transient stannylene  $\text{SnMes}_2$  is produced cleanly from the photolysis of 1,1-dimesityl-3,4-dimethyl-1-stannacyclopent-3-ene (**1**) in hydrocarbon solutions (at ambient temperatures) as shown by the results of product studies and laser flash photolysis experiments. Three stannylene-trapping reactions were studied, the results providing strong evidence for the formation of  $\text{SnMes}_2$  as the key Sn-containing intermediate. The stannylene was trapped as the 1,3,5-cyclotristannoxane **5** when the photolysis of **1** was performed in air saturated  $\text{C}_6\text{D}_{12}$  solution, affording diene **3** as the photolysis co-product. The results of photolysis of **1** in the presence of AcOH indicate that the reaction of the acid with  $\text{SnMes}_2$  affords two equivalents of mesitylene (**4**). When the photolysis of **1** is repeated in the presence of  $\text{Me}_2\text{SnCl}_2$  as the stannylene substrate, the resulting tin containing products dichlorodimesitylstannane (**2**) and the association dimer of 1,3-dichlorotetramethyldistannoxane (**6**) suggest the efficient trapping of  $\text{SnMes}_2$  by the dichlorostannane. The results are complicated by a dark reaction of **1** with  $\text{Me}_2\text{SnCl}_2$  that affords several (but not all) of the same products. The formation of **2** allows for a determination of  $\Phi_{\text{SnMes}_2} = 0.36 \pm 0.05$ .

Laser flash photolysis experiments with **1** in hexanes solution result in the prompt formation of transient absorption bands assigned to  $\text{SnMes}_2$  ( $\lambda_{\text{max}} < 270$ ,  $\sim 330$ (sh), and 550 nm). The transient species decays with second order kinetics ( $2k_{\text{decay}}/\epsilon_{570\text{nm}} = (7.5 \pm 2.7) \times 10^6 \text{ cm}^2 \text{ s}^{-1}$ ) and affords a new transient species assigned to  $\text{Mes}_2\text{Sn}=\text{SnMes}_2$  (**9**,  $\lambda_{\text{max}} = 290, 490 \text{ nm}$ ). The reactions of  $\text{SnMes}_2$  with seven Lewis bases allow several conclusions to be made regarding the kinetic and thermodynamic aspects of stannylene reactivity.  $\text{SnMes}_2$  is the least acidic stannylene in the series  $\text{SnPh}_2 > \text{SnMe}_2 > \text{SnMes}_2$ , but is the most acidic tetrylene within the series  $\text{SnMes}_2 > \text{SiMes}_2 > \text{GeMes}_2$ . This contrasts the ordering of the less-hindered stannylene derivatives:  $\text{SiR}_2 > \text{SnR}_2 > \text{GeR}_2$  (R

= Me, Ph). The reactions of  $\text{SnMes}_2$  with  $\text{O}_2$ ,  $\text{Me}_2\text{SnCl}_2$  and  $\text{AcOH}$  afford rate constants that are consistent with the results of the product studies experiments, which indicate the stannylene is trapped efficiently by these substrates.

A bimolecular rate constant was also measured for the reaction of tetramesityldistannene (**9**) with  $\text{O}_2$ , a reaction for which there is precedent in the distannene literature.<sup>44</sup> The results indicate the distannene is ca. 20 times more reactive than its germanium homolog ( $\text{Mes}_2\text{Ge}=\text{GeMes}_2$ , **20**) under similar conditions.

### 5.5. Supporting Information

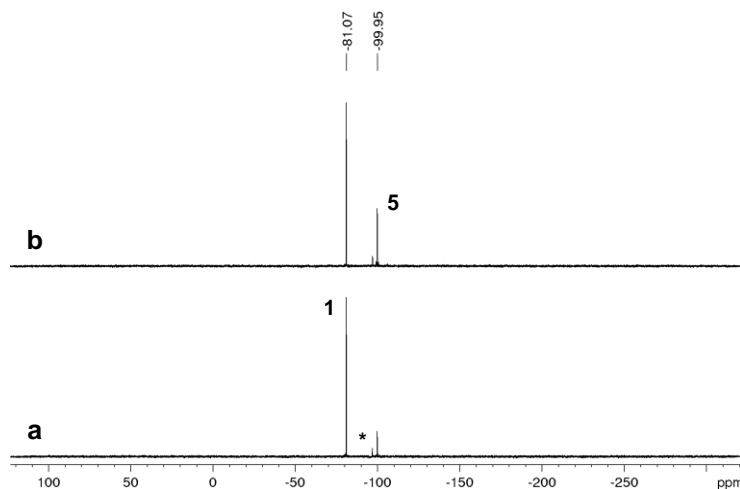


**Figure S5.1.**  $^{119}\text{Sn}$  NMR spectra of an air-saturated 0.045 M solution of **1** in  $\text{C}_6\text{D}_{12}$  (a) after 10 minutes photolysis with 254 nm light, and (b) after spiking the resulting photolyzate with an authentic sample of **5**. (\*Unreactive Impurity) (Samples prepared by J. Woodard)

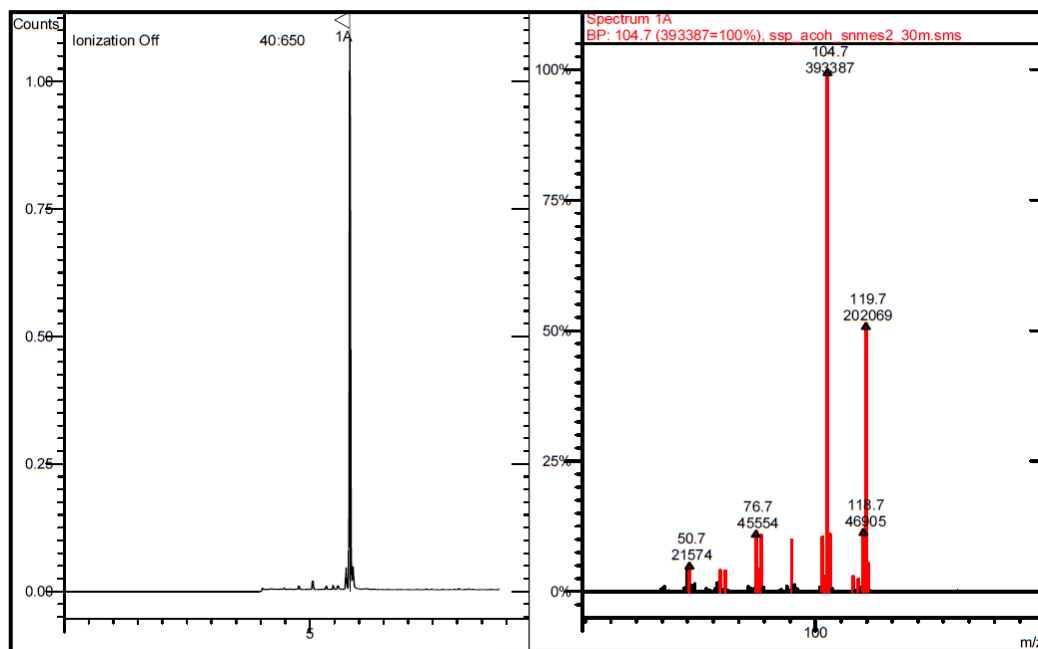


**Figure S5.2.** (a) GC-MS chromatogram (0 - 9.5 minutes retention time) and (b) mass spectrum of the peak at ca. 5.8 minutes retention time from a 0.04 M solution of **1** in  $C_6D_{12}$  containing 0.2 M AcOH after 30 minutes photolysis with 254 nm UV light.

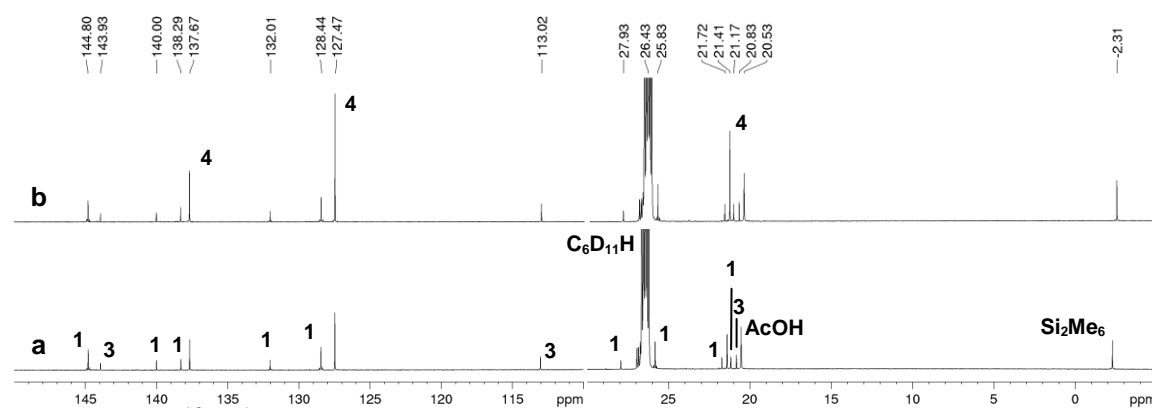


**Figure S5.3.**  $^{13}C\{^1H\}$  NMR spectra of a 0.04 M solution of **1** in  $C_6D_{12}$  containing 0.2 M AcOH (a) after 30 minutes photolysis with 254 nm UV light and (b) after spiking the photolyzate of (a) with an authentic sample of **4**.

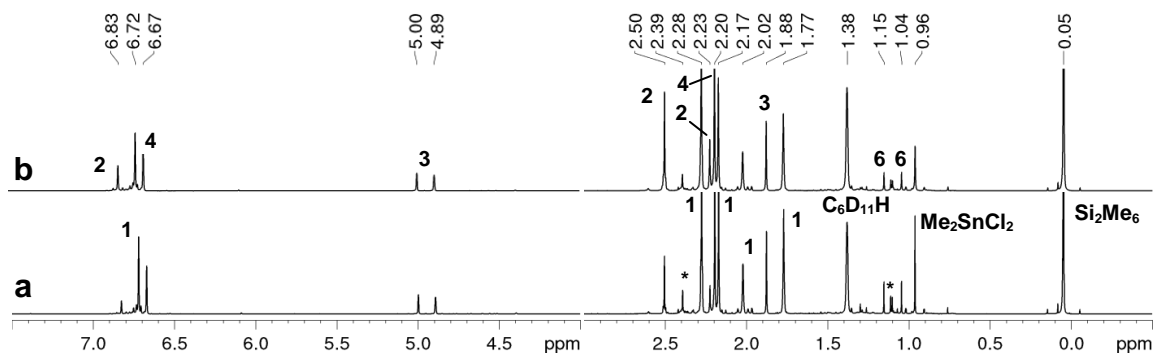


**Figure S5.4.**  $^1\text{H}$  NMR spectra of a 0.045 M solution of **1** in  $\text{C}_6\text{D}_{12}$  containing  $\text{Me}_2\text{SnCl}_2$  (0.035 M) (a) after 10 minutes photolysis with 254 nm light, and (b) after spiking the photolyzate of (a) with an authentic sample of **2**. (\*Unreactive Impurity) (Samples prepared by J. Woodard)

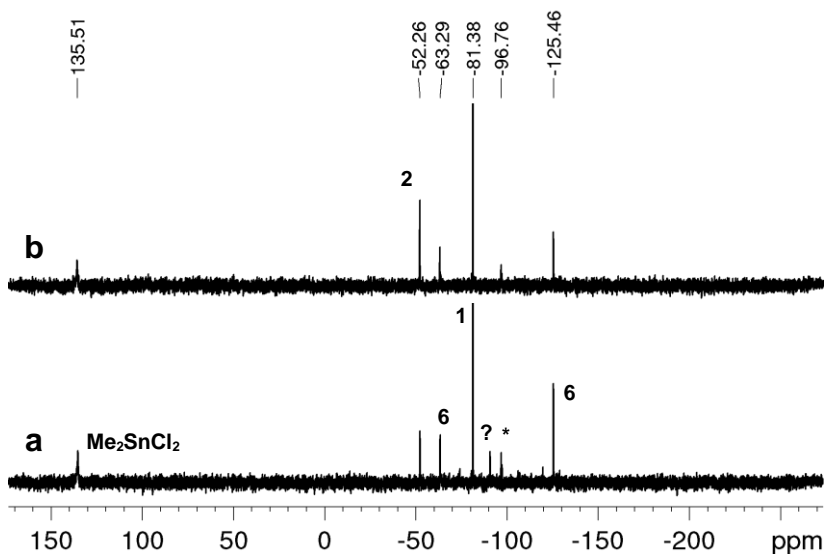


**Figure S5.5.**  $^{119}\text{Sn}\{^1\text{H}\}$  NMR spectra of a 0.045 M solution of **1** in  $\text{C}_6\text{D}_{12}$  containing  $\text{Me}_2\text{SnCl}_2$  (0.035 M) (a) after 10 minutes photolysis with 254 nm light, and (b) after spiking the photolyzate of (a) with an authentic sample of **2**. (\*Unreactive Impurity; ? unidentified tin-containing compound) (Samples prepared by J. Woodard)

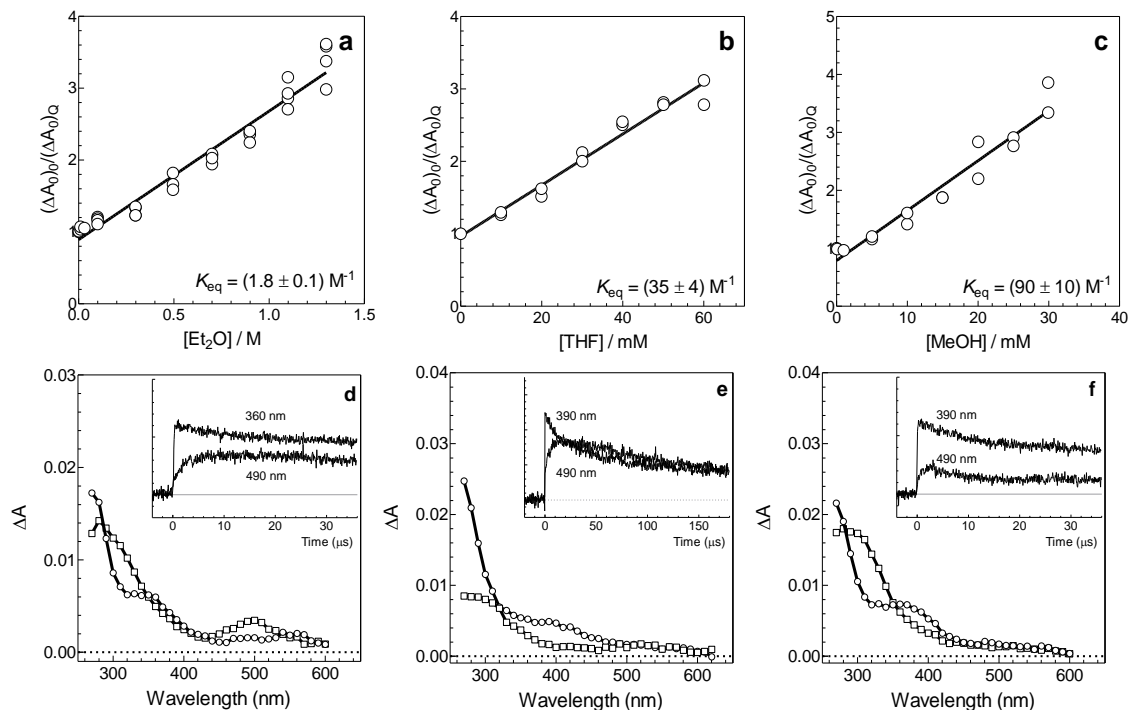


**Figure S5.6.** Plot of  $(\Delta A_0)_0 / (\Delta A_0)_Q$  for reaction of  $\text{SnMes}_2$  (570 nm) with (a)  $\text{Et}_2\text{O}$ , (b) THF and (c) MeOH in hexanes at 25 °C; the solid lines are the linear least squares fit of the data to equation 5.11. (d) Time-resolved UV-vis spectra recorded by laser photolysis of **1** in hexanes containing 2.0 M  $\text{Et}_2\text{O}$ , 0.4-0.5  $\mu\text{s}$  ( $\circ$ ), and 17.3-17.6  $\mu\text{s}$  ( $\square$ ) after the laser pulse (25 °C), and absorbance-time profiles at selected wavelengths (inset). (e) Time-resolved UV-vis spectra recorded by laser photolysis of **1** in hexanes containing 0.12 M THF, 0.32-1.0  $\mu\text{s}$  ( $\circ$ ), and 172-173  $\mu\text{s}$  ( $\square$ ) after the laser pulse (25 °C), and absorbance-time profiles at selected wavelengths (inset). (f) Time-resolved UV-vis spectra recorded by laser photolysis of **1** in hexanes containing 41 mM MeOH, 0.58-0.70  $\mu\text{s}$  ( $\circ$ ), and 34.4-34.6  $\mu\text{s}$  ( $\square$ ) after the laser pulse (25 °C), and absorbance-time profiles at selected wavelengths (inset). (Data in (a)-(c) recorded by J. Woodard)

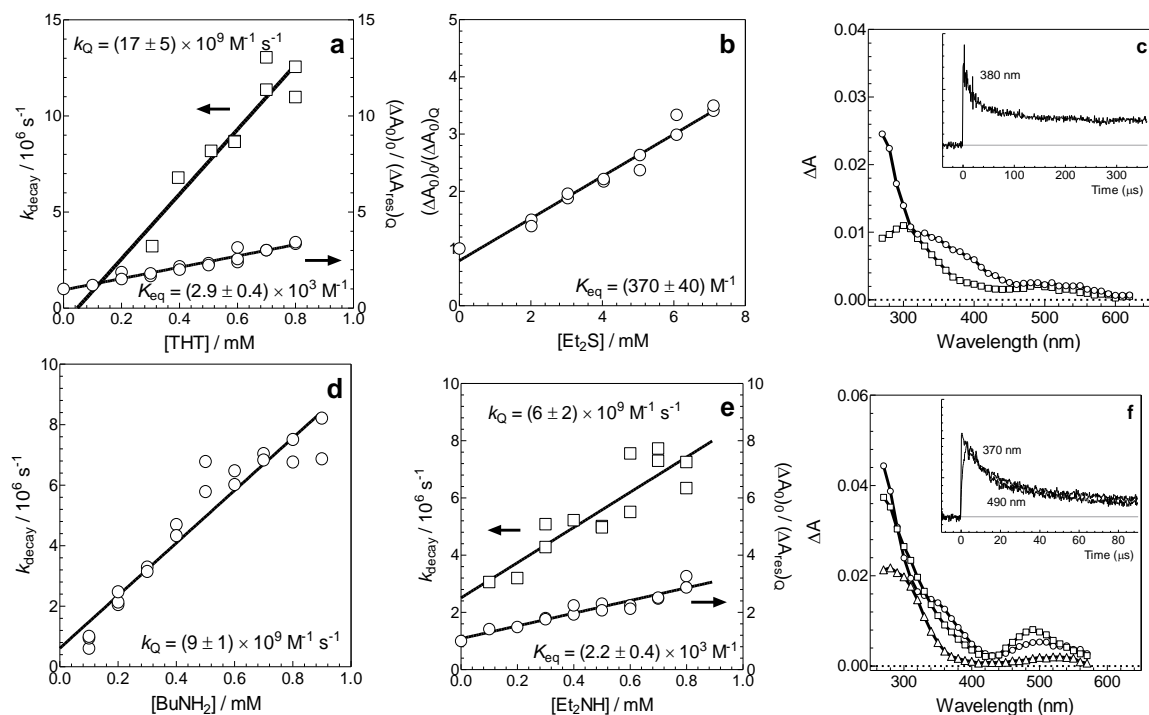


**Figure S5.7.** Plots of  $k_{\text{decay}}$  ( $\square$ ) and  $(\Delta A_0)_0 / (\Delta A_{\text{res}})_Q$  ( $\circ$ ) of SnMes<sub>2</sub> (570 nm) versus (a) [THT] and (e) [Et<sub>2</sub>NH], in hexanes solution at 25 °C; the solid lines are the linear least-squares fits of the data to equations 5.9 and 5.10, respectively. (b) Plot of  $(\Delta A_0)_0 / (\Delta A_0)_Q$  for reaction of SnMes<sub>2</sub> (570 nm) with Et<sub>2</sub>S in hexanes at 25 °C; the solid line is the linear least squares fit of the data to eq. 5.11. (c) Time-resolved UV-vis spectra from laser photolysis of **1** in hexanes containing 7.0 mM Et<sub>2</sub>S, 0.0 - 0.64  $\mu\text{s}$  ( $\circ$ ), and 87.7 - 90.9  $\mu\text{s}$  ( $\square$ ) after the laser pulse (25 °C), and absorbance-time profiles at selected wavelengths (inset). (d) Plot of  $k_{\text{decay}}$  for reaction of SnMes<sub>2</sub> (570 nm) with BuNH<sub>2</sub> in hexanes at 25 °C; the solid line is the linear least squares fit of the data to equation 5.9. (f) Time-resolved UV-vis spectra from laser photolysis of **1** in hexanes containing 1.0 mM Et<sub>2</sub>NH, 0.32 - 0.80  $\mu\text{s}$  ( $\circ$ ), 5.92 - 6.56  $\mu\text{s}$  ( $\square$ ), and 85.9 - 86.6  $\mu\text{s}$  ( $\Delta$ ) after the laser pulse (25 °C), and absorbance-time profiles at selected wavelengths (inset). (Data recorded by J. Woodard)



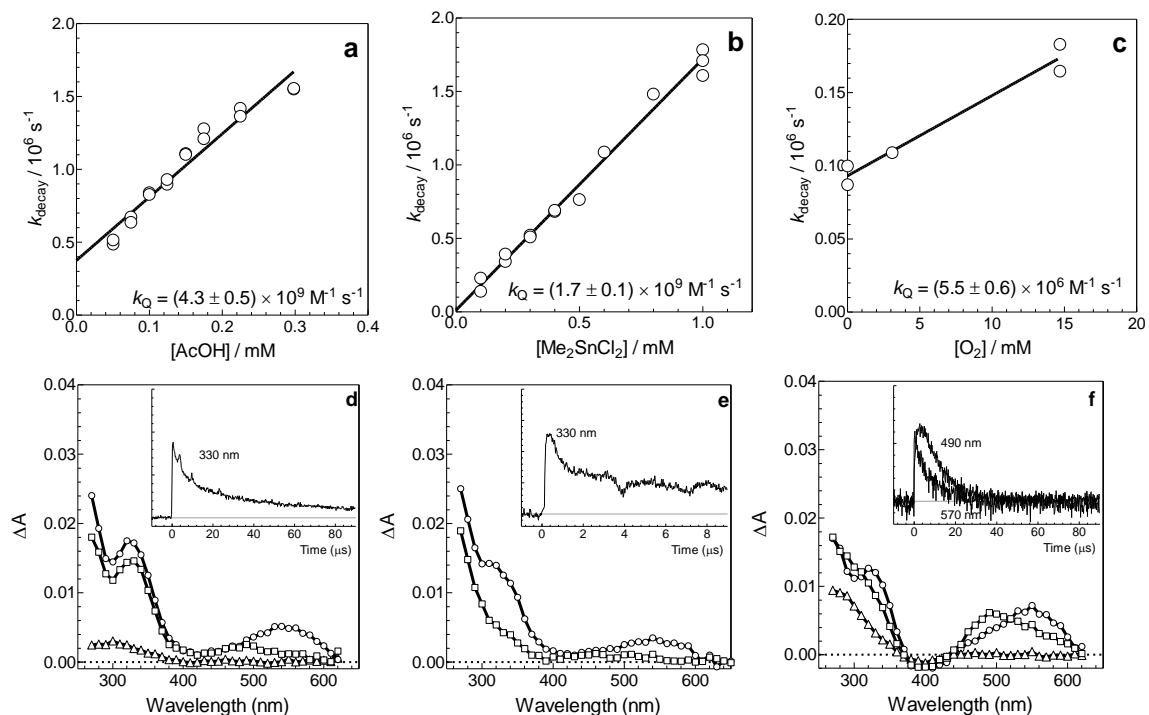


**Figure S5.8.** Plots of  $k_{\text{decay}}$  for reaction of SnMes<sub>2</sub> (570 nm) with (a) AcOH, (b) Me<sub>2</sub>SnCl<sub>2</sub>, and (c) molecular oxygen in hexanes at 25 °C; the solid lines are the linear least squares fit of the data to equation 5.9. (d) Time-resolved UV-vis spectra from laser photolysis of **1** in hexanes containing 0.3 mM AcOH, 0.16 - 0.32 μs (○), 1.3 - 1.6 μs (□), and 85.9 - 86.7 μs (Δ) after the laser pulse (25 °C), and absorbance-time profiles at selected wavelengths (inset). (e) Time-resolved UV-vis spectra from laser photolysis of **1** in hexanes containing 1.0 mM Me<sub>2</sub>SnCl<sub>2</sub>, 0.27 - 0.35 μs (○), and 6.6 - 6.7 μs (□) after the laser pulse (25 °C), and absorbance-time profiles at selected wavelengths (inset). (f) Time-resolved UV-vis spectra from laser photolysis of **1** in hexanes containing 14.7 mM O<sub>2</sub>, 0.16 - 0.32 μs (○), 4.8 - 5.1 μs (□), and 87.5 - 88.3 μs (Δ) after the laser pulse (25 °C), and absorbance-time profiles at selected wavelengths (inset); data from (f) recorded using a neutral density filter (67 % transmittance). (Data in (a)-(e) recorded by J. Woodard)

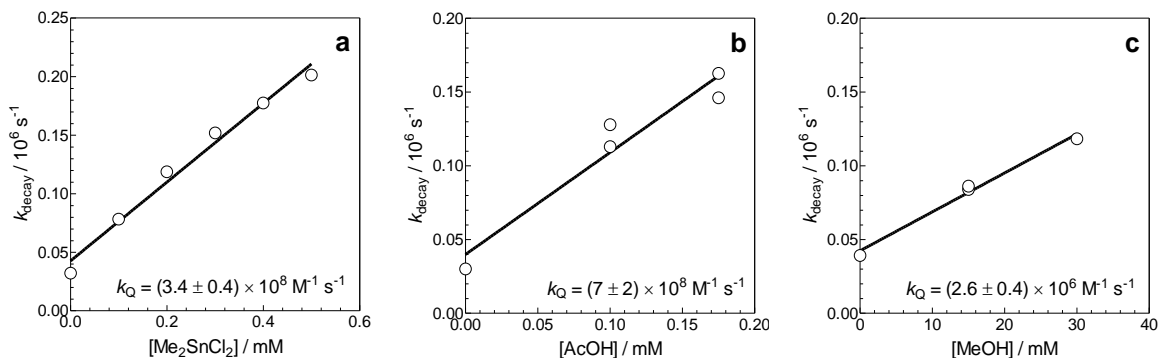


**Figure S5.9.** Plots of  $k_{\text{decay}}$  for the reactions of **9** with (a)  $\text{Me}_2\text{SnCl}_2$ , (b)  $\text{AcOH}$ , and (c)  $\text{MeOH}$  in hexanes at  $25\text{ }^\circ\text{C}$ ; the solid lines are the linear least squares fit of the data to eq. 5.9. (Data recorded by J. Woodard)

## 5.6. References

- (1) Bigwood, M. P.; Corvan, P. J.; Zuckerman, J. J. *J. Am. Chem. Soc.* **1981**, *103*, 7643.
- (2) Jolly, B. S.; Lappert, M. F.; Engelhardt, L. M.; White, A. H.; Raston, C. L. *J. Chem. Soc., Dalton Trans.* **1993**, 2653.
- (3) Peng, Y.; Guo, J.-D.; Ellis, B. D.; Zhu, Z.; Fettingner, J. C.; Nagase, S.; Power, P. P. *J. Am. Chem. Soc.* **2009**, *131*, 16272.
- (4) Wilfling, P.; Schittelkopf, K.; Flock, M.; Herber, R. H.; Power, P. P.; Fischer, R. C. *Organometallics* **2015**, *34*, 2222.
- (5) Moiseev, A. G.; Leigh, W. J. *Organometallics* **2007**, *26*, 6268.
- (6) Moiseev, A. G.; Leigh, W. J. *Organometallics* **2007**, *26*, 6277.
- (7) Leigh, W. J.; Kostina, S. S.; Bhattacharya, A.; Moiseev, A. G. *Organometallics* **2010**, *29*, 662.
- (8) Kostina, S. S.; Singh, T.; Leigh, W. J. *J. Phys. Org. Chem.* **2011**, *24*, 937.
- (9) Kostina, S. S.; Singh, T.; Leigh, W. J. *Organometallics* **2012**, *31*, 3755.
- (10) Leigh, W. J.; Harrington, C. R.; Vargas-Baca, I. *J. Am. Chem. Soc.* **2004**, *126*, 16105.
- (11) Toltl, N. P.; Leigh, W. J.; Kollegger, G. M.; Stibbs, W. G.; Baines, K. M. *Organometallics* **1996**, *15*, 3732.
- (12) Leigh, W. J.; Lollmahomed, F.; Harrington, C. R.; McDonald, J. M. *Organometallics* **2006**, *25*, 5424.
- (13) West, R.; Fink, M.; Michl, J. *Science* **1981**, *214*, 1343.
- (14) Fink, M. J.; Michalczyk, M. J.; Haller, K. J.; West, R.; Michl, J. *Organometallics* **1984**, *3*, 793.
- (15) Hurni, K. L.; Rupar, P. A.; Payne, N. C.; Baines, K. M. *Organometallics* **2007**, *26*, 5569.

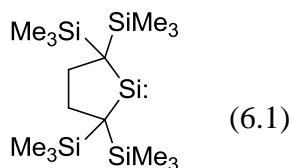
- (16) Zhou, D.; Reiche, C.; Nag, M.; Soderquist, J. A.; Gaspar, P. P. *Organometallics* **2009**, *28*, 2595.
- (17) National Institute of Standards and Technology of the United States (NIST) chemwebbook, Sept 14, 2017, <http://webbook.nist.gov/chemistry>
- (18) Neale, N. R.; Tilley, T. D. *J. Am. Chem. Soc.* **2002**, *124*, 3802.
- (19) Duffy, I. R.; Leigh, W. J. *Organometallics* **2015**, *34*, 5029.
- (20) Phillips, A. D.; Hino, S.; Power, P. P. *J. Am. Chem. Soc.* **2003**, *125*, 7520.
- (21) Spikes, G. H.; Peng, Y.; Fettinger, J. C.; Power, P. P. *Z. Anorg. Allg. Chem.* **2006**, *632*, 1005.
- (22) Murov, S. L.; Carmichael, I.; Hug, G. L. *Handbook of Photochemistry*; 2nd ed.; Dekker: New York, 1993; p 208.
- (23) Scaiano, J. C. In *Reactive Intermediate Chemistry*; Moss, R. A., Platz, M. S., Jones, M., Jr., Eds.; John Wiley & Sons, Inc.: New York, 2004, p 847.
- (24) Saito, M.; Tokitoh, N.; Okazaki, R. *Chem. Lett.* **1996**, *25*, 265.
- (25) Simons, R. S.; Pu, L.; Olmstead, M. M.; Power, P. P. *Organometallics* **1997**, *16*, 1920.
- (26) Tajima, T.; Takeda, N.; Sasamori, T.; Tokitoh, N. *Organometallics* **2006**, *25*, 3552.
- (27) Conlin, R. T.; Netto-Ferreira, J. C.; Zhang, S.; Scaiano, J. C. *Organometallics* **1990**, *9*, 1332.
- (28) Kira, M.; Ishida, S.; Iwamoto, T. *Chem. Record* **2004**, *4*, 243.
- (29) Levin, G.; Das, P. K.; Lee, C. L. *Organometallics* **1988**, *7*, 1231.
- (30) Becerra, R.; Harrington, C. R.; Gaspar, P. P.; Leigh, W. J.; Vargas-Baca, I.; Walsh, R.; Zhou, D. *J. Am. Chem. Soc.* **2005**, *127*, 17469.
- (31) Masamune, S.; Sita, L. R. *J. Am. Chem. Soc.* **1985**, *107*, 6390.
- (32) Henning, J.; Eichele, K.; Fink, R. F.; Wesemann, L. *Organometallics* **2014**, *33*, 3904.
- (33) Schneider, J.; Henning, J.; Edrich, J.; Schubert, H.; Wesemann, L. *Inorg. Chem.* **2015**, *54*, 6020.
- (34) Lee, V. Y.; Fukawa, T.; Nakamoto, M.; Sekiguchi, A.; Tumanskii, B. L.; Karni, M.; Apeloig, Y. *J. Am. Chem. Soc.* **2006**, *128*, 11643.
- (35) Arp, H.; Baumgartner, J.; Marschner, C.; Muller, T. *J. Am. Chem. Soc.* **2011**, *133*, 5632.
- (36) Sturmman, M.; Saak, W.; Klinkhammer, K. W.; Weidenbruch, M. *Z. anorg. allg. Chem.* **1999**, *625*, 1955.
- (37) Hamao, W.; Ken, T.; Norio, F.; Motohiko, K.; Midori, G.; Yoichiro, N. *Chem. Lett.* **1987**, *16*, 1341.
- (38) Ando, W.; Itoh, H.; Tsumuraya, T.; Yoshida, H. *Organometallics* **1988**, *7*, 1880.
- (39) Sekiguchi, A.; Inoue, S.; Ichinohe, M.; Arai, Y. *J. Am. Chem. Soc.* **2004**, *126*, 9626.
- (40) Lee, V. Y.; McNeice, K.; Ito, Y.; Sekiguchi, A. *Chem. Commun.* **2011**, *47*, 3272.
- (41) Grützmacher, H.; Pritzkow, H. *Chem. Ber.* **1993**, *126*, 2409.
- (42) Cotton, J. D.; Davidson, P. J.; Lappert, M. F. *J. Chem. Soc., Dalton Trans.* **1976**, 2275.

- (43) Becerra, R.; Boganov, S. E.; Egorov, M. P.; Faustov, V. I.; Krylova, I. V.; Nefedov, O. M.; Walsh, R. *J. Am. Chem. Soc.* **2002**, *124*, 7555.
- (44) Tsumuraya, T.; Batcheller, S. A.; Masamune, S. *Angew. Chem. Int. Ed. Engl.* **1991**, *30*, 902.
- (45) Masamune, S.; Sita, L. R.; Williams, D. J. *J. Am. Chem. Soc.* **1983**, *105*, 630.
- (46) Huck, L. A.; Leigh, W. J. *Organometallics* **2007**, *26*, 1339.
- (47) Leigh, W. J.; Lollmahomed, F.; Harrington, C. R. *Organometallics* **2006**, *25*, 2055.
- (48) Erickson, J. D.; Vasko, P.; Riparetti, R. D.; Fettinger, J. C.; Tuononen, H. M.; Power, P. P. *Organometallics* **2015**, *34*, 5785.
- (49) Grützmacher, H.; Freitag, S.; Herbst-Irmer, R.; Sheldrick, G. S. *Angew. Chem. Int. Ed. Engl.* **1992**, *31*, 437.
- (50) Donaldson, J. D.; Moser, W.; Simpson, W. B. *J. Chem. Soc.* **1964**, 5942.
- (51) Gross, L. W.; Moser, R.; Neumann, W. P.; Scherping, K. H. *Tetrahedron Lett.* **1982**, *23*, 635.
- (52) Padelkova, Z.; Svec, P.; Pejchal, V.; Růžička, A. *Dalton Trans.* **2013**, *42*, 7660.
- (53) Davies, A. G. *J. Chem. Res.* **2004**, *5*, 309.
- (54) Kira, M.; Ishida, S.; Iwamoto, T.; Yauchibara, R.; Sakurai, H. *J. Organomet. Chem.* **2001**, *636*, 144.
- (55) Weidenbruch, M.; Schäfer, A.; Kilian, H.; Pohl, S.; Saak, W.; Marsmann, H. *Chem. Ber.* **1992**, *125*, 563.
- (56) Schäfer, A.; Weidenbruch, M.; Saak, W.; Pohl, S.; Marsmann, H. *Angew. Chem. Int. Ed. Engl.* **1991**, *30*, 834.
- (57) Wiederkehr, J.; Wolper, C.; Schulz, S. *Chem. Commun.* **2016**, *52*, 12282.
- (58) Jones, C.; Schulten, C.; Stasch, A. *Inorg. Chem.* **2008**, *47*, 1273.
- (59) Fink, M. J.; Haller, K. J.; West, R.; Michl, J. *J. Am. Chem. Soc.* **1984**, *106*, 822.
- (60) McKillop, K.; Gillette, G. R.; Powell, D. R.; West, R. *J. Am. Chem. Soc.* **1992**, *114*, 5203.
- (61) Samuel, M. S.; Jennings, M. C.; Baines, K. M. *J. Organomet. Chem.* **2001**, *636*, 130.

## Chapter 6: Photochemical Generation and Characterization of Di-*tert*-butylsilylene in Solution

### 6.1. Introduction

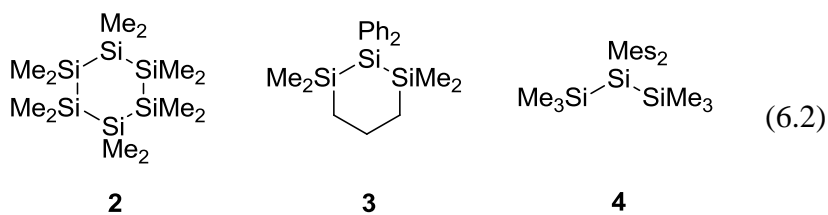
Our understanding of the chemistry of silylenes, formally compounds containing a divalent Si(II) centre, has evolved substantially since their debut as "short-lived intermediates"<sup>1</sup> in organosilicon transformations.<sup>2-5</sup> Contemporary studies are mainly directed at exploring the potential utility of electronically and/or kinetically stabilized isolable silylenes<sup>6,7</sup> in catalytic applications, such as transition-metal-free small molecule activation,<sup>8,9</sup> although interest remains in advancing our understanding of basic reactions of the simpler derivatives. The majority of the known isolable silylenes contain some degree of electronic stabilization: either via intramolecular or intermolecular donor coordination or direct bonding to a heteroatom. Relatively few kinetically stable and electronically-unperturbed silylenes have yet been prepared and studied. The notable exception to this generalization is the well-known compound **1** (eq. 6.1),<sup>10-12</sup> first reported by Kira and coworkers.<sup>13</sup> The rich and diverse reactivity established for this compound has a direct analogy in the chemistry of simple transient dialkyl and diarylsilylenes in solution, which were studied in detail via indirect methods thirty to forty years ago.<sup>2,14,15</sup>



**1**

Transient silylenes have been characterized using UV-vis and infrared spectroscopy in frozen matrices,<sup>16</sup> and in the gas phase<sup>4,17</sup> and fluid solution<sup>18-24</sup> by time-resolved UV-vis spectrophotometry, or flash photolysis. This has allowed the direct detection and

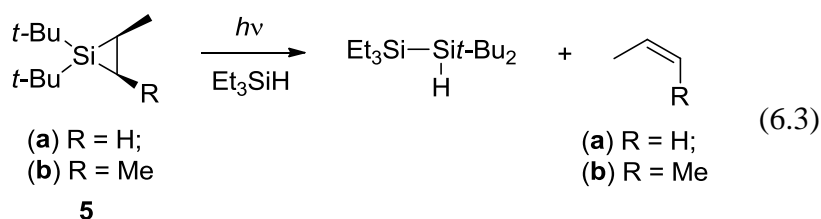
characterization of the simplest carbon substituted silylenes in solution:  $\text{SiMe}_2$  by Levin and Das<sup>18,19</sup> and Shizuka and coworkers,<sup>20</sup>  $\text{SiPh}_2$  by Leigh and coworkers,<sup>21-23</sup> and  $\text{SiMes}_2$  (Mes = 2,4,6-trimethylphenyl) by Conlin and Scaiano,<sup>24</sup> and has been made possible by employing compounds **2-4** (eq. 6.2) that produce strong and well-resolved transient UV-vis absorptions due to their respective silylenes.<sup>22</sup> Simple hydrido, alkyl, and halo-substituted systems have been studied in the gas phase by Strausz,<sup>25</sup> Jasinski,<sup>27</sup> and Walsh and their coworkers.<sup>17,26</sup> In particular, the reactivity of the parent silylene  $\text{SiH}_2$ , which has been described as one of the most reactive transients known,<sup>4,27</sup> has been characterized extensively in the gas-phase toward such substrates as  $\text{SiH}_4$ ,<sup>28,29</sup> ethylene,<sup>30,31</sup> acetylene,<sup>32</sup> acetone,<sup>33</sup> THF,<sup>34</sup> and MeOH,<sup>35</sup> with reactions approaching the collisional rate in many cases.<sup>4</sup> The aim of recent solution phase studies has been to elucidate detailed mechanisms for some of the fundamental reaction pathways of silylenes; some examples of this include the O-H insertion reaction with alcohols,<sup>36</sup> N-H insertion with amines<sup>37</sup> and chalcogen abstraction with oxiranes and thiiranes in solution.<sup>38</sup>



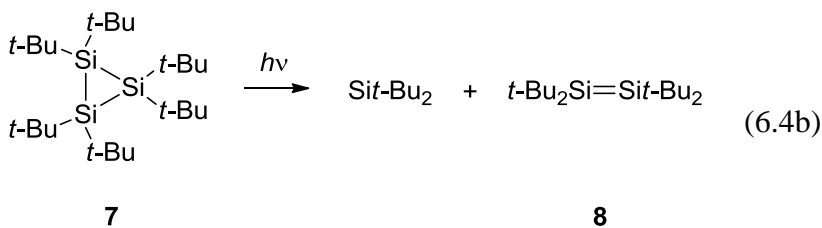
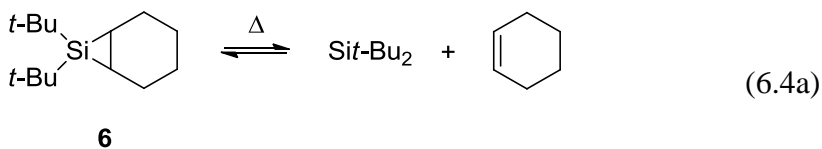
Di-*tert*-butylsilylene (*Sit*-Bu<sub>2</sub>) has been studied extensively as a transfer group in organic synthesis.<sup>39-46</sup> Silver-mediated transfer reactions of *Sit*-Bu<sub>2</sub> from 1,1-di-*tert*-butylsilirane derivatives has been demonstrated by K. Woerpel and coworkers to be a versatile method for the stereoselective formation of organosilicon compounds,<sup>47</sup> and subsequent derivatization directed towards the preparation of natural products. The mechanism of silylene transfer in these reactions is thought to involve silver-assisted

extrusion of  $\text{Si}t\text{-Bu}_2$  from the silirane precursor to form an intermediary silylsilver complex, preceding formal  $\text{Si}t\text{-Bu}_2$  transfer to the substrate.<sup>48</sup>

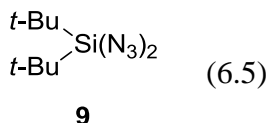
The intermediacy of uncoordinated  $\text{Si}t\text{-Bu}_2$  has been postulated in a number of organosilicon transformations. Thermolysis and/or photolysis of substituted di-*tert*-butylsiliranes (**5a-b**) in the presence of a silylene substrate generally furnish silylene-derived products and the corresponding alkene (eq. 6.3).<sup>49,50</sup>



The thermal (uncatalyzed) transfer of  $\text{Si}t\text{-Bu}_2$  from **6** to mono-substituted alkenes has received particular mechanistic attention, and is thought to proceed via reversible extrusion of free  $\text{Si}t\text{-Bu}_2$  (eq. 6.4a).<sup>51</sup> Irradiation of hexa-*tert*-butylcyclotrisilane (**7**) in the presence of a trapping agent generated compounds consistent with the extrusion of both  $\text{Si}t\text{-Bu}_2$  and tetra-*tert*-butyldisilene (**8**) as photoproducts,<sup>52</sup> and was used exclusively by Weidenbruch and coworkers to isolate a number of novel organosilicon compounds (eq. 6.4b).<sup>53-56</sup>



Efforts to obtain direct evidence for the existence of *Sit*-Bu<sub>2</sub> and to probe its electronic structure have been made both experimentally and theoretically.<sup>57-59</sup> Gordon and coworkers investigated *Sit*-Bu<sub>2</sub> theoretically as a potential ground state triplet silylene,<sup>57</sup> and later studied its (1+2) cycloaddition reaction with acetylene using ab initio calculations.<sup>58</sup> The free silylene (as well as its deuterated isotopomer, *Sit*-Bu<sub>2</sub>-*d*<sub>18</sub>) was generated by two-photon photolysis of diazidodi-*tert*-butylsilane (**9**; eq. 6.5) in an argon matrix at 10 K, and was characterized by its UV-visible and IR absorption spectra.<sup>60</sup>



In the present chapter, the direct detection of *Sit*-Bu<sub>2</sub> is reported in solution under ambient conditions using **6** and **7**, two well-known photochemical precursors to this silylene. We have also characterized its reaction kinetics and thermodynamics in a variety of well-documented silylene reactions, including Lewis acid-base complexation with ethers, sulfides, and amines,  $\sigma$ -bond insertion with O-H and Si-H bonds, ene-addition with ketones and carboxylic acids, cycloaddition with substituted alkenes, and reaction with molecular oxygen. The data enable direct comparisons to be made with the reactivity of SiMe<sub>2</sub> with the same group of substrates, allowing a quantitative assessment of the effects of steric bulk on the kinetics and thermodynamics of dialkylsilylene reactions in solution.

## 6.2. Results and Discussion

Hexa-*tert*-butylcyclotrisilane (**7**) was prepared from di-*tert*-butyldiiodosilane (*t*-Bu<sub>2</sub>SiI<sub>2</sub>)<sup>61</sup> by a procedure adapted from that of Weidenbruch and coworkers.<sup>52</sup> After column chromatography (silica gel, hexanes), **7** was further purified by recrystallization from pentane, to a purity of  $\geq 97\%$  as determined by <sup>1</sup>H NMR spectroscopy (see Chapter 8.5.6). Sealed ampoules of 7,7-di-*tert*-butyl-7-silabicyclo[4.1.0]heptane (**6**) used in this



study were provided by Prof. K. Woerpel and his group. Compound **6** is a colourless, air and moisture sensitive liquid; hence samples were handled in a glovebox and immediately transferred to the reservoirs using a microlitre syringe to minimize contact with air and moisture. Both compounds absorb sufficiently at the excitation wavelength, however **7** exhibits a ca. 100 times larger extinction coefficient ( $\epsilon_{248\text{nm}} \sim 1.6 \times 10^4 \text{ M}^{-1} \text{ cm}^{-1}$ ) compared to **6** ( $\epsilon_{248\text{nm}} \sim 1.7 \times 10^2 \text{ M}^{-1} \text{ cm}^{-1}$ ). See Figure 8.2 for the UV-visible absorption spectra of the *Sit*-Bu<sub>2</sub> precursors, recorded between 220 - 300 nm in hexanes solution.

Laser flash photolysis of rapidly flowed, deoxygenated solutions of **6** (ca.  $4 \times 10^{-3} \text{ M}$ ) in anhydrous hexanes were carried out using a KrF excimer laser for excitation (248 nm, ca. 25 ns, 92 - 100 mJ). Time-resolved UV-vis absorption spectra recorded over the 270 - 650 nm spectral region at selected time intervals after the laser pulse are shown in Figure 6.1. The spectrum recorded immediately after the pulse reveals a broad absorption band with an apparent maximum at  $\lambda_{\text{max}} \approx 490 \text{ nm}$ , which decays over ca. 10  $\mu\text{s}$  with second order kinetics and rate coefficient  $2k/\epsilon_{530\text{nm}} = (8.4 \pm 0.8) \times 10^7 \text{ cm s}^{-1}$  (see eq. 6.6).

$$\Delta A_t = \Delta A_0 / (1 + (2k_{\text{dim}}\Delta A_0 / \epsilon l)t) \quad (6.6)$$

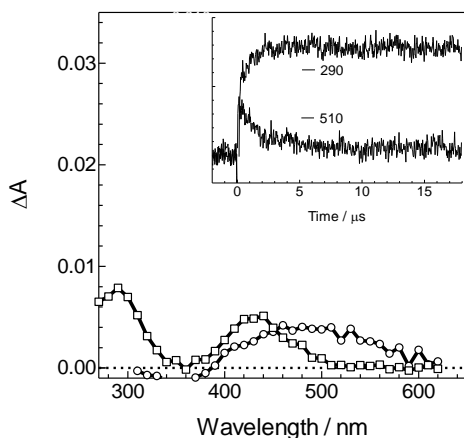
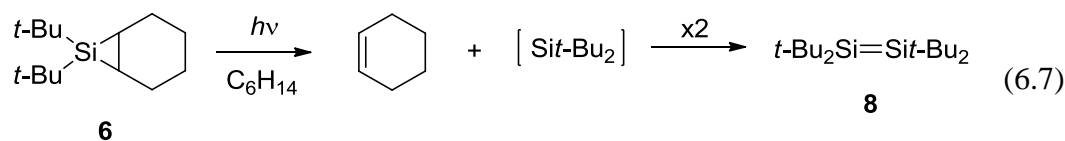


**Figure 6.1.** Transient absorption spectra from laser photolysis of **6** in hexanes solution (ca.  $4 \times 10^{-3} \text{ M}$ ) recorded 0.13 - 0.16  $\mu\text{s}$  (○) and 17.7 - 17.8  $\mu\text{s}$  (□) after the laser pulse. The inset shows absorbance-time profiles recorded at 290 nm and 510 nm.

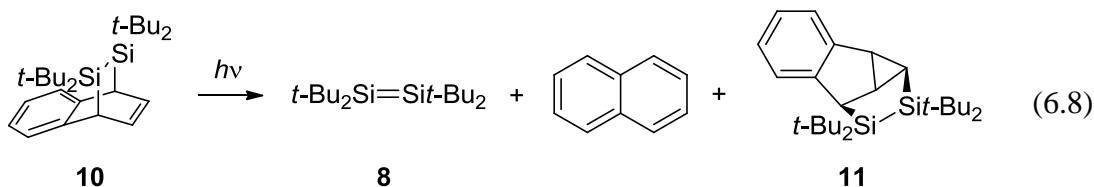
Accompanying the decay of the silylene is the growth of a second species which exhibits  $\lambda_{\text{max}} = 430 \text{ nm}$  and 290 nm and appears to be stable over a timescale of ca. 360  $\mu\text{s}$ . We

assign the promptly formed species to *Sit*-Bu<sub>2</sub>, based on comparisons to the reported spectrum of the species in a 3-methylpentane matrix at 77 K ( $\lambda_{\text{max}} = 480 \text{ nm}$ ).<sup>60</sup> The long wavelength absorption band for *Sit*-Bu<sub>2</sub> also agrees well with the results of TDDFT calculations, which predict  $\lambda_{\text{max}} = 505 \text{ nm}$  (determined at the TDωB97XD/def2-TZVP level of theory). The spectrum is red-shifted compared to those of SiMe<sub>2</sub> ( $\lambda_{\text{max}} = 465 \text{ nm}$ )<sup>18,22</sup> and the stable dialkylsilylene **1** ( $\lambda_{\text{max}} = 440 \text{ nm}$ ; see eq. 6.1),<sup>13</sup> which has been rationalized as due to widening of the C-Si-C bond angle by the sterically bulky substituents.<sup>60</sup> The spectrum of the secondary product and its apparent stability is in reasonable agreement with those reported for disilene **8** ( $\lambda_{\text{max}} = 305 \text{ nm}$  ( $\epsilon = 5200 \text{ M}^{-1} \text{ cm}^{-1}$ ), 433 nm ( $\epsilon = 2800 \text{ M}^{-1} \text{ cm}^{-1}$ )) in methylcyclohexane-*d*<sub>14</sub>.<sup>62</sup> Assuming a value on the order of ca.  $500 \text{ M}^{-1} \text{ cm}^{-1}$  for the molar extinction coefficient of *Sit*-Bu<sub>2</sub> at 530 nm - similar to the value reported for **1** ( $\epsilon_{440\text{nm}} = 500 \text{ M}^{-1} \text{ cm}^{-1}$ )<sup>13</sup> - kinetic analysis of the 530 nm decay profile affords a second order rate constant  $k_{\text{dim}} \approx 2 \times 10^{10} \text{ M}^{-1} \text{ s}^{-1}$ , consistent with a diffusion-controlled process.<sup>63</sup> These observations suggest the 248 nm photolysis of **6** generates cyclohexene and *Sit*-Bu<sub>2</sub> as co-products, with the latter decaying via diffusion-controlled dimerization to yield disilene **8** (see eq. 6.7).



The relative band intensities of **8** generated from **6** (Figure 6.1) are different from those in the spectrum reported by Masamune et al,<sup>62</sup> who generated the disilene by photolysis of **10** in methylcyclohexane (eq. 6.8). The reported spectrum of **8** contains a band at 305 nm that is ca. 1.9 times greater than the band at 433 nm, likely due to a contribution from the expected photolysis co-product naphthalene ( $\epsilon_{300\text{nm}} \sim 300 \text{ M}^{-1} \text{ cm}^{-1}$

<sup>1</sup>),<sup>63</sup> which would account for some of the differences. Furthermore, co-product **11** may also contribute to the 270 - 300 nm region of the UV-vis spectrum.<sup>62</sup>



Flash photolysis of deoxygenated hexane solutions of cyclotrisilane **7** (ca.  $4 \times 10^{-5}$  M) afforded strong, long-lived UV-vis absorptions centred at 295 nm and 435 nm with apparent lifetimes in excess of 300  $\mu\text{s}$ . Figure 6.2 shows time-resolved spectra recorded ca. 0.4  $\mu\text{s}$  and ca. 7.5  $\mu\text{s}$  after the laser pulse, along with the difference spectrum calculated by subtracting the 42 - 43  $\mu\text{s}$  spectrum (not shown) from the 0.2 - 0.5  $\mu\text{s}$  spectrum, and representative absorbance-time profiles at 530 and 430 nm (Figure 6.2b). 42 - 43  $\mu\text{s}$  corresponds to the point in which the signal intensity of the 430 nm trace had decayed back to its value at the end of the laser pulse. Thus, subtracting the 42 - 43  $\mu\text{s}$  spectrum from the end-of-pulse spectrum subtracts the components of the spectrum that do not decay during the first 42 - 43  $\mu\text{s}$  after excitation.

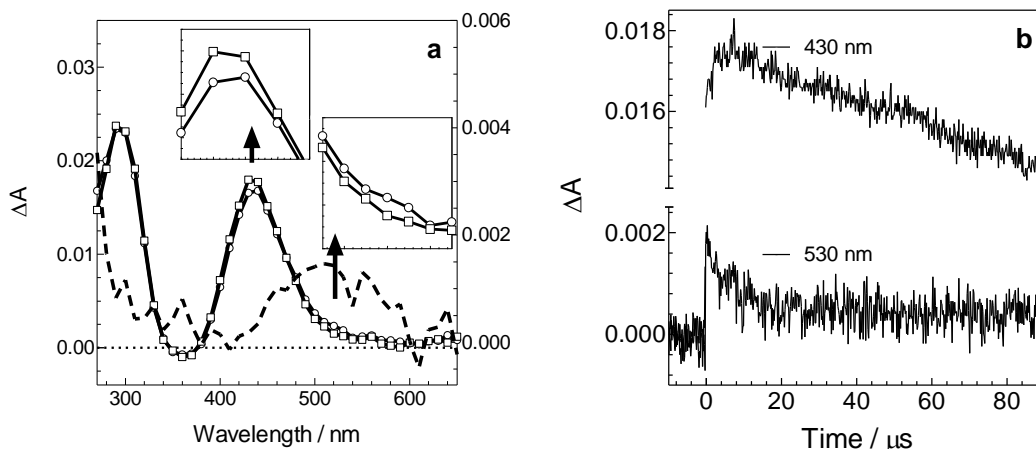
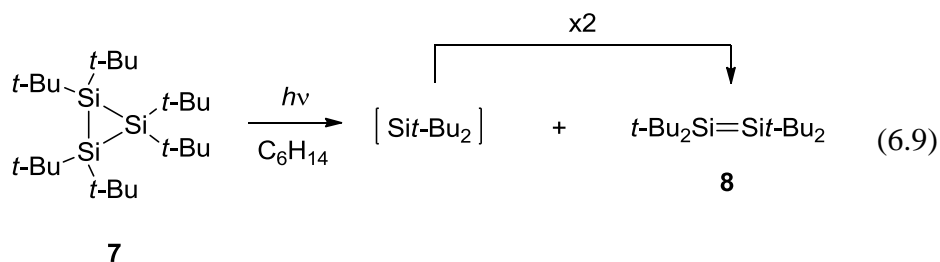


**Figure 6.2.** (a) Transient absorption spectra from laser photolysis of **7** in hexanes solution (ca.  $4 \times 10^{-5}$  M) recorded 0.16 - 0.64  $\mu\text{s}$  ( $\circ$ ) and 7.2 - 7.7  $\mu\text{s}$  ( $\square$ ) after the laser pulse. The dashed spectrum (--) shows the difference between spectra recorded 0.16 - 0.64  $\mu\text{s}$  and 42.1 - 43.0  $\mu\text{s}$  after the laser pulse scaled by a factor of 5. The insets show magnified versions of the spectra at 420 - 460 nm and 490 - 550 nm. (b) Absorbance-time profiles recorded at 430 nm and 530 nm.

Comparing spectra recorded over the first 10  $\mu\text{s}$  after excitation (Figure 6.2a) revealed additional, much weaker transient absorptions, one due to a promptly-formed species that absorbs on the long-wavelength edge of the 435 nm product band and exhibits a lifetime of  $\tau \sim 10 \mu\text{s}$ . A second set of absorptions grows in over  $\sim 10 \mu\text{s}$  and is superimposed on the two main product absorption bands. The short-lived long wavelength edge absorption is assigned to *Sit*-Bu<sub>2</sub>, based on the good agreement between its apparent  $\lambda_{\text{max}}$  ( $\sim 515$  nm) and second-order decay rate coefficient ( $2k/\epsilon_{530\text{nm}} = (8 \pm 2) \times 10^7 \text{ cm s}^{-1}$ ) with that observed from flash photolysis of **6**. The promptly formed, strongly absorbing bands are assigned to **8** generated as a direct photoproduct from **7**. The post-pulse growth in the 435 nm transient absorption band is assigned to the additional amount of **8** that is formed as the product of silylene dimerization. The difference spectrum shown in Figure 6.2a affords the most accurate determination for the absorption maximum of *Sit*-Bu<sub>2</sub> since the contribution to the overall signal from **8** has been eliminated.

Using the reported molar absorptivity value at 435 nm for **8** ( $\epsilon = 2800 \text{ M}^{-1} \text{ cm}^{-1}$ ),<sup>62</sup> the  $\Delta A$  value at 430 nm in the 0.2 - 0.5  $\mu\text{s}$  spectrum of Figure 6.2b ( $\Delta A \sim 0.165$ ) indicates the disilene was generated from **7** at a concentration of ca. 10  $\mu\text{M}$ , which is typical for our instrument. A similar calculation affords an "initial" concentration of ca. 8  $\mu\text{M}$  for *Sit*-Bu<sub>2</sub>, using the estimate of  $\epsilon_{530\text{nm}} \sim 500 \text{ M}^{-1} \text{ cm}^{-1}$  discussed above. The comparable values obtained for both photoproducts are consistent with prior studies of **7** that have suggested they are formed in equimolar quantities.<sup>52,64</sup> The transient absorption spectra recorded immediately following laser excitation of **7** and their temporal behaviour are consistent with the reaction scheme shown in eq. 6.9. If *Sit*-Bu<sub>2</sub> and **8** are the only species responsible for the transient absorption of Figure 6.2, and the only decay pathway available to *Sit*-Bu<sub>2</sub> is dimerization, the post-pulse growth of the 435 nm is expected to lead to a 50 % increase of  $\Delta A_{435\text{nm}}$  from its value immediately after the pulse, in a manner similar to that reported for laser photolysis of hexamethylcyclotrigermane.<sup>65,66</sup> However, the 430 nm absorbance-time profile in Figure 6.2 indicates that  $\Delta A_{430}$  increases by only ca. 10 % from its value immediately after the laser pulse. This suggests that only a portion of the initially produced *Sit*-Bu<sub>2</sub> decays to form **8**.



Given the precedent for triethylsilane (Et<sub>3</sub>SiH) and cyclohexene to be effective trapping agents for *Sit*-Bu<sub>2</sub>,<sup>49-52,60,67</sup> we used these silylene substrates to examine the reactivities of the promptly formed transients from both **6** and **7** to gain evidence for a common assignment to *Sit*-Bu<sub>2</sub>. Indeed, addition of the silane or alkene in millimolar concentrations to solutions of **7** resulted in increases in the rate of decay of the species

(monitored at 530 nm to reduce spectral overlap) and a change in decay kinetics from second-order to pseudo-first order. Non-linear least squares analysis of the decays according to eq. 6.10 at each substrate concentration studied afforded decay rate coefficients ( $k_{\text{decay}}$ ) that increased linearly with concentration, consistent with an overall second order reaction. Linear least squares analysis of the  $k_{\text{decay}}$ -concentration data according to eq. 6.11 afforded bimolecular rate constants of  $k_{\text{Cyclohexene}} = (1.8 \pm 0.2) \times 10^8 \text{ M}^{-1} \text{ s}^{-1}$  (see Figure 6.3) and  $k_{\text{Et}_3\text{SiH}} = (8 \pm 2) \times 10^8 \text{ M}^{-1} \text{ s}^{-1}$  (see Figure S6.2c). The formation of **8** (i.e. growth of the signal at 430 nm) was suppressed in the presence of added substrate, consistent with it being the product of silylene decay; this behaviour is expected if the reaction between the silylene and the substrate is irreversible on the timescale of the experiment. The portion of **8** formed instantaneously was found to be unaffected upon addition of the substrate up to a concentration of ca. 5 mM for  $\text{Et}_3\text{SiH}$  and ca. 10 mM for cyclohexene. Similar observations were made for the silylene and disilene upon addition of these reagents to a solution with **6**, and with the silylene (measured at 530 nm) afforded bimolecular rate constants of  $k_{\text{Q}} = (2.6 \pm 0.3) \times 10^8 \text{ M}^{-1} \text{ s}^{-1}$  and  $k_{\text{Q}} = (1.25 \pm 0.11) \times 10^9 \text{ M}^{-1} \text{ s}^{-1}$  for cyclohexene and  $\text{Et}_3\text{SiH}$ , respectively. These values are in reasonable agreement with those determined using **7**. The value of  $k_{\text{cyclohexene}}$  allows us to conclude that, in our flash photolysis experiments with **6**, the contribution from the reaction between the photolysis co-products towards the overall lifetime of  $\text{Si}t\text{-Bu}_2$  is expected to be negligible: given  $[\text{cyclohexene}] \sim 10 \text{ }\mu\text{M}$  from **6**, the product  $k_{\text{Q}}[\text{Q}] \sim 10^3 \text{ s}^{-1}$  is orders of magnitude smaller than the measured decay coefficient at "0" concentration ( $k_0 \sim 0.2 \times 10^6 \text{ s}^{-1}$ ; see Figure 6.3).

$$\Delta A_t = \Delta A_{\text{res}} + (\Delta A_0 - \Delta A_{\text{res}}) \exp(-k_{\text{decay}}t) \quad (6.10)$$

$$k_{\text{decay}} = k_0 + k_{\text{Q}}[\text{Q}] \quad (6.11)$$

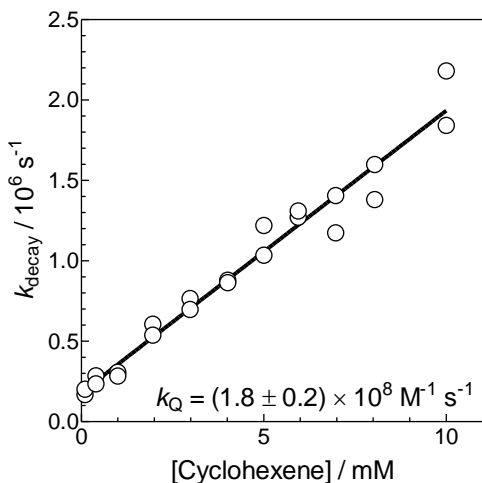


**Figure 6.3.** Plot of  $k_{\text{decay}}$  versus [cyclohexene] for the reaction of  $\text{Si}t\text{-Bu}_2$  with cyclohexene in a hexanes solution of **7** at 25 °C, the silylene is monitored at 530 nm. The solid line is the linear least squares fit of the data to eq. 6.11.

Diethyl ether ( $\text{Et}_2\text{O}$ ) was next examined as the silylene substrate, which is of particular interest as reactions with  $\text{SiMe}_2$ ,  $\text{SiPh}_2$  and  $\text{SiMes}_2$  give rise to measurable  $K_{\text{eq}}$  values, and also lead to the formation of the corresponding Lewis acid-base complexes which can be detected by transient UV-vis spectroscopy.<sup>19,23,68</sup> Addition of  $\text{Et}_2\text{O}$  to a hexanes solution of **7** led to a decrease in the maximum signal intensity at 530 nm but had no effect on the decay rate coefficient. The initial absorbance of the silylene is represented by the term  $(\Delta A_0)_0$ , while in the presence of ether is given the term  $(\Delta A_0)_Q$ . Such behaviour is consistent with rapid and reversible reaction between the transient and the substrate, characterized by an equilibrium constant ( $K_{\text{eq}}$ ) smaller than ca.  $10^3 \text{ M}^{-1}$ .<sup>68,69</sup> The relative decrease in the initial signal intensity (i.e.  $(\Delta A_0)_0 / (\Delta A_0)_Q$ ) is linear with respect to  $[\text{Et}_2\text{O}]$  and, according to eq. 6.12, affords the equilibrium constant  $K_{\text{eq}} = (14 \pm 2) \text{ M}^{-1}$  (Figure 6.4a).

$$(\Delta A_0)_0 / (\Delta A_0)_Q = 1 + K_{\text{eq}}[\text{Q}] \quad (6.12)$$

A transient absorption spectrum, recorded 0.35 - 0.43  $\mu\text{s}$  after the laser pulse with a hexanes solution of **6** containing ca. 0.4 M  $\text{Et}_2\text{O}$  (Figure 6.4b), reveals the presence of a short lived transient species centred at ca. 310 nm with a lifetime of 1.4  $\mu\text{s}$ . These

spectroscopic characteristics resemble those reported for  $\text{SiMe}_2\text{-Et}_2\text{O}$  and  $\text{SiMe}_2\text{-THF}$  complexes under similar conditions,<sup>18,68</sup> and thus can be assigned to the  $t\text{-Bu}_2\text{Si-OEt}_2$  complex (**12**). A spectrum recorded 0.25 - 0.30  $\mu\text{s}$  after the laser pulse with a hexanes solution of **7** containing ca. 0.2 M  $\text{Et}_2\text{O}$  consists of bands due to two transients (see Figure 6.4c). The difference between this early spectrum and a second spectrum recorded ca. 8.6 - 8.7  $\mu\text{s}$  after the pulse resolves a short lived absorption centred at ca. 300 nm with a lifetime of 1.4  $\mu\text{s}$ , superimposed on the more intense absorption bands due to **8**. The short lived species is assigned to the same donor-acceptor pair **12** as observed from **6** in the presence of  $\text{Et}_2\text{O}$  (Figure 6.4b). The spectrum of **12** obtained with **6** is stronger and less obscured by additional transients than that obtained with **7**, and so is considered to provide the more reliable determination of  $\lambda_{\text{max}}$ . The relative absorbances due to **12** obtained from **6** and **7** report on the relative photochemical yields of  $\text{Si}t\text{-Bu}_2$  from the two precursors. Since the laser intensity and static solution OD at the excitation wavelength were quite similar in the two experiments, the absorbance ratio is approximately equal to the ratio of quantum yields for the formation of  $\text{Si}t\text{-Bu}_2$  from the two precursors,  $\Phi_6/\Phi_7 \approx 1.4$ .

Addition of THF in sub-millimolar concentrations to hexanes solutions of **7** also led to decreases in the initial signal intensity due to  $\text{Si}t\text{-Bu}_2$ ; analysis of the data according to eq. 6.12 as discussed above affords the equilibrium constant  $K_{\text{eq}} = (1.4 \pm 0.3) \times 10^3 \text{ M}^{-1}$  (see Figure S6.1a). Transient absorption spectra recorded in the presence of 5.0 mM THF shows an absorption due to a short-lived species ( $\tau = 7.4 \mu\text{s}$ ) centred at  $\lambda_{\text{max}} = 310 \text{ nm}$ , which is assigned to the  $\text{Si}t\text{-Bu}_2\text{-THF}$  complex. The isolated spectrum of the species was calculated as a difference spectrum and is shown in Figure S6.8.



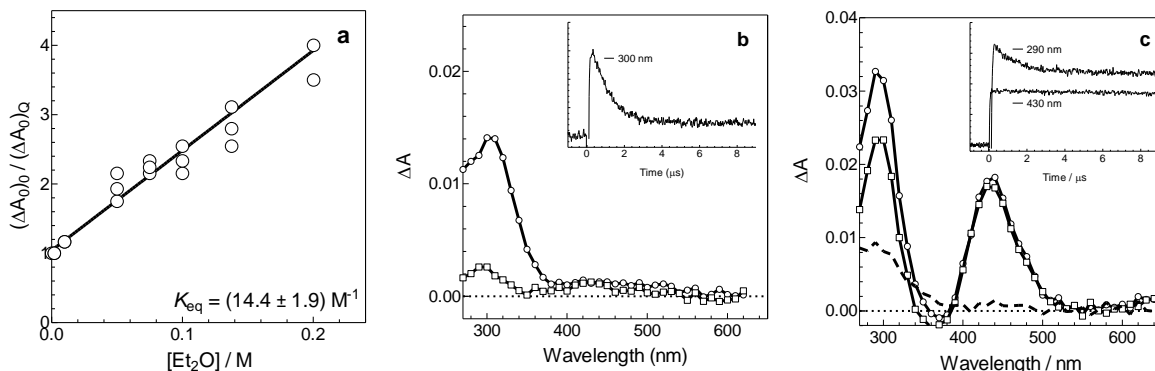


**Figure 6.4.** (a) Plot of  $(\Delta A_0)_0 / (\Delta A_0)_\infty$  versus  $[\text{Et}_2\text{O}]$  for the reaction of *Sit*-Bu<sub>2</sub> with Et<sub>2</sub>O from a hexanes solution of **7** at 25 °C, the silylene is monitored at 530 nm. The solid line is the linear least squares fit of the data to eq. 6.12. (b) Transient absorption spectra from laser photolysis of **6** in hexanes solution (ca.  $4 \times 10^{-3} \text{ M}^{-1}$ ) containing 0.40 M Et<sub>2</sub>O recorded 0.35 - 0.43 μs (○) and 8.6 - 8.7 μs (□) after the laser pulse. The inset shows the transient profile recorded at 300 nm. (c) Transient absorption spectra from laser photolysis of **7** in hexanes solution (ca. 0.04 mM) containing 0.20 M Et<sub>2</sub>O recorded 0.25 - 0.30 μs (○) and 8.6 - 8.7 μs (□) after the laser pulse. The dashed spectrum (--) shows the difference between the spectra recorded 0.25 - 0.30 μs and 8.6 - 8.7 μs after the laser pulse. The inset shows the transient profile recorded at 290 nm and 430 nm.

Absolute rate and/or equilibrium constants for the reactions of *Sit*-Bu<sub>2</sub> with eleven additional substrates were measured using **7** (mainly) as the photoprecursor and are summarized in Table 6.1. Also included in the table are the corresponding values for SiMe<sub>2</sub> to enable direct comparisons. Although **7** exhibits more complicated transient spectra and reduced signal intensity of the silylene relative to those from **6**, it has the advantage of being insensitive to air and moisture, and has a ca. 100 fold higher molar absorptivity at the irradiation wavelength, which means that much smaller amounts of material are required for an experiment. The outcomes of the reactions with *Sit*-Bu<sub>2</sub> have been documented in the cases of Et<sub>3</sub>SiH,<sup>4</sup> methanol (MeOH),<sup>4</sup> acetone,<sup>22</sup> 1-hexene,<sup>6</sup> cyclohexene,<sup>23</sup> and *cis*-cyclooctene.<sup>6</sup> They can be categorized according to the five reaction types shown in equation 6.13: Lewis acid-base complexation (with Et<sub>2</sub>O, tetrahydrofuran (THF), tetrahydrothiophene (THT), and triethylamine (Et<sub>3</sub>N)), σ-bond

insertion (with  $\text{Et}_3\text{SiH}$ , MeOH, and diethylamine ( $\text{Et}_2\text{NH}$ )), ene-addition (with acetic acid (AcOH) and acetone), [2+1] cycloaddition (with cyclohexene, *cis*-cyclooctene, 1-hexene, and 2,3-dimethyl-2-butene (TME)), and reaction with an open shell substrate (molecular oxygen). In all cases except  $\text{Et}_2\text{O}$  and THF, addition of the substrate led to a shortening of the silylene lifetime in an analogous fashion to that observed for  $\text{Et}_3\text{SiH}$  and cyclohexene (*vide supra*), and thus  $k_{\text{decay}}$  versus concentration data were analyzed according to equations 6.10 and 6.11. Rate constants were also determined for the reactions of  $\text{SiMe}_2$  with *cis*-cyclooctene and TME, for comparison to the values obtained for  $\text{Si}t\text{-Bu}_2$ ; these data are shown in Figures S6.6a and S6.7a, and were obtained using **2** as a  $\text{SiMe}_2$  precursor (eq. 6.2). The absolute rate and equilibrium constants determined in these experiments are listed in Table 6.1, along with the reported values for reaction of  $\text{SiMe}_2$  with the same substrates.

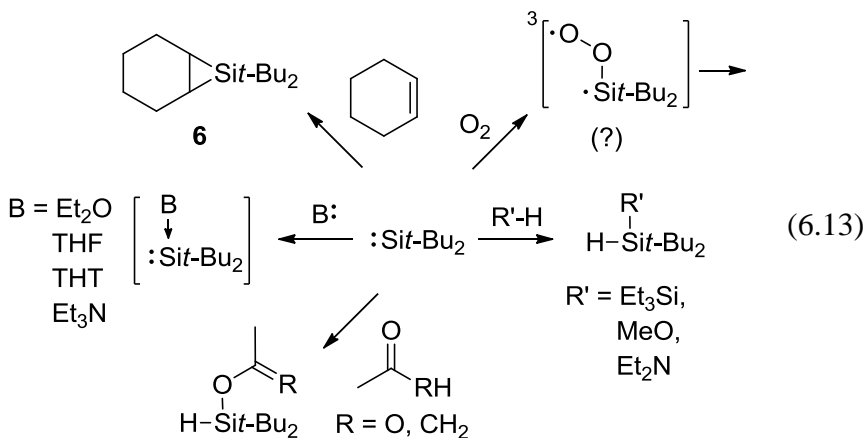


**Table 6.1.** Absolute Rate Constants ( $k_Q$ ) and Equilibrium Constants ( $K_{eq}$ ) for the Reactions of  $Si^t\text{-Bu}_2$  and  $SiMe_2$  with Various Silylene Substrates in Hydrocarbon Solution at 20 - 25 °C.<sup>a</sup>

Substrate	$k_Q^{Si^t\text{-Bu}_2}$ ( $10^9 \text{ M}^{-1} \text{ s}^{-1}$ ) <sup>b</sup> [ $K_{eq}^{Si^t\text{-Bu}_2}$ ( $\text{M}^{-1}$ )] <sup>b</sup>	Figure	$k_Q^{SiMe_2}$ ( $10^9 \text{ M}^{-1} \text{ s}^{-1}$ ) [ $K_{eq}^{SiMe_2}$ ( $\text{M}^{-1}$ )]	Ref. (Figure)
Et <sub>2</sub> O	[14.4 ± 1.9]	6.4a	[1260 ± 50]	68
THF	- [1400 ± 300]	- S6.1a	17.3 ± 1.5 -	23 -
THT	10 ± 4	S6.1c	21 ± 2	38
Et <sub>2</sub> NH	8 ± 2	S6.2b	16 ± 3	37
Et <sub>3</sub> N	0.53 ± 0.09	S6.1b	9.8 ± 0.8	37
Et <sub>3</sub> SiH	0.8 ± 0.2 (1.2 ± 0.1)	S6.2c S6.5b	3.6 ± 0.3	22
MeOH	6.3 ± 1.6	S6.2a	21 ± 3	36
AcOH	4.0 ± 0.6	S6.3a	15.9 ± 1.0	23
Acetone	18.9 ± 3.1	S6.3b	14.1 ± 1.2	23
O <sub>2</sub> <sup>d</sup>	0.19 ± 0.04	S6.3c	0.47 ± 0.04	23
Cyclohexene	0.18 ± 0.02 (0.26 ± 0.03)	6.3 S6.5a	7.8 ± 1.0	23
<i>Cis</i> -Cyclooctene	0.96 ± 0.07	S6.4b	9.0 ± 0.4	(S6.6a)
1-hexene	1.13 ± 0.07	S6.4a	7.3 ± 1.1 <sup>c</sup>	19
TME	0.031 ± 0.002	S6.4c	9.3 ± 1.0	(S6.7a)

<sup>a</sup>In hexanes at 25 °C unless otherwise noted. Errors are quoted as twice the standard error obtained from the least-squares analyses; <sup>b</sup>Measured by laser photolysis of **7**; values determined using **6** as precursor are in parentheses; <sup>c</sup>(cyclohexane; 22 °C; estimated error ± 15%); <sup>d</sup>Estimated using values of  $k_{decay}$  measured in argon, air and O<sub>2</sub> saturated solutions of anhydrous hexane.<sup>63</sup>

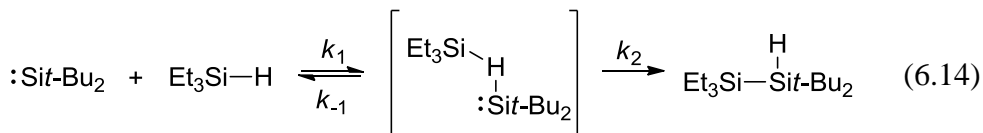
Transient absorption spectra were reported in those cases where a new transient product was observed as a result of the reaction between  $\text{Si}t\text{-Bu}_2$  and the substrate, and were recorded at a sufficiently high concentration of substrate such that the free silylene could not be detected. In most of these cases the spectra were recorded using **6** as precursor, in order to obtain an absorption spectrum of the new transient species with minimal spectral interference from disilene **8**. Of the reactive substrates examined in this study, new transient products were observed in the presence of  $\text{Et}_2\text{O}$ , THF, THT, and  $\text{Et}_2\text{NH}$ , and are assigned to the corresponding Lewis acid-base complexes between the silylene and donor substrate based on the similarities in  $\lambda_{\text{max}}$  to the corresponding  $\text{SiMe}_2$  complexes.<sup>19,37,38</sup> No additional transient products were observed with the other silylene substrates; the spectrum obtained with a solution of **6** with 1.5 mM  $\text{Et}_3\text{N}$  showed a strong transient absorption at 280 nm that has been shown to originate from direct photolysis of the amine,<sup>70</sup> and so a spectrum of the expected complex could not be obtained. Table 6.2 summarizes the UV-vis absorption maxima and lifetimes of each of the Lewis acid-base complexes, along with those reported previously for the corresponding complexes with  $\text{SiMe}_2$ .<sup>19,22,37,38</sup> In both cases, the transient products exhibit intense absorption bands with maxima that range between 290 nm and 340 nm, blue-shifted relative to the spectrum of the free silylene. The spectra of the  $\text{Si}t\text{-Bu}_2$ -donor complexes are red-shifted slightly relative to those of the corresponding  $\text{SiMe}_2$ -donor complexes. This trend is likely due to widening of the C-Si-C bond angles, as in the spectra of the free silylenes.<sup>60</sup>

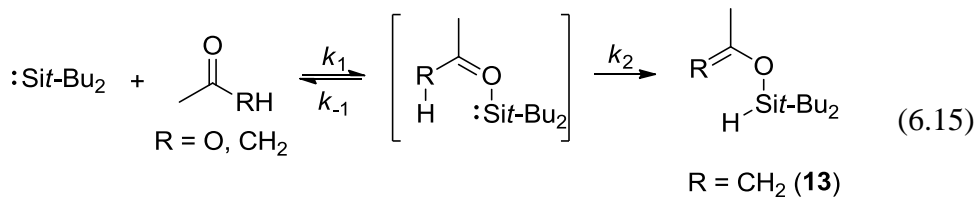
**Table 6.2.** UV-vis Absorption Maxima ( $\lambda_{\max}$ , nm) and Lifetimes ( $\tau$ ,  $\mu\text{s}$ ) of the Lewis Acid-Base Complexes of *Sit*-Bu<sub>2</sub> and SiMe<sub>2</sub> with Chalcogen and Pnictogen Donors in Hydrocarbon Solution at 20 - 25 °C.

Substrate	<i>Sit</i> -Bu <sub>2</sub> <sup>a</sup>			SiMe <sub>2</sub>		
	$\lambda_{\max}$ (nm)	$\tau$ ( $\mu\text{s}$ )	Fig.	$\lambda_{\max}$ (nm)	$\tau$ ( $\mu\text{s}$ )	Ref.
none	515 <sup>b</sup>	1.9 <sup>b</sup>	6.1, 6.2	465	0.25-0.6	22
Et <sub>2</sub> O	310	0.9	6.4b, 6.4c	305 <sup>c</sup>	4.0 <sup>c</sup>	19
THF	310 <sup>b</sup>	7.4 <sup>b</sup>	S6.8	310 <sup>c</sup>	12.5 <sup>c</sup>	19
THT	340	22	S6.9a	325	>10	38
Et <sub>2</sub> NH	290	1.1	S6.9b	280	27	37

<sup>a</sup>Measured by laser flash photolysis of deoxygenated solutions of **6** in anhydrous hexane at 25 °C unless otherwise specified; <sup>b</sup>Values determined using **7** as precursor, obtained from the difference spectrum in Figure S6.8 for THF; <sup>c</sup>Cyclohexane at 22 °C.

The  $\sigma$ -bond insertion reaction of *Sit*-Bu<sub>2</sub> with Et<sub>3</sub>SiH in solution has been well documented, and has been used to provide evidence for the formation of the silylene in early studies of the photochemistry of both **6** and **7** (eq. 6.14).<sup>50,52</sup> Other transient silylenes have been efficiently trapped in solution as the formal ene (or O-H insertion) product with AcOH,<sup>23</sup> while *Sit*-Bu<sub>2</sub> generated from **7** reacts with acetone to afford the silyl enol ether **13** (eq. 6.15).<sup>71</sup> The mechanistic aspects of these reactions in the case of the parent silylene SiH<sub>2</sub> have been the subject of theoretical investigations and gas phase kinetics studies;<sup>17,26,33,72</sup> the accepted mechanisms involve initial, reversible coordination of the silylene with the substrate (with equilibrium constant  $K_1 = k_1/k_{-1}$ ), followed by unimolecular rearrangement with rate constant  $k_2$  (eq. 6.14 - 6.15).





$$k_Q = k_1 k_2 / k_{-1}$$

In our flash photolysis studies of *Si**t*-Bu<sub>2</sub>, the reactions of the silylene with Et<sub>3</sub>SiH, AcOH, and acetone proceed without the formation of an intermediate that could be detected under our conditions. Such behaviour is analogous to earlier kinetic studies carried out for SiMe<sub>2</sub>,<sup>22,23</sup> and indicate that if intermediates are involved, they proceed to product too rapidly to be detected. Thus the overall second order rate constants measured in our own experiments (*k*<sub>Q</sub>), according to the schemes in eq. 6.14 - 6.15, are the product of the terms *K*<sub>1</sub> and *k*<sub>2</sub> (i.e. *k*<sub>Q</sub> = *K*<sub>1</sub>*k*<sub>2</sub>; *K*<sub>1</sub> = *k*<sub>1</sub>/*k*<sub>-1</sub>), assuming the equilibrium approximation holds for the reaction intermediate.

The results of low temperature matrix and solution phase studies indicate that transient silylenes react with O<sub>2</sub> to produce the corresponding dioxasilirane via a triplet silanone oxide intermediate.<sup>23,73-75</sup> However, no new product absorptions could be detected in experiments carried out with **7** in O<sub>2</sub>-saturated hexanes (see Figure S6.10b); similar results were reported previously for SiMe<sub>2</sub> in O<sub>2</sub>-saturated hexane. In both cases it can be concluded that the corresponding dioxasilirane or triplet silanone oxide, if formed, either does not build up to sufficient concentrations or does not absorb strongly enough in the 270 - 620 nm region of the UV-vis spectrum to be detected.

[2+1]-Cycloadditions of *Si**t*-Bu<sub>2</sub> with alkenes have been well documented,<sup>54,64,76</sup> and additional mechanistic insight for this reaction would be informative given its utility in generating 5-membered ring silacycles with high stereospecificity.<sup>40,47,77</sup> In our kinetic examination of *Si**t*-Bu<sub>2</sub>, we report bimolecular rate constants with four aliphatic alkenes (Table 6.1): 1-hexene, cyclohexene, *cis*-cyclooctene, and TME, employing both cyclic

and acyclic alkenes with variable degrees of alkyl substitution. The rate constants decrease with increasing alkyl substitution on the alkene over a 40-fold range in the order: 1-hexene > *cis*-cyclooctene > cyclohexene > TME. Comparing the cycloalkenes also reveals a five-fold difference in the rates obtained between cyclohexene and *cis*-cyclooctene. This latter finding appears to parallel the relative thermal stabilities of the corresponding silirane products,<sup>51</sup> whereby the cyclohexene derived product experiences additional steric interactions. By contrast, the rate constants determined for SiMe<sub>2</sub> exhibited much lower sensitivity to the change in substrate. The differences in reactivity between the alkenes for Sit-Bu<sub>2</sub>, but not with SiMe<sub>2</sub>, support the conclusion that these reactions are influenced by a steric interaction with the larger *tert*-butyl substituents. These findings also support the conclusion that the steric interaction becomes more significant with increased alkyl substitution on the alkene.

With reference to previous studies, the results of our work can be used to make additional inferences into the behaviour of Sit-Bu<sub>2</sub> in solution, assuming the relative rate constants for its reactions do not vary significantly with differences in temperature and solvent. Woerpel and coworkers have proposed the intermediacy of Sit-Bu<sub>2</sub> in the thermal silylene transfer from **6** to substituted alkenes,<sup>51</sup> and determined the relative rate constants for reaction of two cycloalkenes and allylbenzene via competitive silylene trapping experiments (i.e.  $k_{\text{rel}} = k_{\text{cycloalkene}} / k_{\text{allylbenzene}}$ ), affording values of  $k_{\text{rel}} = 1.37 \pm 0.11$  for cyclopentene and  $1.34 \pm 0.08$  for *cis*-cyclooctene.<sup>51</sup> The rate constant determined for *cis*-cyclooctene in this work provides an estimate of that for the reaction with allylbenzene of  $k_{\text{Q}} \sim 0.7 \times 10^9 \text{ M}^{-1} \text{ s}^{-1}$ . This result suggests that allylbenzene is ca. 1.6 times less reactive than 1-hexene towards [2+1] cycloaddition with Sit-Bu<sub>2</sub>.

Table 6.3 expresses the rate and equilibrium constants of Table 6.1 as rate and equilibrium constant ratios, which reflect the relative reactivities of SiMe<sub>2</sub> and Si*t*-Bu<sub>2</sub> with the various substrates that have been studied (eq. 6.16 and 6.17).

$$k_{\text{rel}} = k_{\text{Q}}^{\text{SiMe}_2} / k_{\text{Q}}^{\text{Si-}t\text{-Bu}_2} \quad (6.16)$$

$$K_{\text{rel}} = K_{\text{eq}}^{\text{SiMe}_2} / K_{\text{eq}}^{\text{Si-}t\text{-Bu}_2} \quad (6.17)$$

In almost all cases  $k_{\text{rel}}$  exceeds unity, indicating a general impediment in the reactivity of the silylene with the *tert*-butyl for methyl substitution at the silicon centre. The values for  $k_{\text{rel}}$  range between  $0.8 < k_{\text{rel}} < 300$  and largely reflect the ca. 600 fold variation in  $k_{\text{Q}}^{\text{Si-}t\text{-Bu}_2}$ . Reactions with SiMe<sub>2</sub> by comparison show little variation in  $k_{\text{Q}}^{\text{SiMe}_2}$  between substrates; with the exception of O<sub>2</sub>, all fall within a factor of six of the diffusion controlled rate constant in hexanes solution. With the exclusion of the [2+1] cycloaddition with alkenes, and with the exception of Et<sub>3</sub>N which exhibits higher sensitivity towards steric effects ( $k_{\text{rel}} = 19 \pm 4$ ), the reactions of Si*t*-Bu<sub>2</sub> with THT, Et<sub>2</sub>NH, Et<sub>3</sub>SiH, AcOH, MeOH, acetone and O<sub>2</sub> exhibit a relatively minor sensitivity to steric effects, where the relative rates  $k_{\text{rel}} < 6$ . The smallest values ( $k_{\text{rel}} < 2.5$ ) were obtained with THT, Et<sub>2</sub>NH, acetone and O<sub>2</sub>; with acetone the value approaches unity (i.e.  $k_{\text{rel}} \sim 1$ ) or within error implies an overall rate increase with Si*t*-Bu<sub>2</sub>. The latter statement implies that one or both of the terms  $K_1$  and  $k_2$  (likely  $k_2$  given the values of  $K_{\text{rel}}$  determined in this work (see Table 6.3)) is larger with the increase in steric hindrance; this will be the subject of a broader investigation of the reaction of silylenes with carbonyl compounds. The largest rate reductions were found with cycloaddition reactions, and the substitution pattern on the alkene imparting the greatest effect on  $k_{\text{rel}}$ . The *tert*-butyl for methyl substitution on the silylene also leads to a destabilization of the silylene-ether Lewis acid-base complexes relative to its free reagents, with Et<sub>2</sub>O affording the ratio of equilibrium constants  $K_{\text{rel}} = 90 \pm 10$ .



Also included in Table 6.3 are the ratio of rate and equilibrium constants for the same set of reactions of SiPh<sub>2</sub> and SiMes<sub>2</sub>. In addition to using values that have been previously measured,<sup>22-24,36-38,68,78</sup> we report in this work four additional quenching rate constants with 1-hexene and TME to enable a more comprehensive comparison. The rate constants were determined using **3** and **4** as precursors to SiPh<sub>2</sub> and SiMes<sub>2</sub>, respectively (eq. 6.2). Linear least squares analysis of the plots of  $k_{\text{decay}}$  for the silylene versus substrate concentration (see Figures S6.6b, S6.6c, S6.7b, and S6.7c) according to eq. 6.11 affords bimolecular rate constants  $k_{1\text{-hexene}} = (5.9 \pm 0.3) \times 10^9 \text{ M}^{-1} \text{ s}^{-1}$  and  $k_{\text{TME}} = (4.3 \pm 0.1) \times 10^9 \text{ M}^{-1} \text{ s}^{-1}$  for SiPh<sub>2</sub>, and  $k_{1\text{-hexene}} = (1.02 \pm 0.03) \times 10^7 \text{ M}^{-1} \text{ s}^{-1}$  and  $k_{\text{TME}} = (1.67 \pm 0.09) \times 10^6 \text{ M}^{-1} \text{ s}^{-1}$  for SiMes<sub>2</sub>. The reduction in reactivity with increasing substitution in the diarylsilylene system parallels the observations for the *tert*-butyl for methyl substitution in this work, although it spans a wider range, varying from  $1.7 < k_{\text{rel}} < 2800$ . With the exception of AcOH, the substrates when ranked according to  $k_{\text{rel}}$  (within experimental error) follow the same ordering for both dialkyl- and diarylsilylene systems. A comparison of  $K_{\text{rel}}$  for the complexation with Et<sub>2</sub>O yields the same conclusion as with  $k_{\text{rel}}$ .

**Table 6.3.** Ratio of Absolute Rate Constants ( $k_Q$ ) and Equilibrium Constants ( $K_{eq}$ ) Between the Silylene Pairs SiMe<sub>2</sub>:*Sit*-Bu<sub>2</sub> and SiPh<sub>2</sub>:SiMes<sub>2</sub> with Various Silylene Substrates in Hydrocarbon Solution at Ambient Temperatures.

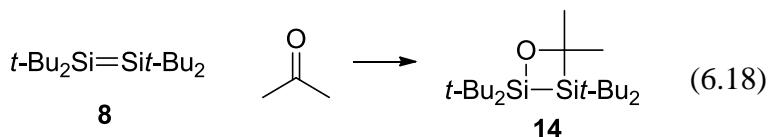
Substrate	$\frac{k_Q^{\text{SiMe}_2} / k_Q^{\text{Si}t\text{Bu}_2}}{[K_{eq}^{\text{SiMe}_2} / K_{eq}^{\text{Si}t\text{Bu}_2}]^j}$	$\frac{k_Q^{\text{SiPh}_2} / k_Q^{\text{SiMes}_2}}{[K_{eq}^{\text{SiPh}_2} / K_{eq}^{\text{SiMes}_2}]}$
Et <sub>2</sub> O	[90 ± 10]	[7900 ± 1100] <sup>a</sup>
THF	[> 18] <sup>k</sup>	[> 10000] <sup>a,k</sup>
THT	2.1 ± 0.9	2.3 ± 0.7 <sup>a,b</sup>
Et <sub>2</sub> NH	2.0 ± 0.6	[> 17] <sup>a,k</sup>
Et <sub>3</sub> N	19 ± 4	2.2 ± 0.4 <sup>c</sup>
Et <sub>3</sub> SiH	4.6 ± 1.0	[> 4.0] <sup>c,k</sup>
AcOH	4.0 ± 0.6	-
MeOH	3.3 ± 1.0	[> 190] <sup>c,k</sup>
Acetone	0.8 ± 0.1	42 ± 3 <sup>d,e</sup>
O <sub>2</sub>	2.5 ± 0.6	2.9 ± 0.4 <sup>f,i</sup>
Cyclohexene	43 ± 7	18 ± 2 <sup>h</sup>
<i>Cis</i> -cyclooctene	9.4 ± 0.8	1.7 ± 0.2 <sup>d</sup>
1-hexene	6.5 ± 1.1	3.8 ± 0.8 <sup>e,f</sup>
TME	300 ± 40	2800 ± 400 <sup>e,f</sup>
		<sup>g</sup>

<sup>a</sup>Data from ref<sup>68</sup>; <sup>b</sup>SiPh<sub>2</sub> data from ref<sup>38</sup>; <sup>c</sup>Data from ref<sup>37</sup>; <sup>d</sup>Data from ref<sup>22</sup>; <sup>e</sup>SiMes<sub>2</sub> data from ref<sup>24</sup> (Cyclohexane; 25 °C); <sup>f</sup>SiPh<sub>2</sub> data from ref<sup>23</sup>; <sup>g</sup>not determined; <sup>h</sup>Data from ref<sup>36</sup>; <sup>i</sup>SiMes<sub>2</sub> data from ref<sup>78</sup>; <sup>j</sup>Calculated using data from Table 6.1; *Sit*-Bu<sub>2</sub> data obtained using **7** as precursor; <sup>k</sup>Upper limit provided  $K_Q^{\text{SiPh}_2}$  and  $K_Q^{\text{SiMe}_2} > 25000 \text{ M}^{-1}$ .

The reactions of tetra-*tert*-butyldisilene (**8**) in solution have been studied by Weidenbruch and coworkers, and have focused largely on the cycloaddition of unsaturated compounds (examples of which include alkenes,<sup>64</sup> alkynes,<sup>71</sup> ketones,<sup>71</sup> and

nitriles<sup>79</sup>) via the preparative-scale photolysis of **7**.<sup>54,55</sup> We have found in our flash photolysis studies of **7** that the quantity of **8** generated with the laser pulse provides an opportunity to analyse its reaction kinetics. Accelerations of the decay rate coefficient for **8** were observed from the photolysis in air- and O<sub>2</sub>-saturated hexane solutions, corresponding to O<sub>2</sub> concentrations of 3.1 and 14.7 mM, respectively.<sup>63</sup> Three-point plots of  $k_{\text{decay}}$  versus [O<sub>2</sub>], according to equation 6.11 afforded a bimolecular rate constant of  $k_Q = (2.3 \pm 0.1) \times 10^7 \text{ M}^{-1} \text{ s}^{-1}$ , regardless of whether the 310 nm or 430 nm band was monitored (see Figure S6.10a). Given the rate constant  $k_{\text{O}_2}$  for **8** in this work, a residual oxygen content of ca. 0.1 mM in the solvent would be sufficient to account for the difference in lifetimes of the disilene when generated from **7** or **6**, solutions of the latter compound would be expected not to contain residual oxygen.

The addition of acetone also results in an acceleration of the decay coefficient of **8**, consistent with the reported formation of **14** from photolysis of **7** in the presence of acetone (see eq. 6.18).<sup>71</sup> The reaction proceeds without the formation of detectable intermediates in the 270 - 620 nm region of the UV-vis spectrum (Figure 6.5b). The absorbance versus time profiles for **8** follows bi-exponential decay characteristics in the presence of substrate, with the slow component roughly constant at  $4.7 \times 10^3 \text{ s}^{-1}$ , while analysis of  $k_{\text{fast}}$  according to eq. 6.11 affords  $k_Q = (5.0 \pm 0.7) \times 10^5 \text{ M}^{-1} \text{ s}^{-1}$  (see Figure 6.5a). The slow component is attributed to the presence of residual oxygen (ca. 0.2 mM given the  $k_Q$  value for the reaction of O<sub>2</sub> with **8**) in the solution (*vide infra*).



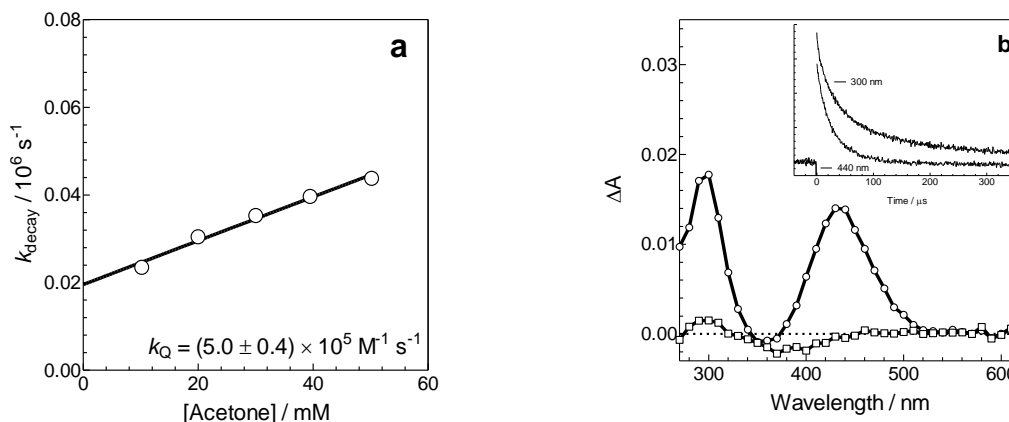


**Figure 6.5.** (a) Plot of  $k_{\text{fast}}$  versus [acetone] for the reaction of **8** with acetone in a hexanes solution of **7** at 25 °C, the disilene is monitored at 440 nm. The solid line is the linear least squares fit of the data to eq. 6.11; (b) Transient absorption spectra from laser photolysis of **7** in hexanes solution (ca. 0.04 mM) containing 50 mM acetone recorded 0.64 - 1.28  $\mu\text{s}$  ( $\circ$ ) and 344 - 347  $\mu\text{s}$  ( $\square$ ) after the laser pulse. The inset shows the transient profile recorded at 300 nm and 440 nm. The apparent negative absorption in the 340 - 430 nm regions of the UV-vis spectra is due to bleaching of **7**, which exhibits absorption maxima in this wavelength region.<sup>52</sup>

Shown in Table 6.4 is a comparison of the kinetic data for **8** to corresponding data reported for tetramethyldisilene<sup>23</sup> ( $\text{Me}_2\text{Si}=\text{SiMe}_2$ ; **15**), trimethylphenyldisilene ( $\text{MePhSi}=\text{SiMe}_2$ ; **16**)<sup>80</sup> and tetrakis(trimethylsilyl)disilene ( $(\text{Me}_3\text{Si})_2\text{Si}=\text{Si}(\text{SiMe}_3)_2$ ; **17**).<sup>81</sup> The data indicate that **8** is more reactive than **17** but less reactive than disilenes containing much smaller substituent groups.

**Table 6.4.** Absolute Rate Constants ( $k_Q$ ;  $10^6 \text{ M}^{-1} \text{ s}^{-1}$ ) for the Reactions of Disilenes with Substrates in Hexane Solution at Ambient Temperatures.

Substrate	$t\text{-Bu}_2\text{Si}=\text{Si}t\text{-Bu}_2$ <b>(8)</b>	$\text{Me}_2\text{Si}=\text{SiMe}_2^{\text{a}}$ <b>(15)</b>	$\text{MePhSi}=\text{SiMe}_2^{\text{b}}$ <b>(16)</b>	$(\text{Me}_3\text{Si})_2\text{Si}=\text{Si}(\text{SiMe}_3)_2^{\text{c}}$ <b>(17)</b>
$\text{O}_2$	$23 \pm 1$	$290 \pm 40$	$1000^{\text{d}}$	$1.1 \pm 0.1^{\text{d}}$
Acetone	$0.50 \pm 0.07$	-	580	-

<sup>a</sup>Data from ref<sup>23</sup>; <sup>b</sup>Data from ref<sup>80</sup>; <sup>c</sup>Data from ref<sup>81</sup>; <sup>d</sup>Single point determination from the lifetimes in air-saturated hexane solution.

General agreement is found between the absorption maximum for **8** in this work and a transient species exhibiting  $\lambda_{\max} = 440$  nm generated from the 266 nm flash photolysis studies of **7** reported by Gaspar et al.<sup>82</sup> In the initial report, the transient product was reported to exhibit a half-life of  $\tau_{1/2} \sim 12$  ms in cyclohexane solution, and react with O<sub>2</sub> with a rate constant of  $k_{\text{O}_2} = 7.1 \times 10^7 \text{ M}^{-1} \text{ s}^{-1}$ .<sup>82</sup> The transient species was assigned to *Sit*-Bu<sub>2</sub>, but its characteristics are clearly in line with that of disilene **8**. The discrepancy in  $k_{\text{O}_2}$  between the value obtained for **8** in this work and the value reported by Gaspar et al. could be attributed to the differences in solvent or how the experiments were carried out, however a more detailed comparison cannot be made as the reported study does not give a description of how  $k_{\text{O}_2}$  was determined.<sup>82</sup>

### 6.3. Summary and Conclusions

Laser flash photolysis of **6** and **7** affords *Sit*-Bu<sub>2</sub>, which has been detected for the first time in solution under ambient conditions. The silylene exhibits a broad absorption band centred at  $\lambda_{\max} = 515$  nm and decays with the concurrent growth of **8**, the spectral characteristics of which ( $\lambda_{\max} = 290, 430$  nm) match those reported. The decay of *Sit*-Bu<sub>2</sub> follows second order decay kinetics, affording a rate coefficient  $2k/\epsilon_{530\text{nm}} = (8.4 \pm 0.8) \times 10^7 \text{ cm s}^{-1}$ . In the case of **7**, formation of the silylene is accompanied by the formation of **8**, which exhibits an intense absorption band centred at  $\lambda_{\max} = 435$  nm, that swamps the much weaker absorption above 500 nm due to *Sit*-Bu<sub>2</sub>. Nevertheless, the silylene could be detected clearly at 520 - 530 nm and was found to decay with second order kinetics and  $2k/\epsilon_{530\text{nm}} = (8 \pm 2) \times 10^7 \text{ cm s}^{-1}$ , in good agreement with the value obtained using **6** as precursor. In spite of the fact that a generally stronger and better resolved signal for *Sit*-Bu<sub>2</sub> is obtained using **6** as the silylene precursor, **7** is the preferred precursor in studies of this type because of its comparatively low sensitivity to oxygen and moisture.

Absolute rate and equilibrium constants for reaction of *Sit*-Bu<sub>2</sub> with 14 substrates have been measured, detailing the reactivity of the silylene towards Lewis acid-base complexation, O-H and Si-H insertion, ene-addition with acetone and AcOH, and [2+1] cycloaddition reactions with aliphatic alkenes. Transient absorption spectra recorded in the presence of Lewis bases reveal the formation of short lived Lewis acid-base complexes, whose spectra are considerably blue-shifted relative to that of the free silylene, and red-shifted by 5 - 15 nm relative to the spectra of the corresponding complexes formed with SiMe<sub>2</sub>. The rate and/or equilibrium constants measured for the 14 reactions indicate that *Sit*-Bu<sub>2</sub> is consistently less reactive than the parent dialkylsilylene, SiMe<sub>2</sub> and exhibits a consistent decrease in reactivity relative to its closest silylene analogue SiMe<sub>2</sub>. The differences in rate constant are relatively small for the complexation, insertion and ene- addition reactions, affording  $k_{\text{rel}}$  values that span a range  $0.8 < k_{\text{rel}} < 19$ , where  $k_{\text{rel}} = k_{\text{Q}}^{\text{SiMe}_2} / k_{\text{Q}}^{\text{Si}t\text{Bu}_2}$ . Cycloaddition reactions exhibit  $k_{\text{rel}}$  values that are much larger and vary strongly with alkene structure, with values that span a range of  $6.5 < k_{\text{rel}} < 300$ . The equilibrium constant for complexation with Et<sub>2</sub>O is also smaller for *Sit*-Bu<sub>2</sub> than SiMe<sub>2</sub> by a factor of ca. 90. The mesityl for phenyl substitution affords a larger decrease in silylene reactivity for the substrates evaluated, and exhibits a parallel trend to the dialkylsilylenes, but the differences are greater.

#### 6.4. Supporting Information

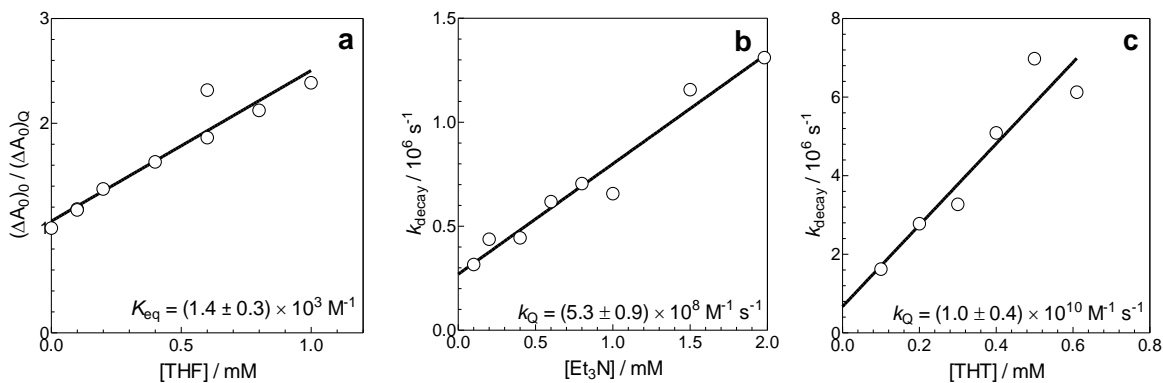


**Figure S6.1.** (a) Plot of  $(\Delta A_0)_0 / (\Delta A_0)_Q$  versus  $[\text{THF}]$  for the reaction of  $\text{Si}t\text{-Bu}_2$  with THF from flash photolysis of a hexanes solution of **7** at 25 °C. Plots of  $k_{\text{decay}}$  versus  $[\text{Q}]$  for the reactions of  $\text{Si}t\text{-Bu}_2$  with (b)  $\text{Q} = \text{Et}_3\text{N}$  and (c)  $\text{Q} = \text{THT}$  in hexanes solutions of **7** at 25 °C. The solid lines are the linear least squares fits of the data to eq. 6.12 (a) and 6.11 (b,c), respectively.

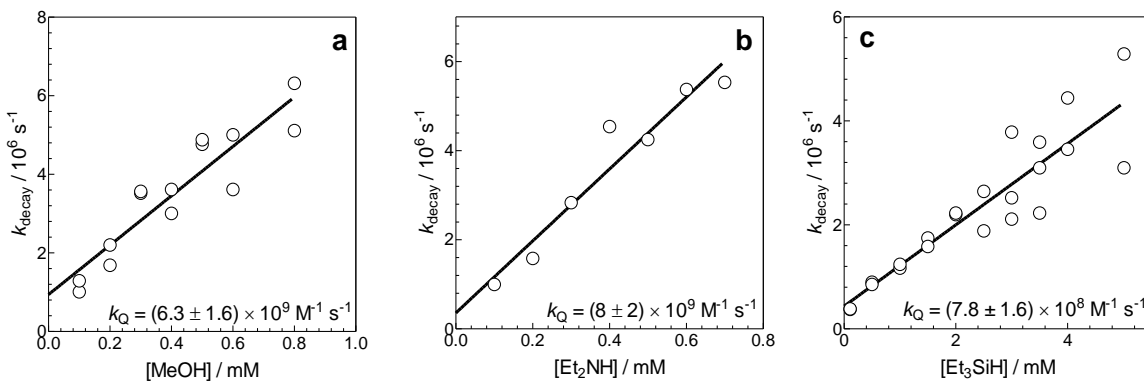


**Figure S6.2.** Plot of  $k_{\text{decay}}$  versus  $[\text{Q}]$  for the reaction of  $\text{Si}t\text{-Bu}_2$  with (a)  $\text{Q} = \text{methanol}$ , (b)  $\text{Q} = \text{Et}_2\text{NH}$  and (c)  $\text{Q} = \text{triethylsilane}$  in hexanes solutions of **7** at 25 °C. The solid lines are the linear least squares fits of the data to eq. 6.11.

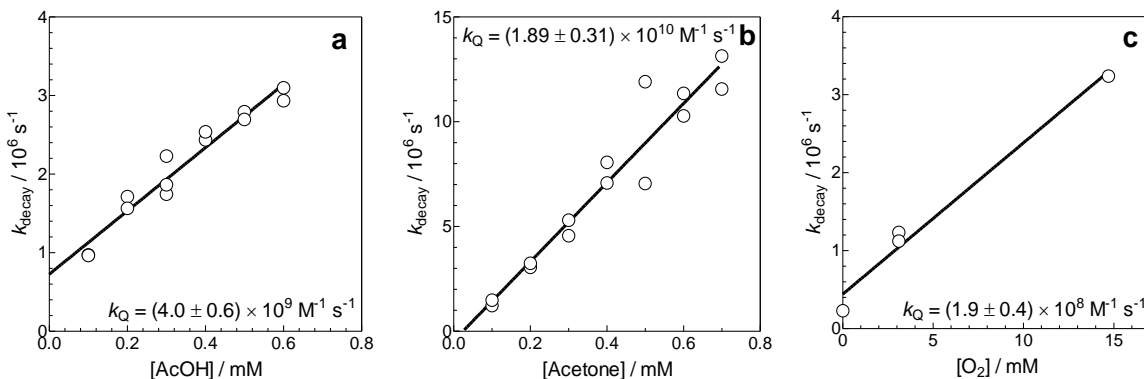


**Figure S6.3.** Plot of  $k_{\text{decay}}$  versus  $[Q]$  for the reaction of  $\text{Si}t\text{-Bu}_2$  with (a)  $Q = \text{AcOH}$ , (b)  $Q = \text{acetone}$  and (c)  $Q = \text{molecular oxygen}$  from flash photolysis of hexanes solutions of **7** at 25 °C. The solid lines are the linear least squares fit of the data to eq. 6.11.

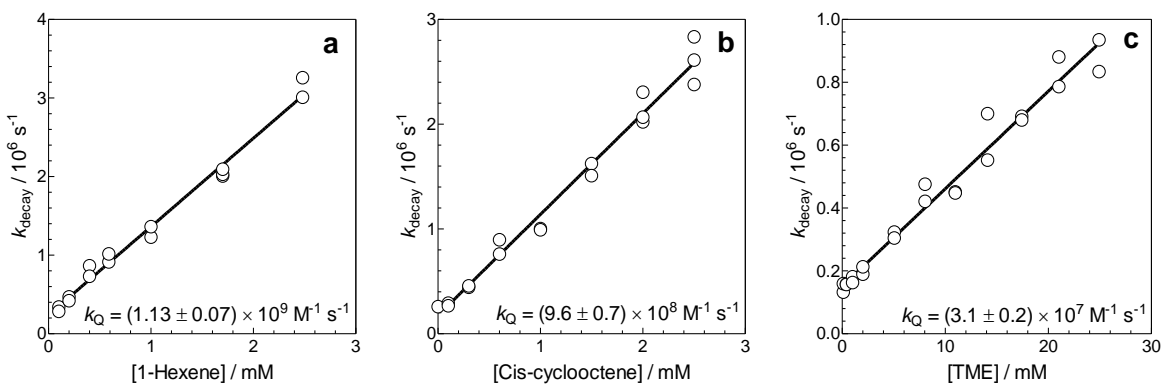


**Figure S6.4.** Plot of  $k_{\text{decay}}$  versus  $[Q]$  for the reaction of  $\text{Si}t\text{-Bu}_2$  with (a)  $Q = 1\text{-hexene}$ , (b)  $Q = \text{cis-cyclooctene}$  and (c)  $Q = \text{TME}$  in hexanes solutions of **7** at 25 °C. The solid lines are the linear least squares fit of the data to eq. 6.11.

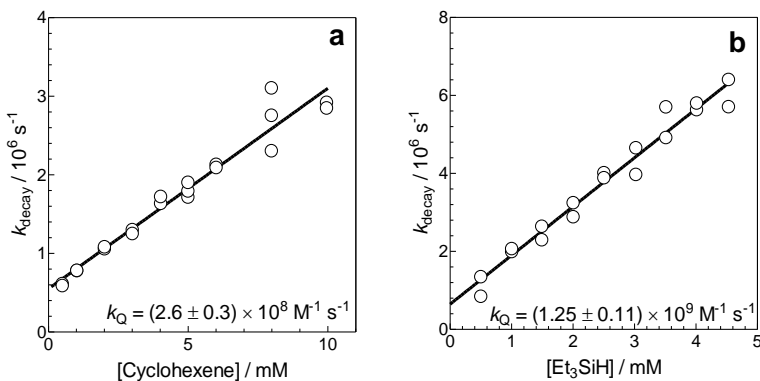


**Figure S6.5.** Plot of  $k_{\text{decay}}$  versus  $[Q]$  for the reaction of  $\text{Si}t\text{-Bu}_2$  with (a)  $Q = \text{cyclohexene}$  and (b)  $Q = \text{triethylsilane}$  in hexanes solutions of **6** at 25 °C. The solid lines are the linear least squares fits of the data to eq. 6.11.



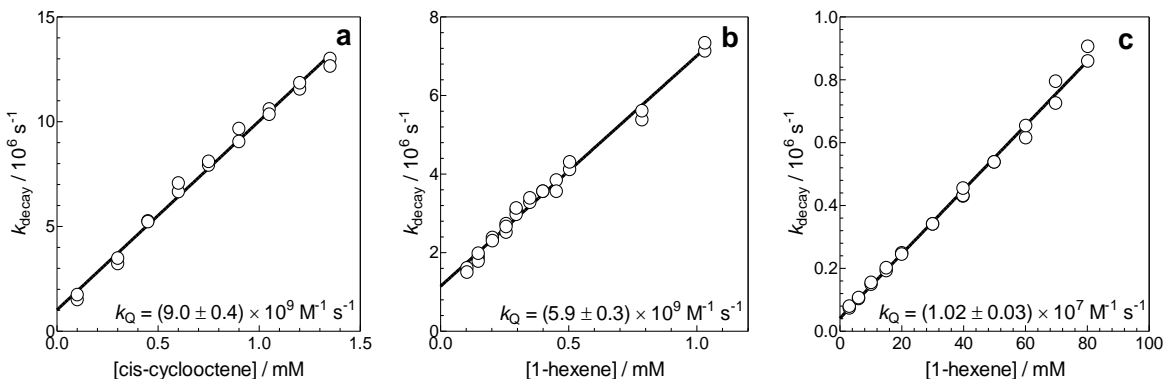


**Figure S6.6.** (a) Plot of  $k_{\text{decay}}$  versus [*cis*-cyclooctene] for the reaction of  $\text{SiMe}_2$  with *cis*-cyclooctene in a hexanes solution of **2** at 25 °C. (b) Plot of  $k_{\text{decay}}$  versus [1-hexene] for the reaction of  $\text{SiPh}_2$  with 1-hexene in a hexanes solution of **3** at 25 °C. (c) Plot of  $k_{\text{decay}}$  versus [1-hexene] for the reaction of  $\text{SiMes}_2$  with 1-hexene in a hexanes solution of **4** at 25 °C. The solid lines are the linear least squares fit of the data to eq. 6.11. (Data from (b) recorded by M. Reid)

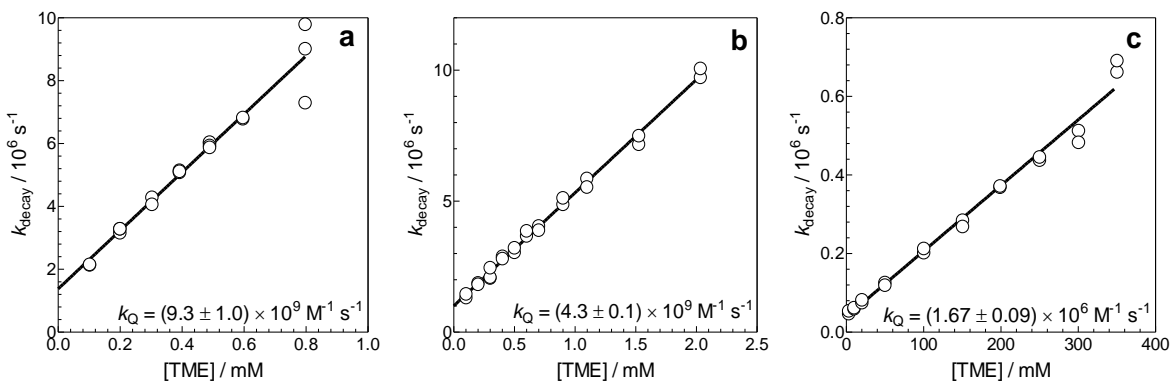


**Figure S6.7.** Plots of  $k_{\text{decay}}$  versus [TME] for the reaction of (a)  $\text{SiMe}_2$ , (b)  $\text{SiPh}_2$ , and (c)  $\text{SiMes}_2$  with TME in hexanes solutions of (a) **2**, (b) **3**, and (c) **4** at 25 °C. The solid lines are the linear least squares fit of the data to eq. 6.11. (Data from (a) and (b) recorded by M. Reid)

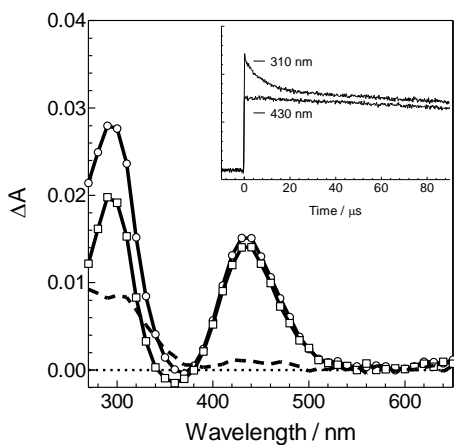


**Figure S6.8.** Transient absorption spectra from laser photolysis of **7** in a hexanes solution (ca. 0.04 mM) containing 5.0 mM THF recorded 0.16 - 0.64  $\mu$ s ( $\circ$ ) and 45.9 - 46.6  $\mu$ s ( $\square$ ) after the laser pulse. The dashed spectrum (--) shows the difference between the spectra recorded 0.16 - 0.64  $\mu$ s and 45.9 - 46.6  $\mu$ s after the laser pulse. The inset shows the transient profile recorded at 310 nm and 430 nm. The apparent negative absorption in the 340 - 430 nm regions of the UV-vis spectra in (a) and (b) is due to bleaching of **7**, which exhibits absorption maxima in this wavelength region.<sup>52</sup>

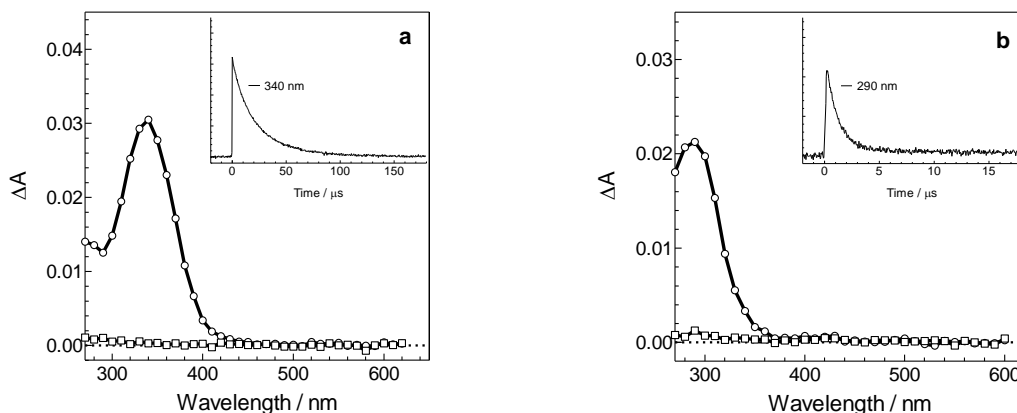


**Figure S6.9.** (a) Transient absorption spectra from laser photolysis of **6** in a hexanes solution (ca. 4 mM) containing 5.1 mM THT recorded 0.32 - 1.28  $\mu$ s ( $\circ$ ) and 172 - 173  $\mu$ s ( $\square$ ) after the laser pulse. The inset shows the transient profile recorded at 340 nm; (b) Transient absorption spectra from laser photolysis of **6** in a hexanes solution (ca. 4 mM) containing 5.0 mM Et<sub>2</sub>NH recorded 0.22 - 0.32  $\mu$ s ( $\circ$ ) and 17.2 - 17.3  $\mu$ s ( $\square$ ) after the laser pulse. The inset shows the transient profile recorded at 290 nm.

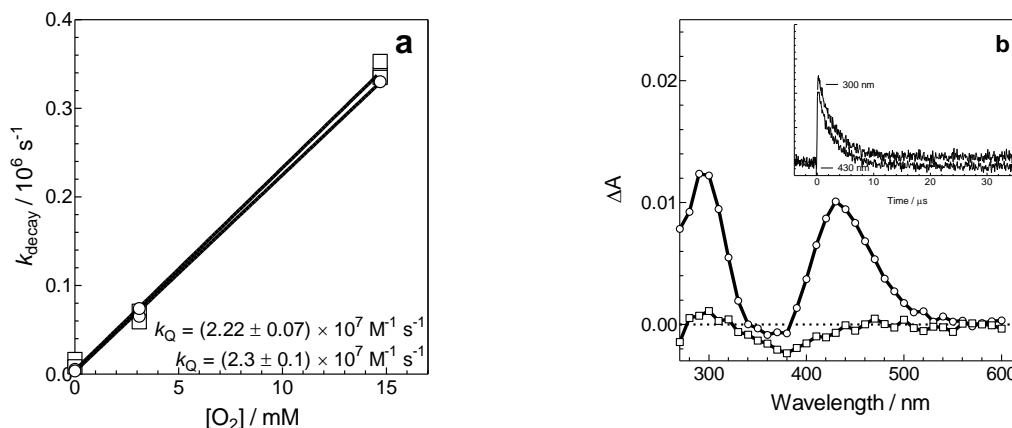


**Figure S6.10.** (a) Plot of  $k_{\text{decay}}$  versus  $[\text{O}_2]$  for the reaction of the 310 nm ( $\circ$ ) and 440 nm ( $\square$ ) transient signals with molecular oxygen in a hexanes solution of **7** at 25 °C. The solid line is the linear least squares for of the data to eq. 6.11. (b) Transient absorption spectra from laser photolysis of **7** in an  $\text{O}_2$  saturated hexanes solution (ca. 0.04 mM) recorded 0.19 - 0.38  $\mu\text{s}$  ( $\circ$ ) and 35.3 - 35.6  $\mu\text{s}$  ( $\square$ ) after the laser pulse. The inset shows the transient profile recorded at 300 nm and 430 nm. The apparent negative absorption in the 340 - 430 nm regions of the UV-vis spectra is due to bleaching of **7**, which exhibits absorption maxima in this wavelength region.<sup>52</sup>

## 6.5. References

- (1) Skell, P. S.; Goldstein, E. J. *J. Am. Chem. Soc.* **1964**, *86*, 1442.
- (2) Gaspar, P. P. In *Reactive Intermediates, Vol. 3*; Jones, M., Jr., Moss, R. A., Eds.; John Wiley & Sons: New York, 1985; Vol. 3, p 333.
- (3) Gaspar, P. P.; West, R. In *The chemistry of organic silicon compounds, Vol. 2*; Rappoport, Z., Apeloig, Y., Eds.; John Wiley and Sons: New York, 1998; Vol. 2, p 2463.
- (4) Becerra, R.; Walsh, R. *Dalton Trans.* **2010**, *39*, 9217.
- (5) Tokitoh, N.; Ando, W. In *Reactive Intermediate Chemistry*; Moss, R. A., Platz, M. S., Jones, M., Jr., Eds.; John Wiley & Sons: New York, 2004, p 651.
- (6) Lee, V. Y.; Sekiguchi, A. In *Organometallic Compounds of Low-Coordinate Si, Ge, Sn and Pb*; John Wiley & Sons, Ltd: Chichester, 2010, p 139.
- (7) Asay, M.; Jones, C.; Driess, M. *Chem. Rev.* **2011**, *111*, 354.
- (8) Yao, S.; Xiong, Y.; Driess, M. *Organometallics* **2011**, *30*, 1748.
- (9) Blom, B.; Driess, M. *Struct. Bond.* **2014**, *156*, 85.
- (10) Kira, M. *J. Chem. Sci.* **2012**, *124*, 1205.
- (11) Kira, M. *Chem. Commun.* **2010**, *46*, 2893.
- (12) Kira, M.; Iwamoto, T.; Ishida, S. *Bull. Chem. Soc. Jpn.* **2007**, *80*, 258.
- (13) Kira, M.; Ishida, S.; Iwamoto, T.; Kabuto, C. *J. Am. Chem. Soc.* **1999**, *121*, 9722.
- (14) Gaspar, P. P. In *Reactive Intermediates, Vol. 1*; Jones, M., Jr., Moss, R. A., Eds.; John Wiley & Sons: New York, 1978; Vol. 1, p 229.

- (15) Gaspar, P. P. In *Reactive Intermediates, Vol. 2*; Jones, M., Jr., Moss, R. A., Eds.; John Wiley & Sons: New York, 1981; Vol. 2, p 335.
- (16) Michalczyk, M. J.; Fink, M. J.; De Young, D. J.; Carlson, C. W.; Welsh, K. M.; West, R.; Michl, J. *Sil. Germ. Tin Lead Cpds.* **1986**, *9*, 75.
- (17) Becerra, R.; Walsh, R. *Phys. Chem. Chem. Phys.* **2007**, *9*, 2817.
- (18) Levin, G.; Das, P. K.; Lee, C. L. *Organometallics* **1988**, *7*, 1231.
- (19) Levin, G.; Das, P. K.; Bilgrien, C.; Lee, C. L. *Organometallics* **1989**, *8*, 1206.
- (20) Yamaji, M.; Hamanishi, K.; Takahashi, T.; Shizuka, H. *J. Photochem. Photobiol. A: Chem.* **1994**, *81*, 1.
- (21) Moiseev, A. G.; Leigh, W. J. *J. Am. Chem. Soc.* **2006**, *128*, 14442.
- (22) Moiseev, A. G.; Leigh, W. J. *Organometallics* **2007**, *26*, 6268.
- (23) Moiseev, A. G.; Leigh, W. J. *Organometallics* **2007**, *26*, 6277.
- (24) Conlin, R. T.; Netto-Ferreira, J. C.; Zhang, S.; Scaiano, J. C. *Organometallics* **1990**, *9*, 1332.
- (25) Safarik, I.; Sandhu, V.; Lown, E. M.; Strausz, O. P.; Bell, T. N. *Res. Chem. Intermed.* **1990**, *14*, 105.
- (26) Becerra, R.; Walsh, R. *Res. Chem. Kinetics* **1995**, *3*, 263.
- (27) Jasinski, J. M.; Becerra, R.; Walsh, R. *Chem. Rev.* **1995**, *95*, 1203.
- (28) Becerra, R.; Frey, H. M.; Mason, B. P.; Walsh, R.; Gordon, M. S. *J. Chem. Soc., Far. Trans.* **1995**, *91*, 2723.
- (29) Becerra, R.; Frey, H. M.; Mason, B. P.; Walsh, R.; Gordon, M. S. *J. Am. Chem. Soc.* **1992**, *114*, 2751.
- (30) Al-Rubaiey, N.; Walsh, R. *J. Phys. Chem.* **1994**, *98*, 5303.
- (31) Al-Rubaiey, N.; Becerra, R.; Walsh, R. *Phys. Chem. Chem. Phys.* **2002**, *4*, 5072.
- (32) Becerra, R.; Cannady, J. P.; Dormer, G.; Walsh, R. *J. Phys. Chem. A* **2008**, *112*, 8665.
- (33) Becerra, R.; Cannady, J. P.; Walsh, R. *J. Phys. Chem. A* **1999**, *103*, 4457.
- (34) Becerra, R.; Cannady, J. P.; Goulder, O.; Walsh, R. *J. Phys. Chem. A* **2010**, *114*, 784.
- (35) Becerra, R.; Cannady, J. P.; Walsh, R. *J. Phys. Chem. A* **2011**, *115*, 4231.
- (36) Leigh, W. J.; Kostina, S. S.; Bhattacharya, A.; Moiseev, A. G. *Organometallics* **2010**, *29*, 662.
- (37) Kostina, S. S.; Singh, T.; Leigh, W. J. *J. Phys. Org. Chem.* **2011**, *24*, 937.
- (38) Kostina, S. S.; Leigh, W. J. *J. Am. Chem. Soc.* **2011**, *133*, 4377.
- (39) Howard, B. E.; Woerpel, K. A. *Org. Lett.* **2007**, *9*, 4651.
- (40) Ottosson, H.; Steel, P. G. *Chem. Eur. J.* **2006**, *12*, 1576.
- (41) Driver, T. G.; Franz, A. K.; Woerpel, K. A. *J. Am. Chem. Soc.* **2002**, *124*, 6524.
- (42) Cirakovic, J.; Driver, T. G.; Woerpel, K. A. *J. Am. Chem. Soc.* **2002**, *124*, 9370.
- (43) Cirakovic, J.; Driver, T. G.; Woerpel, K. A. *J. Org. Chem.* **2004**, *69*, 4007.
- (44) Calad, S. A.; Woerpel, K. A. *J. Am. Chem. Soc.* **2005**, *127*, 2046.
- (45) Nevárez, Z.; Woerpel, K. A. *Org. Lett.* **2007**, *9*, 3773.
- (46) Calad, S. A.; Cirakovic, J.; Woerpel, K. A. *J. Org. Chem.* **2007**, *72*, 1027.
- (47) Driver, T. G. In *Silver in Organic Chemistry*; Harmata, M., Ed.; John Wiley & Sons: New York, 2010, p 183.

- (48) Driver, T. G.; Woerpel, K. A. *J. Am. Chem. Soc.* **2004**, *126*, 9993.
- (49) Boudjouk, P.; Samaraweera, U.; Sooriyakumaran, R.; Chrusciel, J.; Anderson, K. R. *Angew. Chem. Int. Ed. Engl.* **1988**, *27*, 1355.
- (50) Boudjouk, P.; Black, E.; Kumarathasan, R. *Organometallics* **1991**, *10*, 2095.
- (51) Driver, T. G.; Woerpel, K. A. *J. Am. Chem. Soc.* **2003**, *125*, 10659.
- (52) Schäfer, A.; Weidenbruch, M.; Peters, K.; von Schnering, H.-G. *Angew. Chem. Int. Ed. Engl.* **1984**, *23*, 302.
- (53) Weidenbruch, M. *Comment. Inorg. Chem.* **1986**, *5*, 247.
- (54) Weidenbruch, M. *Organometallics* **2003**, *22*, 4348.
- (55) Weidenbruch, M. *Coord. Chem. Rev.* **1994**, *130*, 275.
- (56) Weidenbruch, M. *Chem. Rev.* **1995**, *95*, 1479.
- (57) Gordon, M. S.; Schmidt, M. W. *Chem. Phys. Lett.* **1986**, *132*, 294.
- (58) Chung, G.; Gordon, M. S. *Organometallics* **1999**, *18*, 4881.
- (59) Schoeller, W. W. *J. Mol. Struct.: THEOCHEM* **2010**, *957*, 66.
- (60) Welsh, K. M.; Michl, J.; West, R. *J. Am. Chem. Soc.* **1988**, *110*, 6689.
- (61) Weidenbruch, M.; Schafer, A.; Rankers, R. *J. Organomet. Chem.* **1980**, *195*, 171.
- (62) Masamune, S.; Murakami, S.; Tobita, H. *Organometallics* **1983**, *2*, 1464.
- (63) Murov, S. L.; Carmichael, I.; Hug, G. L. *Handbook of Photochemistry*; 2nd ed.; Dekker: New York, 1993.
- (64) Weidenbruch, M.; Kroke, E.; Marsmann, H.; Pohl, S.; Saak, W. *Chem. Commun.* **1994**, 1233.
- (65) Tolti, N. P.; Leigh, W. J.; Kollegger, G. M.; Stibbs, W. G.; Baines, K. M. *Organometallics* **1996**, *15*, 3732.
- (66) Leigh, W. J.; Harrington, C. R.; Vargas-Baca, I. *J. Am. Chem. Soc.* **2004**, *126*, 16105.
- (67) Kollegger, G. M.; Stibbs, W. G.; Vittal, J. J.; Baines, K. M. *Main Group Metal Chem.* **1996**, *19*, 317.
- (68) Kostina, S. S.; Singh, T.; Leigh, W. J. *Organometallics* **2012**, *31*, 3755.
- (69) Becerra, R.; Harrington, C. R.; Gaspar, P. P.; Leigh, W. J.; Vargas-Baca, I.; Walsh, R.; Zhou, D. *J. Am. Chem. Soc.* **2005**, *127*, 17469.
- (70) Leigh, W. J.; Harrington, C. R. *J. Am. Chem. Soc.* **2005**, *127*, 5084.
- (71) Schäfer, A.; Weidenbruch, M.; Pohl, S. *J. Organomet. Chem.* **1985**, *282*, 305.
- (72) Becerra, R.; Carpenter, I. W.; Gordon, M. S.; Roskop, L.; Walsh, R. *Phys. Chem. Chem. Phys.* **2007**, *9*, 2121.
- (73) Akasaka, T.; Nagase, S.; Yabe, A.; Ando, W. *J. Am. Chem. Soc.* **1988**, *110*, 6270.
- (74) Bornemann, H.; Sander, W. *J. Am. Chem. Soc.* **2000**, *122*, 6727.
- (75) Patyk, A.; Sander, W.; Gauss, J.; Cremer, D. *Angew. Chem. Int. Ed. Engl.* **1989**, *28*, 898.
- (76) Kroke, E.; Willms, S.; Weidenbruch, M.; Saak, W.; Pohl, S.; Marsmann, H. *Tetrahedron Lett.* **1996**, *37*, 3675.
- (77) Franz, A. K.; Woerpel, K. A. *Acc. Chem. Res.* **2000**, *33*, 813.
- (78) Bhattacharya, A. M.Sc. Thesis, McMaster University, 2010.
- (79) Weidenbruch, M.; Flintjer, B.; Pohl, S.; Saak, W. *Angew. Chem. Int. Ed. Engl.* **1989**, *28*, 95.

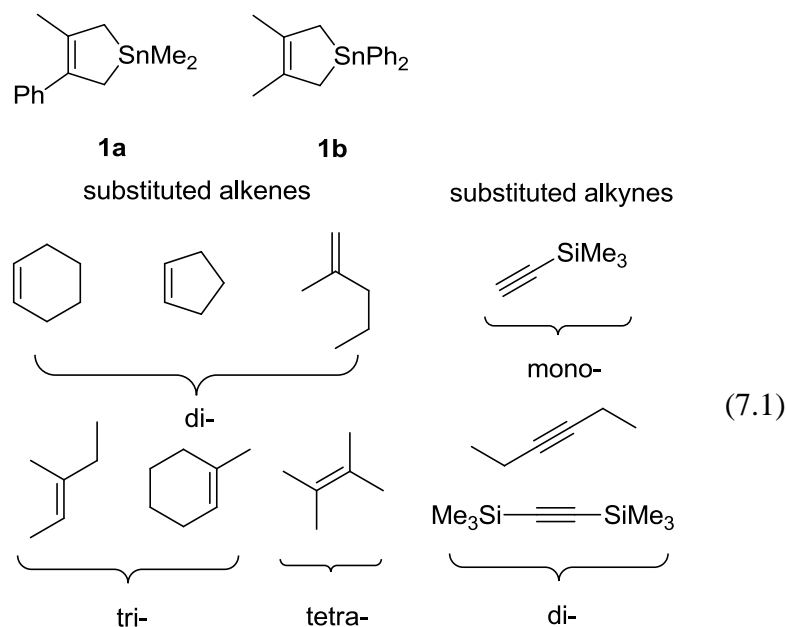
- (80) Morkin, T. L.; Owens, T. R.; Leigh, W. J.; Rappoport, Z.; Apeloig, Y. In *The chemistry of organic silicon compounds, Volume 3*; Rappoport, Z., Ed.; John Wiley and Sons: New York, 2001, p 949.
- (81) Apeloig, Y.; Bravo-Zhivotovskii, D.; Zharov, I.; Panov, V.; Leigh, W. J.; Sluggett, G. W. *J. Am. Chem. Soc.* **1998**, *120*, 1398.
- (82) Gaspar, P. P.; Holten, D.; Konieczny, S.; Corey, J. Y. *Acc. Chem. Res.* **1987**, *20*, 329.

## Chapter 7 - Future Directions

### 7.1. Intra- and Intermolecular $\pi$ -Complexes with Unsaturated Hydrocarbons and Arenes

#### 7.1a. Intermolecular $\pi$ -Complexes with Unsaturated Hydrocarbons

The detection of  $\pi$ -complexes between stannylenes and terminal alkenes and alkynes provided the first examples of such an interaction within the transient tetrylene series with unsaturated hydrocarbons in solution. The substrate scope of the initial investigation of  $\text{SnMe}_2$  and  $\text{SnPh}_2$  (from precursors **1a-b**) can be readily broadened to include di-substituted alkynes as well as di-, tri-, and tetra-substituted alkenes (eq. 7.1).



A sequential increase in alkyl substitution to the  $\text{C}=\text{C}$  and  $\text{C}\equiv\text{C}$  bond would be expected to increase the donor ability of the unsaturated  $\pi$ -bond and increase the exergonicity of interaction, measured by an increase in  $K_{\text{eq}}$ . A similar approach was taken in a previous study by S. Chitnis and Y. Saeidi in their investigations of the (1+2) cycloaddition of  $\text{GePh}_2$  with alkenes (unpublished results). Interestingly, the increase in alkyl substitution of the alkene had a destabilizing effect on the stability of the resulting

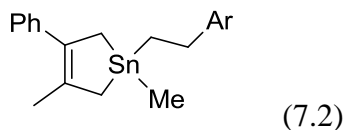
germirane, culminating in a positive linear correlation between  $\Delta G^\circ$  and ionization potential (IP) of the alkene.

### *7.1b. Intramolecular Stannylenes Arene Interactions*

The interaction between Sn(II) compounds and the  $\pi$ -orbitals of neutral aromatic hydrocarbons has been recently reviewed,<sup>1</sup> and has also been evaluated as a potential new bonding motif for supramolecular self-assembly.<sup>2</sup> Broeckeaert et al. studied the possibility of such an interaction between stannylenes and a collection of aromatic compounds with electron-donating and withdrawing character.<sup>3,4</sup> The authors theoretically established the existence of an interaction between benzene and SnMe<sub>2</sub>, but also mention that the interaction with  $\sigma$ -donating substrates such as methanol and THF (wherein experimental benchmarks exist in this work) results in much stronger coordination.<sup>3</sup> The calculations also revealed  $\eta^1$ -type interactions of SnF<sub>2</sub> with the aromatic ring of benzene, and show complexation energies increase with electron donating aryl substitution and decrease with electron withdrawing groups.<sup>3</sup>

The relatively high molar absorptivity ( $\epsilon_{248\text{nm}}$ ) of aromatic compounds coupled with their expected weak interaction with stannylenes preclude their use as scavengers in flash photolysis experiments using 248 nm excitation. One alternative approach would be to use a substituent that incorporates a pendant arene at the terminal position of a linear alkyl chain, for instance in compounds **2a-b** (eq. 7.2). A two carbon alkyl chain was selected based on the structure of calix[4]arene Sn(II) complexes that appear to exhibit interactions with an intramolecular arene.<sup>5</sup> Furthermore, the  $\pi$ -donating character of the arene can be readily modified with methyl substitution, for instance in **2b**. Intramolecular arene  $\pi$ -complexation would likely result in an observable blue-shift in  $\lambda_{\text{max}}$  relative to uncoordinated SnMe<sub>2</sub>, similar to the effects of alkene  $\pi$ -complexation on the absorption maxima of SnMe<sub>2</sub> (see Chapter 4).



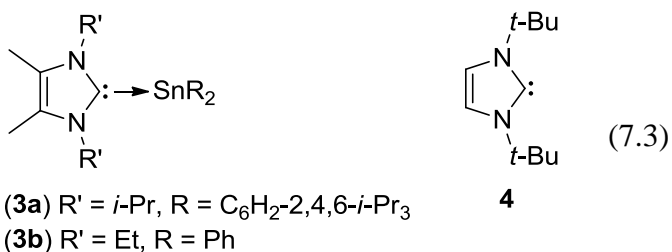


(2a) Ar = Ph

(2b) Ar = C<sub>6</sub>Me<sub>5</sub>

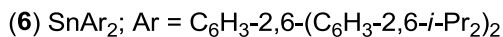
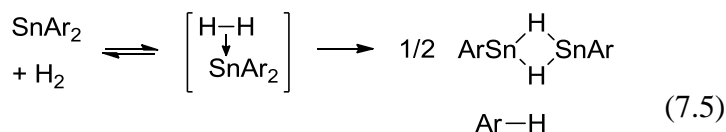
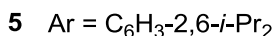
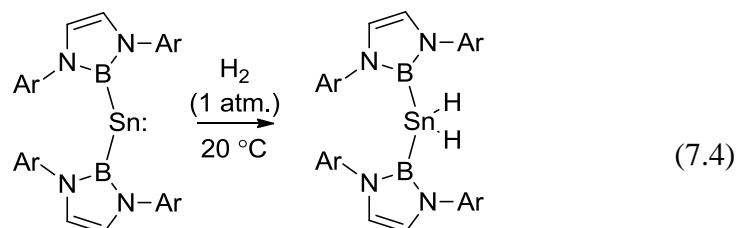
## 7.2. Stannylenes Stabilized by N-heterocyclic Carbenes

Few scavengers still exist that form discrete and isolable transient stannylene derived products. The stabilization of transient diorganostannylenes using Arduengo-type carbenes (also referred to as N-heterocyclic carbenes or NHCs) have been known since 1995 (compound **3a**)<sup>6</sup> (the stabilization of GeMe<sub>2</sub> by a NHC has also been reported<sup>7</sup>), and represent a new and unexplored scavenger of transient stannylenes, especially given the recent advances in the NHC stabilized chemistry of reactive silicon compounds.<sup>8</sup> Wesemann and coworkers recently isolated the 1:1 adduct of (NHC)SnPh<sub>2</sub> (**3b**),<sup>9</sup> demonstrating that even the simplest diorganostannylene derivatives can be isolated as the stannylene-NHC pair. The use of NHCs as stannylene substrates in chemical trapping experiments - and more specifically with the formation of **3b** - serves ultimately to further support the conclusion that the photolysis of **1b** results in the extrusion of SnPh<sub>2</sub>. Importantly, examples of stannylene-NHC adducts utilize alkylated NHC derivatives, the UV-vis spectrum of an alkyl substituted NHC (**4**) exhibits maxima at  $\lambda_{\text{max}} = 214$  and 228 nm, enabling their use in 248 nm flash photolysis experiments.<sup>10,11</sup>



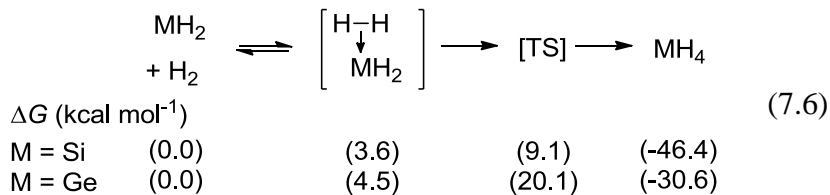
### 7.3. Reaction of Stannylenes with H<sub>2</sub>

The opportunity to observe novel pre-reaction complexes by laser flash photolysis motivates us to study the reaction of stannylenes with dihydrogen (H<sub>2</sub>). To the best of our knowledge, the direct observation of a complex between H<sub>2</sub> and a main group element is unknown experimentally despite its prevalence in transition metal chemistry.<sup>12</sup> The activation of H<sub>2</sub> by main group elements has received growing interest in recent years, the use of heavy carbene analogs to perform such transformations has been motivated by the finding that carbenes can undergo single site activation of H<sub>2</sub>.<sup>13</sup> Recently, the reaction of H<sub>2</sub> with stannylene **5** was found to proceed by oxidative addition<sup>14</sup> (eq. 7.4) while with **6** the reaction proceeds via arene elimination (eq. 7.5).<sup>15</sup> The formation of a pre-reaction complex between **6** and H<sub>2</sub> in eq. 7.5 was theoretically predicted, however the positive  $\Delta G$  of the interaction (8 kcal mol<sup>-1</sup>) made it unlikely to be detected.<sup>16</sup>

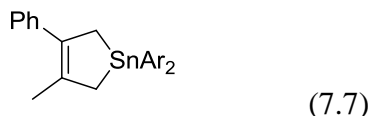


The existence of pre-reaction complexes between MH<sub>2</sub> (M = Si, Ge) and H<sub>2</sub> has been proposed in numerous theoretical studies.<sup>17-19</sup> Boganov et al. predicted the formation of pre-reaction complexes between H<sub>2</sub> and MHX (M = Si, Ge, Sn; X = F, Cl, Br) with stabilities ranging between  $\Delta G = 3.5 - 4.8$  kcal mol<sup>-1</sup>,<sup>20</sup> while Walsh and Becerra predicted the formation of a pre-reaction complex in the oxidative addition of H<sub>2</sub> with

SiH<sub>2</sub> and GeH<sub>2</sub> to be between  $\Delta G = 2.9 - 4.8 \text{ kcal mol}^{-1}$  (eq. 7.6).<sup>21</sup> The authors suggest in the latter study the possibility of its direct observation at low temperatures, and recommend the germylene complex to be more suitable towards detection due to the larger kinetic barrier of the second step.<sup>21</sup>



It remains unlikely that the pre-reaction complex between SnPh<sub>2</sub> (the most Lewis acidic of the stannylenes studied in this work) and H<sub>2</sub> would be observed given the concentration of H<sub>2</sub> in a saturated hexanes solution ( $[\text{H}_2] = 5.5 \text{ mM}$  at 25 °C, 1 atm<sup>22</sup>). One alternative approach is to introduce electron withdrawing groups to the aromatic ring of SnPh<sub>2</sub>. Such a strategy has been found to be effective: introducing electron withdrawing groups to the aromatic ring of diarylgermylenes enhances the Lewis acidity of the central germanium atom and stabilizes their resulting coordination compounds.<sup>23</sup> This was quantified in their reactions with oxygen donors such as THF and EtOAc to dramatically increase the binding energy.<sup>23</sup> Stannylene precursors **7a-b** (eq. 7.7) can generate electrophilic stannylenes Sn(C<sub>6</sub>H<sub>3</sub>-3,5-(CF<sub>3</sub>)<sub>2</sub>)<sub>2</sub> and Sn(C<sub>6</sub>F<sub>5</sub>)<sub>2</sub> upon photolysis, the latter compound having been studied.<sup>24</sup> Alternatively, we can attempt to detect a complex between the electrophilic stannylenes and H<sub>2</sub> using low temperature frozen matrices.

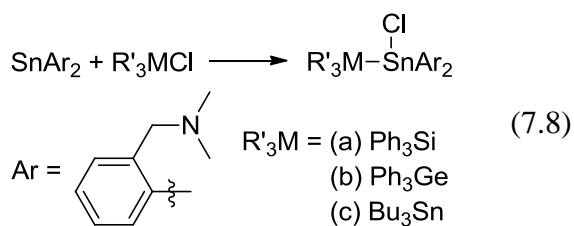


(7a) Ar = C<sub>6</sub>H<sub>3</sub>-3,5-(CF<sub>3</sub>)<sub>2</sub>

(7b) Ar = C<sub>6</sub>F<sub>5</sub>

#### 7.4. $\sigma$ -Bond Insertion of Stannylenes into the M-Cl Bond of Chlorosilanes and Chlorogermanes

Despite the interesting optical properties of catenated group 14 compounds containing tin,<sup>25-28</sup> the preparation of such compounds remains a synthetic challenge, and the direct incorporation of low-valent tin(II) compounds has not been utilized as a viable transformation to prepare these types of molecules. The Sn-Cl insertion of transient stannylenes into chlorostannanes  $\text{Me}_2\text{SnCl}_2$ <sup>29</sup> and  $\text{Bu}_3\text{SnCl}$  presented in this thesis represent just some examples of a potentially more generalized approach: the stannylene unit  $\text{SnR}_2$  in the resulting mono and dichlorodistannanes can be variable, and the resulting products contain a Sn-Cl bond that is amenable to further derivatization. Recently, Růžička and coworkers demonstrated the  $\sigma$ -bond insertion of diarylstannylenes into the Sn-Cl bond of chlorostannanes can be generalized to include Si-Cl and Ge-Cl insertion with compounds of the type  $\text{R}_3\text{MCl}$  ( $\text{M} = \text{Si}, \text{Ge}$ ) (eq. 7.8).<sup>30</sup>



The use of such compounds like  $\text{Me}_3\text{SiCl}$  and  $\text{Me}_3\text{GeCl}$  as scavengers for transient stannylenes has not been previously reported. Understanding the mechanistic aspects and scope of this transformation may be of interest towards the larger goal of preparing highly derivatized compounds containing catenated group 14 elements.

## 7.5. References

- (1) Schmidbaur, H.; Schier, A. *Organometallics* **2008**, *27*, 2361.
- (2) de Lima, G. M. In *Tin Chemistry: Fundamentals, Frontiers, and Applications*; Davies, A. G., Gielen, M., Pannell, K. H., Tiekink, E., Eds.; John Wiley & Sons, Ltd: New York, 2008, p 285.
- (3) Broeckaert, L.; Geerlings, P.; Růžička, A.; Willem, R.; De Proft, F. *Organometallics* **2012**, *31*, 1605.
- (4) Broeckaert, L.; Turek, J.; Olejník, R.; Růžička, A.; Biesemans, M.; Geerlings, P.; Willem, R.; De Proft, F. *Organometallics* **2013**, *32*, 2121.
- (5) Hascall, T.; Pang, K.; Parkin, G. *Tetrahedron* **2007**, *63*, 10826.

- (6) Schafer, A.; Weidenbruch, M.; Saak, W.; Pohl, S. *Chem. Commun.* **1995**, 1157.
- (7) Rugar, P. A.; Jennings, M. C.; Ragogna, P. J.; Baines, K. M. *Organometallics* **2007**, *26*, 4109.
- (8) Scheschke, D. *Functional Molecular Silicon Compounds II. Low Oxidation States*; Springer, 2014; Vol. 156.
- (9) Sindlinger, C. P.; Wesemann, L. *Chem. Sci.* **2014**, *5*, 2739.
- (10) Leites, L. A.; Bukalov, S. S.; Aysin, R. R.; Piskunov, A. V.; Chegerev, M. G.; Cherkasov, V. K.; Zabula, A. V.; West, R. *Organometallics* **2015**, *34*, 2278.
- (11) Leites, L. A.; Magdanurov, G. I.; Bukalov, S. S.; Nolan, S. P.; Scott, N. M.; West, R. *Mendeleev Commun.* **2007**, *17*, 92.
- (12) Crabtree, R. H. *Chem. Rev.* **2016**, *116*, 8750.
- (13) Frey, G. D.; Lavallo, V.; Donnadiu, B.; Schoeller, W. W.; Bertrand, G. *Science* **2007**, *316*, 439.
- (14) Protchenko, A. V.; Bates, J. I.; Saleh, L. M. A.; Blake, M. P.; Schwarz, A. D.; Kolychev, E. L.; Thompson, A. L.; Jones, C.; Mountford, P.; Aldridge, S. *J. Am. Chem. Soc.* **2016**, *138*, 4555.
- (15) Peng, Y.; Ellis, B. D.; Wang, X.; Power, P. P. *J. Am. Chem. Soc.* **2008**, *130*, 12268.
- (16) Peng, Y.; Guo, J.-D.; Ellis, B. D.; Zhu, Z.; Fetting, J. C.; Nagase, S.; Power, P. P. *J. Am. Chem. Soc.* **2009**, *131*, 16272.
- (17) Wang, Y.; Ma, J. *J. Organomet. Chem.* **2009**, *694*, 2567.
- (18) Devarajan, D.; Doubleday, C. E.; Ess, D. H. *Inorg. Chem.* **2013**, *52*, 8820.
- (19) Adamczyk, A. J.; Reyniers, M.-F.; Marin, G. B.; Broadbelt, L. J. *Phys. Chem. Chem. Phys.* **2010**, *12*, 12676.
- (20) Boganov, S. E.; Promyslov, V. M.; Faustov, V. I.; Egorov, M. P.; Nefedov, O. M. *Russ. Chem. Bull.* **2011**, *60*, 2147.
- (21) Becerra, R.; Boganov, S. E.; Egorov, M. P.; Faustov, V. I.; Nefedov, O. M.; Walsh, R. *Can. J. Chem.* **2000**, *78*, 1428.
- (22) Brunner, E. *J. Chem. Eng. Data* **1985**, *30*, 269.
- (23) Huck, L. A.; Leigh, W. J. *Organometallics* **2007**, *26*, 1339.
- (24) Bigwood, M. P.; Corvan, P. J.; Zuckerman, J. J. *J. Am. Chem. Soc.* **1981**, *103*, 7643.
- (25) Zaitsev, K. V.; Lermontova, E. K.; Churakov, A. V.; Tafeenko, V. A.; Tarasevich, B. N.; Poleshchuk, O. K.; Kharcheva, A. V.; Magdesieva, T. V.; Nikitin, O. M.; Zaitseva, G. S.; Karlov, S. S. *Organometallics* **2015**, *34*, 2765.
- (26) Caseri, W. *Chem. Soc. Rev.* **2016**, *45*, 5187.
- (27) Baumgartner, J.; Fischer, R.; Fischer, J.; Wallner, A.; Marschner, C.; Flörke, U. *Organometallics* **2005**, *24*, 6450.
- (28) Sharma, H. K.; Cervantes-Lee, F.; Parkanyi, L.; Pannell, K. H. *Organometallics* **1996**, *15*, 429.
- (29) Duffy, I. R.; Leigh, W. J. *Organometallics* **2015**, *34*, 5029.
- (30) Padelkova, Z.; Svec, P.; Pejchal, V.; Růžička, A. *Dalton Trans.* **2013**, *42*, 7660.

## Chapter 8 - Experimental Details

### 8.1. General

$^1\text{H}$  and  $^{13}\text{C}$  NMR spectra were recorded at 600.13 MHz ( $^1\text{H}$ ) and 150.90 MHz ( $^{13}\text{C}\{^1\text{H}\}$ ) using a Bruker AV600 spectrometer or at 700.17 MHz ( $^1\text{H}$ ) and 176.06 MHz ( $^{13}\text{C}\{^1\text{H}\}$ ) respectively, using a Bruker AV700 spectrometer, and were referenced to the residual solvent proton and  $^{13}\text{C}$  signals, respectively.  $^{119}\text{Sn}$  NMR spectra were recorded at 223.79 MHz ( $^{119}\text{Sn}\{^1\text{H}\}$ ) on a Bruker AV600 spectrometer using the inverse-gated  $^1\text{H}$  decoupling scheme with a 30-degree pulse on  $^{119}\text{Sn}$ , and were referenced to an external solution of tetramethylstannane.  $^{29}\text{Si}\{^1\text{H}\}$  spectra were recorded on a Bruker AV600 spectrometer using the 2D  $^1\text{H}$ - $^{29}\text{Si}$  HMBC pulse sequence and were referenced to an external solution of tetramethylsilane. Spectra were recorded using chloroform-*d*, dichloromethane-*d*<sub>2</sub>, benzene-*d*<sub>6</sub>, or cyclohexane-*d*<sub>12</sub> solution. High-resolution electron impact mass spectra and exact masses were determined on a Waters Micromass GCT Premier mass spectrometer using electron impact ionization (70 eV). High-resolution chemical ionization mass spectra and exact masses were also determined on a Waters Micromass GCT Premier mass spectrometer using ammonia as ionizing agent. Infrared spectra were recorded using a Nicolet 6700 FTIR spectrometer. GC/MS analyses were performed on a Varian Saturn 2200 GC/MS/MS system equipped with a VF-5 ms capillary column (30 m x 0.25 mm; 0.25  $\mu\text{m}$ ; Agilent Technologies). Melting points were measured using a Mettler FP82 Hot Stage mounted on an Olympus BH-2 microscope and controlled by a Mettler FP80 Central Processor, and are uncorrected. Static UV-visible absorption spectra were recorded using a Cary 50 UV-Vis spectrophotometer. Column chromatography and silica micro-columns were prepared using SiliaFlash P60 40–63  $\mu\text{m}$  (230–400 mesh) silica gel (Silicycle). Alumina-packed micro-columns were prepared using neutral (60–325 mesh) Brockmann Activity I alumina (Fisher Scientific).

## 8.2. Steady State Photolysis Experiments

Steady-state photolysis experiments were carried out using a Rayonet® photochemical reactor (Southern New England Ultraviolet Co.) equipped with two RPR-2537 lamps as excitation source. Samples were contained in quartz NMR tubes mounted in a merry-go-round apparatus, and were monitored at selected time intervals by  $^1\text{H}$  NMR spectroscopy; the end photolyzate was also (typically) analyzed by  $^{119}\text{Sn}$  and/or  $^{13}\text{C}$  NMR spectroscopy to further aid in product identification. Cyclohexane- $d_{12}$  solutions containing the desired combinations of stannylene precursor, substrate, and hexamethyldisilane (ca. 0.01 M; internal integration standard) were prepared in 1 or 2 mL volumetric flasks. Solid samples of substrate and stannylene precursor were weighed using an analytical balance while liquid samples were measured volumetrically using a microlitre syringe. The solutions were transferred to the quartz NMR tubes, deoxygenated with a slow stream of dry argon for ca. 5 min, and sealed using an NMR tube cap. Air-saturated or "nondeaerated" solutions in quartz NMR tubes were simply used as prepared under ambient conditions, the oxygen content in the aerated samples was replenished at periodic intervals throughout photolysis as indicated by bubbling air through the solution using a plastic syringe (1 mL). For the quantum yield experiments, a slow stream of air was bubbled through the solutions both before irradiation commenced and in between each photolysis interval in order to maintain air-saturation. Each photolysis experiment was compared to a separate sample containing the same molar ratio of starting compounds but was kept in the dark. Product yields were calculated from the (initial) relative slopes of concentration versus time plots for the products to that of the corresponding plot for the photoprecursor.

### 8.3. Laser Flash Photolysis Experiments

Laser flash photolysis experiments were carried out using a Lambda Physik Compex 120 excimer laser filled with F<sub>2</sub>/Kr/Ne (248 nm, 20 ns, 99 ± 5 mJ) and a Luzchem Research mLFP-111 laser flash photolysis system, modified as described previously;<sup>1</sup> kinetic traces that were recorded with the laser power reduced from the nominal value using neutral density filters (constructed from wire screening) are indicated when appropriate. Photolysis precursors were added to a solution of deoxygenated anhydrous hexanes such that the absorbance of the resulting solution at 248 nm in a 7 x 7 mm quartz cell was between 0.4 and 0.7. The solutions were flowed through a 7 × 7 mm Suprasil flow cell from calibrated 100 mL or 250 mL reservoirs, which contain a glass frit to allow bubbling of argon gas through the solution for 30 min prior to and throughout the experiment. Samples of 7,7-di-*tert*-butyl-7-silabicyclo[4.1.0]heptane (**7**) were handled in a glovebox and immediately transferred to the reservoirs using a microlitre syringe to minimize contact with air and moisture. The flow cell was connected to a Masterflex™ 77390 peristaltic pump fitted with Teflon tubing (Cole-Parmer Instrument Co.) which pulls the solution through the cell at a constant rate of 2-3 mL/min. Solution reservoirs were flame-dried under an atmosphere of nitrogen or argon, while the sample cell and transfer lines were dried in a vacuum oven (55–75 °C) before use. Solution temperatures were measured with a Teflon-coated copper/constantan thermocouple inserted into the thermostated sample compartment in close proximity to the sample cell. Substrates were added directly to the reservoir by microlitre syringe, either as the neat liquid or as aliquots of standard solutions. Standard solutions were prepared in 10 or 25 mL volumetric flasks using known quantities (determined by mass and/or volume, in the latter case using literature densities at 25 °C) of substrate. Air and O<sub>2</sub>-saturated solutions were prepared by



bubbling the appropriate gas through the solution for at least 20 minutes prior to and during measurement.

Transient absorbance-time profiles were recorded by signal-averaging of data obtained from 10-50 individual laser shots. Decay rate coefficients were calculated by non-linear least squares analysis of the transient absorbance-time profiles using the Prism 5.0 software package (GraphPad Software, Inc.) and the appropriate user-defined fitting equations, after importing the raw data from the Luzchem mLFP software. Rate and equilibrium constants were calculated by linear least-squares analysis of transient absorbance data that spanned as large a range in transient decay rate or initial signal intensity as possible. Errors are quoted as twice the standard error obtained from the least-squares analyses.

#### **8.4. Reagents Used**

All commercially-available materials were used as received from the suppliers or further purified prior to use as described below; solvents were all reagent grade or better.

##### **8.4.1. Solvents**

Tetrahydrofuran (THF) for synthesis was distilled under nitrogen from sodium/benzophenone. Hexanes (Caledon) and diethyl ether (Et<sub>2</sub>O; Caledon) were dried by passage through activated alumina under nitrogen using a Solv-Tek solvent purification system (Solv-Tek Inc.). Pentane (Caledon), 35-60 petroleum ether (Caledon), methanol (MeOH, Caledon), and absolute ethanol (EtOH, Commercial Alcohols) were used as received. Sealed ampoules of cyclohexane-*d*<sub>12</sub> (Cambridge Isotope), benzene-*d*<sub>6</sub> (Cambridge Isotope), chloroform-*d* (Cambridge Isotope), and dichloromethane-*d*<sub>2</sub> (Cambridge Isotope) were used as received from the suppliers. Chloroform-*d* was dried when necessary by distillation from CaH<sub>2</sub>.

#### 8.4.2. Reagents used in Synthesis

Naphthalene (99 %, Sigma-Aldrich) was purified by sublimation, while 2,3-dimethyl-1,3-butadiene (DMB; 98 %, Sigma-Aldrich) and 1,2-dibromoethane (98 %, Sigma-Aldrich) were purified by passage through a silica microcolumn immediately prior to use. Lithium wire (99.9 %, Sigma-Aldrich) was freshly cut and washed with dry hexanes. Magnesium turnings (98 %, Sigma-Aldrich), ammonium chloride ( $\text{NH}_4\text{Cl}$ ;  $\geq 99.5$  %, Caledon), pyridine (99 %, Caledon), pinacol (98 %, Sigma-Aldrich), 1-phenyl-1,2-propanedione (98 %, Sigma-Aldrich), iodomethane (99 %, Sigma-Aldrich), 2-bromomesitylene (99 %, Sigma-Aldrich), bromine ( $\text{Br}_2$ , 99 %, Sigma-Aldrich), iodine ( $\text{I}_2$ ; 99.8 %, VWR), and methylmagnesium bromide (3.0 M solution in  $\text{Et}_2\text{O}$ , Sigma-Aldrich) were used as received from the suppliers. Similarly, di-*tert*-butylsilane (*t*- $\text{Bu}_2\text{SiH}_2$ ; 95 %, Gelest), dichlorodimethylstannane ( $\text{Me}_2\text{SnCl}_2$ ; 97 %, Sigma-Aldrich), dichlorodiphenylstannane ( $\text{Ph}_2\text{SnCl}_2$ ; 95 %, Gelest), and tetraphenyltin ( $\text{SnPh}_4$ ; 97 %, Sigma-Aldrich), were used as received from the suppliers. Tin tetrachloride ( $\text{SnCl}_4$ ;  $\geq 97$  %, Gelest) was distilled under an argon or nitrogen atmosphere immediately prior to use.

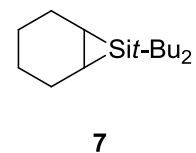
#### 8.4.3. Reagents used in Steady State and Laser Flash Photolysis Experiments

Tetrahydrofuran (THF; Caledon) for flash photolysis experiments was dried by stirring over lithium aluminum hydride ( $\text{LiAlH}_4$ ) overnight and distilling immediately prior to use. Ethyl acetate ( $\text{EtOAc}$ ; Caledon) was dried by passage through a silica gel micro-column immediately prior to use. Methanol ( $\text{MeOH}$ ; Caledon) was distilled from sodium methoxide ( $\text{NaOMe}$ ). Glacial acetic acid ( $\text{AcOH}$ ; Caledon) was used as received from the suppliers. Acetone (Caledon) was distilled from calcium sulfate ( $\text{CaSO}_4$ ).<sup>2</sup> Triethylsilane ( $\text{Et}_3\text{SiH}$ ; 98 %, Gelest) was stirred over  $\text{LiAlH}_4$  overnight before distilling. Butylamine ( $\text{BuNH}_2$ ; 99.5 %, Sigma-Aldrich), diethylamine ( $\text{Et}_2\text{NH}$ ; 99.5 %, Sigma-Aldrich), and triethylamine ( $\text{Et}_3\text{N}$ ;  $\geq 99$  %, Sigma-Aldrich) were stirred over solid sodium

hydroxide (NaOH) or potassium hydroxide (KOH) under nitrogen and distilled immediately prior to use. Diethyl sulfide (Et<sub>2</sub>S; 98 %, Sigma-Aldrich) was dried by passage through a silica gel micro-column immediately prior to use. Tetrahydrothiophene (THT; 99 %, Sigma-Aldrich) was refluxed over anhydrous sodium sulfate (Na<sub>2</sub>SO<sub>4</sub>) and distilled immediately prior to use. Dichlorodimethylstannane (Me<sub>2</sub>SnCl<sub>2</sub>; 97 %, Sigma-Aldrich) was purified by sublimation immediately prior to use. Tributyltin chloride (Bu<sub>3</sub>SnCl; Sigma-Aldrich) was distilled under reduced pressure prior to use (92 °C, 0.02 mmHg), samples used for flash photolysis and product studies contained ca. 3.9 mol % tetrabutyltin (Bu<sub>4</sub>Sn) as an impurity as estimated by <sup>1</sup>H NMR spectroscopy. Tributyltin hydride (Bu<sub>3</sub>SnH; 97 %, Sigma-Aldrich) was passed through a silica gel micro-column to remove the stabilizer (butylated hydroxytoluene, BHT) and dried over lithium aluminum hydride (LiAlH<sub>4</sub>) for 1 hr before distilling under reduced pressure (62 °C, 0.2 mmHg) immediately prior to use. 1-Hexene (99 %, Sigma-Aldrich), 1-hexyne (Lancaster), and 2,3-dimethyl-2-butene (TME; ≥ 99 %, Sigma-Aldrich) were stirred over calcium hydride (CaH<sub>2</sub>) or lithium aluminum hydride (LiAlH<sub>4</sub>) and distilled immediately prior to use. Isoprene (99 %, Sigma-Aldrich) was dried and stabilizer removed by passing through a silica gel micro-column immediately prior to use. Cyclohexene (≥ 99 %, Sigma-Aldrich) was stirred over maleic anhydride overnight before being distilled and passed through a silica gel micro-column.<sup>2</sup> Cis-cyclooctene (95 %, Sigma-Aldrich) was distilled under reduced pressure over NaOH pellets and then passed through an alumina micro-column.<sup>2</sup> The compressed gases from cylinders containing air or O<sub>2</sub> were dried further by passage through anhydrous calcium sulphate (CaSO<sub>4</sub>) prior to use in flash photolysis experiments. Hexamethyldisilane (Si<sub>2</sub>Me<sub>6</sub>, Sigma-Aldrich), mesitylene (≥ 98 %, Alfa Aesar), benzene (≥ 99 %, Caledon), and a cylinder of methane (≥ 99 %, Sigma-Aldrich) were used as received from the suppliers.

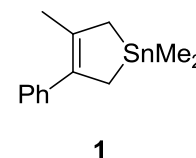
## 8.5. Synthesis and Characterization of Photoprecursors

The 1-stannacyclopent-3-enes **1-5** were prepared according to procedures adapted from those of Gaspar and coworkers,<sup>3</sup> with the requisite organomagnesium reagents being prepared according to the methods of Rieke and Xiong.<sup>4</sup> The preparation of MePhSnCl<sub>2</sub> (**10**), Mes<sub>2</sub>SnCl<sub>2</sub> (**11**), 2,3-dimethyl-1,3-butadiene (**13**), and 2-methyl-3-phenyl-1,3-butadiene (**14**) are described in sections 8.7.2 and 8.7.3. The preparation of **14** used for the synthesis of **4** was performed by K. Jeyakanthan. Di-*tert*-butyldiiodosilane (*t*-Bu<sub>2</sub>SiI<sub>2</sub>) was prepared according to the previously reported procedures of Weidenbruch and co-workers.<sup>5</sup> The samples of 7,7-di-*tert*-butyl-7-silabicyclo[4.1.0]heptane (**7**) used in this study were provided in sealed ampoules by Prof. K. Woerpel and his group.



### 8.5.1. Synthesis of 1,1,3-trimethyl-4-phenyl-1-stannacyclopent-3-ene (**1**)

A THF solution of anhydrous magnesium dibromide (MgBr<sub>2</sub>) was prepared in a flame-dried apparatus, consisting of a two-neck 250 mL round bottom flask equipped with a stir-bar, condenser and septum, by the addition of 1,2-dibromoethane (5.00 mL, 10.85 g, 0.058 mol) to Mg turnings (1.34 g, 0.055 g-atom) in THF (80 mL). The solution was refluxed until all of the magnesium had been consumed (ca. 1.5 h), before being allowed to cool to room temperature. To the resulting grey suspension of MgBr<sub>2</sub> in THF was added finely cut lithium wire (0.78 g, 0.113 g-atom) and naphthalene (2.19 g, 0.0171 mol). The resulting mixture was stirred vigorously at room temperature for 18 h, at which point the lithium was fully consumed. The finely divided activated magnesium (Mg\*) was allowed to settle and the supernatant was removed by syringe and replaced with fresh THF (ca. 135 mL). The procedure was repeated, and then 2-methyl-3-phenyl-1,3-butadiene (**14**, 7.63 g, 0.053 mol) was added as



the neat liquid in a single portion. The resulting orange-brown solution was stirred for an additional 8 h, and the residual solids were allowed to settle.

A 500 mL two-neck round-bottom flask equipped with a stirbar, septum and addition funnel was assembled and then flame-dried. The flask was then charged with  $\text{Me}_2\text{SnCl}_2$  (3.29 g, 0.015 mol) and dry THF (250 mL) under an atmosphere of argon and then cooled to  $-78\text{ }^\circ\text{C}$  in an acetone / dry ice bath. The solution of (2-methyl-3-phenyl-2-butene-1,4-diyl)magnesium in THF prepared above was transferred to the addition funnel and added to the flask dropwise until the reaction mixture tested neutral on moist pH paper. An additional portion of  $\text{Me}_2\text{SnCl}_2$  (2.74 g, 0.012 mol) was added, and dropwise addition of the organomagnesium reagent was resumed until the pH again tested neutral (ca. 2 h). At this point, ca. 108 mL of the THF solution containing (2-methyl-3-phenyl-2-butene-1,4-diyl)magnesium had been added. The reaction mixture was stirred and allowed to warm to room temperature overnight, before being transferred to a separatory funnel and washed with saturated aqueous ammonium chloride (3 x 75 mL). The combined aqueous extracts were extracted with diethyl ether (3 x 40 mL). The organic fractions were combined, dried over  $\text{MgSO}_4$ , filtered, and the solvent was removed to yield a yellow viscous liquid (12.53 g), which was estimated by  $^1\text{H}$  NMR of the crude mixture to contain **1**, naphthalene, and **14** in a ratio of (1):(0.09):(0.09).

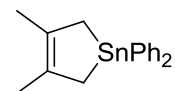
The isolation and purification of **1** from the crude reaction mixture was carried out as follows. Pentane (ca. 25 mL) was added to the oil from above, resulting in the formation of a white precipitate. The supernatant was decanted, the solid washed twice with fresh pentane (ca. 2 x 10 mL), and the solvent was removed from the combined filtrate on a rotary evaporator. The residue was then distilled ( $60\text{ }^\circ\text{C}$ , 0.03 torr) using a Kugelrohr distillation apparatus, collecting 2.23 g of a pale yellow oil. This procedure was repeated twice more with the viscous residue that remained after distillation,

affording pale yellow oils with masses of 0.81 g and 0.57 g. The  $^1\text{H}$  NMR spectra of the three collected fractions showed them to consist of a mixture of **1**, naphthalene, and **14** in relative ratios of (1.0):(0.12):(0.27), (1.0):(0.02):(0.19), and (1.0):(0):(0.10), respectively. The first fraction was pumped under high vacuum for ca. 9 h to obtain a mixture (1.72 g) of **1**, naphthalene, and **14** in a ratio of (1):(0.03):(0.08). The second fraction was further purified by column chromatography (silica gel; hexanes/dichloromethane gradient (100:0 to 70:30)), the fractions containing **1** were collected, and the solvent was removed, affording a clear colourless oil (0.50 g) containing a mixture of **1** and **14** in a molar ratio of (1):(0.06). The three fractions were then combined and distilled (60 °C, 0.03 Torr) to afford a clear colourless oil (0.93 g) in which only **14** could be detected as an impurity. This was then pumped under high vacuum (0.02 Torr) at room temperature for ca. 18 h to afford **1** as a colorless oil (0.59 g, 0.002 mol, 7 %). The purity was estimated to be  $\geq 98\%$  by  $^1\text{H}$  NMR spectroscopy, the major detectable contaminant being **14**.  $^1\text{H}$  NMR ( $\text{CDCl}_3$ ):  $\delta$  0.34 (s, 6 H,  $^2J_{119\text{SnH}} = 56.1$  Hz,  $^2J_{117\text{SnH}} = 54.0$  Hz,  $\text{Me}_2\text{Sn}$ ), 1.71 (m, 3 H, - $\text{CH}_2\text{C}(\text{Me})\text{C}(\text{Ph})\text{CH}_2$ -), 1.76 (m, 2 H,  $^2J_{\text{SnH}} = 36.4$  Hz, - $\text{CH}_2\text{C}(\text{Me})\text{C}(\text{Ph})\text{CH}_2$ -), 1.92 (m, 2 H,  $^5J = 1.8$  Hz,  $^2J_{\text{SnH}} = 37.6$  Hz, - $\text{CH}_2\text{C}(\text{Me})\text{C}(\text{Ph})\text{CH}_2$ -), 7.17 (d, 2 H,  $^3J = 6.9$  Hz, *o*-Ph), 7.19 (t, 1 H,  $^3J = 7.3$  Hz, *p*-Ph), 7.30 (t, 2 H,  $^3J = 7.6$  Hz, *m*-Ph).  $^{13}\text{C}\{^1\text{H}\}$  NMR ( $\text{CDCl}_3$ ):  $\delta$  -9.9 ( $^1J_{119\text{SnC}} = 324.3$  Hz,  $^1J_{117\text{SnC}} = 309.8$  Hz,  $\text{Me}_2\text{Sn}$ ), 21.9 ( $^1J_{119\text{SnC}} = 320.8$  Hz,  $^1J_{117\text{SnC}} = 306.2$  Hz, - $\text{CH}_2\text{C}(\text{Me})\text{C}(\text{Ph})\text{CH}_2$ -), 22.4 ( $^1J_{119\text{SnC}} = 311.7$  Hz,  $^1J_{117\text{SnC}} = 297.6$  Hz, - $\text{CH}_2\text{C}(\text{Me})\text{C}(\text{Ph})\text{CH}_2$ -), 23.0 ( $^3J_{\text{SnC}} = 59.9$  Hz, - $\text{CH}_2\text{C}(\text{Me})\text{C}(\text{Ph})\text{CH}_2$ -), 125.5 (*p*-Ph), 127.9 (*m*-Ph), 128.1 (*o*-Ph), 135.7 ( $^2J_{\text{SnC}} = 17.1$  Hz, - $\text{CH}_2\text{C}(\text{Me})\text{C}(\text{Ph})\text{CH}_2$ -), 137.9 ( $^2J_{\text{SnC}} = 20.4$  Hz, - $\text{CH}_2\text{C}(\text{Me})\text{C}(\text{Ph})\text{CH}_2$ -), 146.2 ( $^3J_{\text{SnC}} = 55.3$  Hz, *ipso*-Ph).  $^{119}\text{Sn}\{^1\text{H}\}$  NMR ( $\text{CDCl}_3$ ):  $\delta$  34.0. IR,  $\text{cm}^{-1}$  (relative intensity): 2976 (w), 2906 (m), 1491 (w), 1439 (w), 1103 (w), 890 (w), 766 (w), 700 (m). EI-MS,  $m/z$  (relative intensity; Sn-containing isotopomeric clusters are represented by the  $^{120}\text{Sn}$  isotopomer and are indicated with an

asterisk): 294.0\* (26, M<sup>+</sup>), 279.0\* (78, M<sup>+</sup>-CH<sub>3</sub>), 144.1 (22, M<sup>+</sup>-C<sub>2</sub>H<sub>6</sub>Sn), 134.9\* (100, MeSn<sup>+</sup>), 129.1 (52, C<sub>10</sub>H<sub>9</sub><sup>+</sup>), 128.1 (37, C<sub>10</sub>H<sub>8</sub><sup>+</sup>), 119.9\* (14, Sn<sup>+</sup>), 115.1 (15, C<sub>9</sub>H<sub>7</sub><sup>+</sup>), 77.0 (11, C<sub>6</sub>H<sub>5</sub><sup>+</sup>) HRMS: C<sub>18</sub>H<sub>20</sub><sup>120</sup>Sn: calc.: 294.0430, found: 294.0447.

**8.5.2. 3,4-Dimethyl-1,1-diphenyl-1-stannacyclopent-3-ene (**2**)<sup>3</sup>**

A 100 mL one-neck round bottom flask equipped with a stir bar was flame-dried under an atmosphere of argon and later charged with THF (38 mL) and lithium wire (0.84 g, 0.121 g-atom). With rapid stirring, a solution of naphthalene (16.94 g, 0.132 mol) dissolved in THF (37 mL) was added via syringe. The resulting dark green THF solution of lithium naphthalenide was allowed to stir for an additional 8 h at which point all of the lithium wire had been consumed. A separate two-neck 250 mL round bottom flask, equipped with a stir-bar, condenser and septum, was flame-dried under an atmosphere of argon and charged with Mg turnings (1.34 g, 0.055 g-atom) in THF (90 mL). 1,2-dibromoethane (5.0 mL, 0.058 mol) was added in one portion and the mixture was allowed to stir at ca. 60 °C until all of the Mg turnings were consumed (ca. 2 h). With rapid stirring and after cooling to room temperature, the previously prepared THF solution of lithium naphthalenide was added dropwise in one-portion via syringe. The resulting dark grey slurry of Mg\* was allowed to settle and the supernatant was removed via syringe and replaced with fresh THF (136 mL). The washing step was repeated, and then 2,3-dimethyl-1,3-butadiene (**13**, 6.2 mL, 0.055 mol) was added in one portion via syringe. The mixture was stirred for an additional 8 hours, the precipitate was allowed to settle, and the resulting orange solution of (2,3-dimethyl-2-butene-1,4-diyl)magnesium in THF was removed by syringe and used directly in the following step.



**2**

A 500 mL two-neck round-bottom flask equipped with a stir bar, septum and addition funnel was assembled and then flame-dried. It was later charged with Ph<sub>2</sub>SnCl<sub>2</sub>

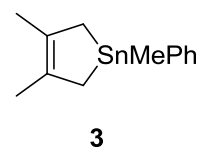
(4.81 g, 0.0140 mol) and THF (250 mL), and the resulting solution was cooled to  $-78\text{ }^{\circ}\text{C}$  in an acetone / dry ice bath. The solution of (2,3-dimethyl-2-butene-1,4-diyl)magnesium in THF prepared above was transferred to the addition funnel and then added dropwise over 8 h. The reaction mixture was monitored periodically using moist pH paper and addition was stopped when the solution reached neutrality. At this point, all of the THF solution containing (2,3-dimethyl-2-butene-1,4-diyl)magnesium had been added. The mixture was stirred while the bath warmed to room temperature overnight, after which it was washed with saturated aqueous  $\text{NH}_4\text{Cl}$  (3 x 75 mL), and the combined aqueous extracts were back-extracted with diethyl ether (3 x 40 mL). The combined organic extracts were dried over anhydrous  $\text{MgSO}_4$  and the solvent was removed to afford a pale yellow oil, to which pentane (ca. 30 mL) was added to precipitate salts. The supernatant was decanted, the solid washed twice with pentane (ca. 2 x 10 mL), and the solvent removed to yield a pale yellow oil (1.87 g). Purification by column chromatography (silica gel; hexanes/dichloromethane gradient (100:0 to 70:30)) followed by recrystallization from hot methanol afforded colourless crystals (1.32 g, 3.72 mmol, 27 %) that were identified as **2** (m.p.  $45.9 - 46.8\text{ }^{\circ}\text{C}$ ) on the basis of their  $^1\text{H}$ ,  $^{13}\text{C}\{^1\text{H}\}$ ,  $^{119}\text{Sn}\{^1\text{H}\}$  NMR, IR, and mass spectra (Sn isotopomeric clusters are represented by the  $^{120}\text{Sn}$  isotopomer and are indicated with an asterisk):  $^1\text{H}$  NMR ( $\text{C}_6\text{D}_6$ ):  $\delta$  1.82 (s, 6 H, *CMe*), 1.92 (s, 4 H,  $^2J_{\text{SnH}} = 39.3\text{ Hz}$ ,  $-\text{CH}_2\text{C}(\text{Me})\text{C}(\text{Me})\text{CH}_2-$ ), 7.18 (m, 6 H, *o,p*-Ph), 7.51 (m, 4 H,  $^4J_{\text{SnH}} = 48.4\text{ Hz}$ , *m*-Ph).  $^{13}\text{C}\{^1\text{H}\}$  NMR ( $\text{C}_6\text{D}_6$ ):  $\delta$  21.5 ( $-\text{CH}_2\text{C}(\text{Me})\text{C}(\text{Me})\text{CH}_2-$ ), 21.7 ( $-\text{CH}_2\text{C}(\text{Me})\text{C}(\text{Me})\text{CH}_2-$ ), 128.7 ( $^2J_{\text{SnC}} = 49.1\text{ Hz}$ , *o*-Ph), 129.0 ( $^4J_{\text{SnC}} = 11.1\text{ Hz}$ , *p*-Ph), 131.7 ( $-\text{CH}_2\text{C}(\text{Me})\text{C}(\text{Me})\text{CH}_2-$ ), 137.1 ( $^3J_{\text{SnC}} = 37.8\text{ Hz}$ , *m*-Ph), 138.7 (*ipso*-Ph).  $^{119}\text{Sn}\{^1\text{H}\}$  NMR ( $\text{C}_6\text{D}_6$ ):  $\delta$  -34.2. IR,  $\text{cm}^{-1}$  (relative intensity): 3063 (w), 2909 (m), 1480 (w), 1428 (m), 1146 (w), 1075 (w), 997 (w), 727 (m), 698 (m). EI-MS,  $m/z$  (relative intensity): 356.1\* (4,  $\text{M}^+$ ), 274.0\* (41,  $\text{M}^+ - \text{C}_6\text{H}_{10}$ ), 196.9\* (62,  $\text{PhSn}^+$ ), 144.9 (5), 119.9\* (100,  $\text{Sn}^+$ ).



HRMS:  $C_{18}H_{20}^{120}Sn$ : calc.: 356.0587, found: 356.0579. Except for a few differences in the  $^{13}C$  spectrum (the reported spectrum assigns a resonance "108.4 (s, Ph)" that was not found in this spectrum, an additional resonance was instead found at 131.7 (- $CH_2C(Me)C(Me)CH_2-$ ) that was not reported), the data are in good agreement with the reported data of Gaspar and coworkers.<sup>3</sup>

### 8.5.3. Synthesis of 1,3,4-trimethyl-1-phenyl-1-stannacyclopent-3-ene (**3**)

A two-neck 250 mL round bottom flask, equipped with a stir-bar, condenser and septum, was flame-dried under an atmosphere of argon and charged with Mg turnings (1.34 g, 0.055 g-atom) and THF (90 mL).



1,2-dibromoethane (5.0 mL, 0.058 mol) was added in one portion via syringe and the mixture was allowed to reflux until all of the Mg turnings were consumed (ca. 2 h). Subsequent cooling to room temperature results in a light grey suspension of magnesium dibromide ( $MgBr_2$ ) in THF solution. A separate one-neck 100 mL round bottom flask equipped with a stir bar was flame-dried under an atmosphere of argon and charged with finely cut lithium wire (0.84 g, 0.121 g-atom) and THF (38 mL). With rapid stirring, a solution of naphthalene (16.93 g, 0.132 mol) dissolved in THF (37 mL) was added in one-portion via syringe, resulting in green colouration of the reaction mixture. The solution was allowed to stir for an additional 8 h at which point all of the lithium wire had been consumed. With rapid stirring, the resulting dark green THF solution of lithium naphthalenide was added dropwise in one-portion via syringe to the previously prepared THF solution of magnesium dibromide. The resulting finely divided  $Mg^*$  precipitate was allowed to settle overnight before the supernatant was removed and fresh THF (130 mL) was added by syringe. This procedure was repeated twice, followed by the addition of 2,3-dimethyl-1,3-butadiene (**13**, 6.2 mL, 0.055 mol) was added in one portion by syringe. The mixture was allowed to stir at room temperature for an additional 8 hours before

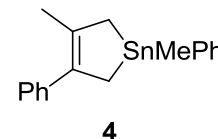
stirring was stopped and the precipitate allowed to settle. The resulting orange solution of (2,3-dimethyl-2-butene-1,4-diyl)magnesium in THF was used as is in the next step without disturbing the settled precipitate.

A 500 mL 2-neck round bottomed flask was fitted with a stir bar, septum and addition funnel and flame-dried. After cooling, it was later charged with MePhSnCl<sub>2</sub> (**10**, 3.37 g, 0.0120 mol) and THF (200 mL). The solution was cooled to -78 °C using a dry ice / acetone bath before the THF solution of the organomagnesium reagent from the previous step was transferred to the addition funnel and then added dropwise with stirring over 6 hours. The pH of the solution was tested periodically using moistened pH paper periodically and addition was stopped when it tested neutral. At this point, all of the THF solution containing (2,3-dimethyl-2-butene-1,4-diyl)magnesium had been added. The mixture was allowed to warm slowly to room temperature overnight, and was then washed with NH<sub>4</sub>Cl (3 x 75 mL). The combined aqueous extracts were then extracted with Et<sub>2</sub>O (3 x 40 mL), the organic extracts were combined, dried with MgSO<sub>4</sub>, and the solvent was removed on the rotary evaporator. To the resulting oily residue was added pentane (ca. 10 mL), which resulted in the formation of a white precipitate. The solution was decanted and the pentane removed on the rotary evaporator to afford 1.6 g (estimated crude yield: 46 %) of an opaque oil. The sample was purified by column chromatography (silica gel; 20 - 25 % dichloromethane / hexane) to first obtain a clear colourless oil of **3** (0.06 g, 0.21 mmol, 2 %), followed by a later fraction found to consist of **3** and naphthalene (0.55 g, 82 wt % **3** by <sup>1</sup>H NMR spectroscopy); from this a crude yield of 15 % for **3** can be estimated. Attempts to re-chromatograph the latter mixture (silica gel; hexanes/dichloromethane gradient 100:0 to 75:25) resulted in no recovery of **3**. The 0.06 g sample of purified **3** was found by <sup>1</sup>H NMR (C<sub>6</sub>D<sub>12</sub>) to contain naphthalene (ca. 0.2 mol %) and additional resonances at δ<sub>H</sub> = 0.88 and 1.29 ppm (see Chapter 3; Figure S3.2a)

that did not change over the course of photochemical experiments. Without knowing the exact structure, integration of the  $\delta_{\text{H}} = 0.88$  ppm signal (assuming the signal is due to 6 equivalent protons) relative to the  $\delta_{\text{H}} = 0.43$  ppm resonance due to **3** affords an approximate mol ratio  $\sim 0.12$ . Compound **3** was identified on the basis of its  $^1\text{H}$ ,  $^{13}\text{C}\{^1\text{H}\}$ ,  $^{119}\text{Sn}\{^1\text{H}\}$  NMR, IR and mass spectra.  $^1\text{H}$  NMR ( $\text{CDCl}_3$ ):  $\delta$  7.52 (m, 2 H,  $^3J_{\text{SnH}} = 45.5$  Hz, *o*-Ph), 7.33 (m, 3 H, *m,p*-Ph), 1.79 (s, 6 H,  $-\text{CH}_2\text{C}(\text{Me})\text{C}(\text{Me})\text{CH}_2-$ ), 1.68-1.86 (m, 4 H,  $-\text{CH}_2\text{C}(\text{Me})\text{C}(\text{Me})\text{CH}_2-$ ), 0.50 (s, 3 H,  $^2J_{\text{SnH}} = 57.0$  Hz, *Me*Sn).  $^1\text{H}$  NMR ( $\text{C}_6\text{D}_{12}$ ):  $\delta$  7.40 (m, 2 H,  $^3J_{\text{SnH}} = 46.9$  Hz, *o*-Ph), 7.18 (m, 3 H, *m,p*-Ph), 1.78 (s, 6 H,  $-\text{CH}_2\text{C}(\text{Me})\text{C}(\text{Me})\text{CH}_2-$ ), 1.64-1.84 (m, 4 H,  $-\text{CH}_2\text{C}(\text{Me})\text{C}(\text{Me})\text{CH}_2-$ ), 0.43 (s, 3 H,  $^2J_{\text{SnH}} = 56.0$  Hz, *Me*Sn).  $^{13}\text{C}\{^1\text{H}\}$  NMR ( $\text{CDCl}_3$ ):  $\delta$  140.8 ( $^1J_{\text{SnC}} = 452$  Hz, *ipso*-Ph), 136.2 ( $^2J_{\text{SnC}} = 36.4$  Hz, *o*-Ph), 131.8 ( $^2J_{\text{SnC}} = 20.6$  Hz,  $-\text{CH}_2\text{C}(\text{Me})\text{C}(\text{Me})\text{CH}_2-$ ), 128.4 ( $^4J_{\text{SnC}} = 10.6$  Hz, *p*-Ph), 128.2 ( $^3J_{\text{SnC}} = 46.2$  Hz, *m*-Ph), 21.8 ( $^1J_{^{119}\text{SnC}} = 335.3$  Hz,  $^1J_{^{117}\text{SnC}} = 320.4$  Hz,  $-\text{CH}_2\text{C}(\text{Me})\text{C}(\text{Me})\text{CH}_2-$ ), 21.6 ( $^3J_{\text{SnC}} = 65.4$  Hz,  $-\text{CH}_2\text{C}(\text{Me})\text{C}(\text{Me})\text{CH}_2-$ ), -11.5 ( $^1J_{^{119}\text{SnC}} = 340.8$  Hz,  $^1J_{^{117}\text{SnC}} = 325.2$  Hz, *Me*Sn).  $^{119}\text{Sn}\{^1\text{H}\}$  NMR ( $\text{CDCl}_3$ ):  $\delta$  -4.8. IR,  $\text{cm}^{-1}$  (relative intensity): 2907 (m), 2887 (m), 1428 (m), 1146 (m), 1075 (m), 834 (w), 747 (m), 726 (s), 697 (s), 673 (m). EI-MS,  $m/z$  (relative intensity; Sn-containing isotopomeric clusters are represented by the  $^{120}\text{Sn}$  isotopomer and are indicated with an asterisk): 294.0\* (22,  $\text{M}^+$ ), 279.0\* (30,  $\text{M}^+ - \text{CH}_3$ ), 212.0\* (53,  $\text{M}^+ - \text{C}_6\text{H}_{10}$ ), 200.5 (17), 196.9\* (98,  $\text{PhSn}^+$ ), 134.9\* (11,  $\text{MeSn}^+$ ), 127.1 (18,  $\text{C}_9\text{H}_{19}^+$ ), 119.9\* (41,  $\text{Sn}^+$ ), 97.0 (10,  $\text{C}_7\text{H}_{13}^+$ ). HRMS: ( $\text{C}_{13}\text{H}_{18}^{120}\text{Sn}$ ) calc.: 294.0430, found: 294.0454.

#### 8.5.4. Synthesis of 1,3-dimethyl-1,4-diphenyl-1-stannacyclopent-3-ene (**4**)

A two-neck round bottom flask equipped with a stir-bar, septum, and condenser was charged with Mg turnings (1.21 g, 0.050 mol) and flame-dried under an atmosphere of argon. After cooling, the flask was charged with THF (150 mL) followed by the addition of 1,2-dibromoethane (4.54 mL, 0.052 mol) in one portion via syringe. The reaction mixture was allowed to reflux until all of the Mg turnings were consumed (ca. 2 h). Afterwards, the solution was allowed to cool to room temperature, affording a grey suspension of magnesium dibromide. To the reaction mixture was added finely cut lithium wire (0.71 g, 0.10 g-atom) and naphthalene (1.98 g, 0.016 mol). The solution was heated to reflux with rapid stirring until the lithium was fully consumed, which required 4 days.



The resulting finely divided black powder of activated magnesium (Mg\*) was allowed to settle; the resulting green supernatant was removed and replaced with freshly distilled THF (124 mL). A mixture of 2-methyl-3-phenyl-1,3-butadiene (**14**, 5.8 g, 40 mmol) in pentane (80 wt %) was added in one portion, the resulting solution was allowed to stir at room temperature for an additional two days before stirring was halted and the residual solids were allowed to settle. The resulting dark orange solution of (2-methyl-3-phenyl-2-butene-1,4-diyl)magnesium in THF was used as is in the next step without disturbing the settled precipitate.

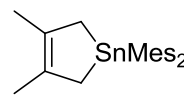
A flame-dried 500 mL three-neck round bottomed flask was fitted with a stir bar, septum, glass stopper and addition funnel. The flask was charged with MePhSnCl<sub>2</sub> (**10**, 4.96 g, 15.0 mmol) and THF (180 mL), and the resulting solution was cooled to -78 °C using an acetone / dry ice bath. The solution of (2-methyl-3-phenyl-2-butene-1,4-diyl)magnesium in THF prepared in the previous step (120 mL) was added dropwise from the addition funnel until the reaction mixture tested neutral on moist pH paper, at which

point all of the THF solution containing (2-methyl-3-phenyl-2-butene-1,4-diyl)magnesium had been added. The reaction mixture was allowed to stir overnight, at which point the bath had warmed up to room temperature. The reaction mixture was washed with saturated aqueous  $\text{NH}_4\text{Cl}$  (3 x 75 mL), and the aqueous washes were back-extracted with  $\text{Et}_2\text{O}$  (3 x 50 - 60 mL). The combined organic extracts were dried with  $\text{MgSO}_4$ , filtered, and the solvent was removed on the rotary evaporator to yield a yellow oil (7.76 g). Pentane (ca. 20mL) was added, resulting in the formation of a white precipitate. The resulting mixture was filtered and the solvent was removed using a rotary evaporator to afford a yellow oil (6.35 g). Residual naphthalene and **14** were removed with mild heating (40 - 50 °C) under vacuum (0.005 torr) for ca. 40 h. The remaining crude oil (5.40 g, 93 %) was purified by column chromatography (basic alumina; 10 % dichloromethane / hexane) to afford a clear colourless oil (2.57 g, 7.77 mmol, 44 %) that was identified as **4** on the basis of its  $^1\text{H}$ ,  $^{13}\text{C}\{^1\text{H}\}$ ,  $^{119}\text{Sn}\{^1\text{H}\}$  NMR, IR and mass spectra; the samples also contained of a hydrocarbon of unknown structure that did not change over the course of steady state photolysis experiments; from the resonances in the  $^1\text{H}$  NMR spectrum a purity of  $\geq 90\%$  was estimated. This estimate was derived from a resonance at  $\delta_{\text{H}}$  7.06 (d, 2 H  $^2J = 8.1$  Hz) for the unknown compound which was interpreted as due to at least 2 H, relative to the resonance due to **4** at  $\delta_{\text{H}}$  1.75 (s, 3 H,  $-\text{CH}_2\text{C}(\text{Me})\text{C}(\text{Ph})\text{CH}_2-$ ).  $^1\text{H}$  NMR ( $\text{CDCl}_3$ ):  $\delta$  0.58 (s, 3 H,  $^2J_{119\text{SnH}} = 57.4$  Hz,  $^2J_{117\text{SnH}} = 55.0$  Hz,  $\text{MeSn}$ ), 1.75 (s, 3 H,  $-\text{CH}_2\text{C}(\text{Me})\text{C}(\text{Ph})\text{CH}_2-$ ), 1.91 (d, 1 H,  $^2J = 16.7$  Hz,  $-\text{CH}_2\text{C}(\text{Me})\text{C}(\text{Ph})\text{CH}_2-$ ), 1.96 (d, 1 H,  $^2J = 17.3$  Hz,  $-\text{CH}_2\text{C}(\text{Me})\text{C}(\text{Ph})\text{CH}_2-$ ), 2.07 (d, 1 H,  $^2J = 16.6$  Hz,  $-\text{CH}_2\text{C}(\text{Me})\text{C}(\text{Ph})\text{CH}_2-$ ), 2.14 (d, 1 H,  $^2J = 16.5$  Hz,  $-\text{CH}_2\text{C}(\text{Me})\text{C}(\text{Ph})\text{CH}_2-$ ), 7.19 (d, 2 H,  $^3J = 7.9$  Hz, *o*-Ph), 7.20 (t, 1 H,  $^3J = 6.6$  Hz, *p*-Ph), 7.31 (t, 2 H,  $^3J = 7.9$  Hz, *m*-Ph), 7.37 (m, 3 H, *m,p*-PhSn), 7.57 (m, 2 H,  $^3J_{\text{SnH}} = 45.6$  Hz, *o*-PhSn).  $^{13}\text{C}\{^1\text{H}\}$  NMR ( $\text{CDCl}_3$ ):  $\delta$  -11.2 ( $^1J_{119\text{SnC}} = 343.8$  Hz,  $^1J_{117\text{SnC}} = 328.7$ ,  $\text{MeSn}$ ),

22.0 ( $^1J_{119\text{SnC}} = 333.6$  Hz,  $^1J_{117\text{SnC}} = 317.7$  Hz,  $-\text{CH}_2\text{C}(\text{Me})-\text{C}(\text{Ph})\text{CH}_2-$ ), 22.4 ( $^1J_{119\text{SnC}} = 322.9$  Hz,  $^1J_{117\text{SnC}} = 310.0$  Hz,  $-\text{CH}_2\text{C}(\text{Me})-\text{C}(\text{Ph})\text{CH}_2-$ ), 22.9 ( $^3J_{\text{SnC}} = 62.2$  Hz,  $-\text{CH}_2\text{C}(\text{Me})-\text{C}(\text{Ph})\text{CH}_2-$ ), 125.7 (*p*-Ph), 127.9 (*m*-Ph), 128.1 (*o*-Ph)), 128.3 ( $^3J_{\text{SnC}} = 46.5$  Hz, *m*-PhSn), 128.6 ( $^4J_{\text{SnC}} = 11.8$  Hz, *p*-PhSn), 135.7 ( $^2J_{\text{SnC}} = 18.8$  Hz,  $-\text{CH}_2\text{C}(\text{Me})-\text{C}(\text{Ph})\text{CH}_2-$ ), 136.2 ( $^2J_{\text{SnC}} = 36.7$  Hz, *o*-PhSn), 137.8 ( $^2J_{\text{SnC}} = 22.2$  Hz,  $-\text{CH}_2\text{C}(\text{Me})-\text{C}(\text{Ph})\text{CH}_2-$ ), 140.7 ( $^1J_{119\text{SnC}} = 455.8$  Hz,  $^1J_{117\text{SnC}} = 438.4$ , *ipso*-PhSn), 145.8 ( $^3J_{\text{SnC}} = 57.3$  Hz, *ipso*-Ph).  $^{119}\text{Sn}\{^1\text{H}\}$  NMR ( $\text{CDCl}_3$ ):  $\delta$  5.1. IR,  $\text{cm}^{-1}$  (relative intensity): 2904 (w), 1491 (w), 1428 (m), 1074 (w), 764 (m), 727 (m), 697 (s), 640 (m), 575 (m), 555 (m). EI-MS,  $m/z$  (relative intensity; Sn-containing isotopomeric clusters are represented by the  $^{120}\text{Sn}$  isotopomer and are indicated with an asterisk): 356.1\* (3,  $\text{M}^+$ ), 341.0\* (17,  $\text{M}^+ - \text{CH}_3$ ), 233.1 (92,  $\text{C}_{18}\text{H}_{17}^+$ ), 196.9\* (63,  $\text{PhSn}^+$ ), 144.1 (78,  $\text{C}_{11}\text{H}_{12}^+$ ), 129.0 (100,  $\text{C}_{10}\text{H}_9^+$ ), 115.0 (95,  $\text{C}_9\text{H}_7^+$ ), 105.1 (54,  $\text{C}_8\text{H}_9^+$ ), 91.1 (79,  $\text{C}_7\text{H}_7^+$ ), 77.0 (65,  $\text{C}_6\text{H}_5^+$ ), 51.0 (17,  $\text{C}_4\text{H}_3^+$ ). HRMS: ( $\text{C}_{18}\text{H}_{20}^{120}\text{Sn}$ ) calc.: 356.0566, found: 356.0587.

### 8.5.5. Synthesis of 1,1-dimesityl-3,4-dimethyl-1-stannacyclopent-3-ene (5)

A two-neck 250 mL round bottom flask, equipped with a stir-bar, condenser and septum, was flame-dried under an atmosphere of argon and charged with Mg turnings (1.21 g, 0.050 g-atom) and THF (150 mL).



5

1,2-dibromoethane (4.50 mL, 0.052 mol) was added in one portion via syringe and the mixture was allowed to reflux until all of the magnesium had been consumed (ca. 1.5 h), after which the solution was allowed to cool to room temperature. To the resulting light grey suspension of magnesium dibromide ( $\text{MgBr}_2$ ) in THF was added naphthalene (1.98 g, 0.016 mol) and finely cut lithium wire (0.71 g, 0.10 g-atom). The reaction mixture was stirred rapidly at room temperature for 18 hours, by which point all of the lithium had been consumed. Stirring was halted, and the finely divided dark grey magnesium ( $\text{Mg}^*$ ) was allowed to settle. The supernatant was removed and replaced with fresh THF (130

mL), followed by the addition of 2,3-dimethyl-1,3-butadiene (**13**, 5.7 mL, 0.050 mol) in a single portion. The reaction mixture was stirred for 8 hours, before stirring was stopped and the residual precipitate was allowed to settle. The orange supernatant containing (2,3-dimethyl-2-butene-1,4-diyl)magnesium in THF was used as is in the next step without disturbing the settled precipitate.

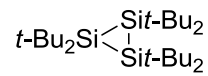
A flame-dried 500 mL 2-neck round bottomed flask was fitted with a stirbar, addition funnel, and septum. The reaction flask was charged with  $\text{Me}_2\text{SnCl}_2$  (**11**, 6.28 g, 14.7 mmol; see section 8.7.2 for the synthesis) in THF (180 mL) and cooled to  $-78\text{ }^\circ\text{C}$  using a dry ice / acetone bath. The addition funnel was charged with the organomagnesium reagent prepared in the previous step, which was then added dropwise to the flask until the pH of the reaction mixture tested neutral on moist pH paper; this required the addition of ca. 100 mL of the Grignard solution. The reaction mixture and cooling bath were allowed to warm to room temperature overnight. The solution was transferred to a separatory funnel and washed with saturated  $\text{NH}_4\text{Cl}$  solution (3 x 75 mL). The combined aqueous extracts were then extracted using  $\text{Et}_2\text{O}$  (3 x 40 mL). The combined organic fractions were dried over  $\text{MgSO}_4$ , filtered, and the solvent was removed on the rotary evaporator to yield a viscous yellow oil (7.79 g), which was found by  $^1\text{H}$  NMR to consist of **5** and naphthalene (ca. 2:1 mol ratio) in addition to small amounts of at least three unidentified tin-containing compounds.

Pentane was added to precipitate salts. After filtration and removal of solvent, the resulting oil was placed under high vacuum ( $60 - 65\text{ }^\circ\text{C}$ ,  $0.02 - 0.05\text{ mmHg}$ , 15 h) to remove residual naphthalene. The remaining impurities were removed by dividing the crude mixture into two, and adding each half to different, rapidly stirred mixtures of basic alumina (20 g) and pentane (ca. 30 mL) for 20 minutes before filtering the solution. Removal of solvent on a rotary evaporator yielded an opaque colourless oil, which was

identified as 1,1-dimesityl-3,4-dimethyl-1-stannacyclopent-3-ene (**5**, combined mass 0.50 g, 1.1 mmol, 8 %) on the basis of its  $^1\text{H}$ ,  $^{13}\text{C}\{^1\text{H}\}$ ,  $^{119}\text{Sn}\{^1\text{H}\}$  NMR, IR and mass spectra. The sample was contaminated with mesitylene (1.9 wt % by  $^1\text{H}$  NMR).  $^1\text{H}$  NMR ( $\text{C}_6\text{D}_6$ ):  $\delta$  6.77 (s, 4 H,  $^4J_{\text{SnH}} = 16.6$  Hz, *m*- $\text{C}_6\text{H}_2\text{Me}_3$ ), 2.36 (s, 12 H,  $^4J_{\text{SnH}} = 6.2$  Hz, *o*- $\text{C}_6\text{H}_2\text{Me}_3$ ), 2.14 (s, 6 H, *p*- $\text{C}_6\text{H}_2\text{Me}_3$ ), 2.09 (s, 4 H,  $^2J_{\text{SnH}} = 37.1$  Hz,  $-\text{CH}_2\text{C}(\text{Me})\text{C}(\text{Me})\text{CH}_2-$ ), 1.83 (s, 6 H,  $-\text{CH}_2\text{C}(\text{Me})\text{C}(\text{Me})\text{CH}_2-$ ).  $^1\text{H}$  NMR ( $\text{C}_6\text{D}_{12}$ ):  $\delta$  6.72 (s, 4 H,  $^4J_{\text{SnH}} = 16.6$  Hz, *m*- $\text{C}_6\text{H}_2\text{Me}_3$ ), 2.28 (s, 12 H,  $^4J_{\text{SnH}} = 6.2$  Hz, *o*- $\text{C}_6\text{H}_2\text{Me}_3$ ), 2.17 (s, 6 H, *p*- $\text{C}_6\text{H}_2\text{Me}_3$ ), 2.02 (s, 4 H,  $^2J_{\text{SnH}} = 37.4$  Hz,  $-\text{CH}_2\text{C}(\text{Me})\text{C}(\text{Me})\text{CH}_2-$ ), 1.77 (s, 6 H,  $-\text{CH}_2\text{C}(\text{Me})\text{C}(\text{Me})\text{CH}_2-$ ).  $^{13}\text{C}\{^1\text{H}\}$  NMR ( $\text{C}_6\text{D}_6$ ):  $\delta$  145.1 ( $^2J_{\text{SnC}} = 34.3$  Hz, *o*- $\text{C}_6\text{H}_2\text{Me}_3$ ), 140.1 ( $^1J_{119\text{SnC}} = 492.8$  Hz,  $^1J_{117\text{SnC}} = 471.1$  Hz, *ipso*- $\text{C}_6\text{H}_2\text{Me}_3$ ), 138.6 ( $^4J_{\text{SnC}} = 9.8$  Hz, *p*- $\text{C}_6\text{H}_2\text{Me}_3$ ), 132.1 ( $^2J_{\text{SnC}} = 22.9$  Hz,  $-\text{CH}_2\text{C}(\text{Me})\text{C}(\text{Me})\text{CH}_2-$ ), 128.7 ( $^3J_{\text{SnC}} = 42.9$  Hz, *m*- $\text{C}_6\text{H}_2\text{Me}_3$ ), 28.0 ( $^1J_{119\text{SnC}} = 330.6$  Hz,  $^1J_{117\text{SnC}} = 316.4$  Hz,  $-\text{CH}_2\text{C}(\text{Me})\text{C}(\text{Me})\text{CH}_2-$ ), 26.1 ( $^3J_{\text{SnC}} = 31.7$  Hz, *o*- $\text{C}_6\text{H}_2\text{Me}_3$ ), 22.1 ( $^3J_{\text{SnC}} = 65.0$  Hz,  $-\text{CH}_2\text{C}(\text{Me})\text{C}(\text{Me})\text{CH}_2-$ ), 21.4 ( $^5J_{\text{SnC}} = 5.1$  Hz, *p*- $\text{C}_6\text{H}_2\text{Me}_3$ ).  $^{119}\text{Sn}\{^1\text{H}\}$  NMR ( $\text{C}_6\text{D}_6$  or  $\text{C}_6\text{D}_{12}$ ):  $\delta$  -81.0. IR,  $\text{cm}^{-1}$  (relative intensity): 3017 (s), 2965 (m), 2917 (m), 2854 (s), 1599 (s), 1447 (m), 1025 (s), 846 (m), 802 (s), 684 (m). CI-MS,  $m/z$  (relative intensity; Sn-containing isotopomeric clusters are represented by the  $^{120}\text{Sn}$  isotopomer and are indicated with an asterisk): 441.2\* (2,  $(\text{M}+\text{H})^+$ ), 358.1\* (46,  $(\text{M}-\text{C}_6\text{H}_{10})^+$ ), 238.0\* (100,  $\text{C}_9\text{H}_{10}\text{Sn}^+$ ), 119.1 (92,  $\text{C}_9\text{H}_{11}^+$ ), 105.1 (41,  $\text{C}_8\text{H}_9^+$ ), 91.1 (31,  $\text{C}_7\text{H}_7^+$ ), 67.1 (31,  $\text{C}_5\text{H}_7^+$ ). HRMS: ( $\text{C}_{24}\text{H}_{32}^{120}\text{Sn}+\text{H}$ ) calcd 441.1604, found 441.1609. The data are in good agreement with the previously reported  $^1\text{H}$ ,  $^{13}\text{C}$ ,  $^{119}\text{Sn}$  NMR and IR spectra of Neale and Tilley.<sup>6</sup> The attempted purification of **5** by silica gel chromatography resulted in no recovery and subsequent isolation of mesitylene.



**8.5.6.** *Hexa-tert-butylcyclotrisilane (6)* was prepared according to the procedure of Weidenbruch and co-workers.<sup>7</sup> Compound **6** was purified



**6**

by column chromatography (silica gel, hexanes), followed by

recrystallization from pentane, to a purity of  $\geq 97\%$  as determined by  $^1\text{H}$  NMR spectroscopy (m.p. 175 - 188 °C (dec)). Spectroscopic data for the compound are in reasonable agreement with the spectra reported by Weidenbruch and coworkers,<sup>7,8</sup> except for the assignment for  $\text{C}(\text{CH}_3)_3$  in the  $^{13}\text{C}$  spectrum which was reported at 31.0 ppm. In this work, the resonance was found at 27.2 ppm, this new assignment is supported by the results of a 1D-DEPTq spectrum:  $^1\text{H}$  NMR ( $\text{C}_6\text{D}_6$ ):  $\delta$  1.42 (s, 54 H);  $^{13}\text{C}\{^1\text{H}\}$  NMR ( $\text{C}_6\text{D}_6$ ):  $\delta$  27.2 ( $\text{C}(\text{CH}_3)_3$ ; determined by 1D-DEPTq), 35.1 ( $\text{C}(\text{CH}_3)_3$ );  $^{29}\text{Si}\{^1\text{H}\}$  NMR ( $\text{C}_6\text{D}_6$ ):  $\delta$  3.58 (Determined by 2D  $^1\text{H}$ - $^{29}\text{Si}$  HMBC experiments). IR,  $\text{cm}^{-1}$  (relative intensity): 2951 (w), 2853 (s), 1483 (m), 1473 (w), 1361 (m), 1165 (m), 937 (w), 810 (s), 481 (w), 438 (m). EI-MS,  $m/z$  (relative intensity): 426.4 (18,  $\text{M}^+$ ), 376.2 (9), 314.2 (9), 285.2 (9,  $(\text{Si}_2t\text{-Bu}_4+1)^+$ ), 228.2 (18,  $(\text{Si}_2t\text{-Bu}_3+1)^+$ ), 185.1 (12), 169.1 (39,  $(\text{Si}_2t\text{-Bu}_2-1)^+$ ), 127.1 (52), 91.1 (51), 73.0 (100), 57.1 (35,  $\text{C}_4\text{H}_9^+$ ). HRMS: ( $\text{C}_{24}\text{H}_{54}\text{Si}_3$ ) calc.: 426.3533, found: 426.3529.

## 8.6. UV-Visible Spectra of Photoprecursors

Hexanes solutions of **1-7** used to record UV-visible absorption spectra were prepared from the addition of the photoprecursors (pre-weighed using an analytical balance) to calibrated 100 mL or 250 mL reservoirs containing dry and deoxygenated hexanes. The data shown in Figures 8.1 - 8.2 (with the exception of **3**) were measured in triplicate.

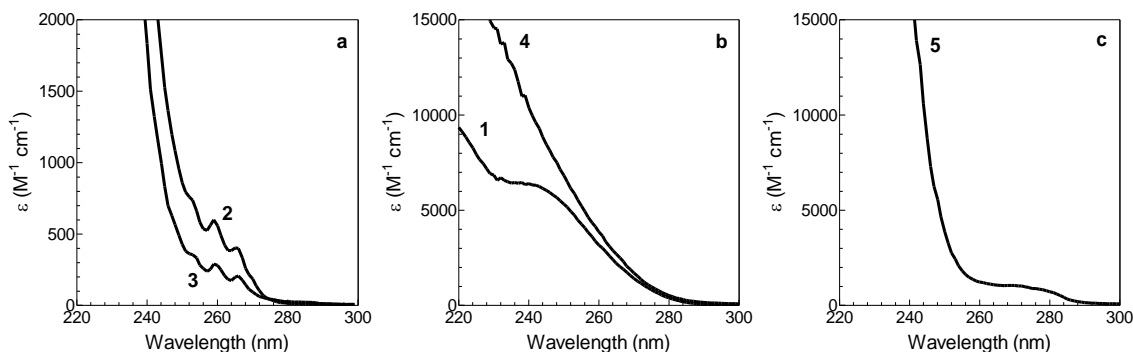


**Figure 8.1.** UV-visible absorption spectra of 1-stannacyclopent-3-enes (a) **2** and **3**, (b) **1** and **4**, and (c) **5**, recorded between 220 - 300 nm in hexanes solution.

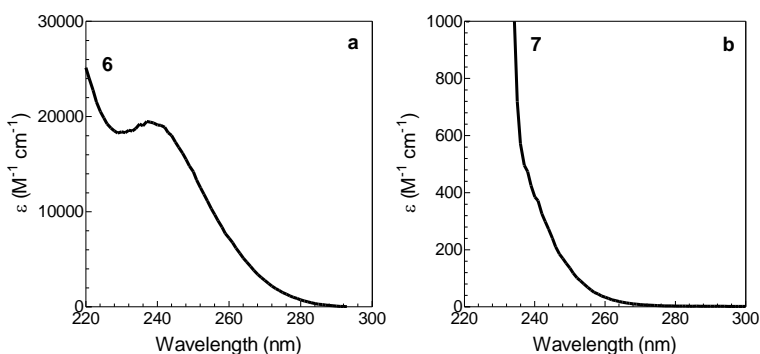


**Figure 8.2.** UV-visible absorption spectra of Sit-Bu<sub>2</sub> precursors (a) **6** and (b) **7** recorded between 220 - 300 nm in hexanes solution.

## 8.7. Identification of Compounds in Steady State Photolysis Experiments

See 8.2 for a description of steady state photolysis experiments, including the preparation and photolysis of solutions, and the identification of compounds.

### 8.7.1. Compounds Identified by Spiking the Photolyzate using Commercially Available

Authentic Samples:

*Ph<sub>2</sub>SnCl<sub>2</sub>*:  $\delta_{\text{H}}$  (C<sub>6</sub>D<sub>12</sub>) 7.39 (m, 6 H, *m,p*-Ph), 7.62 (m, 4 H,  $^3J_{\text{SnH}} = 82.3$  Hz, *o*-Ph);  $\delta_{\text{Sn}}$  (C<sub>6</sub>D<sub>12</sub>) -25.1.

*Me<sub>3</sub>SnCl*:  $\delta_{\text{H}}$  (C<sub>6</sub>D<sub>12</sub>) 0.52 (s, 9 H,  $^2J_{\text{SnH}} = 56.4$  Hz);  $\delta_{\text{Sn}}$  (C<sub>6</sub>D<sub>12</sub>) 152.0.

*Benzene*:  $\delta_{\text{H}}$  (C<sub>6</sub>D<sub>12</sub>) 7.22 (s, 6 H);  $\delta_{\text{C}}$  (C<sub>6</sub>D<sub>12</sub>) 128.7.

*Methane*:  $\delta_{\text{H}}$  (C<sub>6</sub>D<sub>12</sub>) 0.18 (s, 4 H);  $\delta_{\text{C}}$  (C<sub>6</sub>D<sub>12</sub>) -4.7.

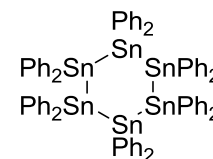
*Mesitylene*:  $\delta_{\text{H}}$  ( $\text{C}_6\text{D}_{12}$ ) 2.20 (s, 9 H,  $\text{CH}_3$ ), 6.67 (s, 3 H,  $H\text{-Ar}$ );  $\delta_{\text{C}}$  ( $\text{C}_6\text{D}_{12}$ ) 21.4, 127.5, 137.7.

### 8.7.2. Compounds Identified by Spiking the Photolyzate using Independently Prepared Authentic Samples:

*Dodecaphenylcyclohexastannane* (**8**) ( $c\text{-Sn}_6\text{Ph}_{12}$ ) was prepared

according to the method of Neumann and König.<sup>9</sup> The compound was obtained as colorless crystals (m.p. > 270 °C (dec)<sup>9</sup>), which exhibited

$^1\text{H}$  and  $^{119}\text{Sn}$  NMR spectra that are in reasonable agreement with



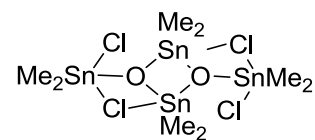
**8**

published data for the compound:<sup>10,11</sup>  $\delta_{\text{H}}$  ( $\text{C}_6\text{D}_6$ ) 6.92 (t, 24 H,  $^3J = 7.3$  Hz,  $m\text{-Ph}$ ), 7.00 (t, 12 H,  $^3J = 7.3$  Hz,  $p\text{-Ph}$ ), 7.60 (d, 24 H,  $^3J = 7.6$  Hz,  $^3J_{\text{SnH}} = 47.8$  Hz,  $o\text{-Ph}$ );  $\delta_{\text{H}}$  ( $\text{CDCl}_3$ ) 7.02 (t, 24 H,  $^3J = 7.4$  Hz,  $m\text{-Ph}$ ), 7.20 (t, 12 H,  $^3J = 7.4$  Hz,  $p\text{-Ph}$ ), 7.25 (d, 24 H,  $^3J = 7.4$  Hz,  $^3J_{\text{SnH}} = 47.5$  Hz,  $o\text{-Ph}$ );  $\delta_{\text{C}}$  ( $\text{CDCl}_3$ ) 128.2 ( $^4J_{\text{SnC}} = 10.5$  Hz,  $p\text{-Ph}$ ), 128.6 ( $^3J_{\text{SnC}} = 44.7$  Hz,  $m\text{-Ph}$ ), 138.3 ( $^2J_{\text{SnC}} = 41.9$  Hz,  $^3J_{\text{SnC}} = 9.9$  Hz,  $o\text{-Ph}$ ), 138.6 ( $^1J_{\text{SnC}} = 284.2$  Hz,  $^2J_{\text{SnC}} = 20.0$  Hz,  $ipso\text{-Ph}$ );  $\delta_{\text{Sn}}$  ( $\text{C}_6\text{D}_6$ ) -207.2 ( $^1J_{\text{SnSn}} = 1100.95$  Hz,  $^2J_{\text{SnSn}} = 771.07$  Hz);  $\delta_{\text{Sn}}$  ( $\text{CDCl}_3$ ) -207.5 ( $^1J_{\text{SnSn}} = 1084.2$  Hz,  $^2J_{\text{SnSn}} = 777.8$  Hz).

*1,3-Dichloro-1,1,3,3-tetramethyldistannoxane dimer* (**9**) was

synthesized and purified by the method of Okawara and

Wada.<sup>12</sup> A one-neck 50 mL round bottom flask was fitted with



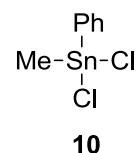
**9**

an addition funnel and stir bar. It was later charged with  $\text{Me}_2\text{SnCl}_2$  (0.51 g, 2.3 mmol) and distilled  $\text{H}_2\text{O}$  (3.7 mL). The addition funnel was charged with pyridine (0.18 mL, 2.2 mmol) dissolved in ethanol (1.4 mL). Dropwise addition of the ethanol/pyridine mixture results in the immediate formation of a white precipitate. After the addition was completed, the reaction mixture was then filtered on a Buchner funnel to collect the precipitate. The precipitate was then washed with ethanol and further dried under vacuum to afford a colorless, high melting (m.p. > 280 °C)<sup>13</sup> powder (0.20 g, 0.26 mmol, 45 %).

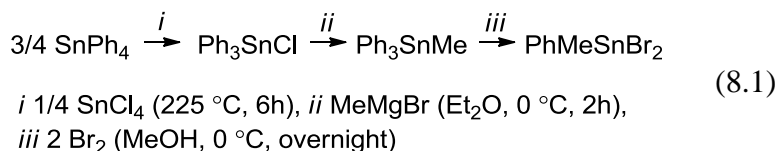
The  $^1\text{H}$ ,  $^{13}\text{C}$ , and  $^{119}\text{Sn}$  NMR spectra of the compound in  $\text{CDCl}_3$  and  $\text{C}_6\text{D}_{12}$  are listed below; the spectra were recorded in the presence of ca. 40 and 25 mM  $\text{Me}_2\text{SnCl}_2$ , respectively, to facilitate dissolution.  $\delta_{\text{H}}$  ( $\text{CDCl}_3$  + 40 mM  $\text{Me}_2\text{SnCl}_2$ ) 1.18 (s, 12 H,  $^2J_{119\text{SnH}} = 79.5$  Hz,  $^2J_{117\text{SnH}} = 76.3$  Hz,  $(\text{Me}_2\text{SnO})_2(\text{Me}_2\text{SnCl}_2)_2$ ), 1.25 (s, 12 H,  $^2J_{119\text{SnH}} = 83.9$  Hz,  $^2J_{117\text{SnH}} = 81.4$  Hz,  $(\text{Me}_2\text{SnO})_2(\text{Me}_2\text{SnCl}_2)_2$ );  $\delta_{\text{H}}$  ( $\text{C}_6\text{D}_{12}$ ) 1.04 (s, 12 H,  $^2J_{119\text{SnH}} = 80.2$  Hz,  $^2J_{117\text{SnH}} = 76.8$  Hz,  $(\text{Me}_2\text{SnO})_2(\text{Me}_2\text{SnCl}_2)_2$ ), 1.15 (s, 12 H,  $^2J_{119\text{SnH}} = 85.4$  Hz,  $^2J_{117\text{SnH}} = 82.6$  Hz,  $(\text{Me}_2\text{SnO})_2(\text{Me}_2\text{SnCl}_2)_2$ );  $\delta_{\text{C}}$  ( $\text{CDCl}_3$ ) 12.4 ( $(\text{Me}_2\text{SnO})_2(\text{Me}_2\text{SnCl}_2)_2$ ), 13.7 ( $(\text{Me}_2\text{SnO})_2(\text{Me}_2\text{SnCl}_2)_2$ );  $\delta_{\text{Sn}}$  ( $\text{CDCl}_3$ ) -61.1 ( $^2J_{\text{SnSn}} = 55.2$  Hz (approx),  $(\text{Me}_2\text{SnO})_2(\text{Me}_2\text{SnCl}_2)_2$ ), -116.1 ( $^2J_{\text{SnSn}} = 57.2$  Hz,  $(\text{Me}_2\text{SnO})_2(\text{Me}_2\text{SnCl}_2)_2$ );  $\delta_{\text{Sn}}$  ( $\text{C}_6\text{D}_{12}$ ) -63.2 ( $(\text{Me}_2\text{SnO})_2(\text{Me}_2\text{SnCl}_2)_2$ ), -125.4 ( $(\text{Me}_2\text{SnO})_2(\text{Me}_2\text{SnCl}_2)_2$ ). The  $^1\text{H}$  and  $^{119}\text{Sn}$  NMR spectra are in reasonable agreement with previously reported spectra.<sup>13-15</sup> (*Synthesis by P. Ho*)

*Dichloromethylphenylstannane* (**10**) was prepared as a white crystalline

solid (m.p. 39.6 - 42.4 °C) using procedures adapted from those of Dakternieks and coworkers<sup>16</sup> using  $\text{MePhSnBr}_2$  as starting reagent.



$\text{MePhSnBr}_2$  in turn was synthesized in three steps from  $\text{SnPh}_4$  according to literature procedures summarized in equation 8.1 (*i*<sup>17</sup>, *ii*<sup>18</sup>, *iii*<sup>19</sup>).



(i) A one-neck 100 mL round bottom flask was fitted with a stir-bar, condenser and purged with nitrogen, before being charged with  $\text{SnPh}_4$  (39.99 g, 0.094 mol) and  $\text{SnCl}_4$  (3.75 mL, 0.032 mol). The mixture was heated using a sand bath to ca. 230-260 °C initially to melt the solid, before being stirred at 225 °C for ca. 3 h, then at 160 °C for ca. 3 h before cooling to room temperature. The resulting brown solid was transferred to a

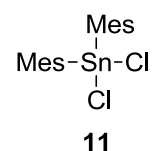
one-neck one litre round bottom flask, where recrystallization from isooctane (with a hot-filtration) afforded pale yellow crystals of  $\text{Ph}_3\text{SnCl}$  (38.09 g, 0.099 mol 79 %). (ii) A three-neck one litre round bottom flask was fitted with a stir-bar, addition funnel, condenser and stopper, and flame-dried under an atmosphere of nitrogen. The flask was then charged with  $\text{Ph}_3\text{SnCl}$  (38.25 g, 0.099 mol) and  $\text{Et}_2\text{O}$  (450 mL). With rapid stirring, the mixture was cooled to 0 °C using an ice/water bath, and 33.5 mL of  $\text{MeMgBr}$  solution (3.0 M in  $\text{Et}_2\text{O}$ ) was added dropwise using the addition funnel. After warming to room temperature and stirring for an additional two hours, the reaction mixture was quenched with an aqueous solution of  $\text{NH}_4\text{Cl}$  (ca. 300 mL). The aqueous layer was extracted with  $\text{Et}_2\text{O}$  (2 x 70 mL) and the organic fractions were combined, dried over  $\text{MgSO}_4$ , filtered, and the solvent removed via rotary evaporator to afford a pale yellow oil that recrystallized on standing to afford white crystals of  $\text{Ph}_3\text{SnMe}$  (33.71 g, 0.092 mol, 93 %). (iii) A one-neck one litre round bottom flask, equipped with a stir-bar and addition funnel, was charged with  $\text{Ph}_3\text{SnMe}$  (34.94 g, 0.096 mol), benzene (30 mL) and  $\text{MeOH}$  (120 mL). With stirring, the mixture was cooled to 0 °C using an ice/water bath before a solution of bromine (10.2 mL, 0.198 mol) and  $\text{MeOH}$  (233 mL) was added dropwise using the addition funnel. The reaction mixture was allowed to warm to room temperature overnight, resulting in a transparent yellow solution. Solvent was removed via a rotary evaporator, after which  $\text{MePhSnBr}_2$  was collected by vacuum distillation (100 °C, 0.02 mmHg) as a clear colourless oil (33.12 g, 0.089 mol, 93 %).

A one neck, one litre round bottom flask was equipped with a stir bar, followed by the addition of  $\text{PhMeSnBr}_2$  (34.60 g, 0.093 mol) and  $\text{Et}_2\text{O}$  (250 mL). Saturated  $\text{NH}_4\text{Cl}$  solution (375 mL) was then added in a single portion and the mixture was stirred vigorously. After one hour, the aqueous layer was removed and extracted with  $\text{Et}_2\text{O}$  (2 x 50 mL), and then an additional 375 mL saturated  $\text{NH}_4\text{Cl}$  solution was added to the

reaction flask. The previous step was repeated twice more, except the saturated  $\text{NH}_4\text{Cl}$  solution was not added the final time. The combined organic fractions were dried over  $\text{MgSO}_4$ , filtered, and the solvent was removed using a rotary evaporator to afford a clear colourless oil (27.40 g). The residue was distilled under vacuum (87 °C, 0.09 mmHg) to afford  $\text{MePhSnCl}_2$  (**10**) as a white crystalline solid (21.55 g, 0.077 mol, 82 %).  $\delta_{\text{H}}$  ( $\text{CDCl}_3$ ) 1.34 (s, 3 H,  $^2J_{\text{SnH}} = 69.3$  Hz), 7.53 (m, 3 H, *o,p*-Ph), 7.65 (m, 2 H, *m*-Ph,  $^3J_{\text{SnH}} = 80.1$  Hz);  $\delta_{\text{C}}$  ( $\text{CDCl}_3$ ) 4.46 ( $^1J_{^{119}\text{SnC}} = 499.4$  Hz,  $^1J_{^{117}\text{SnC}} = 477.4$  Hz,  $\text{SnCH}_3$ ), 129.54 ( $^2J_{\text{SnC}} = 82.0$  Hz, *m*-Ph), 131.62 ( $^4J_{\text{SnC}} = 16.8$  Hz, *p*-Ph), 134.47 ( $^3J_{\text{SnC}} = 64.0$  Hz, *o*-Ph), 138.69 ( $^1J_{^{119}\text{SnC}} = 754.2$  Hz,  $^1J_{^{117}\text{SnC}} = 721.8$  Hz, *ipso*-Ph);  $\delta_{\text{Sn}}$  ( $\text{CDCl}_3$ ) 57.2. IR,  $\text{cm}^{-1}$  (relative intensity): 3023 (w), 1479 (m), 1432 (m), 1333 (w), 1071 (m), 1021 (w), 996 (m), 781 (m), 730 (s), 690 (s). EI-MS,  $m/z$  (relative intensity; Sn-containing isotopomeric clusters are represented by the  $^{120}\text{Sn}$  isotopomer and are indicated with an asterisk): 281.9\* (51,  $\text{M}^+$ ), 266.9\* (38,  $\text{M}^+ - \text{CH}_3$ ), 246.9\* (13,  $\text{M}^+ - \text{Cl}$ ), 206.9\* (5,  $\text{M}^+ - \text{C}_6\text{H}_6$ ), 154.9\* (85,  $\text{SnCl}^+$ ), 119.9\* (20,  $\text{Sn}^+$ ), 77.0 (43,  $\text{C}_6\text{H}_5^+$ ), 51.0 (6,  $\text{C}_4\text{H}_3^+$ ). HRMS: ( $\text{C}_7\text{H}_8^{35}\text{Cl}_2^{120}\text{Sn}$ ) calcd 281.9025, found 281.9022. The  $^1\text{H}$ ,  $^{13}\text{C}$  and  $^{119}\text{Sn}$  NMR and mass spectra are in reasonable agreement with those previously reported.<sup>19,20</sup>

*Dichlorodimesitylstannane* (**11**) was prepared as an off-white solid (m.p.

182.2-183.3 °C<sup>21</sup>) using procedures adapted from those of Dakternieks and coworkers,<sup>16</sup> using a mixture of  $\text{Mes}_2\text{SnXX}'$  ( $\text{XX}' = \text{Cl}_2, \text{ClBr}, \text{Br}_2$ ) as



starting reagent. The mixture of dimesityltin dihalides was prepared by the method of Molloy and coworkers,<sup>22</sup> and was found to contain a mixture of  $\text{Mes}_2\text{SnCl}_2$  (51 %),  $\text{Mes}_2\text{SnClBr}$  (40 %), and  $\text{Mes}_2\text{SnBr}_2$  (9 %). The identity of the compounds and their relative proportions were determined using the  $^{119}\text{Sn}$  NMR spectrum and *o*-Me protons in the  $^1\text{H}$  NMR spectrum, respectively, with comparison to literature spectra.<sup>22,23</sup>

A two-neck, 500 mL round bottom flask fitted with a stir-bar, condenser, and addition funnel, was charged with Mg turnings (3.90 g, 0.160 g-atom) before the glassware was flame-dried under an atmosphere of argon. THF (90 mL) was added to the flask and the solution was cooled to 0 °C using an ice / water bath. A mixture of 2-bromomesitylene (22 mL, 0.145 mol) in THF (25 mL) was added dropwise via the addition funnel, resulting in a brown colouration of the reaction mixture. The resulting THF solution of 2-mesitylmagnesium bromide was allowed to reflux overnight with rapid stirring. A separate three-neck 500 mL round bottom flask was equipped with a stir-bar, addition funnel, condenser and septum, and was flame dried under an atmosphere of nitrogen. THF (50 mL) was added and the solution cooled to ca. -78 °C using a dry ice / acetone bath. SnCl<sub>4</sub> (4.8 mL, 0.041 mol) was slowly added via syringe, followed by the dropwise addition of the Grignard reagent prepared in the previous step, using the addition funnel. The resulting milky white mixture was allowed to stir for an additional ca. 16 hours at room temperature. The solution was quenched with 6 M HCl solution (ca. 20 mL), followed by the addition of Et<sub>2</sub>O (80 mL). The aqueous layer was removed and back extracted with Et<sub>2</sub>O (2 x 20 mL). The combined organic extracts were dried over Na<sub>2</sub>SO<sub>4</sub>, filtered, and the solvent removed on a rotary evaporator to afford a yellow solid (17.04 g) identified by its <sup>1</sup>H and <sup>119</sup>Sn NMR spectra (CDCl<sub>3</sub>) as containing a mixture of Mes<sub>2</sub>SnCl<sub>2</sub> (δ<sub>H</sub> 2.56 (s, 12 H, *o*-Me); δ<sub>Sn</sub> -50.8), Mes<sub>2</sub>SnClBr (δ<sub>H</sub> 2.57 (s, 12 H, *o*-Me); δ<sub>Sn</sub> -96.0), and Mes<sub>2</sub>SnBr<sub>2</sub> (δ<sub>H</sub> 2.58 (s, 12 H, *o*-Me); δ<sub>Sn</sub> -146.0) in relative proportions of (0.51):(0.40):(0.09).

A one neck, 500 mL round bottom flask was charged with a stir bar, the crude product mixture (17.04 g) described above, Et<sub>2</sub>O (40 mL) and toluene (60 mL). Saturated aqueous NH<sub>4</sub>Cl solution (50 mL) was added and the mixture was stirred vigorously. After one hour, the aqueous layer was removed and back-extracted with toluene (15 mL), while

an additional 50 mL saturated  $\text{NH}_4\text{Cl}$  solution was added to the reaction flask. The previous step was repeated twice more, except the saturated  $\text{NH}_4\text{Cl}$  solution was not added the final time. The combined organic fractions were dried over  $\text{Na}_2\text{SO}_4$ , filtered, and the solvent was removed using a rotary evaporator to afford a yellow solid (7.68 g). The solid was recrystallized from hot toluene to afford an off-white solid (4.15 g, 9.70 mmol, 23 % from  $\text{SnCl}_4$ ), which was identified as **11** on the basis of its  $^1\text{H}$ ,  $^{13}\text{C}$  and  $^{119}\text{Sn}$  NMR and mass spectra, which are in good agreement with those previously reported.<sup>21,22</sup>

$\delta_{\text{H}}$  ( $\text{CDCl}_3$ ) 6.94 (s, 4 H,  $^4J_{\text{SnH}} = 36.2$  Hz, *m*- $\text{C}_6\text{H}_2\text{Me}_3$ ), 2.55 (s, 12 H,  $^4J_{\text{SnH}} = 9.4$  Hz, *o*- $\text{C}_6\text{H}_2\text{Me}_3$ ), 2.30 (s, 6 H, *p*- $\text{C}_6\text{H}_2\text{Me}_3$ );  $\delta_{\text{C}}$  ( $\text{CDCl}_3$ ) 21.1 (*p*- $\text{C}_6\text{H}_2\text{Me}_3$ ), 24.7 ( $^3J_{\text{SnC}} = 49$  Hz, *o*- $\text{C}_6\text{H}_2\text{Me}_3$ ), 129.5 ( $^3J_{\text{SnC}} = 75$  Hz, *m*- $\text{C}_6\text{H}_2\text{Me}_3$ ), 139.1 ( $^1J_{\text{SnC}} = 760$  Hz, *ipso*- $\text{C}_6\text{H}_2\text{Me}_3$ ), 141.4 ( $^4J_{\text{SnC}} = 14$  Hz, *p*- $\text{C}_6\text{H}_2\text{Me}_3$ ), 143.5 ( $^2J_{\text{SnC}} = 60$  Hz, *o*- $\text{C}_6\text{H}_2\text{Me}_3$ );  $\delta_{\text{Sn}}$  ( $\text{CDCl}_3$ ) -51.

IR,  $\text{cm}^{-1}$  (relative intensity): 2914 (w), 1596 (m), 1559 (w), 1442 (m), 1408 (w), 1376 (w), 1293 (m), 1036 (m), 849 (s), 700 (m). EI-MS, *m/z* (relative intensity; Sn-containing isotopomeric clusters are represented by the  $^{120}\text{Sn}$  isotopomer and are indicated with an asterisk): 428.0\* (4,  $\text{M}^+$ ), 413.0\* (3,  $\text{M}^+ - \text{CH}_3$ ), 393.0\* (29,  $\text{M}^+ - \text{Cl}$ ), 307.9\* (67,  $\text{M}^+ - \text{C}_9\text{H}_{11}$ ), 238.1 (64,  $\text{C}_{18}\text{H}_{22}^+$ ), 223.13 (59,  $\text{C}_{17}\text{H}_{19}^+$ ), 207.1\* (15,  $\text{M}^+ - \text{C}_9\text{H}_{11}\text{Cl}$ ), 155.0\* (38,  $\text{SnCl}^+$ ), 118.1 (100,  $\text{C}_9\text{H}_{10}^+$ ), 91.1 (41,  $\text{C}_7\text{H}_7^+$ ). An acceptable HRMS (for  $\text{C}_{18}\text{H}_{22}^{35}\text{Cl}_2^{120}\text{Sn}$ ; calcd 428.0121) has yet to be obtained. (*Synthesis by J. Woodard*)

*Hexakis(2,4,6-trimethylphenyl)cyclotristannoxane (12)* was

synthesized according to the method of Lockhart<sup>24</sup> using  $\text{Mes}_2\text{SnCl}_2$

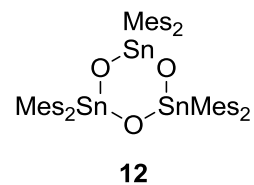
(**11**) as the starting reagent. A 1-neck 250 mL round bottom flask

was charged with a stir-bar,  $\text{Mes}_2\text{SnCl}_2$  (**11**, 0.36 g, 0.84 mmol),

toluene (35 mL) and 7 M NaOH (35 mL). The flask was fitted with a condenser and the

solution refluxed for 17 hours. The aqueous layer was removed and extracted with

toluene (ca. 10 mL). The combined organic fractions were dried with sodium sulphate,

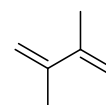




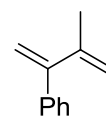
filtered and the solvent removed using a rotary evaporator to afford a crude solid (0.40 g). Recrystallization from hot toluene afforded colourless crystals (m.p. 221-223 °C<sup>25</sup>) identified as **12** (0.30 g, 0.27 mmol, 96 %). Spectroscopic data obtained for **12** is in agreement with those previously reported.<sup>24,25</sup>  $\delta_{\text{H}}$  (CDCl<sub>3</sub>) 6.60 (s, 12 H,  $^4J_{\text{SnH}} = 26.8$  Hz, *m*-C<sub>6</sub>H<sub>2</sub>Me<sub>3</sub>), 2.40 (s, 36 H,  $^4J_{\text{SnH}} = 8.5$  Hz, *o*-C<sub>6</sub>H<sub>2</sub>Me<sub>3</sub>), 2.20 (s, 18 H, *p*-C<sub>6</sub>H<sub>2</sub>Me<sub>3</sub>);  $\delta_{\text{C}}$  (CDCl<sub>3</sub>) 144.1 ( $^2J_{\text{SnC}} = 49$  Hz, *o*-C<sub>6</sub>H<sub>2</sub>Me<sub>3</sub>), 140.7 ( $^1J_{\text{SnC}} = 779$  Hz, *ipso*-C<sub>6</sub>H<sub>2</sub>Me<sub>3</sub>), 138.5 ( $^4J_{\text{SnC}} = 13$  Hz, *p*-C<sub>6</sub>H<sub>2</sub>Me<sub>3</sub>), 127.7 ( $^3J_{\text{SnC}} = 68$  Hz, *m*-C<sub>6</sub>H<sub>2</sub>Me<sub>3</sub>), 23.8 ( $^3J_{\text{SnC}} = 38$  Hz, *o*-C<sub>6</sub>H<sub>2</sub>Me<sub>3</sub>), 21.1 (*p*-C<sub>6</sub>H<sub>2</sub>Me<sub>3</sub>);  $\delta_{\text{Sn}}$  (CDCl<sub>3</sub>) -103 ( $^2J_{\text{SnSn}} = 306$  Hz). IR, cm<sup>-1</sup> (relative intensity): 2917 (m), 1598 (w), 1450 (m), 1410 (w), 1376 (w), 1261 (w), 1028 (m), 844 (m), 801 (m), 724 (s). (*Synthesis by J. Woodard*)

### 8.7.3. Compounds Identified *In-situ* by Comparison with Literature Data:

*2,3-Dimethyl-1,3-butadiene* (**13**) was synthesized according to the method of Allen and Bell,<sup>26</sup> and was collected by fractional distillation (b.p. 69 °C). The spectroscopic data are in agreement with that recorded with an authentic sample (98 %; Sigma-Aldrich).  $\delta_{\text{H}}$  (C<sub>6</sub>D<sub>12</sub>) 1.88 (s, 6 H, CH<sub>3</sub>), 4.89 (s, 2 H, *cis*-H-C=C-Me), 5.00 (s, 2 H, *trans*-H-C=C-Me);  $\delta_{\text{C}}$  (C<sub>6</sub>D<sub>12</sub>) 20.8, 113.0, 143.9.<sup>27</sup>

**13**

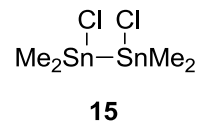
*2-Methyl-3-phenyl-1,3-butadiene* (**14**) was prepared from 1-phenyl-1,2-propanedione by the method of Alder et al.,<sup>28</sup> and was purified by column chromatography (silica gel, hexanes). The compound was obtained as a

**14**

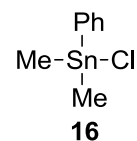
colorless liquid exhibiting <sup>1</sup>H and <sup>13</sup>C NMR spectra that were in good agreement with reported data.<sup>29</sup>  $\delta_{\text{H}}$  (C<sub>6</sub>D<sub>12</sub>) 1.94 (s, 3 H, CH<sub>3</sub>), 4.84 (s, 1 H, H<sub>2</sub>C=CMe), 5.02 (s, 1 H, H<sub>2</sub>C=CMe), 5.03 (s, 1 H, H<sub>2</sub>C=CPh), 5.22 (s, 1 H, H<sub>2</sub>C=CPh), 7.19 (m, 3 H, H-Ar), 7.13 - 7.18 (2 H, resonance obscured);  $\delta_{\text{C}}$  (C<sub>6</sub>D<sub>12</sub>) 21.4, 113.5, 117.2, 127.5, 128.2, 129.2, 142.4, 144.3, 152.4.<sup>29</sup>

$(\text{SnMe}_2)_n$ <sup>30</sup>:  $\delta_{\text{H}}$  ( $\text{C}_6\text{D}_{12}$ ) 0.35 - 0.46 (m);  $\delta_{\text{Sn}}$  ( $\text{C}_6\text{D}_{12}$ ) -242.0, -245.6, -243.8.

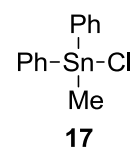
$\text{Me}_2\text{ClSnSnClMe}_2$ <sup>30,31</sup> (**15**):  $\delta_{\text{H}}$  ( $\text{C}_6\text{D}_{12}$ ) 0.81 (s, 12 H,  $^2J_{\text{SnH}} = 51.1$  Hz,  $^3J_{\text{SnH}} = 12.8$  Hz);  $\delta_{\text{Sn}}$  ( $\text{C}_6\text{D}_{12}$ ) 99.2.



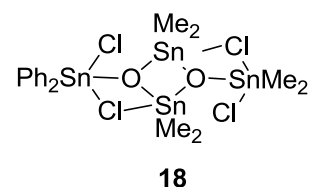
$\text{PhMe}_2\text{SnCl}$ <sup>32</sup> (**16**):  $\delta_{\text{H}}$  ( $\text{C}_6\text{D}_{12}$ ) 0.69 (s, 6 H,  $^2J_{\text{SnH}} = 57.7$  Hz) (The remaining peaks could not be resolved);  $\delta_{\text{Sn}}$  ( $\text{C}_6\text{D}_{12}$ ) 85.0.



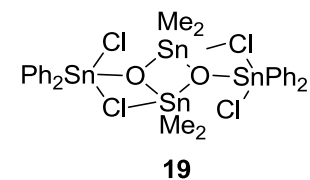
$\text{Ph}_2\text{MeSnCl}$  (**17**):  $\delta_{\text{H}}$  ( $\text{C}_6\text{D}_{12}$ ) 0.84 (s, 3 H,  $^2J_{\text{SnH}} = 58.4$  Hz) (The remaining peaks could not be resolved);  $\delta_{\text{Sn}}$  ( $\text{C}_6\text{D}_{12}$ ) 19.1.



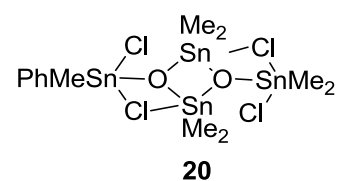
$(\text{Ph}_2\text{SnCl}_2)(\text{Me}_2\text{SnO})_2(\text{Me}_2\text{SnCl}_2)$  (**18**):  $\delta_{\text{H}}$  ( $\text{C}_6\text{D}_{12}$ ) 8.09 (d, 4 H,  $^3J = 7.8$  Hz, *o*-Ph). The remaining peaks could not be resolved.



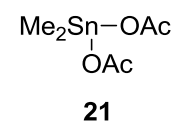
$(\text{Ph}_2\text{SnCl}_2)_2(\text{Me}_2\text{SnO})_2$  (**19**):  $\delta_{\text{H}}$  ( $\text{C}_6\text{D}_{12}$ ) 8.06 (d, 8 H,  $^3J = 7.5$  Hz, *o*-Ph). The remaining peaks could not be resolved.



$(\text{MePhSnCl}_2)(\text{Me}_2\text{SnO})_2(\text{Me}_2\text{SnCl}_2)$  (**20**):  $\delta_{\text{H}}$  ( $\text{C}_6\text{D}_{12}$ ) 8.08 (d, 2 H,  $^3J = 7.4$  Hz, *o*-Ph). The remaining peaks could not be resolved.

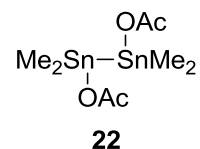


$\text{Me}_2\text{Sn}(\text{OAc})_2$ <sup>33</sup> (**21**):  $\delta_{\text{H}}$  ( $\text{C}_6\text{D}_{12}$ ) 0.81 (s, 6 H,  $^2J_{\text{SnH}} = 83.7$  Hz,  $\text{SnCH}_3$ ) (other resonances could not be resolved);  $\delta_{\text{H}}$  ( $\text{CDCl}_3$ ) 1.01 (s, 6 H,  $^2J_{\text{SnH}} = 80.3$  Hz,  $\text{SnCH}_3$ ), 2.06-2.10 (s, 6 H,  $\text{O}=\text{C}-\text{CH}_3$ );  $\delta_{\text{H}}$  ( $\text{CD}_2\text{Cl}_2$ ) 0.95 (s, 6 H,



$^2J_{\text{SnH}} = 84.1$  Hz,  $\text{SnCH}_3$ ), 2.05 (s, 6 H,  $\text{O}=\text{C}-\text{CH}_3$ );  $\delta_{\text{C}}$  ( $\text{C}_6\text{D}_{12}$ ) 3.76 (other resonances could not be resolved);  $\delta_{\text{C}}$  ( $\text{CDCl}_3$ ) 4.10, 21.40 (resonance obscured due to **22**), 181.34 (resonance obscured due to **22**);  $\delta_{\text{C}}$  ( $\text{CD}_2\text{Cl}_2$ ) 4.18, 20.72, 181.71,  $\delta_{\text{C}}$  ( $\text{C}_6\text{D}_6$ ) 3.67;  $\delta_{\text{Sn}}$  ( $\text{C}_6\text{D}_{12}$ ) -130.29;  $\delta_{\text{Sn}}$  ( $\text{CDCl}_3$ ) -115.87;  $\delta_{\text{Sn}}$  ( $\text{CD}_2\text{Cl}_2$ ) -120.01.

$Me_2(OAc)SnSn(OAc)SnMe_2$ <sup>34</sup> (**22**):  $\delta_H$  ( $C_6D_{12}$ ) 0.55 (s, 12 H,  $^2J_{SnH} = 60.0$  Hz,  $^3J_{SnH} = 12.7$  Hz,  $SnCH_3$ ) (other resonances could not be resolved);  $\delta_H$  ( $CDCl_3$ ) 0.67 (s, 12 H,  $^2J_{SnH} = 59.2$  Hz,  $^3J_{SnH} = 12.9$  Hz,  $SnCH_3$ ), 2.05-2.07 (s, 6 H,  $O=C-CH_3$ ) (resonance obscured due to **21**);  $\delta_C$  ( $C_6D_{12}$ ) -2.98 ( $^1J_{119SnC} = 372.0$  Hz,  $^1J_{117SnC} = 356.7$  Hz,  $^2J_{SnC} = 84.8$  Hz,  $SnCH_3$ ) (other resonances could not be resolved);  $\delta_C$  ( $CDCl_3$ ) -2.48 ( $^1J_{119SnC} = 365.7$  Hz,  $^1J_{117SnC} = 348.8$  Hz,  $^2J_{SnC} = 83.0$  Hz,  $SnCH_3$ ), 21.40 (resonance obscured due to **21**), 181.34 (resonance obscured due to **21**);  $\delta_{Sn}$  ( $C_6D_{12}$ ) -130.71;  $\delta_{Sn}$  ( $CDCl_3$ ) -117.08.



$H_2$ <sup>35</sup> (**23**):  $\delta_H$  ( $C_6D_{12}$ ) 4.54 (s, 2 H).

H-H

**23**

$HD$ <sup>35</sup> (**24**):  $\delta_H$  ( $C_6D_{12}$ ) 4.50 (s, 1 H,  $^1J_{HD} = 42.5$  Hz).

H-D

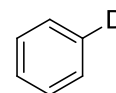
**24**

$CH_3D$ <sup>36</sup> (**25**):  $\delta_H$  ( $C_6D_{12}$ ) 0.17 (s, 3 H,  $^2J_{HD} = 1.9$  Hz);  $\delta_C$  ( $C_6D_{12}$ ) -4.9 ( $^1J_{CD} = 19.6$  Hz).

$H_3C-D$

**25**

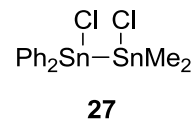
$Benzene-d^{37}$  (**26**):  $\delta_H$  ( $C_6D_{12}$ ) 7.22 (s, 5 H, obscured by the resonance due to benzene);  $\delta_C$  ( $C_6D_{12}$ ) 128.4 ( $^1J_{CD} = 24.5$  Hz, *ipso*-Ph), 128.6 (*o*-Ph), 128.7 (*m,p*-Ph, obscured by the resonance due to benzene).



**26**

#### 8.7.4. New Compounds Identified *In-situ*:

$Ph_2ClSnSnClMe_2$  (**27**):  $\delta_H$  ( $C_6D_{12}$ ) 0.89 (s, 6 H,  $^2J_{SnH} = 52.4$  Hz,  $^3J_{SnH} = 13.7$  Hz,  $SnCH_3$ ). The remaining peaks could not be resolved. Compound **27** was tentatively assigned on the basis of its diagnostic methyl-tin

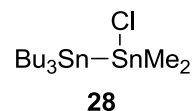


resonance, and is the expected primary product of insertion of  $SnPh_2$  into a  $Sn-Cl$  bond of  $Me_2SnCl_2$ . **27** was identified as the primary product generated from the photolysis of a deaerated  $C_6D_{12}$  solution of **2** (0.04 M) containing  $Me_2SnCl_2$  (0.035 M) after a ca. 3% conversion of **2** (see Chapter 2, Figure S2.9). In addition, the concentration versus time plots for **27** indicate light sensitivity at higher conversion rates, and reactivity with

molecular oxygen. These are all qualitatively consistent with what would be expected for **27**.<sup>38,39</sup> The formation of  $\text{Ph}_2\text{SnCl}_2$ , **9**, **16**, **17**, and **18** can all be attributed to the initial formation of **27** followed by air oxidation or secondary photolysis.

*1,1,1-Tributyl-2-chloro-dimethyldistannane (28)*:  $\delta_{\text{H}}$  ( $\text{C}_6\text{D}_{12}$ ): 0.64 (s, 6

H,  $^2J_{\text{SnH}} = 41.6$  Hz,  $^3J_{\text{SnH}} = 6.4$  Hz, Sn-Me), 0.89-0.94 (t, 9 H, n-



Bu( $\text{C}^{\delta}\text{H}_3$ )), 1.11-1.26 (m, 6 H, n-Bu( $\text{C}^{\alpha}\text{H}_2$ )), 1.32-1.40 (m, 6 H, n-

Bu( $\text{C}^{\gamma}\text{H}_2$ )), 1.57-1.65 (m, 6 H, n-Bu( $\text{C}^{\beta}\text{H}_2$ ));  $\delta_{\text{C}}$  ( $\text{C}_6\text{D}_{12}$ ) 0.72 ( $^1J_{119\text{SnC}} = 198.6$  Hz,  $^1J_{117\text{SnC}}$

= 190.4 Hz,  $^2J_{\text{SnC}} = 44.2$  Hz, Sn-Me), 11.61 ( $^1J_{119\text{SnC}} = 277.2$  Hz,  $^1J_{117\text{SnC}} = 264.7$  Hz,

$^2J_{\text{SnC}} = 59.4$  Hz, n-Bu( $\text{C}^{\alpha}$ )), 13.96 (n-Bu( $\text{C}^{\delta}$ )), 28.15 ( $^3J_{\text{SnC}} = 54.9$  Hz, n-Bu( $\text{C}^{\gamma}$ )), 31.26

( $^2J_{\text{SnC}} = 20.5$  Hz,  $^3J_{\text{SnC}} = 6.4$  Hz, n-Bu( $\text{C}^{\beta}$ ));  $\delta_{\text{Sn}}$  ( $\text{C}_6\text{D}_{12}$ ) 100.4 ( $\text{Me}_2\text{ClSn}$ ), -48.4 ( $\text{Bu}_3\text{Sn}$ ).

Compound **28** (the expected primary product of insertion of  $\text{SnMe}_2$  into the Sn-Cl bond of  $\text{Bu}_3\text{SnCl}$ ) was tentatively identified as the major Sn containing product, generated from the photolysis of a deaerated  $\text{C}_6\text{D}_{12}$  solution of **1** (0.04 M) containing  $\text{Bu}_3\text{SnCl}$  (0.04 M), on the basis of its diagnostic  $^1\text{H}$ ,  $^{13}\text{C}$  and  $^{119}\text{Sn}$  NMR resonances and splitting pattern that indicate the expected connectivity for **28** (see Chapter 3.3.1).<sup>40-42</sup>

## 8.8. References

- (1) Leigh, W. J.; Harrington, C. R.; Vargas-Baca, I. *J. Am. Chem. Soc.* **2004**, *126*, 16105.
- (2) Armarego, W. L. F.; Chai, C. L. L. In *Purification of Laboratory Chemicals (Sixth Edition)*; Butterworth-Heinemann: Oxford, 2009, p 88.
- (3) Zhou, D.; Reiche, C.; Nag, M.; Soderquist, J. A.; Gaspar, P. P. *Organometallics* **2009**, *28*, 2595.
- (4) Rieke, R. D.; Xiong, G. *J. Org. Chem.* **1991**, *56*, 3109.
- (5) Weidenbruch, M.; Schafer, A.; Rankers, R. *J. Organomet. Chem.* **1980**, *195*, 171.
- (6) Neale, N. R.; Tilley, T. D. *J. Am. Chem. Soc.* **2002**, *124*, 3802.
- (7) Schäfer, A.; Weidenbruch, M.; Peters, K.; von Schnering, H.-G. *Angew. Chem. Int. Ed. Engl.* **1984**, *23*, 302.
- (8) Weidenbruch, M.; Thom, K.-L.; Pohl, S.; Saak, W. *J. Organomet. Chem.* **1987**, *329*, 151.
- (9) Neumann, W. P.; König, K. *J. Liebigs Ann. Chem.* **1964**, 677, 1.

- (10) Dräger, M.; Mathiasch, B.; Ross, L.; Ross, M. *Z. Anorg. Allg. Chem.* **1983**, 506, 99.
- (11) Saito, M.; Okamoto, Y.; Yoshioka, M. *Appl. Organomet. Chem.* **2005**, 19, 894.
- (12) Okawara, R.; Wada, M. *J. Organomet. Chem.* **1963**, 1, 81.
- (13) Beckmann, J.; Dakternieks, D.; Kuan, F. S.; Tiekink, E. R. T. *J. Organomet. Chem.* **2002**, 659, 73.
- (14) Fujiwara, H.; Sakai, F.; Sasaki, Y. *J. Chem. Soc., Perkin Trans. 2* **1983**, 11.
- (15) Yano, T.; Nakashima, K.; Otera, J.; Okawara, R. *Organometallics* **1985**, 4, 1501.
- (16) Zobel, B.; Lim, A. E. K.; Dunn, K.; Dakternieks, D. *Organometallics* **1999**, 18, 4889.
- (17) Kozeschkow, K. A.; Nadj, M. M.; Alexandrow, A. P. *Ber. Dtsch. Chem. Ges. (A and B Series)* **1934**, 67, 1348.
- (18) Smith, S. E.; Sasaki, J. M.; Bergman, R. G.; Mondloch, J. E.; Finke, R. G. *J. Am. Chem. Soc.* **2008**, 130, 1839.
- (19) Gielen, M.; Vanden Eynde, I. *J. Organomet. Chem.* **1981**, 217, 205.
- (20) Lloyd, N.; Nicholson, B.; Wilkins, A. *J. Organomet. Chem.* **2006**, 691, 2757.
- (21) Berwe, H.; Haas, A. *Chem. Ber.* **1987**, 120, 1175.
- (22) Brown, P.; Mahon, M. F.; Molloy, K. C. *J. Organomet. Chem.* **1992**, 435, 265.
- (23) Chandrasekhar, V.; Thirumoorathi, R. *J. Chem. Sci.* **2010**, 122, 687.
- (24) Lockhart, T. P.; Puff, H.; Schuh, W.; Reuter, H.; Mitchell, T. N. *J. Organomet. Chem.* **1989**, 366, 61.
- (25) Weber, U.; Pauls, N.; Winter, W.; Stegmann, H. B. *Z. Naturforsch.* **1982**, 37b, 1316.
- (26) Allen, C. F. H.; Bell, A. *Org. Syn.* **1942**, 22, 39.
- (27) Leigh, W. J.; Harrington, C. R. *J. Am. Chem. Soc.* **2005**, 127, 5084.
- (28) Alder, K.; Heimbach, K.; Neufang, K. *Liebigs Ann. Chem.* **1954**, 586, 138.
- (29) Leigh, W. J.; Lollmahomed, F.; Harrington, C. R. *Organometallics* **2006**, 25, 2055.
- (30) Watta, B.; Neumann, W. P.; Sauer, J. *Organometallics* **1985**, 4, 1954.
- (31) Mathiasch, B. *Inorg. Nucl. Chem. Lett.* **1977**, 13, 13.
- (32) Apodeca, P.; Cervantes-Lee, F.; Pannell, K. H. *Main Group Metal Chem.* **2001**, 24, 597.
- (33) Lockhart, T. P.; Calabrese, J. C.; Davidson, F. *Organometallics* **1987**, 6, 2479.
- (34) Mathiasch, B.; Mitchell, T. N. *J. Organomet. Chem.* **1980**, 185, 351.
- (35) Billone, P. S.; Beleznyay, K.; Harrington, C. R.; Huck, L. A.; Leigh, W. J. *J. Am. Chem. Soc.* **2011**, 133, 10523.
- (36) Skakovskii, E. D.; Stankevich, A. I.; Tychinskaya, L. Y.; Shirokii, O. V.; Choban, Y. P.; Murashko, V. L.; Rykov, S. V. *Russ. J. Gen. Chem.* **2004**, 74, 1719.
- (37) Berger, S.; Diehl, B. W. K. *Tetrahedron Lett.* **1987**, 28, 1243.
- (38) Scherping, K. H.; Neumann, W. P. *Organometallics* **1982**, 1, 1017.
- (39) Sawyer, A. K.; Brown, Y. E.; Hanson, E. L. *J. Organomet. Chem.* **1965**, 3, 464.
- (40) Duffy, I. R.; Leigh, W. J. *Organometallics* **2015**, 34, 5029.
- (41) Padelkova, Z.; Svec, P.; Pejchal, V.; Růžička, A. *Dalton Trans.* **2013**, 42, 7660.
- (42) Mitchell, T. N.; Walter, G. *J. Chem. Soc., Perkin Trans. 2* **1977**, 1842.